

LEABHARLANN CHOLÁISTE NA TRÍONÓIDE, BAILE ÁTHA CLIATH | TRINITY COLLEGE LIBRARY DUBLIN
Ollscoil Átha Cliath | The University of Dublin

Terms and Conditions of Use of Digitised Theses from Trinity College Library Dublin

Copyright statement

All material supplied by Trinity College Library is protected by copyright (under the Copyright and Related Rights Act, 2000 as amended) and other relevant Intellectual Property Rights. By accessing and using a Digitised Thesis from Trinity College Library you acknowledge that all Intellectual Property Rights in any Works supplied are the sole and exclusive property of the copyright and/or other IPR holder. Specific copyright holders may not be explicitly identified. Use of materials from other sources within a thesis should not be construed as a claim over them.

A non-exclusive, non-transferable licence is hereby granted to those using or reproducing, in whole or in part, the material for valid purposes, providing the copyright owners are acknowledged using the normal conventions. Where specific permission to use material is required, this is identified and such permission must be sought from the copyright holder or agency cited.

Liability statement

By using a Digitised Thesis, I accept that Trinity College Dublin bears no legal responsibility for the accuracy, legality or comprehensiveness of materials contained within the thesis, and that Trinity College Dublin accepts no liability for indirect, consequential, or incidental, damages or losses arising from use of the thesis for whatever reason. Information located in a thesis may be subject to specific use constraints, details of which may not be explicitly described. It is the responsibility of potential and actual users to be aware of such constraints and to abide by them. By making use of material from a digitised thesis, you accept these copyright and disclaimer provisions. Where it is brought to the attention of Trinity College Library that there may be a breach of copyright or other restraint, it is the policy to withdraw or take down access to a thesis while the issue is being resolved.

Access Agreement

By using a Digitised Thesis from Trinity College Library you are bound by the following Terms & Conditions. Please read them carefully.

I have read and I understand the following statement: All material supplied via a Digitised Thesis from Trinity College Library is protected by copyright and other intellectual property rights, and duplication or sale of all or part of any of a thesis is not permitted, except that material may be duplicated by you for your research use or for educational purposes in electronic or print form providing the copyright owners are acknowledged using the normal conventions. You must obtain permission for any other use. Electronic or print copies may not be offered, whether for sale or otherwise to anyone. This copy has been supplied on the understanding that it is copyright material and that no quotation from the thesis may be published without proper acknowledgement.

P.hD

TRINITY COLLEGE DUBLIN
27 SEP 2017
ACADEMIC REGISTRY

School of Medicine



Trinity College Dublin

Coláiste na Tríonóide, Baile Átha Cliath

The University of Dublin

Molecular mechanisms linking excess adipose tissue with esophageal cancer: Targeting tumor metabolism and 5-lipoxygenase

A dissertation submitted to the University of Dublin for the degree of Doctor of Philosophy

Zivile Useckaite

Under the supervision of Dr. Graham Pidgeon

Departmental Head: Prof. John V. Reynolds

Department of Surgery

School of Medicine

Trinity College Dublin

2017

TRINITY LIBRARY
05 APR 2018
DUBLIN

Thesis 11468

I declare that this thesis has not been submitted as an exercise for a degree at this or any other university and it is entirely my own work. I agree to deposit this thesis in the University's open access institutional repository to do so on my behalf, subject to Irish Copyright Legislation and Trinity College policy on fair use and acknowledgement.

Signed: _____ 20.03.2018

Declaration

I hereby declare that this thesis has not been submitted as an exercise for a degree at this or any other University and that it is entirely my own work except where otherwise acknowledged.

I agree that the Library may lend or copy this thesis upon request.

Zivile Useckaite
June 2017

Summary

Oesophageal adenocarcinoma (OAC) is the fastest growing cancer in the developed world. Visceral obesity, and in particular factors secreted from metabolically active visceral adipose tissue, may alter tumour glycolytic pathways resulting in a more aggressive phenotype. Despite major improvements to patient outcomes, less than 20% of OAC patients remain alive 5 years after diagnosis.

The rising incidence of OAC is attributed to increases in the prevalence of obesity. The mechanisms linking obesity and OAC are not fully understood, however, it is thought that visceral obesity has more relevance to the pro-carciogenic alterations than subcutaneous obesity. Strong preliminary data using an Affymetrix array platform demonstrated glycolysis to be one out of three most upregulated pathways (alongside with EMT and cytokine signalling) following co-culture of oesophageal adenocarcinoma cells with adipose explants from OAC patients. Subsequent KEGG pathway analysis showed 5-lipoxygenase (5LOX) to be one of the top ten significantly upregulated genes in OAC. 5LOX is an enzyme involved in the metabolism of arachidonic acid to pro-inflammatory bioactive lipids. It has been linked to cancer with roles in inflammation, tumourigenesis and overall survival.

The aim of this project was to delineate how excess visceral adiposity affects tumour metabolism and to investigate the role of commercially available and novel inhibitors of the glycolytic pathway and 5LOX as anti-cancer agents in obesity-driven oesophageal cancer.

Glucose transporter protein Glut 4 and glycolysis associated enzymes HK2, PKM2 GAPDH and ENO3, alongside with 5LOX were significantly higher in treatment-naive OAC tumor biopsies from viscerally obese compared to non-obese patients, suggesting that glycolysis was upregulated and was more active process in obese OAC patients. Expression of glycolytic enzymes, 5LOX and marker of hypoxia HIF1A, was confirmed by immunohistochemistry (IHC) in tumours from both obese and non-obese OAC patients. Obese patients expressed significantly higher levels of glycolytic enzymes, 5LOX and HIF1A and were associated with significantly lower five-year disease specific survival compared to normal weight patients, suggesting that visceral adiposity was

contributing to the prognosis of the disease and that there was a need of novel targets for treatment of OAC in obese patients.

The Seahorse XFe24 analyser was used to investigate the ability of commercially available and novel inhibitors of 5LOX to alter glycolysis in OE33 cells and whether the alterations were maintained or became more significant following induction of glycolysis by ACM. Results revealed that commercially available inhibitors of 5LOX MK886 and Ketoconazole significantly reduced glycolysis in OE33 cells following 24-hour treatment maintaining the same level of reduction in the presence of ACM. Interestingly, novel inhibitors HS6 and NIH4, both significantly reduced glycolytic OE33 cell activity following 24-hour treatment and the reduction was significantly greater following treatment of OE33 cells in the presence of ACM, suggesting that the novel inhibitors could potentially be more beneficial in reducing obesity driven glycolysis in OAC. Following the findings that HS6 and NIH4 may be potentially more effective in reducing obesity-induced glycolysis in OE33 cells, NIH4 was shown to have a significantly greater effect in reducing glycolysis in OE33 cells under hypoxic (0.5% O_2) conditions compared to normoxic environment.

Inflammation I and Oncology II multiplex immunoassays were employed to assess pathways altered *ex vivo* using esophageal tumor explants and treating them with novel inhibitors of 5LOX. Results suggested that the novel inhibitor NIH4 exhibited anti-inflammatory and anti-tumourigenic effects by downregulating a number of secreted growth factors, cytokines, pro-inflammatory and pro-tumourigenic factors. NIH4 reduced OAC tumor secretions included VEGFA, TGF-alpha, SCF, MCP3, WISP1, CTSV, ESM-1 and CYR61.

In conclusion, this study demonstrated that glycolysis, hypoxia and 5-lipoxygenase were involved in progression of OAC and were associated with visceral obesity. High expression of markers of glycolysis, hypoxia and 5LOX were associated with more aggressive cancer type and poor OAC-specific survival. Assessment of novel 5LOX inhibitors in both *in vitro* and *ex vivo* models of OAC have indicated the importance of these pathways in the regulation of cell growth and survival. Therefore, targeting 5LOX may be a therapeutic strategy in the treatment of OAC. Further studies are required to determine whether 5LOX is preferentially expressed in early or later stages of the disease, and at what point of the disease targeting this enzyme would be the most efficacious.

Acknowledgements

First and foremost, I would like to thank Dr. Graham Pidgeon for the endless hard work and dedication that you put into my project throughout the duration of the PhD. I simply can't thank you enough for being a supervisor and a friend, helping me to become, I feel, a better all-round scientist. I feel very privileged to have worked with you.

Within the Department of Surgery, I would like to single out Dr. Jacintha O'Sullivan and Dr. Joanne Lysaght, Prof. Reynolds and Dr. Niamh Lynam-Lennon for all their constructive input and support throughout the Ph.D. In addition, I also would like to acknowledge all the girls in the reading room: Emma Folley, Amy Buckley, Aoife Dunne, Aoife Cannon, Róisín Byrne, Gill Moore, Maria Kavanagh, Niamh Gilmartin, Niamh Clarke and our only boy James Phelan. Thank you for making the years of my PhD so enjoyable and a rather entertaining experience.

To my parents, thank you for your constant support- financial, emotional and everything in between.

Last but not least, my sister Egle, thank you so much for always being there for me. Thanks for all the late night lifts home, listening to all my "failed Western Blot" drama, numerous cups of tea and everything in between. I couldn't have done without you.

Table of Contents

Declaration ---- i
Summary ---- ii
Acknowledgements ---- iv
List of Figures ---- xii
List of Tables ---- xxi
Abbreviations ---- xxiv
Units ---- xxvi
Poster Presentations ---- xxviii
Awards ---- xxviii
Courses Attended ---- xxviii

Chapter 1

Introduction ---- 1

1.1 Oesophageal adenocarcinoma ---- 2
1.1.1 Pathology and epidemiology ---- 2
1.1.2 Other risk factors ---- 5
1.1. Clinical presentation, diagnosis and staging ---- 5
1.1.4 Biology of oesophageal adenocarcinoma ---- 6
1.1.5 Molecular mechanisms of oesophageal adenocarcinoma ---- 7
1.1.6 Recurrence pattern ---- 9
1.1.7 Inflammatory sequence to cancer / Barrett's ---- 10
1.1.8 Standard treatment regimen ---- 14
1.1.9 Potential targeted therapies in oesophageal adenocarcinoma ---- 16
1.1.10 Potential novel therapies in oesophageal adenocarcinoma ---- 17
1.1.10.1 Eicosanoids ---- 17
1.1.10.2 The potential role of 5-lipoxygenase in cancer progression ---- 18
1.1.10.3 Blocking 5-lipoxygenase signaling in cancer ---- 20
1.1.10.4 5-lipoxygenase in oesophageal cancer ---- 21
1.2 Obesity ---- 22
1.2.1 Obesity and cancer ---- 22
1.2.1.1 Obesity and oesophageal adenocarcinoma ---- 23
1.2.2 Obesity epidemiology ---- 26
1.2.3 Adipose tissue distribution ---- 26
1.2.3.1 White and brown fat ---- 28
1.2.4 Measuring obesity ---- 30

1.2.5 The tumour microenvironment ---- 32
1.2.6 The role of adipose tissue in the tumour microenvironment ---- 34
1.2.7 Hallmarks of cancer and potential role of visceral obesity in tumourigenesis ---- 38
1.2.8 Epithelial Mesenchymal Transition (EMT) ---- 41
1.2.8.1 Cadherin switching in EMT ---- 42
1.3 Tumour metabolism ---- 43
1.3.1 Metabolic pathways ---- 43
1.3.2 Glycolysis ---- 43
1.3.2.1 Glucose transporter proteins ---- 45
1.3.2.2 Hexokinases ---- 47
1.3.2.3 Pyruvate kinase M2 ---- 48
1.3.2.4 Glyceraldehyde-3-phosphate dehydrogenase ---- 48
1.3.2.5 Enolase 3 ---- 49
1.3.3 Oxidative phosphorylation ---- 50
1.3.3.1 ATP synthase subunit beta (ATP5B) ---- 51
1.3.4 The Warburg effect ---- 52

Chapter 2

Materials and Methods ---- 55

2.1 Reagents and general lab equipment ---- 56
2.2 Drugs, chemical reagents and other materials ---- 56
2.3 *In-vitro* cell culture ---- 56
2.3 Cell culture ---- 57
2.3.1 Cell line ---- 57
2.3.2 Cell counting ---- 58
2.3.3 Reverse cell transfection with siRNA ---- 58
2.3.4 Mycoplasma testing ---- 58
2.4 Patient tissue samples ---- 59
2.5 Anthropometry ---- 60
2.6 Isolation of RNA from epithelial tissue ---- 61
2.7 Isolation of RNA from cells ---- 61
2.8 RNA quantification ---- 62
2.9 cDNA synthesis ---- 63
2.10 Probe-based quantitative reverse transcription polymerase chain reaction ---- 64
2.11 Screening via RT^2 Profiler PCR Arrays ---- 65

2.12 SYBR-based quantitative reverse transcription polymerase chain reaction ---- 67
2.13 Immunohistochemistry ---- 69
2.13.1 Construction of tissue microarrays ---- 69
2.13.2 Staining procedure using tissue microarrays ---- 70
2.13.3 Imaging and scoring stromal and epithelial staining ---- 71
2.14 Cell and tissue lysate preparation ---- 71
2.14.1 Cultured cells ---- 71
2.14.2 Tissue ---- 72
2.15 Protein quantification ---- 72
2.16 Acetone precipitation of proteins ---- 73
2.17 Protein SDS-PAGE and Western blotting ---- 73
2.17.1 Protein separation by SDS-PAGE ---- 73
2.17.2 Protein Transfer ---- 74
2.17.3 Visualization of proteins – Ponceau S Stain ---- 74
2.17.4 Western Blotting ---- 74
2.18 Drug Screening ---- 75
2.18.1 MTT - Cell viability assay ---- 75
2.18.2 BrdU – Cell proliferation assay ---- 76
2.18.3 xCeLLigence RTCA for cell proliferation ---- 77
2.18.4 Seahorse XFe24 analyser ---- 77
2.18.5 Crystal Violet Assay ---- 78
2.19 Investigation of pathways altered *ex vivo* in oesophageal tumour explants using Olink Platform ---- 78
2.19.1 Tumour explant culture ---- 78
2.19.2 Proseek® Multiplex Inflammation I and Oncology II 96x96 multiplex OAC immunoassay ---- 79
2.20 Enzyme-linked Immunosorbent Assay ---- 80
2.20.1 Competitive ELISA ---- 80
2.20.2 DuoSet sandwich ELISA ---- 81
2.21 Statistical analysis ---- 82

Chapter 3

Expression of markers of glycolysis, OXPHOs, hypoxia and 5LOX in oesophageal adenocarcinoma, and their association with clinical and pathological features ---- 83

3.1 Introduction ---- 84

3.2 Aims and objectives ---- 87
3.3.1 Oesophageal adenocarcinoma tissue microarray demographics -- 88
3.3.2 Association of glucose transporter proteins and glycolytic markers with obesity and clinical data ---- 89
3.3.2.1 Differential expression of glucose transporter proteins and glycolytic markers and tissue type ---- 89
3.3.2.2. Glucose transporter protein and glycolytic marker expression and lymph node involvement in oesophageal adenocarcinoma ---- 97
3.3.2.3. Glucose transporter protein and glycolytic marker expression and venous involvement in oesophageal adenocarcinoma ---- 99
3.3.2.4 Association between, glucose transporter proteins and glycolytic markers and metabolic tumour activity (PET SUV) ---- 101
3.3.2.5 Epithelial expression of the glucose transporters and the markers of glycolysis and their association with disease-specific survival 103
3.3.3 Association of markers of hypoxia, oxidative phosphorylation and 5-LOX with clinical parameters in OAC ---- 107
3.3.3.1 Differential expression of 5-LOX, ATP5B, HIF1A and CAIX and tissue type ---- 107
3.3.3.2 Association of 5-LOX, ATP5B, HIF1A and CAIX with lymph node involvement in oesophageal adenocarcinoma ---- 112
3.3.2.3 5-LOX, ATP5B, HIF1A and CAIX expression and their association with venous involvement in oesophageal adenocarcinoma ---- 112
3.3.3.4 Association between 5-LOX, ATP5B, HIF1A and CAIX with metabolic tumour activity (PET SUV) ---- 115
3.3.3.5 Epithelial expression of 5LOX, markers of hypoxia and OXPHOS and their association with disease-specific survival ---- 115
3.4 Discussion ---- 119

Chapter 4

The link between glycolysis, OXPHOS, 5LOX and obesity in oesophageal adenocarcinoma ---- 126

4.1 Introduction ---- 127
4.2 Aims and Objectives ---- 130
4.3 Results ---- 131
4.3.1 The link between glycolysis, oxidative phosphorylation, hypoxia, 5- Lipoxygenase and obesity ---- 131
4.3.1.1 Assessment of 5-Lipoxygenase, glucose transporter protein, glycolysis, OXPHOS and hypoxia associated genes in OE33 cells co-cultured with ACM ---- 131

4.3.1.2 Assessment of 5-Lipoxygenase, glucose transporter protein, glycolysis, OXPHOS and hypoxia associated genes in OAC tumour ---------- 133

4.3.1.3 Epithelial expression of glucose transporter proteins, markers of glycolysis, OXPHOS and 5-lipoxygenase and their association with obesity---------- 140

4.3.2 Molecular delineation of the EMT process in OAC driven by adipose tissue ---------- 147

4.3.2.1 Assessment of EMT-associated genes in OE33 cells co-cultured with ACM ---------- 147

4.3.2.2 Assessment of EMT-associated genes in OAC tumour and their association with visceral obesity ---------- 150

4.3.2.3 Epithelial expression EMT markers and their association with obesity status determined by BMI ---------- 152

4.4 Discussion ---------- 155

Chapter 5

5LOX, glycolysi, OXPHOS marker association with visceral obesity in OAC patients ---------- 161

5.1 Introduction---------- 162

5.2 Aims and Objectives ---------- 165

5.3 Results---------- 166

5.3.1 Oesophageal adenocarcinoma tissue microarray demographics 166

5.3.2 Epithelial expression of glucose transporter proteins, markers of glycolysis, OXPHOS and 5-lipoxygenase and their association with visceral obesity ---------- 167

5.3.3 The association of glucose transporter protein, markers of glycolysis, OXPHOS, hypoxia and 5-lipoxygenase with clinical data ---------- 171

5.3.3.1 Differential expression of glucose transporter protein, marker of glycolysis, OXPHOS, hypoxia and 5-lipoxygenase and tissue type ---------- 171

5.3.3.2 Glucose transporter protein, glycolysis marker, 5-lipoxygenase, ATP5B and HIF1A expression and lymph node involvement in oesophageal adenocarcinoma ---------- 175

5.3.3.3 Glucose transporter protein, marker of glycolysis, 5-lipoxygenase, ATP5B and HIF1A expression and venous involvement in oesophageal adenocarcinoma ---------- 178

5.3.3.4 The association between visceral fat area, glucose transport protein, markers of glycolysis, OXPHOS, hypoxia, 5-lipoxygenase and metabolic tumour activity---------- 180

5.3.3.5 Association between metabolic tumour activity and disease-specific survival ---------- 183

5.3.3.6 Association between visceral obesity and metabolic tumour volume ---------- 184

5.3.3.7 The association between the epithelial expression of markers of metabolism and metabolic tumour volume ---------- 185

5.3.3.8 Association between metabolic tumour volume and disease-specific survival ---------- 187

5.3.3.9 Epithelial expression of glucose transporter proteins, markers of glycolysis, OXPHOS, hypoxia and 5-lipoxygenase and their association with disease-specific survival ---------- 189

5.4 Discussion ---------- 192

Chapter 6

Delineation whether visceral adiposity results in metabolic shift in glcose metabolism in oesophageal adenocarcinoma 195

6.1 Introduction ---------- 196

6.2. Aims and objectives ---------- 199

6.3 Results ---------- 200

6.3.1 Assessment of lactate secretion levels by OE33 cells following co-culture with adipose conditioned media ---------- 200

6.3.2 Assessment whether co-culture of oesophageal adenocarcinoma cells with ACM result in metabolic shift in glucose metabolism - 201

6.3.3 Delineating the expression of human glucose metabolism associated gene expression in response to ACM treatment ------ 202

6.3.3.1 Validation of glucose metabolism associated genes in OE33 cells co-cultured with ACM ---------- 206

6.3.3.2 Validation of glucose metabolism associated genes in OAC tumour biopsies ---------- 209

6.3.4 Delineation of human mitochondrial energy metabolism associated genes on OE33 cells cultured with ACM ---------- 212

6.3.4.1 Validation of human mitochondrial function associated genes in OE33 cells co-cultured with ACM ---------- 217

6.3.4.2 Validation of human mitochondrial function associated genes in OAC tumour ---------- 219

6.3.5 Investigation of the effect of hypoxia on metabolic activity in oesophageal adenocarcinoma ---------- 223

6.3.5.1 Determining the optimum concentration of $CoCl_2$ to induce hypoxia in oesophageal adenocarcinoma ---------- 223

6.3.5.2 Investigation of $CoCl_2$ effect on glycolysis and oxidative phosphorylation in oesophageal adenocarcinoma cells ---------- 225

6.3.5.3 Investigation of the optimum time required for $CoCl_2$ to induce hypoxia in oesophageal adenocarcinoma cells ---------- 227

6.3.5.4 Assessment of HIF1A expression in OAC tumour and its association with visceral obesity ---------- 229

6.4 Discussion ---------- 231

Chapter 7

Assessment of anti-cancer potential of novel 5LOX inhibitors in models of OAC ---------- 235

7.1 Introduction ---------- 236

7.2 Aims and objectives ---------- 238

7.3 Results ---------- 239

7.3.1 Oesophageal adenocarcinoma cell viability following treatment with potential glycolytic and 5-lipoxygenase inhibitors ---------- 239

7.3.2 Oesophageal adenocarcinoma cell proliferation following treatment with potential glycolytic and 5-lipoxygenase inhibitors ---------- 240

7.3.3 Assessing 5LOX activity in OAC *ex vivo* ---------- 242

7.3.4 Effect of glycolytic and 5LOX inhibitors on ECAR in oesophageal adenocarcinoma cells ---------- 246

7.3.5 Effect of novel inhibitors of 5LOX on glycolysis and mitochondrial metabolism in oesophageal adenocarcinoma cells in hypoxia --- 251

7.3.6 Human Glucose Metabolism Arrays: alterations in OE33 gene expression following novel 5-lipoxygenase inhibitor treatment 253

7.3.7 Validation of selected genes from human glucose metabolism genes from Human Glucose Metabolism RT^2 Profiler arrays ---------- 255

7.3.8 Human Mitochondrial Function Arrays: alterations in OE33 gene expression following novel 5-lipoxyhenase inhibitor treatment 258

7.3.9 Validation of selected genes from human Mitochondrial Metabolism RT^2 Profiler arrays ---------- 261

7.3.10 Investigation of pathways altered *ex vivo* using oesophageal tumour explants ---------- 263

7.3.11 Validation of pathways altered *ex vivo* using oesophageal tumour explants ---------- 272

7.3.12 Association between secreted levels of LTB4 and VEGF by OAC patient biopsies *ex vivo* ---------- 273

7.4 Discussion ---------- 275

Chapter 8

Assessment of role of ENO3 and PKM2 in OAC cell model driven by adipose conditioned media: therapeutic targetting of a specific pathway ---------- 282

8.1 Introduction ---- 283
8.2 Aims and objectives ---- 285
8.3 Results ---- 286
8.3.1 siRNA-mediated ENO3 and PKM2 knockdown in OE33 cells *in vitro* ---- 286
8.3.1.1 Relative expression of ENO3 and PKM2 in OE33 cells silenced for these genes ---- 288
8.3.1.2 Assessment of ENO3 and PKM2 protein expression in OE33 cells following targeted transfection ---- 290
8.3.2 Assessment of efficacy of novel small molecule inhibitors following silencing of ENO3 and PKM2 in OE33 cells ---- 292
8.3.3 Assessment of ENO3 and PKM2 role in glycolysis *in vitro* ---- 295
8.3.3.1 Assessment of ENO3 and PKM2 role in glycolysis *in vitro* ---- 295
8.3.3.2 Assessment of ENO3 and PKM2 role in ACM-driven glycolysis *in vitro* ---- 296
8.3.3.3 Effect of novel inhibitors of 5LOX on glycolysis in OE33 cells following transfection of ENO3, PKM2 and the combination of both ENO3 and PKM2 ---- 297
8.4 Discussion ---- 299

Chapter 9

Concluding Discussion ---- 301

9.1 Concluding discussion ---- 302
9.2 Future directions ---- 312

References ----313
Appendices ----345

List of Figures

Figure 1.1 Number of cases of esophageal cancer diagnosed per year by sex and age with age-specific incidence rate (ASIR) per 100,000 persons: 2000-2004 ---- 3

Figure 1.2 5 year survival rates for all cancers ---- 4

Figure 1.3 Molecular factors driving esophageal adenocarcinoma----8

Figure 1.4 The endoscopic detection and histology of Barrett's oesophagus---12

Figure 1.5 Pathological sequence of neoplastic transformation in esophageal adenocarcinoma ----------12

Figure 1.6 Disease-specific survival has improved in esophageal adenocarcinoma patients treated with curative intent----------15

Figure 1.7 Arachidonic acid metabolism---------- 18

Figure 1.8 Overexpression of 5-LOX in esophageal samples of EGDA rats and humans----------19

Figure 1.9 Association between body mass index and cancer incidence----------25

Figure 1.10 Association between body mass index and cancer incidence----------25

Figure 1.11 Distribution of adipose tissue----------27

Figure 1.12 Adipose tissue is stained with hematoxylin and eosin ---------- 29

Figure 1.13 Computed tomography of the abdomen----------31

Figure 1.14 The tumor microenvironment----------34

Figure 1.15 Adipose tissue constitutes an active endocrine organ----------35

Figure 1.16 Obesity is associated with a great infiltration of cells from both the innate and adaptive immune systems----------37

Figure 1.17 Hallmarks of cancer and potential role of visceral obesity in tumourigenesis----------40

Figure 1.18 Top differentially expressed genes in three significantly upregulated pathways in esophageal adenocarcinoma cells following co-culture with ACM from viscerally obese OAC patients----------41

Figure 1.19 Epithelial mesenchymal transition in cancer----------42

Figure 1.20 Glycolysis----------45

Figure 1.21 The mitochondrial electron transport chain----------51

Figure 1.22 The Warburg effect----------53

Figure 2.1 Representative image of standard curve obtained when measuring RNA----------62

Figure 2.2 Effect of phenol on UV absorbance----------63

Figure 2.3 Proseek® Multiplex Inflammation I and Oncology II^{96x96} immunoassay panel----------79

Figure 3.1 Potential glucose transporter protein and glycolytic enzyme targets in Glycolysis----------84

Figure 3.2 Tissue microarray construction ----------88

Figure 3.3 Tissue microarray Glut1 and Glut4 staining pattern in esophageal adenocarcinoma----------91

Figure 3.4 Tissue microarray HK1 and HK2 staining pattern in esophageal adenocarcinoma----------92

Figure 3.5 Tissue microarray PKM2 and GAPDH staining pattern in esophageal adenocarcinoma----------93

Figure 3.6 Tissue microarray ENO3 staining pattern in esophageal adenocarcinoma----------94

Figure 3.7 Comparison of glucose transporter protein and glycolytic marker expression in leading edge and non-leading edge esophageal adenocarcinoma----------95

Figure 3.8 Comparison of glycolytic marker expression in leading edge and non-leading edge esophageal adenocarcinoma----------96

Figure 3.9 Epithelial expression of glucose transporter proteins and glycolytic marker was associated with more aggressive tumor phenotype in OAC----------98

Figure 3.10 Epithelial expression of glucose transporter proteins and glycolytic markers and their association with venous involvement in OAC patients----------100

Figure 3.11 Association between the markers of glycolysis and tumor metabolism In OAC patients----------102

Figure 3.12 The link between epithelial Glut1 and Glut4 expression and OAC specific 5-year post-operative survival----------104

Figure 3.13 Association between epithelial HK1 and HK2 expression and OAC specific 5-year post-operative survival----------105

Figure 3.14 Association betweenPKM2 and GAPDH expression and OAC specific survival----------106

Figure 3.15 Association between ENO3 epithelial expression and disease-specific survival----------107

Figure 3.16 Tissue microarray 5-LOX staining pattern in esophageal adenocarcinoma----------109

Figure 3.17 Tissue microarray ATP5B staining pattern in esophageal Adenocarcinoma----------109

Figure 3.18 Tissue microarray HIF1A and CAIX staining pattern in esophageal adenocarcinoma----------110

Figure 3.19 Expression of 5-LOX, ATP5B, HIF1A and CAIX at the leading edge versus non-leading edge in esophageal adenocarcinoma----------111

Figure 3.20 Epithelial expression of hypoxia and OXPHOS markers and their association with tumor aggressiveness in OAC----------113

Figure 3.21 Epithelial expression of glucose transporter proteins and glycolytic markers and their association with venous involvement in OAC patients----------114

Figure 3.22 Association between 5LOX, ATP5B, HIF1A, CAIX and tumor metabolism in OAC tissue microarrays----------116

Figure 3.23 Association between 5LOX and ATP5B expression and OAC specific survival----------117

Figure 3.24 Association between HIF1A and CAIX expression and OAC specific survival----------118

Figure 4.1 Glucose transporter protein, but not hexokinase levels are higher in OE33 cells co-cultured with ACM from overweight and obese OAC patients----------132

Figure 4.2 PKM2 and GAPDH, but not ENO3 and 5LOX are associated with ACM-induced glycolysis in OE33 cells----------133

Figure 4.3 Glut1 but not Glut4 expression is associated with visceral obesity in OAC tumor----------135

Figure 4.4 HK2 but not HK1 expression is associated with visceral obesity in OAC tumor----------136

Figure 4.5 PKM2 and GAPDH expression is associated with visceral obesity in OAC patients----------137

Figure 4.6 High ENO3 and 5LOX expression is associated with visceral obesity in OAC patient tumor----------138

Figure 4.7 High level of ATP5B expression is associated with visceral obesity--139

Figure 4.8 An increase in epithelial Glut4 expression, but not Glut1 expression Is associated with obesity in OAC tissue microarrays----------142

Figure 4.9 High epithelial HK2, but not HK1 expression is associated with obesity in OAC tissue microarrays----------143

Figure 4.10 High epithelial PKM2 and GAPDH expression is associated with obesity in OAC tissue microarrays----------144

Figure 4.11 An increase in epithelial ENO3 and 5LOX expression is associated With obesity in OAC tissue microarrays----------145

Figure 4.12 Significantly higher epithelial expression of HIF1A and CAIX in overweight and obese OAC patients is not associated with increasing BMI----------146

Figure 4.13 High epithelial ATP5B expression is associated with obesity in OAC tissue microarrays----------147

Figure 4.14 Expression of EMT-associated genes in OE33 cells co-cultured with ACM----------149

Figure 4.15 The link between EMT-associated genes and visceral obesity in OAC tumor----------151

Figure 4.16 Low epithelial expression of Beta-catenin, but not E-cadherin, is associated with obesity in OAC tissue microarrays----------153

Figure 4.17 The association between epithelial E-cadherin and Beta-catenin expression and OAC-specific 5-year post-operative survival----------154

Figure 5.1 CT scans from two subjects with comparable BMI illustrating Adiposity phenotypes characterized mainly by intra-abdominal adiposity and subcutaneous adiposity----------163

Figure 5.2 High epithelial Glut4 and HK2 expression is associated with visceral obesity in OAC tissue microarrays----------169

Figure 5.3 High epithelial GAPDH and ATP5B expression is observed in viscerally obese patients but high expression is not correlated with VFA in OAC tissue microarrays ----------170

Figure 5.4 High epithelial expression of 5LOX, but not PKM2, ENO3 or HIF1A is correlated with visceral obesity in OAC tissue microarrays----------171

Figure 5.5 Comparison of glucose transport protein and glycolytic marker expression in the leading edge and non-leading edge esophageal adenocarcinoma----------173

Figure 5.6 Comparison of epithelial expression of ENO3, 5LOX, ATP5B and HIF1A in the leading edge and non-leading edge esophageal adenocarcinoma----------174

Figure 5.7 There is no association between epithelial Glut4, HK2, PKM2 or GAPDH expression and more aggressive phenotype of OAC in this cohort of patients ----------176

Figure 5.8 There is no association between epithelial ENO3, 5LOX, ATP5B or HIF1A expression and venous involvement in this cohort of OAC patients----------177

Figure 5.9 There is no association between epithelial Glut4, HK2, PKM2 or GAPDH expression and venous involvement in this cohort of OAC patients----------179

Figure 5.10 There is no association between epithelial ENO3, 5LOX, ATP5B or HIF1A expression and venous involvement in this cohort of OAC patients----------180

Figure 5.11 Association between tumor metabolism and increasing visceral fat

area ----------181

Figure 5.12 Association between markers of glycolysis and tumor metabolism in OAC patients----------182

Figure 5.13 Association between ENO3, 5LOX, ATP5B and HIF1A and tumor metabolism in OAC patients----------183

Figure 5.14 An increase in metabolic tumor activity is associated with poor survival in OAC patients ----------184

Figure 5.15 There is no positive association between increasing VFA measurement and metabolic tumor volume in OAC patients----------185

Figure 5.16 There is a significant association between GAPDH, but not GLUT4, HK2 or PKM2 with metabolic tumor volume in OAC patients --------186

Figure 5.17 There is no significant association between ENO3, 5LOX, ATP5B And HIF1A with metabolic tumor volume in this cohort of OAC patients----------187

Figure 5.18 There is no association between metabolic tumor volume and disease specific survival in this cohort of OAC patients----------188

Figure 5.19 There is no association between visceral obesity and disease-specific survival in this cohort of OAC patients----------189

Figure 5.20 There is no association between the epithelial expression of Glut4, HK2, PKM2 or GAPDH and disease-specific survival in this cohort of OAC patients----------190

Figure 5.21 There is no association between epithelial expression of ENO3, 5LOX, ATP5B or HIF1A and disease-specific survival in this cohort of OAC patients----------191

Figure 6.1 Oncogenic and tumor-suppressive pathways contributing to the cellular transformation----------198

Figure 6.2 Adipose conditioned media induces lactate secretion----------201

Figure 6.3 Co-culture of ACM with esophageal adenocarcinoma cells results in a metabolic shift in-vitro----------202

Figure 6.4 Glucose metabolism, glycolysis and TCA cycle associated genes are expressed at significantly higher level in ACM co-cultured OE33-----208

Figure 6.5 Pentose phosphate pathway and TCA cycle associated gene expression in ACM co-cultured OE33 cells compared to media only treated control----------209

Figure 6.6 Assessment of glucose metabolism, glycolysis and TCA cycle associated genes in viscerally obese and non-obese OAC patient tumor----------211

Figure 6.7 Pentose phosphate pathway and TCA cycle associated gene expression In OAC patient tumor----------212

Figure 6.8 Mitochondrial energy metabolism associated gene expression: Complex I and Complex III are not upregulated by co-culture of OE33 cells with ACM----------218

Figure 6.9 Mitochondrial energy metabolism associated gene expression: Complex V and pathway activity signature genes are upregulated by co-culture of OE33 cells with ACM ----------219

Figure 6.10 Mitochondrial energy metabolism associated gene expression: Complex I and Complex III associated gene expression in AOC patient tumor----------221

Figure 6.11 Mitochondrial energy metabolism associated gene expression: Complex V and pathway activity signature gene expression in the OAC tumor----------222

Figure 6.12 HIF1A protein levels are significantly increased following 24-hour treatment of OE33 cells with 100 μM of CoCl2 ----------224

Figure 6.13 Investigating the ability of CoCl2 to induce changes in glycolysis And mitochondrial respiration in esophageal adenocarcinoma cells *in vitro*----------226

Figure 6.14 The optimum time required for CoCl2 to induce hypoxia in OE33 cells is 8 hours----------228

Figure 6.15 HIF1A expression is significantly higher in tumor from viscerally obese compared to non-obese OAC patients----------230

Figure 7.1 OAC tumor LTB4 secretion is decreased following 5LOX inhibitor treatment----------243

Figure 7.2 5LOX inhibitors, with the exception of Zileuton, significantly reduced OE3 cell proliferation at dose of 10 μM----------244

Figure 7.3 Glycolysis pathway inhibitors significantly reduce OE33 cell proliferation at dose of 10 μM----------245

Figure 7.4 Inhibitors of 5LOX, with the exception of Zileuton, reduce glycolysis in OE33 cells----------249

Figure 7.5 Inhibitors of glycolysis, with the exception of 2-Deoxy D-Glucose, reduce glycolysis in OE33 cells----------250

Figure 7.6 Hypoxia induces the ability of NIH4, but not HS6 of reducing ECAR in OE33 cells----------252

Figure 7.7 Validation of glucose metabolism, glycolysis and TCA cycle associated gene expression following treatment with novel small molecule inhibitors HS6 and NIH4----------257

Figure 7.8 Validation of pentose phosphate pathway and TCA cycle associated gene expression following treatment with novel small molecule inhibitors HS6 and NIH4----------258

Figure 7.9 Complex I and Complex III associated gene expression in OE33 cells following treatment with novel small molecule inhibitors HS6 and NIH4----------262

Figure 7.10 Complex V and Pathway Activity associated gene expression in OE33 cells following treatment with novel small molecule inhibitors HS6 and NIH4. Treatment of OE33 cells with HS6----------263

Figure 7.11 Clustering heat map of NPX-levels of significantly altered proteins on the INF panel----------267

Figure 7.12 Assessment of inflammation-related protein marker secretions by *ex vivo* cultured biopsies following novel 5LOX inhibitor treatment: INF panel----------268

Figure 7.13 Clustering heat map of NPX-levels of significantly altered proteins on the ONC2 panel----------269

Figure 7.14 Assessment of inflammation-related protein marker secretions by

ex vivo cultured biopsies following novel 5LOX inhibitor treatment: ONC2 panel----------270

Figure 7.15 Assessment of inflammation-related protein marker secretions by *ex vivo* cultured biopsies following novel 5LOX inhibitor treatment: ONC2 panel----------271

Figure 7.16 Validation of VEGF secretions by ex vivo cultured biopsies following novel 5LOX inhibitor treatment ----------272

Figure 7.17 There is a significant association between tumor secretion levels of LTB4 and VEGF ----------273

Figure 8.1 Two methods of siRNA-targeted transfection in vitro ----------287

Figure 8.2 A 100% knock down knockdown of ENO3 and PKM2 gene expression in OE33 cells is achieved at 72 hours----------289

Figure 8.3 A 100% knockdown of ENO3 and PKM2 protein expression in OE33 cells is achieved at 72 hours----------291

Figure 8.4 Preliminary results indicate the utility of the xCELLigence platform to investigate the functional effect of novel inhibitors of 5LOX treatment on OE33 cells ----------293

Figure 8.5 Preliminary results indicate the utility of the xCELLigence platform to investigate the functional effect of novel inhibitors of 5LOX treatment on OE33 cells following ENO3 and PKM2 knockout----------294

Figure 8.6 Silencing of ENO3 and PKM2 significantly reduces glycolysis in OE33 cells----------296

Figure 8.7 Silencing of ENO3 and PKM2 significantly reduces ACM-induced glycolysis in OE33 cells----------297

Figure 8.8 Effect of ACM and HIH4 on glycolytic activity in OE33 cells following transfection of ENO3, PKM2 and the combination of both-298

List of Tables

Table 1.1 Tumour-node-metastasis (TNM) staging for esophageal Adenocarcinoma----------6

Table 1.2 Representative mutated genes in esophageal adenocarcinoma----------9

Table 1.3 Summary of inhibitors of 5LOX signaling in cancer----------21

Table 1.4 Relative risk association with obesity in cancer----------23

Table 1.5 Overview of the characteristics of white and brown adipose tissue------29

Table 1.6 Measuring obesity by Body Mass Index (BMI) ----------30

Table 1.7 Visceral fat area measurement by CT----------32

Table 2.1 Reagents and volumes used in cDNA synthesis----------64

Table 2.2 List of FAM-labelled primer probes and corresponding configuration numbers ----------65

Table 2.3 Key genes involved in the regulation and enzymatic pathways of glucose and glycogen metabolism----------66

Table 2.4 The list of key genes involved in mitochondrial respiration, components of electron transport chain and oxidative phosphorylation complexes--67

Table 2.5 Primer sequences for SYBR-based PCR----------67

Table 2.6 List of antibodies used for IHC ----------71

Table 2.7 List of primary and secondary antibodies used for western blotting with their corresponding dilutions----------75

Table 3.1 Summary of markers that have been shown to be involved in tumourigenesis in cancer----------85

Table 3.2 Patients demographic for esophageal adenocarcinoma microarrays ----89

Table 3.4 Summary of findings from Chapter 3----------119

Table 4.1 List of markers associated with tumor metabolism and cancer spread ----------129

Table 4.2 Details of patient demographic used for preparation of ACM and gene analysis study ----------132

Table 4.3 Details of patient demographic used for tumor biopsy gene analysis study----------134

Table 4.4 Summary of findings from Chapter 4----------155

Table 5.1 Patient demographic for esophageal adenocarcinoma microarrays-----167

Table 5.2 Summary of significant findings from Chapter 5----------192

Table 6.1 Patient demographics for preparation of ACM for lactate assay secretion study----------200

Table 6.2 Glucose metabolism gene microarray screen between media only and ACM co-cultured OE33 cells: the effect of ACM on the genes of glycolysis, gluconeogenesis and glucose metabolism----------204

Table 6.3 Glucose metabolism gene microarray screen between media only and ACM co-cultured OE33 cells: the effect of ACM on the genes of TCA cycle----------205

Table 6.4 Glucose metabolism gene microarray screen between media only and ACM co-cultured OE33 cells: the effect of ACM on the genes of glycogen metabolism----------206

Table 6.5 Human mitochondrial function gene microarray screen between media only and ACM co-cultured OE33 cells: the effect of ACM on Complex I gene expression----------214

Table 6.6 Human mitochondrial function gene microarray screen between media only and ACM co-cultured OE33 cells: the effect of ACM on Complex II, Complex III and Complex V gene expression ----------215

Table 6.7 Human mitochondrial function gene microarray screen between media only and ACM co-cultured OE33 cells: the effect of ACM on Pathway activity signature genes----------216

Table 7.1 IC50 doses for OE33 viability by commercially available inhibitors of glycolysis pathway and 5LOX determined by non-linear regression analysis----------239

Table 7.2 IC50 doses for OE33 viability by commercially available inhibitors of glycolysis pathway and 5LOX determined by non-linear regression analysis----------240

Table 7.3 IC50 doses for OE33 cell proliferation by commercially available and novel inhibitors of glycolysis pathway and 5LOX determined by non-linear regression analysis----------241

Table 7.4 OE33 cell proliferation following 24-hour treatment in normoxic and hypoxic conditions----------242

Table 7.5 List of OE33 gene alterations following ACM and 5LOX inhibitor treatment----------254

Table 7.6 List of OE33 gene alterations following 5LOX inhibitor treatment----260

Table 8.1 Variations on the protocols trialed in order to achieve ENO3 and PKM2 knockout in OE33 cells----------287

Abbreviations

18S	18S ribosomal RNA
2-DG	2-deoxy-D-glucose
5LOX	5-lipoxygenase
5-FU	5-fluorouracil
AA	Arachidonic acid
ACM	Adipose conditioned media
ADP	Adenosine diphosphate
APS	Ammonium persulfate
AKT	Protein kinase B
AMPK	AMP-activated protein kinase
ANOVA	Analysis of variance
ARID1A	AT-rich interactive domain-containing protein 1A
ATP	Adenosine Triphosphate
ATP5B	Adenosine triphosphate isoform 5B
BAK1	Bcl-2 homologous antagonist killer
BAT	Brown adipose tissue
BCA	Bicinchoninic acid assay
BMI	Body mass index
BO	Barratt's oesophagus
BSA	Bovine serum albumin
B2M	β-2-microglobulin
CDK4	Cyclin-dependant kinase 4
CI	Cell index
CML	Chronic myeloid leukemia
CRT	Chemo-radiation therapy
Ct	Cycle threshold
COX6C	Cytochrome c oxidase subunit 6
COX8C	Cytochrome c oxidase subunit 8
CRY1/2	Cryptochrome protein ½
CO_2	Carbon Dioxide
DAB	3, 3'-diaminobenzidine
DCA	Deoxycholic acid
DFS	Disease free survival
DMSO	Dimethylsulfoxide

DNA	Deoxyribonucleic acid
dNTP	Nucleoside triphosphate
DSS	Disease specific survival
dH_2O	Distilled water
ECAR	Extracellular acidification rate
ECM	Extracellular matrix
EDTA	Ethylenedeminetetraacetic acid
ELISA	Enzyme-linked immunosorbent assay
ELMO1	Engulfment and cell motility 1
EMT	Epithelial mesenchymal transition
ENO3	Enolase 3
FAK	Focal adhesion kinase
FBS	Fetal bovine serum
FCCP	Trifluorocarbonylcyanide phenylhydrazone
FDA	Food and Drug Administration
FLAP	5-lipoxygenase activating protein
ERK	Extracellular signal-regulated kinase
FIS1	Mitochondrial fission 1 protein
G6P	Glucose 6-phosphate
GAPDH	Glyceraldehyde 3-phosphate dehydrogenase
GI	Gastrointestinal
GLUT1	Glucose transporter 1
GLUT4	Glucose transporter 4
GORD	Gastroesophageal reflux disease
HIF1A	Hypoxia induced factor alpha
HK1	Hexokinase 1
HK2	Hexokinase 2
HRP	Horse radish peroxidase
MMP	Matrix metalloproteinase
mRNA	Messenger RNA
MTT	3-(4,5-Dimethyl-2-thiazolyl)-2,5-diphenyl-2H-tetrazolium bromide
NCRI	National Cancer Registry Ireland
NLE	Non-leading edge
NSAID	Non-steroid anti-inflammatory drug
NSB	Non-specific binding
NSCLC	Non-small cell lung cancer
OAC	Oesophageal adenocarcinoma
OE33	Oesophageal adenocarcinoma cell line
OS	Overall survival
OXPHOS	Oxidative phosphorylation
PET-CT	Positron emission tomography-computed tomography
HGD	High-grade dysplasia
HIF1A	Hypoxia-inducible factor 1-alpha
IBD	Inflammatory bowel disease
ICAM	Intercellular adhesion molecule-1
IgG	Immunoglobulin G
IGFR	Insulin-like growth factor receptor
IL-8	Interleukin-8
LE	Leading edge
LDH	Lactate dehydrogenase

LGD	Low-grade dysplasia
LPS	Lipopolysaccharide
MMP	Mitochondrial membrane potential
MMP1	Matrix metallopeptidase 1
MMP7	Matrix metallopeptidase 7
mtDNA	Mitochondrial DNA
mTOR	Mammalian target of rapamycin
NADH	Nicotinamide adenine dinucleotide
NADPH	Nicotinamide adenine dinucleotide phosphate
NFκB	Nuclear factor kappa-light-chain-enhancer of activated B cells
NLE	Non-leading edge
OAC	Oesophageal adenocarcinoma
OCR	Oxygen consumption rate
OSCC	Oesophageal squamous cell carcinoma
OXPHOS	Oxidative phosphorylation
p53	Tumour protein p53
PBS	Phosphate-buffered saline
PCR	Polymerase chain reaction
PDK1	Pyruvate dehydrogenase kinase 1
PIK3CA	phosphatidylinositol-4, 5-bisphosphate 3-kinase
PI3K	Pphosphoinositide 3-kinase
PKM2	Pyruvate kinase isoform 2
PPP	Pentose phosphate pathway
PVDF	Polyvinylidene difluoride
qRT-PCR	Quantitative/real-time reverse transcription polymerase chain reaction
RB	Retinoblastoma
rcf	Relative centrifugal force
RNA	Ribonucleic acid
ROS	Reactive oxygen species
RPMI	Roswell Park Memorial Institute Medium
RT-PCR	Reverse transcription polymerase chain reaction
SCC	Squamous cell carcinoma
SCJ	Squamocolumnar junction
siRNA	Small interfering RNA
SMAD4	SMAD family member 4
TIMP	Tissue inhibitor of metalloproteinases 3
TMAs	Tissue microarrays
TME	Tumour microenvironment
TNFα	Tumour necrosis factor alpha
VEGF	Vascular endothelial growth factor
VFA	Visceral fat area
WAT	White adipose tissue

Units

^{0}C	degrees Celsius
bp	base pairs
cm	centimetre
g	grams
Hz	Hertz

kD	kilodalton
kg	kilogram
M	molar
m	metre
mA	milliamp
mg	milligram
mL	milliliter
mm	millimeter
mM	millimolar
µg	microgram
µL	microliter
µM	micromolar
ng	nanogram
nm	nanometre
nM	nanomolar
pg	pictogram
px	pixel
rpm	revolutions per minute
U	units
V	volts
v/v	volume per volume
w/v	weight per volume
X	magnification

Research Presentations

Poster Presentations

- International Bioactive Lipids Conference, Puerto Rico – November 2013
- Irish Association for Cancer Research Meeting, Galway – February 2014
- TCD Conference, Dublin – September 2014
- IMM Annual Meeting – Translational Medicine, Dublin – November 2014
- Irish Association for Cancer Research Meeting, Limerick – February 2015
- International Bioactive Lipids Conference, Budapest – July 2015
- Irish Association for Cancer Research Meeting, Cork – February 2016
- International Aegan Conference on Tumour Microenvironment and Cellular Stress – July, 2016
- Irish Association for Cancer Research Meeting, Kilkenny- February 2017

Awards

- Poster Prize. Irish Association for Cancer Research Meeting, Kilkenny- February 2017

Courses Attended

- Certificate of Good Clinical Practice, January 2015, Clinical Research Facility, St. James's hospital, Dublin, Ireland

Chapter 1

General Introduction

1.1 Oesophageal adenocarcinoma

1.1.1 Pathology and epidemiology

Oesophageal cancer is the eight most common cause of cancer worldwide and the sixth most common cause of cancer-related deaths, accounting for an estimated 4.9% of all cancer mortalities [1] Oesophageal cancer can be divided into two major histological types - adenocarcinoma (OAC) and squamous cell carcinoma (SCC). The two sub-types are known to differ greatly in terms of risk factors. Oesophageal adenocarcinoma predominantly arises from intestinal glandular epithelium in the lower third of the oesophagus, squamous cell carcinoma occurs mostly in flat cells lining the upper two-thirds of the oesophagus [2]. Males are more likely to develop OAC, with a three to four times greater incidence [3]. According to a comprehensive report of cancer in Ireland between 1994 and 2004, esophageal cancer has a median age of diagnosis of 69 years among males compared to 75 years for females (National Cancer Registry, 2014). Male cases are highest among those aged 75-79, and among females cases peak in the 85 and over age group (Figure 1.1). OAC rates also higher in Caucasian population compared to African-Americans, with a five-fold greater incidence [4]. The rate of OAC has increased rapidly in Western countries since the 1980s [5, 6] and now exceeds the incidence of SCC [7]. This rise could be potentially associated with steadily increasing obesity epidemic. Obesity Worldwide has more than doubled since 1980. According to the data provided by WHO, in 2014, more than 1.9 billion adults, 18 years and older, were overweight, indicating that 39% of adults aged 18 years and over were overweight in 2014, and 13% were obese (WHO 2016). Published studies predominantly show a causal association between obesity and gastro-esophageal reflux disease (GORD) [8]. Abdominal obesity plays a major part in this association by increasing intragastric pressure, gastro-esophageal gradient, and esophageal acid exposure [2, 9]. People with GORD have a higher risk of getting adenocarcinoma of the esophagus and this risk seems to be higher in people who have more frequent symptoms [2].

The rising number of OAC cases seen in Ireland and UK are primarily due to the prominent OAC subtype in these countries. The National Cancer Registry reports that the incidence of esophageal cancer has risen by 27% in the past 15 years. The incidence of SCC has declined by 0.9% in females and 1.4% in males between 1994 and 2009. The decline of SCC rates in Ireland could be potentially linked to the smoking ban in

workplaces in Ireland since 29th of March 2004. Ireland was the first country in the world to institute a ban on smoking in workplaces [10]. From 29th of March 2004 onwards, under the Public Health (Tobacco) Acts, it has been illegal to smoke in all enclosed workplaces including bars, restaurants, offices, company cars, taxis. A private residence is considered a workplace when tradespeople are working there [11]. Data collected by HSE between March 2004 and December 2013 report a drop in smoking rate from 29% to 22% of the overall population in Ireland [12]. Tobacco and alcohol consumption has been shown to be the primary causes of SCCs of the esophagus [12]. There may be a potential link between the dropping rate of smokers and the decline in incidence of SCC in Ireland. On the other hand, the incidence rate of OAC has increased by 2.2% in Irish females and 3% in Irish males, per annum (National Cancer Registry, 2011).

Five-year relative survival is estimated to be 12.8% for males and 17.0% for females diagnosed with OAC between 2000 and 2004 (National Cancer Registry Ireland, a comprehensive report April, 2009) (Figure 1.2).

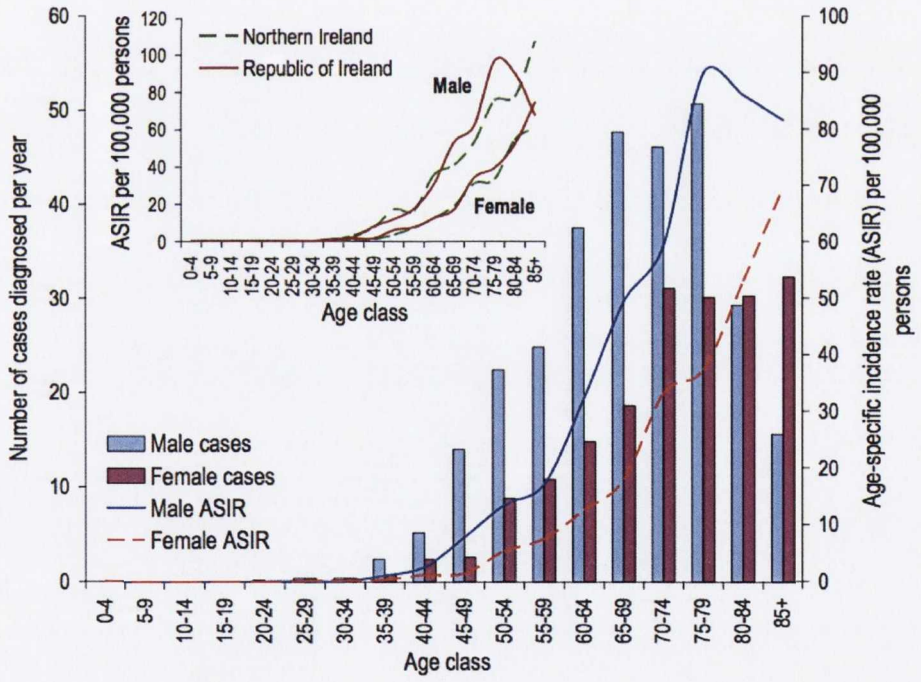


Figure 1.1 Number of cases of esophageal cancer diagnosed per year by sex and age with age-specific incidence rate (ASIR) per 100,000 persons: 2000-2004. Figure reproduced from the National Cancer Registry report, 2009.

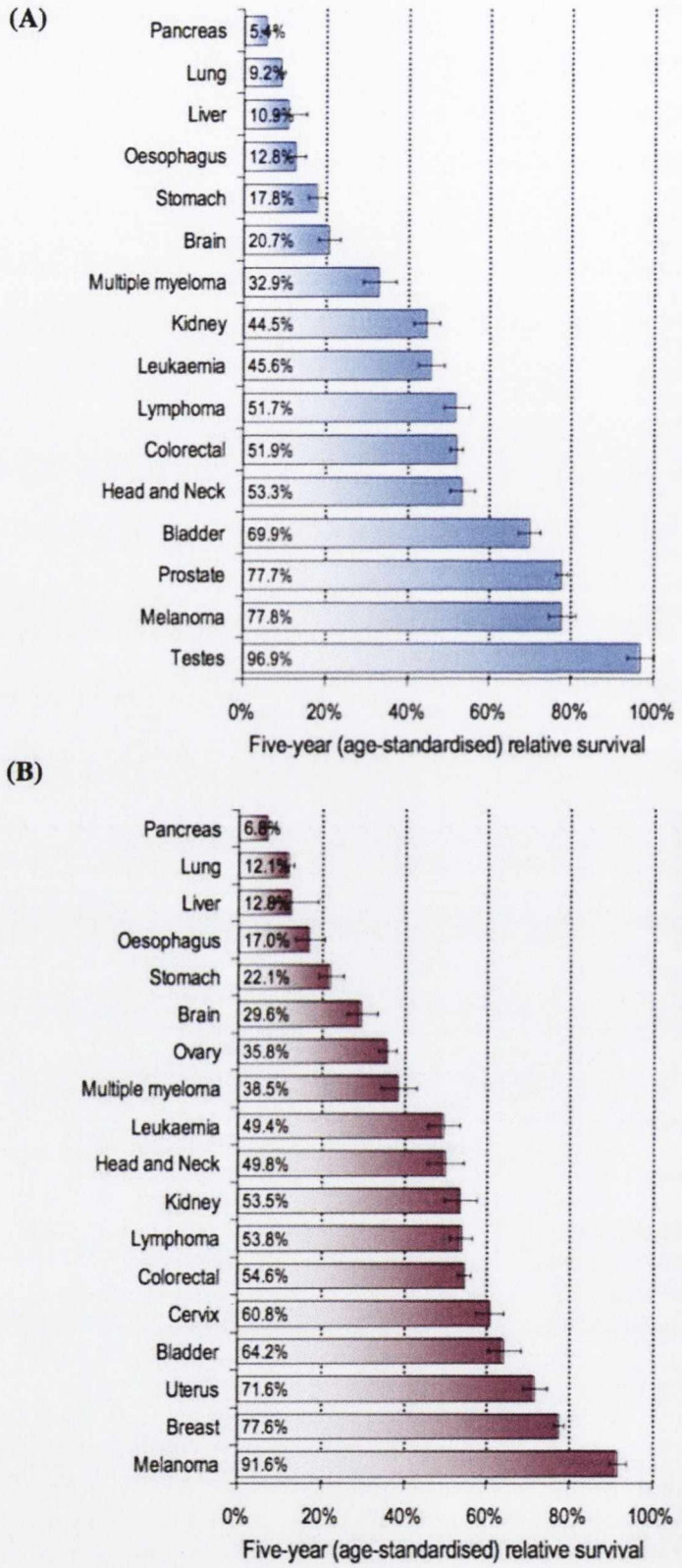


Figure 1.2 5-year survival rates for all cancers. 5-year survival rates for (A) males and (B) females, for all cancers. Figure reproduced from the National Cancer Registry report, 2009.

1.1.2 Other risk factors

Medication, diet and *Helicobacter pylori* infection are moderate modifiable protective factors in the development of OAC [13]. It was proposed that aspirin and other non-steroidal anti-inflammatory drugs (NSAIDs), however, evidence is limited [14, 15]. Low fruit and vegetable consumption is a moderate risk of OAC development [16]. It has been shown that reduced rates of *Helicobacter pylori* infection in general population correlate with increased risk of GORD and OAC [17].

1.1.3 Clinical presentation, diagnosis and staging

Dysphagia (difficulty swallowing) is the most common symptom of OAC (74%), alongside other symptoms like weight loss (57.3%), GORD (20.5%), and dyspnea (shortness of breath) (12.1%) [18]. At the time of diagnosis, approximately half of the OAC patients have metastatic disease [19].

OAC is diagnosed by histological examination of biopsies taken during esophagogastroduodenoscopy (OGD), which also allows examination of the tumor. Endoscopic ultrasound (EUS) determines invasion depth and allows biopsies of local lymph nodes to be taken [18]. Computed tomography (CT) along with FDG-PET scanning (PET-CT) can determine if metastasis has occurred [19, 20].

Staging of the disease is conducted according to the American Joint Committee on Cancer tumor-node-metastasis (TNM) [9]. This system allows to classify tumours based on depth of invasion (T stage), lymph node involvement (N stage) and presence of metastasis (M stage) (Table 1.1). Non-anatomic classifications include tumor location and histological type (i.e. Grade 1 (G1), G2 and G3) where higher grade is associated with decreasing survival.

Table 1.1 Tumour-node-metastasis (TNM) staging for esophageal adenocarcinoma. TNM staging according to the American Joint Committee on Cancer tumor-node-metastasis, 7th Ed. (2010) [9].

TNM Definitions	
Primary tumor (T)	
TX	Primary tumor cannot be assessed
T0	No evidence of primary tumor
Tis	Carcinoma in situ
T1	
-T1a	Tumour invades lamina propria
-T1b	Tumour invades submucosa
T2	Tumour invades muscularis propria
T3	Tumour invades adventitia
T4	Tumour invades adjacent structures
-T4a	Resectable
-T4b	Unresectable
Regional lymph nodes (N)	
NX	Regional lymph nodes cannot be assessed
N0	No regional lymph nodes metastasis
N1	Regional lymph nodes metastasis
-N1a	1-3 nodes involved
-N1b	4-7 nodes involved
-N1c	More than 7 nodes involved
Distant metastasis (M)	
MX	Distant metastasis cannot be assessed
M0	No distant metastasis
M1	Distant metastasis

1.1.4 Biology of esophageal adenocarcinoma

Oesophageal adenocarcinoma was believed to be systemic at the time of diagnosis, however, it is now well understood that it follows a pattern where lymphatic metastases precede systemic disease in most patients [21]. Clear evidence for this comes from studies demonstrating that intramucosal cancer is curable in nearly all patients and is associated with a low prevalence of lymph node metastases [11].

It is well established that the depth of tumor invasion predicts the risk of lymph node metastases, but the presence and extent of lymph node involvement is the major determinant of survival in patients with esophageal adenocarcinoma [11]. The risk of lymph node involvement increases from a low 2% to 4% for intramucosal tumors to 30% for submucosal tumor invasion and more than 80% with intramural and transmural

invasion [12]. Single-center and multi-center Surveillance Epidemiology and End Results (SEER) data analysis suggested that survival of esophageal adenocarcinoma patients improves with increasing numbers of resected nodes [22, 23].

The tumor margin, also called the invasive edge or the leading edge of the tumor, is an area where recruited immune and stromal cells are highly active and interactive with the tumor [24]. The microenvironment at the invasive edge of tumors is quite different than that of the tumor core [24]. Hypoxia tends to be associated with the center of a tumor, while oxygen is largely available at the invasive edge of the tumor. Macrophages play important roles during invasion at the tumor margin [25]. They have also been shown to thrive in hypoxic conditions in tumors and ischemic tissues, and thereby facilitate angiogenesis [26]. The relationship between oxygen and immune cells may inadvertently promote metastatic dissemination in multiple respects. Hypoxia mediates immune cell recruitment, these cells concentrate at the tumor periphery to support cancer invasion at the leading edge [21]. In the tumor core, hypoxia contributes to cancer cell escape by providing an aggressive selection pressure for resilient stem-like tumor cells that subsequently migrate away to the tumor margin. Differential distribution of immune cells at the tumor edge versus the tumor center is critical for fully understanding tumor-stroma dynamics [27].

1.1.5 Molecular mechanisms of esophageal adenocarcinoma

Recent progress in molecular biology has revealed that several genetic and epigenetic alterations are implicated in both carcinogenesis and progression of esophageal cancer. Genetic alterations include a chromosomal loss or gain, loss of heterozygosity (LOH), and amplification or mutations of genes. Epigenetic changes, such as DNA methylation, histone modifications, and altered expression of microRNAs regulate gene expression through mechanisms other than changes in DNA sequence. It has become evident that molecular mechanisms also differ greatly across the sequence of neoplastic transformation from normal esophageal tissue to esophageal adenocarcinoma (Figure 1.3). An increase in pro-inflammatory factors: NFκB, IL-8, RB, CDK4, MMP1 and downregulation of TIMP3 results in an increase of genomic instability and progression from normal to metaplastic phenotype in the oesophagus. TIMP3 belongs to a family of genes that inhibit matrix metalloproteinases, a group of peptides involved in degeneration

of extracellular matrix. Loss of tumor suppressor P53, an increase in VEGF and activation of arachidonic acid metabolism (5LOX, COX2 and prostaglandins) drives metaplasia to dysplasia.

Subsequently, upregulation of MMP9, VEGF, Leptin Receptor, IGF-R, EMT and FAK pathway activation allows progression to cancer, where cancer cells exhibit immortalization, increased invasive and metastatic capacity.

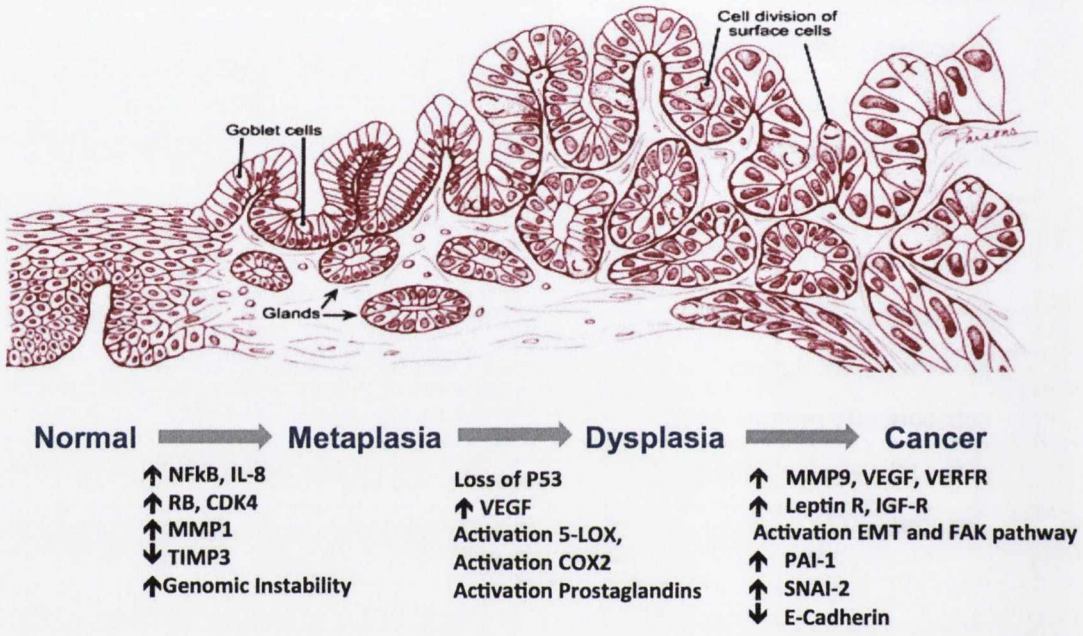


Figure 1.3 Molecular factors driving esophageal adenocarcinoma. An increase in pro-inflammatory factors: NFκB, IL8, RB, CDK4, MMP1 and downregulation of TIMP3 results in an increase of genomic instability and progression from normal to metaplastic phenotype in the oesophagus. Loss of tumor suppressor P53, an increase in VEGF and activation of arachidonic acid metabolism (5LOX, COX2 and prostaglandins) drives metaplasia to dysplasia. TP53 is a major tumor-suppressor gene responsible for the maintenance of genetic stability and DNA repair capacity. Subsequently, upregulation of MMP9, VEGF, Leptin R, IGF-R, EMT and FAK pathway activation allows progression to cancer, where cancer cells exhibit immortalization, increased invasive and metastatic capacity.

A number of frequently mutated genes in OAC are shown in Table 1.2. For example, PIK3CA is a kinase activator of the phosphoinositide 3-kinase (PI3K)/AKT pathway and is frequently mutated in many types of human cancers including OAC [28]. SMAD4 is a key intracellular mediator of transforming growth factor-beta signaling and is known to act as a tumor suppressor [29]. ARID1A, which is one of the chromatin remodeling genes, is frequently mutated in a variety of human cancers [29][30]. Mutations of TP53 and SMAD4 were stage-specific, confined to HGD and OAC, respectively [30].

Table 1.2 Representative mutated genes in esophageal adenocarcinoma

Gene Symbol	Gene Name
TP53	Tumour protein 53
CDKN2A	Cyclin-dependent kinase Inhibitor 2A
SMAD4	SMAD family member 4
AR1D1A	AT-rich interactive domain-containing protein 1A
PIK3CA	Phosphatidylinositol-4,5-Bisphosphate 3-Kinase Catalytic Subunit Alpha
SPG20	Spastic Paraplegia 20
TLR4	Toll-like receptor 4
ELMO1	Engulfment And Cell Motility 1
DOCK2	Dedicator of cytokinesis 2

[31]. MicroRNAs can act as tumor promoters through targeting expression of tumor suppressor genes or as tumor suppressors through targeting expression of oncogenes. miR-21 functions as a tumor promoter because it is overexpressed in many types of cancers, including OAC [32]. Another MicroRNA, miR-375, is considered as tumor suppressor in several cancers, including OAC [33]. Reduced levels of miR-375 in cancerous tissue of EAC patients with Barrett's have been shown to be strongly associated with a worse prognosis [33].

1.1.6 Recurrence pattern

Esophageal cancer is an aggressive malignancy with high rates of recurrence, even if treated with curative intent. Current National Comprehensive Cancer Network guidelines recommend more-frequent follow-up, with medical history and physical examination, during the first 5 years. The assumed benefit of a surveillance program is that the detection of recurrences at an earlier stage might result in improved survival and better quality of life [34].

A number of published studies have evaluated recurrence patterns in esophageal cancer. Lou *et al,* similarly to other investigators, reported that distant, locoregional, and mixed recurrences represented 55%, 28%, and 17% of all new events, respectively. In this particular study 75% of all recurrences occurred in the first 2 years after surgery. Proportion was significantly lower (63%) for patients who had not received neoadjuvant therapy than for those who had (83%). The median time to recurrence was 5.5 years and the overall recurrence rate was 27 per 100 person-years in postoperative year 1 and then

rapidly decreased to 4 per 100 person-years by postoperative year 6. The site of the first recurrence was correlated with survival. It was evident that patients with locoregional disease did the best, and patients with both distant and locoregional disease did the worst. This finding likely represents the overall tumor burden at the time of detection [34]. Parry *et al* reported that distant recurrence and more than three recurrent locations may be used as independent factors associated with a worse survival, irrespective of primary tumor characteristics [35].

A number of published studies suggest that post-operative recurrence of esophageal cancer is relatively common, therefore close follow-up should be performed for 2-3 years after surgery in order to timely detect tumor recurrence [36].

1.1.7 Inflammatory sequence to cancer / Barrett's

Barrett's oesophagus is an intestinal metaplasia of the distal oesophagus that predominantly arises from gastroesophageal reflux disease (GORD) and is a precursor lesion in the majority of patients with esophageal and gastroesophageal adenocarcinoma [37, 38]. Normally, the lower esophageal sphincter closes as soon as food passes. Failure of the sphincter to close allows acid produced by your stomach to move up into oesophagus. This can cause symptoms such as a burning chest pain called heartburn. If acid reflux symptoms occur more than twice a week, it is defined as gastroesophageal reflux disease (GERD).

The main risk factors in developing Barrett's oesophagus include gastro-esophageal reflux disease (GORD), medications, age, race, sex, diet, obesity, alcohol, smoking, socioeconomic status, and *Helicobacter pylori* infection [8]. Sontag et al proposed that development of GORD may be congenital, where the antireflux barrier does not completely develop due to a developmental anomaly, due to acute trauma, where the antireflux barrier in adults suffering acute traumatic injury to the abdomen or chest is permanently disrupted or by chronic trauma, there the antireflux barrier in children and adults is gradually weakened over time as a result of chronic straining to defecate and straining in an unphysiologic position. Sontag *et al* proposed that development of GORD may be congenital, where the antireflux barrier does not completely develop due to a developmental anomaly, due to acute trauma, where the antireflux barrier in adults suffering acute traumatic injury to the abdomen or chest is permanently disrupted or by

chronic trauma, there the anti-reflux barrier in children and adults is gradually weakened over time as a result of chronic straining to defecate and straining in an unphysiologic position [39].

Main symptoms of GORD include pain, regurgitation and throat problems. The most common feeling a person with GORD experiences is a persistent burning sensation in the chest. GERD can cause some of the stomach contents to go all the way through the oesophagus and back into the mouth. A bitter or sour taste is left in the mouth and subsequently followed by vomiting. This is more likely to occur in children. Individuals with GORD may also complain of having throat problems, including swallowing difficulties, frequent cough, sore throat [39].

Specifically, Barrett's oesophagus is a metaplastic alteration in the esophageal cell lining from a squamous epithelial mucosa to a columnar-lined epithelium [38]. It can be determined endoscopically as a transition from a pink squamous epithelium to dark, salmon-pink columnar lined epithelium [38] (Figure 1.4A). In normal individuals, the squamocolumnar junction (SCJ) and the gastroesophageal junction are situated in the same place, however, in the Barrett's patients the SCJ is displaced [38]. Barrett's oesophagus can be classified as either a short-segment disease of less than 3 cm or a long-segment disease, greater than 3 [38, 40] Histologically, the surface and crypts in Barrett's oesophagus are typically composed of various cells including mucinous cells, goblet cells, enterocytes, endocrine cells and Paneth cells (Figure 1.4B) [41, 42].

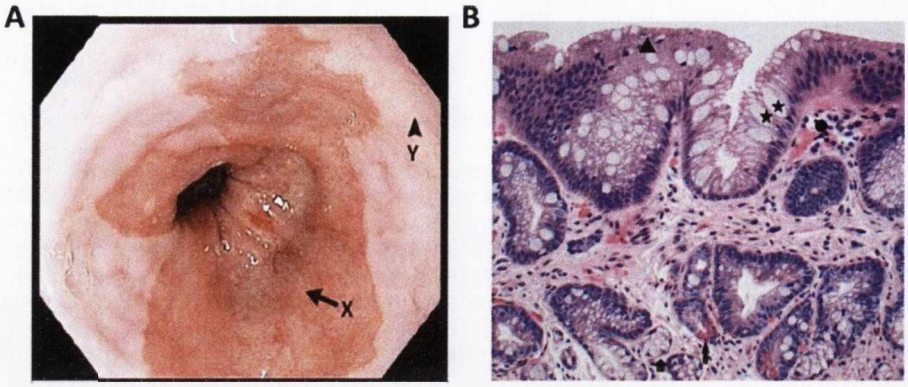


Figure 1.4 The endoscopic detection and histology of Barrett's oesophagus. (A) The salmon-pink, columnar- lined oesophagus (X), and the contrast between the light-pink squamous epithelium (Y) are characteristic of Barrett's oesophagus. (B) The epithelium consists of columnar epithelium with goblet cells (star asterisks) and non-goblet cells (arrowheads). Paneth cells may also be present (arrows). The epithelial crypts show slight architectural budding and distortion. The lamina propria additionally shows some evidence of lymphoplasmacytic infiltrate (circle). The mucous glands that are present in the basal mucosa (wide arrow). Endoscopic image (A) reproduced from Sharma *et al.*, (2009) [38]. Histological Image (B) reproduced from Naini *et al.*,[42].

The risk of developing OAC is approximately 30-40 times greater among patients with Barrett's oesophagus compared to those without intestinal metaplasia making it the greatest risk factor for OAC [40]. It is diagnosed in approximately 10-15% of patients with reflux, however, it is still reported in patients without chronic reflux symptoms thereby making diagnosis of Barrett's oesophagus a greater clinical problem. A study by Rex *et al* reported that among 556 patients who never presented reflux symptoms, the prevalence of Barrett's oesophagus was 5.6% [43]. Barrett's oesophagus progresses to OAC in a sequential manner from intestinal metaplasia through low-grade dysplasia (LGD), high-grade dysplasia (HGD) followed by OAC (Figure 1.5) [44, 45].

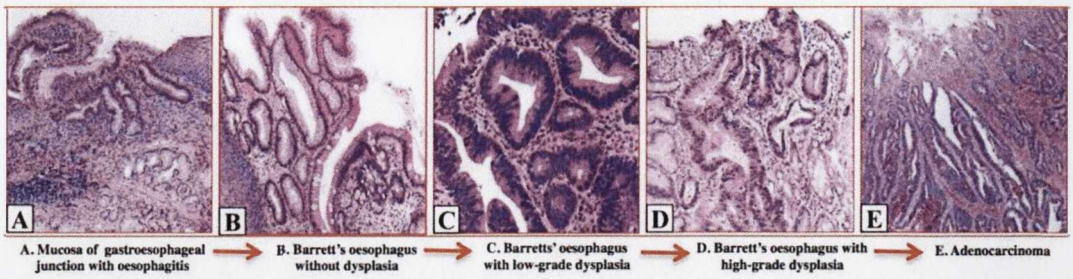


Figure 1.5 Pathological sequence of neoplastic transformation in esophageal adenocarcinoma. Normal squamous epithelial acquires an intestinal metaplastic histology following prolonged exposure to bile acids (Barrett's oesophagus). This can give a rise to dysplasia and eventually to invasive adenocarcinoma. Image reproduced from Conteduca *et al* [45].

In a large population study, Bhat *et al* used data available from Northern Ireland Barrett's esophagus Register for 1993– 2005 matched with cancer registry records to calculate the risk for individuals with Barrett's oesophagus developing OAC [46]. In the entire cohort of 8522 patients with Barrett's oesophagus, the incidence of esophageal, gastric cancer and high-grade dysplasia combined was 0.22% per year. In patients with specialized intestinal metaplasia (SIM), the combined incidence was 0.38% per year. The risk of cancer was significantly elevated in patients with SIM versus patients without SIM at index biopsy (0.38% per year vs 0.07% per year), in men compared with women (0.28% per year vs 0.13% per year) [46].

In a multicentre clinical trial, the LOTUS trial, 554 patients with chronic reflux and Barrett's oesophagus, were randomly assigned to either anti-reflux surgery or proton pump inhibitor treatment groups. Data from the trial showed that patients in the surgery group had a better esophageal pH control. Quality of life measures did not statistically differ between the anti-reflux surgery and proton pump inhibitor treatment regimes [47]. A meta-analysis of over 30 studies by Corey *et al* found no significant difference in the risk of OAC between patients who received anti-reflux surgery and those who received medical treatment [48].

In St. James's hospital, HALO® ablative treatment is employed in Barrett's patients with HGD and intra-mucosal cancer. HALO® ablative technology delivers heat in a very precise and highly controlled manner and therefore achieves a complete removal of affected tissue without damage to underlying tissue. If pathological staging of the disease suggests HGD or mucosal cancer, the patient undergoes either endoscopic therapy, such as EMR and HALO® ablative therapy, or surgery. The best treatment option is decided by an interdisciplinary collaboration of experts in the hospital. Treatment with EMR, with or without ablation, appears an acceptable alternative to surgery in St. James's hospital. Morbidity has been shown to be higher in the surgery group compared to those who obtained EMR ± ablative therapy [49]. In addition, after approximately 13 months, following EMR ± ablative therapy, 72% of patients had no endoscopic or histological evidence of Barrett's oesophagus [49]. However, upon progression to OAC, oesophagectomy remains the primary gold standard treatment approach [50].

The precise risk of cancer in Barrett's esophagus remains unclear. Reported estimates of cancer risk continue to vary widely, and it is not clear how biases, statistical aberrations,

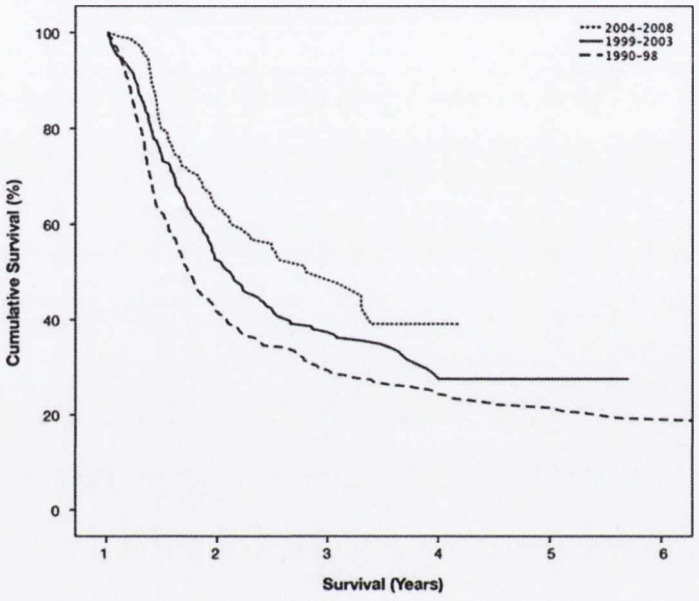
and regional differences in incidence rates contribute to the disparities among the published reports, however, many published studies agree that patients with dysplasia in Barrett's epithelium, have a substantially higher risk of developing esophageal cancer than the ones with no dysplasia.

1.1.8 Standard treatment regimen

Despite improvements in early diagnosis in esophageal adenocarcinoma, up to 75% of patients are not treated with curative intent, due to advanced poor physical condition [51]. These patients receive palliative care involving a combination of chemotherapy, radiotherapy, feeding interventions and pain relief [52]. Patients with localized disease are treated with curative intent. The standard of care usually involves neoadjuvant chemotherapy (CRT) followed by surgery [53]. The neoadjuvant treatment regimen typically consists of a course of chemotherapy on week 1 and week 6 (15mg/kg 5-fluorouracil (5-FU) or 75mg/m^2 cisplatin) while the radiation is administered concurrently with chemotherapy from week 1 to t3 weeks (40Gy (Gray) in 15 fractions)) [53]. Tumour response to neoadjuvant CRT is used as a predictor of disease-free survival (DFS) and overall survival (OS). It has been shown that only about 30% of patients achieve a complete pathological response [54, 55]. Results from the largest neoadjuvant CRT trial show an absolute OAC benefit of only 7% at 5 years for patients receiving CRT prior surgery versus surgery alone [55] therefore a large fraction of patients are not benefiting by receiving this treatment.

The recent ICORG 10-14 randomized clinical trial is led by St. James's Hospital, comparing neoadjuvant and adjuvant chemotherapy (MAGIC protocol) [56] to neoadjuvant CRT (CROSS protocol) [50] in OAC. The trial began in 2013 and involves six locations around Ireland. The MAGIC protocol consists of administration of etoposide, cisplatin and 5-FU chemotherapy pre- and post-surgery while the CROSS protocol consists of administration of carboplatin and paclitaxel chemotherapy with fractioned radiotherapy of 41.4Gy over five weeks. The primary end point of the trial which is still ongoing is overall survival, with a minimum of 3 years follow up. The secondary end-points are disease-free survival, response rates, recurrence rates, toxicity, operative complications and quality of life.

Despite the advances in clinical procedures and patient care demonstrated by a decreasing post-operative mortality rate of less than 2% [57] and significantly improved disease-specific-survival (DSS) in patients treated with curative intent during the period of 2004-2008 compared to earlier data from 1990-2003 (DFS increased by 17%) (Figure 1.6), prognosis is still poor [58]. A large percentage of OAC patients are not suitable for curative treatment and those who are suitable have a high cancer-specific mortality incidence. New treatment strategies, such as molecular targeted therapies, are urgently required to boost patient responses to current treatment regimes.



	1990-1998		1999-2003		2004-2008		p-value (long rank)
	N	95% CI	N	95% CI	N	95% CI	
Median survival (months)	17.38	14.89-18.87	22.93	18.29-27.58	32.85	24.34-38.15	0.001

Survival	1990-1998			1999-2003			2004-2008		
	No at risk	Deaths	% Survival	No at risk	Deaths	% Survival	No at risk	Deaths	% Survival
0 years	471	0	100	254	0	100	342	0	100
1 year	462	151	65	208	51	75	253	65	80
3 years	241	103	36	144	60	43	144	60	55
5 years	151	27	27	99	13	35	84	13	44
10 years	102	15	19	63	8	28	n/a	n/a	n/a

Figure 1.6 Disease-specific survival has improved in esophageal adenocarcinoma patients treated with curative intent. Data from St. James's Hospital demonstrates improved disease-specific survival during the period of 2004-2008 compared to the preceding 15 years. Figure reproduced from Reynolds *et al.*, 2012 [58].

1.1.9 Potential targeted therapies in esophageal adenocarcinoma

Systemic therapy for OAC tumours is based primarily on cytotoxic chemotherapy however the outcome remains poor. Due to the poor outcome of the OAC in patients, a major research focus in the past decade has been to understand the molecular pathways involved in the progression of esophageal cancer [59]. Published research shows that targeted medicine, where treatments are tailored to specific molecular abnormalities of tumors, holds a great promise for improving prognosis for patients with this disease [60]. One of the most promising potential targets in OAC is human epidermal growth factor-2 (HER-2). HER-2 is overexpressed in approximately 15% of OAC however the prognostic value still remains unclear [61]. The international TOGA Phase III randomized clinical trial reported a significant increase in the response rate in metastatic HER-2 positive gastric cancer and esophageal junction (OGJ) patients treated with HER-2 monoclonal antibody trastuzumab in combination with chemotherapy. Following these findings Food and Drug Administration (FDA) approved the trastuzumab for the treatment of HER-2 positive treatment-naive gastric cancers [62]. The RTOG Phase III 1010 clinical trial evaluating the addition of trastuzumab to trimodality treatment of Her2-overexpressing OAC is still ongoing (https://www.rtog.org/ClinicalTrials). The findings from this study will help to elucidate the benefit of the use of trastuzumab in combination with chemo-radiation (CRT) therapy.

EGFR belongs to the same family of growth factor receptors as HER-2, however, targeting EGFR so far does not show any clinically significant results. EGFR has been selected as a potential target due to the evidence of being overexpressed in 30-70% of OAC patients [63, 64] and has been shown to be a prognostic marker in OAC [65]. Despite this evidence, a number of Phase II clinical trials using monoclonal antibodies failed to demonstrate any benefit in patients or increase in overall survival [66]. The tyrosine kinase inhibitor gefitinib also failed to improve overall survival in a Phase III multi-centre randomized trial however it showed palliative advancements in OAC patients [67].

Another potential area for targeted treatments of OAC at an earlier stage of tumor development is anti-angiogenic therapies. VEGF is overexpressed in 30-60% of OAC patients and high expression of levels of VEGF correlate with poor prognosis [68, 69]. A recent phase II trial has reported an improved response and survival for HER-2 positive

gastric and OAC patients when bevacizumab was used in combination with trastuzumab, capecitabine (CAPOX) and oxaliplatin. The study is still ongoing however early reports show that patients receiving combination of treatments, have a median overall survival (OS) of 21 months and the response rate to the treatment is at 81% [70]. These preliminary results are already an improvement on the previous results published by Bang *et al* for ToGA (Trastuzumab for Gastric Cancer) study. ToGA was an international, phase III, randomised control trial undertaken in 122 centers in 24 countries [62], where trastuzumab treatment was used in combination with CAPOX [62]. Patients were randomly assigned to treatment group (trastuzumab plus chemotherapy) or chemotherapy alone. Median overall survival was 13.8 months in those assigned to trastuzumab plus chemotherapy compared with 11.1 months in those assigned to chemotherapy alone [62].

To date, studies have concentrated on single mutations or proteins in the hope to discover relevant therapeutic targets in OAC however with little translational success. Further studies on biomarkers and combination therapies for increased therapeutic response are needed to increase clinical benefits to the patients.

1.1.10 Potential novel therapies in esophageal adenocarcinoma

1.1.10.1 Eicosanoids

Eicosanoids represent a diverse group of bioactive lipids synthesized from polyunsaturated fatty acids (PUFA) to either proinflammatory omega-6 arachidonic acid (AA) or anti-inflammatory omega-3 eicosapentaenoic acid (EPA) and docosahexaenoic acid (DHA). These eicosanoids are synthesized from two essential fatty acids (FAs), ω-6 linoleic acid (C18:2n6) and ω-3 linoleic acid (LA) (C18:3n3), by a series of denaturize andelongase enzymes [71]. AA is 20-carbon polyunsaturated fatty acid that is the major precursor of several classes of signal molecules. Alteration of AA metabolism is thought to be involved in human carcinogenesis, because some of the AA metabolites enhance cell proliferation and increase cell survival and suppress apoptosis [72]. AA is stored in cell membrane phospholipids and it can be mobilized by various phospholipase enzymes therefore the release free fatty acids provides the substrate for the enzymes of the eicosanoid synthesis pathway. There are three known classes of enzymes involved in AA metabolism: cyclooxygenases (COX), lipoxygenases (LOX) and cytochrome P450. COX

metabolises AA to prostanoids, LOX metabolises AA to hydroxylated eicosatetraenoic acid (HETEs), lipoxins and leukotrienes and cytochrome P450 has been shown to metabolise AA to epoxides [73] (Figure 1.7). Eicosanoids trigger signals for gene transcription responsible for apoptosis, cell proliferation and immune system modulation, just to mention a few, which may create an inflammatory environment supporting cancer development.

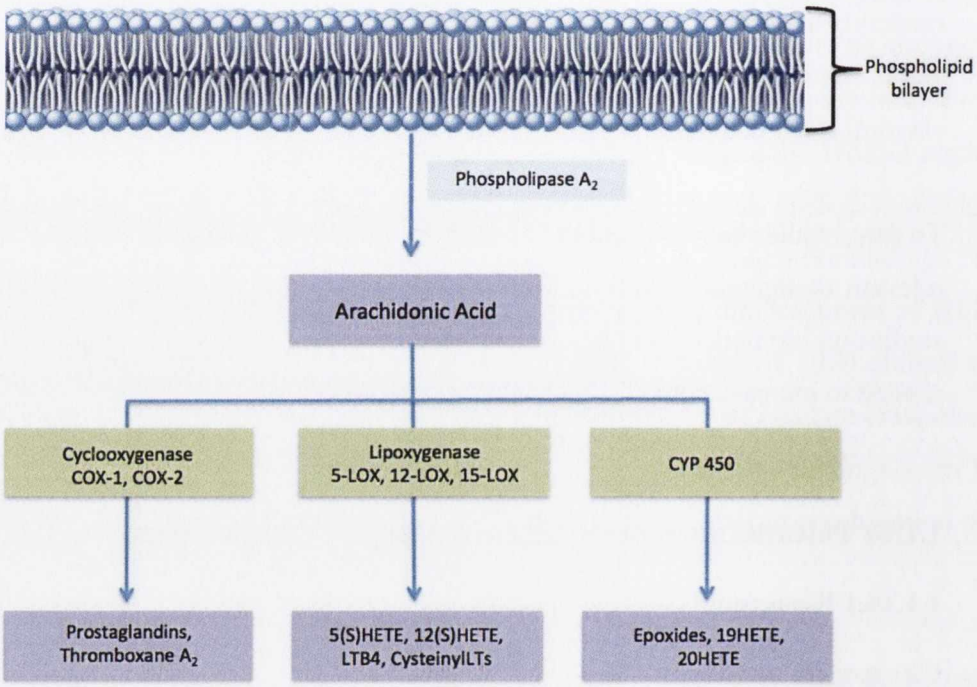


Figure 1.7 Arachidonic acid metabolism. Upon stimulation, Phospholipase A_2 induces the release of arachidonic acid (AA) from the lipid bilayer. The released AA is metabolized into eicosanoids by one out of three enzymatic pathways: COX1 and COX2 metabolises AA to Prostaglandins and Thromboxane A2; 5-LOX metabolises AA to 5(S) HETE, LTB4 and cysteinyl leukotrienes; 12-LOX metabolises to 12(S) HETE, 15-LOX to 15(S) HETE and to a lesser extent 12(S) HETE; Cytochrome P450 (CYP P450) metabolises AA to epixodes and to a lesser extent 19HETE and 20HETE.

1.1.10.2 The potential role of 5-lipoxygenase in cancer progression

Lipoxygenases are the least studied of the three families of enzymes in eicosanoid signaling pathway however they have been shown to have a role in various cancers.

In resting cancer cells, 5LOX is located in the nucleus [74]. 5LOX is translocated to

nuclear membrane where the interaction with FLAP results in the AA metabolism [75]. AA is metabolized to 5(S) HETE which can be further metabolized to 5-oxo-HETE [76] or LTA4 [77]. LTA4 is further oxidised to either LTB4, a potent chemoattractant for monocytes, neutrophils, oesinophils, stimulating cell adhesion and extravasation [78] or converted to one of the cysteinyl leukotrienes that may play a role in the recruitment of inflammatory cells, blood vessel dilation and permeability [79].

A number of studies report the link between 5LOX and tumorigenesis. 5LOX has been shown to have a potential contribution to tumorigenesis in colorectal cancer [80]. It has been documented that colorectal cancer is often caused by mutation of the tumor suppressor Adenomatous polyposis coli (APC) gene [81]. A study investigating the link between 5LOX and colorectal cancer reports that ApcΔ468 mice that bear a truncated APC, developed severe polyposis by four months [82]. A published study exploiting 5LOX in colorectal cancer reported that deficiency in 5LOX led to impairment in ApcΔ468 mice, implying that LOX5 has as an important role in colorectal tumorigenesis [82]. A summary of experimental findings accounting for the role of 5LOX in tumorigenesis can be found in Figure 1.8. Some evidence suggests that low 5LOX expression in tumors found in humans might lead to greater 15-LOX expression followed by cancer formation through impaired apoptotic activity [82-84].

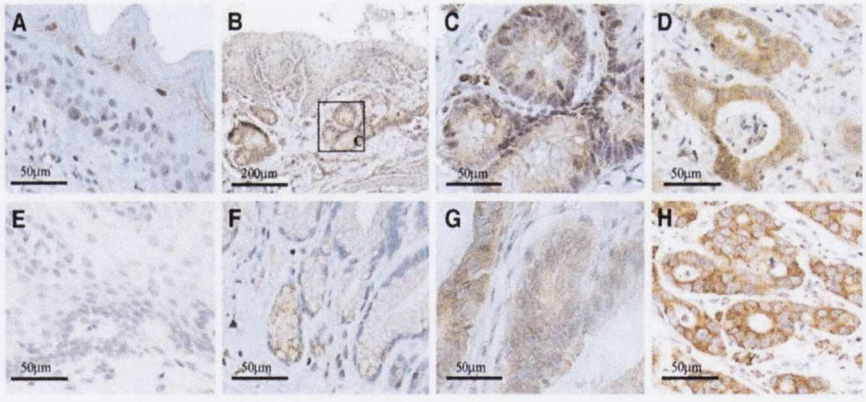


Figure 1.8 Overexpression of 5-LOX in esophageal samples of EGDA rats and humans. In rat normal esophagus (A) 5LOX expression is very low. In reflux esophagitis and Barrett's oesophagus (B and C) there is a positive 5LOX overexpressed in both epithelial and infiltrating inflammatory cells. In OAC (D) 5LOX is strongly expressed in epithelial cells. Similar to the rat model, normal human oesophagus (E) display very low levels of 5LOX. In human Barrett's oesophagus (F) 5LOX expression is higher than compared to (E). In dysplasia (G) 5LOX is further overexpressed. In OAC (H) a high staining intensity is observed. Image adapted from Chen *et al.*, 2004) [85].

1.1.10.3 Blocking 5-lipoxygenase signaling in cancer

Research is still limited in this area however there have been efforts to determine the role of 5LOX and leukotrienes in many cancer types. Published research predominantly delineates the benefit of using 5LOX inhibitors in various cancer types (Table 1.3). A study in 1986 was one of the first to describe the potent anti-proliferative effects of the 5LOX inhibitor AA-861 in a human leukemic cell line [86]. The treatment resulted in great reduction in cellular DNA, RNA, and protein synthesis. It was proposed that LTs potentially play an essential role in cancer cell viability [86]. A similar *in vitro* effect was observed using the lipoxygenase inhibitor nordihydroguaiaretic acid (NDGA) in stomach cancer cells, suggesting a potential role of LTs in cancer progression [87]. Prostate cancer cells have been shown to produce 5(S) HETE in unstimulated conditions *in vitro* [88]. Treatment of the cells with MK886 (sodium salt hydrate, a FLAP inhibitor) resulted in inhibition of 5LOX signaling pathway, and subsequently a large proportion of cells died by apoptosis [88]. This data highlights a potential role of FLAP in cancer cell survival and cancer progression. An *in vivo* study in prostate cancer reported that the 5(S)HETE production was significantly higher in the tumours in metastatic prostate tumor mouse xenografts compared to the treatment group where zileuton, a selective inhibitor of 5LOX was used [89], suggesting a potential positive association between 5LOX and metastatic tumor potential in prostate cancer. A number of in vitro studies reported that the inhibition of 5LOX pathway by addition of exogenous 5(S) HETE result in reduces proliferation and induce apoptosis in cancer cells [90-92].

To conclude, various 5LOX inhibitors were shown to suppress the growth of different types of tumor cells by cytotoxic mechanisms, primarily through activation of the apoptotic pathway. In addition to the pro-apoptotic activity of the drugs, it should be noted that additional whether any additional anti-proliferative effects were observed, such as a decrease in DNA synthesis or induction of cell cycle arrest, which could harbor great significance [87].

Table 1.3 Summary of inhibitors blocking 5LOX signaling in cancer

5LOX Inhibitor	Cancer Type	Reference
AA-861	Leukaemia	Grichenko *et al.*, 2004 (205)
NDGA	Gastric	Toyoda *et al.*, 2007 (206)
MK886	Prostate	Gosh & Meyers, 1998 (207)
Zileuton	Prostate	Meng *et al.*, 2013 (208)
REV5901	Pancreatic	Ding *et al.*, 1999 (209)

1.1.10.4 5-lipoxygenase in esophageal cancer

There is little research investigating the association of 5LOX and esophageal cancer. An immunohistochemical study assessing 5LOX expression in formalin-fixed, paraffin-embedded tissue sections from 161 esophageal cancer cases (81 from Anhui Medical University in China and 80 cases from MD Anderson Cancer Center) was conducted [72]. The Chinese cases consisted of only SCC but the Anderson cases consisted of both SCC (27 cases) and adenocarcinoma (53 cases). 5LOX expression was detected in 4 out of 32 cases (13%) of the normal epithelium and in 127 out of 161 cases (79%) of the esophageal cancer. There was a significant difference observed between 5LOX expression between normal and tumor tissues ($p<0.00001$). There was no difference observed in 5LOX expression between SCC and adenocarcinoma, or between Chinese and Anderson cases. 5LOX protein was expressed in cancerous epithelial cells and stromal cells [72]. Another immunohistochemical study was exploiting 5LOX expression in the esophageal samples of 67 patients [85]. 5LOX expression was negative in most samples of normal esophagus, however, 5LOX expression was markedly increased in Barrett's Oesophagus and dysplasia. In OAC, overexpression was obvious in 50% of the cases (28 of 56), with moderate and strong expression [85]. In the same study, in parallel to the human IHC study, 5LOX expression was measured in 20 esophagogastroduodenal anastomosis (EGDA) rats. In the proximal esophagus, 5LOX was barely detectable in the epithelial cells however the areas of EGDA-induced esophagitis and Barrett's oesophagus, 5LOX was overexpressed [85]. This study reported a progressive increase in 5LOX expression during histologic progression to EAC in both human OAC samples and EGDA rat tumours. More importantly, 5LOX was overexpressed in Barrett's oesophagus indicating that 5LOX overexpression begins at an early stage of esophageal adenocarcinogenesis.

1.2 Obesity

1.2.1 Obesity and cancer

Obesity has been shown to increase both the rate of cancer progression and the risk of developing cancers [93]. Many types of cancers including colon, breast (in postmenopausal women), endometrium, kidney, oesophagus, stomach, pancreas, gallbladder and liver are linked to obesity [94]. It has been estimated that 15–20% of all cancer deaths in the United States are associated with increased adiposity [93]. To date, the strongest evidence linking obesity and cancer risk are due to metabolic and endocrine effects of obesity [93, 94].

The risk ratio (RR) analysis was used to determine whether individuals with increasing levels of BMI are at higher risk of developing cancer than the ones with lower BMI. In statistics and epidemiology, RR is the ratio of the probability of an event occurring, for example developing a cancer, in an exposed group to the probability, for example varied levels of obesity. In all cancers that have been investigated, increasing BMI was positively correlated with the risk of developing cancer (Table 1.4).

The incidence of OAC has been rapidly increasing in westernized countries in recent decades [95], whereas the rates for the other main histological subtype of cancer, squamous-cell carcinoma (SCC), have remained stable or decreased [96]. As a result, an increasing proportion of all esophageal cancers in the western countries are OACs. Obesity increases risk of developing OAC by 2-3-fold [97] (Table 1.3) but is not associated with an increased risk SCC. Independent of obesity, gastro-esophageal reflux disease (GERD) has also been associated with esophageal adenocarcinoma alongside with its metaplastic precursor, Barrett's oesophagus [98]

Table 1.4 Relative risk association with obesity status in cancer

Type of cancer	Relative risk with BMI25-30kg/m^2	Relative risk with BMI>30kg/m^2
Colorectal (men)	1.5	2
Colorectal (women)	1.2	1.5
Female breast (postmenopausal)	1.3	1.5
Endometrial	2	3.5
Kidney	1.5	2.5
Oesophageal (adenocarcinoma)	2	3
Pancreatic	1.3	1.7
Liver	ND	1.5-4.0
Gallbladder	1.5	2
Gastric cardia	1.5	2

Adipose tissue from obese individuals exhibit an altered endocrine function and secretory profile, resulting in the increase of pro-inflammatory molecules that have been shown to be linked to the development many cancers [99].

Research suggests that the increased risk of developing various cancers in obese individuals is due to the ability of adipose tissue to secrete factors that collectively contribute to proinflammatory, procoagulant and insulin resistant state known as the metabolic syndrome [99, 100].

1.2.1.1 Obesity and esophageal adenocarcinoma

Obesity has been strongly implicated in the pathogenesis of esophageal adenocarcinoma (Figure 1.9, Figure 1.10) [101, 102]. The rising incidence of esophageal adenocarcinoma parallels with the obesity epidemic [103]. There have been multiple studies looking at the association between visceral obesity and OAC. A prospective cohort study using the European Prospective Investigation into Cancer and Nutrition (EPIC) population revealed a positive association between the risk OAC and BMI or waist circumference [104]. On multivariate analysis, neither of the factors were of statistical significance, however the sample size was relatively small, of only 88 cases of OAC, therefore a larger sample size would be required to determine whether visceral obesity is an independent predictor of risk above BMI alone.

To measure the risk of developing gastro-esophageal cancer with increasing visceral

obesity rather than BMI alone, they used a waist circumference and waste hip ratio (WHR) and reported a significant positive correlation of gastro-esophageal adenocarcinoma [105]. The Melbourne Collaborative Cohort Study (MCCS), a prospective cohort study of 41,528 people (17,049 men and 24,479 women) aged between 27 and 75, reported that the risk of developing esophageal adenocarcinoma and gastric carcinoma was positively associated with BMI with a higher risk for people with BMI $\geq$ 30 kg/m^2 compared with those <25 kg/m^2 [105]. To measure the risk of developing gastro-esophageal cancer with increasing visceral obesity rather than BMI alone, they used a waist circumference and waste hip ratio (WHR) and reported a significant positive correlation of gastro-esophageal adenocarcinoma [105].

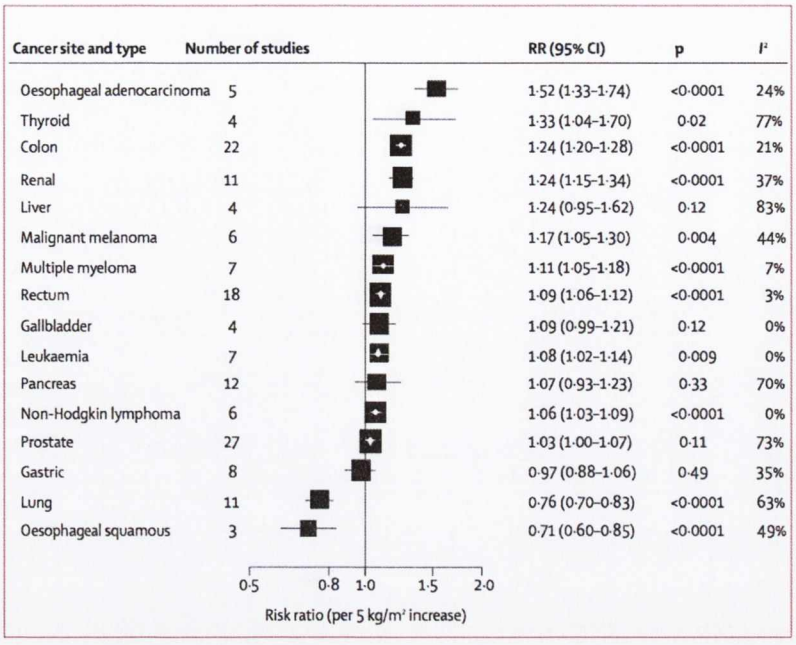


Figure 1.9 Association between body mass index and cancer incidence: summary risk estimates by cancer sites for men. Meta-analysis of risk ratios (per 5 kg/m2 increase in BMI) in men. Increased BMI is strongly associated with esophageal adenocarcinoma (RR 1·52, p<0·0001) and thyroid (1·33, p=0·02), colon (1·24, p<0·0001), and renal (1·24, p<0·0001) cancers. Adapted from Renehan *et al.*, 2008 [102].

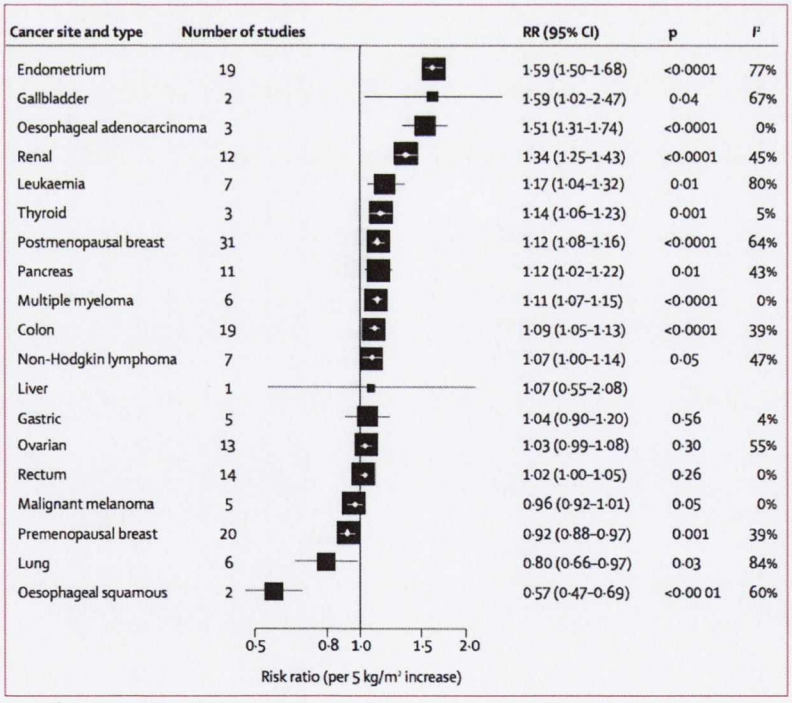


Figure 1.10 Association between body mass index and cancer incidence: summary risk estimates by cancer sites for women. Meta-analysis of risk ratios (per 5 kg/m^2 increase in BMI) in women. An increase in BMI is strongly associated with endometrial (1·59, p<0·0001), gallbladder (1·59, p=0·04), and renal (1·34, p<0·0001) cancers and with esophageal adenocarcinoma (1·51, p<0·0001). Adapted from Renehan *et al.*, 2008 [102].

1.2.2 Obesity epidemiology

According to the WHO report in 2014, 39% of adults were overweight (BMI $\geq$ 25 kg/m^2) and 13% were obese (BMI $\geq$30 kg/m^2) [WHO, 2014]. Thus, nearly 2 billion adults worldwide are overweight and, of these, more than half a billion are obese. The prevalence of obesity in Irish adults is currently 25.6% (with a prevalence of 25.9% in males and 25.3% in females) [WHO, 2014].

According to a study published in The Lancet [106], Ireland, with the United Kingdom, is set to become the most obese country in Europe. Irish men already have the highest body mass index (BMI), while Irish women rank third. It is predicted that by 2025, 37 % of Irish women will be obese, just behind 38 % in the UK [106].

Obesity rates are also steadily increasing in children and adolescents [107]. In the USA, the average weight of a child has risen by more than 5 kg within three decades, to a point where a third of the country's children are overweight or obese [107]. Research shows that overweight children become overweight adults [108].
The Commission on Ending Childhood Obesity (ECHO) presented its final report to the WHO in January, 2016 culminating a two-year process to address the alarming levels of childhood obesity globally. At least 41 million children under the age of five are obese or overweight, with the greatest rise in the number of children being obese or overweight coming from low- and middle-income countries [WHO report, 2014].

1.2.3 Adipose tissue distribution

Adipose tissue is principally deposited in two compartments: centrally and subcutaneously (Figure 1.11). Central fat is stored within the abdominal cavity and is therefore stored around a number of important internal organs such as the liver, pancreas and intestines [109]. It is also be referred as 'visceral fat' or 'active fat'. Subcutaneous fat is found just beneath the skin and it acts as padding and as an energy reserve, as well as providing some minor thermoregulation via insulation [101]. It has been shown that centrally deposited visceral fat is more metabolically active than subcutaneous fat [101]. Visceral fat secretes a number of pro-inflammatory adipokines, such as interleukin (IL)-6 [110], tumor necrosis factor (TNF), macrophage chemoattractant protein-1 (MCP-1) and resistin, that induce insulin resistance and diabetes [111, 112]. All of these visceral

fat secreted factors collectively contribute to proinflammatory, procoagulant and insulin resistant state known as the metabolic syndrome [100].

The location of adipose tissue is important in terms of dysmetabolism risk as central obesity is more strongly associated with insulin resistance, metabolic syndrome, cardiovascular diseases rather than BMI alone [101]. Metabolic syndrome is also associated with physical inactivity and aging [113, 114].

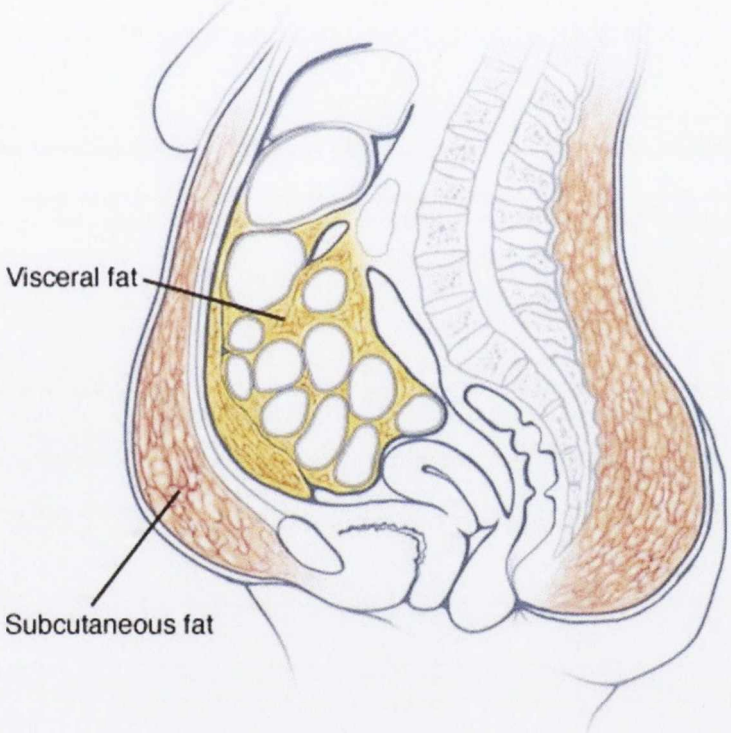


Figure 1.11 Distribution of adipose tissue. Adipose tissue is deposited in two main compartments: centrally (visceral adipose tissue) and peripherally (subcutaneous adipose tissue). Image adapted from http://xbodyconcepts.com/visceral-fat-causes-intestinal-cancer/ accessed on 7/9/2016.

1.2.3.1 White and brown fat

There are two types of adipose tissue, which have antagonistic functions [115, 116]. White adipose tissue (WAT) stores excess energy as triglycerides and brown adipose tissue (BAT) is specialized in the dissipation of energy through the production of heat [116]. BAT is abundant in newborns but it has been considered to be absent or have no relevance in adults [116]. White and brown fat differs both structurally and physiologically (Figure 1.12). White adipocytes are spherical and variable in size. Mitochondria in white adipocytes are thin, elongated and present in variable amounts [117]. In brown adipocytes, most characteristic organelles of BAT cells are the mitochondria [117]. Mitochondria are large, spherical, packed with laminar cristae and are present in higher numbers than in WAT [117]. The brown color of BAT is a result of high mitochondrial density and high vascularization [117]. BAT can also increase the uptake of blood glucose and lipids resulting in a decrease in blood glucose and lipids and increase in insulin sensitivity leading to anti-dyslipidemic effects [118, 119]. Characteristics for white and brown adipose tissue are summarized in Table 1.5.
BAT activity has been shown to be negatively associated with BMI [120]. Interestingly, obese individuals have very small amounts detectable BAT [121]. Published studies suggest that, low BAT activity might be a result of obesity and low BAT activity might increase the susceptibility to develop obesity [122]. Published studies suggest that the presence and activation of BAT may result in a hypermetabolic state in cancer patients and be partially responsible for weight loss [123]. Shellock *et al* examined necropsy samples of periadrenal tissues in order to identify the prevalence of brown adipose tissue in 25 cachectic patients, who died from cancer and 15 age-matched subjects who died from other illnesses. Brown adipose tissue was observed in 20 of the cancer patients (80%) compared to 2 of the age-matched subjects (13%), indicating that a high prevalence BAT is associated with cancer-induced cachexia [123].

Jones *et al* investigated whether brown fat is associated with breast cancer development [124]. In their immunohistochemical study they used a marker for BAT, UCP1. They reported that the expression of UCP1 mRNA in the BRCA1 mutant mice was significantly greater (approximately 50-fold) than in the age matched mammary glands from wild type mice, therefore suggesting the link between BAT and breast cancer development in BRCA1 mouse model [124].

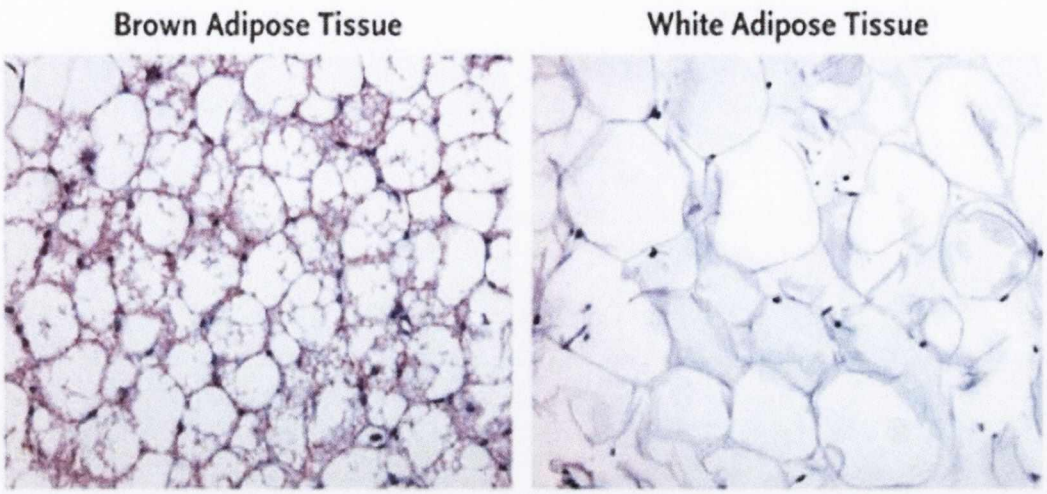


Figure 1.12 Adipose tissue is stained with hematoxylin and eosin. BAT contains multiple lipid droplets (white areas) and mitochondria (purple lining). Picture adapted from van Marken Lichtenbelt *et al.*,2009 [125].

Table 1. 5 Overview of the characteristics of brown and white adipose tissue

	Brown adipose tissue	**White adipose tissue**
Function	Uses energy when activated to generate heat	Stores energy
Location	Cervical-supraclaviculair area and paravertebral area	Ubiquitous
Tissue Characteristics	Fleshy like appearance High vascularization	Yellowish colour Low vascularization
Cell Characteristics	Polygonal shape Nucleus located in the centre Multiple lipid droplets of varying size High number of mitochondria UCP1 present	Generally rounded shape Nucleus compressed to the cell membrane Single large lipid droplet Few small mitochondria No UCP1

1.2.4 Measuring obesity

The World Health Organization defines obesity as abnormal or excessive fat accumulation that may impair health. The classification of obesity for epidemiological purposes defines overweight and obese body mass index greater than 25kg/m^2 and 30kg/m^2 respectively [WHO, 2000] (Table 1.6).

Table 1.6 Measuring obesity by Body Mass Index (BMI)

Category	BMI (kg/m^2)
Underweight	<18.5
Normal Weight	18.5-25
Overweight	25-30
Obese Class I	30-35
Obese Class II	35-40
Obese Class III	>40

It is important to consider that there is a large variation between total and visceral adiposity in individuals even within the same BMI category. This is also true when determining the BMI category, as BMI does not distinguish adipose tissue from lean tissue mass or reflect adipose tissue distribution [126]. BMI is defined as weigh-for-height index and it is calculated as a person's weight in kilograms divided by his height in meters (kg/m^2) [WHO, 2000]. Since the biological activity is of the adipose tissue compartments (i.e. subcutaneous versus visceral fat) is distinct, discrimination between the two has important implications for disease [126].

Considering the increase in the number of obese patients in the clinic, more knowledge on the effects of the visceral obesity is emerging. In the assessment of visceral obesity, the abdominal computed tomography (CT) scan is used as it enables the direct measurement of visceral fat area (VFA) with far more precision than the indirect anthropometric measurements like BMI [126, 127].

Cross-sectional abdominal and subcutaneous fat areas are measured by obtaining a cross-sectional scan at the disk space between the L3 and L4 vertebral body and a radiograph of the skeleton is taken for reference [128]. The total fat area (TFA) is calculated by drawing a line around the skin surface with a cursor (Figure 1.12; yellow line) therefore the software is able to calculate the area within the highlighted area. The visceral fat area (VFA) is calculated by repeating the technique with an area delineated by a line drawn around the abdominal wall muscle (Figure 1.13; red line). The subcutaneous fat area (SFA) is calculated by subtracting VFA from TFA [128].

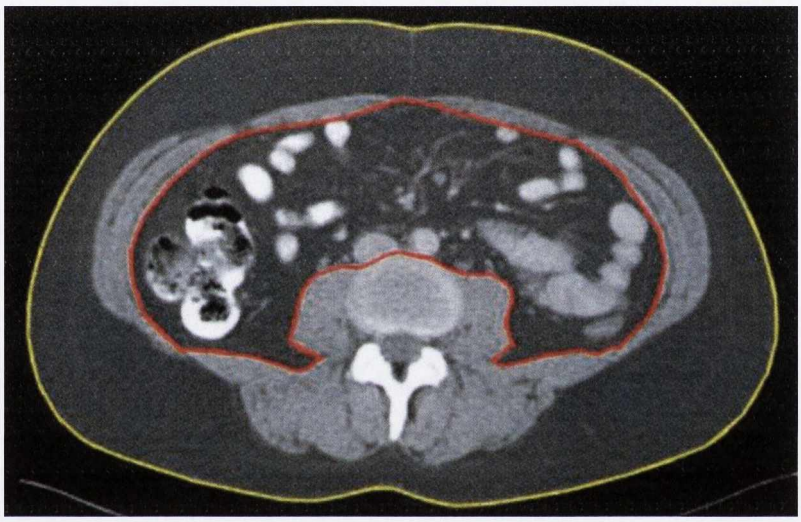


Figure 1.13 Computed tomography of the abdomen. The area inside the yellow line is the total fat area; the area inside the red line is the visceral fat area. The subcutaneous fat area is calculated by subtracting visceral fat area from the total fat area. Image reproduced from Beddy *et al.*, 2010 [128].

The patients can be stratified to obese and non-obese based on the value of VFA measurement. The cut of value for the measurement of obesity is different in males in females. Males with a measurement of visceral fat area greater than 163.8 cm^2, and females with a measurement greater than 80.1 cm^2 are considered to be obese (Table 1.7) [129]. Given the accuracy in determining the distribution of the body fat, CT measurement of visceral adiposity is considered to be the gold standard [127, 130, 131].

Table 1.7 Visceral fat area measurement by CT

Category	VFA cm^2
Obese	
Male	>163.8
Female	>80.1
Non-Obese	
Male	<163.8
Female	<80.1

When the technology and the expertise required to measure VFA is not available, waist circumference (WC) is a simple and reliable measurement of visceral obesity that positively correlates with VFA measurement [132]. Only a tape measure is required to measure WC and the technique appears to be straightforward, however it is difficult to standardize between patients and different studies at different locations [133].

1.2.5 The tumor microenvironment

Stephen Paget first highlighted the importance of the tumor microenvironment (TME) over a century ago when he described his 'seed and soil' hypothesis. The concept that cancer cells (seeds) require a specific TME (soil) in order to establish or propagate a tumor. The concept is still valid today and is recognised as the first key milestone in the numerous discoveries in cancer research [134]. The tumor microenvironment, in addition to harbouring carcinoma cells, consists of various components that have a major role in influencing the outcome of the malignancy (Figure 1.14) [135]. These can be widely classified into three main groups: cells of hematopoietic origin (includes T-Cells, B-Cells, macrophages, neutrophils, myeloid derived suppressor), cells of mesenchymal origin (fibroblasts, myo-fibroblasts, mesenchymal stem cells (MSC), adipocytes, endothelial cells) and non-cellular components (extracellular matrix (ECM) which contains of proteins, glycoproteins and proteoglycans). Tumours of different origins and different stages of progression will inevitably contain components in various proportions. Nonetheless, these three classes of stromal components represent the most abundant elements present in the microenvironment of solid tumours [135].

A number of published studies have highlighted the tissue microenvironment as a potential therapeutic target [136]. Cells within the TME are genetically stable than cancer cells. They have less mutations and they have lower chance of developing resistance. Furthermore, cells in the tissue microenvironment are highly dependent on factors in their environment for their pro-tumorigenic characteristics [24].

The tissue microenvironment has been shown to contribute to treatment resistance in many cancers, including esophageal cancer [137]. One of the most studied treatment approach in esophageal cancer, by targeting the tissue microenvironment, entails inhibition of angiogenesis (VEGF), preventing new blood vessel formation and the delivery of on oxygen and nutrients to sustain its growth.

Published research predominantly shows that chronic inflammation contributes to cancer development [137]. Clinical and experimental data indicate that the activation of certain immune cell types, for example neutrophils, macrophages and mast cells promote cancer development [138].

A number anti-inflammatory drugs have been shown to slow down tumor progression and reduce mortality [139]. For example, cyclooxygenase 2 (COX2) inhibitors have been shown to slow down tumor progression in colorectal cancer and breast cancers, including chemoresistant colorectal cancer [140, 141]. Published research shows that chronic activation of NF-κB causes resistance to chemotherapy and radiotherapy in many cancers [142]. STAT3, inhibitors of NF-κB been shown to enhance the effect of therapeutic agents in the treatment of bone metastasis in prostate cancer [143]. However, sustained NF-κB inhibition can result in severe side effects caused by immune deficiency and enhanced acute inflammation and subsequently liver damage [144].

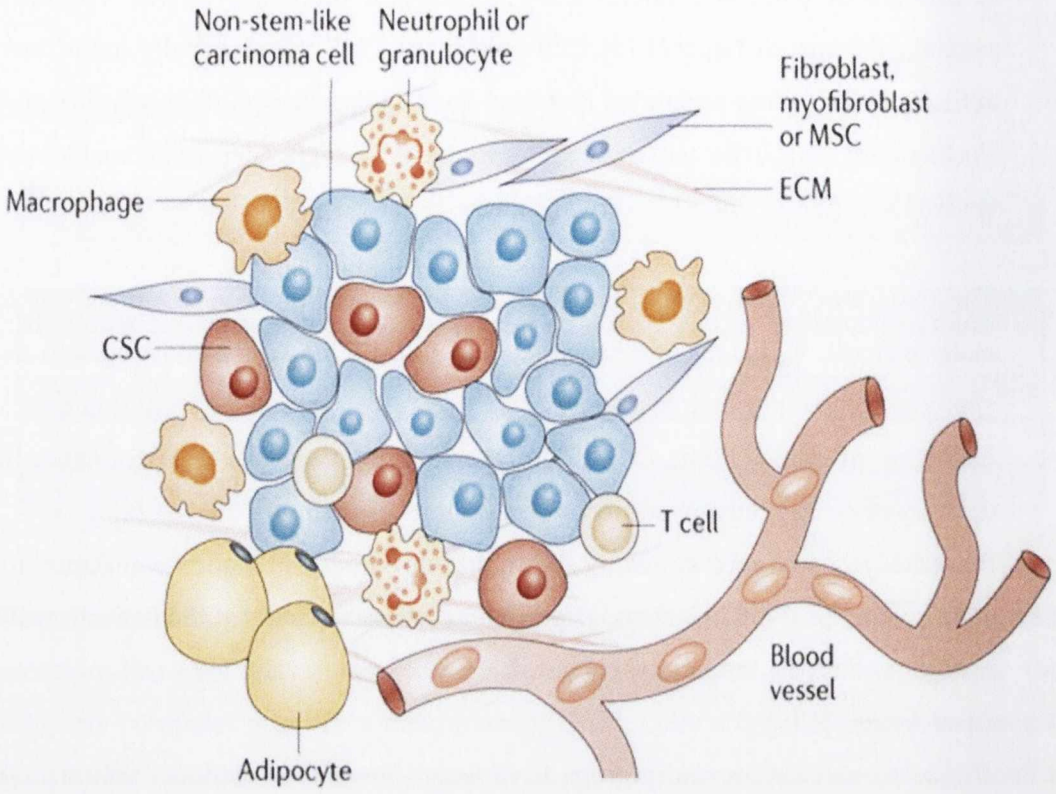


Figure 1.14 The tumor microenvironment. The figure depicts various components that have a major role in influencing the outcome of the malignancy. Image adapted from Nature Reviews Drug Discovery 13, 497–512 (2014) [135].

1.2.6 The role of adipose tissue in the tumor microenvironment

Inflammation is a well-studied hallmark of cancer, and growing evidence continues to emerge that chronic inflammation is highly associated with increased cancer risk [145]. In the lean state, adipose tissue supports metabolic homeostasis however in obesity, adipocytes undergo hypertrophy and release adipocytes that promotes increased production of pro-inflammatory factors (Figure 1.15).

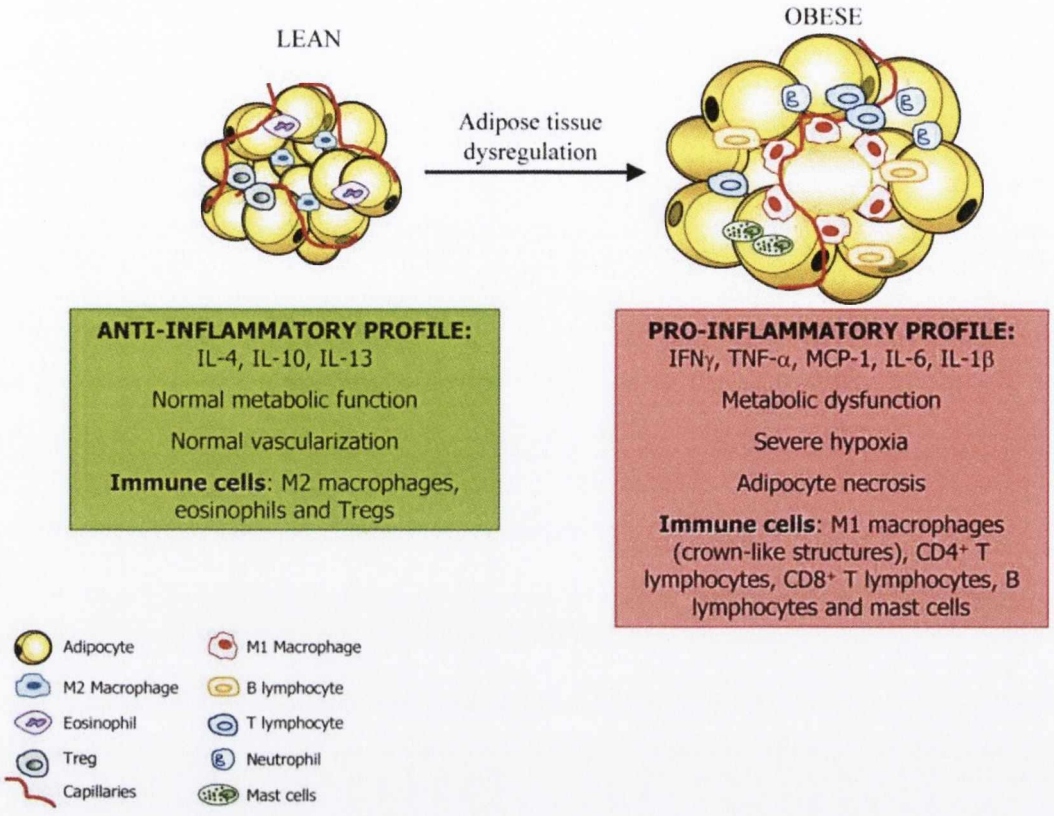


Figure 1.15 Adipose tissue constitutes an active endocrine organ. In the lean state, adipose tissue exhibits resident macrophages polarized toward an M2 status and Treg cells supporting metabolic homeostasis. The inflammation is controlled through the eosinophil-derived interleukin (IL)-4 and IL-13 and IL-10. In obesity, adipocytes undergo hypertrophy and release adipocytes that promotes the acquisition of an M1 macrophage phenotype with increased production of pro-inflammatory factors such as tumor necrosis factor-α (TNF-α), monocyte chemotactic protein (MCP)-1, and IL-6. This tissue microenvironment is infiltrated with mast cells and T lymphocytes, which collectively contribute to the dysregulation of adipose tissue and causing inflammation. Image reproduced from Catalan *et al.*, 2013 [146].

Due to the ability of fat to produce and secrete inflammatory cytokines by adipocytes or infiltrating macrophages [112] the adipose tissue constitutes an important initiator of the microenvironment favorable for tumor development (Figure 1.16) [146]. Novel adipokines (lipocalin-2 (LCN-2), osteopontin (OPN) and YKL40) which are linked to inflammation and insulin resistance with emerging roles in tumor development have been reported to be increased in adipose tissue from patients with colon cancer [146]. Adipose tissue also alters the B lymphocyte antigen CD20 encoded by the MS4A1 gene with a functional role in B-cell activation and FFAR2 that encodes a protein reported to modulate the differentiation and/or activation of leukocytes [147]. As a result of

expanding adipose tissue, enlarged adipocytes become distant from the vasculature resulting in hypoxic regions and subsequently necrosis. Adipose tissue hypoxia is considered to underlie the inflammatory response [148-150]. Hypoxia-inducible factor (HIF1A), the regulator of oxygen homeostasis, is increased in the adipose tissue of obese patients and its expression is reduced following weight loss [151]. HIF1A also influences both the innate and the adaptive immunity regulating functions of myeloid cells, neutrophils, macrophages, mast cells, dendritic cells, natural killer cells and lymphocytes [152, 153]. Similarly to the hypoxia-induced events in tumor tissue, adipose tissue hypoxia is also associated with the presence of macrophages, which migrate to the hypoxic regions and alter their expression profile increasing inflammation [146].

Induction of hypoxia is a vital micro environmental factor during tumor progression [154, 155]. HIF1A is overexpressed in many solid tumors [156, 157], therefore the elevated levels of HIF1A are being associated with cancer-related mortalities in oligodendroglioma, breast, cervix, oropharynx, ovarian, and endometrial cancers [158]. Published studies predominantly show that hypoxia alters the function of adipocytes and appears to be an important factor in adipose tissue dysfunction in obesity leading to an increased risk of cancer development [148, 158]. By adipose tissue induced hypoxia, adipose tissue indirectly induces angiogenesis as hypoxia is a primary physiological signal for angiogenesis [148-150]. Adipocytes may also regulate angiogenesis by cell-to-cell contact and by adipokine secretion [159]. Many cytokines produced by adipose tissue such as leptin, TNF-α, IL-6, IL-8, vascular endothelial growth factor (VEGF) and tumor growth factor β (TGF-β) show pro-angiogenic properties [160-162]. Emerging evidence shows that modulation of angiogenesis is a possible therapeutic intervention to impair the development of obesity by regulating the growth and remodeling of the adipose tissue vasculature [163, 164].

In cases of severe obesity, adipose tissue can constitute up to 50–60% of the total body mass being the expanded adipose tissue [165]. The mechanisms linking obesity and cancer are not fully understood however a low grade chronic inflammation, dysregulation of growth signaling pathways, chronic hyperinsulinemia, and hypoxia associated to obesity are widely accepted as important factors in cancer pathogenesis [102]. Published studies predominantly show the link between obesity and inflammation, while focusing on the involvement of infiltrated immune cells into adipose tissue. Adipose tissue has

been shown to exhibit high infiltration by innate and adaptive cell types, which may have potential roles in insulin resistance in type II diabetes [146, 166, 167].

The understanding of the regulatory mechanisms that lead obesity-induced inflammation may provide new avenues to target adipose tissue inflammation (Figure 1.16).

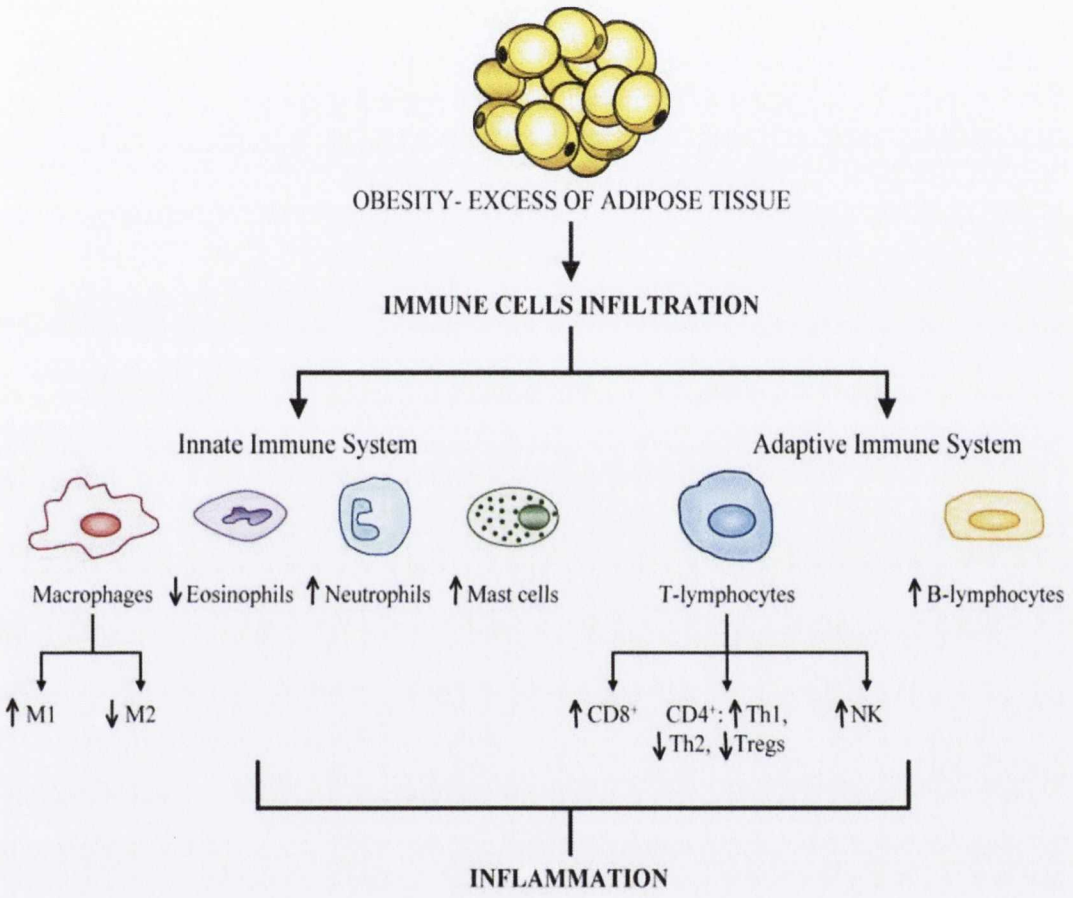


Figure 1.16 Obesity is associated with a great infiltration of cells from both the innate and adaptive immune systems. The aberrant population expansion of these cells is related to the onset of obesity-related cancer development. Image reproduced from Catalan *et al.*, 2013 [146].

1.2.7 Hallmarks of cancer and potential role of visceral obesity in tumourigenesis

Hanahan and Weinberg originally described six principle traits of cancer hallmarks essential for the transformation of normal cell to a malignant cell. The original six principles included self-sufficiency in growth signals, evading apoptosis, insensitivity to anti-growth signals, sustained angiogenesis, tissue invasion and metastasis and limitless replicative potential [168]. Progress in understanding the development of cancer, resulted in the addition of two new hallmarks of cancer: reprogramming of energy metabolism and evading immune destruction. Two enabling characteristics are described as environment supportive of cancer development: genomic instability and tumor promoting inflammation [169].

The cellular and molecular pathways linking obesity with established and emerging hallmarks of cancer [169] are unclear, but are of considerable research focus investigating the link between obesity and various hallmarks of cancer. These include pathways relevant to inflammation, angiogenesis, immune regulation, invasion and metastasis (EMT), genomic instability, and altered cellular energetics [170] (Figure 1.17).

There is a number of published studies undertaken St. James's hospital, that show the link between central adiposity and different hallmarks of cancer. Study by Lysaght *et al* reported an increase in pro-inflammatory and proliferative properties of excess visceral adiposity in OAC [171]. Significantly higher levels of VEGF and IL-6, along with significantly higher proportions of CD8+T cells and NKT cells were observed in visceral adipose tissue compared to subcutaneous fat in OAC patients [171]. Significantly higher levels of VEGF were observed in the conditioned media from visceral adipose tissue of centrally obese compared to non-obese patients. They also seen a significant increase in esophageal and colorectal tumor cell proliferation following culture with conditioned media from visceral adipose tissue of centrally obese patients [171].

Another study by Lysaght *et al* reported that visceral fat from OAC patients displayed elevated levels of activated proinflammatory CD4(+) and CD8(+) T cells compared to peripheral blood, suggesting that this pro-inflammatory cell activation in visceral adipose tissue may fuel chronic inflammation via T cell-mediated pathways [172].

Published study by Allott *et al* demonstrated that visceral obesity plays a role in upregulation of pro-tumor pathways contributing to aggressive tumor biology [173]. Following co-culture of OAC cell lines with visceral adipose tissue explants, expression of genes involved in tumor cell invasion and metastasis (matrix metalloproteinases) MMP2 and MMP9 were upregulated between 10-fold (MMP2) and 5000-fold (MMP9), and expression of tumor suppressor p53 was downregulated 2-fold in OAC cell lines [173]. MMP9 expression has been shown to be associated with angiogenesis and neovascularization in many cancers including breast and lung, therefore, a 5000-fold upregulation of MMP9 in OAC cell lines following co-culture with adipose tissue explants from viscerally obese OAC patients suggests that visceral obesity plays a role in tumor aggressiveness [173]. In a different study Allott *et al* documented that visceral adiposity is responsible for upregulation of PAI-1 and SNAI2, therefore inducing invasion and metastasis in OAC [174]. In this study, OE33 were co-cultured with adipose tissue from viscerally obese patients and subsequently, pathways altered in OE33 cells following co-culture were determined. Pathway analysis revealed that cytokine signaling, focal adhesion/EMT, and glycolysis were the top three significantly upregulated pathways in OE33 following co-culture with adipose tissue, when compared with co-culture with control medium (Figure 1.18). The top 9 significantly altered genes in each pathway belonging to the glycolysis pathway, cytokine signaling pathways and focal adhesion/EMT pathways (Figure 1.18) [174].

Lynam-Lennon *et al* demonstrated that excess visceral adiposity induces alterations in mitochondrial function in OAC [175], therefore altering cellular energetics hallmark of cancer. This study revealed that ACM from obese OAC patients significantly increased mitochondrial mass and mitochondrial membrane potential in OAC cells. This mitochondrial dysfunction was associated with altered expression of 19 mitochondrial-associated genes and significantly reduced intracellular ATP levels. Additionally, ACM from obese OAC patients induced a metabolic shift to glycolysis in OAC cells [175].

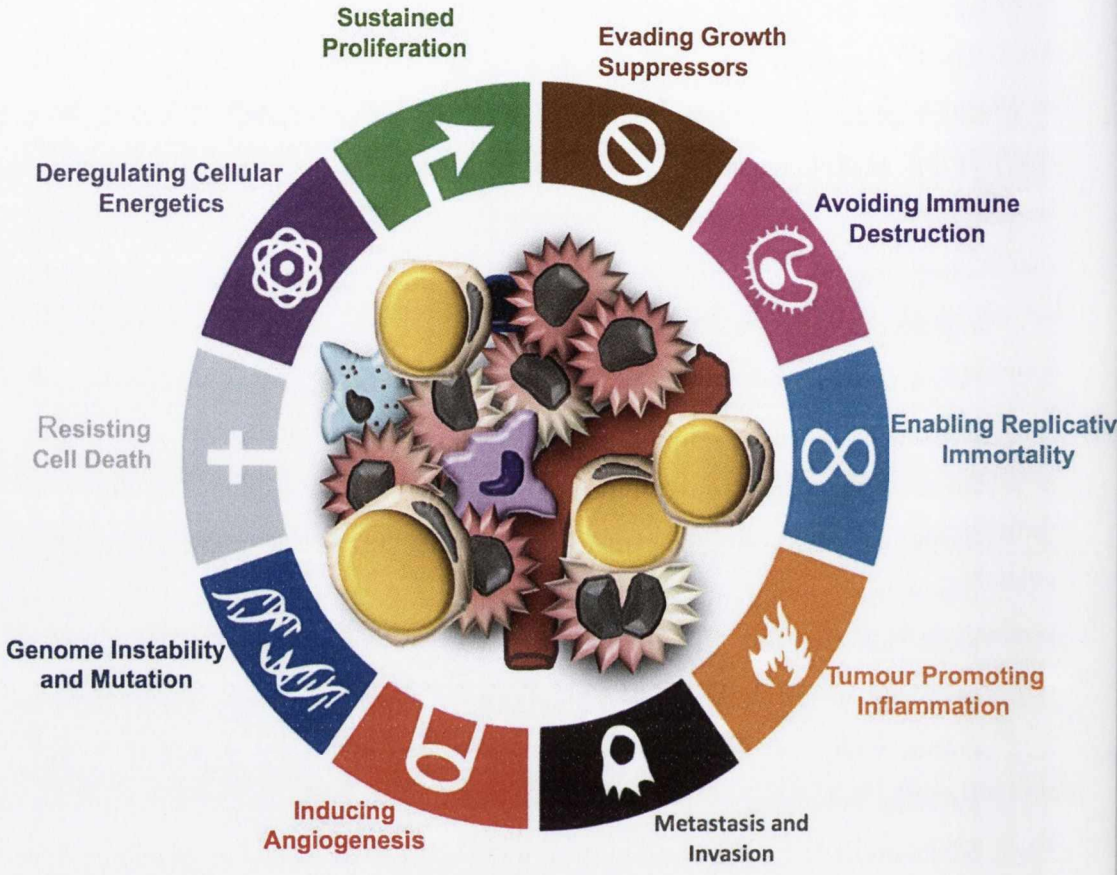


Figure 1.17 Hallmarks of cancer and potential role of visceral obesity in tumourigenesis. Hannah and Weinberg, in 2000, proposed six hallmarks that define properties that tumours acquire in order to sustain a malignant phenotype. Mantovani, in 2009, proposed an addition of seventh property: an inflammatory microenvironment. In 2011, Hannah and Weinberg added the eighth and the ninth hallmarks: genomic instability and mutation, and deregulating cellular energetics. Adipose tissue through the systemic alterations associated with obesity may support the development of a malignant phenotype in susceptible cells through supporting invasion and metastases (EMT), evasion and apoptosis, promotion of angiogenesis, genomic instability and systemic inflammation.

Pathway	LogFC	Gene	Description
Cytokine signaling*	6.941	*CXCL5***	*Chemokine (C–X–C motif) ligand 5*
	4.370	*PPBP*	*Pro-platelet basic protein (chemokine (C–X–C motif) ligand 7)*
	1.871	*OSMR***	*Oncostatin M receptor*
	1.580	*SOCS3**	*Suppressor of cytokine signaling 3*
	1.501	*IL1B**	*Interleukin 1, beta*
	1.082	*CCL7**	*Chemokine (C–C motif) ligand 7*
	0.873	*IL4R***	*Interleukin 4 receptor*
	0.840	*IL1R1*	*Interleukin 1 receptor, type I*
	0.424	*IL7R**	*Interleukin 7 receptor*
	0.351	*STAT5A*	*Signal transducer and activator of transcription 5A*
Focal adhesion/EMT*	4.919	*SPP1**	*Secreted phosphoprotein 1*
	2.867	*SERPINE1*	*Serpin peptidase inhibitor E1 (plasminogen activator inhibitor-1)*
	2.496	*SNAI2**	*Snail homolog 2*
	1.353	*LAMB3**	*Laminin, beta 3*
	1.255	*ITGA3***	*Integrin, alpha 3*
	1.149	*LAMC2**	*Laminin, gamma 2*
	0.656	*SERPINB6**	*Serpin peptidase inhibitor, B6*
	0.504	*ITGA6**	*Integrin, alpha 6*
	0.410	*LAMC1*	*Laminin, gamma 1*
	0.269	*PXN*	*Paxillin*
Glycolysis*	1.555	*PDK4**	*Pyruvate dehydrogenase kinase, isozyme 4*
	1.406	*ALDOC*	*Aldolase C, fructose-bisphosphate*
	1.110	*PFKFB3**	*6-phosphofructo-2-kinase/fructose-2,6-biphosphatase 3*
	1.071	*HK1***	*Hexokinase 1*
	1.036	*PDK1**	*Pyruvate dehydrogenase kinase, isozyme 1*
	0.716	*PFKP**	*Phosphofructokinase, platelet*
	0.697	*PKM2**	*Pyruvate kinase, muscle*
	0.589	*LDHC*	*Lactate dehydrogenase C*
	0.350	*ALDOA*	*Aldolase A, fructose-bisphosphate*

Figure 1.18 Top differentially expressed genes in three significantly upregulated pathways in esophageal adenocarcinoma cells following co-culture with ACM from viscerally obese OAC patients. Figure adapted from Allott *et al.*, [174].

1.2.8 Epithelial Mesenchymal Transition (EMT)

The epithelial-mesenchymal transition was first recognized as a feature of embryogenesis [176]. EMT, and its reverse process, MET (mesenchymal-epithelial transition) are both critical for normal tissue and organ development in the embryo, and in numerous embryonic events such as gastrulation, crest formation, heart valve formation, pathogenesis and myogenesis [176]. Epithelial and mesenchymal cells differ in their phenotype and function. Epithelial cells are closely connected to each other by tight junctions, gap junctions and adherent junctions; whereas mesenchymal cells have a spindle-shaped morphology and interact with each other only through focal points [177]. It is now understood that mesenchymal transition (EMT) is due to downregulation of the cell the adhesion molecule E-cadherin, while substituting it with another cadherin such as N-cadherin. N-Cadherin enables the cell to dissociate from the neighboring cells and migrate through tissue, to lymphatic or blood vessels and subsequently to a new location [178]. It has been shown that EMT occurs during tissue injury and is likely to promote cancer invasion and metastasis [179].

Various biomarkers have been screened to explore the EMT process, including the loss of E-cadherin, cytokeratin, as well as the upregulation of matrix metalloproteinase, fibronectin, α-smooth muscle actin, vimentin, Zeb 1 / 2 , snail, and slug (Figure 1.19) [109, 180].

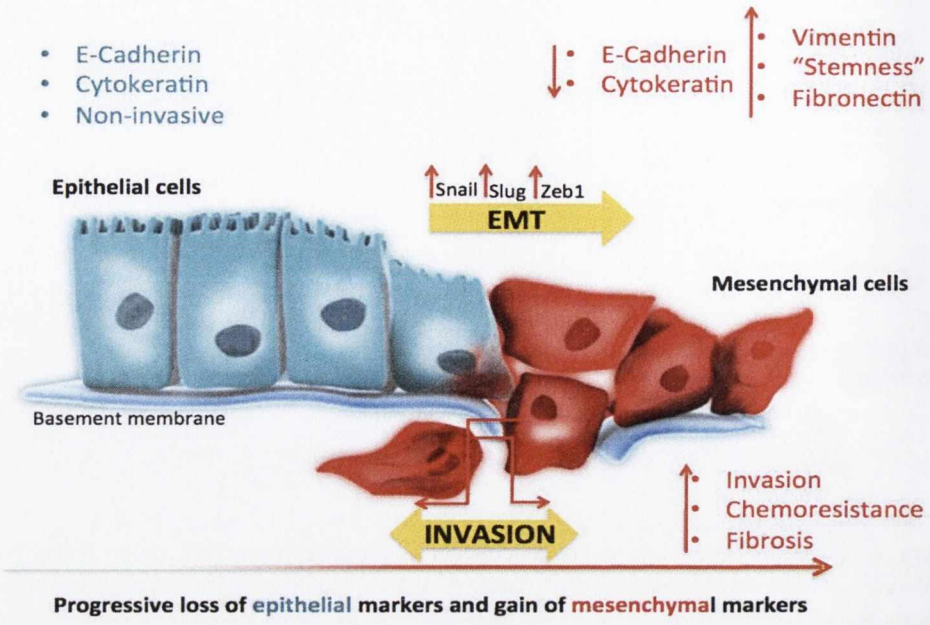


Figure 1.19 Epithelial mesenchymal transition in cancer. Figure shows a progressive loss of epithelial markers such as E-cadherin and cytokeratin and gain of mesenchymal markers such as SNAI1, SNAI2, Zeb1, vimentin, leading to cancer metastasis and chemoresistance.

1.2.8.1 Cadherin switching in EMT

It is widely documented that a process called Cadherin Switching often happens during EMT [181, 182]. Most normal epithelial tissues in which cells are polarized express the epithelial adhesion molecule E-Cadherin, while mesenchymal cells, which are more motile and less polarized, typically express N-cadherin [183].

Both EMT and MET are dependent on E-cadherin, therefore cells undergoing EMT downregulate E-Cadherin. E-Cadherin is required for normal embryonic development and homeostasis and it has been shown to act as a potential tumor suppressor because following the silencing transcription of its gene in different cancer types, and re-expression of a native form of E-Cadherin in carcinomas *in vitro* is sufficient to reduce the aggressiveness of tumor cells [184]. During EMT cell-cell junctions and basoapical polarity acquiring mesenchymal characteristics are lost resulting in increased motility and invasive potential, stem like characteristics and resistance to apoptosis that are essential for the development of metastatic disease. Major signaling pathways involved in EMT include Ras, transforming growth factor-β (TGF-β), Wnt, epidermal growth factor (EGF), Notch and Hedgehog. These signaling pathways are activated by extrinsic or intrinsic stimuli and they will ultimately converge on any of the transcription factors, including

nuclear factor kappa B (NFκB) and zinc finger proteins Snail and Slug, Twist, ZEB 1/2 and Smads that will likely culminate in transcriptional repression of E-cadherin. These transcription factors are able to interact with each other and with other proteins providing a crosstalk mechanism between the relevant signaling pathways and regulate the phenotypic changes of cancer cells. EGF and TGF-β promote EMT by regulating Snail, Slug and Twist through direct regulation of genes involved in cellular adhesion, migration, and invasion [185]. Snail and Slug have been previously described as direct repressors of E-cadherin and inducers of EMT and subsequent metastases when overexpressed in epithelial cells [185, 186]. The clinical relevance of Slug expression has been demonstrated in multiple human cancers including breast, prostate, head and neck, pancreas and endometrial carcinomas [187-191]. Some studies report that Slug expression correlates with loss of E-cadherin in breast cancer cell lines to a stronger extent than correlation of SNAIL expression at the same setting, suggesting Slug is a likely *in vivo* repressor of E-cadherin expression in breast cancer [192, 193]. Expression of Slug, especially in the E-cadherin preserved tumors, has been shown to be related to prognosis in esophageal cancer [194].

1.3 Tumour metabolism

1.3.1 Metabolic pathways

Metabolism describes the process whereby cells extract energy from their environment to produce new cellular components. There are a number of metabolic pathways however the one a cell uses is influenced by the source of energy (i.e. amino acids, glucose, fatty acids) and the resources available to the cell to drive the metabolic pathway (i.e. oxygen) [195].

1.3.2 Glycolysis

The dysregulation of energy metabolism is an emerging hallmark of cancer [196]. Glucose is the most important fuel in the body. It is the only fuel used by the brain during non-starvation conditions and the only fuel used by red blood cells [189, 197]. The information about these metabolic pathways included in this section is from the textbook 'Biochemistry' [190]. Glycolysis is anaerobic and takes place in cystol [134]. During this process, one molecule of glucose is converted into two molecules of pyruvate in a series

of chemical reactions with production of ATP [190]. Following formation of glucose-6-phosphate from glucose, glucose-6-phosphate is converted to fructose-6-phosphate and fructose 1, 6-biphosphate using one molecule of ATP. Fructose and galactose do not have catabolic pathways of their own therefore they also feed into glycolysis as two intermediates fructose-6-phosphate and glucose-6-phosphate, respectively. Fructose 1, 6-biphosphate is split into glyceraldehyde 3-phosphate and dihydroxyacetone phosphate. Dihydroxyacetone phosphate is an isomer of glyceraldehyde 3-phosphate therefore this conversion allows the remaining reactions of glycolysis to proceed twice. Glyceraldehyde 3-phosphate is converted into 1, 3-bibiphosphoglycerate and 2-phosphoglycerate respectively, resulting in generation of ATP. Finally, phosphoenolpyruvate is formed and is converted into pyruvate, generating one more molecule of ATP [122]. Pyruvate is either processed to form lactate or gets oxidized during anaerobic conditions (i.e. OXPHOS), to yield a larger number of ATP molecules [122] (Figure 1.20).

Glycolysis involves the use of numerous enzymes that are potential druggable targets [198]. These include hexokinases that phosphorylate glucose after it is transported across the cell membrane producing glucose-6-phosphatase [122] (Figure 1.19).

Due to an increase of glycolytic enzymes in cancer cells, they are attractive potential targets in cancer treatment [199].

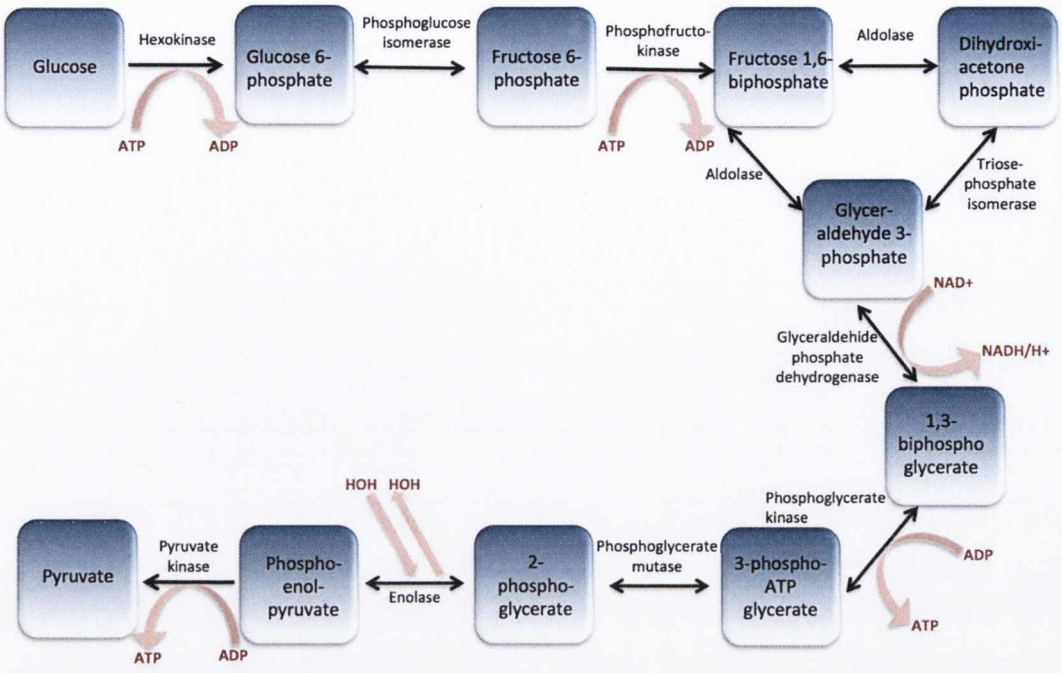


Figure 1.20 Glycolysis. Following formation of glucose-6-phosphate from glucose, glucose-6-phosphate is converted into fructose 6-phosphate and then fructose 1, 6-biphosphate, using up a molecule of ATP. Fructose and galactose also feed into glycolysis as intermediates (fructose-6-phosphate and glucose-6-phosphate respectively). Fructose 1, 6-biphosphatase is split into glyceraldehyde, 3-phosphate and dihydroxyacetone phosphate. Glyceraldehyde 3-phosphate is converted into 1, 3-biphospholycerate (generating one molecule of NADH), 3-phosphoglycerate (generating one molecule of ATP) and 2-phosphoglycerate. Finally, phosphoenolpyruvate is formed and converted into pyruvate, generating one more molecule of ATP.

1.3.2.1 Glucose transporter proteins

Glucose enters the cells via a family of glucose transporter proteins (GLUTs) [200]. Glucose transporter proteins mediate the transport of glucose and other monosaccharides into and out of mammalian cells and therefore play a pivotal role in maintaining blood glucose concentrations in a normal range between 4.5 and 6 mM [201]. The GLUT transporters have different expression patterns in different tissues and play various roles. Published research show that the expression of glucose transporter genes, GLUT1 (erythrocyte type), GLUT2 (liver type), GLUT3 (brain type), GLUT4 (muscle/ fat type) and GLUT5 (small intestine type), is relatively tissue specific [202].

Glucose transporter protein 1 (GLUT1) is generally absent from normal epithelial cells, but increased Glut1 expression has been observed in many epithelial malignancies [203]. A recent immunohistological study by Sawayama *et al* investigated the link between an esophageal SCC and the effects of GLUT1 expression in 145 patients [204]. They reported that GLUT1 positivity was associated with depth of invasion and vascular invasion, and in tumors where GLUT1 expression was up-regulated, high microvessel density was detected and GLUT1 positivity was correlated with hematogenous recurrence. Overall, GLUT1 positivity led to a patient's poor prognosis in colorectal cancer [204]. In another immunohistochemical study, Tohma *et al* investigated the expression of GLUT1 at the different stages of esophageal cancer in 63 patients [205]. He reported that pathological later stage esophageal cancers (T3-T4) presented a higher level of GLUT1 than at the earlier stages of the disease (T1-T2), and lesions with lymph node metastasis showed a higher level of expression of GLUT1 than lesions without lymph node metastasis. A study by Chiba *et al* employed 25 esophageal SCC patients and investigated the link between GLUT1 expression and response to concurrent chemo radiotherapy (CRT) [206]. They reported that GLUT1 expression was significantly correlated with initial response to concurrent chemo radiotherapy (CRT) where patients with a high GLUT1 expression had a significantly poorer local control than those with a low expression [206].

GLUT4 displays an interesting connection with cancer because it is transcriptionally repressed by p53 [207], a tumor suppressor protein is important for cell cycle control and apoptosis, therefore it is an attractive target in different types of cancer. A recent study by Acharya *et al* reported that high GLUT4 expression was associated with increased progression of ER-/HER2+ breast cancer at an early stage disease model [208]. They also showed that treatment with lapatinib inhibited HER2 signaling and downregulated GLUT4, which contribute to decreased cell proliferation and increased cell death, and consequently, a significant delay of mammary tumor progression in the MMTV-neu ER-/HER2+ transgenic mice model [208]. Garrido *et al* demonstrated that shRNA-mediated down-regulation of GLUT4 inhibited glucose uptake and induced metabolic reprogramming by reallocating metabolic flux to oxidative phosphorylation. This reallocation resulted in increased activity of the mitochondrial oxidation of pyruvate and lower lactate release, therefore potentially reducing glycolysis [209]. GLUT4 inhibition also reduced cell proliferation and cell viability under hypoxic conditions, suggesting

GLUT4 as a potential pharmacological target for the induction of metabolic reprogramming *in vivo* in breast cancer models [208].

1.3.2.2 Hexokinases

Hexokinase 1 (HK1) and hexokinase 2 (HK2) are unique enzymes in the glycolytic pathway due to their ability to bind the outer mitochondrial membrane. They are structurally and functionally similar to each other and both are inhibited by their catalytic product G6P. Both HK1 and HK2 are highly expressed in embryonic tissues. However, while HK1 is ubiquitously expressed in the majority of adult tissues, HK2 is expressed at relatively high level only in adipose tissues, skeletal muscles, and heart [210]. HK1 is also one of the key regulators in glycolysis and oncogenic markers in cancers [211]. Li *et al* retrospectively recruited 141 surgically resected specimens of primary esophageal SCC and investigated the link between HK1 and SCC by immunohistochemical staining [212]. They found that the expression of HK1 was associated with disease progression, invasion, poor survival of patients with esophageal SCC and HK1 was an independent predictor for the disease. Moreover, when HK1-shRNA was used to knock out the expression of HK1 in esophageal SCC cell model, silencing of HK1 expression by ShRNA also induced a reduction of phospho-S6 kinase, an important kinase in the mTOR pathway therefore inhibited cell proliferation and colony formation of esophageal SCC cells [212]. A recent retrospective study Anderson *et al* examined the expression of genes involved in glucose metabolism using a previously described dataset of tumors from primary and metastatic sites of 143 pancreatic ductal adenocarcinoma (PDAC) patients [213]. A list of 153 unique genes of interest was compiled using existing KEGG and Reactome gene lists for glucose metabolism, glycolysis and gluconeogenesis, the pentose phosphate pathway and O-glycan biosynthesis. HK2 has been shown to be one of the top four upregulated genes in primary tumors compared to normal pancreas and in metastases compared to primary tumors [213].

A study investigating the natural compound resveratrol reports that the natural compound inhibits HK2 activity in hepatocellular carcinoma (HCC) cell lines and subsequently reduces tumor growth in mice bearing HCC [214]. A recent study indicated that reduction of HK2 activity by metformin (used in treatment of Type 2 Diabetes Mellitus (T2DM), partially reduces the rate of glycolysis in triple negative breast cancer cell line [215]. The

most recent evidence suggests HK2 as a target for miRNA-143 and the downregulation of HK2 results in reduced glycolysis in prostate and lung cancers [215, 216].

1.3.2.3 Pyruvate kinase M2

Pyruvate kinase M2 (PKM2) is the key enzyme in catalyzing the final glycolysis reaction, which is expressed mainly in the embryonic tissues and proliferative cells, especially in cancer cells [217, 218]. In recent years, several studies reported that PKM2 had a high sensitivity in auxiliary diagnosis in melanoma [219], renal cell carcinoma [220], lung cancer [221], cervical cancer [222] and colorectal cancer (CRC) [223], indicating the significance of PKM2 in early detection of cancer and prognosis. In an immunohistochemical study Zhan *et al* investigated the link between PKM2 expression and esophageal SCC. The retrospective analysis of 210 SCC patients with additional 59 adjacent normal tissue cases taken from the same cohort of patients were investigated [217]. Out of 210 patients, 151 cases (with complete following up data) were included for analysis. Patients with moderate PKM2 expression in tumor tissues possessed a higher risk of locoregional recurrence compared with patients with weak PKM2 expression and patients with strong PKM2 expression in tumor tissues, were shown to be at the highest risk. This study also reported that PKM2 expression had a strong correlation with survival. The estimated 5-year survival rate of patients with weak PKM2 expression was 65.6%, moderate 49.6%, and strong 24.9%. PKM2 expression was identified as a predictor of the prognosis of as well as TNM stage in esophageal SCC [217].

1.3.2.4 Glyceraldehyde-3-phosphate dehydrogenase

Glyceraldehyde-3-phosphate dehydrogenase (GAPDH) is a glycolytic enzyme catalyzing the reversible conversion of glyceraldehyde-3-phosphate to 1, 3-diphosphoglycerate [224]. Bioinformatics Group in the European Molecular Biology Laboratory in Germany used NIH public database revealed that GAPDH was overexpressed in 24 types of cancer including brain, testicular, prostate, gastric cancers [225]. Bazzocco *et al* showed that inhibition of GAPDH efficiently reduced the growth of 52 types of colon cancer cells *in vitro* by both, using a pharmacological GAPDH inhibitor and RNAi-based knockdown, outlining the importance of GAPDH expression in colorectal cancer in vitro [226]. Puzone *et at* retrospectively investigated the expression of GAPDH in 82 consecutive

early stages resected non-small cell lung cancer (NSCLC) patients and compared the results to the publicly available NSCLC microarray datasets collecting data from 6 large publically available NSCLC microarray datasets with over 1250 total patients [227]. In their retrospective study GAPDH gene over expression was found to be an adverse prognostic factor in early stages NSCLC and this result was confirmed in 5 of 6 public datasets analyzed: Shedden *et al* 2008 [228], Lee *et al* 2008 [229], Tomida *et al* 2009 [230], Roepman *et al* 2009 [231], Okayama *et al* 2012 [232], Botling *et al* 2013 [233], all confirming the prognostic value of glucose metabolism assessment in NSCLC. A recent prospective study by Hjerpe *et al* in Sweden investigated the link between the expression levels of GAPDH and disease prognosis and response to treatment in 62 ovarian adenocarcinoma patients with the median follow up time of 59.9 months [234]. They reported that high GAPDH expression was associated with early disease progression, shorter platinum free interval (PFI) and poor overall survival in patients with advanced high-grade serous adenocarcinomas of the ovary, fallopian tube or peritoneum [234]. Their findings were supported by a study by Revillion *et al* where 404 breast cancer patients with a median follow-up of 82 months were assessed. The study revealed that GAPDH was not an independent prognostic factor, but its expression was inversely correlated to estradiol and progesterone receptor concentrations, young age and grading therefore GAPDH expression in breast cancer seemed to reflect tumor aggressiveness [235].

1.3.2.5 Enolase 3

Enolase in another enzyme abundant in the glycolytic pathway. It is responsible for the conversion 2-phosphoglycerate to phosphoenolpyruvate. There is no published work showing the benefit of targeting enolase in glycolysis however, a preliminary Affymetrix study in our department reported significant upregulation of Enolase-3 in OAC cells treated with fresh visceral fat taken during oesophagectomy from obese OAC patients. This has subsequently been validated at the gene level in the obese cohort of OAC patient tumors therefore it is of interest for further investigation.

1.3.3 Oxidative phosphorylation

Oxidative phosphorylation (OXPHOS) occurs in the inner mitochondrial membrane and it involves transfer of electrons from NADH or $FADH_2$ to O_2 by a series of electron carriers to form ATP. The electron transport chain plays a central role in oxidative phosphorylation (Figure 1.21) and it has been shown that respiratory impairment plays a key role in tumourigenesis [236]. Complex I is the entry point for most electrons into the respiratory chain, therefore complex I has been suggested as the rate-limiting step in electron transfer [237]. Recently, mitochondrial DNA (mtDNA) mutations in genes encoding Complex I subunits have been found in various cancer cells such as lung [238], breast, thyroid, and bladder cancers [239]. Published studies show that Complex II deficiency gives rise to cancer, however, it is also speculated that Complex II subunits function as tumor suppressors [240]. One particular study reported that the activity of Complex II in gastrointestinal stromal tumours bearing Complex II mutations is compromised [241]. Research shows that Complex II-deficient tumours accumulate succinate which stabilises HIF1A and results in various protumourigenic effects [242].

Complex III is also linked with a role in carcinogenesis. It has been reported that an increase in superoxide radicals inactivates Complex III resulting in the impairment of mitochondrial respiration in rat hepatomas [243]. Complex III mutations have been linked to ovarian, colorectal and breast cancer [244-246]. Many studies are reporting the link between alterations and defects in Complex IV with disease progression. The Complex IV subunits COX4I2 and COX8C have been reported to be differentially altered across the in-vitro and in-vivo metaplastic-dysplastic-OAC sequence in Barrett's oesophagus [247]. Multiple studies outline the link between defects in Complex V with disease progression. Furthermore, increased expression of the Complex V subunit ATP5B has been reported to be significantly upregulated in OAC patients who have a poor pathological response to neoadjuvant chemoradiation suggesting a role for Complex V, mitochondrial alterations and oxidative phosphorylation in the radioresistance of OAC [248].

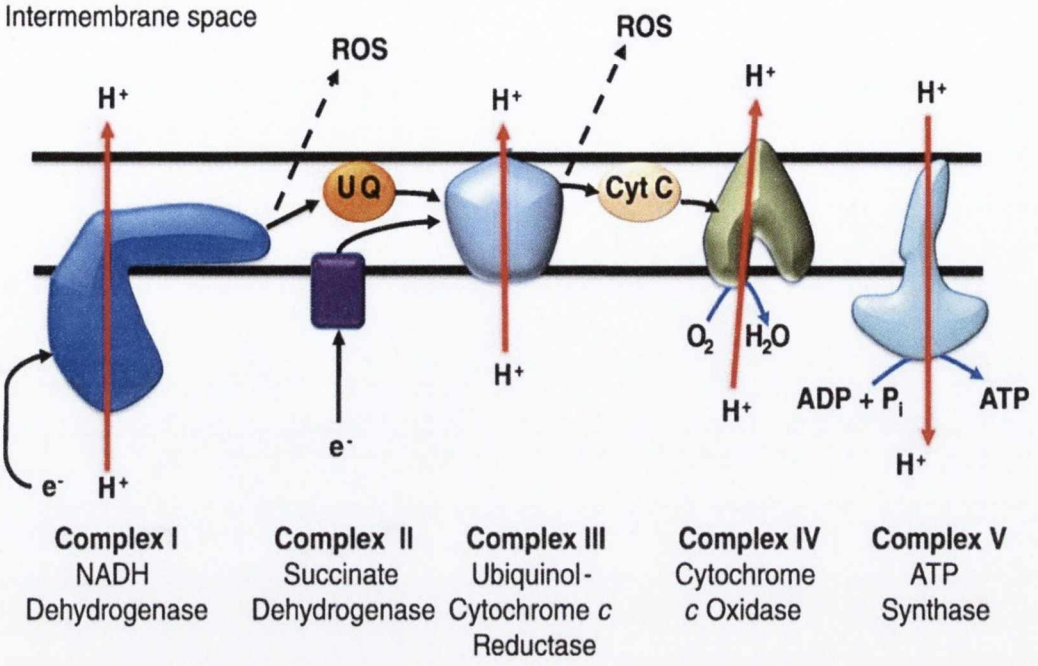


Figure 1.21 The mitochondrial electron transport chain. Composed of five mitochondrial protein complexes, the electron transport chain extrudes hydrogen ions into the intermembrane space to produce an electrochemical gradient. The subsequent influx of hydrogen ions from the intermembrane space into the mitochondrial matrix through complex V produces ATP thereby playing a central role in mitochondrial respiration. Dotted arrows show ROS production as a result of the electron leak. UQ refers to ubiquinone; Cyt C refers to Cytochrome C. Image reproduced from Ghouleh *et al.*, 2011 [249].

1.3.3.1 ATP synthase subunit beta (ATP5B)

ATP5B gene encodes a subunit of mitochondrial ATP synthase. Mitochondrial ATP synthase catalyzes ATP synthesis, utilizing an electrochemical gradient of protons across the inner membrane during oxidative phosphorylation [250]. Previous research from St. James's hospital demonstrated that oxidative phosphorylation and glycolysis are reprogrammed early in the inflamed Barrett disease sequence and may act mutually to promote disease progression in Barrett's oesophagus [247]. They showed that high levels of ATP5B segregated Barrett's patients who progressed to HGD/OAC from non-progressors, highlighting the possible prognostic advantage of assessing metabolic profiles in these preneoplastic patients [247]. Hjerpe *et al* also investigated the link between the expression levels of ATP5B and disease prognosis and response to treatment in 62 ovarian adenocarcinoma patients with the median follow up time of 59.9 months [234]. They reported that similarly to GAPDH expression, high of ATP5B expression

was associated with early disease progression, shorter platinum free interval (PFI) and poor overall survival in patients with advanced high-grade serious ovarian adenocarcinomas [234].

1.3.4 The Warburg effect

About 70% of ATP in normal cells is generated through OXPHOS, with the remaining 30% produced by fermentation. The ratio slightly varies depending on the cell type and their environment [251]. The conversion of pyruvate to lactate in normal cells occurs only in the absence of oxygen, in the process called 'aerobic glycolysis' [252].

Otto Warburg's initial observation in 1956 demonstrated that tumours exhibit increased levels of aerobic glycolysis [253]. This observation has since resulted in numerous studies investigating the role of mitochondrial energy metabolism in disease progression across many disease entities. As a result of its importance in the development of various cancers, the reprogramming of cellular energetics is now beginning to establish itself as one of the new hallmarks of cancer [254, 255].

Malignant tumors are able to switch their metabolism towards highly elevated rates of glycolysis [256]. This switch gives tumor cells an advantage over normal cells due to the rapid intake of glucose for which all cells are competing. This allows cancer cells to metabolise in the presence and absence of oxygen (Figure 1.22) [257].

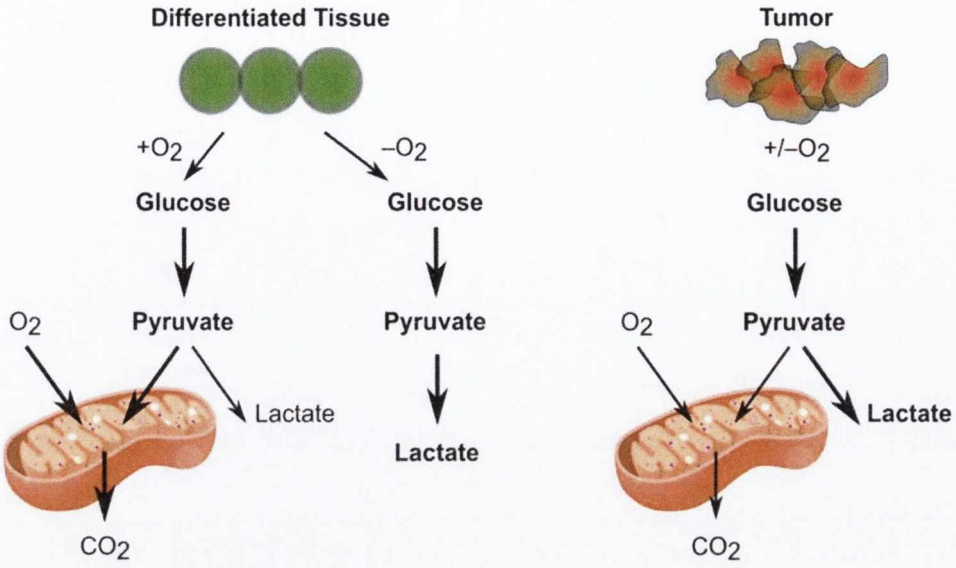


Figure 1.22 The Warburg effect. In the presence of oxygen, normal tissues metabolise glucose to pyruvate via glycolysis, and subsequently, oxidise the majority of the pyruvate in the mitochondria during oxidative phosphorylation. When the cells are oxygen deprived they redirect pyruvate away from oxidative phosphorylation by generating lactate (anaerobic glycolysis). The continued lactate production results in minimal production of ATP. Warburg observed that cancer cells are able to convert the majority of glucose to lactate regardless of both: the presence and absence of oxygen. Image reproduced from Vander Heiden *et al.*, 2009 [134].

The switch from OXPHOS to aerobic glycolysis is regulated by multiple mechanisms such as oncogene activation, the loss of tumor suppressors, mutations to metabolic enzymes and hypoxia [258]. Mutations to the RAS oncogene result in aerobic glycolysis [259] by activating the mTOR (mechanistic target of rapamycin) via the PI3K (phosphoinositide 3-kinase)-Akt-mTOR signaling pathway. mTOR activates HIF1and promotes aerobic glycolysis [260-262]. Many genes, including glucose transporter genes GLUT1 and GLUT3, are regulated by HIF1 [263]. HIF1 has also been reported to inhibit pyruvate dehydrogenase kinase 1 (PDK1), which is responsible for the conversion of pyruvate to acetyl-CoA thus inhibiting OXPHOS [264]. Also, HIF1 has been shown to upregulate pyruvate kinase muscle 2 (PKM2) [265] and Myc oncogene [266]. Myc is responsible for the induction of hexokinase 2 (HK2) resulting in conversion of glucose to glucose-6-phosphatase and lactate dehydrogenase A (LDHA) (328), therefore promoting glycolysis [266].

Overall Hypothesis

Tumour metabolism and 5-lipoxygenase are associated with obesity and play a role in the development and progression of esophageal adenocarcinoma

Objective

Evaluate the expression of markers of glycolysis, OXPHOS, hypoxia and 5-lipoxygenase in esophageal adenocarcinoma and effect of targeting these pathways with novel compounds

Specific Aims:

- Investigation of markers of glycolysis, OXPHOS, hypoxia and 5LOX in OAC, and their association with clinical and pathological features (Chapter 3)
- Investigation of the link between glycolysis, OXPHOS, 5LOX and obesity in OAC (Chapter 4)
- Investigation of markers of glycolysis, OXPHOS, hypoxia and 5LOXmarker in OAC, and their association with visceral obesity (Chapter 5)
- Delineation whether visceral adiposity results in metabolic shift in glucose metabolism in OAC (Chapter 6)
- Assessment of anti-cancer potential of novel 5LOX targeted inhibitors in models of OAC (Chapter 7)
- Assessment of the role of ENO3 and PKM2 in OAC cell model driven by ACM therapeutic targeting of specific pathway (Chapter 8)

Chapter 2 Materials and Methods

2.1 Reagents and general lab equipment

All laboratory chemicals and reagents were stored according to manufacturer's recommendations. All reagents were purchased from Sigma-Aldrich Chemical Company (Dublin, Ireland) unless otherwise stated. Solid chemicals were weighed out using Radwag AS110.R2 analytic balance (Radwag, USA) and made up according to manufacturer's instructions. The pH of solutions was measured using a pH meter (Thermo Fisher Scientific, USA). Gilson pipettes (Gilson, PA, USA) were used to transfer liquid volumes up to 1 mL, electronic pipette aids (Drummond Scientific Company, PA, USA) and disposable plastic 10 mL pipettes were used (Sarstedt, Wexford, Ireland) unless otherwise stated. All plastics such as cell culture flasks were purchased from Sarstedt (Wexford, Ireland). All cell culture reagents were purchased from Lonza (Basel, Switzerland) unless otherwise indicated.

2.2 Drugs, chemical reagents and other materials

Ketoconazole, REV5901 and zileuton were purchased from Cayman Chemical (Ann Arbor, MI, USA). Novel 5LOX inhibitor NIH4, was provided by Dr. David Maloney (NIH, Bethesda, MD, USA), novel inhibitors and natural plant extracts, HS1-HS17 were provided by Dr. Helen Sheridan (School of Pharmacy, TCD, Ireland). All novel inhibitors were received in lyophilized from upon receipt. NIH4, HS1-6 and HS13-17 were reconstituted using dimethyl sulfoxide (DMSO). Inhibitors HS7-HS12 were reconstituted using sterile distilled water. All drugs were stored at -20°C. All cell-based experiments included a vehicle control of DMSO to ensure the effects observed were related to drug treatment specifically.

2.3 *In-vitro* cell culture

All cell culture work was carried out using aseptic technique within a grade II laminar air- flow cabinet while wearing a clean lab coat with elasticated cuffs and disposable latex gloves. The cabinet was cleaned with 70% (v/v) industrial methylated spirits (Lennox Laboratory Supplies, Dublin, Ireland) before and after use. All cell lines were examined

daily using an inverted phase contrast microscope (Optika, XDS-1R) and subcultured upon reaching approximately 70%-80% confluency. For sub-culturing, growth medium was decanted from the flask and the cells were washed with 10 mL of PBS to remove residual serum. 1 mL of trypsin ethylene-diamine tetra-acetic acid (EDTA) (0.05% (w/v) trypsin, 0.02% (w/v) EDTA) was added to the cell culture flasks. Flasks were incubated at 37°C for 3-5 minutes to allow the cells to detach from the surface of the cell culture flask. 10 mL of complete medium was added into the flask to inactivate the trypsin. Cells were transferred into a sterile 15 mL tube and pelleted by centrifugation at 180 x g for 2 minutes. The pellet was re-suspended in 3ml of compete medium and used to seed fresh flasks at desired ratio. All culturing experiments were carried out within 20 passages from the starting passage number.

All culture media, phosphate buffered saline (PBS) and other reagents were heated to 37°C in a water bath prior use. Cells were incubated in 75cm^2 vented flasks and kept in humidified atmosphere with 5% CO_2 at 37°C.

Cell stocks were stored at -80°C. Cells were prepared from cells in exponential phase of growth. Cells were trypsinised and pelleted as previously described. The pellet was re-suspended in 1 mL of freezing medium (compete medium and 10% (v/v) DMSO) and placed into -80°C immediately. For long-term storage the vials were stored in liquid nitrogen. When breaking out the frozen stocks, the vials were incubated at 37°C in the water to thaw rapidly. The cell suspension was transferred to a 15 mL tube with compete medium and spun at 180 x g for 3 minutes to pellet he cells and to remove as much DMSO as possible. The pellet was re-suspended in 5 mL of complete medium and transferred to a 25cm^2 cell culture flask. After 24 hours media was replaced to remove any residual DMSO and dead cells. Once confluent, cells were transferred to a T75 cell culture flask and maintained as previously described.

2.3 Cell culture

2.3.1 Cell line

Oesophageal adenocarcinoma derived cell line OE33 was maintained in Roswell Park Memorial Institute (RPMI) 1640 medium supplemented with penicillin (50 U/mL), streptomycin (50U/mL) and 10% (v/v) foetal bovine serum (FBS).

2.3.2 Cell counting

Cell counting was carried out for all experiments requiring a particular seeding densities. Pelleted cells were re-suspended in 1 mL of medium, briefly pipetted up and down and 20 μL of cell suspension was added to 180 μL of 0.4% (v/v) trypan blue, mixed and 20 μL of the suspension was added to the counter chamber of the slide (bright-line haemocytometer, Hausser Scientific, PA, USA). The numbers of viable cells (unstained with trypan blue) were counted using a light microscope (40X magnification). The average number of cells was multiplied by the dilution factor and by $1x10^4$ to give an estimate of the cell density (cells/mL). The density can be adjusted using cell culture medium for the required density for a particular experiment.

2.3.3 Reverse cell transfection with siRNA

Freshly split OE33 cells were suspended in 3mL of media (RPMI 1640, 10% FBS, -antibiotics) and counted (Section 2.3.2). 200 μL OptiMEM (Gibco) was added to 4 of the 6 wells on the 6-well plate. Silencing of siRNA in OE33 cells was optimized at two different siRNA concentrations (10nM and 30nM). For 10 nM samples 1.25 μL of the 20 μM stock smart pool (created from 4 stock siRNA, Qiagen) added to the OptiMEM along with 2.5 μL Lipofectamine. The mixture was left to stand for 5 minutes to allow the RNA to create a complex with the Lipofectamine. The 30 nM samples were treated under the same conditions with 3.75 μL of the smart pool along with 7.5 μL Lipofectamine. A negative control was set up for each concentration witch utilized a scrambled RNA control. The OE33 cells were seeded into the RNA-Lipofectamine complex at a density of 150,000 cells/mL. Plates were gently agitated to encourage even growth distribution and incubated at 37^0C, 5% CO_2. This experiment was done in triplicate (3 separate 6-well plates, matched cell passage number) to allow transfection analysis at three different time points of 24hr, 48hr and 72 hr.

2.3.4 Mycoplasma testing

Cell lines were routinely tested for mycoplasma contamination using MycoAlert® Mycoplasma detection kit (Lonza). This assay is a biochemical test that exploits the

activity of certain mycoplasma enzymes. These enzymes react with the MycoAlert® substrate, catalyzing the conversion of ADP to ATP. Cells were maintained in antibiotic free medium for two passages before carrying out this assay. 2 mL of culture medium was transferred into a centrifuge tube and spun at 200 x g for 3 minutes to pellet the floating cells. 100 µL of the supernatant was transferred to a luminescence compatible 96 well plate. MycoAlert® reconstitution buffer was added as a negative control and supernatant from in-house mycoplasma positive cell line provided a positive control. 100 µL of reconstituted MycoAlert® Reagent was then added to each sample and incubated for 5 minutes before a 1 second integrated reading was taken using the luminometer (reading A) (Victor^{TM,} Perkin, Elmer, Columbus, OH, USA). 100 µL of MycoAlert® substrate was then added to each sample for 10 minutes and a second reading was taken (reading B). The ratio between the reading A and reading B was used to determine the presence of mycoplasma in the cell culture medium. A ratio greater than 1 was indicative of mycoplasma contamination.

2.4 Patient tissue samples

All patients provided an informed consent for utilizing their samples in this project. All samples were biobanked in accordance with ethically approved standardized operating procedures of the department of surgery. All tissue samples were collected from the patient who underwent oesophagectomy for esophageal cancer at St. James's hospital, Dublin. 120 esophageal adenocarcinoma patients from 1999-2009 with 60 month clinical follow up had paraffin imbedded tumor sections arrayed on a tissue micro arrays (TMA). 48 esophageal adenocarcinoma patients from 2007-2013 with digital CT scan and visceral fat area calculated were selected for TMA construction utilizing paraffin imbedded tissue from the department of pathology in St. James's hospital. Frozen biobanked tumor samples and adipose conditioned media (ACM) from esophageal adenocarcinoma patients undergoing resection between 2007 and 2014 were used in other studies. Additionally, a small number of fresh OAC diagnostic tumor biopsies from January to September 2016 were used in an *ex vivo* study. Data containing patient demographics, clinicopathological stage and outcomes were obtained for all patients from a dedicated patient database.

2.4.1 Adipose conditioned media

Omental fat collected at oesophagectomy was distributed into separate Petri dishes (5g of adipose tissue/10 mL culture media (M199 culture media and gentamycin (50ug/mL). Fat was cut into pulp using surgical scissors. Petri dishes were labeled with biobank number, sampling date, date of surgery, date and time. Fat was incubated for 72 hours at 37^0C, 5% CO_2, solids were sieved using a sterile 40 micron filter and discarded.

Supernatants were aliquoted into 2ml screw cap Eppendorf tubes and stored at -80^0C. ACM was prepared by different users, however, standardized protocol was used.

Important notes:

- Blood vessels (if present) were removed from omental fat before cutting it into pulp. Failing to remove vascularization from adipose tissue results in protein-rich ACM. Treating OE33 cells with protein-rich ACM kills esophageal adenocarcinoma cells. ACM dark red in colour indicates the presence of blood therefore these samples would be excluded from the study.
- ACM was filtered using a sterile 60 micron filter prior every experiment in order to eliminate remaining adipocytes. Failure to remove any remaining adipocytes results in inconsistencies in the experimental set up and often cell death.
- ACM was thawed/heated in cell culture water bath set to 37^0C for 10 minutes prior use.

2.5 Anthropometry

Anthropometric data was required for patient studies in this project. Patients were separated into obese and non-obese categories based on body mass index (BMI) or visceral fat area (VFA). BMI was calculated by weight/height (kg/m^2) and a BMI greater than 25 and 30 were considered overweight and obese respectively. VFA was calculated by computed tomography staging scans. Patients were considered to be viscerally obese as VFA exceeding 163.8 cm^2 in males and 80.1 cm^2 in females [129].

2.6 Isolation of RNA from epithelial tissue

Total RNA from tumor tissue was extracted from approximately 20 mg sample using standardized protocol (RNAeasy® Mini Kit, Qiagen, Crawley, UK) following manufacturer's instructions. Tissue was disrupted and homogenized by rapid agitation in the presence of 7 mm metal beads and 600 µL lysis buffer (buffer RLT with 10% β-mercaptoethanol) using a Qiagen TissueLyser (RETSCH MM200) at 30 Hz for 40-60 seconds or until the lysate was homogenous. The lysate was centrifuged at 200 x g for 3 minutes and the supernatant was transferred to a microcentrifuge tube. 1 volume of 70% ethanol was added and the sample was mixed by pipetting. Up to 700 µL of the sample was transferred to an RNeasy spin column placed in a 2 mL collection tube and centrifuged at 8000 x g for 15 seconds. The flow though was discarded; 700 µL of RW1 buffer was added to the column and spun again at 8000 x g for 15 seconds. The flow through was discarded, 500 µL of RPE buffer was added and the column was centrifuged again at 8000 x g for 15 seconds. The flow through was discarded and the step was repeated and centrifuged at 8000 x g for 2 minutes. The column was plated into new 2 mL collection tube and centrifuged for 2 minutes without the addition of the buffer (in order to remove any residual RPE flow through). The column was placed in a 1.5 mL collection tube and 30-50 µL of RNase-free water was added directly to the column membrane. The column was centrifuged at 8000 x g for 1 minute to elute the RNA. The RNA was quantified and qualified as detailed in Section 2.10 and stored at -80°C.

2.7 Isolation of RNA from cells

Cellular RNA for Qiagen PCR profiler arrays was isolated using RNeasy® Mini Kit. Cells were grown in a monolayer in a 6-well plate, washed with PBS and 350 µL of Buffer RLT was added to each well in order to disrupt cell membranes and lyse the cells). Lysate was collected and pipetted into 1.5 mL centrifuge tube. DNA in the sample was sheared by passing the lysate through a 20-gauge needle and syringe. The cell lysate was then processed in the same manner as human tissue lysate described in Section 2.6 to yield total cellular RNA.

Cellular RNA for qPCR was isolated using TRI reagent. Cells were grown in a monolayer, washed with PBS and 1 mL of TRI reagent was added. The cell lysate was collected into a microfuge tube and either stored at -80°C for up to one month prior RNA isolation or RNA isolation was carried out immediately. On the day of RNA isolation 100 µL of bromo-3-chloro-propane was added to the sample per 1 mL of TRI reagent. The samples were vortexed and left to stand for 15 minutes. The samples were then centrifuged at 12,000 x g for 15 minutes at 4°C to allow phase separation. The clear layer (overlying a pink layer and separated by a white interface) contains the RNA and it was removed carefully, pipetted into a new microfuge tube and 500 µL isopropanol was added, the samples were vortexed. The samples were centrifuged at 8000 x g for 8 minutes. The isopropanol was decanted and the RNA pellet was washed with 75% ethanol by centrifugation at 12,000 x g for 2 minutes. The ethanol was decanted and the pellet was allowed to air-dry before re-suspending the pellet in 25-40 µL RNAse free water. RNA was quantified and qualified as described in Section 2.8 and stored at -80°C.

2.8 RNA quantification

RNA was quantified by measuring absorbance at 260 nm using the Nanodrop® ND-100 spectrophotometer (Nanodrop Technologies Inc., DE, USA). 1 µL of RNA was added to the pedestal of the instrument and the concentration was measured in ng/µL. The A260/280 ratios were used to measure the purity of the extracted RNA, with ratio greater than 1.8 indicating low phenol and protein contamination. Figure 2.1 shows a typical standard curve obtained measuring pure RNA with 260/280 ratio highlighted in red. Samples were kept on ice to prevent degradation.

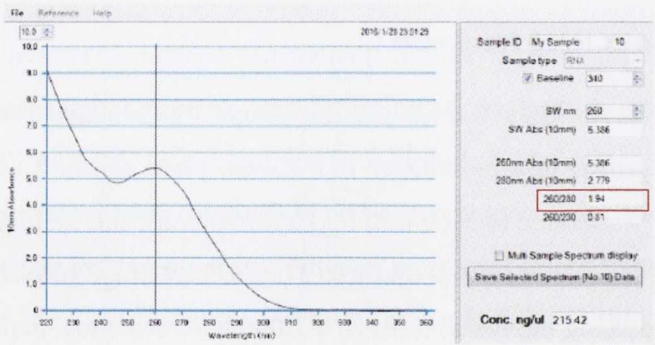


Figure 2.1 Representative image of standard curve obtained when measuring RNA. Standard curve indicated pure RNA with 260/280 of 1.94 ratio highlighted in red.

Phenolic solutions absorbs the UV both at 230nm and with maximum at ~270nm. Phenol contamination imitates higher content of the sample (Figure 2.2).

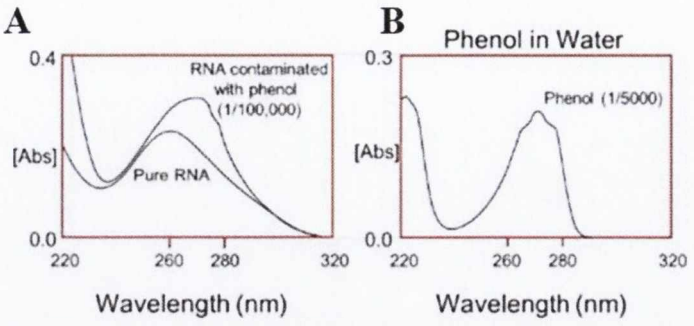


Figure 2.2 Effect of phenol on UV absorbance. (A) Phenol contamination present in the sample indicates higher sample content (concentration). (B) Representative image of phenol absorbance (between 230-270nm).

2.9 cDNA synthesis

All cDNA synthesis was carried out in a sterile environment using 1 μg of RNA and the reagents and volumes listed in Table 2.1. The RNA, RNase free water and 0.5 μg/μL random hexamer primers (40ng/μL) were heated to 70°C for 10 minutes using a thermocycler (Applied Biosystems GeneAmp PCR system 9700) and placed on ice for 1 minute. A master mix of RNaseOUT recombinant ribonuclease inhibitor (1 U/μL), deoxyribose nucleoside triphosphates (dNTPs)(10 mM: prepared as 1:1:1:1 ratio of dATP, dGTP, dTTP, dCTP), Bioscript reverse transcriptase (200 U/μL) and 5x reaction buffer was added to the reaction and heated for 2 hours at 37°C. The resulting cDNA was stored at -20°C.

The reverse transcriptase enzyme and 5x Bioscript reaction buffer were purchased from Bioline (Bioline, Kilkenny, Ireland), all other reagents from Invitrogen (Invitrogen Corp, CA, USA).

Table 2.1 Reagents and volumes used in cDNA synthesis

Step 1: Random primer annealing	
RNA + RNase-free water mix	11μL
Random hexamer primers	1μL
Step 2: cDNA synthesis with master mix	
Bioscript reverse transcriptase	0.5μL
dNTP mix	1μL
RNaseOUT	0.5μL
5X Bioscript reaction buffer	4μL
RNase-free water	2μL
Total volume	20μL

2.10 Probe-based quantitative reverse transcription polymerase chain reaction

Probe-based quantitative polymerase chain reaction (qPCR) was used to quantify mRNA expression in samples relative to the 18S ribosomal RNA endogenous control. Sequence primers were designed with a fluorescent reporter molecule at the 5' end and a fluorescence quencher at 3' end. Upon transcription of gene of interest, the Taq polymerase enzyme removes the quencher molecule from the probe and allows fluorescence emission to be detected following laser excitation of the sample at a particular wavelength.

A master mix containing 10 μL of Taqman® Gene Expression Master Mix (Applied Biosystems), 8 μL RNase-free water, 1 μL primer probe (Applied Biosystems) and 1 μL cDNA was added to each well of a MicroAMP™ Optical 96-well reaction plate (Applied Biosystems) in triplicate for each sample. 18S primer probe was used for every sample (in triplicate) and acted as endogenous control. RNase-free water was added instead of cDNA to wells that acted as a non-template control. Endogenous control was run for every sample and a non-template control was added to every plate that was run. All predesigned primer probes were sourced from Applied Biosystems (Table 2.2). Real time PCR detection was performed on the ABI Prism 7500 real-time thermal cycler.

The relative quantification of target gene expression was performed using the comparative cycle threshold (Ct) method. A sample with median expression of the target gene is set at the calibrator (RQ value=1) that permits the quantification of all other samples. Relative target gene expression was calculated by the following formula:

$2^{(\Delta\Delta Ct)}$, where $\Delta\Delta Ct = \Delta Ct$ sample – ΔCt sample calibrator sample,
with ΔCt=Ct target gene-Ct 18S

Table 2.2 List of FAM-labeled primer probes and corresponding configuration numbers

Gene name of primer probe	Applied Biosystems Ref.
ALCOC	Hs00902800_g1
ALOX5	Hs01095330_m1
ATP5B	Hs00969569_m1
COX6C	Hs00269977_m1
ENO2	Hs01577360_m1
ENO3	Hs01093275_m1
GAPDG	Hs99999905_m1
HIF1A	Hs00936378_m1
HK1	Hs00175976_m1
HK2	Hs00606086_m1
LDHC	Hs00255650_m1
MMP7	Hs01042796_m1
MMP9	Hs00234579_m1
PKM2	Hs00987255_m1
SLCA3 (GLUT3)	Hs00359840_m1
SLC2A1 (GLUT1)	Hs00892681_m1
SNAI1 (Slug)	Hs00195591_m1
SNAI2 (Snail)	Hs00950344_m1
TWIST1	Hs001675818_si
VEGFA	Hs00900055_m1
ZEB2	Hs00207691_m1
18S	Hs03003631_g1

2.11 Screening via RT ^{2} Profiler PCR Arrays

Following strong laboratory data from affymetrix arrays study {Allott et al. 2012), the focus was on the glycolysis pathway. Human Glucose Metabolism RT2 Profiler PCR Arrays (Qiagen) were used to examine 84 key genes associated with glucose metabolism. Firstly, the role of ACM on glucose metabolism in OAC cells was examined by co-culturing OE33 cells with ACM from viscerally obese OAC patients for 24 hours and compared to media alone (M199) cultured cells using real-time PCR arrays. Additionally, in order to determine whether novel inhibitors (HS6 and NIH4) have an effect on ACM-induced alterations in glucose metabolism in OE33 cells, cells were treated with the two small molecule inhibitors of interest NIH4 and HS6 alone and in presence of ACM. The

Human Glucose Metabolism RT^2 Profiler PCR Array profiles the expression of 84 key genes involved in the regulation and enzymatic pathways of glucose and glycogen metabolism summarized in Table 2.3.

Mitochondrial dysfunction also contributes to metabolic syndrome and obesity, where excess β-oxidation overloads oxidative phosphorylation by generating excessive amounts of NADH (). A focus on the mitochondria is warranted as evidence now suggest that the metabolic switch may provide a benefit to the tumor not only by increasing glycolysis but by decreasing mitochondrial activity. Human Mitochondrial Energy Metabolism Plus RT^2 Profiler PCR Arrays (Qiagen), a focused panel of 84-key genes involved in mitochondrial energy metabolism were used (Table 2.4).

For both, glucose metabolism and Mitochondrial metabolism arrays, OE33 cells were subcultured as described in Section 2.3 and treated with the two small molecule inhibitors of interest NIH4 and HS6 alone, in presence of ACM, ACM alone or M199 media alone. RNA was isolated and cDNA was made by the procedures previously described. PCR was performed using RT^2 Real-time SYBR Green PCR mix on a 7900HT Fast Real-time PCR Light-Cycler System (Applied Biosystems). Differentially expressed genes were defined as those that changed by >2-fold. Genes that exhibited the greatest fold change between the different treatment groups were selected for further validation by SYBR-based qPCR.

Table 2.3 Key genes involved in the regulation and enzymatic pathways of glucose and glycogen metabolism

Glucose Metabolism	
Glycolysis	ALDOA, ALDOB, ALDOC, BPGM, ENO1, ENO2, ENO3, GALM, GCK,GPI, HK2, HK3, PFKL, PGAM2, PGK1, PGK2, PGM1, PGM2, PGM3, PKLR, TPI
Gluconeogenesis	FBP1, FBP2, G6PC, G6PC3, PC, PCK1, PCK2
Glucose Metabolism	PDK1, PDK2, PDK3, PDK4, PDP2, PDPR
Tricarboxylic Acid Cycle (TCA)	ACLY, ACO1, ACO2, CS, DLAT, DLD, DLST, FH, IDH1, IDH2, IDH3A,IDH IDH3G, MDH1, MDH1B, MDH2, OGDH, PC, PCK1, PCK2, PDHA1, PDHB, SDHA, SDHB, SDHC,SDHD, SUCLA2, SUCLG1, SUCLG2
Pentose Phosphate Pathway	G6PD, H6PD, PGLS, PRPS1, PRPS1L1, PRPS2, RBKS, RPE, RPIA,TALDO1
	TKT
Glycogen Metabolism	
Glycogen Synthesis	GBE1, GYS1, GYS2, UGP2
Glycogen Degradation	AGL, PGM1, PGM2, PGM3, PYGL, PYGM
Glycogen Metabolism	GSK3A, GSK3B, PHKA1, PHKB, PHKG1, PHKG2

Table 2.4 The list of key genes involved in mitochondrial respiration, components of electron transport chain and oxidative phosphorylation complexes

Complex I	NDUFA1, NDUFA10, NDUFA11, NDUFA2, NDUFA3, NDUFA4, NDUFA5, NDUFA6, NDUFA8, NDUFAB1,NDUFB10, NDUFB2, NDUFB3, NDUFB4, NDUFB5, NDUFB6, NDUFB7, NDU
Complex II	SDHA, SDHB, SDHC, SDHD
Complex III	CYC4I1, COX5A, COX5B, COX6A1,COX6A2, COX6B1, COX6C, COX7A2, COX7A2L,COX7B, COX8A
Complex V	ATP5A1, ATP5B, ATP5C1, ATP5F1, ATP5G1, ATP5G2, ATP5G3, ATP5H, ATP5I, ATP5J, ATP5J2, ATP5L,ATP5O, PPA1
Pathway Activity Signature Genes	ARRDC3, ASB1, CYB561D1, DNAJB1, EDN1, GADD45B, HSPA1A (HSP70-1A), HSPA1B, LRP5L, RNU11, SLC25A25.

2.12 SYBR-based quantitative reverse transcription polymerase chain reaction

A panel of genes was selected from the RT^2 Profile PCR Arrays (Section 2.11) for validation with SYBR green dye based qPCR. cDNA from five independent experiments was synthesized for the validation study. The cell culture set up, RNA isolation and cDNA synthesis were identical to the ones described in Section 2.7 and Section 2.9 respectively. Mastermix containing 10 µL GoTaq® qPCR master with BRYT Green® dye (Promega, WI, USA), 8 µL RNase-free water, 1 µL cDNA and 0.5 µL of 10 µM forward primer and 0.5 µL of 10 µM reverse primer (IDT, Integrated DNA Technologies, Iowa, USA) was added to each well of a MicroAMP™ Optical 96-well qPCR reaction plate (Applied Biosystems), in triplicate for each sample. Predesigned primer sets were sourced using online IDT PrimerQuest® design tool and the forward and reverse sequences are listed in the table 2.5. Real time PCR detection was performed using ABI Prism 7500 real time thermal cycler. The relative quantification of target gene expression was performed using the comparative cycle threshold (Ct) method as described in Section 2.10.

Table 2.5 Primer sequences for SYBR-based PCR

Gene	Primer Sequence
ALDOB	FWD: 5' -TGG TAG GTT GGG AAG GAG ATA G -3'
	REV: 5' - CTG AGT CTT TGG ACA GCA AGA G -3'
ATP5G2	FWD: 5' -GGG AGC CTC ATC ATT GGT TAT -3'
	REV: 5' - GGA TGA GAA AGG CTA CCA TCA G -3'

ATP5L	FWD: 5' - CTG CGG AAT CCT ACT GTT CTT C - 3'
	REV: 5' - GCA GAA TCC AGC CTG TCA AT -3'
COX5B	FWD: 5' -AAG GGA CTG GAC CCA TAC A -3'
	REV: 5' -TTC ACA GAT GCA GCC TAC TAT TC -3'
COX6C	FWD: 5' - TTT GAA CTC CTT CGG CTA CC -3'
	REV: 5' - CCA ACG TCC TTC CTG ACT AAA -3'
CYB561D1	FWD: 5' - CTG ACT GCA GTG TAG GGA ATA G -3'
	REV: 5'- TGG TGA TGG AGG GAG AAA TG -3'
ENO3	FWD: 5'- CGC AAT GGG AAG TAC GAT CT -3'
	REV: 5' - TGC ATG GAG ACC ACA GGA TA -3'
G6PC	FWD: 5' - GCA ATG GGC ACT GGT ATT TG -3'
	REV: 5' - TGG AGT CAC ACA TGG GAA TAA G -3'
HSPA1B	FWD: 5' - AGG ACA TCA GCC AGA ACA AG -3'
	REV: 5' - GTA GAA GTC GAT GCC CTC AAA -3'
H6PD	FWD: 5' - GCA ATG GGC ACT GGT ATT TG -3'
	REV: 5' - TGG AGT CAC ACA TGG GAA TAA G -3'
NDUFA1	FWD: 5' - TTT GAA CTC CTT CGG CTA CC -3'
	REV: 5' - CCA ACG TCC TTC CTG ACT AAA -3'
NDUFA8	FWD: 5' - CCT TTA CCG GAG AAT CCC TAT C -3'
	REV: 5' - CCA CGG ACC CAT CTT TAC TT -3'
NDUFA11	FWD: 5' - CCT ACA GCA CCA GTA TT -3'
	REV: 5' - CAA CCT TAG CCA CTC CTT CA -3'
NDUFS2	FWD: 5' - CTA AGC GAG CAG AGA TGA AGA C -3'
	REV: 5' - GAG CCT CAA TGG CAG TAT ATG T -3'
PC	FWD: 5' - ATG CGC TTC CTG TAT GAG TG -3'

	REV: 5' - GTT GTC TGG GTA GTT GGT GTA G -3'
PCK2	FWD: 5' - CTG AGA ATA CTG CCA CAC TGA C -3'
	REV: 5' - CAA TCA CCG TCT TGC TCT CTA C -3'
PDK1	FWD: 5' - CTG AGA ATA CTG CCA CAC TGA C -3'
	REV: 5' - CAA TCA CCG TCT TGC TCT CTA C -3'
PGM1	FWD: 5' - AAG ATC GGT CGC TTG GTT ATC -3'
	REV: 5' - TGT GAC TGG CTG TCA GAA TG - 3'
RBKS	FWD: 5' - AAG ATC GGT CGC TTG GTT ATC -3'
	REV: 5' - TGT GAC TGG CTG TCA GAA TG -3'
TKT	FWD: 5' - CCG CCA ATA CAA AGG GTA TCT -3'
	REV: 5' - CCT GGT CAT CCT TGC TCT TC -3'
18S	FWD: 5' - CTG AGA AAC GGC TAC CAC ATC -3'
	REV: 5' - GCC TCG AAA GAG TCC TGT ATT G -3'

2.13 Immunohistochemistry

2.13.1 Construction of tissue microarrays

48 esophageal adenocarcinoma patients from 2007-2013 with digital CT scan available and visceral fat area calculated were selected for TMA construction utilizing paraffin imbedded tissue from the department of pathology in St. James's hospital. A 5 µm full-face section was cut from each block using a microtome (Thermo scientific, Microm HM 355S), transferred to a 50°C water bath for stretching and collected on microscopic adhesive glass slides (Thermo Scientific). Sections were allowed to dry and were incubated at 60°C overnight in a Heraeus Instruments Function line incubator (Thermo Scientific). All sections were stained with Haemotoxylin (Merk, Germany) and Eosin (Morphisto, Germany) the following day. The presence of tumor was confirmed and the exact location of the tumor was marked on H&E slides by the pathologist at St. James's Hospital, Dublin. The areas marked on the H&E slide were matched to the areas on the

paraffin blocks, 2mm cores were taken from the blocks and the tissue microarrays were constructed. Three 2mm cores were taken for each patient.

2.13.2 Staining procedure using tissue microarrays

Immunohistochemistry was performed using tissue microarrays (TMAs) utilizing the Vectastain Kit (Elite). All sections for the chosen marker were stained on the same day. All sections were pre-treated with Trilogy (Cell Marque) in an electric pressure cooker for 12 minutes at low pressure to avail deparaffinization, rehydration and antigen retrieval. Following this step the sections were placed into fresh trilogy and allowed to stand for further 5 minutes and incubated in distilled water for further 5 minutes. Endogenous peroxidases were quenched in 3% hydrogen peroxide (diluted in methanol) for 30 minutes at room temperature, in the dark. Following incubation sections were washed for 5 minutes in PBS, the washing step was repeated three times. Primary antibodies used were either rabbit anti-human or mouse anti-human therefore the sections were blocked using goat or horse serum respectively (150 µL in 10 mL of PBS) (Vectasatin Kit) at room temperature for 30 minutes. Following the blocking step, 150 µL of primary antibody was added to the slides and incubated at 4°C overnight. The list of antibodies and dilution used described in Table 2.4. A negative control section was used for each stain where the section was incubated in PBS only rather than a primary antibody. The following day all section were washed 3 x 5 minutes in PBS, covered in appropriate secondary antibody (150 µL of secondary antibody diluted in 10 mL PBS) (Vectastain Kit) and incubated for 30 minutes at room temperature. Following 3 x 5 minute washes in PBS a diluted avidin-biotin complex reagent (100 µL of reagent A and 100 µL of reagent B in 5 mL PBS) (Vectastain Kit) was incubated on the sections for 30 minutes at room temperature. The avidin-biotin reagent was prepared and allowed to stand at room temperature for 15 minutes prior incubation. Following 3 x 5 minute washes with PBS diaminobenzene (DAB) was added to the sections for 4-10 minutes (in the dark) or until sufficient colour development was observed. The excess DAB was rinsed with distilled water and the sections were counterstained with haematoxylin for 30 seconds and rinsed with water for 5 minutes and incubated in PBS for 1 minute. Lastly, the slides were dehydrated with methanol and xylene (Cell Path, UK) and mounted using DPX (B.H.D. Prolabo Chemicals Ltd., UK).

Table 2.6 List of antibodies used for IHC

Antibody	Isotype	IHC	Cat. No.	Manufacturer
Anti-HSP60	Rabbit Monoclonal	1/250	ab45134	abcam
Anti-HK2	Mouse Monoclonal	1/200	ab104836	abcam
Anti-HK1	Rabbit Monoclonal	1/100	ab55144	abcam
Anti-HIF1A	Rabbit Monoclonal	1/100	ab51608	abcam
Anti-GLUT3	Rabbit Polyclonal	1/200	ab41525	abcam
Anti-GLUT1	Mouse Monoclonal	1/200	ab40084	abcam
Anti-GAPDH	Rabbit Monoclonal	1/750	2118	Cell Signaling
Anti-ENO3	Rabbit Polyclonal	1/200	ab203203	abcam
Anti-ATP5B	Mouse Monoclonal	1/150	ab14730	abcam
Anti-5-LOX	Rabbit Polyclonal	1/150	160402	Cayman
Anti-PKM2	Rabbit Monoclonal	1/500	4053	Cell Signaling

2.13.3 Imaging and scoring stromal and epithelial staining

Slides were digitally scanned using NanoZoomer C210 digital scanner and analyzed using NDP View2 viewing software. The staining intensity and positivity was assessed under 40X magnification by 2-3 independent observers (at least 1 pathologist and 1 scientist). For each protein, both epithelial and stromal cells were evaluated for both percentage positivity and intensity of the cytoplasmic staining. Intensity was graded as 0 (negative), 1 (weak), 2 (moderate) and 3 (strong) and positivity was categorized as 0%, 10% 25%, 50%, 75%, 90% or 100%. The values of the two parameters were multiplied to get an overall score for each core of 0-300. There were three 2mm cores available for each patient therefore the mean score of the three cores was collated with clinicopathological and survival data from the database. This scoring mechanism has been previously published by Cathart *et al* in non-small cell lung cancer [337].

2.14 Cell and tissue lysate preparation

2.14.1 Cultured cells

Culture medium was removed from cells grown in a monolayer, washed with ice-cold PBS and lysed directly in the culture vessel using ice-cold lysis buffer (RIPA buffer (50mM Tris HCl, pH 7.4, 150 mM NaCl, 1 mM EDTA, 0.5% (w/v) sodium deoxycholate, 0.1% sodium dodecyl sulfate(SDS), 1% Triton-X) with added protease inhibitor cocktail

(cOmplete™ protease inhibitor tablets, Roche)). 10 µL of lysis buffer was added per cm^2 and cells were incubated on ice for 1 hour. The lysed cells were scraped using a rubber cell scraper, collected into microfuge tube and the lysate was passed through a 20-gauge needle and syringe to shear DNA. Isolated protein lysates were stored at -80°C.

2.14.2 Tissue

Tissue was disrupted and homogenized by rapid agitation in the presence of 7 mm metal beads and 50 µL of lysis buffer (RIPA buffer (50mM Tris HCl, pH 7.4, 150 mM NaCl, 1 mM EDTA, 0.5% (w/v) sodium deoxycholate, 0.1% sodium dodecyl sulfate(SDS), 1% Triton-X) with added protease inhibitor cocktail (cOmplete™ protease inhibitor tablets, Roche)) using a Qiagen TissueLyser at 25 Hz for 30-40 seconds or until the sample was homogenous. The sample was left on ice for 30 minutes, vortexing occasionally. The lysate was centrifuged at 10,000 x g for 30 minutes at 4°C to pellet any debris. The clear cell lysate was transferred to 1.5 mL microfuge tube and sheared DNA by passing the lysate through a 20-gauge needle and syringe. The sample was stored at -80°C.

2.15 Protein quantification

The Pierce Bicinchoninic Acid (BCA) protein assay (Thermo Scientific, IL, USA) was used to determine protein concentration in the sample of interest. A seven point standard curve of bovine serum albumin (BSA) between 0 and 2,000 µg/mL was used to determine protein concentration of the unknown samples (representative standard curve in the Appendix I). 10 µL of each the standard and unknown sample was pipetted in triplicate into a 96-well microplate. 200 µL of BSA working reagent (BCA reagent A and reagent B in ratio 1:50 accordingly) was added to each well. If the concentration of the protein lysate is high, the unknown sample can be pre-diluted to fit the range of the standard curve. The plate was shaken briefly and incubated at 37°C for 30-60 minutes. The absorbance was read at 562 nm on a Versamax microplate reader. The concentration of the samples was determined by extrapolation of the standard curve to give the final concentration of the unknown samples.

2.16 Acetone precipitation of proteins

Acetone precipitation of proteins enables concentration of the protein sample. The required volume of acetone was allowed to cool to -20°C. Protein sample of required concentration was placed into 1.5 mL microfuge tube and four times the sample volume of cold acetone was added to the tube. The tube was vortexed and incubated at -20°C overnight. The sample was centrifuged at 13,000 x g for 30 minutes. Following centrifugation, supernatant was removed, being careful not to dislodge protein pellet. The tube was left uncapped for 30 minutes at room temperature, allowing the acetone to evaporate. The pellet was dissolved in 25 µL of 1X Laemmle buffer ((4X Laemmle buffer (for 10 mL stock: 2 mL 1 M Tris HCl, pH 6.8, 0.8 g SDS, 4 mL 100% glycerol, 0.4 mL 14.7 M β-mecaptoethanol, 1 mL 0.5 M EDTA, 8 mg bromophenol blue, 2.6 mL distilled water)). The sample was stored short-term at -20°C until required for Sodium Dodecyl Sulfate PolyAcrilamide Gel Electrophoresis (SDS-PAGE).

2.17 Protein SDS-PAGE and Western blotting

2.17.1 Protein separation by SDS-PAGE

SDS-PAGE is a standard technique for separating proteins according to their molecular weight. Polyacrylamide gel electrophoresis was carried out using the Mini-PROTEAN Tetra Cell (Bio-Rad, CA, USA) hand cast gel apparatus and electrophoresis tank. A 12% (w/v) SDS_PAGE separation gel was made using 9.2 mL30% (w/v) bisacrylamide, 4.5 mL 1.875 M Tris HCl (pH 8.8), 8.3 mL distilled water, 176 µL 10% (w/v) sodium dodecyl sulfate (SDS), 120 µL 10% (w/v) fresh ammonium persulfate (APS) and 10 µL N,N,N',N'-tetramethylethane-1,2-diamine (TEMED). This solution was sufficient to make two gels. The gels were cast between upright glass plates and absolute alcohol was layered onto the gels to aid polymerization. After polymerization the absolute (1 hour approximately) alcohol was removed and the surface was rinsed with distilled water before adding the stacking gel. Stacking gel was prepared using 1.7 mL 30% (w/v) bisacrylamide, 2 mL 0.6 M Tris HCl (pH 6.8), 6 mL distilled water, 100 µL 10% (w/v) SDS, 150 µL 10% (w/v) APS and 10 µL TEMED. The stacking gel solution was layered over the polymerized stacking gel and 15-well plastic comb was inserted immediately. Protein lysates were diluted to required protein concentration (20-30 µg/µL) in distilled water to a total volume of 20 µL and 5 µL of 4X Laemmle buffer was added to all protein

samples. All samples were denatured by heating at 95°C for 10 minutes. 8 μL of pre-stain Spectra™ Multicolour Broad Range Protein Ladder (Thermo Fisher Scientific, USA) was loaded into the first well in the gel and 20 μg of protein to the maximum of the total volume of 25 μL) was loaded into the gel for all cell lysate samples. Samples were separated by electrophoresis at a constant current of 50 mA for two gels in electrode buffer (50 mM Base Trizma, 384 mM glycine, 0.1% (w/v)SDS) for approximately 1 hour 15 minutes or until the dye reached the bottom of the gel.

2.17.2 Protein Transfer

Separated proteins were transferred onto polyvinylidene fluoride (PVDF) membrane (Pall corp., FL, USA) using a semi-dry transfer apparatus. The PVDF membrane was pre-activated in 100% methanol for 1 minute and soaked in transfer buffer (0.15 M glycine, 20 mM Trizma base, 0.1% (w/v) SDS, 20% (w/v) methanol) alongside with Whatman filter paper (Whatman Laboratory Division, Kent, UK). The gel and PVDF membrane were sandwiched between 5 layers of filter paper with PVDF membrane orientated towards the positive electrode. Proteins were transferred for 1 hour at a constant current of 200mA.

2.17.3 Visualization of proteins – Ponceau S Stain

Ponceau S Stain is a rapid and reversible staining method for locating protein bands on Western blots. Following the transfer of proteins, PVDF membrane was incubated in Ponceau S staining solution (0.1% (w/v) Ponceau S in 5% (v/v) acetic acid) for 2 minutes with gentle agitation. The membrane was rinsed in Tris-buffered saline (25mM Tris HCl (pH 7.6), 150 mM NaCl) containing 0.1% Tween 20 (TBST) until the background was clear and protein bands were visualized. The stain was completely removed by continued washing in TBST.

2.17.4 Western Blotting

Following the transfer of proteins the PVDF membrane was blocked with 5% (w/v) BSA in TBST on a shaker for 1 hour at room temperature. The membrane was then transferred to a 50 mL conical tube containing 5 mL of primary antibody diluted in 5% (w/v) BSA

in TBST and incubated on an electrical roller overnight at 4°C. Following 3x5minute washes with TBST, the membrane was incubated in 10 mL horse-radish peroxidase (HRP) conjugated secondary antibody on the plate shaker, for 1 hour at room temperature. Following 3x5 minute washes with TBST, 5 mL of Supersignal®West Pico Chemiluminescent Substrate Kit (Thermo Scientific, IL, USA) was added to the membrane to detect bound antibody complexes. The working solution was prepared by mixing 2.5 mL of the stable peroxidase solution and the luminol/enhancer solution. The membrane was incubated in chemiluminescent substrate for 2 minutes, excess was drained off and the blot was placed between two acetate sheets for exposure and imaging using an automated chemiluminescent imager (Fusion-FX7 Advance SUPER_BRIGHT). Densitometric analysis was carried out using ImageJ software (NIH, MD, USA). β-actin or β-tubulin protein levels were used as a house keeping protein loading control. Values were represented as a ratio of sample band intensity to that of corresponding loading control.

Table 2.7 List of primary and secondary antibodies used for western blotting with their corresponding dilutions

Antibody	Isotope	Dilution	Size WB (kDa)	Cat. No.	Manufacturer
Anti-PDK1	Rabbit Polyclonal	1/1000	49	ab92959	abcam
Anti-HIF1A	Rabbit Monoclonal	1/1000	93	ab51608	abcam
Anti-GLUT3	Rabbit Polyclonal	1/5000	47	ab41525	abcam
Anti-G6PC	Rabbit Polyclonal	1/2000	40	ab83690	abcam
Anti-COX6C	Mouse Monoclonal	1/1000	9	ab156775	abcam
Anti-COX6C	Mouse Monoclonal	1/4000	9	ab156775	abcam
Anti-COX5B	Mouse Polyclonal	1/1000	14	ab88440	abcam
Anti-ATP5L	Rabbit Polyclonal	1/1000	11	ab126181	abcam
Anti-ATP5B	Mouse Monoclonal	1/500	52	ab14730	abcam
Anti-ALDOB	Rabbit Monoclonal	1/1000	39	ab75751	abcam
Anti-5-LOX	Rabbit Polyclonal	1/200	78	160402	Cayman

2.18 Drug Screening

2.18.1 MTT - Cell viability assay

OE33, OE21, SW480 and SW620 cells were seeded in a 96-well plate at $5x10^3$ cells/well. Cells were left to adhere for 5-6 hours and serum depleted (0.5% FBS) over night (for at least 12 hours). The media was decanted and the vehicle control or treatment (drug

treatments dissolved in M199 media (0.5% FBS) for a total treatment time of 24 hours. 100 µL of 2.5 mg of MTT reagent (3-(4, 5-Dimethylthiazol-2-yl)-2, 5-Diphenyltetrazolium Bromide) dissolved per 1 mL of PBS was added directly to the cell culture medium and incubated for 2 hours at 37°C or until a sufficient crystal formation in the cells was observed. The media was removed by pipetting and 100 µL of DMSO was added to each well to lyse the cells. The plate was shaken briefly and the absorbance was read at 595 nm on a Versamax plate reader.

2.18.2 BrdU – Cell proliferation assay

The effect of the drugs on cell proliferation was measured by BrdU cell proliferation ELISA (Roche). The amount of BrdU incorporation in cells correlates with the amount of DNA synthesis. OE33 cells were seeded in a 96-well plate at the density of $5x10^3$ and allowed to adhere for 5-6 hours and serum depleted (M199 medium, 0.5% FBS) over night (for at least 12 hours). The media was decanted and the vehicle control or treatment (drug treatments dissolved in M199 medium (0.5% FBS) for a total treatment time of 24 hours. At the 24 hour time point 10 µL of working BrdU-labeling reagent (100 µM) was added directly to the culture media to each well and the plate was incubated for 4 hours at 37°C, 5% CO_2 to allow BrdU incorporation into synthesized cellular DNA. The labeling medium was removed and 200 µL of FixDenat was added to each well. The plate was incubated at room temperature for 30 minutes, FixDenat solution was removed and 100 µL of working solution (anti-BrdU-POD antibody conjugate) was added to each well. The plate was incubated for 1 hour 30 minutes at room temperature. The antibody conjugate was removed ant the cells were washed with 300 µL washing buffer, the washing step was repeated three times. After the removal of the washing buffer, 100 µL of substrate solution was added to each well and the plate was incubated in the dark, at room temperature for 10 minutes or until the sufficient colour development was observed. 25 µL of stop solution (2N H_2SO_4) was added directly to the substrate solution, the plate was shaken briefly and the absorbance was read at 450 nm using the Versamax microplate reader.

2.18.3 xCeLLigence RTCA for cell proliferation

Cell proliferation was monitored using xCeLLigence ™ RTCA DP (Real Time Cell Analyser Dual Plate) (ACEA Biosciences, San Diego, CA, USA). The specialist 16 well E-Plate was used to measure proliferation. The bottom of each well contains microelectrode sensors. When the cells adhere to the bottom of the wells and proliferate. Impedance signals are recorded by the xCeLLigence software. This platform allows to observe changes in cell behavior in response to stimuli or inhibitors in real time. 100 µL of culture media was added to each well and left to equilibrate for 1 hour at room temperature. Following equilibration, the plate was inserted into the machine and Step 1 was performed. Step 1 records the background impedance signal of each well. OE33 cells that were previously transfected by reverse transfection (Section 2.3.3) and freshly split not transfected OE33 cells (matched passage), were seeded into each well of the E-plate at a density of $1.5x10^4$ cells/well/100 µL giving a total volume of 200 µL in each well. The plate was left to stand for 30 minutes at room temperature to allow the cells to settle and to distribute evenly across the bottom of the wells. The plate was inserted into the machine and impedance signals of the plate were read every 30 minutes for a total of 200 recordings (i.e. 100 hours). The following day, 12-14 hours post seeding, the machine was paused, the plate was carefully removed and cells were serum depleted (0.5% FBS). The pate was returned to the machine and impedance signals were recorded for another 12 hours. Following serum depletion, the machine was paused, media was carefully removed taking care not to touch the bottom of the well and appropriate treatments were added in serum depleted medium (0.5% FBS). The plate was returned to the machine and the impedance signals were recorded for the next 72 hours.

2.18.4 Seahorse XFe24 analyser

Day 1

OE33 cells were seeded in 20 wells of XFe 24-well plate at $1x10^4$ cells/well in 100µL of complete media (5% FBS) and 100 µL of media only was added to calibration wells A1, B4, C3 and D6. Cells were left to adhere for 3 hours and additional 150 µL of media (5% FBS) was added to all wells. The plate was incubated for 4 hours at 37°C, 5% CO_2. Following incubation, cells were serum depleted (0.5% FBS) over night (for at least 12 hours).

Day 2

24 hours after initial seeding, 200 µL media was removed (without the pipette tip touching the cells) and 200 µL of treatment was added. All treatments and the media-only control were done in duplicate. The plate was incubated for 24 hours at 37°C, 5% CO_2.

In the evening prior day 3, 1mL of Seahorse XF Calibrant was added to each well of the Seahorse Callibrant plate and the plate was incubated overnight in non-CO_2 incubator.

Day 3

Cells were rinsed with assay medium (unbuffered DMEM supplemented with 10mM glucose and 20mM sodium pyruvate, pH 7.4) before incubation with assay medium for 1 hour at 37°C in a non-CO2 incubator. Four baseline OCR and ECAR measurements were obtained over 28 minutes. The experiment was repeated at least 3 times with technical replicates. All measurements were normalised to cell number using the crystal violet assay as described in Section 2.18.4.1

2.18.5 Crystal Violet Assay

All assays undertaken were normalised to cell number using a crystal violet assay. Cell growth media was removed from cells and 50µL of 1% glutaraldehyde in PBS (Sigma) per well was added to cells in a 96 well plate (or 24 well plate for Seahorse XFe24 experiments) for 15 minutes at room temperature. The glutaraldehyde was removed and gentle washed with 1x PBS twice. 50µL 0.1% crystal violet (Sigma) (in dH2O) was added to each well for 30 minutes at room temperature, all wells gently washed with tap water and the plate left inverted to dry overnight. 40µL of 1% triton-X (Sigma) (in PBS) was added to each well and the plate put on a plate shaker for 15 minutes at room temperature. Each corresponding well solution was then transferred into a new 96 well plate and the absorbance read at 590nm using a Versa-max spectrophotometer (Molecular Devices).

2.19 Investigation of pathways altered *ex vivo* in esophageal tumor explants using Olink Platform

2.19.1 Tumour explant culture

Fresh treatment-naive OAC biopsies were collected from the clinic and cut into equally sized pieces. Each piece of tissue was cultured for 24 hours at 37^0C in *ex vivo* medium (M199, 10% FBS, 1 µg insulin, 50 U/mL penicillin) plus a drug (HS6 or NIH4) or vehicle control (i.e. 0.1%DMSO). After 24 hours the piece of tumor was transferred to a 1.5mL

screw cap microfuge tube and tissue conditioned media (TCM) was transferred to another 1.5mL screw cap microfuge tube. All tubes containing TCM and corresponding tissue were snap frozen in liquid nitrogen and stored at -80^{0}C until further processing.

2.19.2 Proseek® Multiplex Inflammation I and Oncology II 96x96 multiplex OAC immunoassay

In order to discover and validate OAC related protein biomarkers, we selected Proseek® Multiplex Oncology II ^{96x96} multiplex OAC immunoassay (Olink Proteomics). Biomarkers associated with cell proliferation, cell differentiation and adhesion, apoptosis, angiogenesis, exploratory, immune response, metastasis and tumor specific markers were included in the panel (Image 2.3). The full list of biomarkers is outlined in Appendix II.

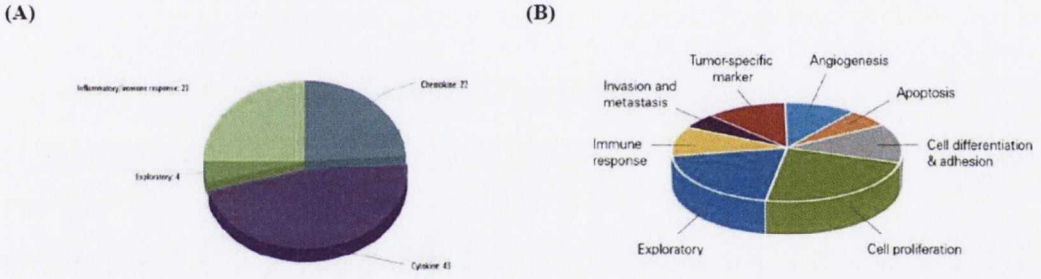


Figure 2.3 Proseek® Multiplex Inflammation I and Oncology II ^{96x96} immunoassay panel. Image adapted from http://www.olink.com/proseek-multiplex/oncology/

Tissue conditioned media and tissue from 5 treatment-naive OAC patients were used for OLINK targeted protein discovery. The biopsy tissue pieces (Section 2.19.1) were homogenized and total protein concentration was determined by BSA assay to normalize protein secretions detected to the size of biopsy pieces. 30 µL of tissue conditioned media (TCM) and protein lysates from the three treatment groups (vehicle control, HS6 and NIH4) from 5 treatment-naive OAC patients, were shipped to OLINK Proteomics, Uppsala, Sweden for analysis. Detection and sample analysis was performed by high-throughput real-time PCR analysis using the Fluidigm® BioMark™ HD System. This PCR platform enables simultaneous detection of 96 analytes in every sample of interest.

The raw data received from Olink contained normalized protein expression (NPX) values (Log2 scale) for all samples. Values below limit of detection were flagged and were not used for statistical analysis. Normalized Protein expression values (NPX) for all proteins were returned as raw values for statistical analysis. All samples sent to Olink Proteomics were blinded and the samples of 2 patients were included in duplicate in order to measure the reproducibility and quality of the experiment. Raw data received from Olink Proteomics in Appendix II.

2.20 Enzyme-linked Immunosorbent Assay

2.20.1 Competitive ELISA

LTB4 levels in tissue conditioned media (TCM) from *ex vivo* cultured OAC tumor explants (Section 2.19.1), were measured by competitive ELISA. Competitive ELISAs use a polyclonal antibody to bind competitively bind to antigen in the sample. The more antigen present in the sample the less recombinant analyte is bound to the antibody and the less signal is produced following addition of substrate. The amount of signal produced is inversely proportional to the amount of antigen in the sample.

The 96-well assay plate was pre-coated with goat antibody specific to rabbit IgG by the manufacturer. 100 µL of Assay Buffer diluent was added into non-specific binding (NSB) and Bo (0pg/mL standard) wells. The stock of supplied antigen standard was diluted with Assay Buffer to the appropriate concentration of the highest standard (see Table 2.6) that was subsequently serially diluted to create a 5-point standard curve. 100 µL of Standards were added to the appropriate wells in duplicate. 100 µL of neat sample (tissue conditioned media) were added to appropriate wells in duplicate. 50 µL of blue conjugate was added to all wells, with the exception of Blank and total activity (TA) wells. 50 µL of yellow polyclonal antibody was added to all wells, with the exception of Blank and TA and NSB wells. The plate was sealed with a plastic seal and incubated at room temperature on a plate shaker set to 500 rpm. Following two hour incubation, the contents of the wells were decanted and 3 x 400 µL washes with Wash Buffer was carried out. Following the final wash step, the Wash Buffer was decanted and the plate was tapped on tissue paper to remove any residual Wash Buffer. 5 µL of Blue Conjugate was added to the TA wells and 200 µL of pNpp Substrate solution was added to all 96 wells. The plate was sealed and incubated for 2 hours without shaking. Following the incubation, 50

µL of Stop Solution was added to each well and the plate was read at 450 nm using the microplate reader.

Results were calculated as follows:

1. The average Net Optical Density (OD) bound for each standard and sample was calculated by subtracting the average NSB OD from the average OD bound.

Average Net OD = Average Bound OD – Average NSB OD

2. The binding of each pair of standard wells as a percentage of the maximum binding wells (Bo), was calculated the following formula:

Percent Bound= (Net OD / Net Bo OD) x 100

3. Percent Bound versus Concentration of LTB4 for the standards was plotted with an approximate straight line through the points. Metabolite concentrations for the unknown samples were determined using 4-parameter non-linear regression curve fitting.

2.20.2 DuoSet sandwich ELISA

DuoSet® sandwich VEGF ELISA was carried out as per manufacturer's protocol. In principle, a capture antibody pre-coated on the plate surface binds to an antigen present in the sample. Any bound antigen is bound by a detection antibody and subsequently bound by enzyme-linked secondary antibody and the signal emitted is proportional to the amount of bound antigen.

A high binding 96-well ELISA plate (Greiner-Bio, Frickenhousen, Germany) was coated with 100 µL of diluted capture antibody overnight, at room temperature, in the dark. The following day, the capture antibody was decanted and 3x washes with Wash Buffer (0.5% Tween-20 in PBS) were carried out. Following the final wash, the Wash Buffer was removed by tapping the plate on tissue paper. The plate was blocked using Reagent Diluent (1% BSA in PBS) for 2 hours at room temperature (to prevent non-specific binding). Antigen standard stock (supplied by the manufacturer) was diluted with Reagent Diluent to the concentration of the highest standard (2000pg/mL) and serially diluted 1:2 using Reagent Diluent to create a 7-point standard. 100 µL of Standards were

added to appropriate wells on the 96-well plate in duplicate. Additionally, Reagent only and cell culture medium (M199) only wells were loaded in duplicate. Neat samples (tissue conditioned media) were added to the appropriate wells, plate was sealed and incubated at room temperature for 2 hours on a plate shaker. Following 3x 400 μL washes with Wash Buffer, 100 μL of Detection antibody was added to each well and incubated for 2 hours at room temperature with no agitation.

2.21 Statistical analysis

All statistical analysis was performed using GraphPad Prism software version 6.0 (Graph Pad Prism, San Diego, CA, USA). All data are expressed at mean ± the standard error of the mean (S.E.M), unless otherwise stated. The normality of the data was assessed and non-parametric analysis was used as appropriate. Differences between continuous variables of matched patient groups were measured by Wilcoxon signed rank test and Mann-Whitney test was used to measure unmatched groups. A paired student t-test was used for all parametric paired data (i.e. untreated controls versus treated samples). One way ANOVA was employed for statistical analysis involving three or more groups. Dunnett's multiple comparisons *post-hoc* test was used to compare multiple groups to one group (i.e. control). Tukey multiple comparison *post-hoc* analysis was used to determine significance between groups. Kruskal-Wallis test with Dunn's post-hoc was used for multiple comparisons between non-parametric data. Patient data correlations between variables (non-parametric) were assessed by Spearman correlation coefficients. Kaplan Meier method was used to perform survival statistics and the differences in survival between two groups were assessed using the log rank test (Mantel-Cox test). The disease specific survival was assessed with survival time was measured from the date of surgery to the last follow up. Differences of $p<0.05$ (*), $p<0.01$(**) and $p<0.001$(***) were considered to be statistically significant. All p-values reported are two-tailed.

Chapter3

Expression of markers of glycolysis, oxidative phosphorylation, hypoxia and 5LOX in esophageal adenocarcinoma, and their association with clinical and pathological features

3.1 Introduction

Most cancer cells exhibit increased glycolysis and use it for their energy supply [90]. Published studies suggest, that mitochondrial defects and malfunction, adaptation to hypoxic tumor microenvironment, oncogenic signaling, and abnormal expression of metabolic enzymes, all contribute to cancer development [267]. Glycolysis involves the use of various enzymes that are attractive potential therapeutic targets to concur cancer. In this study, we examined whether if there is a link between the expression of glucose transporter proteins, glycolytic enzymes, markers of hypoxia and 5-lipoxygenase and outcome in esophageal adenocarcinoma. A simplified diagram of the glucose metabolism pathway with glucose transporter proteins and glycolytic enzymes of interest and their steps are summarised in Figure 3.1 below.

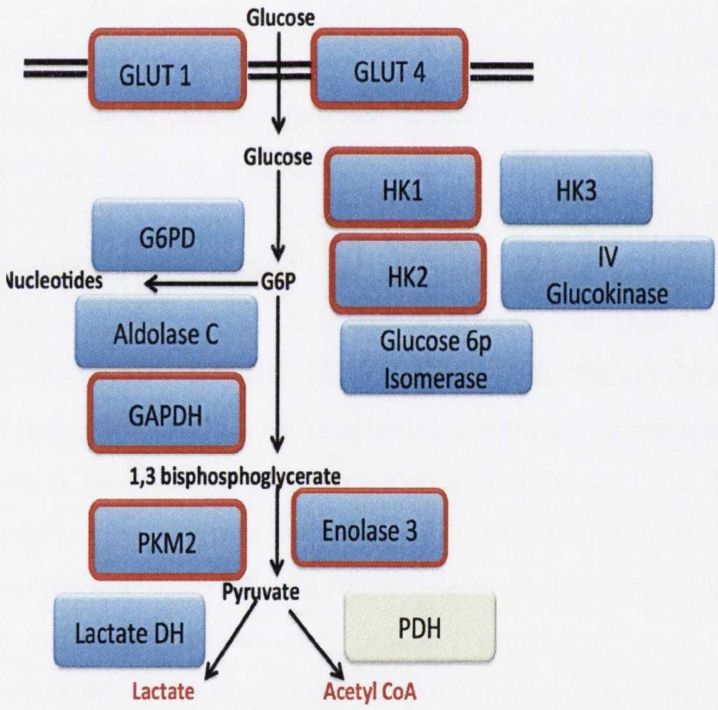


Figure 3.1 Potential glucose transporter protein and glycolytic enzyme targets in glycolysis. A simplified diagram of glucose metabolism pathway with glucose transporter proteins and glycolytic enzymes of interest in the project outlined in red.

Published studies predominantly show glucose transporter proteins, markers of glycolysis, OXPHOS, hypoxia and 5-lipoxygenase to be altered in many cancers. We selected a range of markers based on the evidence in published literature and preliminary studies done in St. James's hospital. A panel of markers of interest and the list of studies showing the link between them and various cancers are summarised in Table 3.1.

Table 3.1 Summary of markers that have been shown to be involved in tumourigenesis in cancer

Marker	Role	References
GLUT1	Glucose transport	Carvalno *et al.*, 2011 [203]; Tohma *et al.*, 2005 [205]
GLUT4	Glucose transport	Gerrido *et al.*, 2015 [209]; Acharya *et al.*, 2016 [208]
HK1	Glycolysis	Li *et al.*, 2014 [212] ; Gao *et al.*, 2015 [211]
HK2	Glycolysis	Anderson *et al.*, 2016 [213] ; Krushana *et al.*, 2013 [268]
PKM2	Glycolysis	Zhan *et al.*, 2013 [217] ; Dong *et al.*, 2016 [269]
GAPDH	Glycolysis	Bazzocco *et al.*, 2015 [226] ; Rezaee-Rad *et al.*, 2014 [270]
ENO3	Glycolysis	Peshavaria *et al.*, 1991 [271]
ATP5B	OXPHOS	Phelan *et al.*, 2016 [247]; Hjerpe *et al.*, 2013 [234]
HIF1A	Hypoxia	Baba *et al.*, 2010 [272]; Fillies *et al.*, 2005 [273]
CAIX	Hypoxia	Lock *et al.*, 2013 [274], McDonald *et al.*, 2014 [275]
5LOX	Eicosanoid signaling	Hoque *et al.*, 2005 [72]; Chen *et al.*, 2004 [85]

In addition to markers of glucose transport, glycolysis and OXPHOS, a particular interest in this study was to investigate the role of hypoxia in OAC. The ability of cancer cells to adapt to hypoxic tumor microenvironment suggests the importance of investigation of markers of hypoxia [267]. HIF1A is a major regulator of oxygen homeostasis within cells [276] and it is a regulator of anaerobic metabolism [277]. When oxygen is available, most cells produce ATP via oxidative phosphorylation. However, in hypoxic environments, there is a shift to anaerobic metabolism for cellular energy production [278] . HIF1A is among the principal genes coordinating this shift, by inducing a variety of glycolytic enzymes and glucose transporters [276]. Due to its role in hypoxia, HIF1A plays a critical part in tumor proliferation [276].

5-Lipoxygenase (5LOX), an enzyme in eicosanoid signaling pathway, has been shown to have a role in various cancers [279]. Published studies show 5-LOX expression in Barrett's oesophagus, indicating that 5-LOX overexpression begins at an early stage of esophageal adenocarcinogenesis [280], therefore it was of a great interest in this study.

With all this evidence from past studies in mind, the main aim of this chapter was to

retrospectively assess the relevance of each marker summarised in Table 3.1, in a cohort of esophageal adenocarcinoma tissue microarrays and correlate them with clinical and pathological parameters, including OAC- specific survival.

3.2 Aims and objectives

The aim of this chapter was to retrospectively examine the expression of oxidative phosphorylation and glycolytic protein biomarkers, the role of hypoxia and 5LOX expression in tissue microarrays of OAC tumours linked to full anthropometric and clinical data.

Specific objectives were:

- To delineate whether expression of glucose transporter proteins, markers of glycolysis, OXPHOS, hypoxia and 5LOX is associated with tissue type in OAC tumor (leading edge or non-leading edge of the tumor) using OAC tissue micro arrays

- To correlate the expression of markers of glycolysis, oxidative phosphorylation, hypoxia and 5LOX with nodal and venous involvement is OAC patients using OAC tissue microarrays

- To correlate the expression of markers of glycolysis, oxidative phosphorylation, hypoxia and 5LOX with metabolic tumor activity (SUVmax) in OAC patients

- To correlate the expression of markers of glycolysis, oxidative phosphorylation, hypoxia and 5LOX with OAC-specific survival in OAC patients using OAC tissue microarrays

3.3.1 Oesophageal adenocarcinoma tissue microarray demographics

The study population consisted of 120 esophageal adenocarcinoma patients, 96 (80%) were male and 24 (20%) were female. The mean age was 63.2 years. Patient and tumor characteristics are summarized in Table 3.2.

Paraffin-embedded tumor sections from 120 esophageal adenocarcinoma patients with a minimum of 36 months of clinical follow up data were used to construct tissue microarrays (TMAs) (Figure 3.2). Matched tumor leading edge cores were also included where available.

TMAs were stained for a number of glucose transporter proteins, markers of glycolysis, hypoxia and EMT. Optimisation of primary antibodies for each marker was carried out prior to staining TMAs. Optimisation was carried out using full-face esophageal adenocarcinoma tissue at a number of different dilutions. The list of markers of interest, primary antibody selection and optimisation delineated in Table 2.6.

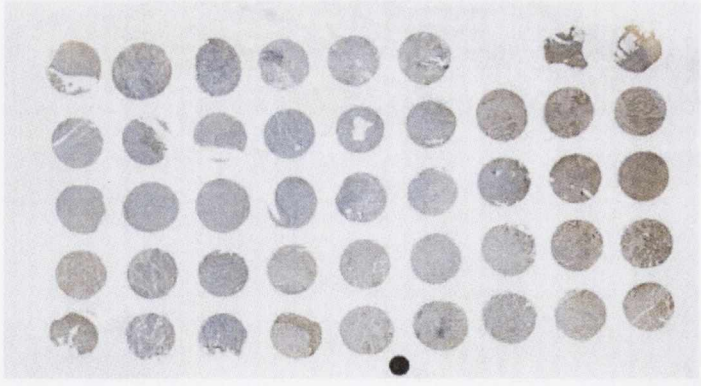


Figure 3.2 Tissue microarray construction. Representative image of a TMA slide containing 2 mm tissue cores for 14 patients in triplicate.

Table 3.2 Patient demographic for esophageal adenocarcinoma microarrays

n=120	Mean (S.D.) or n (%) as appropriate	
Morphology (OAC)	120 (100%)	
Male: female	96:24 (80%: 20%)	
Age	63.22 (12.1)	
Pathological T-stage	T1	7 (5.8%)
	T2	20 (16.7%)
	T3	79 (65.8%)
	T4	1 (0.8%)
	Missing	13 (10.8%)
Pathological N-stage	N0	71 (59.2%)
	N1	39 (32.5%)
	N2	0 (0%)
	N3	0 (0%)
	Missing	10 (8.3%)
Neoadjuvant treatment	38 (31.7%)	

3.3.2 Association of glucose transporter proteins and glycolytic markers with obesity and clinical data

3.3.2.1 Differential expression of glucose transporter proteins and glycolytic markers and tissue type

An average tumor epithelial and stromal score was assigned to each patient with an exception of cases where tissue cores were damaged and impossible to score. The intensity score was obtained by scoring the cores between 0 and 3, where 0= negative, 1= weak, 2=moderate and 3=strong expression. Positivity was categorized as 0%, 10% 25%, 50%, 75%, 90% or 100%. The values of the two parameters were multiplied to get an overall score for each core of 0-300. There were three 2mm cores available for each patient therefore the mean score of the three cores was collated with clinicopathological and survival data from the database. This scoring mechanism has been previously published by Cathart *et al* in non-small cell lung cancer [337].

Representative images for GLUT1 (Figure 3.3a), GLUT4 (Figure 3.3b), HK1 (Figure 3.4a), HK2 (Figure 3.4b), PKM2 (Figure 3.5a), GAPDH (Figure 3.5b), ENO3 (Figure 3.6).

A subset of OAC patients with matched NLE and LE tissue (85/120cases) were analysed for stromal and epithelial expression. Differences between different tissue type of matched patient groups were measured by Wilcoxon signed rank test. Data was not

normally distributed, therefore a non-parametric test was used. There was no difference in epithelial GLUT1 expression between LE and NLE tissue (155.5 ±5.610 versus 164.8 ±5.699, n=85 in both groups, p=0.4986) (Figure 3.7a). However, epithelial GLUT4 levels were significantly higher in the LE compared to NLE tissue (204.00 ±7.242 versus 181.1, n=85 in each group, $p<0.05$) (Figure 3.7c). There was no differential expression of HK1 between LE and NLE tissue (143.8 ±7.112 versus 159.3 ±6.556, n=85 in both groups, p=0.0553) (Figure 3.7e), but HK2 levels were significantly higher in the LE compared to NLE tissue (162.5 ±6.189 versus 156.6 ±6.762, n=85 in each group, $p<0.05$) (Figure 3.7g). There was no difference in epithelial PKM2 expression between LE and NLE tissue (151.9 ±7.911 versus 158.4 ±6.983, n=85 in each group, p=0.4986) (Figure 3.8a). GAPDH levels were significantly higher in the NLE compared to LE tissue (175.8 ±7.229 versus 157.4 ±7.167, n=85 in each group, $p<0.05$) (Figure 3.8c). Finally, was no difference in epithelial ENO3 expression between LE and NLE tissue (150.1 ±7.309 versus 152.5 ±6.887, n=85 in each group, p=0.7347) (Figure 3.8e).

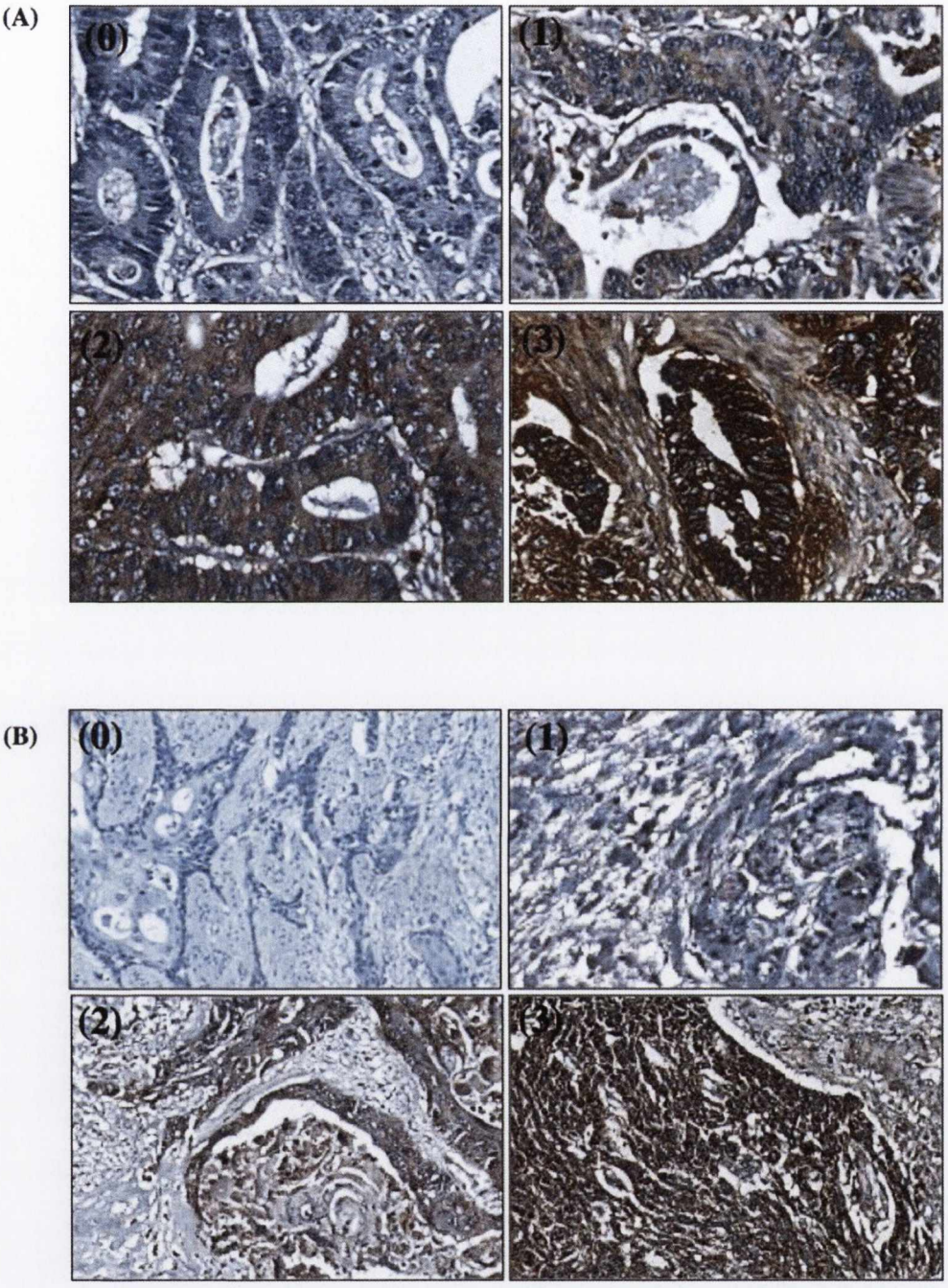


Figure 3.3 Tissue microarray GLUT1 and GLUT4 staining pattern in esophageal adenocarcinoma. Following immunohistochemical staining for (A) GLUT1 and (B) GLUT4, the intensity score was obtained by scoring the cores between 0 and 3, where 0= negative, 1 = weak, 2=moderate and 3=strong expression. The quantity of positive staining within the tissue microarray core was scored between 0 and 100% to obtain the percentage positivity measure. The intensity score and percentage positivity were multiplied giving an overall score for each core 0 to 300. Representative images are 10X magnification.

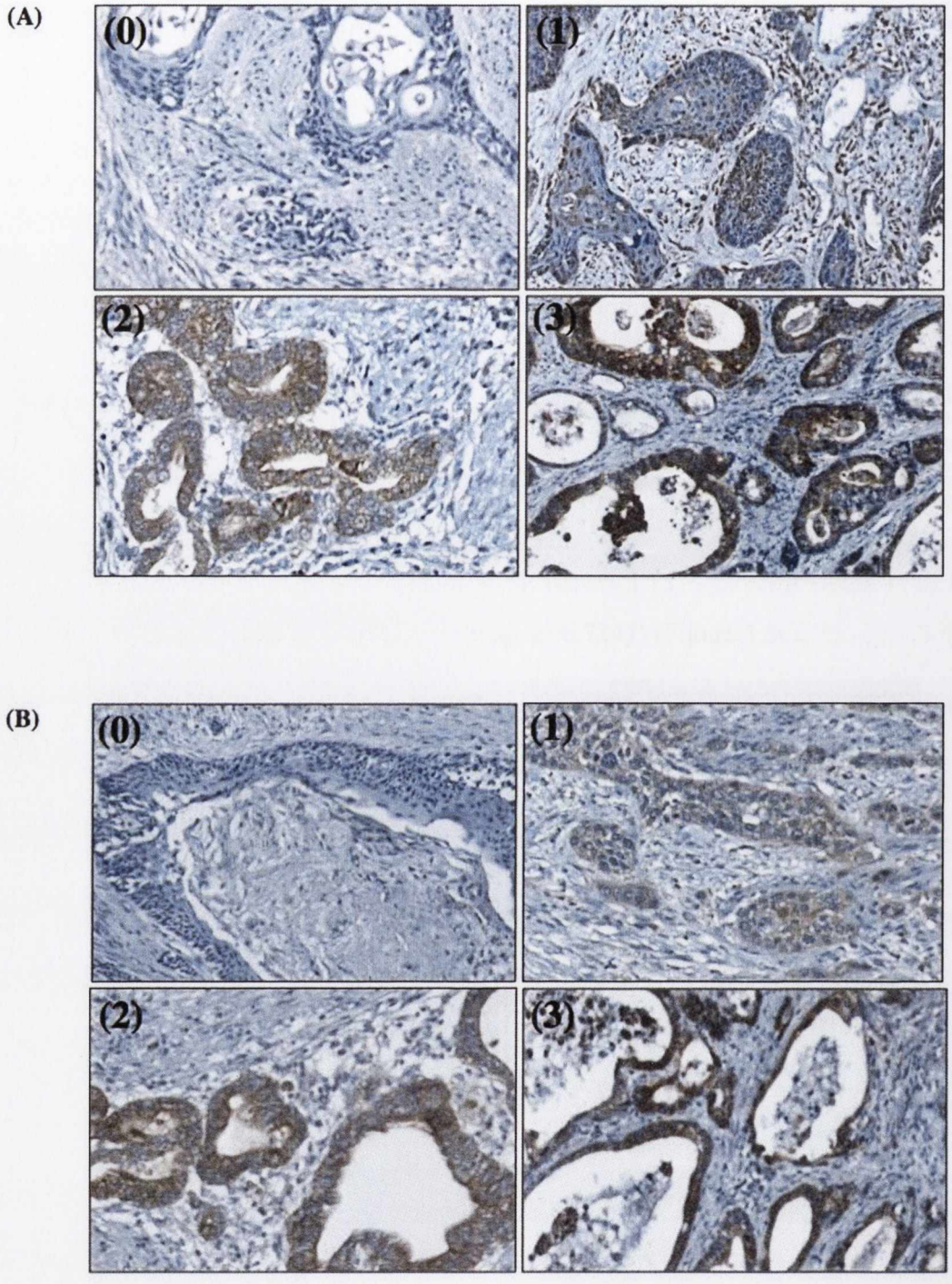


Figure 3.4 Tissue microarray HK1 and HK2 staining pattern in esophageal adenocarcinoma. Following immunohistochemical staining for (A) HK1 and (B) HK2, the intensity score was obtained by scoring the cores between 0 and 3, where 0= negative, 1 = weak, 2=moderate and 3=strong expression. The quantity of positive staining within the tissue microarray core was scored between 0 and 100% to obtain the percentage positivity measure. The intensity score and percentage positivity were multiplied giving an overall score for each core 0 to 300. Representative images are 10X magnification.

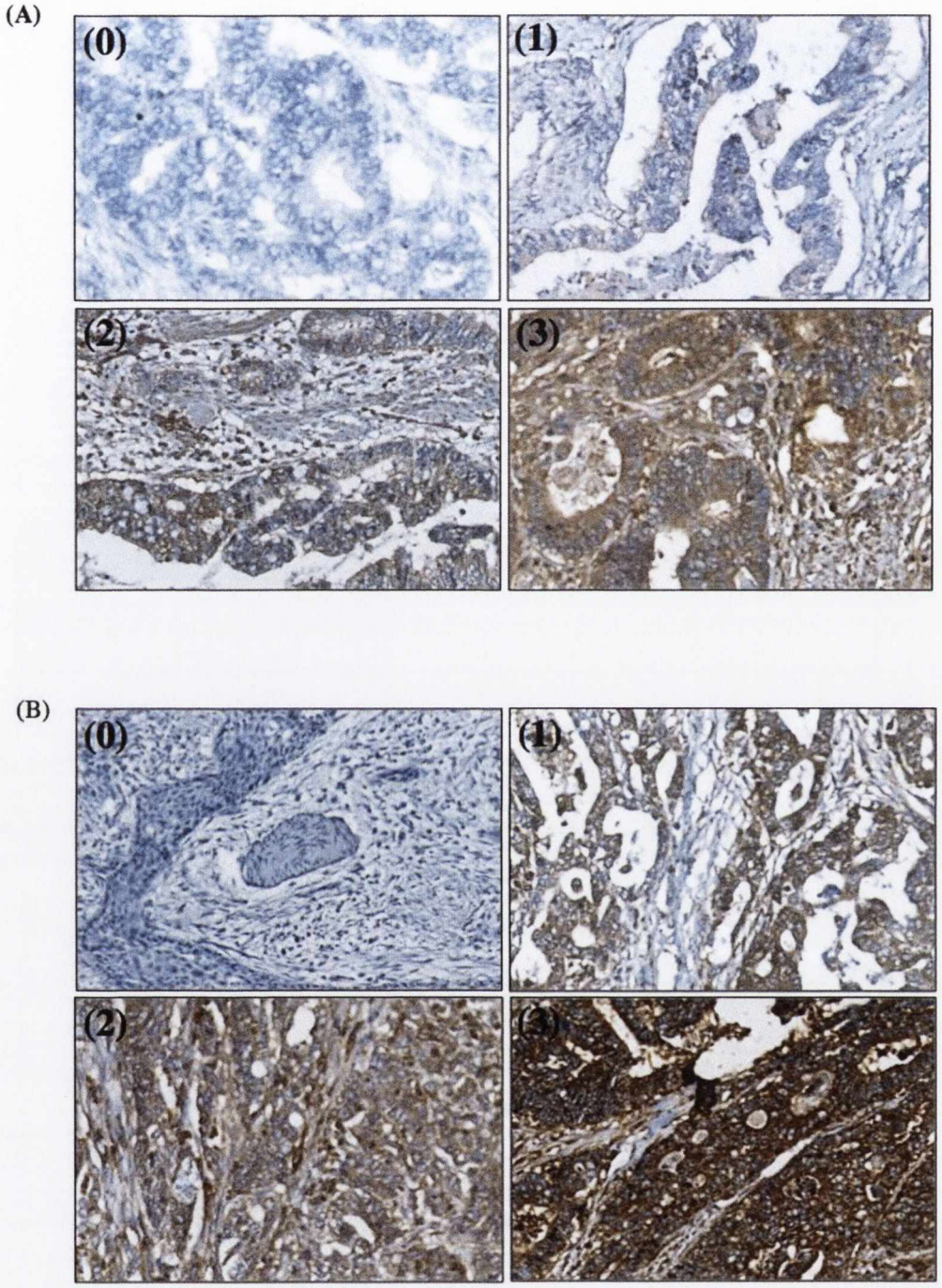


Figure 3.5 Tissue microarray PKM2 and GAPDH staining pattern in esophageal adenocarcinoma. Following immunohistochemical staining for(A) PKM2 and (B) GAPDH, the intensity score was obtained by scoring the cores between 0 and 3, where 0=negative, 1=weak, 2=moderate and 3=strong expression. The quantity of positive staining within the tissue microarray core was scored between 0 and 100% to obtain the percentage positivity measure. The intensity score and percentage positivity were multiplied giving an overall score for each core 0 to 300. Representative images are 10X magnification.

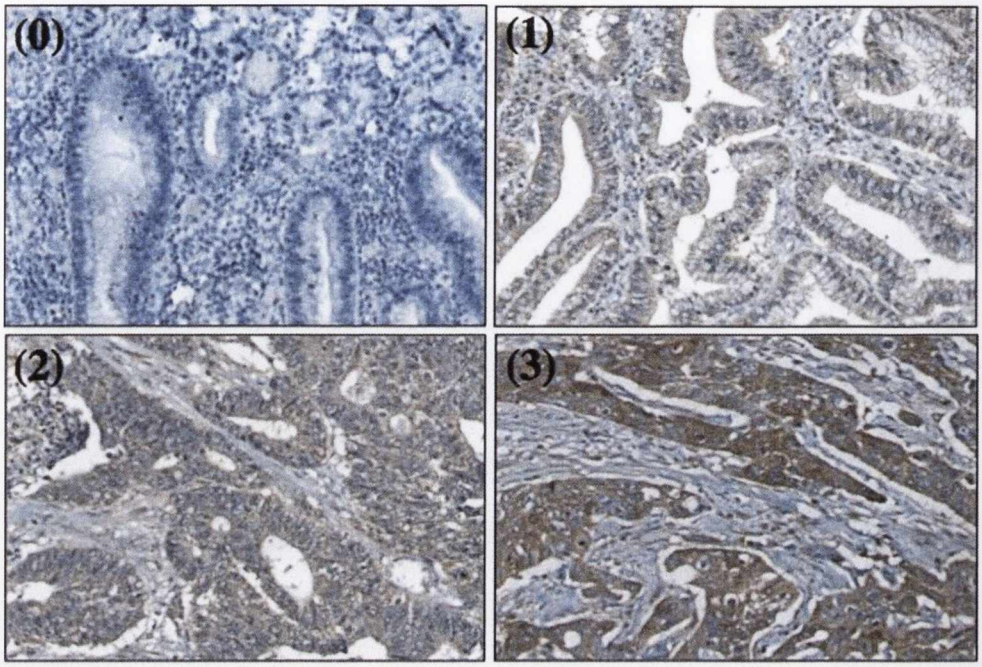


Figure 3.6 Tissue microarray ENO3 staining pattern in esophageal adenocarcinoma. Following immunohistochemical staining for ENO3, the intensity score was obtained by scoring the cores between 0 and 3, where 0= negative, 1=weak, 2=moderate and 3=strong expression. The quantity of positive staining within the tissue microarray core was scored between 0 and 100% to obtain the percentage positivity measure. The intensity score and percentage positivity were multiplied giving an overall score for each core 0 to 300. Representative images are 10X magnification.

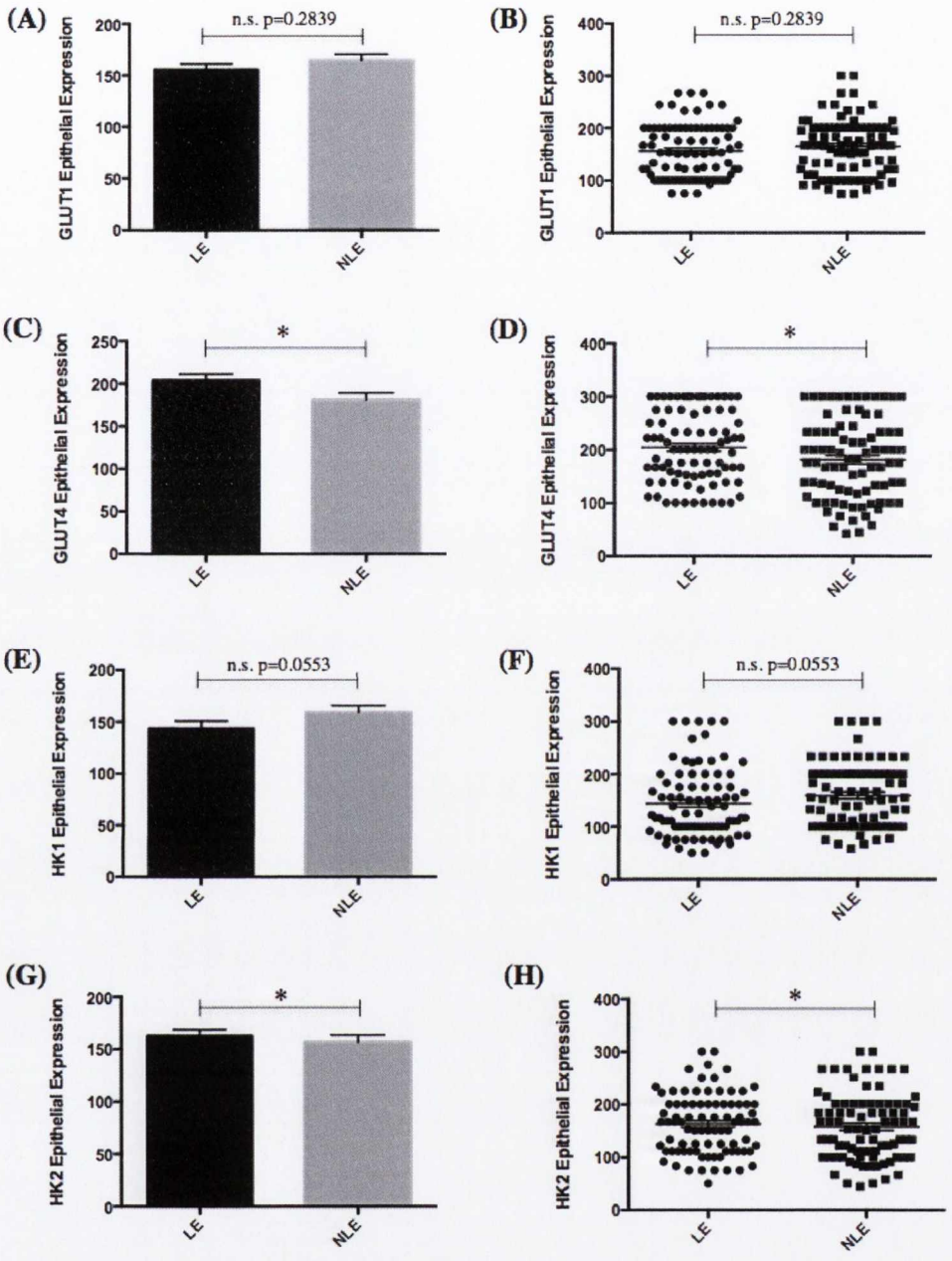


Figure 3.7 Comparison of glucose transporter protein and glycolytic marker expression in leading edge and non-leading edge esophageal adenocarcinoma. (A) There was no difference in epithelial GLUT1 expression between LE and NLE tissue. (B) The distribution of GLUT1 expression across OAC patient cores shown by scatter plot. (C) GLUT4 levels were significantly higher in the LE compared to NLE tissue ($p<0.05$). (D) The distribution of GLUT4 expression across OAC patient cores shown by scatter plot. (E) There was no difference in epithelial HK1 expression between LE and NLE tissue. (F) The distribution of HK1 expression across OAC patient cores shown by scatter plot. (G) HK2 levels were significantly higher in the LE compared to NLE tissue ($p<0.05$). (H) The distribution of HK2 expression across OAC patient cores shown by scatter plot. Statistical used was Wilcoxon signed rank test. $p<0.05$ (*). Error bar denotes mean ± S.E.M.

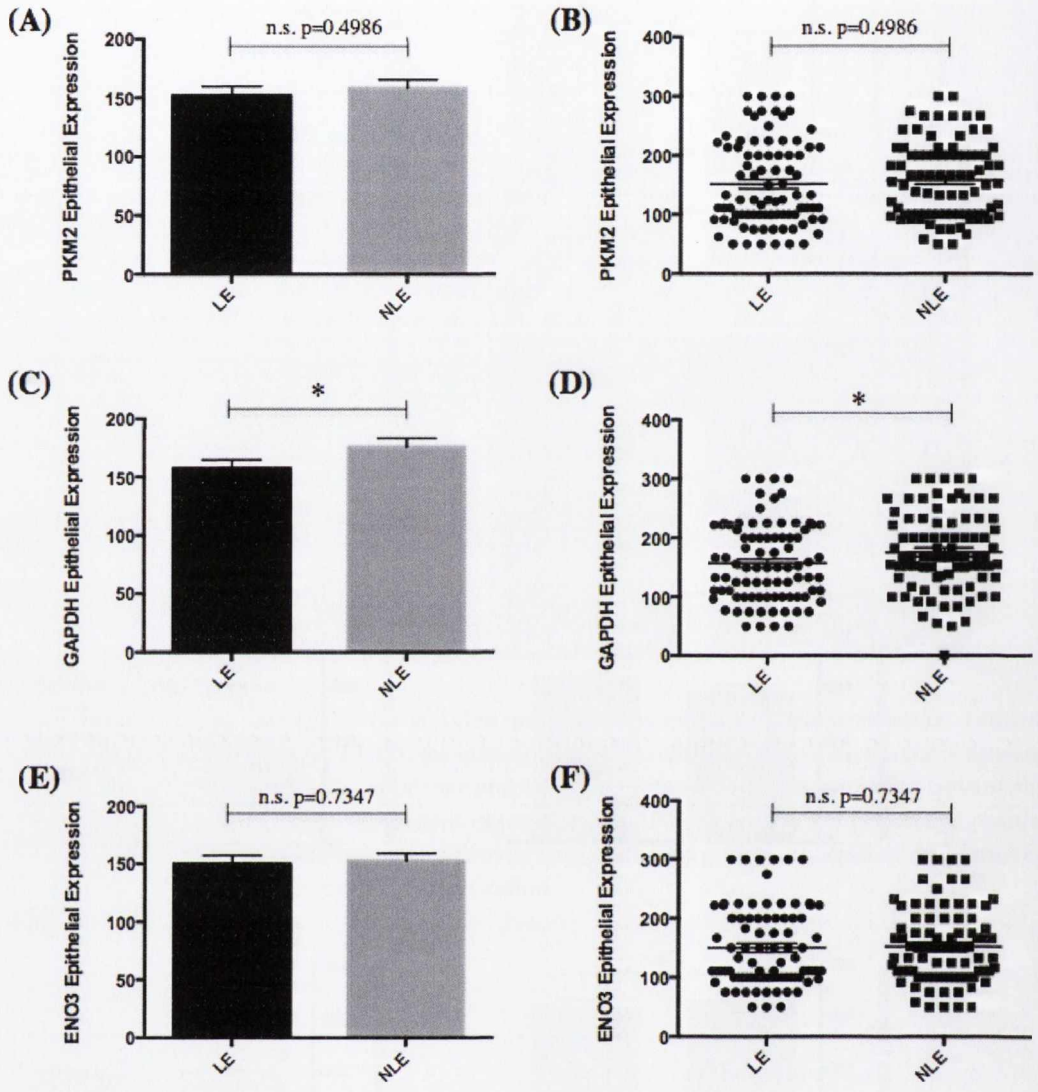


Figure 3.8 Comparison of glycolytic marker expression in leading edge and non-leading edge esophageal adenocarcinoma. (A) There was no difference in epithelial PKM2 expression between LE and NLE tissue. (B) The distribution of PKM2 expression across OAC patient cores shown by scatter plot. (C) GAPDH levels were significantly higher in the NLE compared to LE tissue ($p<0.05$). (D) The distribution of GAPDH expression across OAC patient cores shown by scatter plot. (E) There was no difference in epithelial ENO3 expression between LE and NLE tissue. (F) The distribution of ENO3 expression across OAC patient cores shown by scatter plot. Statistical used was Wilcoxon signed rank test. $p<0.05$ (*). Error bar denotes mean ± S.E.M.

3.3.2.2. Glucose transporter protein and glycolytic marker expression and lymph node involvement in esophageal adenocarcinoma

Glucose transporter protein and glycolytic marker expression in OAC was correlated with lymph node involvement. Differences between nodal involvement of measured by Mann-Whitney test because the two groups were unmatched and independent of each other. Non-parametric test was used as data was not normally distributed.

GLUT1 epithelial expression was significantly higher in patients with the presence of lymph involvement compared to lymph node negative patients (171.3 ±5.58 versus 149.2 ±8.64, n=80 versus n=39, $p<0.05$) (Figure 3.9a). Epithelial expression of the second glucose transporter protein, GLUT4 was also higher in patients with the presence of lymph node involvement compared to lymph node negative patients (185.3 ±7.9 versus 157 ±12.72, n=80 versus n=39, $p<0.05$) (Figure 3.9b). Similarly, there was a significant association between higher epithelial HK2 expression and presence of lymph nodes compared to lymph node absent patients (172 7.06 versus 140.4 ±9.47, n=80 versus n=39, $p<0.05$) (Figure 3.9d). However, there was no association between epithelial HK1 expression levels and patients with the absence of lymph involvement compared to lymph node positive patients (165.6 ±11.44 versus 161.1 ±6.49, p=0.9739) (Figure 3.9c). Similarly, there was no association between epithelial PKM2, GAPDH and ENO3 expression levels and patients with the absence of lymph nodes compared to lymph node positive patients (170.5 ±11.02 versus 159.5 ±7.47, p=0.4648; 156.5 ±11.81 versus 169 ±7.18, p=0.2948 and 150.5 ±11.04 versus 161.7 ±6.59, p=0.1832, respectively) (Figure 3.8e, Figure 3.9f and Figure 3.9g).

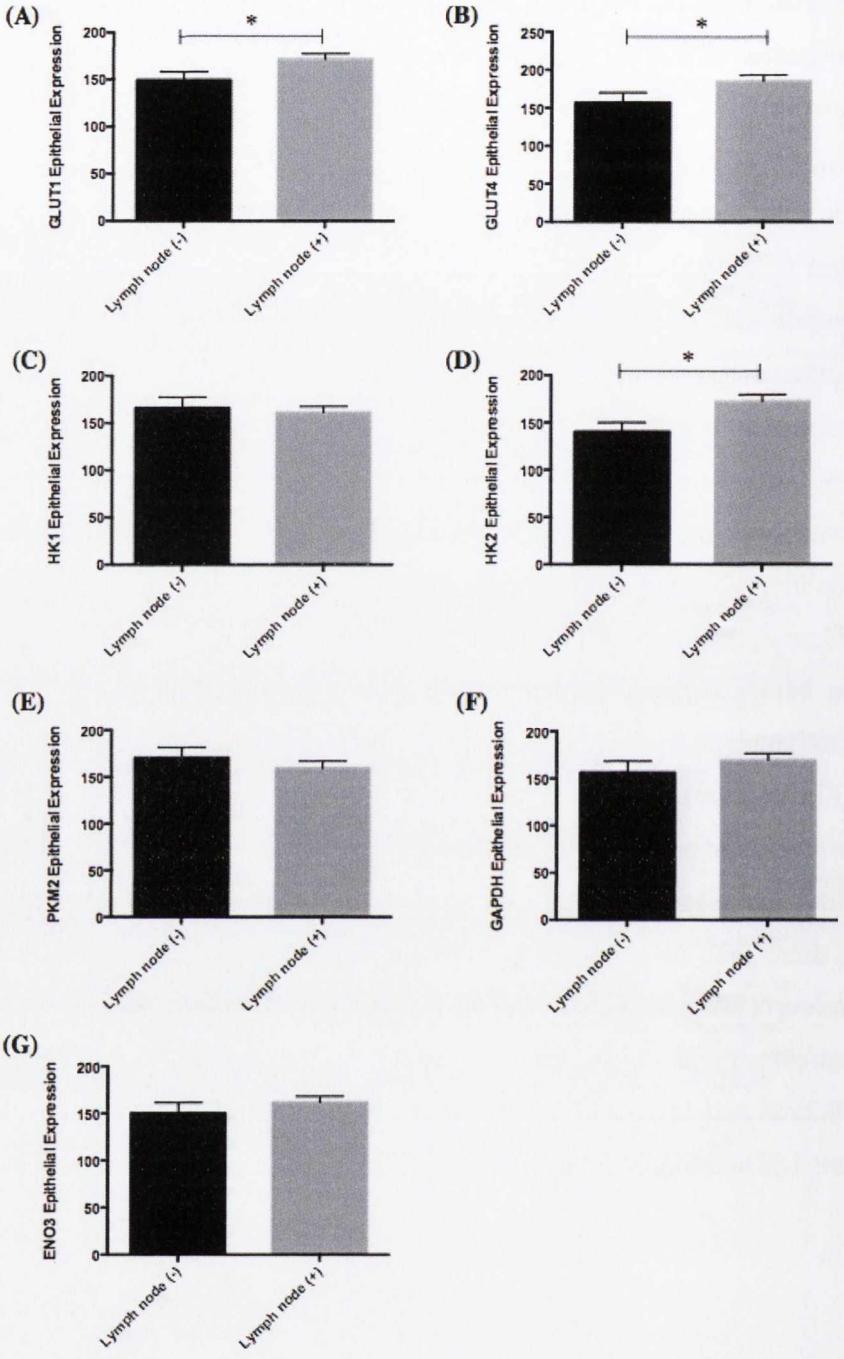


Figure 3.9 Epithelial expression of glucose transporter proteins and glycolytic marker was associated with more aggressive tumor phenotype in OAC. (A) Higher epithelial GLUT1 expression was associated with presence of lymph involvement ($p<0.05$, n=80 versus n=39). (B) Higher epithelial GLUT4 expression was also associated with presence of lymph node involvement ($p<0.05$, n=80 versus n=39). (C) There was no association between epithelial HK1 expression and lymph involvement in OAC patients ($p=0.9739$). (D) Higher epithelial HK2 expression was associated with presence of lymph nodes ($p<0.05$, n=80 versus n=39). (E), (F) and (G) There was no association between PKM2, GAPDH and ENO3 epithelial expression and lymph node involvement in OAC patients ($p=0.4648$, $p=0.2948$ and $p=0.1832$ respectively, n=80 versus n=39). Statistic test used was Mann Whitney U test $p<0.05$(*). Error bar denotes mean ± S.E.M.

3.3.2.3. Glucose transporter protein and glycolytic marker expression and venous involvement in esophageal adenocarcinoma

Following investigation whether expression of glucose transporter proteins and markers of glycolysis had an association with nodal involvement in OAC, we investigated the link between the same markers of glycolysis and glucose transporter proteins and their association with venous involvement in the same cohort of OAC patients. Differences between venous involvement was measured by Mann-Whitney test because the two groups were not matched and the two groups were independent of each other.

The only significant association observed was between HK2 and venous positivity in OAC patients. Epithelial expression of HK2 was significantly higher in patients with the presence of venous involvement compared to the patients that showed the absence of venous involvement (177.9 ±9.96 versus 150.2 ±7.06, n=47 versus n=69, $p<0.05$) (Figure 3.10d). There was no association between epithelial expression of glucose transporter proteins and other glycolytic makers in the OAC patients, with the absence versus the presence of venous involvement. Epithelial Glut1 and Glut4 expression was very similar between the venous positive and venous negative patient groups (163.7 ±6.76 versus 164.8 ±6.57 and 173.5 ±9.16 versus 185.1 ±10.65, n=69 versus n=47, p=0.7536 and p=0.3924 respectively) (Figure 3.10a and Figure 3.10b respectively). Similarly, there was no difference in epithelial HK1 expression between venous negative and venous positive OAC patients (161.7 ±8.23 versus 166.9 ±7.85, n=69 versus n=47, p=0.4526) (Figure 3.10c). There was no difference in epithelial expression of PKM2 between patients associated with venous positivity and the ones without venous involvement (160.5 ±7.84 versus 157.3 ±9.31, n=69 versus n=47, p=0.7308) (Figure 3.10e). Similar results with no significant association between the level of epithelial expression of the marker and venous involvement were seen in tissue microarrays stained for GAPDH (155.9 ±8.24 versus 176.9 ±9.49, n=69 versus n=47, p=0.1022) (Figure 3.10f) and ENO3 (155.2 ±8.01 versus 172.7 ±9.27, n=69 versus n=47, p=0.1763) (Figure 3.10g).

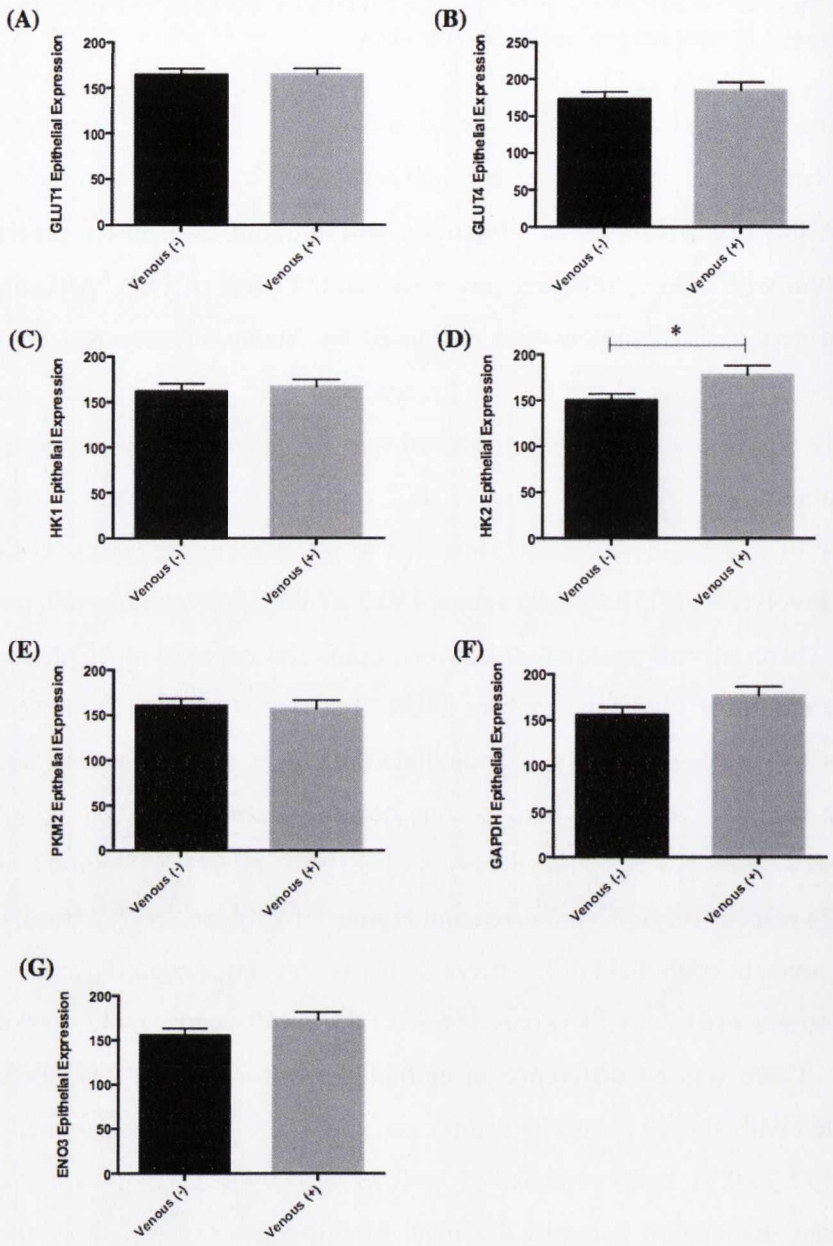


Figure 3.10 Epithelial expression of glucose transporter proteins and glycolytic markers and their association with venous involvement in OAC patients. (A) and **(B)** There was no association between epithelial expression of glucose transporter proteins Glut1 and Glut 4 and venous involvement in OAC patients ($p=0.7536$ and $p=0.3924$ respectively, n=69 versus n=47). (C) Similarly, there was no association between epithelial HK1 expression and venous involvement ($p=0.4526$, n=69 versus n=47). (D) Higher HK2 expression was associated with the presence of venous involvement compared to venous absence ($p<0.05$, n=47 versus n=69). (E), (F) and (G) There was no association between PKM2, GAPDH and ENO3 epithelial expression and venous involvement in OAC patients ($p=0.7308$, $p=0.1022$ and $p=0.1763$ respectively, n=69 versus n=47). Statistic test used was Mann Whitney U test $p<0.05$(*). Error bar denotes mean ± S.E.M.

3.3.2.4 Association between, glucose transporter proteins and glycolytic markers and metabolic tumor activity (PET SUV)

In collaboration with Dr. Vinod Malik we investigated the link between glucose transporter proteins, markers of glycolysis and metabolic tumor activity. PET scans were used to evaluate the presence of tumor and metastases in OAC patients in St. James's Hospital. During a diagnostic PET scan, glucose analogue fluorodeoxyglucose (FDG) was injected and the uptake of the analogue was visualized and quantified to demonstrate the presence of the tumor and to calculate the metabolic activity of the tumor by assigning a FDG standardized uptake value (SUVmax). SUVmax values were calculated by Dr. Malik and provided to us for correlation with data obtained from the tissue microarray study.

Non-paramentric Spearman's correlation was used to determine statistical dependence by ranking two variables (metabolic tumor activity and the level of expression of biomarker). Results showed a significant positive correlation between epithelial GLUT4 expression and SUVmax ($r=0.3857$, $p<0.01$, $n=50$) (Figure 3.11b). Similarly, there was a significant positive correlation between epithelial HK2 expression and SUVmax ($r=0.3874$, $p<0.01$, $n=50$) (Figure 3.11d). There was no association between epithelial Glut1, HK1, PKM2, GAPDH or ENO3 expression and the metabolic activity of tumor in this cohort of OAC patients ($p=0.33$, $p=0.3289$, $p=0.3236$ and $p=0.3641$ respectively, $n=50$) (Figure 3.11).

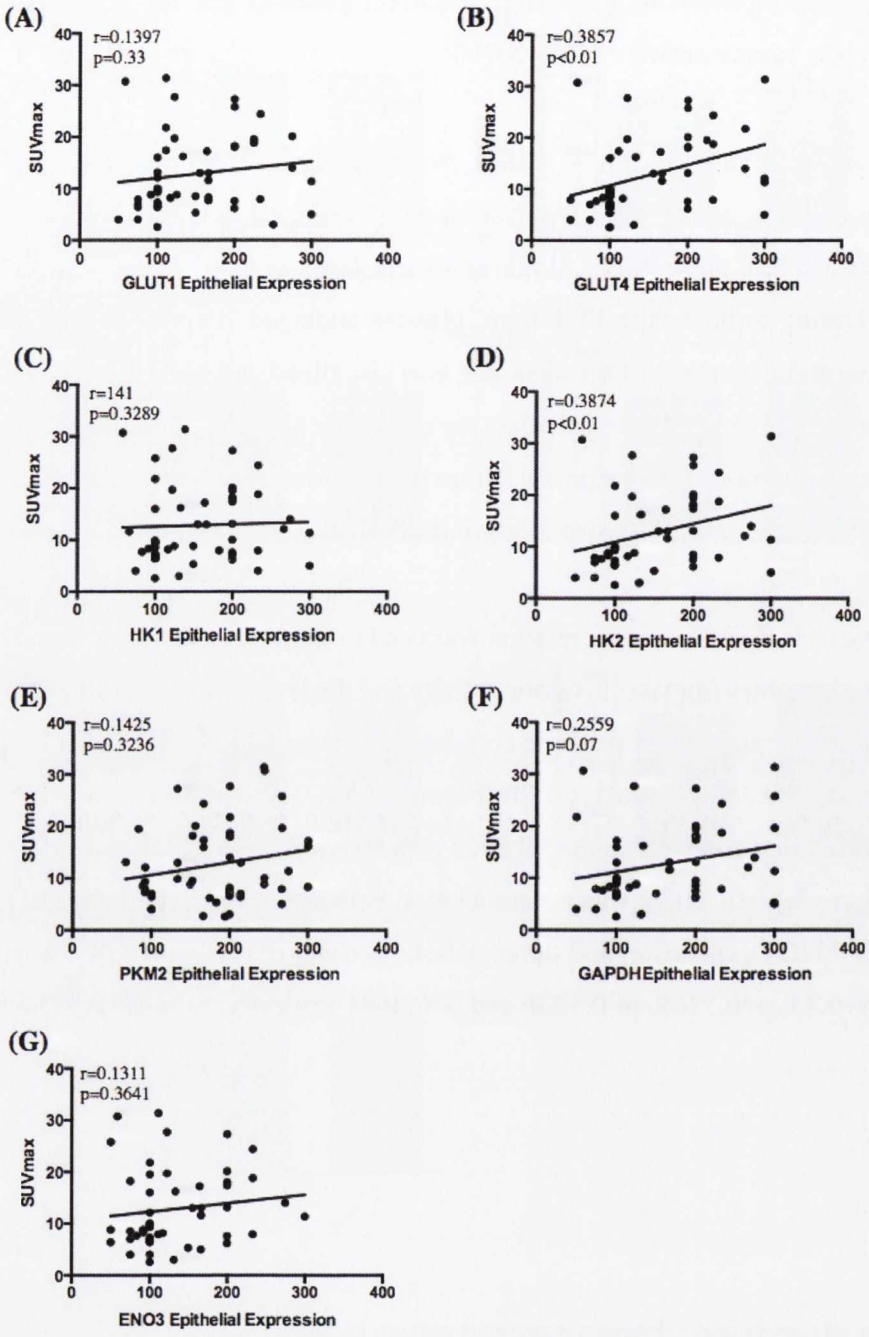


Figure 3.11 Association between the markers of glycolysis and tumor metabolism in OAC patients. (A) There was no association between the measure of tumor metabolism, SUVmax, and GLUT1 (r=0.1397, p=0.33). (B) There was a significant positive correlation between epithelial GLUT4 expression and SUVmax (r=0.3857, p<0.01). (C) There was no association between HK1 and SUVmax (r=0.141, p=0.3289). (D) There was a significant positive correlation between epithelial expression levels of HK2 and SUVmax (r=0.3874, p<0.01). (E), (F) and (G) There was no correlation between epithelial expression of PKM2, GAPDH and ENO3 and SUVmax in OAC patients (p=0.3236, p=0.07 and p=0.3641 respectively). n=50, p<0.01(**).Statistical test used was Spearman's test.

3.3.2.5 Epithelial expression of the glucose transporters and the markers of glycolysis and their association with disease-specific survival

Following immunohistochemical analysis, grade for each marker was divided into greater and less than the median value and disease specific survival was investigated by Kaplan-Meier survival analysis. The log rank test (Mantel-Cox test) was used to assess difference in survival between two groups.

GLUT4 expression above the median value of epithelial expression was significantly associated with poor 5-year disease specific survival (median survival: 35 months versus 12 months, both n=44, log-ranks test $p<0.05$) (Figure 3.12b). There was no significant association between epithelial GLUT1 expression and 5-year disease specific survival (median survival: 36 months versus 20 months, both n=44, log-rank test p=0.092) (Figure 3.12a). High epithelial HK2 expression in OAC patients was associated with significantly poorer 5-year disease specific survival, compared to low expressers of HK2 (median survival: 35 months versus 12 months, both n=44, log-ranks test $p<0.05$) (Figure 3.13b), however, there was no significant association between HK1 epithelial expression and disease-specific survival (median survival: 24 months versus 22 months, both n=44, log-ranks test p=0.5323) (Figure 3.13a). Similarly, there was no significant association between PKM2 and ENO3 epithelial expression and disease-specific survival (median survival: 26 months versus 18 months, log-ranks test p=0.7419 and 32 months versus 18 months, log-ranks test p=0.8066 respectively) (Figure 3.14a and Figure3.15 respectively). High epithelial GAPDH expression was significantly associated with poor 5-year disease-specific survival (median survival: 36 months versus 15 months, both n=44, log-rank test $p<0.05$) (Figure 3.14b).

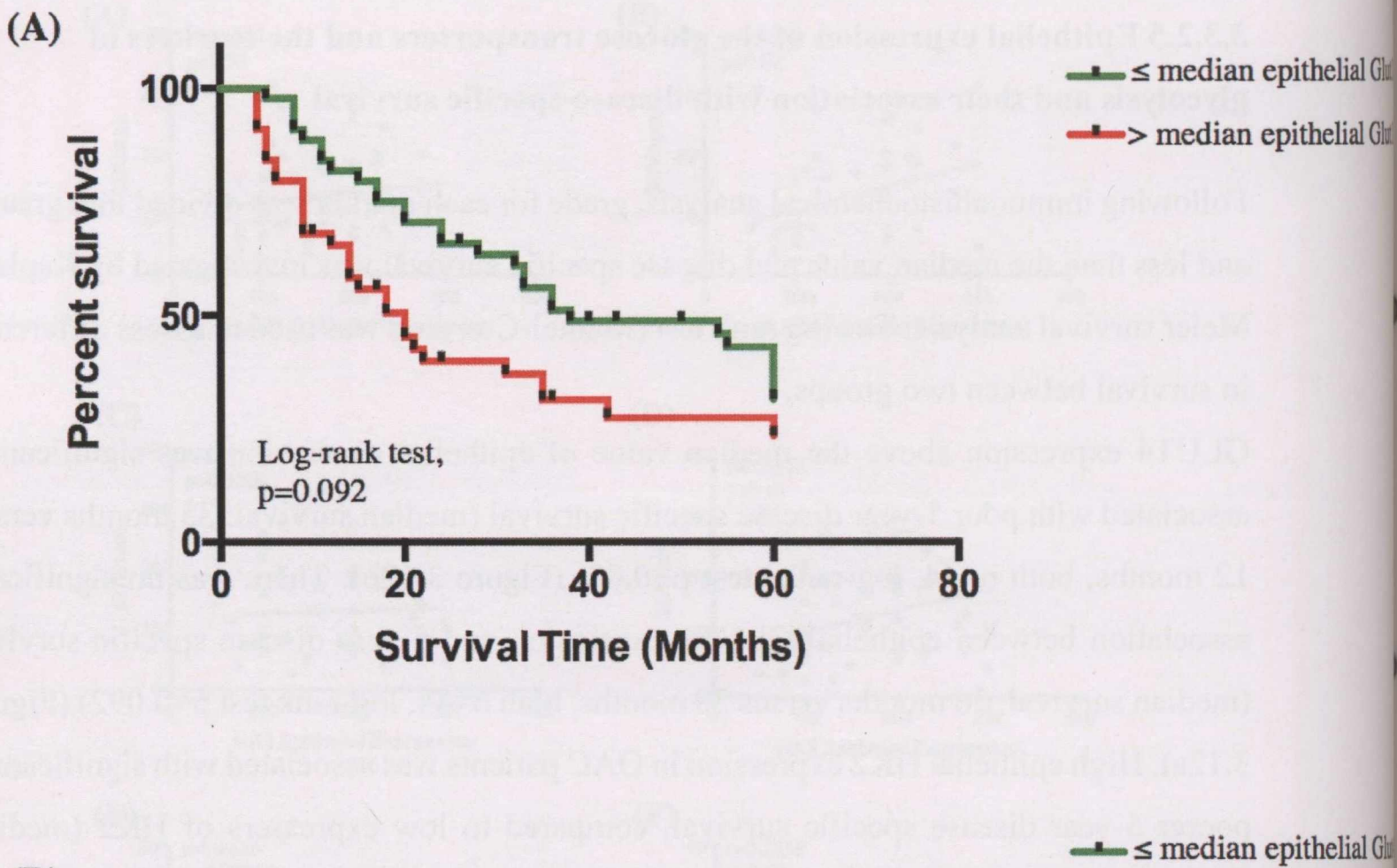
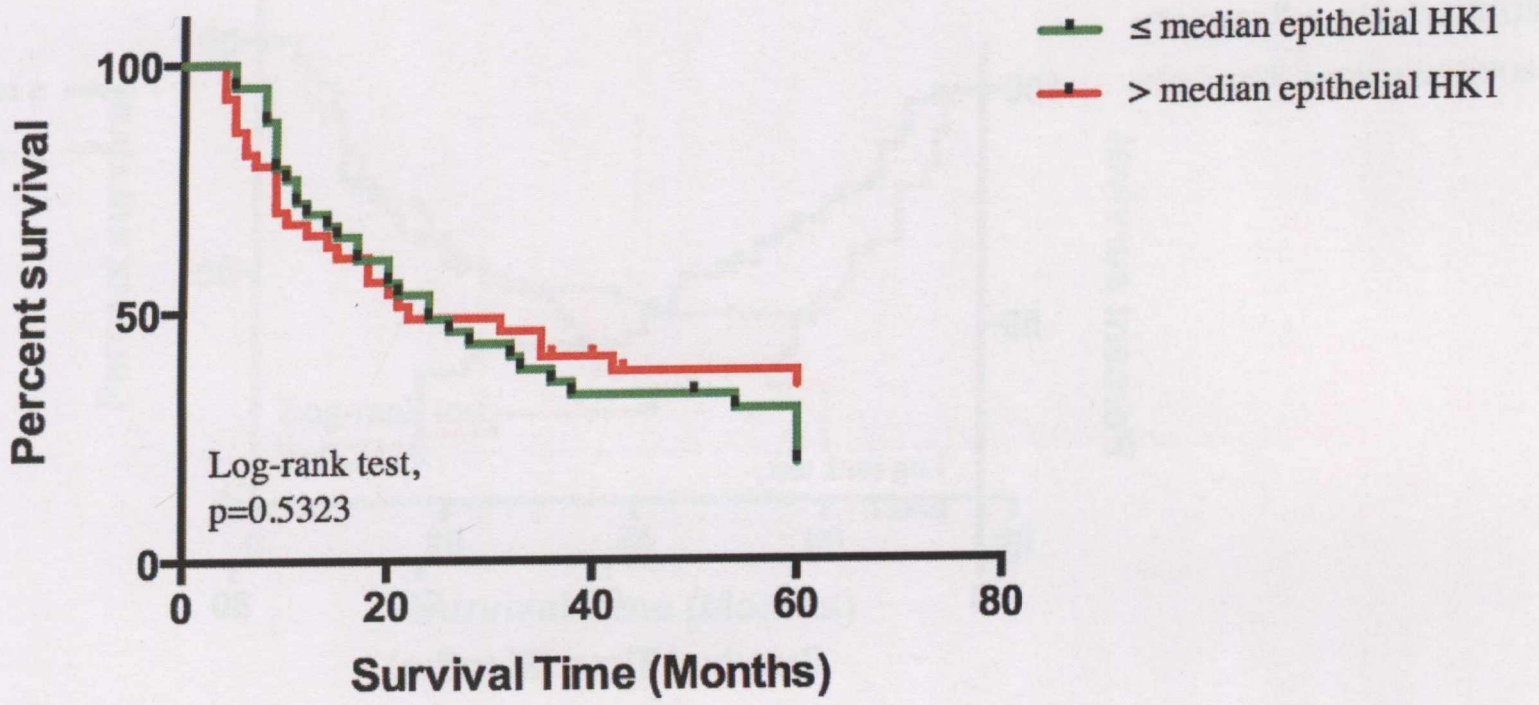


Figure 3.12 The link between epithelial GLUT1 and GLUT4 expression and OAC specific 5-year post-operative survival. (A) There was no significant association between epithelial GLUT1 expression in OAC patients and overall disease-specific 5- year post-operative survival (median survival: 36 months versus 20 months, p=0.092). (B) Higher epithelial GLUT4 expression was significantly associated with poor prognosis (median survival: 35 months versus 14 months, p<0.05). Statistical test used was Kaplan Meier survival curve with Log-rank (Mantel-Cox) test.

(A)



(B)

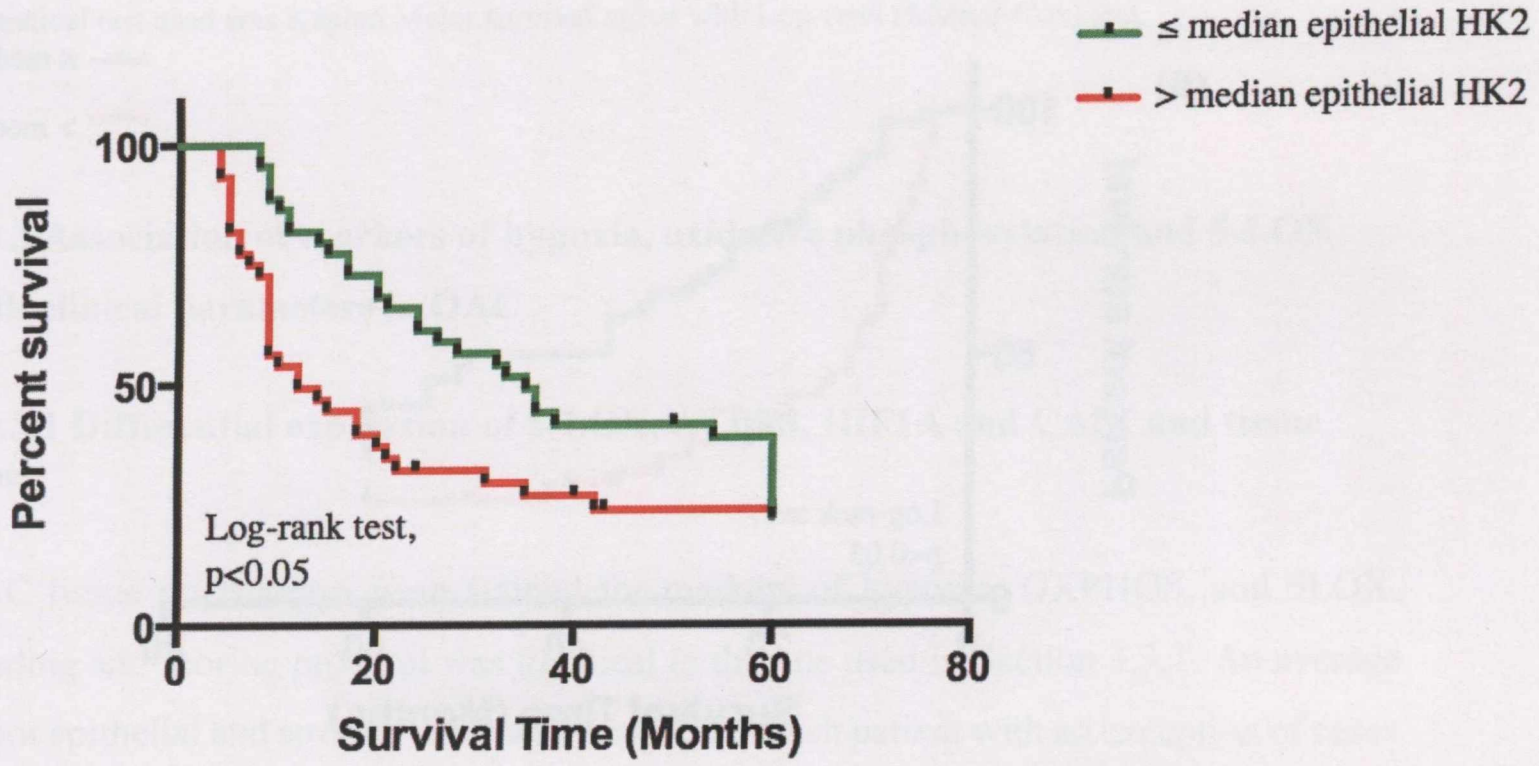
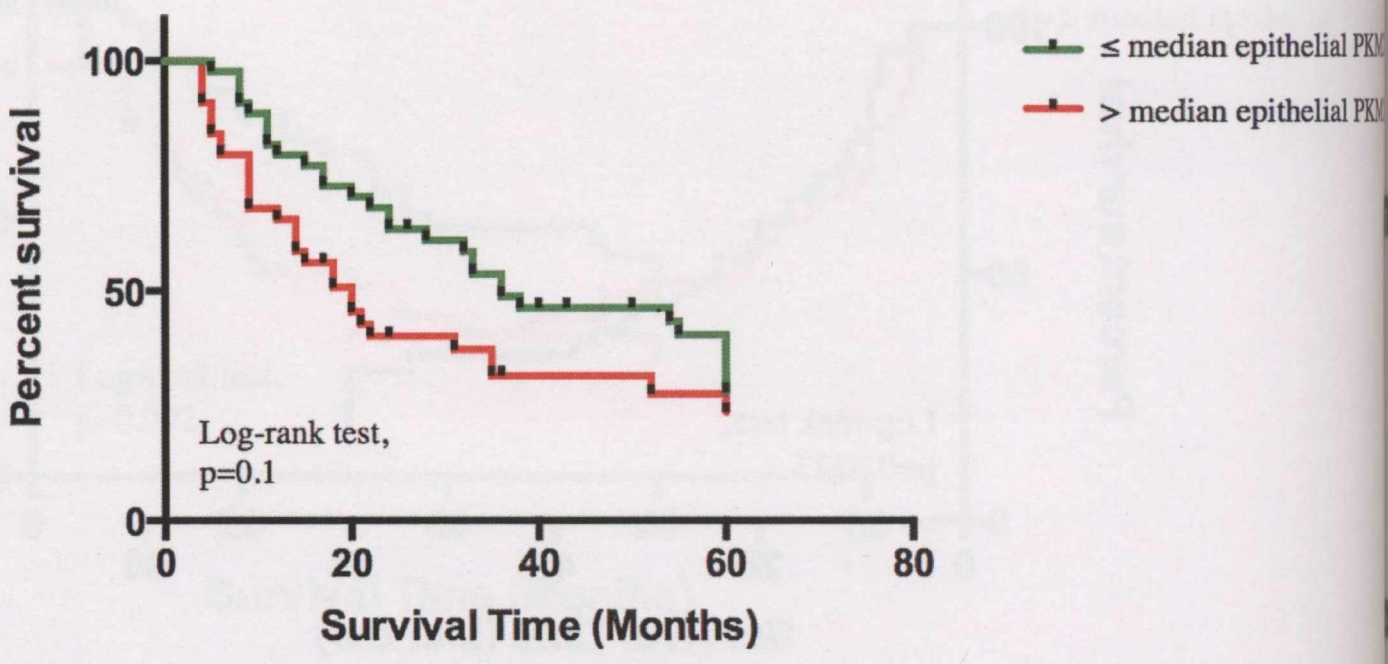


Figure 3.13 Association between epithelial HK1 and HK2 expression and OAC specific 5-year post-operative survival. (A) There was no significant association between epithelial HK1 expression in OAC patients and overall disease-specific post-operative survival (median survival: 24months versus 22 months, p=0.5323). (B) Higher epithelial HK2 expression was significantly associated with poor prognosis (median survival: 35 months versus 12 months, p<0.05) in OAC patients. Statistical test used was Kaplan Meier survival curve with Log-rank (Mantel-Cox) test.

(A)



(B)

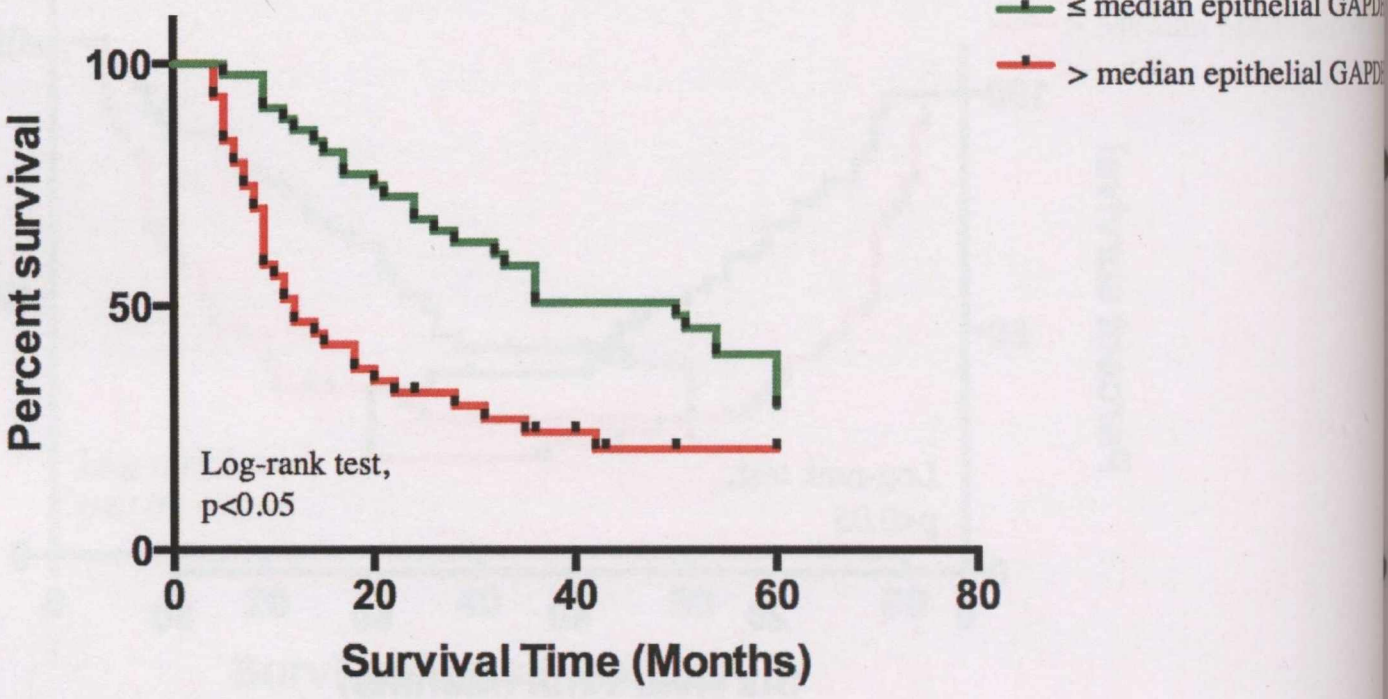


Figure 3.14 Association betweenPKM2 and GAPDH expression and OAC specific survival. (A) There was no significant association between epithelial PKM2 expression in OAC patients and overall disease-specific 5- year post-operative survival (median survival: 26 months versus 18 months, p=0.7519). (B) High epithelial GAPDH expression was significantly associated with poor prognosis (median survival: 36 months versus 15 months, p<0.05). Statistical test used was Kaplan Meier survival curve with Log-rank (Mantel-Cox) test.

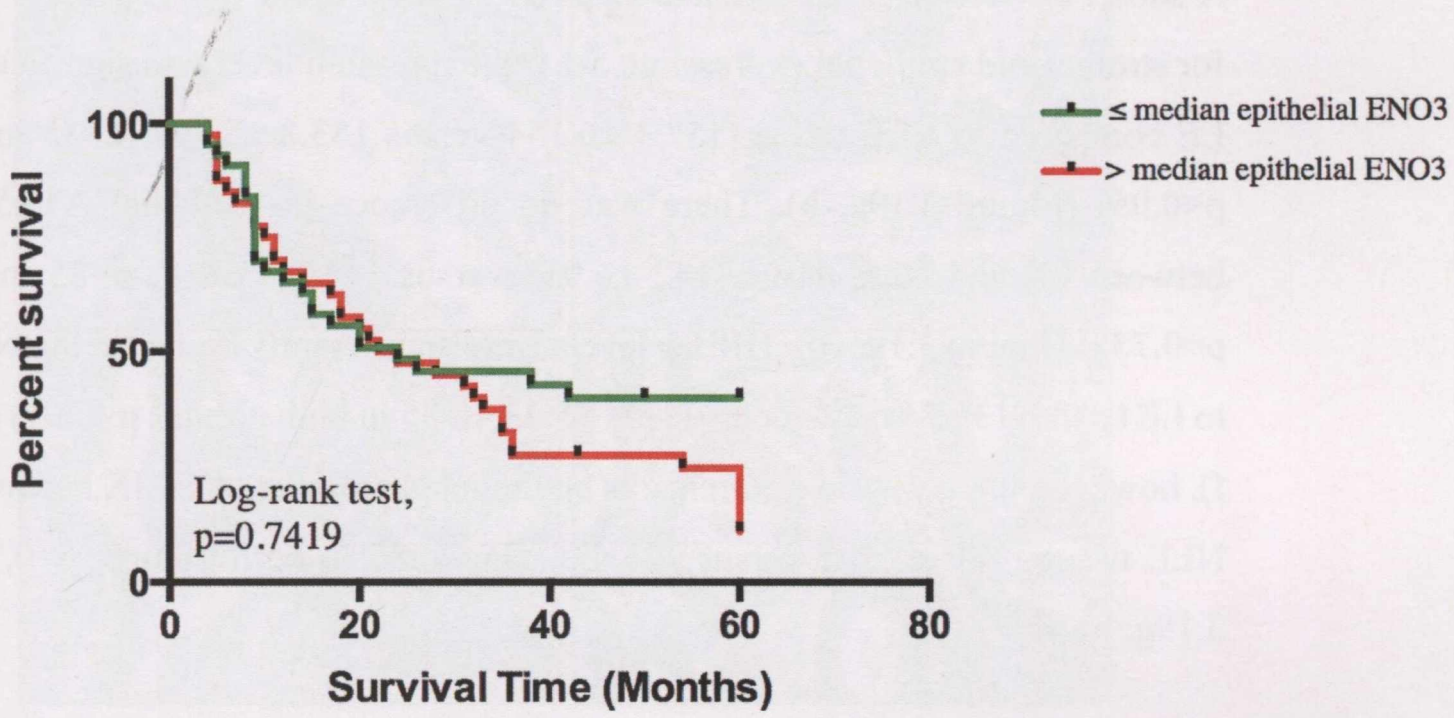


Figure 3.15 Association between ENO3 epithelial expression and disease-specific survival (A) There was no association between the level of epithelial ENO3 expression in OAC patients and overall disease-specific 5- year post-operative survival (median survival: 32 months versus 18 months, p=0.8066). Statistical test used was Kaplan Meier survival curve with Log-rank (Mantel-Cox) test.

3.3.3 Association of markers of hypoxia, oxidative phosphorylation and 5-LOX with clinical parameters in OAC

3.3.3.1 Differential expression of 5-LOX, ATP5B, HIF1A and CAIX and tissue type

OAC tissue microarrays were stained for markers of hypoxia, OXPHOS, and 5LOX. Grading and scoring protocol was identical to the one used in Section 3.3.1. An average tumor epithelial and stromal score was assigned to each patient with an exception of cases where tissue cores were damaged and impossible to score. The intensity score was obtained by scoring the cores between 0 and 3, where 0= negative, 1 = weak, 2=moderate and 3=strong expression. The quantity of positive staining within the tissue microarray core was scored between 0 and 100% in order to obtain the percentage positivity measure. The intensity score and percentage positivity were multiplied giving an overall score for each OAC tumor core between 0 and 300. Representative images for epithelial expression of 5LOX (Figure 3.16), ATP5B (Figure 3.17), HIF1A (Figure 3.18a) and CAIX (Figure 3.18b).

A subset of OAC patients with matched NLE and LE tissue (85/120cases) were analysed for stromal and epithelial expression. 5-LOX expression level was significantly higher in LE compared to NLE tissue (157.3 ±6.154 versus 133.8 ±5.992, n=85 in both groups, $p<0.05$) (Figure 3.19a, b). There was no difference in epithelial ATP5B expression between LE and NLE tissue (142 ±6.915 versus 144.2 ±7.815, n=85 in both groups, $p=0.733$) (Figure 3.19c, d). HIF1A levels were significantly higher in the NLE compared to LE tissue (136.7 ±6.12 versus 113.7 ±5.73, n=85 in both groups, $p<0.05$) (Figure 3.19e, f), however, there was no difference in epithelial expression of CAIX between the LE and NLE tissue (120 ±5.597 versus 136.4 ±6.45, n=85 in both groups, $p>0.7234$) (Figure 3.19g, h).

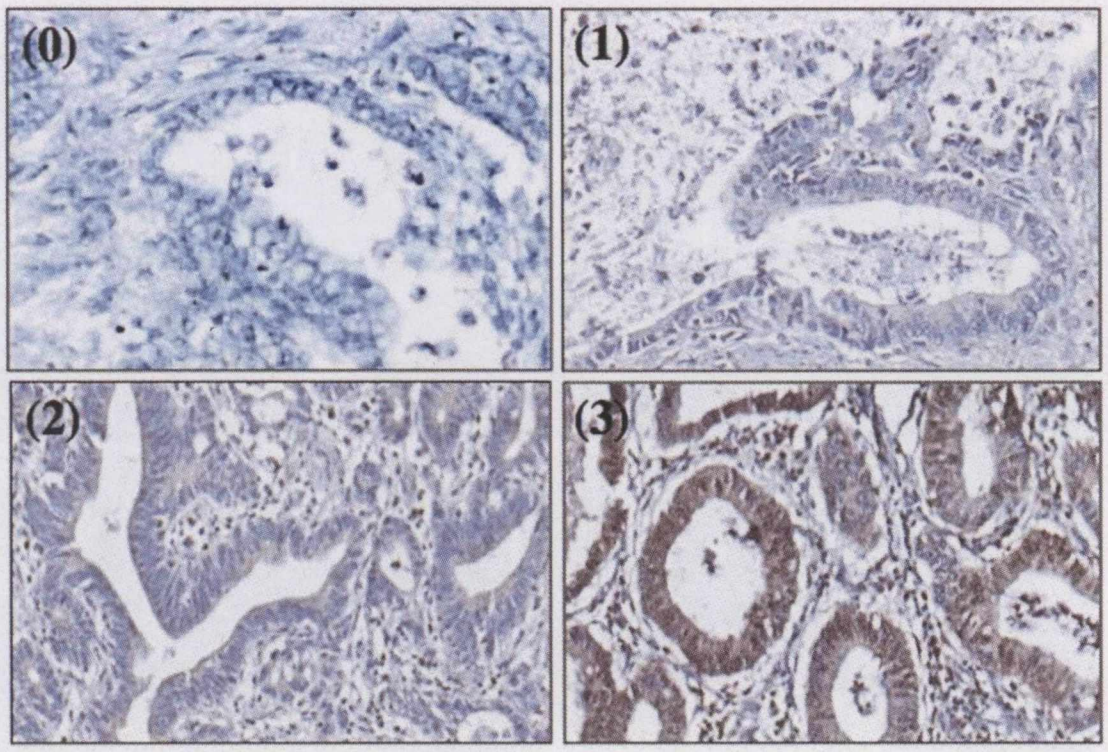


Figure 3.16 Tissue microarray 5-LOX staining pattern in esophageal adenocarcinoma. Following immunohistochemical staining for 5LOX, the intensity score was obtained by scoring the cores between 0 and 3, where 0= negative, 1 = weak, 2=moderate and 3=strong expression. The quantity of positive staining within the tissue microarray core was scored between 0 and 100% to obtain the percentage positivity measure. The intensity score and the percentage positivity were multiplied giving an overall score for each core 0 to 300. Representative images are 10X magnification.

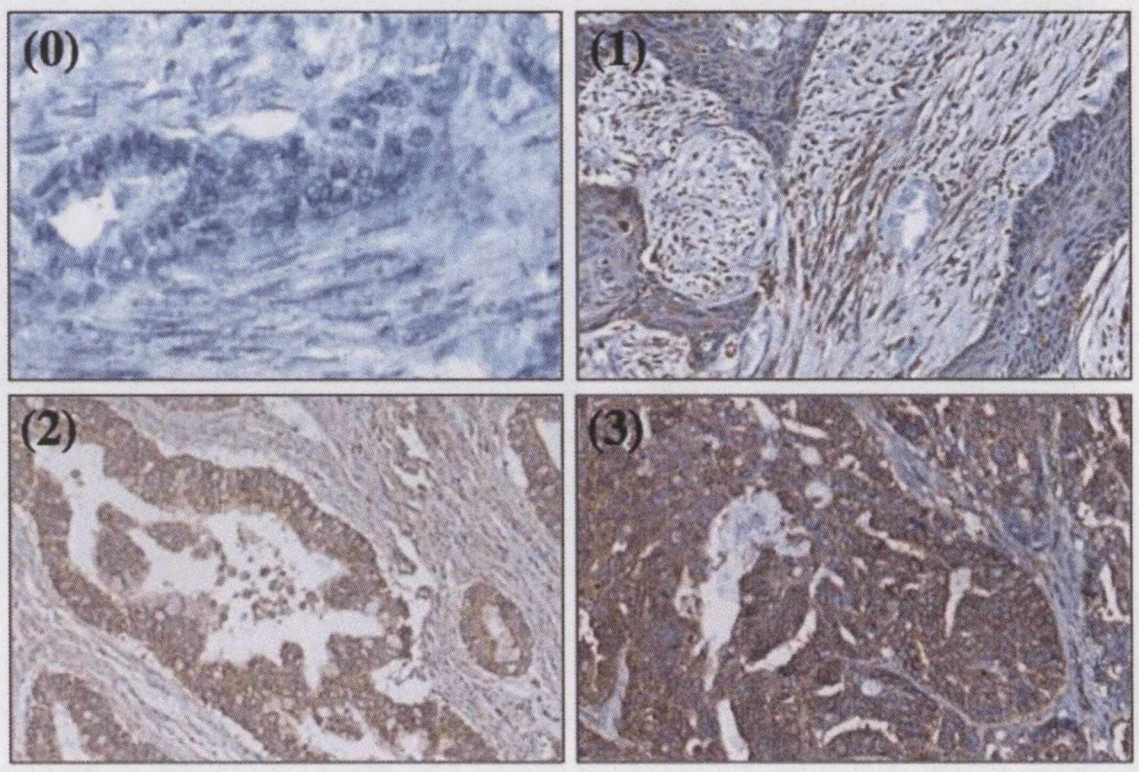


Figure 3.17 Tissue microarray ATP5B staining pattern in esophageal adenocarcinoma. Following immunohistochemical staining for ATP5B, the intensity score was obtained by scoring the cores between 0 and 3, where 0=negative, 1= weak, 2=moderate and 3=strong expression. The quantity of positive staining within the tissue microarray core was scored between 0 and 100% to obtain the percentage positivity measure. The intensity score and percentage positivity were multiplied giving an overall score for each core 0 to 300. Representative images are 10X magnification.

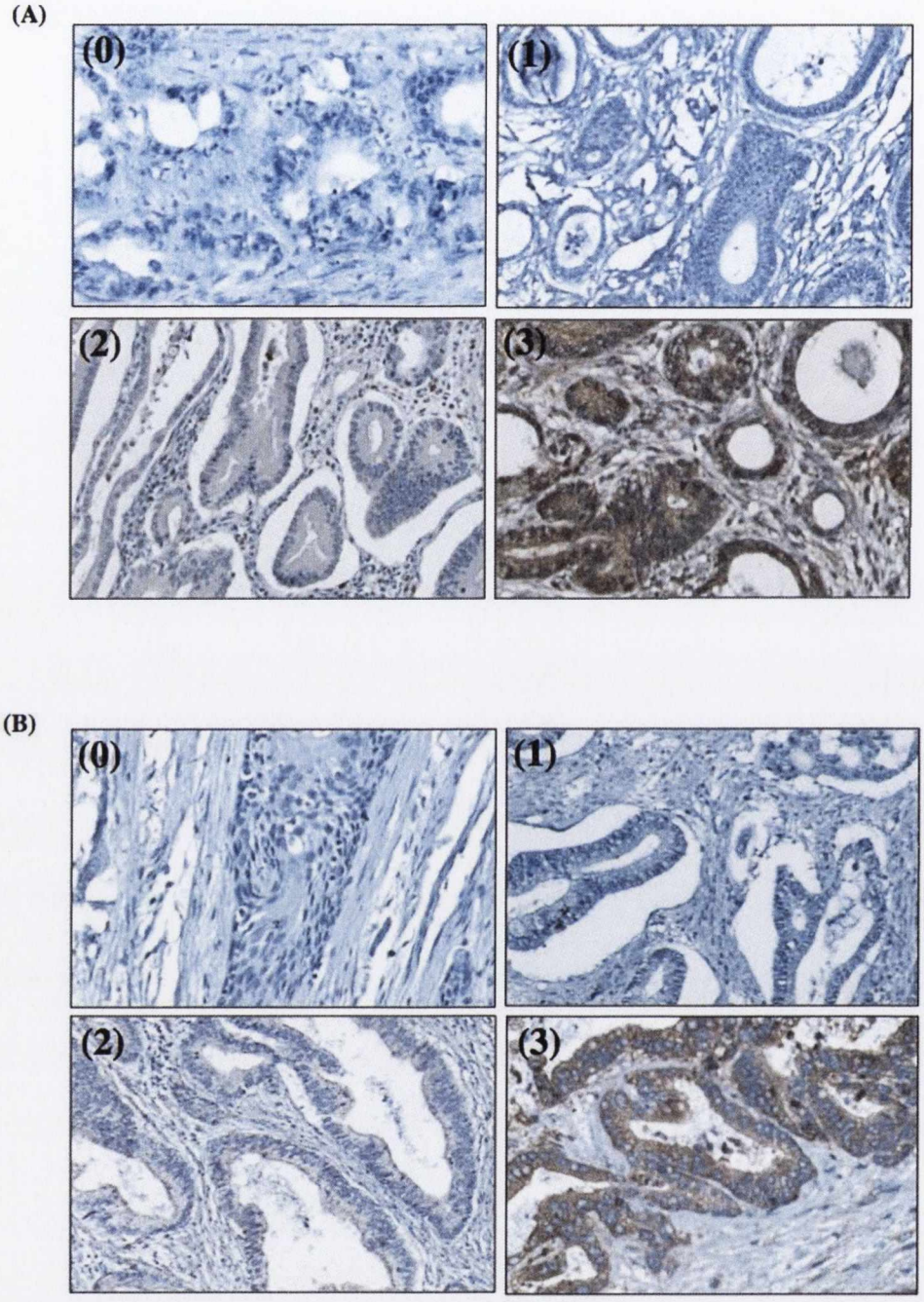


Figure 3.18 Tissue microarray HIF1A and CAIX staining pattern in esophageal adenocarcinoma. Following immunohistochemical staining for (A) HIF1A and (B) CAIX, the intensity score was obtained by scoring the cores between 0 and 3, where 0=negative, 1=weak, 2=moderate and 3=strong expression. The quantity of positive staining within the tissue microarray core was scored between 0 and 100% to obtain the percentage positivity measure. The intensity score and percentage positivity were multiplied giving an overall score for each core 0 to 300. Representative images are 10X magnification.

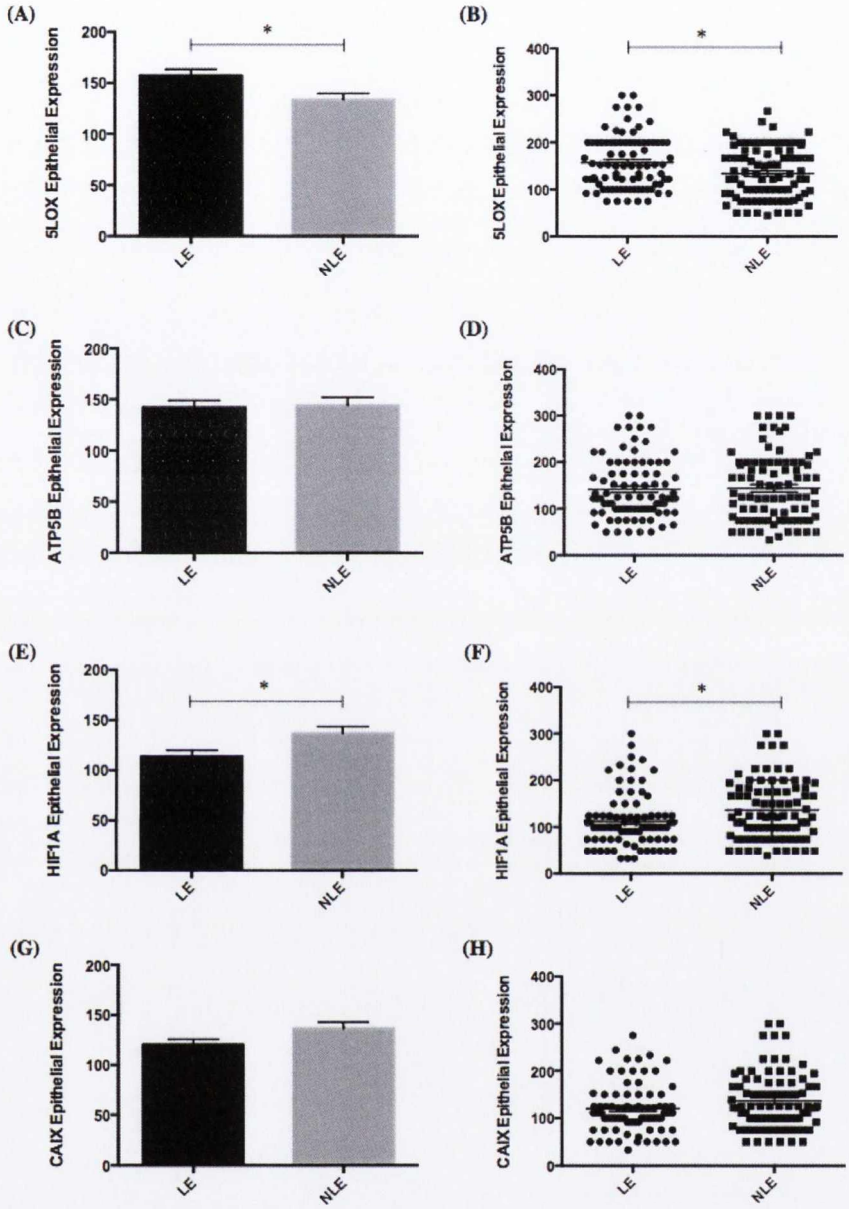


Figure 3.19 Expression of 5-LOX, ATP5B, HIF1A and CAIX at the leading edge versus non-leading edge in esophageal adenocarcinoma. (A) 5-LOX levels were significantly higher in the LE compared to NLE tissue ($p<0.05$). (B) The distribution of 5-LOX expression across OAC patient cores shown by scatter plot. (C) There was no difference in epithelial ATP5B expression between LE and NLE tissue ($p>0.05$). (D) The distribution of ATP5B expression across shown by scatter plot. (E) HIF1A levels were significantly higher in the NLE compared to LE tissue ($p<0.05$). (F) The distribution of HIF1A expression across OAC patient cores shown by scatter plot. (G) There was no difference in epithelial CAIX expression levels between the LE and NLE tissue ($p>0.05$). (H) The distribution of CAIX expression across OAC patient cores shown by scatter plot. Statistical used was Wilcoxon signed rank test. $p<0.05$ (*). Error bar denotes mean ± S.E.M.

3.3.3.2. Association of 5-LOX, ATP5B, HIF1A and CAIX with lymph node involvement in esophageal adenocarcinoma

Expression of markers for hypoxia, oxidative phosphorylation and 5-LOX were correlated with lymph node involvement in OAC. There was no significant difference in epithelial 5-LOX expression in patients with the presence of lymph node involvement compared to lymph node negative patients (162.2 ±7.69 versus 147.4 ±11.39, n=79 versus n=39, p=0.3357) (Figure 3.20a). Significantly higher level of ATP5B was present in lymph node positive OAC tumours (171.8 ±8.398 versus 137.4 ±10.68, n=80 versus n=39, $p<0.01$) (Figure 3.20b). Epithelial expression of HIF1A was significantly higher in the tumours with positive lymph node involvement (183 ±7.67 versus 150 ±11.06, n=80 versus n=39, $p<0.05$) (Figure 3.20c), however, there was no difference between epithelial CAIX expression between OAC tumours that were positive and negative for lymph node involvement (163.8 ±7.105 versus 146.3 ±11.52, n= 79 versus n=39, p=0.3129) (Figure 3.20d).

3.3.2.3. 5-LOX, ATP5B, HIF1A and CAIX expression and their association with venous involvement in esophageal adenocarcinoma

Epithelial expression of 5-LOX, ATP5B, HIF1A and CAIX was correlated with venous involvement in OAC tissue microarrays. HIF1A expression was significantly higher in patients with the presence of venous involvement compared to the patients that showed the absence of venous involvement (177.4 ±10.71 versus 140.6 ±7.988, n=69 versus n=47, $p<0.01$) (Figure 3.21c). However, there was no association between epithelial expression of 5LOX, ATP5B and CAIX in OAC patients with the venous involvement compared to the OAC patients with the absence of venous involvement (170.0 ±9.847 versus 154.0 ±7.89, p=0.1704, 162.5 ±9.728 versus 148.7 ±7.638, p=0.2603 and 177.5 ±9.9862 versus 159.1 ±8.647, p=0.1678 respectively) (Figure 3.21a, Figure 3.21b, Figure 3.21d respectively).

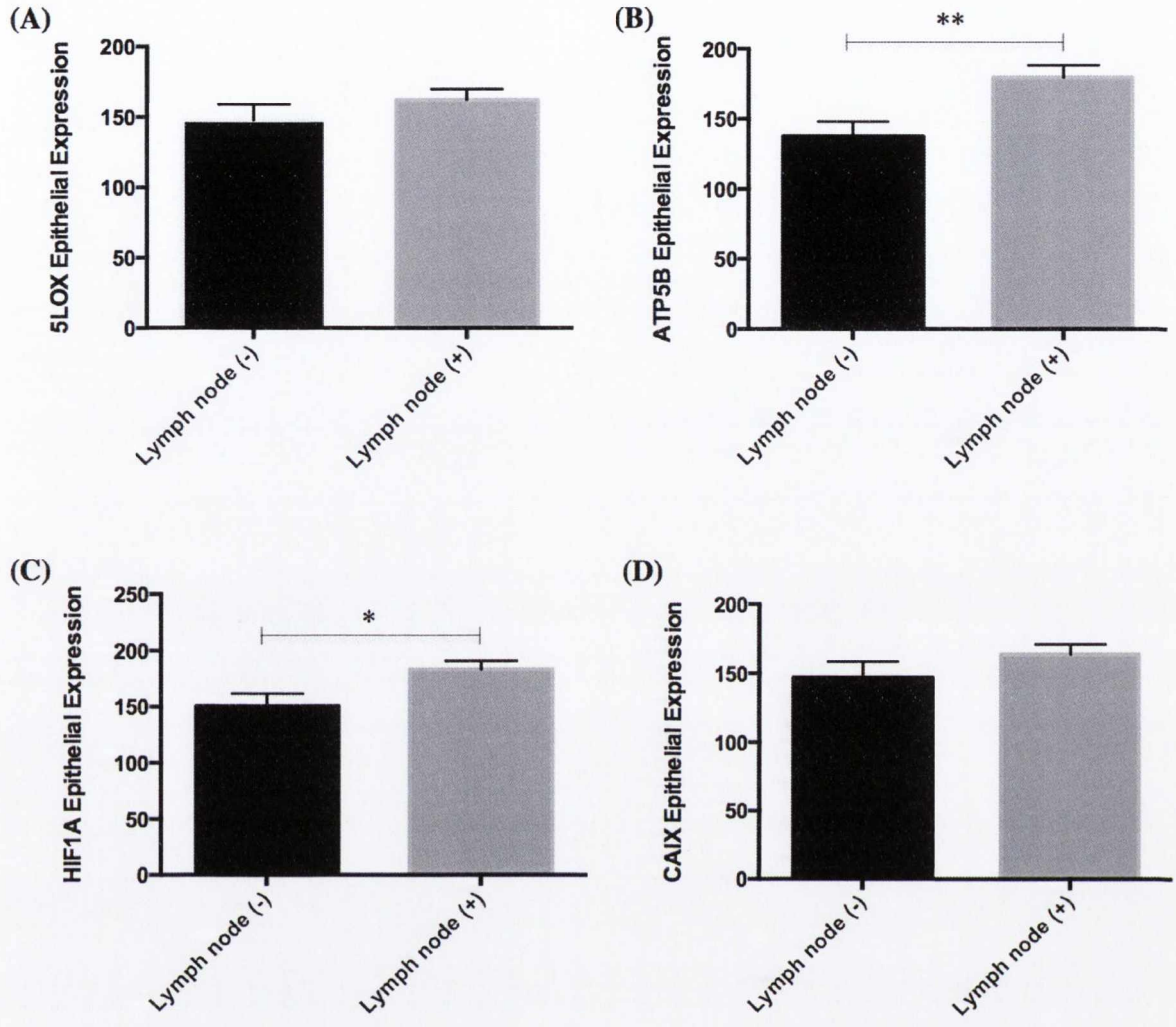


Figure 3.20 Epithelial expression of hypoxia and OXPHOS markers and their association with tumor aggressiveness in OAC. (A) There was no significant difference in epithelial 5-LOX expression in lymph node positive versus lymph node negative tumours ($p>0.05$). (B) Significantly higher levels of ATP5B were present in lymph node positive tumours ($p<0.01$). HIF1A levels were significantly higher in OAC tumours with positive lymph node involvement ($p<0.05$). (D) There was no difference in epithelial CAIX expression between lymph node positive versus lymph node negative tumours ($p>0.05$). Statistic test used was Mann Whitney U test $p<0.05$(*), $p<0.01$(**). Error bar denotes mean ± S.E.M.

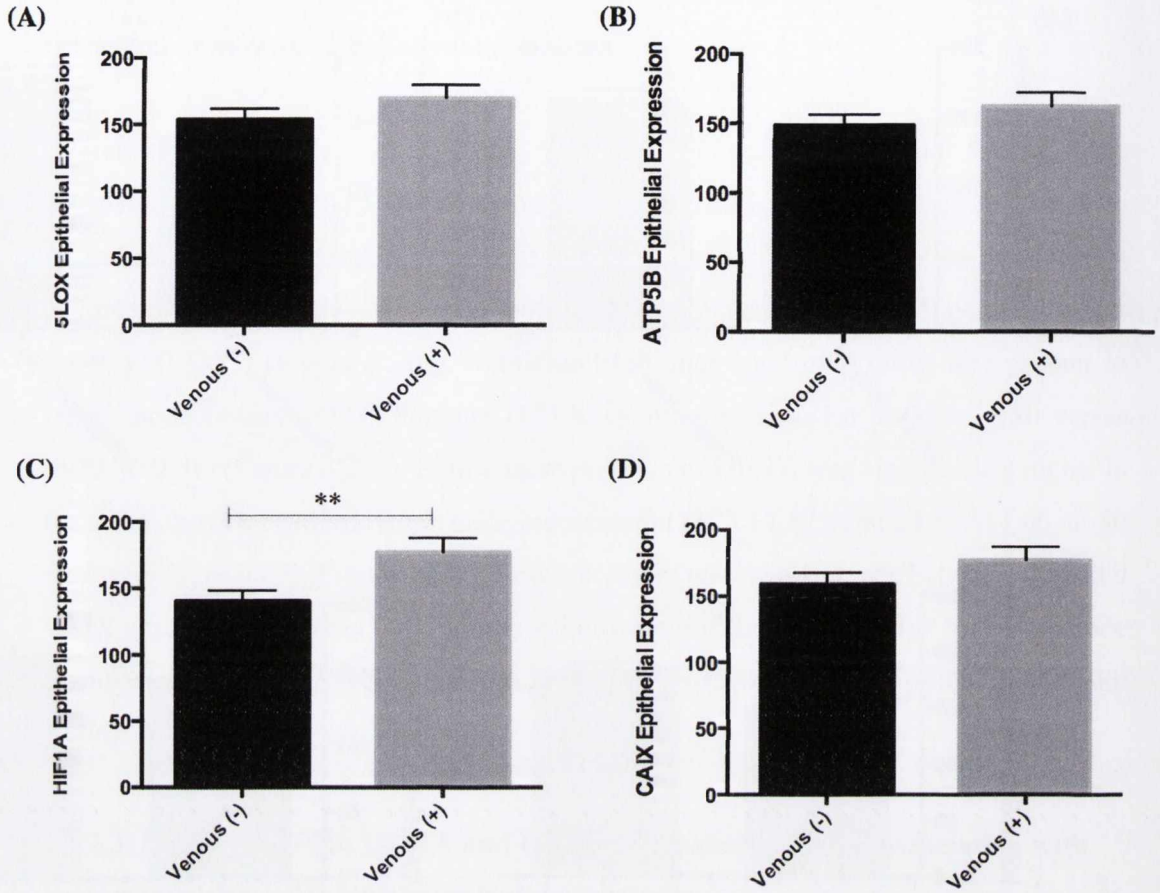


Figure 3.21 Epithelial expression of 5-LOX, hypoxia and OXPHOS markers and their association with venous involvement in OAC patients. (A) and (B) There was no association between epithelial expression of 5-LOX and ATP5B and venous involvement in OAC patients (p=0.1704 and p=0.2603 respectively, n=69 versus n=47). (C) An increase in HIF1A epithelial expression was associated with venous involvement in OAC tumours ($p<0.01$, n=69 versus n=47). (D) There was no association with epithelial CAIX expression and venous involvement in OAC tumours (p=0.1678, n=47 versus n=69). Statistic test used was Mann Whitney U test $p<0.01$(**). Error bar denotes mean ± S.E.M.

3.3.3.4 Association between 5-LOX, ATP5B, HIF1A and CAIX with metabolic tumor activity (PET SUV)

In collaboration with Dr. Vinod Malik in St. James's hospital, we investigated whether there was an association between 5LOX, ATP5B and hypoxic markers HIF1A and CAIX and metabolic tumor activity in OAC patients. Following grading and scoring OAC tissue microarrays, epithelial expression of these markers was correlated with SUVmax measurement for these patients. There was a significant correlation between epithelial 5LOX expression and the measure of tumor metabolism, SUVmax ($r=0.3344$, $p<0.05$) (Figure 3.22a). There was no correlation between ATP5B and increased metabolic tumor activity in this cohort of OAC patients ($r=0.0558$, $p=0.7015$) (Figure 3.22b). There was a significant positive correlation between epithelial expression levels of hypoxic marker HIF1A and SUVmax ($r=0.3465$, $p<0.05$) (Figure 3.22c). However, there no positive association between CAIX and increasing metabolic tumor activity. We observed a significant negative correlation between epithelial expression CAIX and SUVmax in OAC patients ($r=-0.3381$, $p<0.05$) (Figure 3.22d).

3.3.3.5 Epithelial expression of 5LOX, markers of hypoxia and OXPHOS and their association with disease-specific survival

Following grading OAC tissue microarrays, the grade for each marker was divided into greater and less than the median value, and disease specific survival was investigated by Kaplan-Meier survival analysis (Figures 3.23 -3.24). High epithelial 5LOX expression was significantly associated with poor overall survival ($p<0.05$) (Figure 3.23a). There was no association between PKM2 expression levels and overall survival in this cohort of OAC patients ($p=0.7972$) (Figure 3.23b). Epithelial HIF1A expression levels above the median value were associated with significantly reduced 5-year disease-specific survival in OAC patients ($p<0.01$) (Figure 3.24a), however, there was no association between epithelial expression level of CAIX and disease-specific survival in OAC patients ($p=0.558$) (Figure 3.24b).

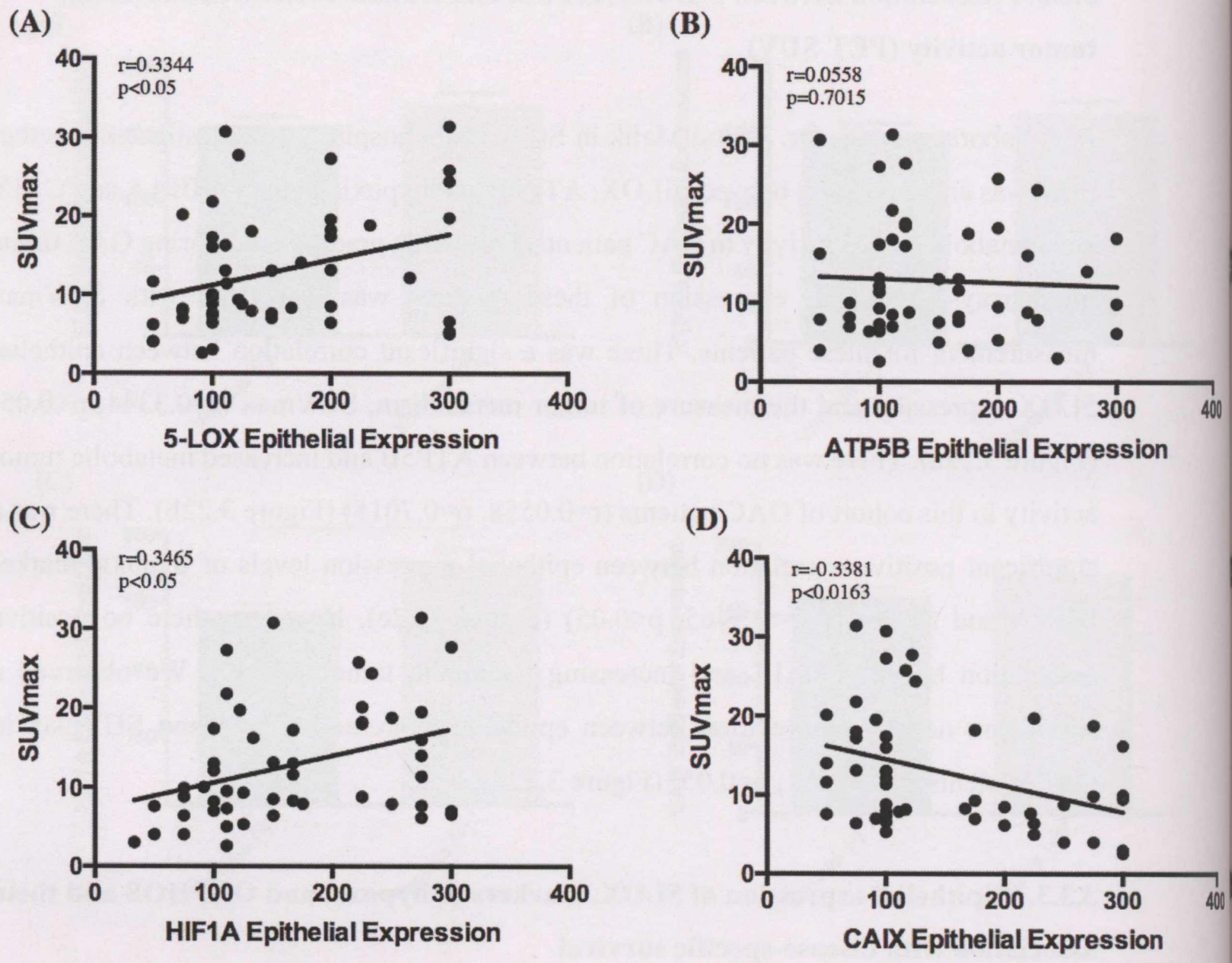
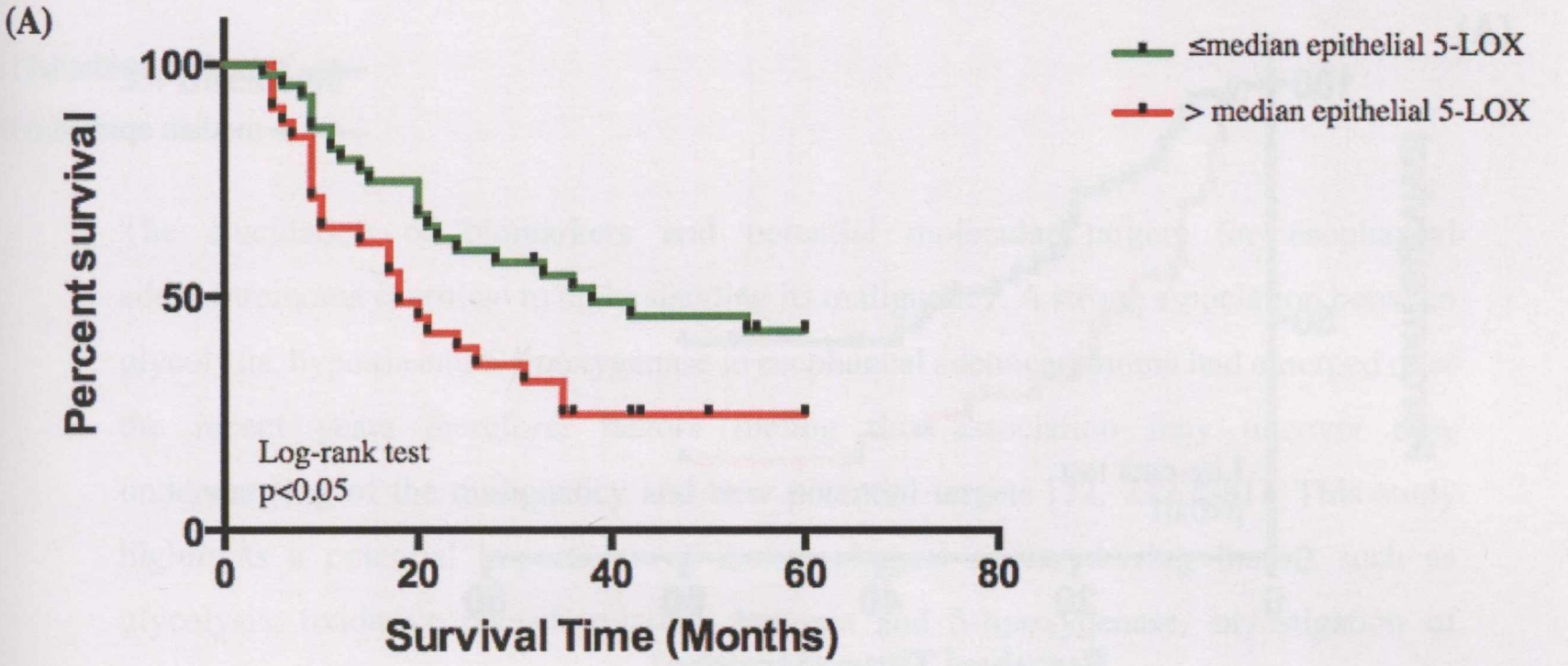


Figure 3.22 Association between 5LOX, ATP5B, HIF1A, CAIX and tumor metabolism in OAC tissue microarrays. (A) There was a significant correlation between epithelial 5LOX expression and the measure of tumor metabolism, SUVmax ($r=0.3344$, $p<0.05$). (B) There was no association between ATP5B and SUVmax ($r=0.0558$, $p=0.7015$). (C) There was a significant positive correlation between epithelial expression of HIF1A and SUVmax ($r=0.3465$, $p<0.05$). (D) There was a significant negative correlation between epithelial expression CAIX and SUVmax in OAC patients ($r=-0.3381$, $p<0.05$). $p<0.05$(*). Statistical test used was Spearman's test.



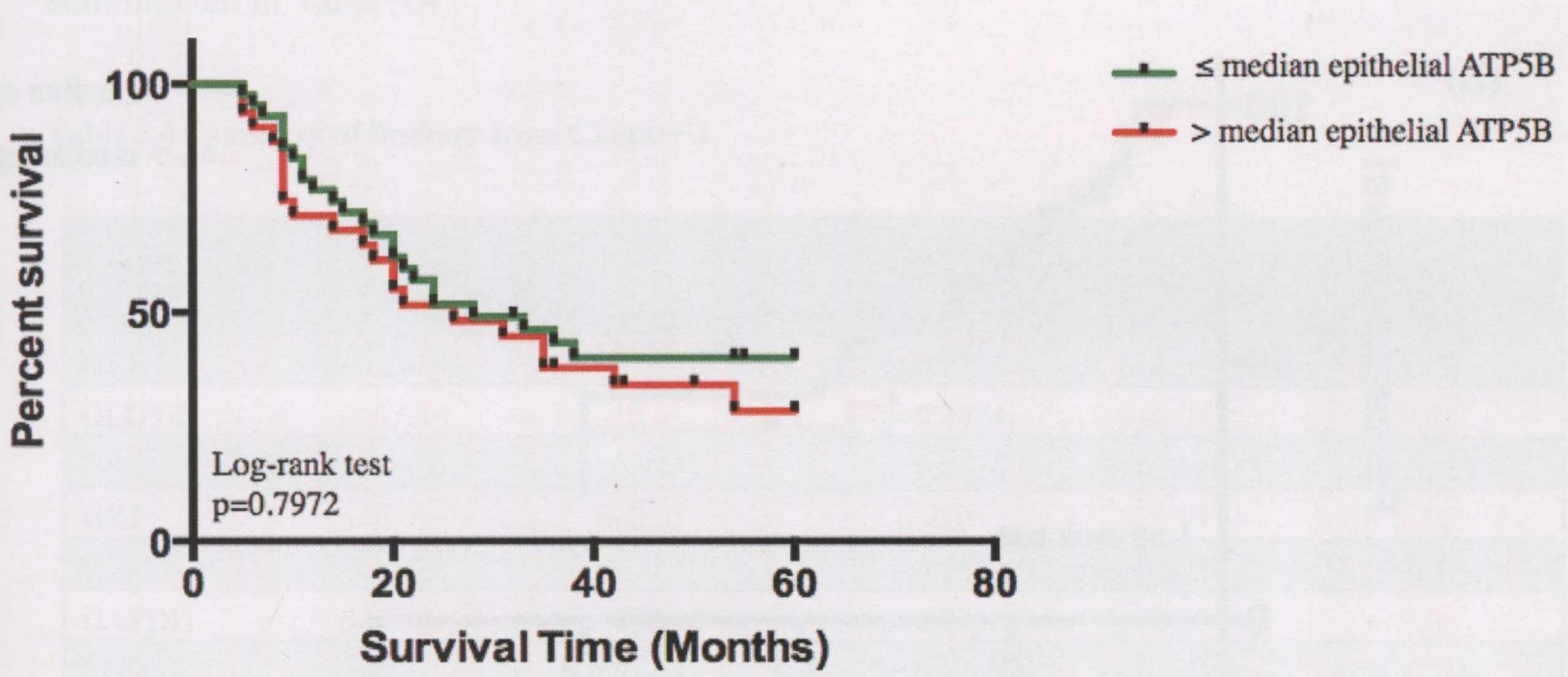


Figure 3.23 Association between 5LOX and ATP5B expression and OAC specific survival. (A) There was a significant association between high epithelial 5LOX expression in OAC patients and reduced overall disease-specific 5-year post-operative survival ($p<0.05$). (B) There was no association between the expression of ATP5B and overall survival ($p>0.05$). Statistical test used was Kaplan Meier survival curve with Log-rank (Mantel-Cox) test.

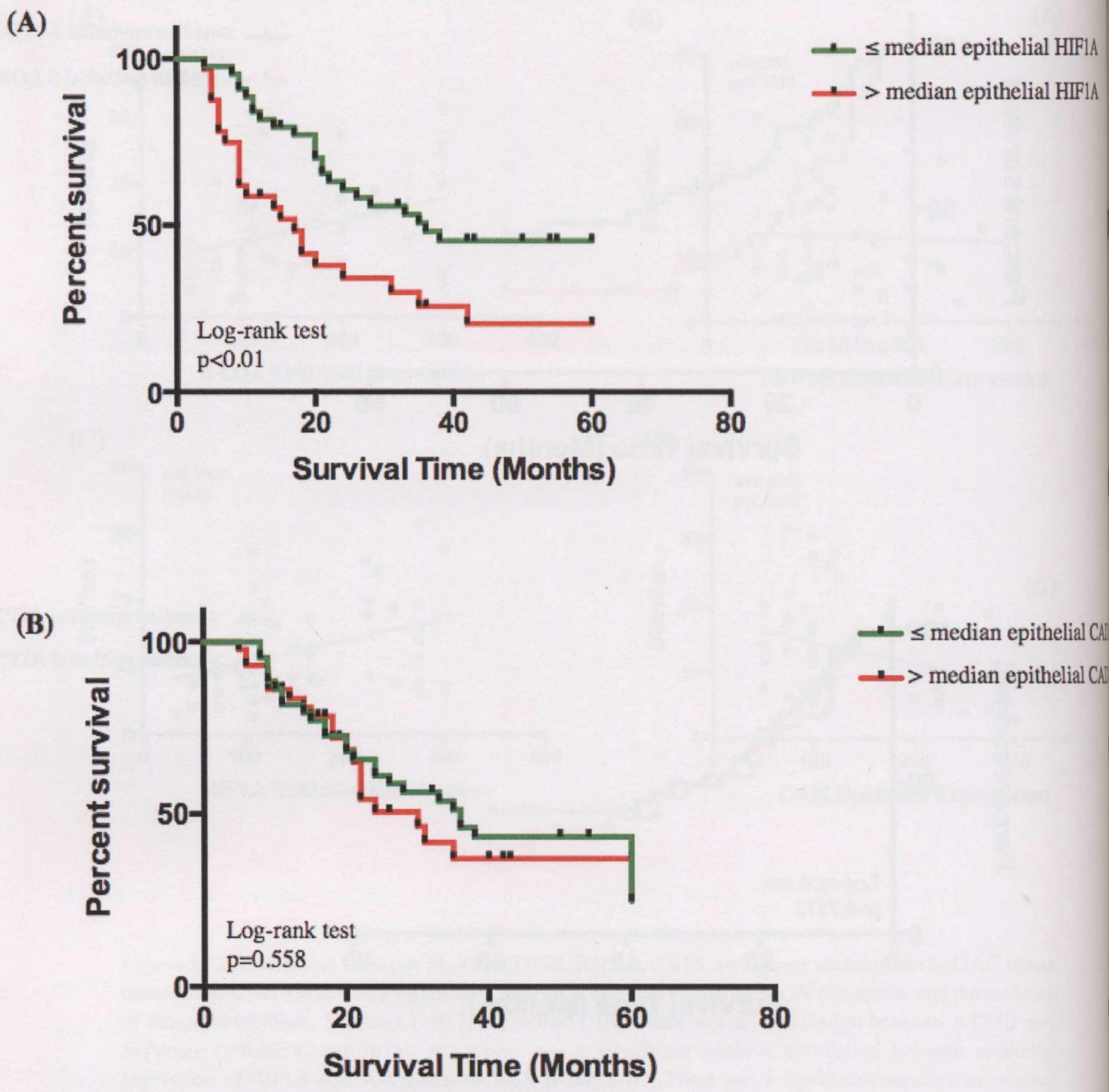


Figure 3.24 Association between HIF1A and CAIX expression and OAC specific survival. (A) There was a significant association between high epithelial HIF1A expression in OAC patients and reduced survival ($p<0.01$). (B) There was no association between the expression of CAIX and OAC patient overall disease-specific survival ($p>0.05$). Statistical test used was Kaplan Meier survival curve with Log-rank (Mantel-Cox) test.

3.4 Discussion

The elucidation of biomarkers and potential molecular targets for esophageal adenocarcinoma is critical to understanding its malignancy. A strong association between glycolysis, hypoxia and 5-lipoxygenase in esophageal adenocarcinoma had emerged over the recent years therefore, factors fueling this association may uncover new understanding of the malignancy and new potential targets [72, 212, 281]. This study highlights a potential importance of the esophageal cancer driving factors such as glycolysis, oxidative phosphorylation, hypoxia and 5-lipoxygenase. Investigation of glycolytic markers in esophageal adenocarcinoma tissue microarrays revealed their potential contribution to the outcome of the disease. All findings from this study were summarized in Table 3.4

Table 3.4 Summary of findings from Chapter 3.

Marker	Tissue type (LE vs NLE)	Lymph node Involvement	Venous Involvement	SUVmax	OAC – specific Survival
GLUT1	p=0.2839	p<0.05	p=0.7536	p=0.33	p=0.092
GLUT4	p<0.05	p<0.05	p=0.3924	p<0.01	p<0.05
HK1	p=0.0553	p=0.9739	p=0.4526	p=0.3289	p=0.5323
HK2	p<0.05	p<0.05	p<0.05	p<0.01	p<0.05
PKM2	p=0.4986	p=0.4648	p=0.7308	p=0.3236	p=0.1
GAPDH	p<0.05	p=0.2948	p=0.1022	p=0.07	p<0.05
ENO3	p=0.7347	p=0.1832	p=0.1763	p=0.3641	p=0.7419
5LOX	p<0.05	p=0.1856	p=0.1704	p<0.05	p<0.05
ATP5B	p=0.9027	p<0.01	p=0.2603	p=0.7015	p=0.7972
HIF1A	p<0.05	p<0.05	p<0.05	p<0.05	p<0.01
CAIX	p=0.0858	p=0.1376	p=0.1678	p<0.05	p=0.558

This study investigated the role of two glucose transporter proteins GLUT1 and GLUT4. GLUT1 has been shown to be expressed in many epithelial malignancies [203] including SCC and a high expression of this glucose transporter has been shown to be positively associated with depth of invasion and vascular invasion, leading to patients poor prognosis and overall survival in colorectal cancer [282]. In this particular cohort of OAC patients, epithelial GLUT1 expression was significantly associated with lymph node

involvement suggesting the association between GLUT1 expression and more aggressive cancer type, however, an increase in epithelial GLUT1 expression did not have any association with cancer-specific survival. GLUT4, the second glucose transporter of interest in this study, has been shown to display an interesting connection with cancer due to an ability of p53, a tumor suppressor protein, to transcriptionally repress GLUT4, making GLUT4 an attractive target in many cancer types including breast, lung and gastric cancer [283]. In this study, a significant increase of GLUT4 expression in the leading edge of the tumor was observed. Unlike the center of cancer which may have a relatively poor blood supply, resulting in hypoxic environment and relatively low metabolic activity, the leading edge of the tumor, also called an invasive front of a tumor, has a high oxygen and nutrient supply from both normal vasculature and the co-opted blood supply, enabling the tumor to grow and thrive [284]. The leading edge of cancer has been shown to be an area where cancer progression could potentially be stopped by an adequate immune response of the host, however in more aggressive cancers the host response often fails allowing tumor to spread to the rest of the body [285], therefore an increase of GLUT4 expression in the invasive edge of the tumor suggested it's potential role in the spread of cancer, therefore suggested it as an attractive potential target in OAC. Additionally, results revealed that high epithelial GLUT4 expression was associated with lymph node involvement in OAC patients, therefore suggested an association of high GLUT4 expression and cancer aggressiveness [286]. Interestingly, there was a significant positive correlation between GLUT4 expression and metabolic tumor activity measured by standardized uptake value (SUVmax). SUVmax measurement has been reported to be a reliable and accurate measuring tool in evaluating metabolic tumor activity and metastases [287, 288]. Following a single infection of glucose analogue fluorodeoxyglucose (FDG), metabolic tumor activity can be quantified by assigning a FDG standardized uptake value [289, 290]. It has been previously shown that the more aggressive, metastatic tumours are associated with high FDG uptake therefore higher SUVmax in non-small cell lung cancer (NSCLC) and breast cancer [291, 292]. This evidence suggested that GLUT4 was highly expressed in metabolically active, aggressive and metastatic tumours, hence in this study, an increase in epithelial GLUT4 expression was associated with poor disease-free survival. To conclude, both glucose transporters show a role in OAC however, in this cohort of patients GLUT1 showed less association with OAC, possibly because GLUT1 has been shown to be the major glucose transporter found in most cells [200] and GLUT4 has been shown to be expressed in insulin-

responsive tissues and white and brown adipose tissue [293], therefore exhibiting more significant association in our cohort where a large proportion of patients were obese and were potentially associated with an increased glycolytic activity.

The role of two hexokinases, HK1 and HK2, in OAC was investigated in this study. They have been shown to be structurally and functionally similar to each other [294], however, in this cohort of OAC patients, HK1 showed no differential expression in the different tissue type (LE versus NLE), nor the link with tumor aggressiveness (lymph node and venous involvement), no association with tumor metabolism (the uptake or FDG) or overall disease-specific survival of OAC patients. Published studies show HK1 to be one of the key regulators in glycolysis and oncogenic markers in cancers [295] and its expression has been shown to be associated with disease progression, invasion, poor survival of patients with esophageal cancer [212]. However, in our cohort of OAC patients, there was no significant association with any of the above. On the other hand, HK2 (that has been shown to be structurally similar to HK1), in this immunohistological study it was significantly associated with all clinical parameters of interest. High HK2 expression was observed in the invasive edge of the tumor, was associated with nodal and venous involvement therefore suggesting its link with tumor aggressiveness. It was also positively correlated with high FDG uptake, suggesting a high metabolic tumor activity and most importantly, high HK2 expression was associated with poor prognosis and disease-specific survival in this cohort of OAC patients. This could potentially be linked with the specificity of the tissue where the enzymes were expressed. HK1 has been shown to be ubiquitously expressed in the majority of adult tissues, whereas HK2, similarly to GLUT4, has been shown to be expressed in high level in adipose tissue [294], therefore potentially due to its area of expression (adipose tissue) it may be exhibiting more significant effect in this cohort of patients. HK2 has been shown to have a prognostic value in human glioblastoma and hepatocellular carcinoma, however, the role of HK2 in esophageal adenocarcinoma has not been previously published. This novel finding forms basis for further studies looking at the link between HK2 expression and obesity and the benefit of therapeutic targeting HK2 in esophageal adenocarcinoma.

PKM2 has been selected for this study based on the literature and the evidence of PKM2 involvement in cancers including esophageal cancer [217]. PKM2 has also been shown to be the key enzyme in catalyzing the final glycolysis reaction, which is expressed mainly in proliferative cells, especially in cancer cells [296]. The results of this study contradict the results of other studies as there was no significant association between

PKM2 and disease phenotype, progression or disease-specific survival in this particular cohort of OAC patients. PKM2 has been shown to have multiple roles, and the intracellular mechanisms induced by PKM2 were more complicated than previously hypothesized [269]. Studies in prostate and colon cancer had suggested PKM2 as a potential biomarker, however, the use of PKM2 as a biomarker has been shown to be controversial and additional studies are required for confirmation [269]. Some contradictory studies report that knockdown of PKM2 resulted in a modest inhibitory effect on *in-vitro* proliferation of cancer cells and xenograft tumors without any signs of inhibition, which indicates that PKM2 is not a requirement for tumor growth [269].

GAPDH has been shown to be glycolytic enzyme catalyzing the reversible conversion of glyceraldehyde-3-phosphate to 1,3-diphosphoglycerate [297]. A Bioinformatics Group in the European Molecular Biology Laboratory in Germany used NIH public database to investigate the expression of GAPDH in a number of cancers. They have shown that GAPDH was overexpressed in 24 types of cancer including brain, testicular, prostate, gastric cancers [225]. In this study, GAPDH was significantly higher expressed in the invasive edge of the tumor suggesting its potential role as a target to avoid cancer spreading into surrounding tissues. High GAPDH expression was also associated with poor patient prognosis and disease-specific survival. This result was supported by a recent prospective study by Hjerpe *et al* where the link between the expression levels of GAPDH and disease prognosis and response to treatment in 62 ovarian adenocarcinoma patients as they reported that high GAPDH expression was associated with early disease progression, shorter platinum free interval (PFI) and poor overall survival in patients with advanced high-grade serous adenocarcinomas of the ovary, fallopian tube or peritoneum [234]. To conclude, their findings were supported in another cancer type in a study by Revillion *et al* where 404 breast cancer patients were assessed and the study revealed that GAPDH was not an independent prognostic factor but GAPDH expression in breast cancer seemed to reflect tumor aggressiveness [235].

ENO3 enzyme was of interest in this study as it has been previously shown to be responsible for catalysing the reversible conversion of 2-phosphoglycerate to phosphoenolpyruvate. It has been associated with energy metabolism in cancer cells, however, very limited research was available [271]. In a pilot study, in St. James's hospital, ENO3 has been shown to be significantly upregulated in obese and overweight

compared to normal weight OAC patients at the gene level (by qPCR analysis) therefore we hypothesised that potentially the glycolytic activity of this enzyme was obesity-induced therefore was of interest. In this study, there was no association between ENO3 and any of the clinical parameters of interest. Published literature concentrates on two other isoforms of Enolase, ENO1 and ENO2, and their role in cancer [298], however based on our pilot study and potential association of ENO3 and obesity, we included ENO3 for further analysis in follow-up studies.

5-LOX has been shown to have a role in various cancers including colorectal and esophageal cancers [87, 299]. In this study, a significantly higher epithelial 5LOX expression was observed in the invasive edge of the tumor suggesting a pro-inflammatory role of 5LOX in OAC. The link between inflammation and 5LOX has been previously described by delineating the biological functions of leukotrienes, 5LOX biological products, with their main function being described as pro-inflammatory mediators in the activation of the NF-κB pathway [300]. High epithelial expression of 5-LOX was associated with poor prognosis and significantly lower OAC-specific survival suggesting that this potentially pro-inflammatory enzyme is an attractive immunological and druggable target in OAC.

ATP5B gene has been shown to encode a subunit of mitochondrial ATP synthase. Previous research from St. James's hospital demonstrated that oxidative phosphorylation and glycolysis were reprogrammed early in the inflamed Barrett's disease sequence and may act mutually to promote disease progression in Barrett's oesophagus [247]. They also showed that high levels of ATP5B segregated Barrett's patients who progressed to HGD/OAC from non-progressors, highlighting the possible prognostic advantage of assessing metabolic profiles in these pre-neoplastic patients [247]. In this immunohistological OAC study, ATP5B was associated with nodal involvement therefore was potentially associated with more aggressive disease phenotype. This result is in line with the previous BO study where the progressors from BO to OAC have shown an increase of ATP5B suggesting an association with a more aggressive phenotype.

HIF-1A has been shown to be a major regulator of oxygen homeostasis within cells and it is a regulator of anaerobic metabolism [276]. In this study, high HIF1A expression was significantly associated with all clinical parameters of interest. Differently to all other markers described above, it was expressed at significantly higher levels in NLE of tumor than the invasive edge suggesting its role in hypoxia, as it has been well documented that

oxygen levels, blood and nutrient supply was lower in the core of the tumor compared to the surrounding tissues [301, 302]. High HIF1A expression was significantly associated with nodal and venous involvement suggesting its role in tumor aggressiveness. High expression was also positively correlated with high FDG uptake suggesting a more aggressive cancer type [303] and most importantly, high HIF1A expression was significantly associated with overall poor prognosis and significantly reduced 5-year disease-specific survival in this cohort of OAC patients. These findings were in line with studies in other types of cancer, for example, an immunohistochemical study by Baba *et al* where the link between HIF1A and disease prognosis was shown in 731 colorectal cancer and HIF1A expression was significantly associated with shorter colorectal cancer-specific survival and overall survival [272].

Carbonic anhydrase IX (CAIX) has been shown to be a hypoxia-inducible enzyme overexpressed by cancer cells in various tumor types [275]. A number of recent immunohistochemical studies have examined the expression of CAIX in cohorts of hundreds to thousands of patients and CAIX has been validated as a biomarker of poor prognosis [304] including studies by Lou *et al* in 3630 breast cancer patients [305], Illie *et al* in 555 NSCLC patients [306], Chochzik *et al* in 205 ovarian cancer patients [307], Klatte *et al* in 340 bladder cancer patients [308], indicating the suitability of CAIX as a biomarker in these cancer types [309]. In this study, there was no association between CAIX and any of the clinical parameters of interest. There was no indication of CAIX having an effect on OAC-specific survival, therefore despite all the evidence in the literature, in this particular cohort of OAC patients, it was not indicative of the patient outcome and could not be used as a biomarker of the disease. Due to high HIF1A expression in this cohort we hypothesized that CAIX, hypoxia-inducible enzyme should be upregulated in the hypoxic regions therefore positively correlate with HIF1A expression, however this hypothesis failed. The possible explanation that the CAIX antibody had a large level of non-specific binding therefore altering the outcome of the study.

With all the significant findings from this study (Table 3.4) and past studies in mind, we conclude that glucose transporter proteins, markers of glycolysis, oxidative phosphorylation, hypoxia and 5-lipoxygenase contribute to the outcome of esophageal adenocarcinoma in this cohort of patients. It is important to note that univariate analysis was performed in this study. In order to have a better understanding whether significant

alterations are seen when a combination of factors are considered, multivariate analysis will be performed. However, when stage of tumor was taken into consideration and expression of markers was compared between different tumor stages, we seen no significant differences. Therefore, stage of tumor had no influence on levels of expression of markers of tumor metabolism, hypoxia and 5LOX in this cohort of patients.

The aim of the follow up study is to investigate the association of all of these markers with obesity.

Chapter 4

The link between glycolysis, OXPHOS, 5LOX and obesity in esophageal adenocarcinoma

4.1 Introduction

Overweight and obesity are linked to increased incidence and mortality in multiple cancer types and increases in body mass index (BMI) and increases in BMI over the lifetime are associated with a higher risk of cancer [110-112]. The earliest reports about a possible link between obesity and esophageal adenocarcinoma were published in the mid 1990's [5]. Current research predominantly shows that obesity, visceral obesity in particular, can alter tumor metabolism, therefore is associated with poor prognosis in patients in different cancers, including esophageal adenocarcinoma [103].

In the clinical setting, obesity is measured by BMI or visceral fat area (VFA) by a computed tomography (CT) scan [310]. Given the accuracy in determining the distribution of body fat, CT measurement of visceral adiposity is considered to be the gold standard [126]. The importance of using VFA measurement rather than BMI in central obesity studies, where the focus is metabolically active fat, is outlined in Chapter 5.

It has been shown that metabolically active fat is able to produce and secrete inflammatory cytokines by adipocytes or infiltrating macrophages [311]. Therefore adipose tissue is an important initiator of the microenvironment favorable for tumor development [146]. As a result of expanding adipose tissue, enlarged adipocytes become distant from the vasculature resulting in hypoxic regions and subsequently necrosis. Adipose tissue hypoxia is considered to underlie the inflammatory response [312]. Hypoxia-inducible factor (HIF1A), the regulator of oxygen homeostasis, is increased in the adipose tissue of obese patients and its expression is reduced following weight loss [150]. Similarly to the hypoxia-induced events in tumor tissue, adipose tissue hypoxia is also associated with the presence of macrophages, which migrate to the hypoxic regions and alter their expression profile increasing inflammation [146].

HIF1A is overexpressed in many solid tumors [313]. Elevated levels of HIF1A have been shown to be associated with cancer-related mortalities in oligodendroglia, breast, cervix, oropharynx, ovarian, and endometrial cancers. Published studies show that adipose tissue is able to induce hypoxia and indirectly induce angiogenesis [150]. Adipocytes may also

regulate angiogenesis by cell-to-cell contact and by adipokine secretion [159]. Many cytokines produced by adipose tissue such as leptin, TNF-α, IL-6, IL-8, vascular endothelial growth factor (VEGF) and tumor growth factor β (TGF-β) show pro-angiogenic properties [150, 160, 162]. Emerging evidence shows that inhibition of angiogenesis is a possible therapeutic intervention to impair the development of obesity by regulating the growth and remodeling of the adipose tissue vasculature [163, 164].

In cases of severe obesity, adipose tissue can constitute up to 50–60% of the total body mass [146]. The mechanisms linking obesity and cancer are not fully understood however a low grade chronic inflammation, dysregulation of growth signaling pathways, chronic hyperinsulinemia, and hypoxia associated to obesity are widely accepted as important factors in cancer pathogenesis [146].

It has been previously shown that adipose conditioned media (ACM) from obese OAC patients has a distinct metabolic profile and is able to alter tumor metabolism, with ACM from obese OAC patients supporting the metabolic shift in glucose metabolism [314]. Additionally, obesity has been shown to be associated with poor prognosis in esophageal cancer [17]. Glycolysis [212], OXPHOS [315], hypoxia [316], epithelial-mesenchymal transition [317] and 5-lipoxygenase [318] have been shown to have a link with obesity and prognosis in cancer.

The main aim in this chapter was to assess the expression of markers of glycolysis, OXPHOS, hypoxia, EMT and 5-lipoxygenase, summarized in Table 4.1, in overweight and obese compared to normal weigh OAC patients having the hypothesis in mind, that obesity alters tumor metabolism and spread.

Table 4.1 List markers associated with tumor metabolism and cancer spread.

Pathway	Marker	Reference
GLYCOLYIS	GLUT1	Freemerman *et al.*, 2014 [319]
	GLUT4	Acharya *et al.*, 2016 [208]
	HK1	Moon *et al.*, 2015 [320]
	HK2	Wolf *et al.*, 2011 [321]
	PKM2	Lynam-Lennon *et al.*, 2014 [103]
	GAPDH	Phelan *et al.*, 2015 [247]
	ENO3	Peshavoria *et al.*, [271]
EICOSANOID	5LOX	Steinhilber *et al.*, 2011 [87]
OXPHOS	ATP5B	Lynam-Lennon *et al.*, 2014 [248]
HYPOXIA	HIF1A	Phan *et al.*, 2014 [322]
	CAIX	Phan *et al.*, 2014 [322]
EMT	E-Cadherin	Larue *et al.*, 2005 [323]
	β-Catenin	Jiang *et al.*, 2007 [324]
	SNAI1	Heerboth et *al.*, 2015 [325]
	SNAI2	Allott *et al.*, 2012 [326]
	Zeb1	Liu *et al.*, 2016 [327]
	MMP9	Lin *et al.*, 2010 [328]

4.2 Aims and Objectives

The aim of this chapter was to delineate the link between glycolysis, OXPHOS, hypoxia, EMT, 5-lipoxygenase and obesity using a number of different biological sample types including adipose conditioned media, tumor biopsy RNA and tumor tissue microarrays. We aimed to investigate whether there is a link between individual markers of these pathways and obesity in OAC.

Specific Objectives:

- Investigate the link between gene expression of tumor metabolism and EMT associated genes in OE33 cells co-cultured with ACM from overweight and obese compared to normal weight OAC patients

- Investigate the link between gene expression of tumor metabolism and EMT associated genes in overweight and obese compared to normal weight OAC patients, using treatment-naive OAC tumor biopsies

- Investigate the link between the expression of tumor metabolism and EMT markers at the protein level in the tissue microarrays and to delineate the link with obesity, obesity status measured by BMI and VFA

- To correlate expression levels of tumor metabolism and EMT markers with BMI and VFA

4.3 Results

4.3.1 The link between glycolysis, oxidative phosphorylation, hypoxia, 5-Lipoxygenase and obesity

4.3.1.1 Assessment of 5-Lipoxygenase, glucose transporter protein, glycolysis, OXPHOS and hypoxia associated genes in OE33 cells co-cultured with ACM

OE33 cells were co-cultured with ACM that was prepared from visceral fat collected from OAC patients who underwent oesophagectomy for esophageal cancer at St. James's hospital and stored in the designated ACM biobank. Cells were co-cultured with ACM for 24 hours in humidified atmosphere with 5% CO_2 at 37°C. RNA was isolated as described in Section 2.6 and gene expression was measured by qPCR as described in Section 2.10. Details for gene primer probes used are summarized in Table 2.2. The RQ value for one patient sample was set as the calibrator to allow normalisation of the data set. Gene expression levels were compared between two groups: OE33 cells treated with ACM from overweight and obese versus normal weight patients (BMI $\geq$25 versus BMI 18.5-25). Samples with a Ct values above 35 were deemed to have negligible expression and omitted from analysis.

Glucose transporter protein GLUT1 and GLUT4 expression was significantly higher in OE33 cells treated with ACM from overweight and obese compared to normal weight patients (1.438 ±0.157 versus 0.8429 ±0.1006 and 1.668 ±0.1315 versus 1.238 ±0.116 respectively, n=5 in each group, $p<0.05$) (Figure 4.1a and Figure 4.1b respectively). There was no significant difference in HK1 and HK2 expression levels between overweight and obese versus normal weight groups (1.439 ±0.1663 versus 0.9973 ±0.09359 and 1.863 ±0.2212 versus 1.272 ±0.1389 respectively, n=5 in each group, $p=0.0952$) (Figure 4.1c and Figure 4.1d respectively). There was no significant difference in PKM2 expression levels in OE33 cells treated with ACM from overweight and obese versus normal weight patients (1.637 ±0.3409 versus 1.020 ±0.064, $p=0.5317$) (Figure 4.2a), however, GAPDH expression was found to be significantly higher in the cells treated with ACM from overweight and obese compared to normal weight OAC patients (2.369 ±0.2077 versus 1.655 ±0.1907, n=5 in each group, $p<0.01$) (Figure 4.2b). There

was no significant difference found in ENO3 expression levels between the overweight and obese compared to normal weight groups (1.436 ±0.1371 versus 1.074 ±0.0728, n=5 in each group, p=0.0556) (Figure 4.2c). Similarly, there was no significant difference found in 5LOX expression between overweight and obese compared to normal weight groups (1.359 ±0.1733 versus 1.237 ±0.1279, n=5 in each group, p=0.5317) (Figure 4.2d).

Table 4.2 Details of patient demographic used for preparation of ACM for gene analysis study

n=10	Mean (S.D.) or n (%) as appropriate
Morphology (OAC)	10 (100%)
Male: female	7:3 (70%: 30%)
Age	69.3 (12.72)
Normal weight: overweight and obese	5:5 (50%: 50%)
Normal weight BMI (kg/m^2)	20.66 (1.318)
Overweight and obese BMI (kg/m^2)	34.2 (5.168)
T Stage	
T Stage T3: T4	3(30%): 7(70%)

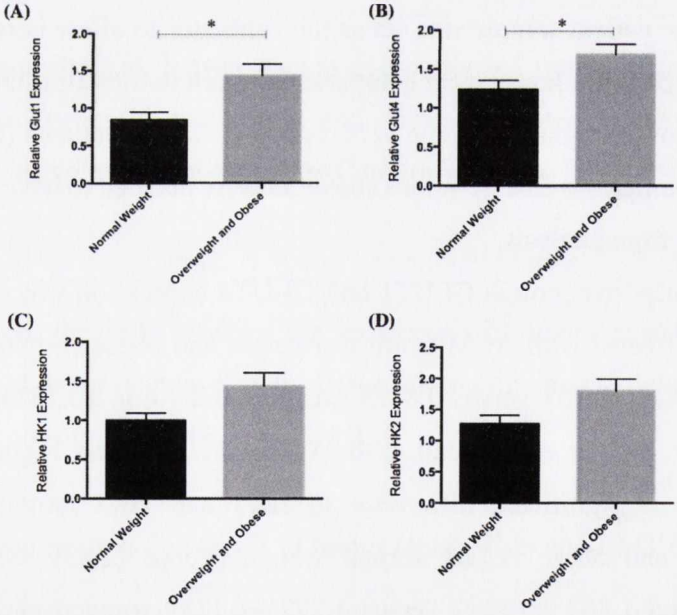


Figure 4.1 Glucose transporter protein, but not hexokinase levels are higher in OE33 cells co-cultured with ACM from overweight and obese OAC patients. (A) The level of GLUT1 was significantly higher in OE33 cells co-cultured with ACM from overweight and obese compared to normal weight OAC patients ($p<0.05$). (B) The level of GLUT4 was significantly higher in OE33 cells co-cultured with ACM from overweight and obese compared to normal weight OAC patients ($p<0.05$). (C) There was no significant difference in HK1 expression between the overweight and obese versus normal weight groups ($p=0.0952$). (D) There was no significant difference in HK2 expression between the cells treated with ACM from overweight and obese versus normal weight patients ($p=0.1508$). Statistical test used was Man-Whitney U test. $p<0.05$(*).Error bar denotes mean ± S.E.M.

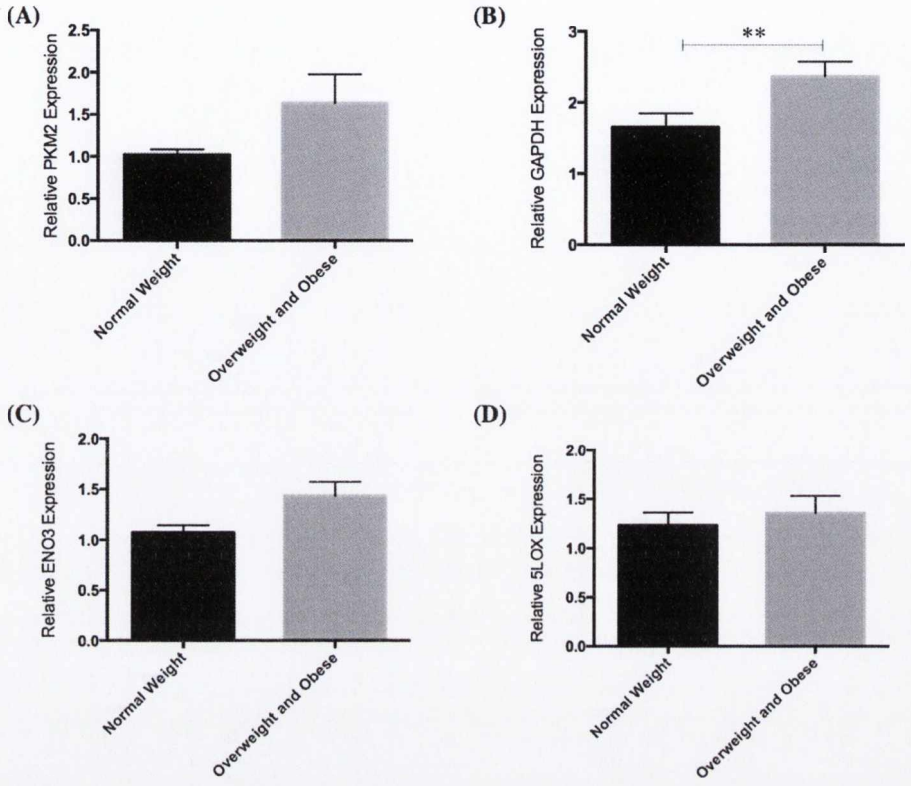


Figure 4.2 PKM2 and GAPDH, but not ENO3 and 5LOX are associated with ACM-induced glycolysis in OE33 cells. (A) There was no significant difference in the level of PKM2 expression between the overweight and obese versus normal weight groups ($p=0.5317$). (B) The level of GAPDH was significantly higher in OE33 cells co-cultured with ACM from overweight and obese compared to normal weight OAC patients ($p<0.01$). (C) There was no significant difference in ENO3 expression between the overweight and obese versus normal weight groups ($p=0.0556$). (D) There was no significant difference in 5LOX expression between the cells treated with ACM from overweight and obese versus normal weight patients ($p=0.5317$). Statistical test used was Mann-Whitney U test. $p<0.01$(**) Error bar denotes mean ± S.E.M.

4.3.1.2 Assessment of 5-Lipoxygenase, glucose transporter protein, glycolysis, OXPHOS and hypoxia associated genes in OAC tumor

Biopsy samples were collected from the main specimen post-surgical resection from OAC patients as described in Section 2.4. The patient demographic is summarized in Table 4.3. RNA was isolated as described in Section 2.6 and gene expression was measured in real time by qPCR as described in Section 2.10. Details for gene primer probes used were summarized in Table 2.2. The RQ value for one patient sample was set as the calibrator to allow normalisation of the data set. Gene expression levels were

compared in tumor from obese versus non-obese OAC patients with obese VFA cut off value of 163.8 cm^2 in males and 80.1 cm^2 in females, n=10 in each group.

There was no significant difference in GLUT1 expression between obese and non-obese OAC patient tumor tissue (1.817 ±0.1850 versus 1.364 ±0.1349, p=0.122) (Figure 4.3a, b), however, GLUT4 expression was found to be significantly higher in OAC tumor from viscerally obese compared to non-obese patients (2.195 ±0.1721 versus 1.568 ±0.1579, $p<0.05$) (figure 4.3c, d). There was no significant difference observed in HK1 expression between obese and non-obese OAC patient tumor tissue (1.349 ±0.1216 versus 1.215 ±0.105, p=0.4727) (Figure 4.4a, b), however, HK2 expression was found to be significantly higher in viscerally obese compared to non-obese patients (2.321 ±0.170 versus 1.557 ±0.1797, $p<0.05$) (figure 4.4c, d). PKM2 and GAPDH were both upregulated in obese patients (1.700 ±0.1131 versus 1.254 ±0.1084 and 2.153 ±0.2073 versus 1.316 ±0.1377 respectively, $p<0.05$ and $p<0.01$ respectively) (Figure 4.5a, b and Figure 4.5c, d respectively). ENO3 expression was found to be significantly higher in OAC tumor from viscerally obese compared to non-obese patients (1.454 ±0.096 versus 1.145 ±0.0625, $p<0.05$) (figure 4.6a, b). 5LOX was expressed at significantly higher level in viscerally obese versus non-obese patients (1.836 ±0.1783 versus 1.312 ±0.1414, $p<0.05$) (Figure 4.6c, d). ATP5B expression has also been found to be higher in obese group (2.889 ±0.2481 versus 1.95 ±0.1994, $p<0.05$) (Figure 4.7a, b).

Table 4.3 Details of patient demographic used for tumor biopsy gene analysis study

n=20	Mean (S.D.) or n (%) as appropriate
Morphology (OAC)	20 (100%)
Male: female	7:3 (70%: 30%)
Age	57.3 (11.53)
Neoadjuvant therapy	0
Normal weight: overweight and obese	10: 10 (50%: 50%)
Normal weight VFA (cm^2)	72.96 (57.75)
Overweight and obese VFA (cm^2)	271 (40.52)
T Stage	
T Stage T2: T3: T4	3(15%): 8(40%): 9(45%)

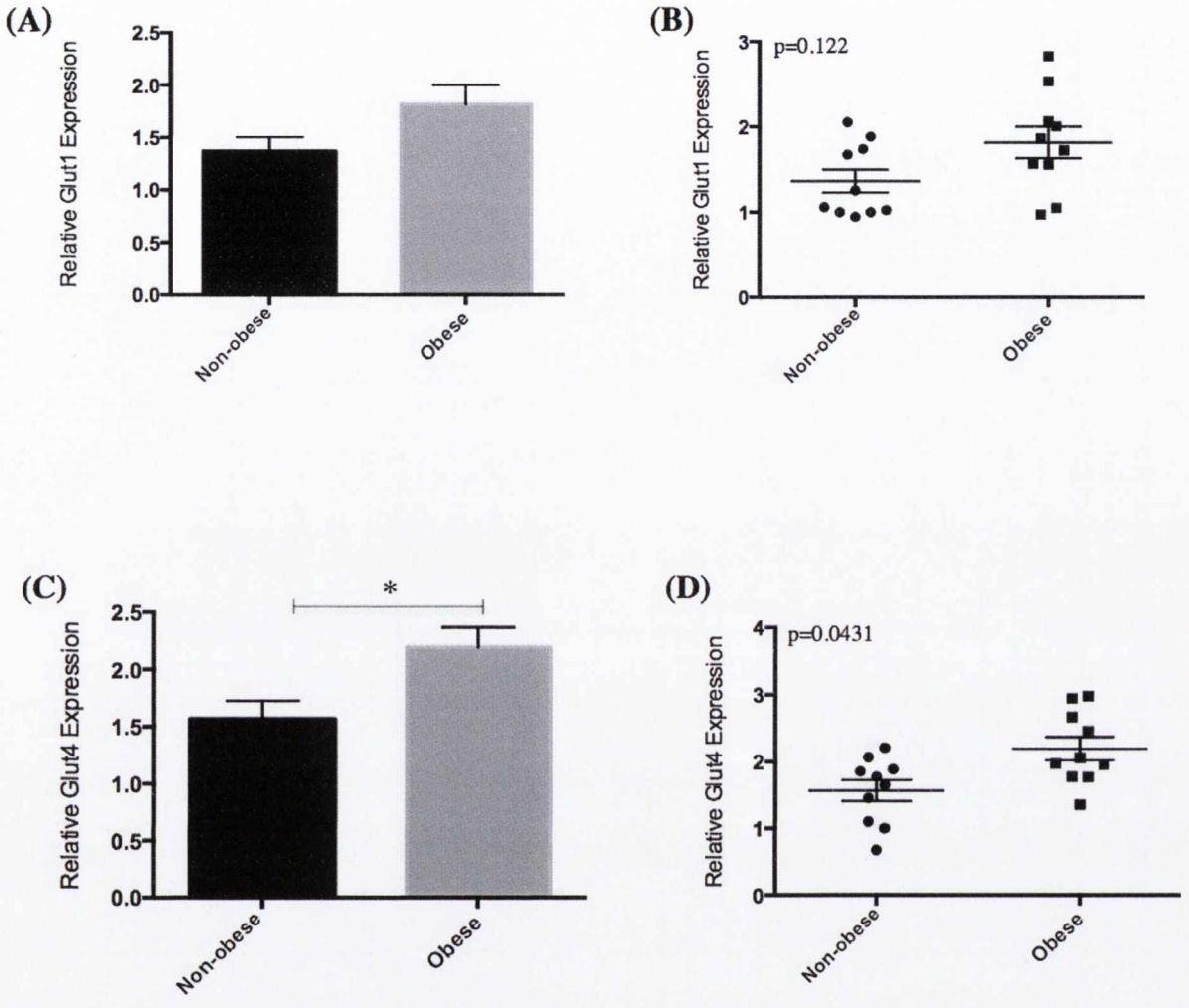


Figure 4.3 GLUT1 but not GLUT4 expression is associated with visceral obesity in OAC tumor. Patients were segregated into obese and non-obese groups based on VFA measurement, 10 patients in each group. (A) There was no significant difference in Glut1 expression between obese and non-obese patient tumor tissue ($p=0.122$). (B) The distribution of Glut1 expression across OAC patient tumor biopsies shown by scatter plot. (C) Glut4 level has been shown to be significantly higher in viscerally obese compared to non-obese patients ($p<0.05$). (D) The distribution of Glut4 expression across OAC patient tumor biopsies shown by scatter plot. Statistical test used was Man-Whitney U test. $p<0.05$ (*). Error bar denotes mean ± S.E.M.

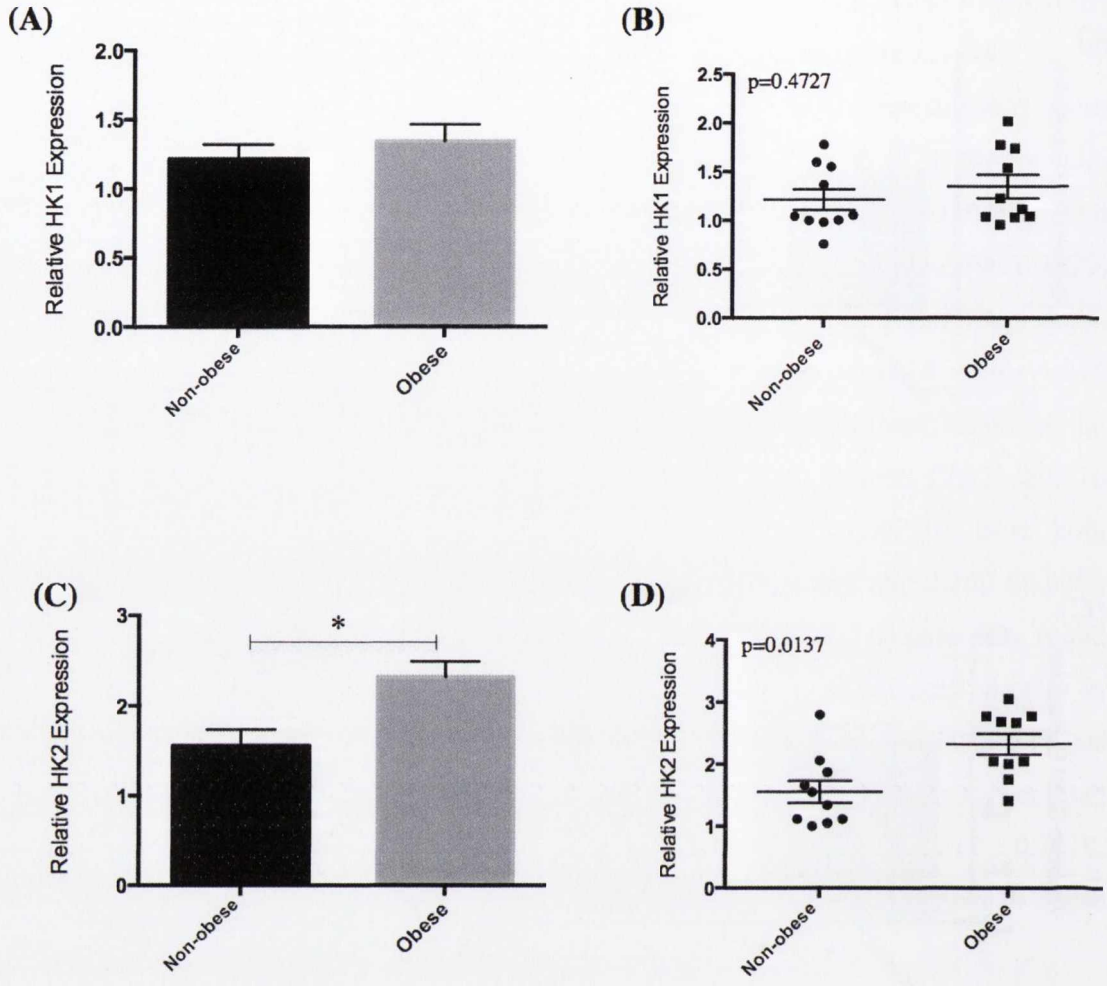


Figure 4.4 HK2 but not HK1 expression is associated with visceral obesity in OAC tumor. Patients were segregated into obese and non-obese groups based on VFA measurement, 10 patients in each group. (A) There was no significant difference in HK1 expression between obese and non-obese patient tumor tissue ($p=0.4727$). (B) The distribution of HK1 expression across OAC patient tumor biopsies shown by scatter plot. (C) HK2 level was significantly higher in viscerally obese compared to non-obese patients ($p<0.05$). (D) The distribution of HK2 expression across OAC patient tumor biopsies shown by scatter plot. Statistical test used was Man-Whitney U test. $p<0.05$ (*). Error bar denotes mean ± S.E.M.

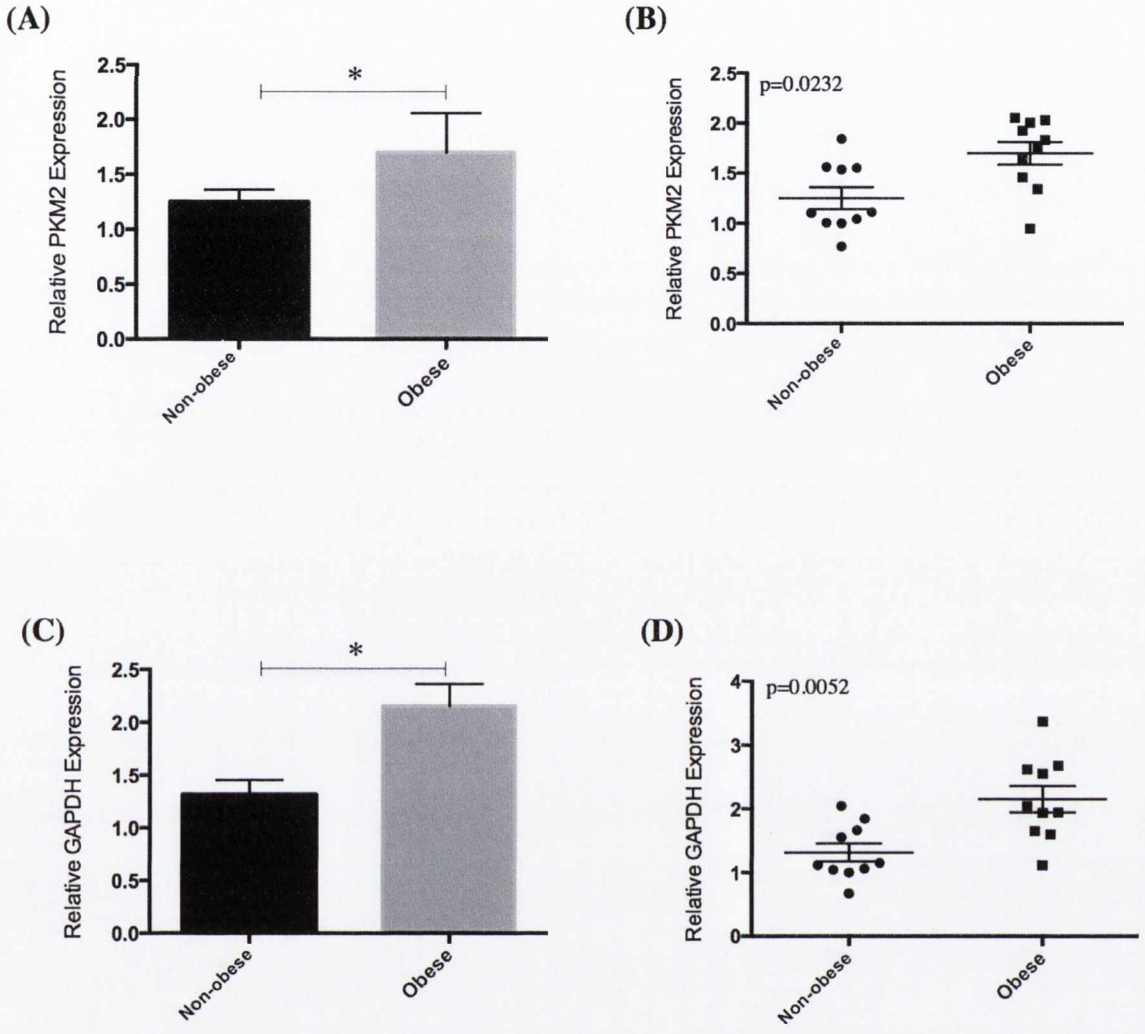


Figure 4.5 PKM2 and GAPDH expression is associated with visceral obesity in OAC patients. Patients were segregated into obese and non-obese groups based on VFA measurement, 10 patients in each group. (A) PKM2 was expressed at significantly higher level in viscerally obese patients ($p<0.05$). (B) The distribution of PKM2 expression across OAC patient tumor biopsies shown by scatter plot. (C) GAPDH level has been shown to be significantly higher in viscerally obese compared to non-obese patients ($p<0.01$). (D) The distribution of GAPDH expression across OAC patient tumor biopsies shown by scatter plot. Statistical test used was Man-Whitney U test. $p<0.05$ (*), $p<0.01$ (**). Error bar denotes mean ± S.E.M.

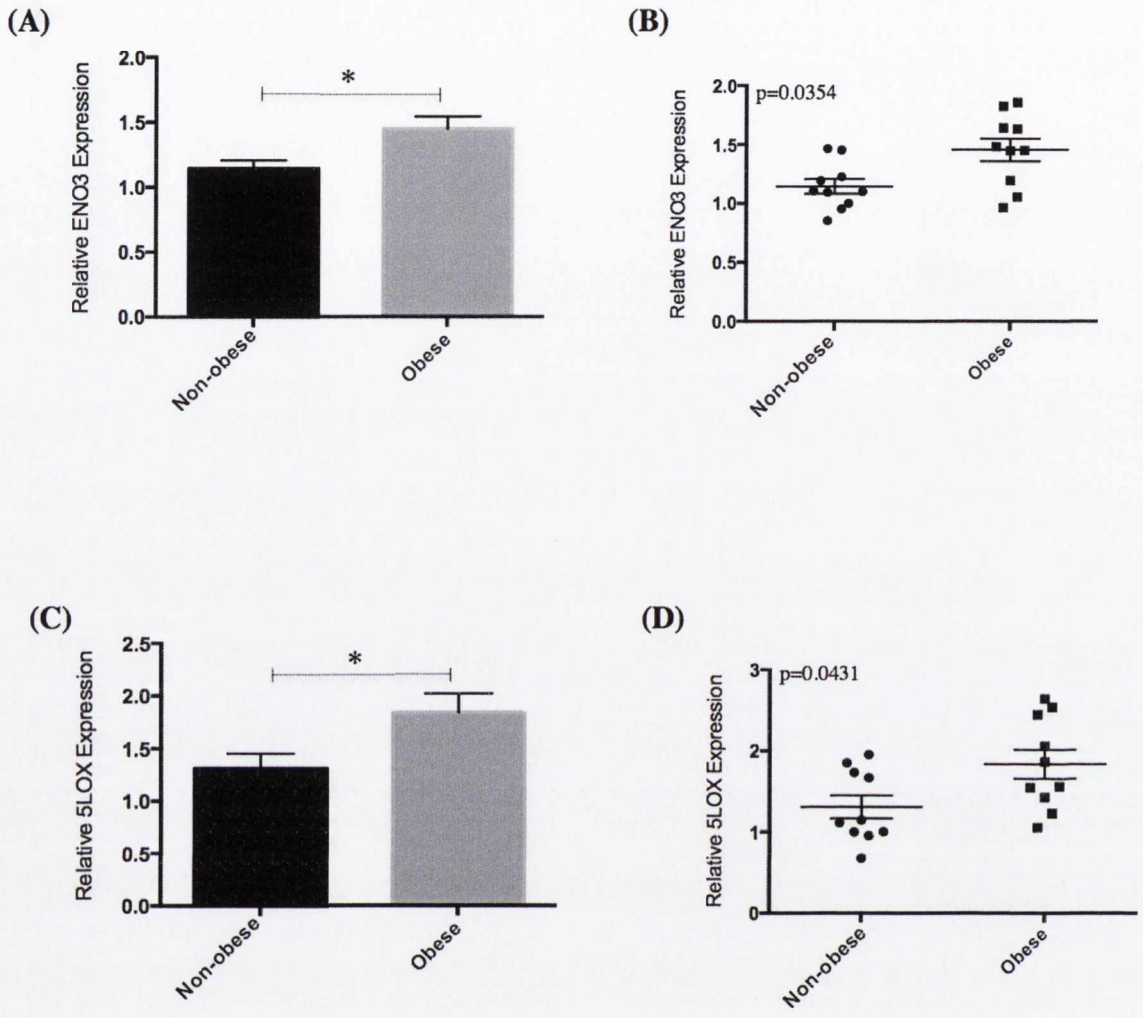


Figure 4.6 High ENO3 and 5LOX expression is associated with visceral obesity in OAC patient tumor. Patients were segregated into obese and non-obese groups based on VFA measurement, 10 patients in each group. (A) ENO3 was expressed at significantly higher level in viscerally obese patients ($p<0.05$). (B) The distribution of ENO3 expression across OAC patient tumor biopsies shown by scatter plot. (C) 5LOX level has been shown to be significantly higher in viscerally obese compared to non-obese patients ($p<0.05$). (D) The distribution of 5LOX expression across OAC patient tumor biopsies shown by scatter plot. Statistical test used was Man-Whitney U test. $p<0.05$ (*), $p<0.05$. Error bar denotes mean ± S.E.M.

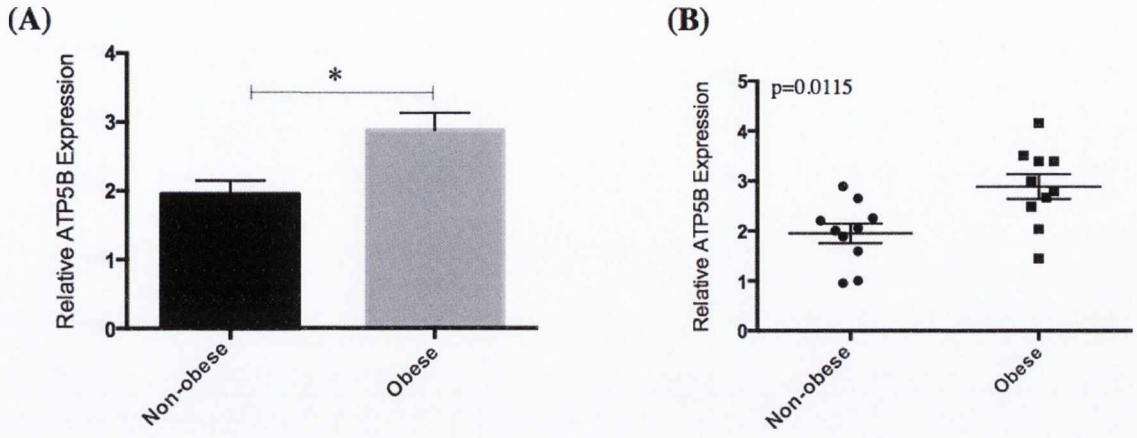


Figure 4.7 High level of ATP5B expression is associated with visceral obesity. Patients were segregated into obese and non-obese groups based on VFA measurement, 10 patients in each group. (A) ATP5B was expressed at significantly higher level in viscerally obese patients ($p<0.05$). (B) The distribution of ATP5B expression across OAC patient tumor biopsies shown by scatter plot. Statistical test used was Man-Whitney U test. $p<0.05$ (*). Error bar denotes mean ± S.E.M.

4.3.1.3 Epithelial expression of glucose transporter proteins, markers of glycolysis, OXPHOS and 5-lipoxygenase and their association with obesity

The study population consisted of 120 OAC patients, 96 (80%) were male and 24 (20%) were female. Patient demographics are described in Table 3.2. Paraffin-embedded tumor sections with a minimum of 36 months of clinical follow up data were used to construct tissue microarrays (TMAs). TMAs were stained for a number of glucose transporter proteins, markers of glycolysis, hypoxia and EMT. Optimisation was carried out using full-face OAC tissue at a number of different dilutions recommended by the manufacturer. The list of primary antibody selection and optimisation is outlined in Table 2.6.

An average tumor epithelial and stromal score was assigned to each patient with an exception of cases where tissue cores were damaged and impossible to score. The intensity score was obtained by scoring the cores between 0 and 3, where 0=negative, 1 =weak, 2=moderate and 3=strong expression. The quantity of positive staining within the tissue microarray core was scored between 0 and 100% to obtain the percentage positivity measure. The intensity score and percentage positivity were multiplied giving an overall score for each core 0 to 300. Representative images in Section 3.3.2.1 and Section 3.3.3.1. 120 OAC patients were segregated into two groups, based on their obesity status: overweight and obese (BMI$\geq$25 kg/m^2) and normal weight (BMI 18.5-25 kg/m^2).

Results showed no significant difference in epithelial GLUT1 expression in OAC tissue samples from overweight and obese versus normal weight patients (157 $\pm$6.063 versus 169.4 $\pm$7.616, n=70 versus 49, p=0.243) (Figure 4.8a). There was a negative correlation between the levels of epithelial GLUT1 expression and increasing BMI (r=-0.0751, p=0.4150) (Figure 4.8b). There was a significant difference in epithelial GLUT4 expression in overweight and obese compared to normal weight OAC patients (190.9 $\pm$7.312 versus 150.8 $\pm$12.12, n=70 versus n=49, p<0.01) (Figure 4.8c). There was also a significant positive correlation between the levels of epithelial GLUT4 expression and increasing BMI (r=0.2805, p=0.0019) (Figure 4.8d). Similar pattern of epithelial hexokinase expression was observed. There was no significant difference between epithelial HK1 expression in obese and overweight versus normal weight OAC patients

(162.3 ±7.095± versus 163 ±9.6, p=0.7976) (Figure 4.9a) and there was no association between HK1 levels and increasing BMI (r=0.0886, p=0.3358) (Figure 4.9b). Interestingly, epithelial HK2 expression was significantly higher in overweight and obese compared to normal weight patients (172.9 ±6.889 versus 136.3 ±9.415, p<0.001) (Figure 4.9c). There was also a significant positive correlation between the levels of HK2 epithelial expression and increasing BMI (r=0.2339, p=0.05) (Figure 4.9d). There was a significant difference in epithelial PKM2 expression in overweight and obese compared to normal weight OAC patients (172.4 ±7.357 versus 147.1 ±10.00, n=70 versus n=49, p<0.01) (Figure 4.10a). There was a significant positive correlation between the levels of PKM2 epithelial expression and increasing BMI (r=0.2316, p<0.05) (Figure 4.10b). Similarly, there was a significant difference in GAPDH expression levels between overweight and obese and normal weight patients (187.0 ±7.792 versus 139.5 ±9.149, n=70 versus n=49, p<0.0001) (Figure 4.10c), and there was a significant positive correlation between the level of GAPDH epithelial expression and increasing BMI (r=0.4633, p<0.0001) (Figure 4.10d). There was also a significant difference between epithelial ENO3 expression in overweight and obese versus normal weight OAC patients (151.1 ±9.82 versus 126.21 ±11.13, n=70 versus n=39, p<0.05) (Figure 4.11a), and there was a significant positive correlation between the levels of epithelial ENO3 expression and increasing BMI (r=0.2283, p<0.05) (Figure 4.11b). There was a significant difference in epithelial 5-LOX expression in overweight and obese versus normal weight OAC patients (178.0 ±8.735 versus 140.4 ±10.23, r=70 versus n=49, p<0.01) (Figure 4.11c), and there was a significant positive correlation between epithelial 5-LOX expression and increasing BMI (r=0.1087, p<0.05) (Figure 4.11d). We investigated the role of OXPHOS in obesity. Results showed that epithelial ATP5B expression, a marker of OXPHOS, was significantly higher in overweight and obese versus non-obese OAC patients (178.8 ±8.406 versus 149.7 ±9.678, n=70 versus n=49, p<0.05) (Figure 4.12a). There was also a significant positive correlation between high level of ATP5B and increasing BMI (r=0.2661, p<0.01) (Figure 4.12b). In terms of hypoxia, there was a significant difference in the HIF1A expression levels between overweight and obese versus normal weight patients (159.9 ±8.342 versus 135.8 ±9.03, n=69 versus 39, p<0.05) (Figure 4.13a), however, there was no correlation between the increasing levels of HIF1A and BMI (r=0.105, p=0.1017) (Figure 4.13b). Finally, there was a significant difference in epithelial expression levels of CAIX, another marker of hypoxia, in overweight and obese versus normal weight OAC patients (180 ±7.497 versus 152.1 ±10.88, n=70 versus n=49,

p<0.05) (Figure 4.13c). However, similarly to HIF1A, there was no significant correlation between epithelial CAIX expression levels and increasing BMI (r=0.1623, p=0.0716) (Figure 4.13).

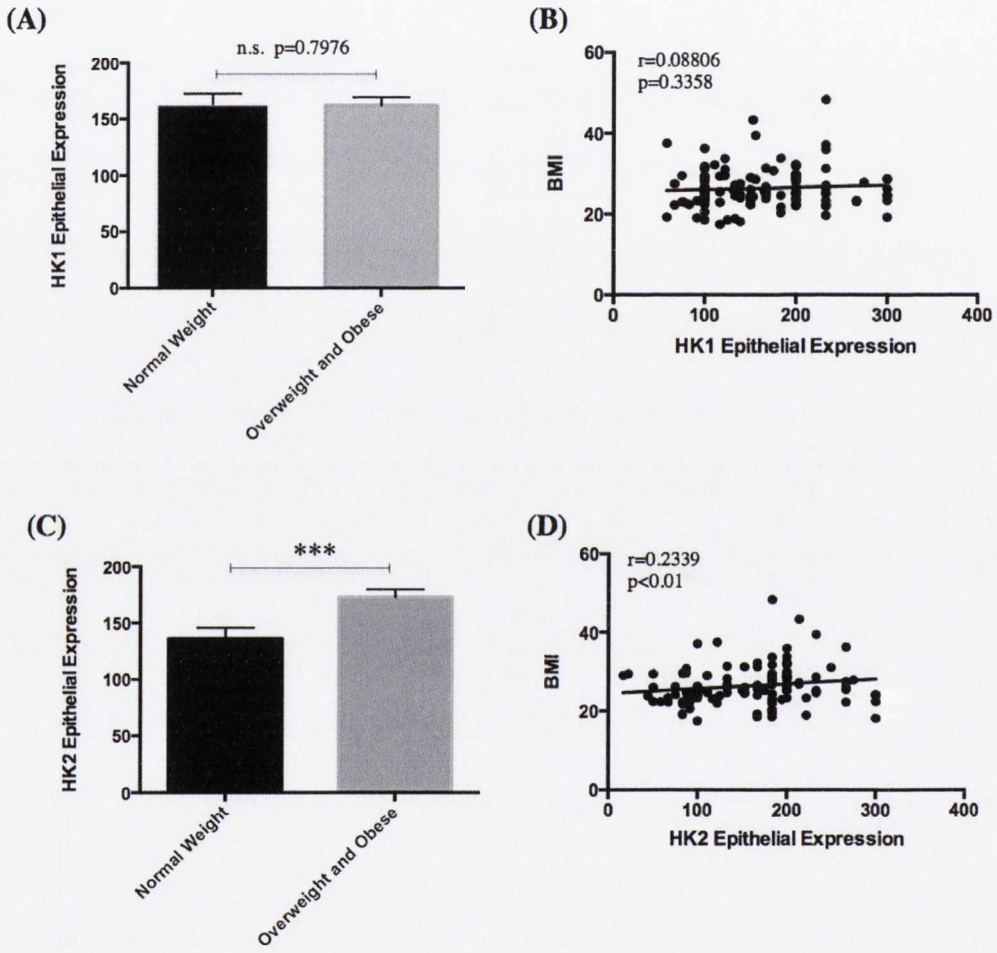


Figure 4.8 Increase in epithelial GLUT4 expression, but not GLUT1 expression is associated with obesity in OAC tissue microarrays. (A) There was no significant difference (p=0.243) in epithelial GLUT1 expression levels between overweight and obese (BMI≥25 kg/m^2) compared to normal weight (BMI 18.5-25 kg/m^2) OAC patients; (B) There was a negative correlation between the levels of GLUT1 epithelial expression and increasing BMI (r=-0.0751, p=0.4150). (C) Epithelial GLUT4 expression was significantly higher (p<0.01) in overweight and obese (BMI≥25 kg/m^2) compared to normal weight (BMI 18.5-25 kg/m^2) OAC patients; (D) There was a significant positive correlation between the levels of Glut4 epithelial expression and increasing BMI (r=0.2805, p<0.01). Statistical test used was Mann Whitney U test for comparison and Spearman's test was used for correlations with anthropomorphic measurements. p<0.01 (**). Error bar denotes mean ± S.E.M.

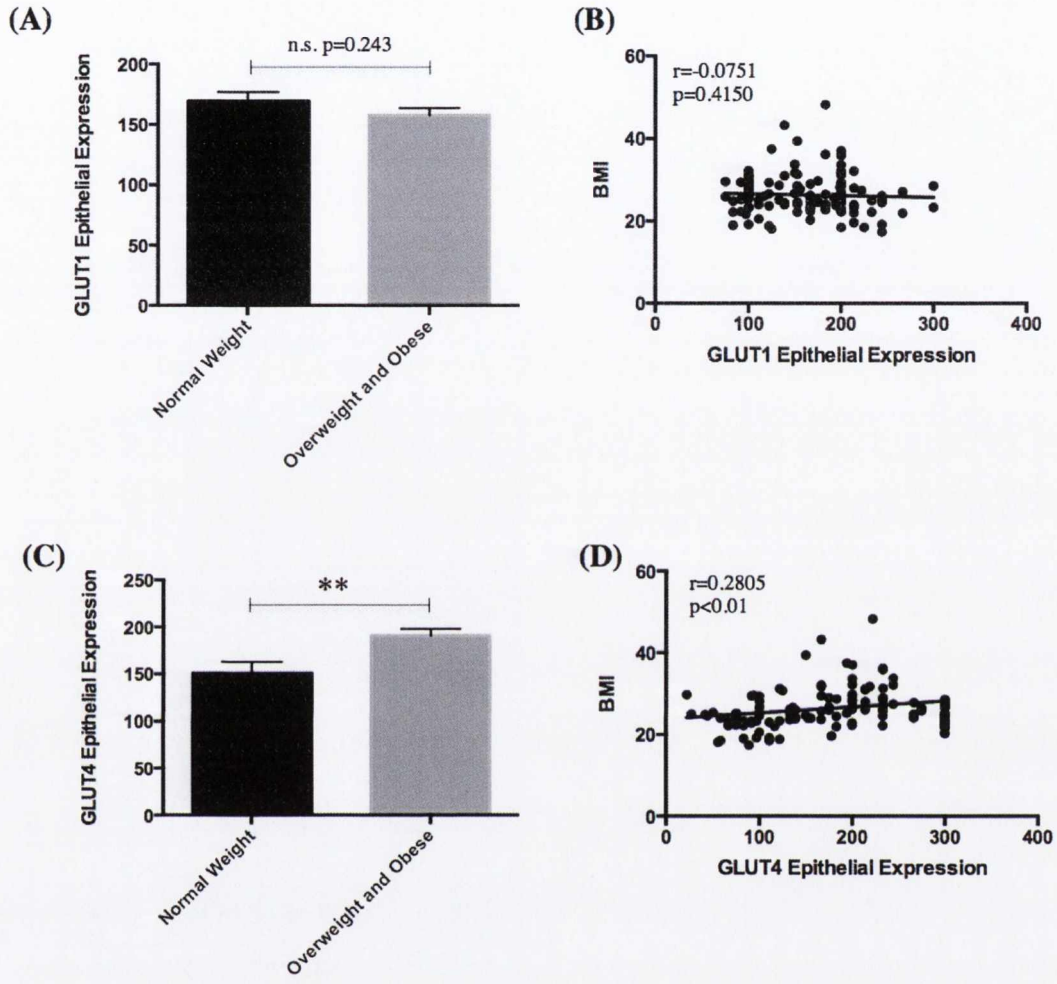


Figure 4.9 High epithelial HK2, but not HK1 expression is associated with obesity in OAC tissue microarrays. (A) There was no significant difference (p=0.7976) in epithelial HK1 expression levels between overweight and obese (BMI≥25 kg/m^2) compared to normal weight (BMI 18.5-25 kg/m^2) OAC patients. (B) There was no correlation between the levels of HK1 epithelial expression and increasing BMI (r=0.0886, p=0.3358). (C) Epithelial HK2 expression was significantly higher (p<0.001) in overweight and obese (BMI≥25 kg/m^2) compared to normal weight (BMI 18.5-25 kg/m^2) OAC patients. (D) There was a significant positive correlation between the levels of HK2 epithelial expression and increasing BMI (r=0.2339, p<0.05). Statistical test used was Mann Whitney U test for comparison and Spearman's test was used for correlations with anthropomorphic measurements. p<0.05 (*), p<0.001 (***). Error bar denotes mean ± S.E.M.

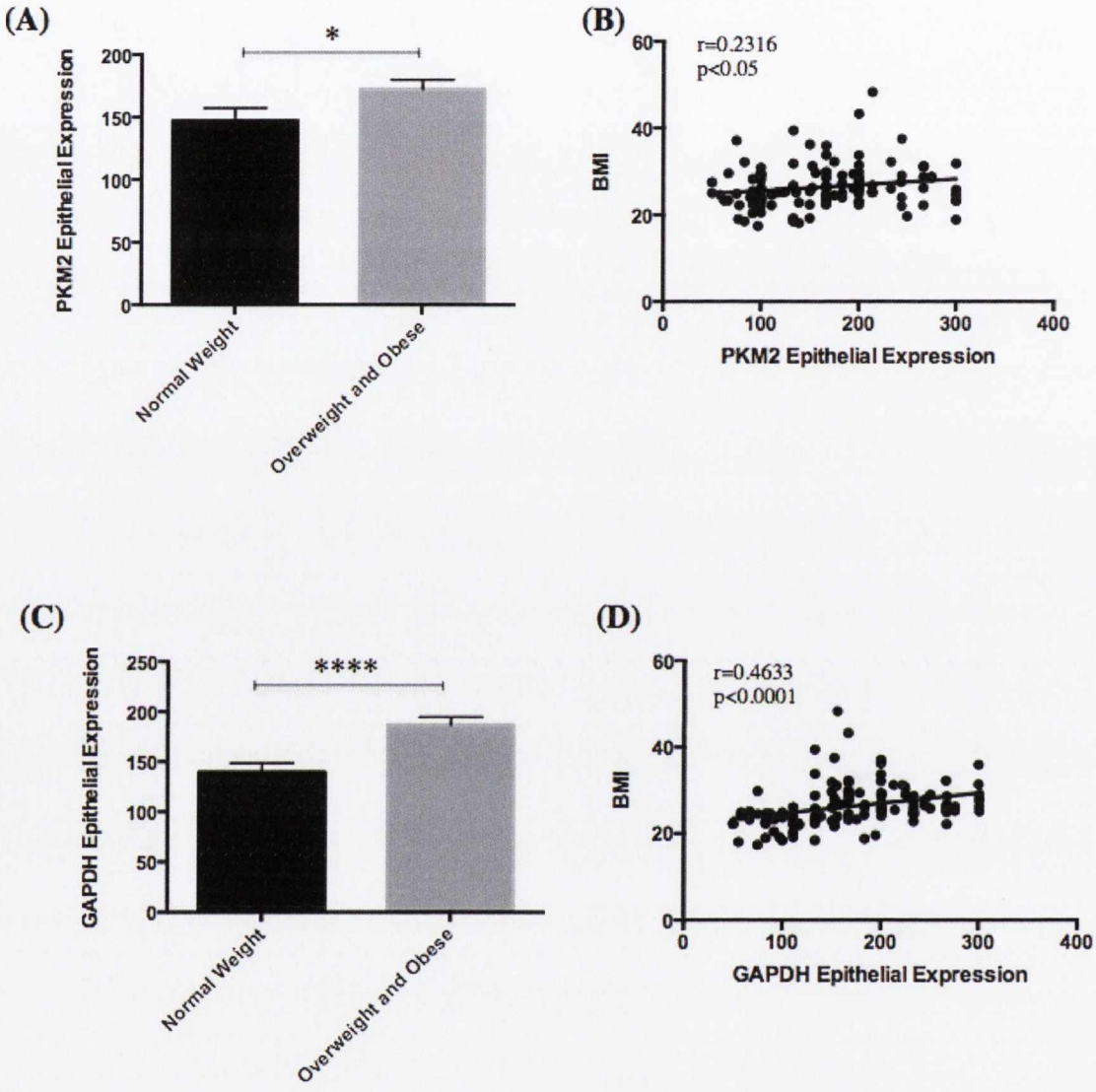


Figure 4.10 High epithelial PKM2 and GAPDH expression is associated with obesity in OAC tissue microarrays. (A) Epithelial PKM2 expression was significantly higher ($p<0.05$) in overweight and obese (BMI≥25 kg/m^2) compared to normal weight (BMI 18.5-25 kg/m^2) OAC patients. (B) There was a significant positive correlation between the levels of PKM2 epithelial expression and increasing BMI ($r=0.2316$, $p<0.05$). (C) Epithelial GAPDH expression was significantly higher ($p<0.0001$) in overweight and obese (BMI≥25 kg/m^2) compared to normal weight (BMI 18.5-25 kg/m^2) OAC patients. (D) There was a significant positive correlation between the levels of GAPDH epithelial expression and increasing BMI ($r=0.4633$, $p<0.0001$). Statistical test used was Mann Whitney U test for comparison and Spearman's test was used for correlations with anthropomorphic measurements. $p<0.05$ (*), $p<0.0001$ (****). Error bar denotes mean ± S.E.M.

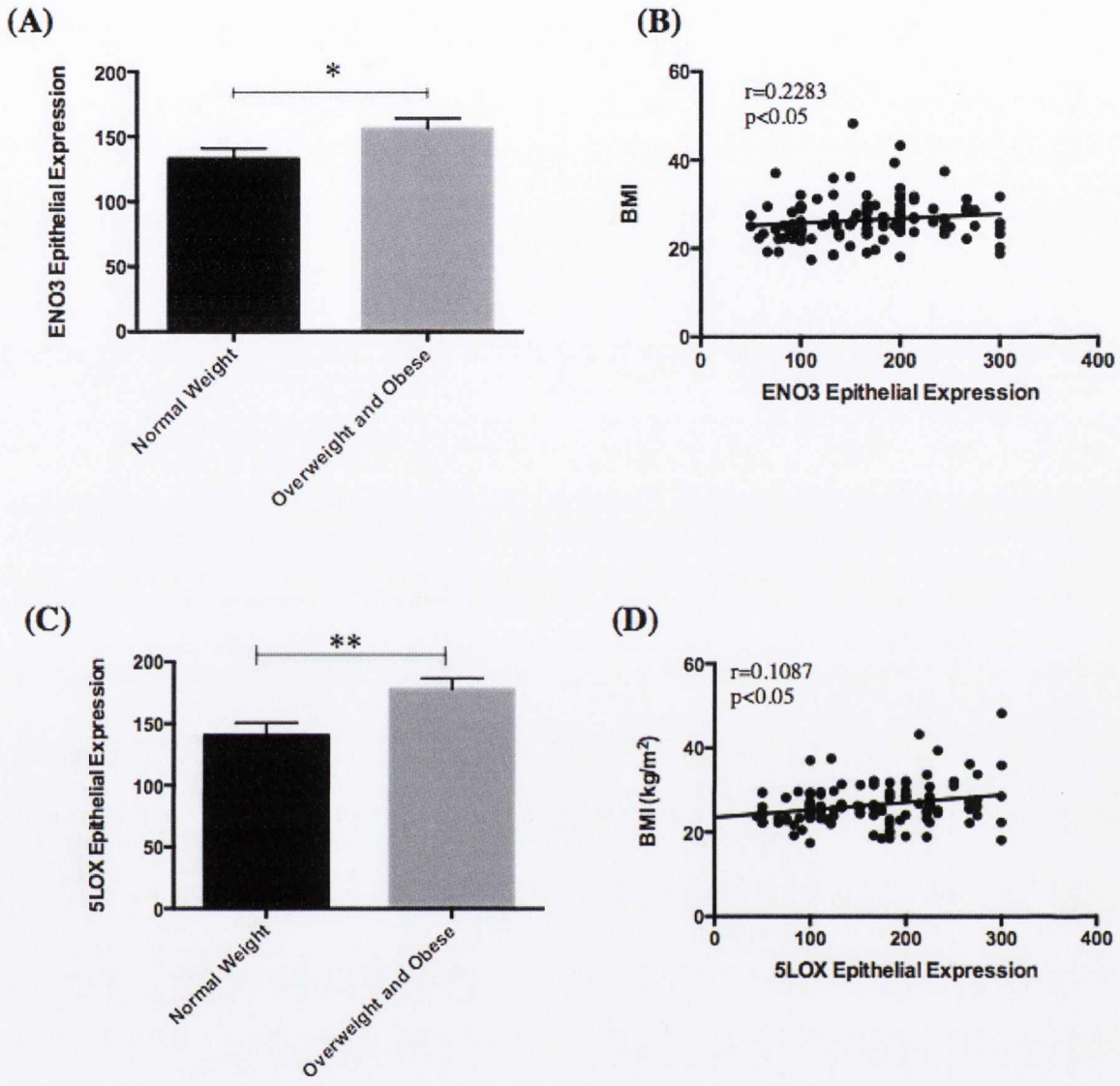


Figure 4.11 Increase in epithelial ENO3 and 5LOX expression is associated with obesity in OAC tissue microarrays. (A) Epithelial ENO3 expression was significantly higher ($p<0.05$) in overweight and obese (BMI≥25 kg/m^2) compared to normal weight (BMI 18.5-25 kg/m^2) OAC patients. (B) There was a significant positive correlation between the levels of epithelial ENO3 expression and increasing BMI ($r=0.2283$, $p<0.05$). (C) There was a significant difference in epithelial 5LOX expression in overweight and obese versus normal weight OAC patients ($p<0.01$). (D) There was a significant positive correlation between epithelial 5LOX expression and increasing BMI ($r=0.1087$, $p<0.05$). Statistical test used was Mann Whitney U test for comparison and Spearman's test was used for correlations with anthropomorphic measurements. $p<0.05$ (*), $p<0.01$ (**). Error bar denotes mean ± S.E.M.

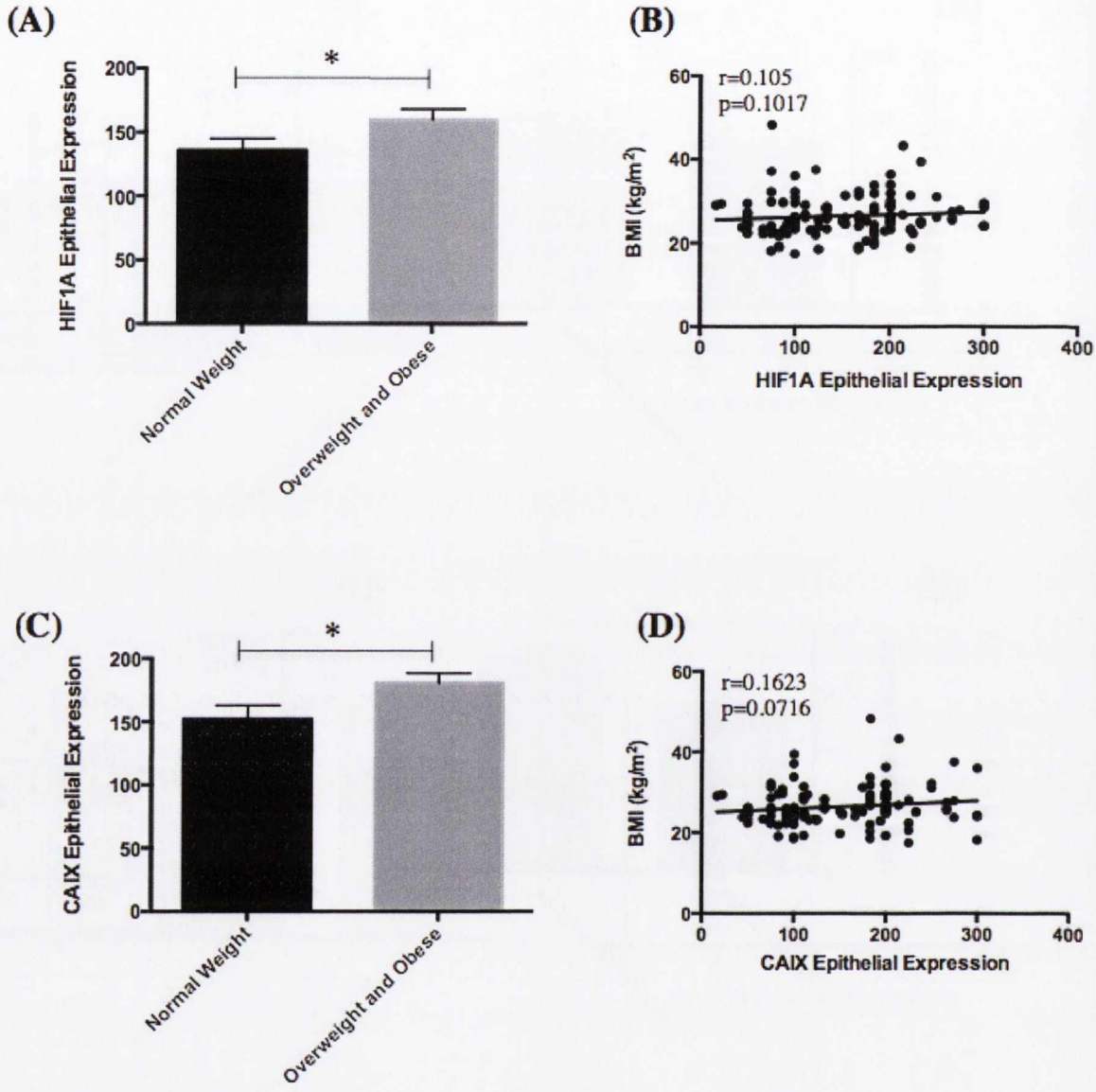


Figure 4.12 Significantly higher epithelial expression of HIF1A and CAIX in overweight and obese OAC patients is not associated with increasing BMI. (A) There was a significant difference in the HIF1A expression levels between overweight and obese versus normal weight patients ($p<0.05$). (B) There was no correlation between HIF1A and BMI ($r=0.105$, $p=0.1017$) (C) There was a significant difference in epithelial expression levels of CAIX in overweight and obese versus normal weight OAC patients ($p<0.05$). (D) There was no significant correlation between epithelial CAIX expression BMI ($r=0.1623$, $p=0.0716$). Statistical test used was Mann Whitney U test for comparison and Spearman's test was used for correlations with anthropomorphic measurements. $p<0.05$ (*). Error bar denotes mean ± S.E.M.

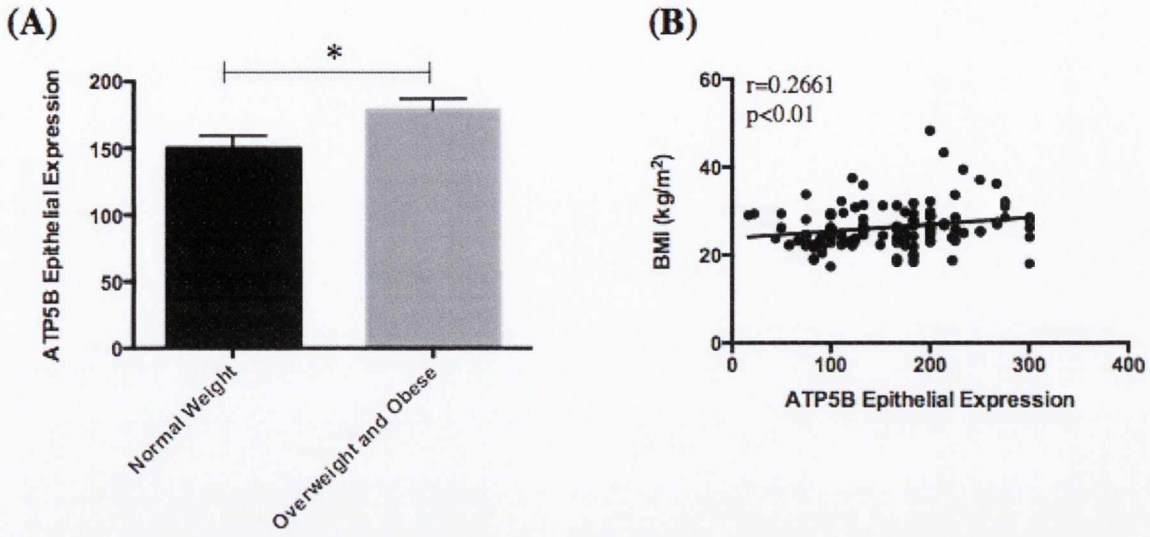


Figure 4.13 High epithelial ATP5B expression is associated with obesity in OAC tissue microarrays. (A) There was a significant difference in the epithelial ATP5B expression levels in overweight and obese versus non-obese patients ($p<0.05$). (B) There was a significant positive correlation between ATP5B and BMI ($r=0.2661$, $p<0.01$). Statistical test used was Mann Whitney U test for comparison and Spearman's test was used for correlations with anthropomorphic measurements. $p<0.05$ (*), $p<0.01$(**). Error bar denotes mean ± S.E.M.

4.3.2 Molecular delineation of the EMT process in OAC driven by adipose tissue

4.3.2.1 Assessment of EMT-associated genes in OE33 cells co-cultured with ACM

OE33 cells were co-cultured with ACM that was prepared from visceral fat collected from OAC patients who underwent oesophagectomy for esophageal cancer at St. James's hospital and stored in the designated ACM biobank.

Cells were co-cultured with ACM for 24 hours in humidified atmosphere with 5% CO_2 at 37°C. RNA was isolated as described in Section 2.7 and gene expression was measured by qPCR as described in Section 2.10. Expression of EMT-associated genes such as E-cadherin, β-catenin, SNAI1, SNAI2, Zeb1 and MMP9 were assessed. The RQ value for one patient sample was set as the calibrator to allow normalisation of the data set. Gene expression levels were compared between two groups: OE33 cells treated with ACM from overweight and obese versus normal weight patients (BMI ≥25 versus BMI 18.5-

25). Samples with a Ct values above 35 were deemed to have negligible expression. There was no significant difference in E-cadherin and β-catenin levels between the cells treated with ACM from overweight and obese compared to normal weight patients (2.465 ±0.2774 versus 1.669 ±0.1855 and 1.393 ±0.2069 versus 1.678 ±0.2613 respectively, n=5 in each group, p=0.0952 and p=0.222 respectively (Figure 4.14a and Figure 4.14b respectively). SNAI1 and SNAI2 expression has been found to be significantly elevated in the cells treated with ACM from overweight and obese compared to normal weight OAC patients (4.455 ±0.2834 versus 2.656 ±0.5316 and 2.365 ±0.4025 versus 1.129 ±0.1274 respectively, n=5 in each group, $p<0.05$) (Figure 4.14c and Figure 4.14d respectively). ZEB1 has been found to be elevated in the cells treated with ACM from overweight and obese in comparison to normal weight patients (1.359 ±0.1733 versus 1.232 ±0.1279, n=5 in each group, $p<0.05$) (Figure 4.14e), however, there was no difference in MMP9 expression levels between the two groups (3.892 ±0.79 versus 2.349 ±0.8371, n=5 in each group, p=0.4127) (Figure 4.14f).

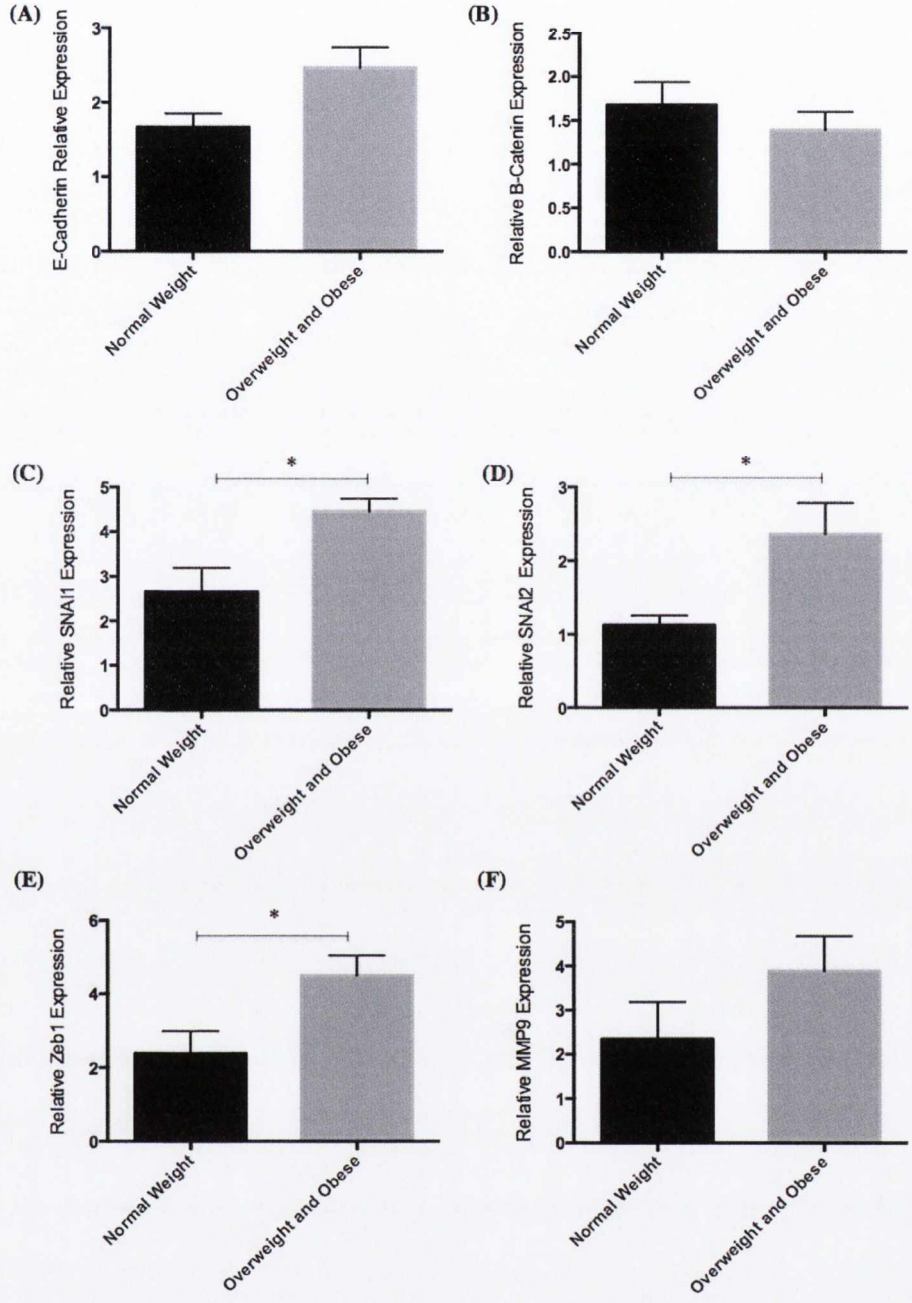


Figure 4.14 Expression of EMT-associated genes in OE33 cells co-cultured with ACM. (A) There was no significant difference in E-cadherin expression level between OE33 cells treated with ACM from overweight and obese versus normal weight OAC patients ($p=0.0952$). (B) There was no significant alterations in β-catenin expression level between the two groups ($p=0.222$). (C) SNAI1 expression level was significantly higher in OE33 cells co-cultured with ACM from overweight and obese compared to normal weight OAC patients ($p<0.05$). (D) SNAI2 expression level was significantly higher in OE33 cells co-cultured with ACM from overweight and obese OAC patients ($p<0.05$). (E) Zeb1 expression was significantly higher in OE33 cells treated with ACM from overweight and obese compared to normal weight patients ($p<0.05$). (F) There was no difference in MMP9 expression between the cells treated with ACM from overweight and obese versus normal weight groups ($p=0.4127$). Statistical test used was Man-Whitney U test. $p<0.05$ (*). Error bar denotes mean ± S.E.M.

4.3.2.2 Assessment of EMT-associated genes in OAC tumor and their association with visceral obesity

Biopsy samples were collected from the main specimen post-surgical resection from OAC patients as described in Section 2.4. The patient demographic is summarized in Table 4.5. RNA was isolated as described in Section 2.6 and gene expression was measured in real time by qPCR as described in Section 2.10. Expression of EMT-associated genes such as E-cadherin, β-catenin, SNAI1, SNAI2, Zeb1 and MMP9 were assessed. Details for gene primer probes used summarized in Table 2.2. The RQ value for one patient sample was set as the calibrator to allow normalisation of the data set. Gene expression levels were compared in tumor from obese versus non-obese OAC patients with obese VFA cut off value of 163.8 cm^2 in males and 80.1 cm^2 in females, n=10 in each group.

There was no significant difference in E-cadherin expression between obese and non-obese OAC tumor tissue (1.892 ±3.097 versus 1.892 ±0.3733, n=10 in each group, p=0.7796) (Figure 4.15a). The level of β-catenin was significantly higher in tumor tissue from viscerally obese compared to non-obese patients (1.525 ±0.3346 versus 2.675 ±0.3727, $p<0.05$) (Figure 4.15b). SNAI1 and SNAI2 levels were significantly higher in viscerally obese compared to non-obese OAC patients (3.958 ±0.5847 versus 2.242 ±0.4155 and 3.388 ±0.9888 versus 2.106 ±0.5537 respectively, $p<0.05$) (Figure 4.15c and Figure 4.15d respectively). There was a trend towards significance in relative Zeb1 expression, Zeb1 being higher in viscerally obese OAC patients (3.398 ±0.4888 versus 2.106 ±0.553, p=0.0522) (Figure 4.15e). MMP9 level was significantly higher in tumor tissue from viscerally obese AOC patients (3.222 ±0.5367 versus 1.698 ±0.3672, $p<0.05$) (Figure 4.15f).

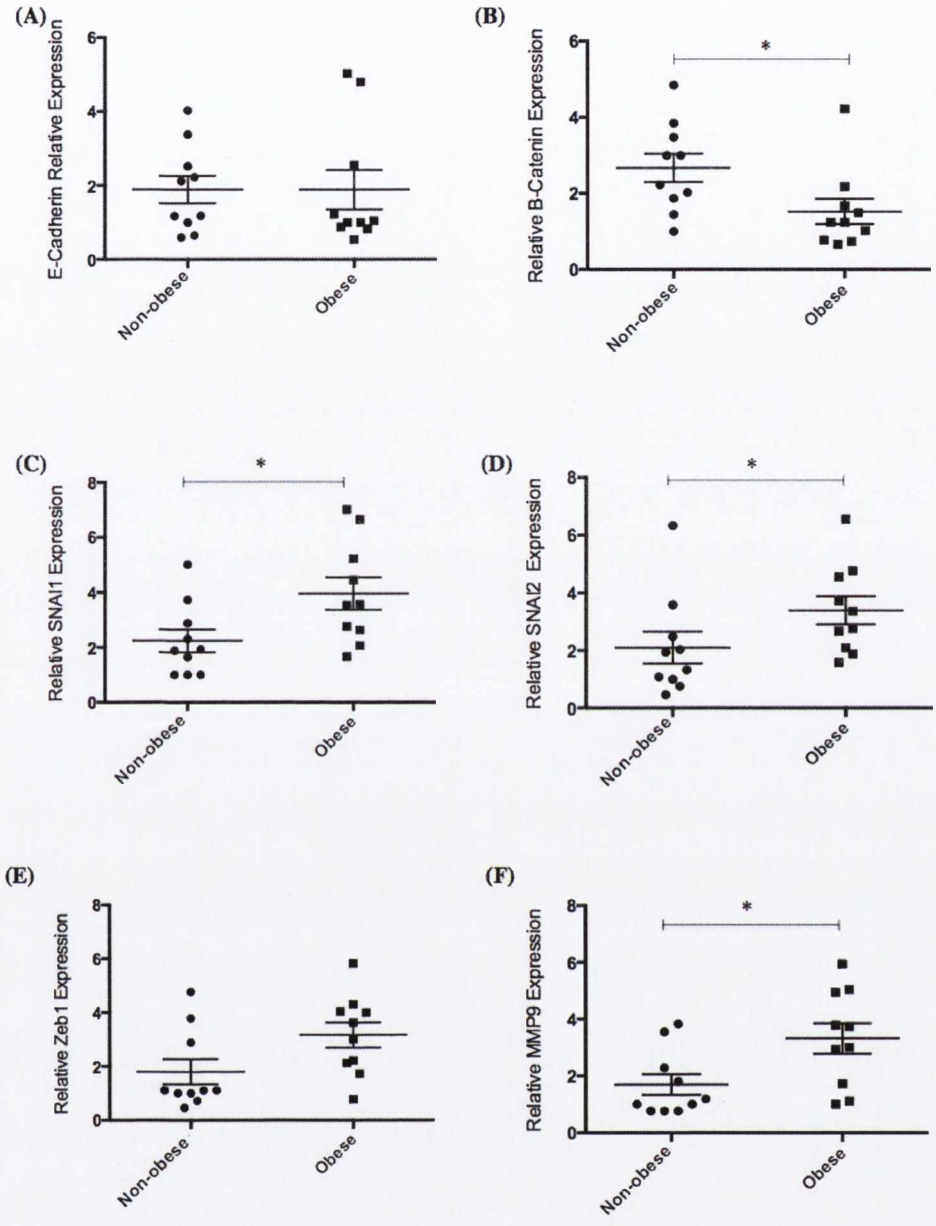


Figure 4.15 The link between EMT-associated genes and visceral obesity in OAC tumor (A) There was no difference in E-cadherin expression in OAC tumor from obese and non-obese patients ($p=0.7796$). (B) β-catenin expression level was significantly lower in viscerally obese compared to non-obese patients ($p<0.05$). (C) SNAI1 expression level was significantly higher in tumour from viscerally obese OAC patients ($p<0.05$). (D) SNAI2 expression level was significantly higher in viscerally obese compared to non-obese patients ($p<0.05$). (E) There appeared to be a higher expression of Zeb1 in OAC tumour from obese patients, however it just failed to reach significance ($p=0.0522$). (F) MMP9 expression level was significantly higher in tumour from viscerally obese compared to non-obese patients ($p<0.05$). n=10 in each group. Statistical test used was Man-Whitney U test. $p<0.05$(*). Error bar denotes mean ± S.E.M.

4.3.2.3 Epithelial expression EMT markers and their association with obesity status determined by BMI

Tissue microarrays (the same cohort as described in Section 3.3.3.1) were stained (staining procedure explained in 2.15.2) for E-cadherin and β-catenin. An average tumour epithelial score was assigned to each patient with an exception of cases where tissue cores and the scoring protocol was followed as described in Section 3.3.2.1 and Section 3.3.3.1. 120 OAC patients were segregated into two groups, based on their obesity status: overweight and obese (BMI≥25 kg/m^2) and normal weight (BMI 18.5-25 kg/m^2). Patient demographics described in Table 3.1. The grade for each marker was divided into greater and less than the median value and disease specific survival was investigated by Kaplan-Meier survival analysis. Patients that died within three months post-surgery, died of other causes or the cause of death was not known, were excluded from survival analysis therefore 95/120 patients were deemed to be suitable for E-cadherin and 92/120 for β-catenin expression analysis.

There was no significant difference in epithelial E-cadherin expression between overweight and obese compared to normal weight patients (157.4 ±6.776 versus 147.8 ±7.84, n=70 versus n=50, p=0.3446) (Figure 4.16b). There was no association between epithelial E-cadherin expression and BMI (r=0.0428, p=0.6423) (Figure 4.16c). β-catenin was expressed at significantly higher level in normal weight compared to overweight and obese patients (178 ±9.536 versus 154 ±7.69, n=50 versus n=70, p<0.05) (Figure 4.16e). There was no significant association between epithelial β-catenin expression and BMI, however negative correlation shows a reduction of β-catenin expression with increasing BMI (r=-0.1101, p=0.2887) (Figure 4.16f). There was no significant association with disease-specific survival between the two groups (median survival: 24 versus 31 months, n=43 versus n=42, log-rank test p=0.6222) (Figure 4.17a). There was no significant association between the level of epithelial β-catenin expression and 5-year post-operative, disease-specific survival (median survival: 28 months versus 18 months, n=46 in each group, p=0.0669) (Figure 4.17b).

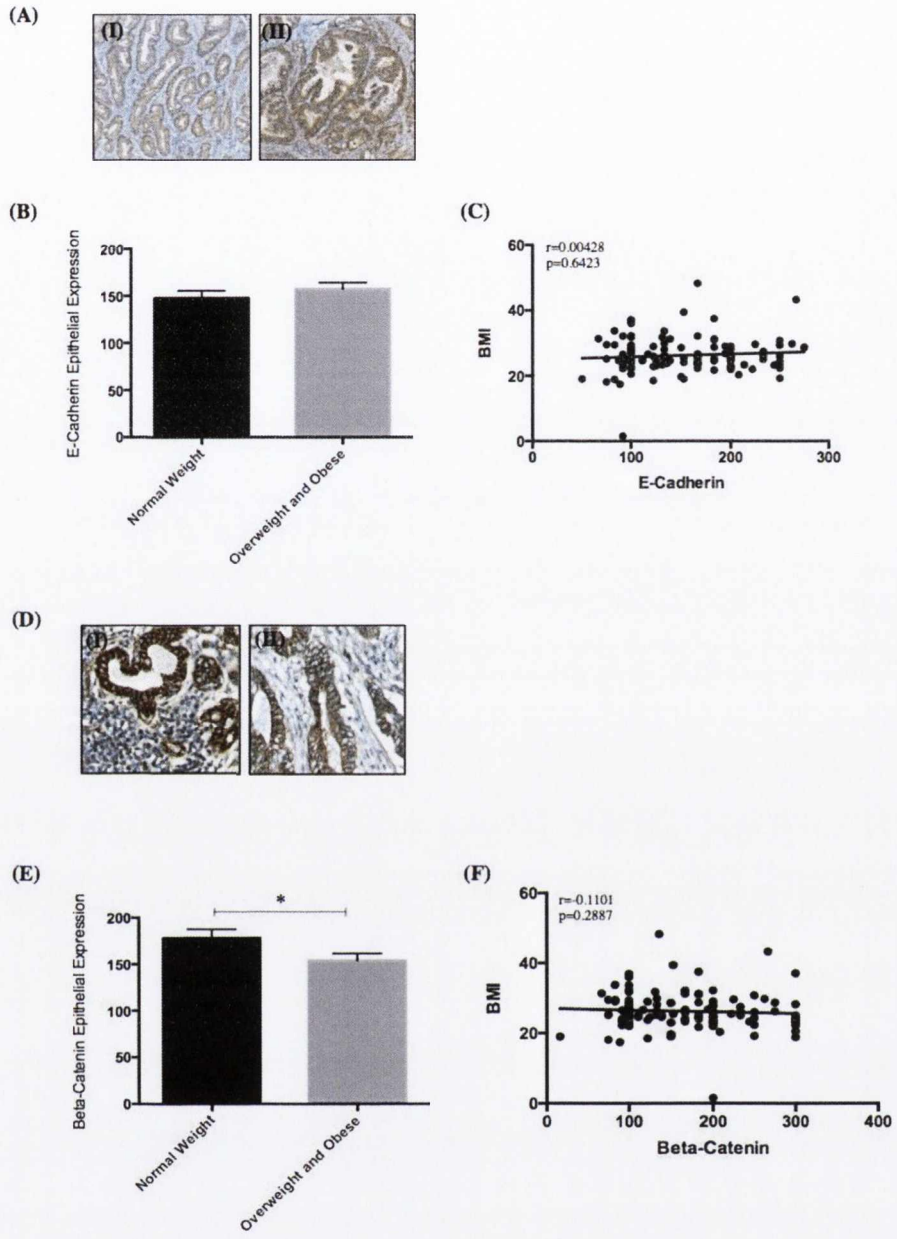


Figure 4.16 Low epithelial expression of β-catenin, but not E-cadherin, is associated with obesity in OAC tissue microarrays. (A) Representative image of E-cadherin expression in OAC tissue microarray. Panel (I) indicates the level of E-cadherin expression in normal weight patients and panel (II) indicates the level of the protein in overweight and obese OAC patients. (B) There was no significant difference in E-cadherin expression between obese and non-obese patients (p=0.3446). (C) There was no association between epithelial E-cadherin expression and BMI (r=0.0428, p=0.6423). (D) Representative image of β-catenin expression in OAC tissue microarray. Panel (I) indicates high level of β-catenin expression and panel (II) indicates reduced levels of the protein in overweight and obese OAC patients. (E) β-catenin was expressed at significantly higher level in normal weight compared to overweight and obese patients ($p<0.05$). (F) There was no significant association between epithelial β-catenin expression and BMI, however negative correlation shows a reduction of β-catenin expression with increasing BMI (r=-0.1101, p=0.2887). Statistical test used was Man-Whitney U test for comparison and Spearman's test was used for correlations with anthropomorphic measurements. $p<0.05$ (*). Error bar denotes mean ± S.E.M.

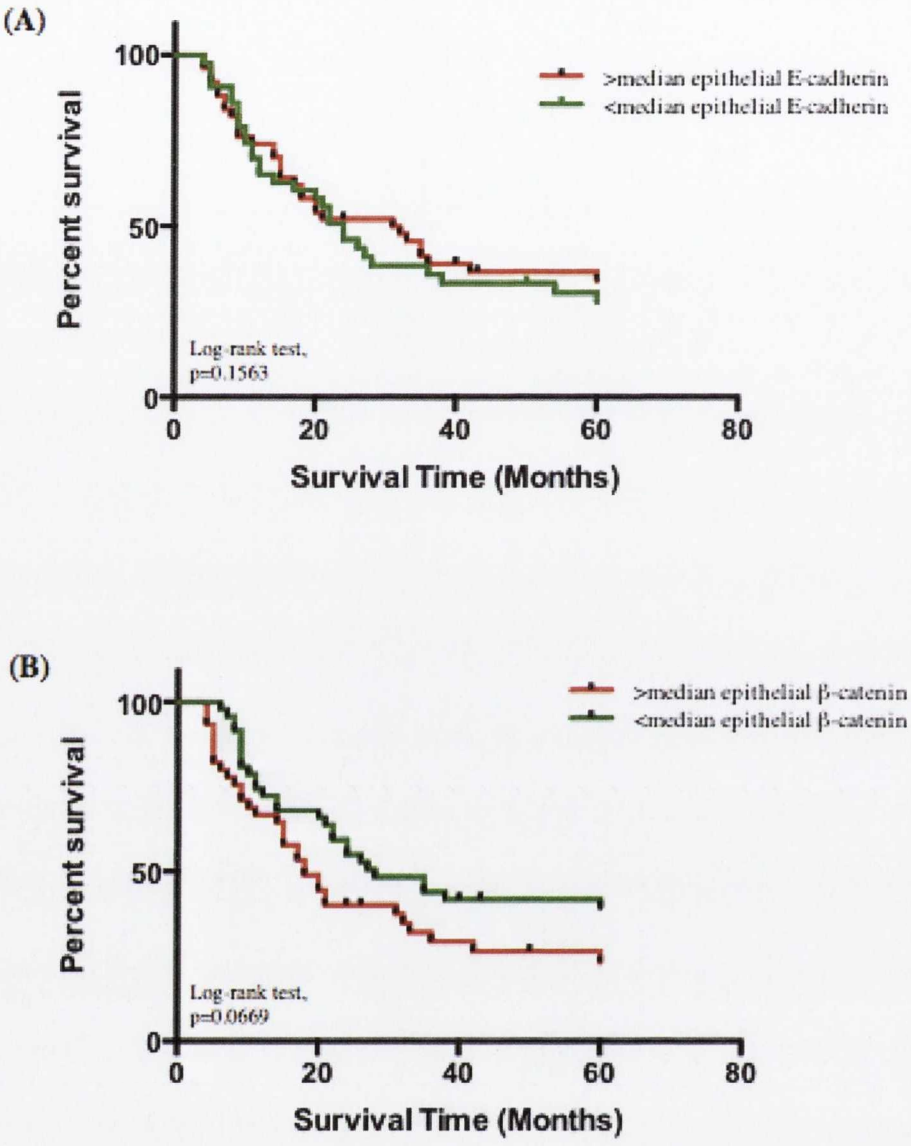


Figure 4.17 The association between epithelial E-cadherin and β-catenin expression and OAC-specific 5-year post-operative survival. (A) There was no association between epithelial E-cadherin expression and disease-specific survival (median survival: 24 versus 31 months, n=43 versus n=42, log-rank test p=0.6222). (B) There was no significant association between the level of epithelial β-catenin expression and 5-year post-operative, disease-specific survival (median survival: 28 months versus 18 months, n=46 in each group, p=0.0669). Statistical test used was Kaplan Meier survival curve with Log-rank (Mantel-Cox) test.

4.4 Discussion

Alterations in mitochondrial function and energy metabolism is an emerging hallmark of cancer, however, the potential role that obesity plays in driving these alterations in OAC is currently unknown [329]. A strong association between obesity and oesophageal adenocarcinoma has emerged over the recent years [330], therefore the factors fueling this association may uncover new understanding of the malignancy and new potential targets. This study highlights a potential importance of obesity driven factors including increased glycolysis, oxidative phosphorylation, hypoxia, 5-lipoxygenase expression and activation of EMT. The list of pathways, markers and all significant findings summarized in Table 4.4.

Table 4.4 Summary of findings from Chapter 4

Pathway	Marker	OE33+ACM	OAC Tumour	TMA (BMI) n=120	
		n=5	n=10	epithelial exp.	correlation
GLYCOLYIS	Glut1	p<0.05	p=0.122	p=0.243	p=0.4150
	Glut4	p<0.05	p<0.05	p<0.01	p<0.05
	HK1	p=0.0952	p=0.4727	p=0.7976	p=0.3358
	HK2	p=0.1508	p<0.05	p<0.01	p<0.05
	PKM2	p=0.317	p<0.05	p<0.05	p<0.05
	GAPDH	p<0.01	p<0.05	p<0.0001	p<0.0001
	ENO3	p=0.0556	p<0.05	p<0.05	p<0.05
EICOSANOID	5LOX	p=0.5317	p<0.05	p<0.01	p<0.05
OXPHOS	ATP5B	-	p<0.05	p<0.05	p<0.01
HYPOXIA	HIF1A	-	-	p<0.05	p=0.1056
	CAIX	-	-	p<0.05	p=0.07
EMT	E-Cadherin	p=0.0952	p=0.7796	p=0.3446	p=0.6423
	β-Catenin	p=0.222	p<0.05	p<0.05	p=0.2887
	SNAI1	p<0.05	p<0.05	-	-
	SNAI2	p<0.05	p<0.05	-	-
	Zeb1	p<0.05	p=0.0522	-	-
	MMP9	p=0.4127	p<0.05	-	-

It has been previously published that ACM from obese OAC patients have a distinct metabolic profile and that ACM is able to alter tumour metabolism [174]. Following co-culture of OE33 cells with ACM from overweight and obese patients, we observed alterations in expression levels of a number of enzymes associated with tumour glycolysis

at the gene level. Glucose transporter proteins GLUT1 and GLUT4 were both significantly upregulated following the co-culture of cells with ACM from overweight and obese OAC patients. An increase in GLUT1 expression levels has been previously shown to be a marker of poor prognosis in oesophageal SCC, however, there has been limited research linking GLUT1 with obesity [204]. GLUT4 has been widely documented to have a significant association with obesity. This study demonstrated that ACM from obese OAC patients resulted in a significant GLUT4 upregulation, however, this result was supported findings in other studies. It has been documented that GLUT4 was upregulated in breast cancer cell lines and a knockout of GLUT4 in breast cancer cell lines have been shown to impair glucose uptake, reduced lactate production, which was also observed in our early breast disease model, suggesting that blocking GLUT4 or its upstream activating signals may empower cancer treatment and prevention [331]. In this study, the increase in GLUT4 expression at the gene level was validated utilizing resected OAC tumour biopsies, with obesity status measured by VFA. GLUT4 expression was significantly higher in tumour from viscerally obese compared to non-obese patients, suggesting a positive association between high GLUT4 expression and induction of glycolysis. Immunohistochemical analysis in this study showed that epithelial expression of GLUT4 was significantly higher in overweight and obese OAC patient tumours compared to normal weight group, and there was a significant correlation between obesity and increasing levels of GLUT4. This result suggests a positive link between GLUT4 upregulation and obesity-induced glucose metabolism.

This study reports an increase in HK2 expression in viscerally obese OAC patient tumour when HK2 expression level in resected OAC tumour was measured in real time by qPCR. The association between HK2 expression and obesity was confirmed at the protein level, where the expression level of HK2 was significantly elevated in overweight and obese compared to normal weight patients. There was a positive correlation between the increasing levels of HK2 and obesity. This study showed a link between an increase in HK2 and obesity (and potentially glycolysis) and not an increase HK1. This link between aerobic glycolysis and HK2 but not HK1 has been previously shown in human glioblastoma, where altered glucose metabolism was observed with altering HK2 expression but not HK1 and is suggestive of aberrant HK2 expression being an important regulator of aerobic glycolysis in GBMs, but does not rule out the possibility of its working in conjunction with other specific downstream glycolytic enzyme isoforms [321].

This study revealed the link between obesity and elevated levels of PKM2 at both gene and protein level in OAC. PKM2 expression was significantly higher in tumour from overweight and obese compared to normal weight OAC patients. The result of elevated PKM2 expression being elevated in obese and overweight OAC patients at the gene level was supported by immunohistochemical study where the increase in epithelial PKM2 expression was positively correlated with increasing BMI. These findings were in line with other studies as PKM2 has been shown to be the key enzyme in catalyzing the final glycolysis reaction [269] and the expression of the glycolytic marker PKM2 in OAC tumours was positively associated with obesity [175].

This study reported a positive association between GAPDH and obesity. The level of GAPDH was significantly upregulated in OE33 cell treated with ACM from overweight and obese OAC patients. It was also upregulated in the tumour tissue from viscerally obese patients and positively correlated with obesity in the immunohistological study. This data has been supported by findings of another study in St. James's hospital where the positive correlation between visceral obesity and increasing GAPDH levels has been shown in Barrett's oesophagus [247]. It has been shown that GAPDH was overexpressed in 24 types of cancer including brain, testicular, prostate, gastric cancers [225] and GAPDH gene over expression was found to be an adverse prognostic factor in early stages NSCLC and this result was confirmed in 5 of 6 public datasets analyzed: Shedden *et al* [228], Lee *et al* [229], Tomida *et al* [230], Roepman *et al* [231], Okayama *et al* [232], Botling *et al* 2013 [233], all confirming the prognostic value of glucose metabolism assessment in NSCLC.

Enolase 3 (ENO3) enzyme was of interest in this study as it has been previously shown to be glycolytic enzyme that was responsible for catalysing the reversible conversion of 2-phosphoglycerate to phosphoenolpyruvate [271]. This study showed a link between OAC and obesity. The level of ENO3 was significantly upregulated in tumour tissue from viscerally obese OAC patients and was positively correlated with increasing BMI suggesting the role in obesity-induced glycolysis in this cohort of patients.

Published studies show HIF1A to be a major regulator of oxygen homeostasis within cells [276]. Results from immunohistochemical study showed an increase in epithelial expression of HIF1A in overweight and obese compared to normal weight OAC patients (Table 4.4). An increase in HIF1A expression has been previously shown in adipose tissue and adipocytes [332]. An increase in HIF1A has also been shown to be associated

with more aggressive disease phenotype, increase in inflammation that may stimulate cancer development and poor overall survival in colorectal cancer [272].

To further investigate the link between hypoxia and obesity in OAC, we assessed expression of CAIX, a second marker of hypoxia, in OAC tissue microarrays. There was no difference in epithelial CAIX expression levels between the normal weight versus overweight and obese OAC patients. There was no correlation between the level of epithelial expression in OAC tissue microarrays and increasing BMI. CAIX been previously shown to be a hypoxia-inducible enzyme overexpressed by cancer cells in various tumour types [304]. Due to high HIF1A expression in overweight and obese OAC patients in this cohort, we hypothesized that CAIX, hypoxia-inducible enzyme should be upregulated in the hypoxic regions therefore positively correlate with HIF1A expression, however, this hypothesis has failed. The possible explanation is that the CAIX antibody had a large level of non-specific binding therefore altered the outcome of the study.

The link between 5LOX expression and obesity was assessed in the same cohort of OAC tissue microarrays. Immunohistochemistry results showed a link between epithelial 5LOX expression in OAC and obesity. Additionally, increasing levels of 5LOX were positively associated with increasing BMI in OAC patients. 5LOX has been previously shown to have a role in various cancers including colorectal and oesophageal cancers. Obesity has also been shown to be associated with poor prognosis in oesophageal cancer, suggesting that 5LOX enzyme may be an attractive immunological and druggable target in OAC.

It has been reported that OAC has a strong link with obesity [333], therefore we hypothesized that adipose tissue would affect the expression of genes associated with EMT, which has been shown to contribute to cancer progression by increasing cell migration, invasive potential and leading to invasive and metastatic cancer [17]. This study showed that genes coding for SNAI1 and SNAI2 were significantly upregulated in OE33 cells following a 24 hour co-culture with ACM from overweight and obese compared to normal weight OAC patients (Table 4.4). These findings were supported by other studies where SNAI1 and SNAI2 genes have been shown to be associated with higher metastatic potential and poor prognosis suggesting that overweight and obese individuals had a higher risk of tumour metastasis and poorer prognosis [326, 334]. E-cadherin and Beta-catenin expression levels were observed to be downregulated in cell lines following treatment with ACM from obese individuals, however this decrease did

not reach a statistical significance. This may be due to the fact that SNAI1 and SNAI2 are upstream of these factors and are the 'master regulators' affected by adipose derived factors, and the expression of E-cadherin and Beta-catenin may be altered at a later time point.

Following the promising results obtained from the cell line work, SNAI1, SNAI2, E-cadherin and β-catenin expression levels were investigated in oesophageal cancer patient tumour biopsies. SNAI1 and SNAI2 confirmed to be expressed at significantly higher levels of expression in obese compared to non-obese individuals. Again, there was no decrease in E-cadherin levels, however, β-catenin levels were significantly downregulated with obese individuals having a lower expression of these adhesion molecules consistent with an activation of the EMT pathway. The activation of this pathway has been shown to confer a poor prognosis of the disease [335].

The expression of E-cadherin and Beta-catenin at the protein level was investigated in tissue-micro arrays of 120 patients with OAC. Kaplan Meyer survival analysis indicated that individuals with reduced levels of β-catenin, had a trend towards the lower probability of survival and individuals that expressed higher levels of these cell adhesion proteins, were more likely to be non-obese with increased survival probability. However, there was no difference in survival between high and low E-cadherin expressers.

This study also showed an increase of Zeb1 and MMP9 gene expression in overweight and obese OAC patients. These findings were in line with proof available in the literature. Zeb1 has been previously shown to be a transcriptional factor, similarly like SNAI1, repressing E-cadherin and inducing EMT [336]. It has been documented that high expression of Zeb1 was associated with an increased in VEGFA, facilitating a more metastatic phenotype in breast cancer cell line [327].

Matrix metaloproteinases have been viewed as one of the most promising targets of cancer treatments [337]. It has been reported that SNAI1, SNAI2, Twist and Zeb1 family of transcription factors were turned on during EMT process [338]. In cancer, EMT may be an important step that contributes to carcinoma progression by increasing cell migration, invasive activity and ability to pass through the basement membrane [178], thus leading to more invasive and metastatic cancers [339]. At the molecular level, EMT has been shown to express reduced levels of epithelial cell markers, including cell adhesion protein.

The limitation in this study was the unavailability of VFA measurements. CT-determined fat area is considered the most accurate and reproducible technique of body fat measurement and has been demonstrated to be a better predictor of cancer development, when compared to BMI. Therefore, the subsequent studies assessing the expression of metabolic markers in tumors from patients with VFA measurements will be utilized in order to fully elucidate the relationship between obesity, altered energy metabolism and OAC.

With all the significant findings from this study (Table 4.6) and past studies in mind, we conclude that glucose transporter proteins, markers of glycolysis, oxidative phosphorylation, hypoxia, EMT and 5-lipoxygenase contribute to the outcome of oesophageal adenocarcinoma in this cohort of patients. The aim of the follow up study is to investigate the functional role of these markers and the avenues to target them.

Chapter 5

5-lipogygenase, glycolysis, oxidative phosphorylation and hypoxia marker association with visceral obesity in OAC patients

5.1 Introduction

Adipose tissue is the primary storage site for excess energy. It has become increasingly clear that visceral adipose tissue has multiple endocrine, metabolic and immunological functions and is central to the pathogenesis of the metabolic syndrome [340], which is associated central obesity, dyslipidemia, hypertension and elevated fasting plasma glucose.

BMI is a simple index of weight-for-height that is commonly used to assess obesity, however, it is an imperfect measurement of abnormal or excessive fat accumulation, because this value does not distinguish fat mass from lean body mass components and because the distribution of fat tissue differs greatly between individuals [340-342]. For example, Figure 5.1 shows a CT scan of two males with the same amount of total body fat and similar BMI. However, it is evident that the VFA of one of the patients is approximately 50% higher compared to the other man, even though they both have similar BMI [341]. Accordingly, VFA has been proposed as an alternative to BMI for assessment of the impact of obesity and fat distribution [343].

Yoshikawa *et al* investigated the link between BMI and VFA in gastric cancer and reported that 33.3% of patients that were assigned to low BMI group were in fact viscerally obese following the measurement of VFA, supporting the usefulness of VFA as a good parameter to assess abdominal obesity even in patients with a normal BMI [343, 344].

The Third National Health and Nutrition Survey (a recent large study in the US) followed more than 15,000 participants for an average of 14 years. They measured the obesity status (by both BMI and waist-hip ratio) and overall survival. Using the data provided by this study, Sahakyan *et al* revealed that people who had normal body mass but had central obesity, had a significantly lower long-term survival compared to participants with normal fat distribution. The lower life expectancy in viscerally obese individuals (defined by WHR measurement) was mainly due to cardiovascular mortalities and it was independent of their BMI, once again, suggesting the importance of measuring visceral obesity by VFA rather than BMI and not even in the cancer setting [345].

There are a number of studies reporting a threshold level of VFA, above which, metabolic and inflammatory processes are altered. However, these studies have been conducted in Asian populations who, due to ethnic differences in fat distribution and metabolism, are not representative of white populations [310, 346, 347]. Doyle *et al* conducted a study aiming to determine VFA threshold level in white population. 170 males and 66 females undergoing gastrointestinal resection recruited and, for the first time, a gender-specific threshold level of VFA in white populations of $\geq$163.8 cm^2 for men and $\geq$80.1 cm^2 for women was reported [310].

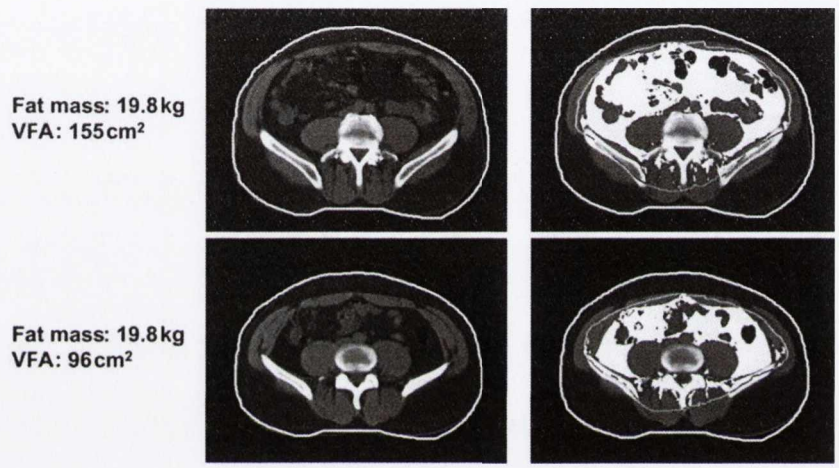


Figure 5.1 CT scans from two subjects with comparable BMI illustrating adiposity phenotypes characterized mainly by intra-abdominal adiposity and subcutaneous adiposity. Subcutaneous fat is shown in black under the skin, and visceral fat area (VFA) in white. Scans were made at the L4-L5 level. Reproduced from Ness-Abramof *et al.*, 2008 [348]. Imagine originally from Tchernof A, Després JP. Obesity and lipoprotein metabolism. In: Kopelman PG, ed. Clinical Obesity. London: Blackwell Science Ltd; 1998:176–204.

Visceral fat activity can be measured by SUVmax, which is a reliable and accurate measuring tool in evaluating metabolic tumour activity and metastases [290, 349]. Measuring SUVmax entails a single injection of radiolabeled glucose analogue fluorodeoxyglucose (FDG). PET scanners are used to measure the *in vivo* radioactivity concentration, which is directly linked to the FDG concentration [350]. An increase in FDG accumulation in tumour is measured relative to normal tissue. Changes in FDG accumulation have been shown to be useful as an imaging biomarker for assessing response to therapy in many cancers [350, 351].

Phank *et al* measured functional visceral fat activity by SUVmax of visceral fat/SUVmax of subcutaneous fat (V/S) ratio with the aim to predict lymph node and distant metastasis in CRC dependent on the metabolic ratio [349]. The study reported that a higher visceral

fat/subcutaneous fat (V/S) ratio had significant association with distant metastasis, therefore they hypothesised that distal metastasis might be associated with a greater inflammatory response than regional lymph metastasis [349]. This work was in line with previous studies showing that metabolically active, more aggressive, metastatic tumours were associated with high FDG uptake therefore higher SUVmax in non-small cell lung cancer (NSCLC) and breast cancer [288, 352] and high V/S ratio was associated with poor overall survival in metastatic melanoma [349].

With all the evidence of VFA measurement being superior to BMI in measuring visceral obesity and being a better indicator of the outcome of the disease, in this chapter, we aimed to investigate the significant findings from the immunohistological study in Chapter 3 (where the obesity status was based on BMI) in a newly-constructed cohort of OAC tissue microarrays with obesity status based on the VFA. This could potentially give us a better insight of the impact of visceral adiposity in oesophageal adenocarcinoma.

5.2 Aims and Objectives

The aim of this chapter was to retrospectively examine the expression of biomarkers of glycolysis, oxidative phosphorylation, hypoxia and 5-lipoxygenase in a newly constructed set of tissue-microarrays of OAC tumours linked to full anthropometric and clinical data with obesity status defined by VFA measurement.

Specific objectives:

- To correlate epithelial expression of glucose transporter proteins, markers of glycolysis, OXPHOS and 5-lipoxygenase and their association with visceral obesity.

- To correlate the expression of markers of glycolysis, oxidative phosphorylation hypoxia and 5-lipoxygense with clinical and pathological features.

- To investigate the link between visceral adiposity and tumour metabolism (SUVmax) in OAC patients

- To investigate the link between markers of glycolysis, OXPHOS, hypoxia and 5LOX, and tumour metabolism (SUVmax) in OAC patients

5.3 Results

5.3.1 Oesophageal adenocarcinoma tissue microarray demographics

The study population consisted of 48 oesophageal adenocarcinoma patients, 41 (85.4%) were male and 7 (14.6%) were female. The mean age was 63.72 years. Patient and tumour characteristics summarized in Table 5.1.

Paraffin-embedded tumour sections from 48 oesophageal adenocarcinoma patients with digital CT scan/VFA measurement and clinical follow up data available, were used to construct the tissue microarrays (Figure 3.2). Matched tumour leading edge cores were also included where available. Three 2mm cores were collected for each patient for TMA construction. Cores were taken from different paraffin-embedded tumour blocks (where available) in order to have a better representation of OAC tumour.
TMAs were stained for a range of markers of glycolysis, OXPHOS, hypoxia and 5-lipoxygenase. Optimisation was carried out using full-face oesophageal adenocarcinoma tissue at a number of different dilutions, as described in Section 2.13.

Table 5.1 Patient demographic for oesophageal adenocarcinoma microarrays

n=48	Mean (S.D.) or n (%) as appropriate	
Morphology (OAC)	48 (100%)	
Male:female	41:7 (85.4% : 14.6%)	
Age	63.7 (8.91)	
Tissue type	Leading edge (LE)	24(50%)
	Non-leading edge (NLE)	24(50%)
Nodal positivity	Lyph node (-)	21(44.6%)
	Lymph node (+)	26(55.3%)
	Missing	1(0.1%)
Venous positivity	Venous (-)	26(55.3%)
	Venous (+)	21(44.6%)
	Missing	1(0.1%)
SUVmax	8.709 (4.79)	
Metabolic tumour volume (MTV)	17.33 (14.93)	
VFA		
Male: female	174 (97.76): 103 (99.22)	
Non-obese: obese	23:25 (47.9%: 52.1%)	
Non-obese VFA	Male: 99.92 (56.13) Female: 45.29 (27.79)	
Obese VFA	Male: 251.3 (57.08) Female: 222 (51.65)	

5.3.2 Epithelial expression of glucose transporter proteins, markers of glycolysis, OXPHOS and 5-lipoxygenase and their association with visceral obesity

VFA measurement has been shown to be a gold standard measurement for central adiposity (483). To delineate the effect of visceral obesity in OAC, an additional TMA study was conducted where the obesity status OAC patients was based on VFA measurement rather than BMI, with obese VFA cut off value of 163.8 cm^2 in males and 80.1 cm^2 in females. Patient demographics are summarized in Table 4.5. 48 oesophageal adenocarcinoma patients samples from 2007-2013 with digital CT scan available and visceral fat area calculated were used to construct a set of TMAs, construction described in Section 2.13.1. Staining intensity, positivity and overall score was obtained as described in Section 3.3.2.1 and Section 3.3.3.1.

GLUT4 expression was significantly higher in obese compared to non-obese patients (188.6 ±14.37 versus 144.8 ±10.48, n=27 versus n=29, $p<0.05$) (Figure 5.2b) and there was also a significant positive correlation between the levels of Glut4 epithelial expression and VFA ($r=0.3094$, $p<0.05$, n=56) (Figure 5.2c). HK2 expression was also

significantly higher in viscerally obese versus non-obese patients (191.7 ±14.55 versus 150.1 ±10.56, n=27 versus n=29, $p<0.05$) (Figure 5.2e), however, there was no correlation between epithelial HK2 expression and increasing VFA (r=0.1376, p=0.3117, n=56) (Figure 5.2f). The level of GAPDH was significantly higher in obese compared to non-obese OAC patients (1.772 ±12.4 versus 143.4 ±9.512, n=27 versus n=29, $p<0.05$) (Figure 5.3b), and the levels of GAPDH appear to correlate with VFA, however, this just failed to reach significance (r=0.2583, p=0.0546) (Figure 5.3c). ATB5B expression was significantly upregulated in viscerally obese compared to non-obese OAC patients (185.6 ±12.55 versus 143.7 ±10.25, n=25 versus n=22, $p<0.05$) (Figure 5.3e), and again there appeared to be a positive association between the visceral obesity measurement and the epithelial ATP5B expression, but this just failed to reach significance (r=0.2819, p=0.0577, n=47) (Figure 5.3f). There was no difference in epithelial PKM2 expression between the two groups (176.2 ±12.79 versus 157.0 ±11.74, p=0.2385, n=56) (data not shown) and no association between the epithelial PKM2 expression and VFA (r=0.0205, p=0.8807, n=56) (Figure 5.4a). Similarly, there was no difference in epithelial ENO3 levels between obese and non-obese OAC patients (162.3 ±11.52 versus 141.4 ±13.17, n=24 versus n=19, p=0.1922) (data not shown) and subsequently there was no association between visceral obesity measurement and epithelial ENO3 expression (r=0.1527, p=0.3284, n=43) (Figure 5.4b). There was no significant difference between 5LOX expression between obese and non-obese patients (153.5 ±11.84 versus 128.5 ±8.193, n=24 versus n=29, p=0.116) (data not shown), however, there was an association between visceral obesity measurement and 5LOX expression levels (r=0.3026, $p<0.05$, n=43) (Figure 5.4c). There was no difference in HIF1A levels between the two groups (158.7 ±12.37 versus 132.1 ±10.73, n=29 versus n=27, p=0.0793) (data not shown) and there was no association between the levels of epithelial HIF1A and VFA (r=0.2186, n=56, p=0.1056) (Figure 5.4d).

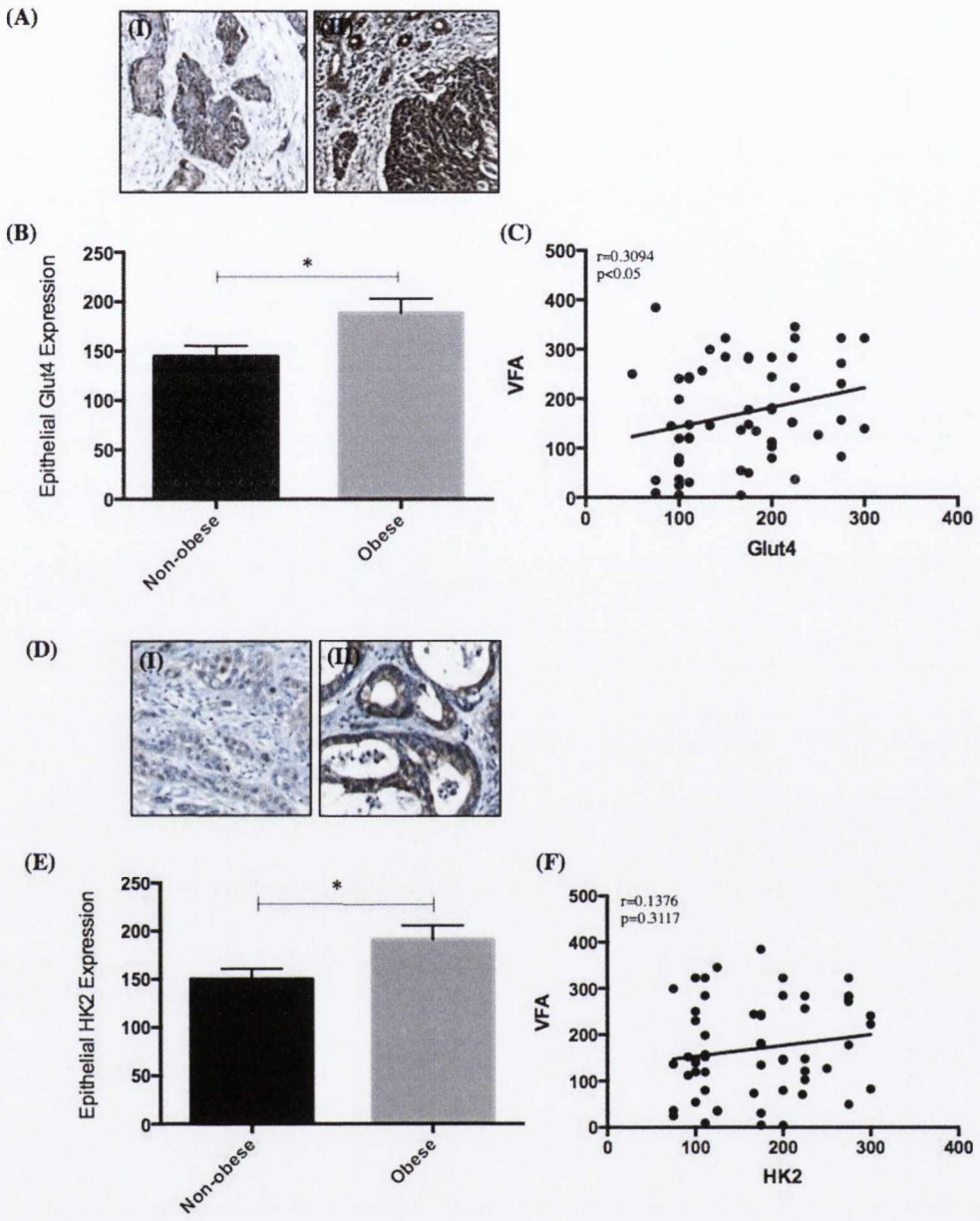


Figure 5.2 High epithelial GLUT4 and HK2 expression is associated with visceral obesity in OAC tissue microarrays. (A) Image (I) represents low/moderate level of GLUT4 expression in non-obese patients and Image (II) represents moderate/high level of epithelial GLUT4 expression in viscerally obese OAC patients. (B) Epithelial GLUT4 expression was significantly higher ($p<0.05$) in viscerally obese compared to non-obese OAC patients. (C) There was a significant positive correlation between the levels of epithelial GLUT4 expression and increasing VFA ($r=0.3094$, $p<0.05$). (D) Panel (I) represents low/moderate level of HK2 expression in non-obese patients and Panel (II) represents moderate/high level of epithelial (E) HK2 expression was significantly higher ($p<0.05$) in viscerally obese compared to non-obese OAC patients. (F). There was a significant positive correlation between the levels of epithelial HK2 expression and increasing VFA ($r=0.3117$, $p<0.05$). Statistical test used was Mann Whitney U test for comparison and Spearman's test was used for correlations with anthropomorphic measurements. $p<0.05$ (*). Error bar denotes mean ± S.E.M.

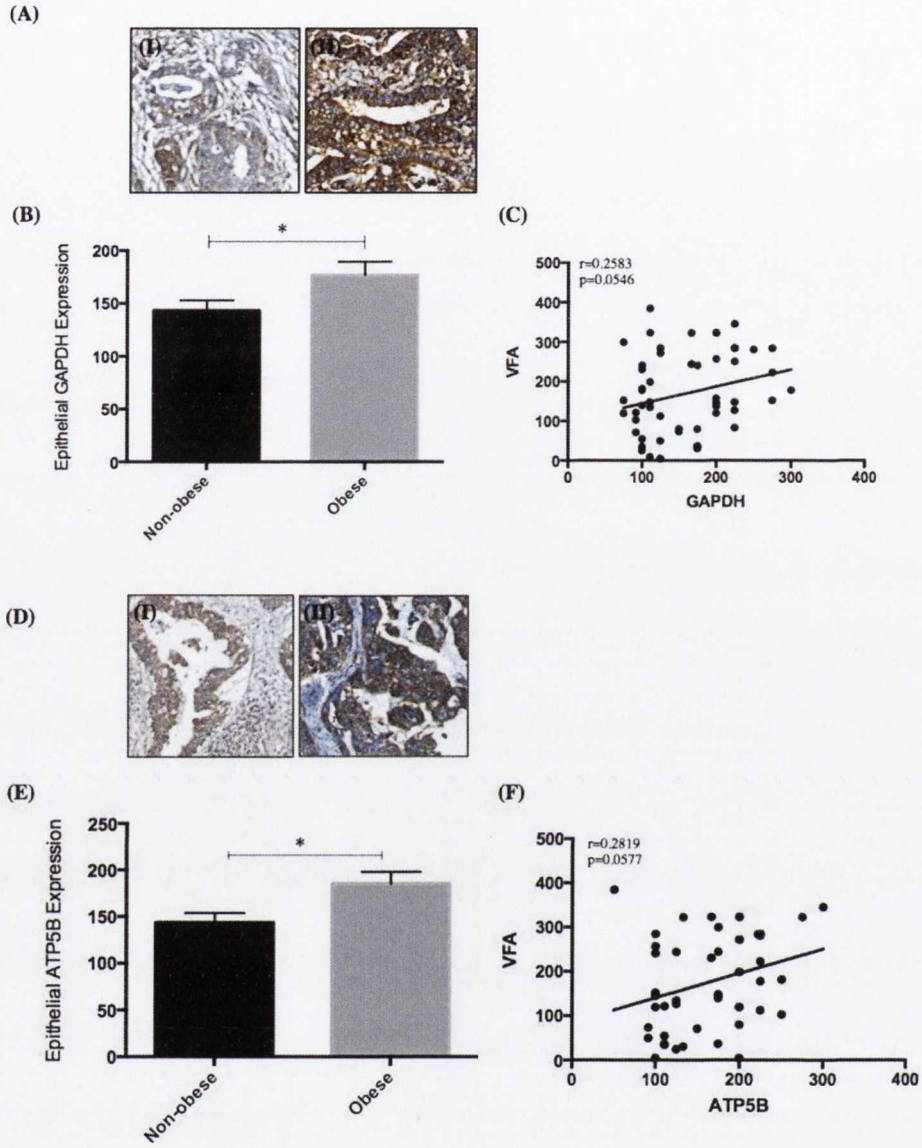


Figure 5.3 High epithelial GAPDH and ATP5B expression is observed in viscerally obese patients but high expression is not correlated with VFA in OAC tissue microarrays. (A) Panel (I) represents low/moderate level of GAPDH expression in non-obese patients and Panel (II) represents moderate/high level of epithelial GAPDH expression in viscerally obese OAC patients. (B) Epithelial GAPDH expression was significantly higher ($p<0.05$) in viscerally obese compared to non-obese OAC patients. (C) There was no significant positive correlation between the level of epithelial GAPDH expression and increasing VFA ($r=0.2583$, $p=0.0546$). (D) Panel (I) represents low/moderate level of ATP5B expression in non-obese patients and Panel (II) represents moderate/high level of epithelial ATP5B expression in viscerally obese OAC patients. (E) Epithelial ATP5B expression was significantly higher ($p<0.05$) in viscerally obese compared to non-obese OAC patients. (F) There was no significant positive correlation between the levels of epithelial ATP5B expression and increasing VFA ($r=0.2819$, $p=0.0577$). Statistical test used was Mann Whitney U test for comparison and Spearman's test was used for correlations with anthropomorphic measurements. $p<0.05$ (*). Error bar denotes mean ± S.E.M.

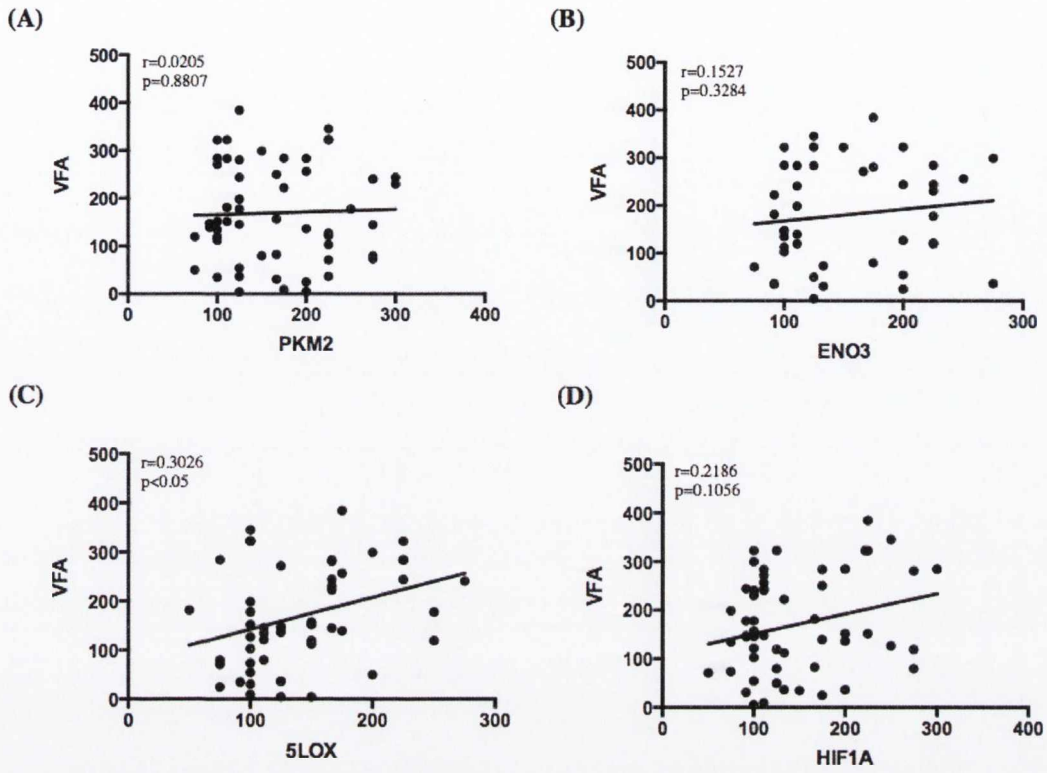


Figure 5.4 High epithelial expression of 5LOX, but not PKM2, ENO3 or HIF1A is correlated with visceral obesity in OAC tissue microarrays (A) There was no significant positive correlation between the level of epithelial PKM2 expression and increasing VFA (r=0.0205, p=0.8807). (B) There was no significant positive correlation between the level of epithelial ENO3 expression and increasing VFA (r=0.1527, p=0.3284). (C) There was a significant association between the level of epithelial 5LOX expression and increasing VFA (r=0.3026, p<0.05). (D) There was no significant difference in epithelial HIF1A expression in obese compared to non-obese patients (p=0.0793). (D) There was no significant association between the level of epithelial HIF1A expression and increasing VFA (r=0.2186, p=0.1056). Statistical test used was Spearman's test. p<0.05(*). Error bar denotes mean ±S.E.M.

5.3.3 The association of glucose transporter protein, markers of glycolysis, OXPHOS, hypoxia and 5-lipoxygenase with clinical data

5.3.3.1 Differential expression of glucose transporter protein, marker of glycolysis, OXPHOS, hypoxia and 5-lipoxygenase and tissue type

An average tumour epithelial and stromal score was assigned to each patient with an exception were cores were damaged or missing. The intensity score was obtained by scoring the cores between 0 and 3, the quantity of staining was obtained as described in Section 3.3.2.1. A subset of OAC patients with matched LE and NLE tissue (24/48 cases)

were analysed for stromal and epithelial expression. There was no difference in epithelial Glut4 expression between LE and NLE tissue (144.8 ±12.41 versus 153.2 ±13.62, n=24 in each group, p=0.6841) (Figure 5.5a, b) and also no difference in HK2 expression (160.9 ±11.94 versus 166.8 ±13.48, n=24 in each group, p=0.5379) (Figure 5.5c, d). Epithelial PKM2 expression was significantly higher in NLE tissue compared to LE (166.8 ±12.96 versus 132.4 ±10.91, n=24 in each group, $p<0.05$) (Figure 5.5e, f). There was no significant difference in epithelial GAPDH expression between LE and NLE tissue (170.3 ±13.45 versus 151.7 ±12.06, n=23 in each group, p=0.1477) (Figure 5.5g, h). Additionally, no significant difference in epithelial expression of ENO3 was observed between LE and NLE tissue (146.6 ±11.21 versus 144.2 ±13.73, n=20 in each group, p=0.8345) (Figure 5.6a, b). Similarly, there was no difference in expression between LE and NLE for 5LOX (132.2 ±9.55 versus 125.4, n=23 in each group, p=0.4673) (Figure 5.6c, d), ATP5B (153.9 ±12.06 versus 167.8 ±11.36, n=20 in each group, p=0.07753) (Figure 5.6e, f) and HIF1A (112.6 ±4.929 versus 110.0 ±7.331, n=24 in each group, p=0.4063) (Figure 5.6g, h). No difference between LE and NLE tissue in stromal expression was observed for any of the markers examined (data not shown).

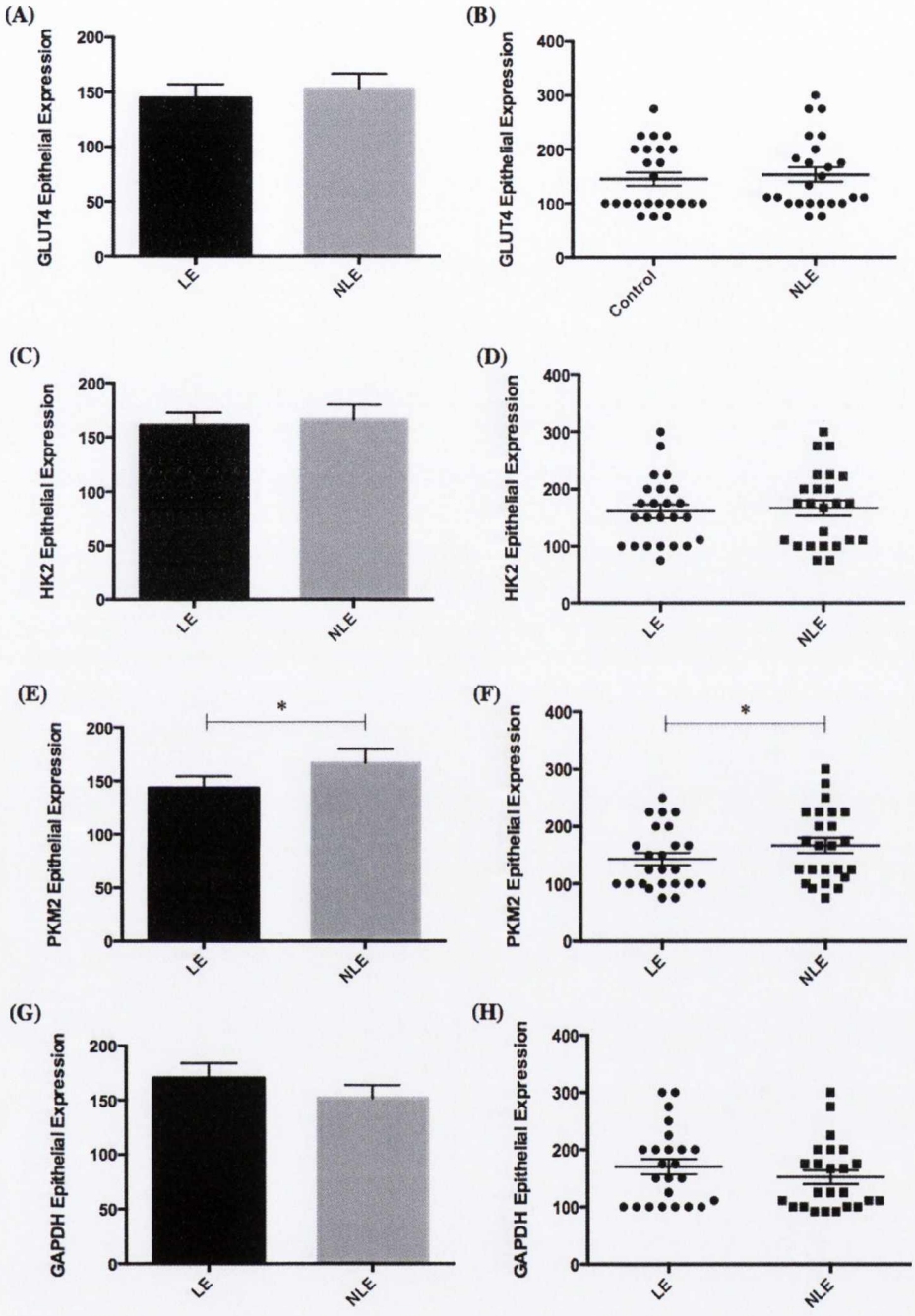


Figure 5.5 Comparison of glucose transport protein and glycolytic marker expression in the leading edge and non-leading edge oesophageal adenocarcinoma. (A) There was no significant difference in epithelial GLUT4 expression between LE and NLE tissue ($p=0.6841$, $n=24$). (B) The distribution of GLUT4 expression across OAC patient cores shown by scatter plot. (C) There was no significant difference in HK2 expression between LE and NLE tissue ($p=0.5379$, $n=24$). (D) The distribution of HK2 expression across OAC patient cores shown by scatter plot. (E) Epithelial PKM2 expression was significantly higher in NLE tissue ($p<0.05$, $n=24$). (F) The distribution of PKM2 expression across OAC patient cores shown by scatter plot. (G) There was no significant difference in epithelial GAPDH expression between LE and NLE tissue ($p=0.1477$, $n=24$). (H) The distribution of GAPDH expression across OAC patient cores shown by scatter plot. Statistical test used was Wilcoxon signed rank test. $p<0.05$(*). Error bar denotes mean ± S.E.M.

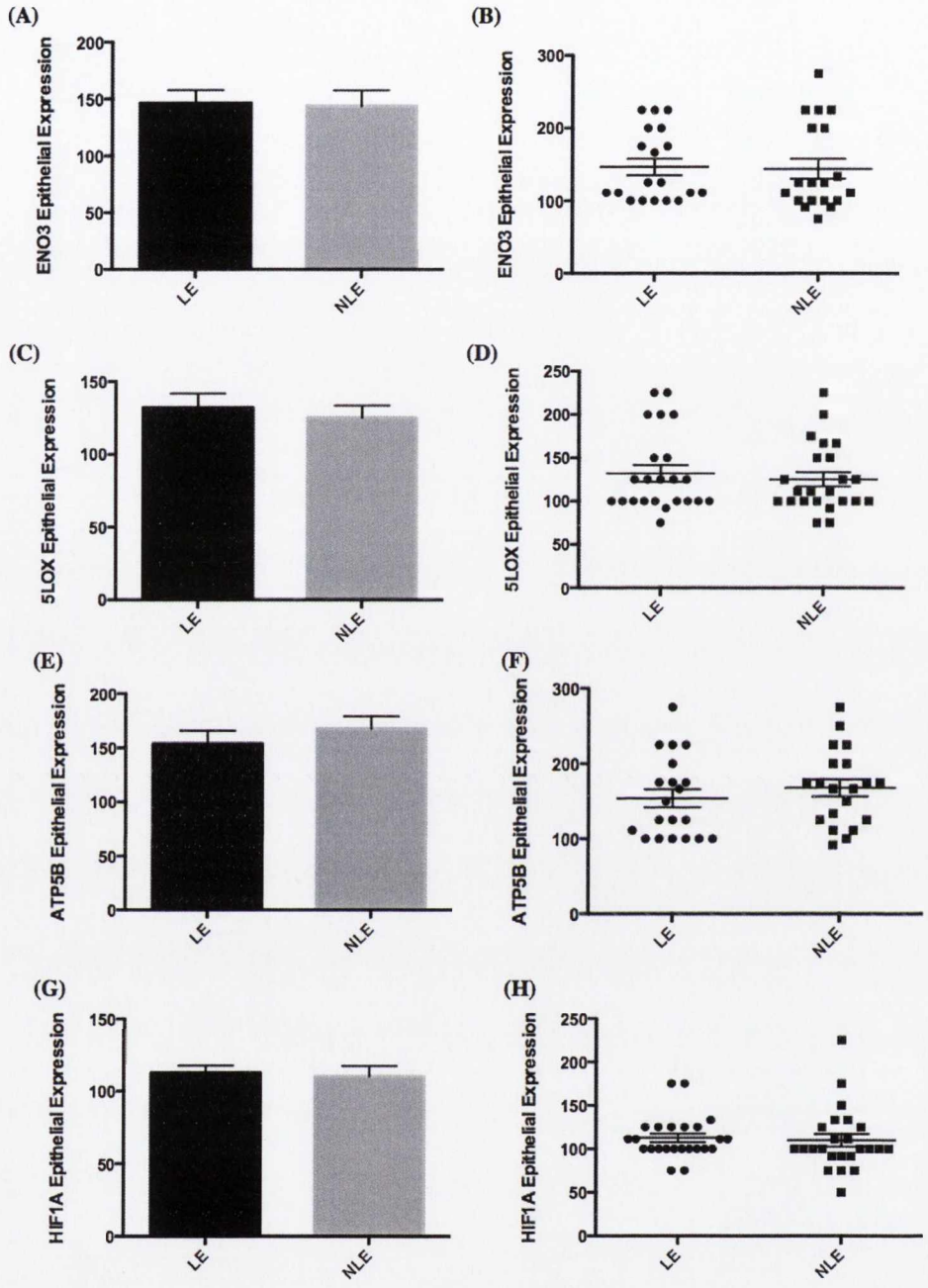


Figure 5.6 Comparison of epithelial expression of ENO3, 5LOX, ATP5B and HIF1A in the leading edge and non-leading edge oesophageal adenocarcinoma. (A) There was no significant difference in epithelial ENO3 expression between LE and NLE tissue (p=0.8345, n=20). (B) The distribution of ENO3 expression across OAC patient cores shown by scatter plot. (C) There was no significant difference in 5LOX expression between LE and NLE tissue (p=0.4673, n=23). (D) The distribution of 5LOX expression across OAC patient cores shown by scatter plot. (E) There was no significant difference in epithelial ATP5B expression between LE and NLE tissue (p=0.0753, n=20). (F) The distribution of ATP5B expression across OAC patient cores shown by scatter plot. (G) There was no significant difference in epithelial HIF1A expression between LE and NLE tissue (p=0.4063, n=24). (H) The distribution of HIF1A expression across OAC patient cores shown by scatter plot. Statistical test used was Wilcoxon signed rank test. Error bar denotes mean ± S.E.M.

5.3.3.2 Glucose transporter protein, glycolysis marker, 5-lipoxygenase, ATP5B and HIF1A expression and lymph node involvement in oesophageal adenocarcinoma

Epithelial expression of glucose transporter protein (GLUT4), markers of glycolysis (HK2, PKM2, ENO3, GAPDH), OXPHOS (ATP5B), hypoxia (HIF1A) and 5-lipoxygenase, was correlated with lymph node involvement in OAC patients. There was no difference in the epithelial expression of any of the markers outlined above, between the patients with the presence of lymph involvement compared to lymph node negative patients. Glucose transport protein GLUT4 was expressed at similar levels in both groups of patients (164.7 ±14.72 versus 168.8 ±11.60, n=26 versus n=21, p=0.6584) (Figure 5.7a). Epithelial HK2 expression showed very similar result. There was no difference in the epithelial HK2 expression levels between OAC patients with the presence and the ones with the absence of lymph node involvement (164.2 ±13.07 versus 158.2 ±14.32, n=26 versus n=21, p=0.7855) (Figure 5.7b). Similarly, no differential epithelial expression of PKM2 (162.4 ±13.07 versus 170.5 ±14.34, n=26 and n=21, p=0.5465) (Figure 5.7c) or GAPDH (140 ±8.987 versus 164.2 ±15.35, n=26 versus n=21, p=0.378) (Figure 5.7d) observed between the two groups of OAC patients. Once again, epithelial expression of glycolysis associated ENO3 expression levels were similar between OAC patients with the presence and with the absence of lymph node involvement (147.5 ±13.5 versus 157.5 ±14.91, n=21 in each group, p=0.5526) (Figure 5.8a). Non-significant findings followed for epithelial expression of 5LOX (137.2 ±11.4 versus 127.5 ±9.349, n=24 versus n=21, p=0.4886) (Figure 5.8b), OXPHOS marker ATP5B (150.8 ±9.684 versus 177.1 ±16.42, n=21 in each group, p=0.2619) (Figure 5.8c) and marker of hypoxia, HIF1A (122.7 ±8.45 versus 164.3 ±16.66, n=26 versus n=21, p=0.0847) (Figure 5.8d) where there was no difference observed in epithelial expression of these markers between the two patient groups: the OAC patients with and without lymph node involvement.

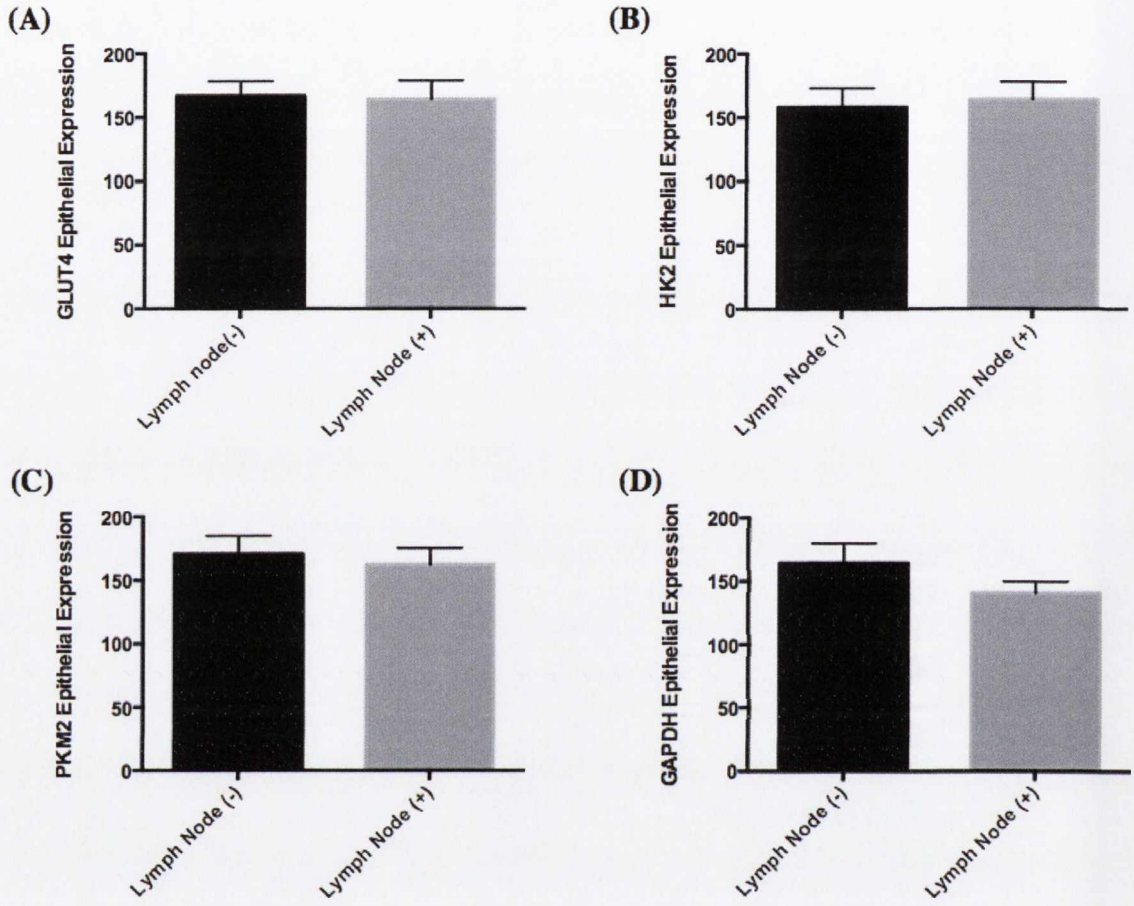


Figure 5.7 There is no association between epithelial GLUT4, HK2, PKM2 or GAPDH expression and more aggressive phenotype of OAC in this cohort of patients. (A) There was no significant difference between epithelial GLUT4 expression in lymph node positive and negative patients (p=0.6504, n=21 versus n=21). Similarly, there was no significant difference between (B) HK2 expression (p=0.7855, n=26 versus n=21), (C) PKM2 expression (p=0.5465, n=26 versus n=21) and (D) GAPDH expression (p=0.378, n=26 versus n=21) in lymph node positive and lymph node negative OAC patients. Statistical test used was Mann Whitney U test. Error bar denotes mean ± S.E.M.

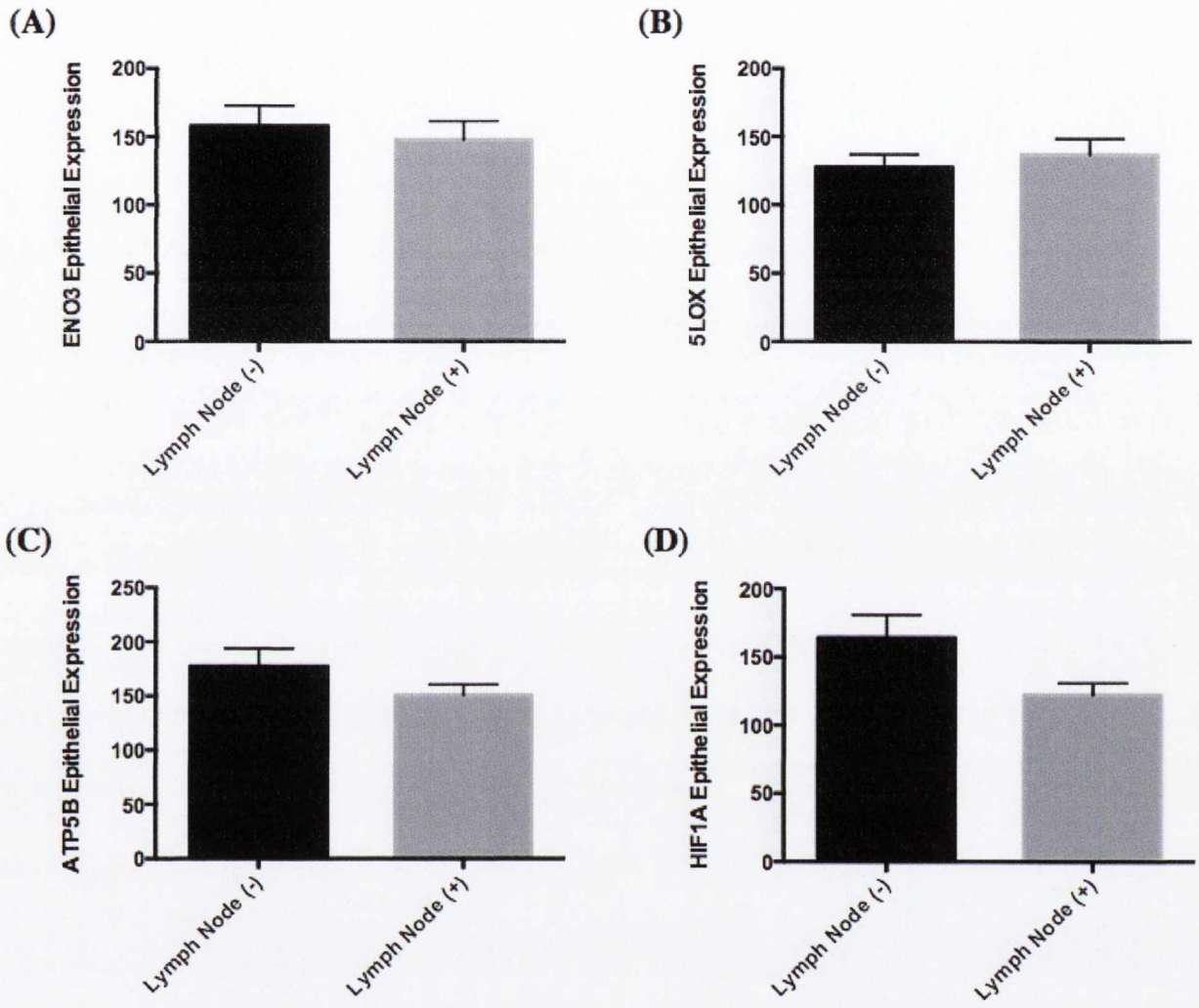


Figure 5.8 There is no association between epithelial ENO3, 5LOX, ATP5B or HIF1A expression and venous involvement in this cohort of OAC patients. (A) There was no significant difference between epithelial ENO3 expression in lymph node positive and negative patients (p=0.5526, n=21 in each group). Similarly, there was no significant difference between (B) 5LOX expression (p=0.4886, n=24 versus n=21), (C) ATP5B expression (p=0.2619, n=21 in each group) and (D) HIF1A expression (p=0.0847, n=26 versus n=21) in lymph node positive and lymph node negative OAC patients. Statistical test used was Mann Whitney U test. Error bar denotes mean ± S.E.M.

5.3.3.3 Glucose transporter protein, marker of glycolysis, 5-lipoxygenase, ATP5B and HIF1A expression and venous involvement in oesophageal adenocarcinoma

Epithelial expression of GLUT4, HK2, PKM2, GAPDH, ENO3, 5LOX, ATP5B and HIF1A was correlated with venous involvement in OAC patients. There was no significant difference in epithelial expression of any of the markers between the patients with and without venous involvement. Epithelial GLUT4 expression was similar in OAC patients with and without venous involvement (159.4 ±14.84 versus 170.7 ±12.61, n=21 versus n=21, p=0.4021) (Figure 5.9a). Similarly, there was no difference in epithelial HK2 expression between the patients with and without venous involvement (157.5 ±14.11 versus 164.7 ±14.25, n=21 versus n=26, p=0.7938) (Figure 5.9b). Similarly, no difference in PKM2 expression (156.9 ±15.61, n=19 versus n=26, p=0.3325) (Figure 5.9c) and GAPDH expression (139.2 ±9.466 versus 160.9 ±13.29, n=21 versus n=26, p=0.4076) (Figure 5.9d) observed between the two OAC patient groups. ENO3 expression also did not vary between the patients with and without venous involvement (149.8 ±16.07 versus 153.6 ±12.71, n=16 versus n=20) (Figure 5.10a). The non-significant findings followed for 5LOX (122.5 ±9.262 versus 142.7 ±11.57, n=18 versus n=24, p=0.4871) (Figure 5.10b), ATP5B (154.3 ±10.9 versus 169.3 ±14.21, n=17 versus n=21, p=0.53) (Figure 5.10c) and HIF1A expression (121.6 ±8.64 versus 158.6 ±14.87, n=22 versus n=25, p=0.204) (Figure 5.10d) and there was no difference observed between venous positive and venous negative OAC patients.

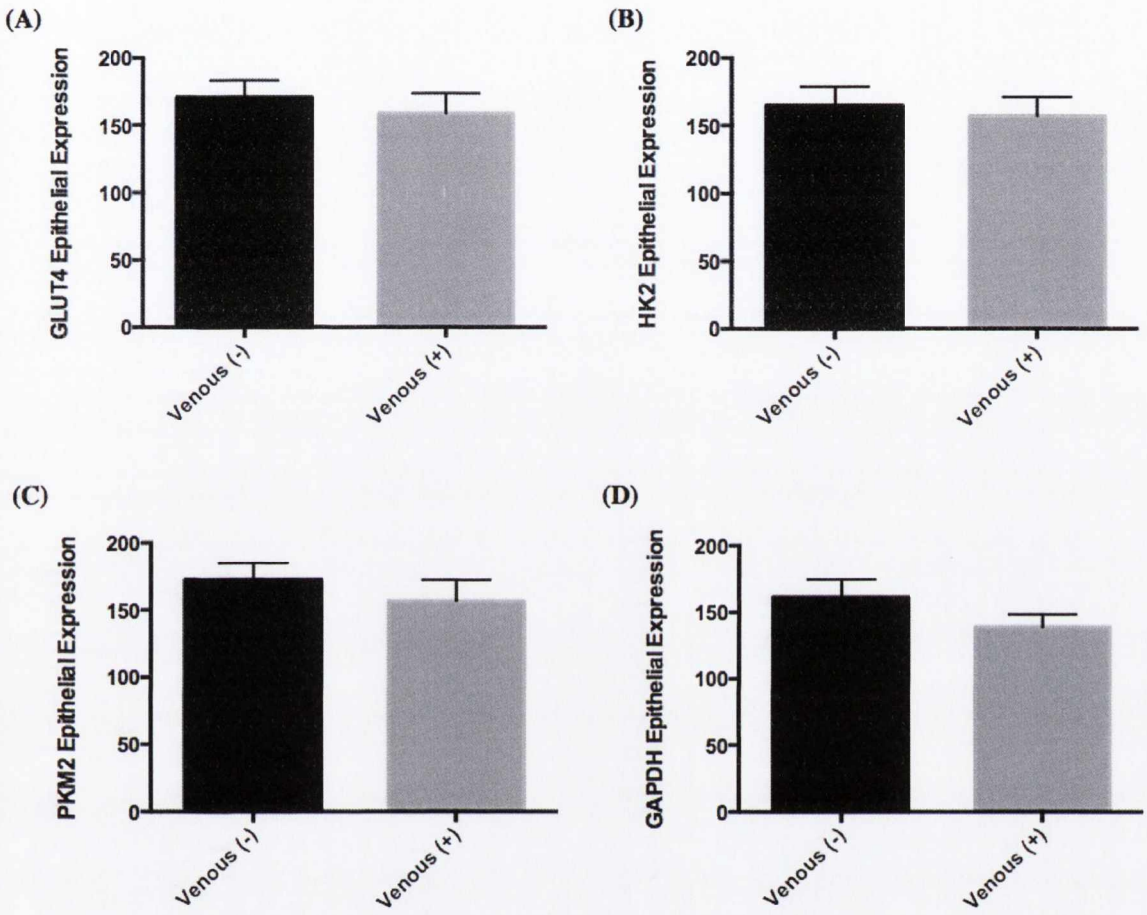


Figure 5.9 There is no association between epithelial GLUT4, HK2, PKM2 or GAPDH expression and venous involvement in this cohort of OAC patients. (A) There was no significant difference between epithelial GLUT4 expression between OAC patients with and without venous involvement (p=0.4021, n=21 versus n=26). Similarly, there was no significant difference between (B) HK2 expression (p=0.7938, n=21 versus n=26), (C) PKM2 expression (p=0.3325, n=19 versus n=26) and (D) GAPDH expression (p=0.4076, n=21 versus n=26) between venous involvement positive and negative OAC patients. Statistical test used was Mann Whitney U test. Error bar denotes mean ± S.E.M.

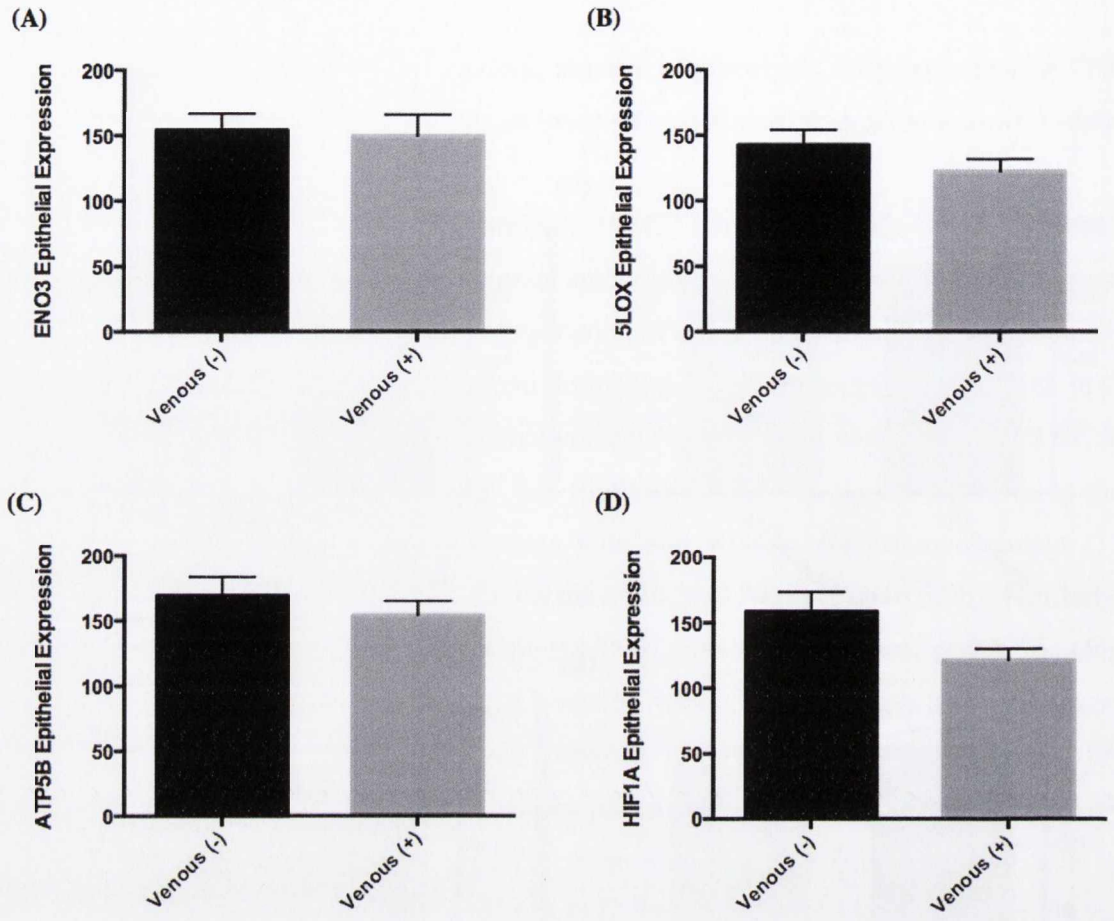


Figure 5.10 There is no association between epithelial ENO3, 5LOX, ATP5B or HIF1A expression and venous involvement in this cohort of OAC patients. (A) There was no significant difference between epithelial ENO3 expression between OAC patients with and without venous involvement (p=0.7757, n=16 versus n=20). Similarly, there was no significant difference between (B) 5LOX expression (p=0.4871, n=18 versus n=26), (C) ATP5B expression (p=0.5346, n=17 versus n=21) and (D) HIF1A expression (p=0.204, n=22 versus n=25) between venous involvement positive and negative OAC patients. Statistical test used was Mann Whitney U test. Error bar denotes mean ± S.E.M.

5.3.3.4 The association between visceral fat area, glucose transport protein, markers of glycolysis, OXPHOS, hypoxia, 5-lipoxygenase and metabolic tumour activity

PET/CT scans were used to evaluate the presence of tumour and metastasis. During the diagnostic PET scan FDG was injected and FDG standardized uptake value was assigned as SUVmax. There was a significant positive correlation between an increase in VFA and increasing SUVmax in male OAC patients ($p<0.05$, n=36) (Figure 5.11a), however, there was no correlation between an increase in VFA and metabolic tumour activity in female patients, presumably due to very low numbers of female patients in the cohort (r=-0.0357, p=0.9635, n=7) (Figure 5.11b).

There was no correlation between epithelial GLUT4 (r=-0.0212, p=0.89, n=45), HK2 (r=0.0185, p=0.9038, n=45), PKM2 (r=-0.03163, p=0.8366n n=45) or GAPDH (r=-0.07304, p=0.6335, n=45) expression and SUVmax (Figure 5.12a, Figure 5.12b, Figure 5.9.c and Figure 5.9d respectively). However, there was a significant correlation between epithelial ENO3 expression and SUVmax (r=0.4177, p<0.05, n=36) (Figure 5.13a). There was no significant association between epithelial expression of 5LOX (r=0.1347, p=0.3796, n=45), ATP5B (r=-0.0536, n=38) or HIF1A (r=0.01143, p=0.9406, n=45) with SUVmax (Figure 5.13b, Figure 5.13c and Figure 5.13d respectively.

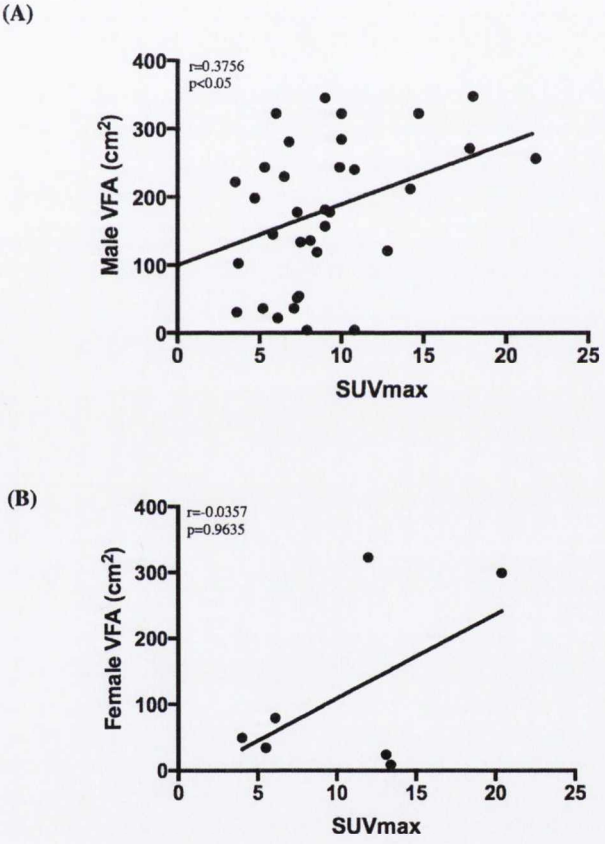


Figure 5.11 Association between tumour metabolism and increasing visceral fat area. (A) There was a significant positive correlation between increasing VFA measurement and increasing tumour metabolism (SUVmax) in males with OAC (r=0.3756, p<0.05, n=36). (B) There was no positive correlation between increasing VFA measurement and tumour metabolism (SUVmax) in females with OAC (r=-0.0357, p=0.9635, n=7). Statistical test used was Spearman's test. p<0.05(*).

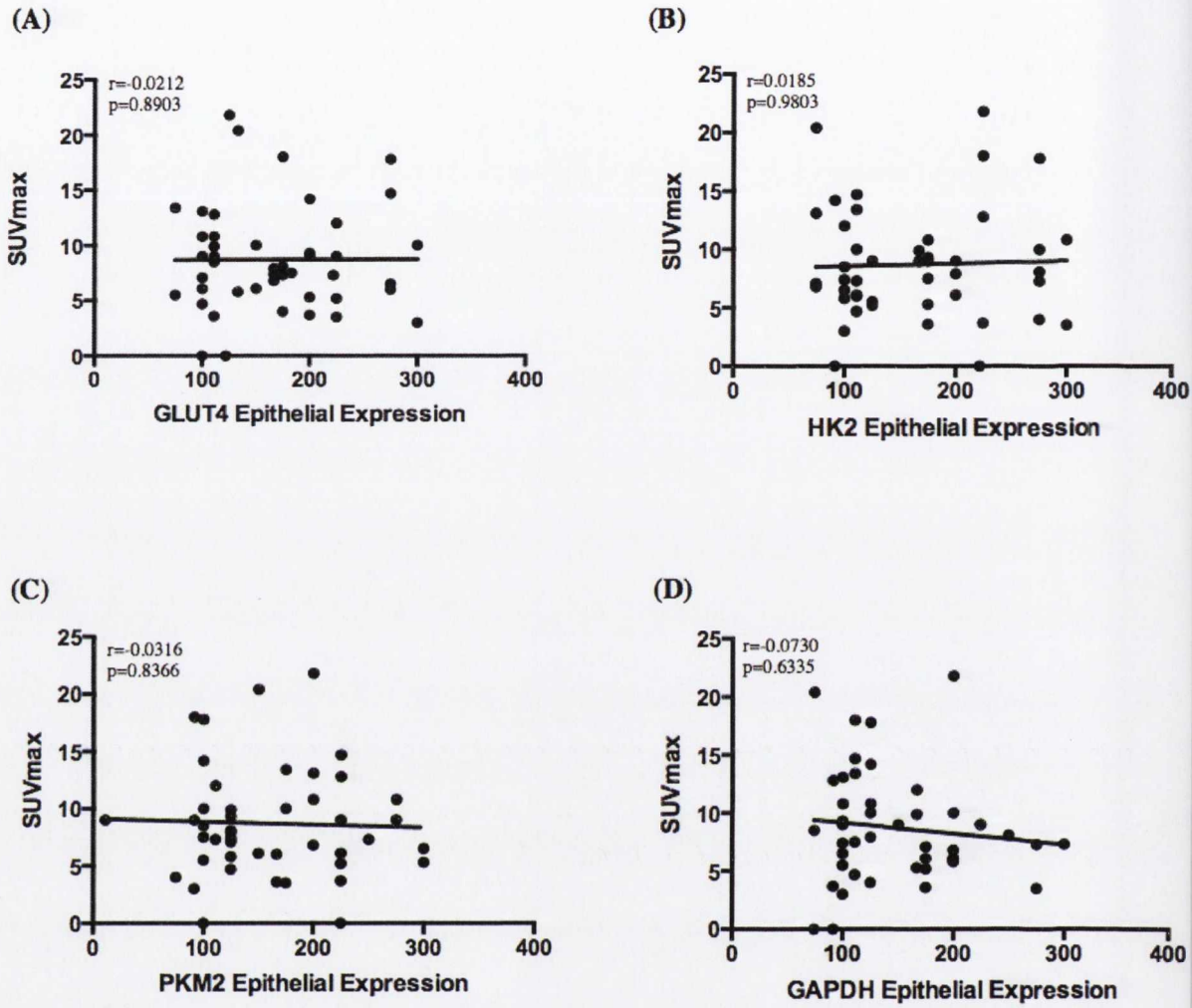


Figure 5.12 Association between markers of glycolysis and tumour metabolism in OAC patients. (A) There was no significant positive correlation between epithelial GLUT4 (r=-0.0212, p=0.89, n=45) (B) HK2 (r=0.0185, p=0.9038, n=45), (C) PKM2 (r=-0.03163, p=0.8366n n=45) or (D) GAPDH (r=-0.07304, p=0.6335, n=45) expression and SUVmax in OAC patients. Statistical test used was Spearman's test.

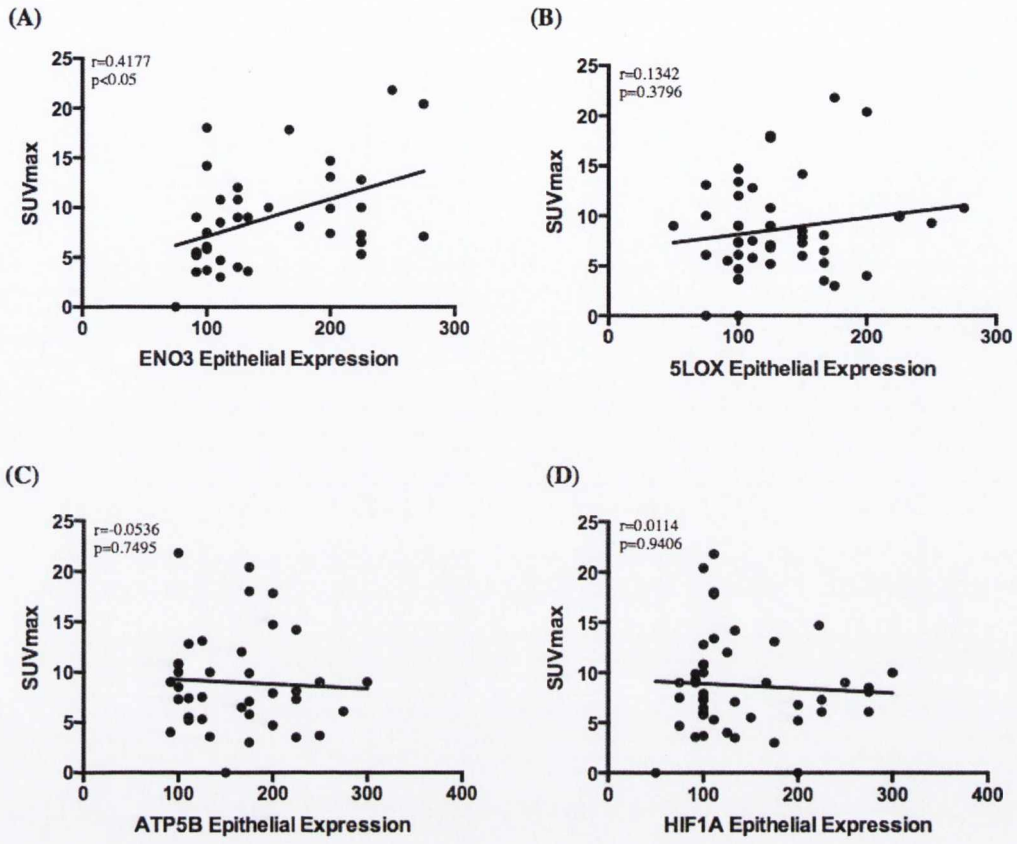


Figure 5.13 Association between ENO3, 5LOX, ATP5B and HIF1A and tumour metabolism in OAC patients. (A) There was a significant positive correlation between epithelial ENO3 expression and increasing SUVmax (r=0.4177, p<0.05, n=36). (B) There was no significant correlation between epithelial 5LOX expression and SUVmax (r=0.1342, p=0.3797, n=45), (C) ATP expression and SUVmax (r=-0.0536, p=0.7495, n=38) and (D) HIF1A expression and SUVmax (r=0.01143, p=0.9406, n=45) in OAC patients. Statistical test used was Spearman's test.

5.3.3.5 Association between metabolic tumour activity and disease-specific survival

SUVmax values were divided into greater and less than the median value and disease-specific survival was calculated by Kaplan-Meier survival analysis (Figure 5.10). Recent OAC tumour samples were used for the construction of tissue microarrays, therefore, follow-up and the survival data was only available for 2-3 years (rather than 5 years follow-up data available in the previous cohort of tissue microarrays were the obesity status was based on BMI). In order to maximize the accuracy of OAC-specific survival in this cohort of patients, survival was measured in days rather than months. Patients with less metabolically active tumours (SUVmax value bellow median) were associated

with significantly higher disease free survival, compared to the patients with more metabolically active tumours (median survival: 1240 days versus 595 days, n=22 versus n=23, log-ranks test $p<0.01$) (Figure 5.14).

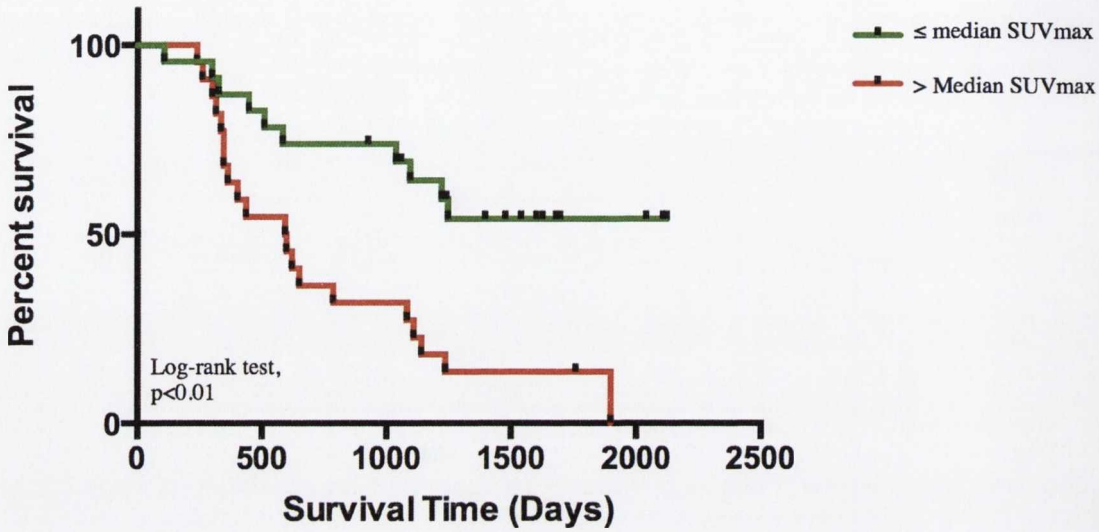


Figure 5.14 An increase in metabolic tumour activity is associated with poor survival in OAC patients. There was a significant association between a high metabolic tumour activity (SUVmax) and poor disease-specific survival in OAC patients (median survival: 1240 days versus 595 days, n=22 versus n=23, $p<0.01$). Statistical test used was Kaplan Meier survival curve with Log-rank (Mantel-Cox) test. $p<0.01$(**).

5.3.3.6 Association between visceral obesity and metabolic tumour volume

At the time of the diagnostic PET/CT scans FDG was injected and FDG standardized uptake value was assigned as SUVmax, metabolic tumour volume (MTV) – the volume of the disease was also calculated.

There was no significant correlation between increasing VFA measurement and metabolic tumour volume in male OAC patients ($r=0.0926$, $p=0.3342$, n=24) (Figure 5.15).

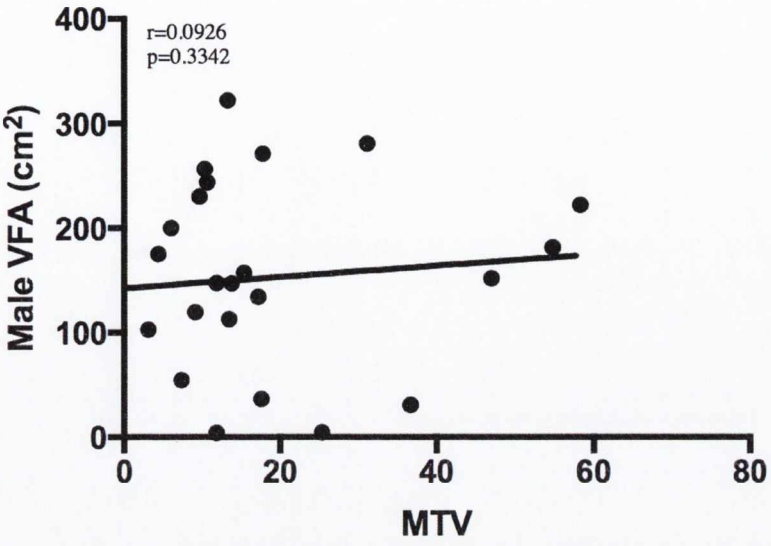


Figure 5.15 There is no positive association between increasing VFA measurement and metabolic tumour volume in OAC patients. There was no significant correlation between increasing VFA measurement and metabolic tumour volume in male OAC patients (r=0.0926, p=0.3342, n=24). Statistical test used was Spearman's test.

5.3.3.7 The association between the epithelial expression of markers of metabolism and metabolic tumour volume

Metabolic tumour volume measurement in OAC patients was correlated with epithelial expression of the glucose transporter GLUT4 and markers of glycolysis: HK2, PKM2, GAPDH, and ENO3. Additionally ATP5B was assessed as a marker of oxidative phosphorylation and the hypoxic marker HIF1A assessed in the TMAs and correlated with metabolic tumour volume (MTV). There was no association between high epithelial expression of Glut4 (r=0.0657, p=0.7299, n=30) (Figure 5.16a), HK2 (r=-0.2273, p=02271,n=30) (Figure 5.16b), PKM2 (r=-0.2256, p=0.2485, n=28) (Figure 5.16c) and MTV, however there was a significant positive correlation between high epithelial GAPDH expression (the marker of oxidative phosphorylation) and MTV (r=0.5706, p<001, n=30) (Figure 5.16d). No association between ENO3 (r=-0.0376, p=0.8682, n=22) (Figure 5.17a), 5LOX (r=0.1202, p=0.5269, n=30) (Figure 5.17b), ATP5B (r=0.1240, p=0.5638, n=24) (Figure 5.17c), HIF1A (r=0.2729, p=0.1445, n=30) (Figure 5.17d) and MTV was observed in the cohort.

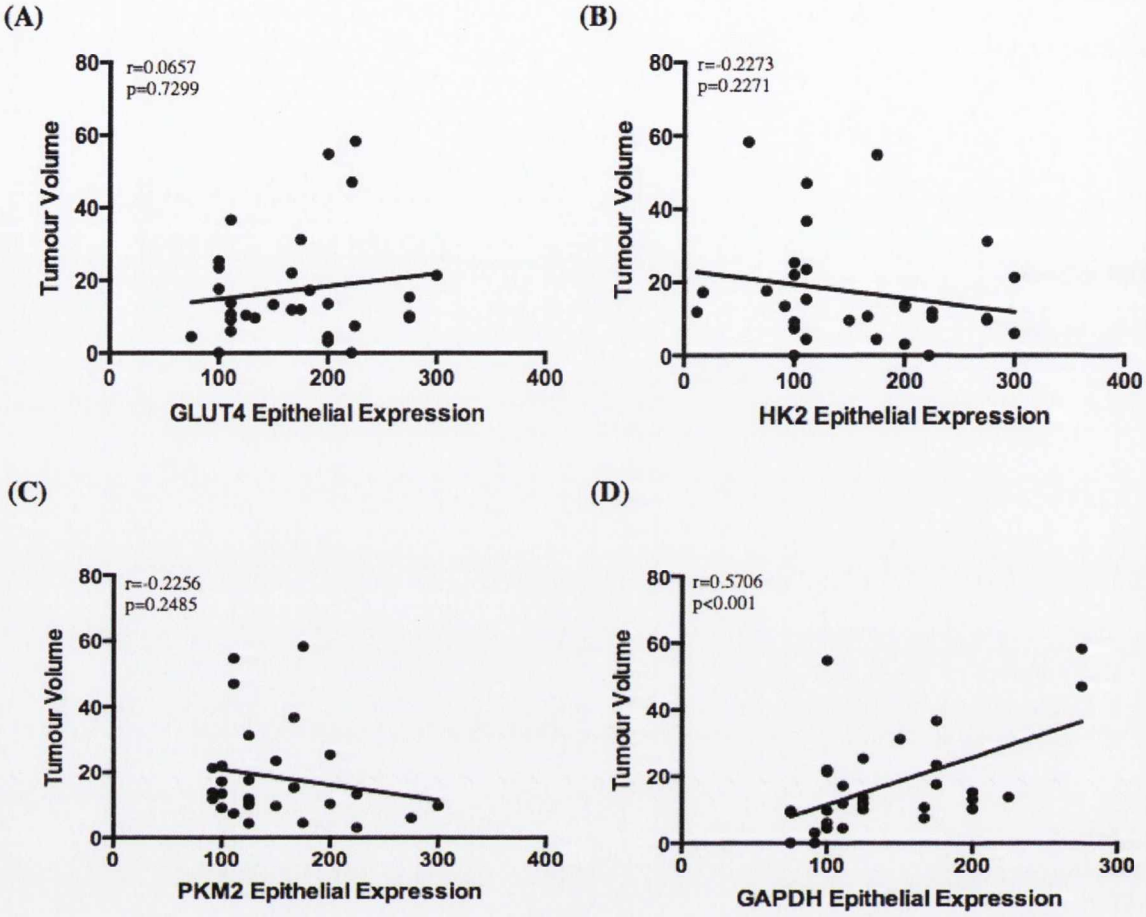


Figure 5.16 There is a significant association between GAPDH, but not GLUT4, HK2 or PKM2 with metabolic tumour volume in OAC patients (A) There was no positive correlation between epithelial Glut4 expression and increasing MTV (r=0.0657, p=0.7299, n=30). (B) There was no significant correlation between epithelial HK2 expression and MTV (r=-0.2273, p=0.2271, n=30) and (C) PKM2 (r=-0.2256, p=0.2485, n=28). (D) There was a significant positive correlation between high epithelial GAPDH expression and increasing MTV (r=05706, p<0.001, n=30) in OAC patients. Statistical test used was Spearman's test. p<0.001(***).

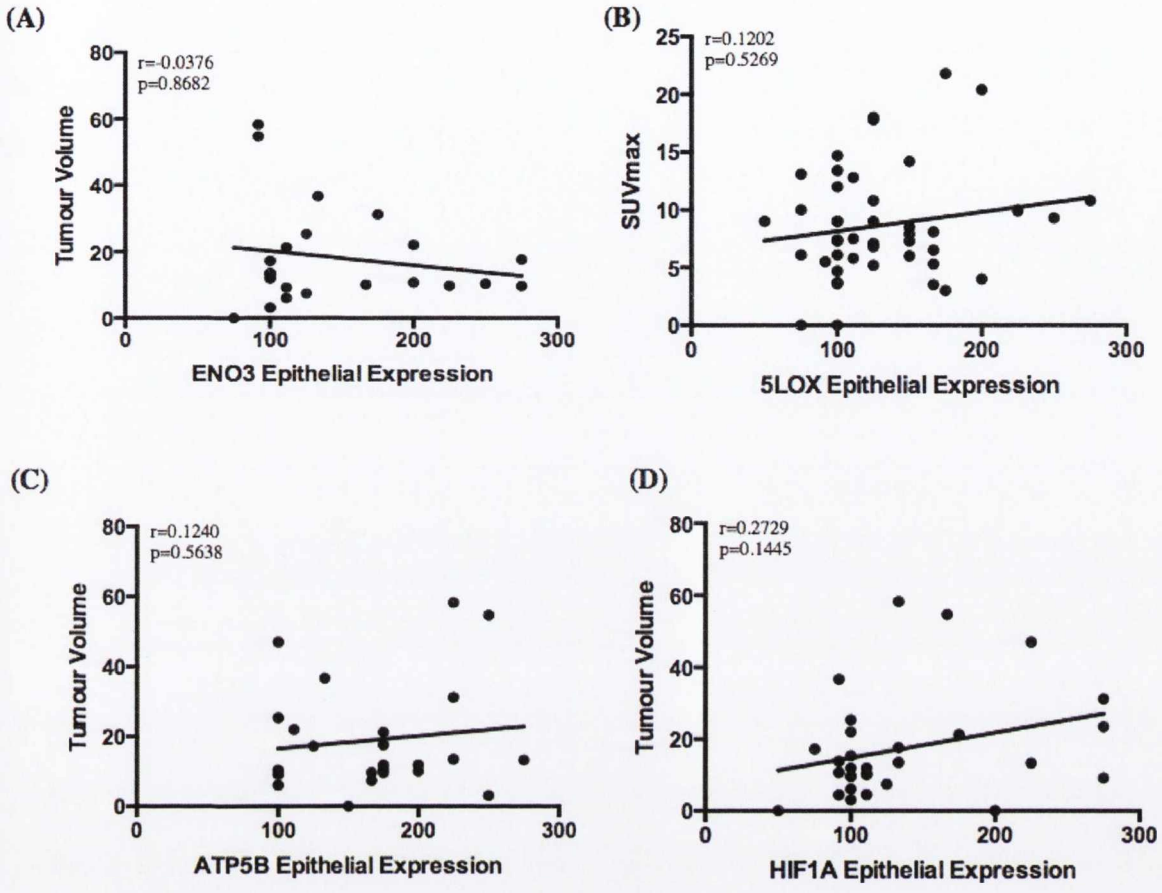


Figure 5.17 There is no significant association between ENO3, 5LOX, ATP5B and HIF1A with metabolic tumour volume in this cohort of OAC patients. (A) There was no significant positive correlation between epithelial (A) epithelial ENO3 (r=-0.03757, p=0.8682, n=22), (B) 5LOX (r=0.1202, p=0.5269, n=30), (C) ATP5B (r=0.1240, p=0.5638, n=24) and (D) HIF1A (r=0.2729, p=0.1445, n=30) with MTV in OAC patients. Statistical test used was Spearman's test.

5.3.3.8 Association between metabolic tumour volume and disease-specific survival

Metabolic tumour volume (MTV) values were divided into greater and less than the median value and disease-specific survival was calculated by Kaplan-Meier survival analysis (Figure 5.18). There was no association between a high MTV and disease-specific survival in OAC patients (median survival: 1081 days versus 1898 days, n=29 in each group, Log-rank test p=0.2862).

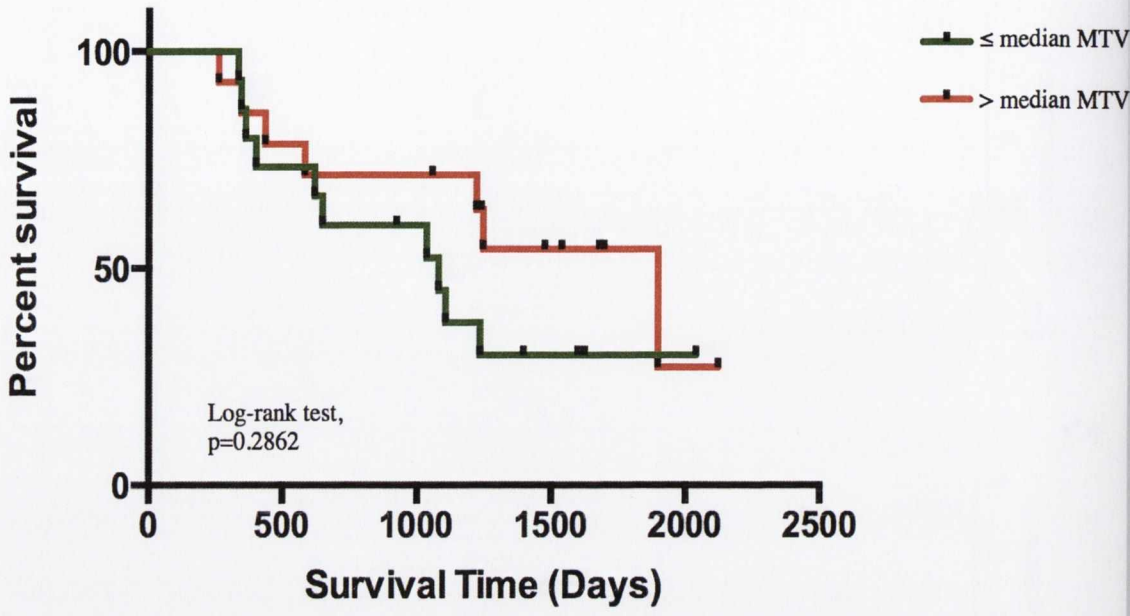


Figure 5.18 There is no association between metabolic tumour volume and disease-specific survival in this cohort of OAC patients. There was no association between a high metabolic tumour volume (MTV) disease-specific survival in OAC patients (median survival: 1081 days versus 1898 days, n=29 in each group, p=0.2862). Statistical test used was Kaplan Meier survival curve with Log-rank (Mantel-Cox) test.

5.3.3.9 Association between visceral obesity and disease-specific survival

In this cohort of OAC patients the obesity status was measured by visceral fat area rather than the body mass index. VFA values were divided into greater and less than the median value (median VFA was 157 for males and 73.50 for females) and disease-specific survival was calculated by Kaplan-Meier survival analysis (Figure 5.16). There was no significant association between patients with VFA bellow or greater than the median value (median survival 620 days versus 1836 days, n=23 in each group, Log-rank test p=0.6440) (Figure 5.19).

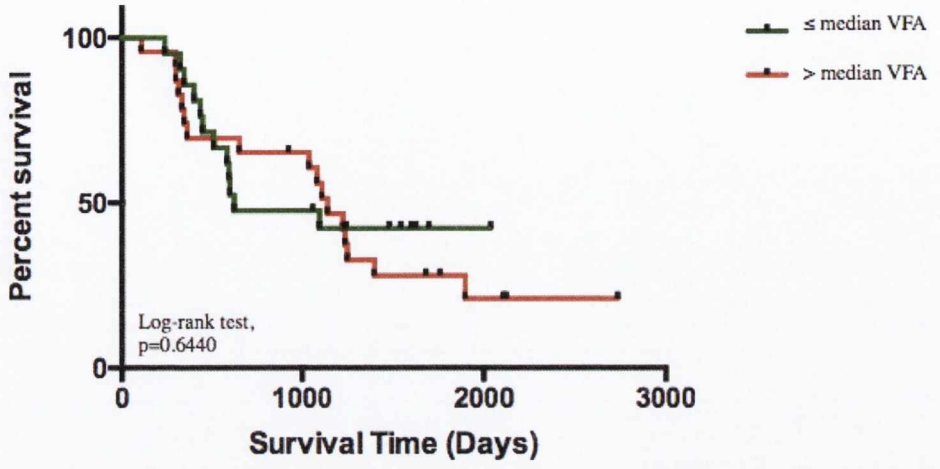


Figure 5.19 There is no association between visceral obesity and disease-specific survival in this cohort of OAC patients. There was no association between VFA measurement and disease-specific survival in this cohort of OAC patients (median survival: 620 days versus 1836 days, n=23 in each group, p=0.6440). Statistical test used was Kaplan Meier survival curve with Log-rank (Mantel-Cox) test.

5.3.3.9 Epithelial expression of glucose transporter proteins, markers of glycolysis, OXPHOS, hypoxia and 5-lipoxygenase and their association with disease-specific survival

The grade for each marker was divided into greater and less than the median value and disease-specific survival was calculated by Kaplan-Meier survival analysis (Figure 5.20-Figure 5.21). There was no significant difference between epithelial expression of any of the markers and disease-specific survival in this recent cohort of OAC patients with survival data available for less than 5 years. There was no statistical significance observed between epithelial GLUT4 expression in patients with the expression greater and less than the median value (median survival: 1108 days versus 1081 days, n=47, Log-rank test p=0.6467) (Figure 5.20a). Similar findings were observed in HK2 (median survival: 1556 days versus 649 days, n=46, Log-rank test p=0.0794) (Figure 5.20b), PKM2 (median survival: 1088 days versus 1081 days, n=46, Log-rank test p=0.4127) (Figure 5.20c), GAPDH (median survival: 1235 days versus 649 days, n=46, Log-rank test p=0.1427)

(Figure 5.20d), ENO3 (median survival: 1037 days versus 509 days, n=36, Log-rank test p=0.6545) (Figure 5.21a), 5LOX (median survival: 1108 days versus 609 days, n=46, Log-rank p=0.6501) (Figure 5.21b), ATP5B (median survival: 1081 days versus 1037 days, n=36, Log-rank test p=0.9370) (Figure 5.21c) and HIF1A (median survival: 1094 days versus 1081 days, n=45, Log-rank test p=0.4890) (Figure 5.21d).

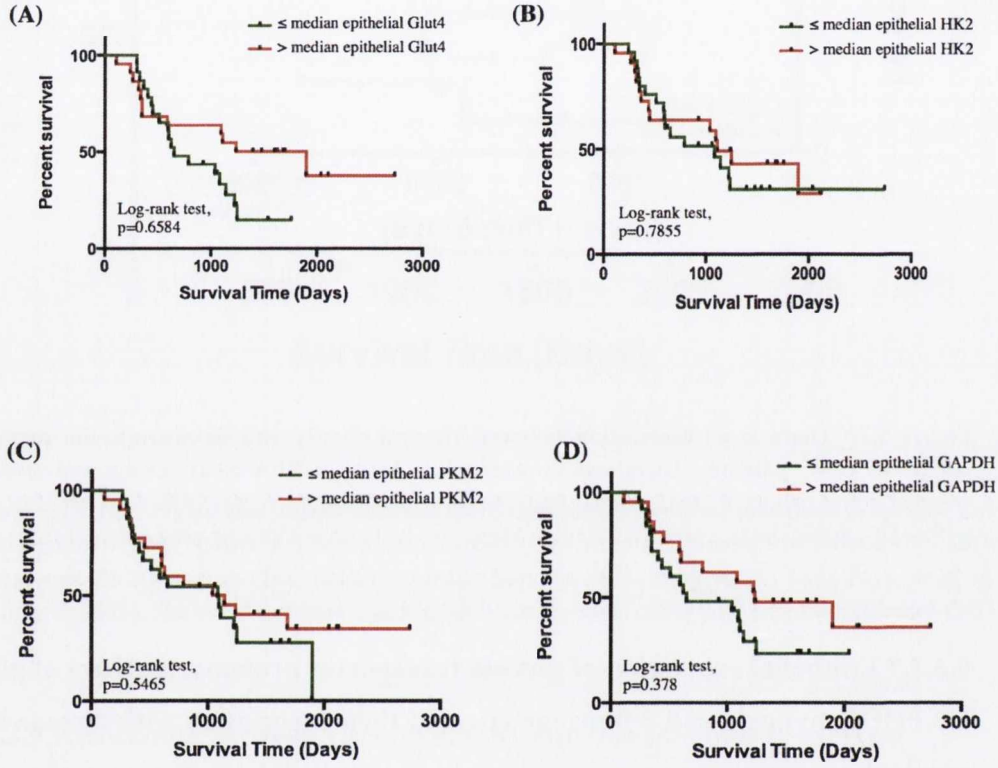


Figure 5.20 There is no association between the epithelial expression of GLUT4, HK2, PKM2 or GAPDH and disease-specific survival in this cohort of OAC patients. (A) There was no statistical significance observed between epithelial GLUT4 expression in patients with the expression greater and less than the median value (median survival: 1108 days versus 1081 days, n=47, Log-rank test p=0.6467). (B) There was no association between the level of epithelial HK2 expression and disease-specific survival (median survival: 1556 days versus 649 days, n=46, Log-rank test p=0.0794). (C) There was no statistically significant difference observed between patients with epithelial expression of PKM2 greater and less than the median value and disease-specific survival (median survival: 1088 days versus 1081 days, n=46, Log-rank test p=0.4127) and (D) GAPDH (median survival: 1235 days versus 649 days, n=46, Log-rank test p=0.1427). Statistical test used was Kaplan Meier survival curve with Log-rank (Mantel-Cox) test.

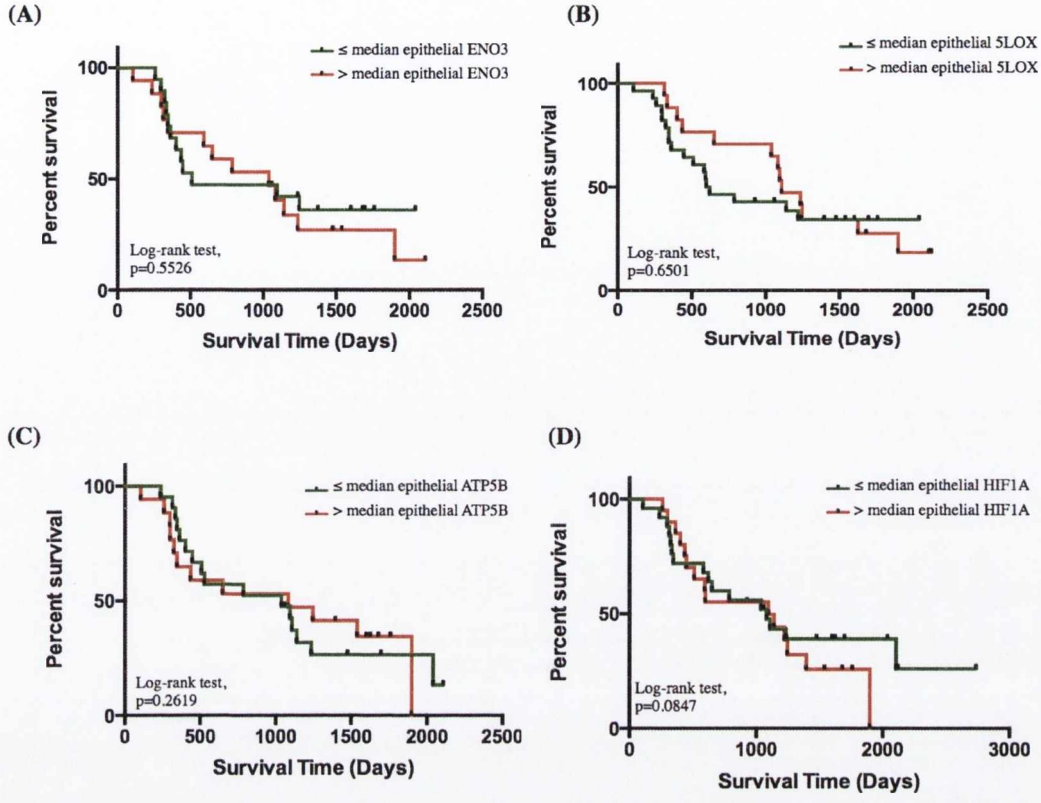


Figure 5.21 There is no association between epithelial expression of ENO3, 5LOX, ATP5B or HIF1A and disease-specific survival in this cohort of OAC patients. (A) There was no statistically significant difference in disease-specific survival between the patients with epithelial expression of 5LOX greater and less than the median value (median survival: 1037 days versus 509 days, n=36), and (B) there was no statistical significance between disease-specific survival between high and low-expressers of 5LOX (median survival: 1108 days versus 609 days, n=46, p=0.6501). (C) There was no statistically significant difference in disease-specific survival between patients with epithelial expression of ATP5B greater and less than the median value (median survival: 1081 days versus 1037 days, n=36, p=0.9370), and (D) there was no statistical significance between disease-specific survival between high and low-expressers of HIF1A (median survival: 1094 days versus 1081 days, n=45, p=0.4890). Statistical test used was Kaplan Meier survival curve with Log-rank (Mantel-Cox) test.

5.4 Discussion

It is widely documented that BMI does not provide a reliable indication of the extent of central adiposity [310], because this value does not distinguish fat mass from lean body mass components and the distribution of fat tissue differs greatly between individuals [348]. This study was conducted using a newly constructed set of tissue microarrays with obesity status of the oesophageal adenocarcinoma patients determined by the visceral fat area. All significant finding from this part of the study are summarized in Table 5.2.

Table 5.2 Summary of the significant findings from Chapter 5

Marker	Obese vs Non-obese epithelial exp.	Correlation (VFA)	Tissue type (LE vs NLE)	Lymph node involvement	Venous involvement	SUVmax*	MTV	OAC - specific survival
OBESITY			-	-	-	p<0.05 (male)	n.s.	-
Glut4	p<0.01	p<0.01	n.s.	n.s	n.s	n.s.	n.s.	n.s.
HK2	p<0.05	n.s.	n.s.	n.s	n.s	n.s.	n.s.	n.s.
PKM2	n.s.	ns.s	p<0.05	n.s.	n.s	n.s	n.s.	n.s.
GAPDH	p<0.05	n.s.	n.s.	n.s	n.s	n.s.	p<0.001	n.s.
ENO3	n.s.	n.s.	n.s.	n..s	n.s.	p<0.05	n.s.	n.s.
5LOX	n.s.	p<0.05	n.s.	n.s	n.s	n.s.	n.s.	n.s.
ATP5B	p<0.05	n.s.	n.s.	n.s	n.s	n.s.	n.s.	n.s.
HIF1A	n.s.	n.s.	n.s.	n.s	n.s	n.s.	n.s.	n.s.

Above median SUVmax value was significantly associated with poor disease-specific survival in OAC patients (Log-rank test $p<0.05$, Kaplan-Meier survival curve).

Epithelial expression of glucose transporter, markers of glycolysis, OXPHOS, hypoxia and 5LOX, was investigated in a newly constructed cohort of oesophageal adenocarcinoma TMAs. Obesity status in these patients was based on the VFA measurement. Even a small population size of OAC patient tumours (n=46) lead to significant association between visceral obesity and high glycolytic marker expression. Epithelial GLUT4 expression was significantly higher in tumour from viscerally obese compared to non-obese OAC patients, and there was a significant correlation between high levels of epithelial GLUT4 expression and increasing VFA measurement. This result is suggesting a positive association between GLUT4 and induction of glycolysis in OAC patients. Epithelial HK2 expression was significantly elevated in obese compared to non-

obese OAC patients, however, there was no significant positive correlation between epithelial HK2 expression and VFA in this cohort of patients. Epithelial GAPDH expression was also significantly higher in viscerally obese compared to non-obese OAC patients. GAPDH expression levels appeared to correlate with VFA, however, just failed to reach significance (p=0.0546), suggesting a link between GAPDH and visceral obesity in this cohort of patients. On the other hand, there was no significant difference in epithelial 5LOX expression between viscerally obese and non-obese OAC patients, however, elevated 5LOX expression positively correlated with increasing VFA. This result suggested a strong association between 5LOX and visceral obesity in this cohort of OAC patients. Epithelial ATP5B levels were significantly higher in tumour from viscerally obese compared to non-obese patients in this cohort of OAC patients. An increase in ATP5B expression levels seemed to correlate with increasing VFA, however, similarly like GAPDH, failed to reach significance (p=0.0577). The sample size was relatively small, consisting of only 46 OAC patients, therefore any findings close to reaching statistical significance were considered important.

Following the immunohistochemical analysis, we investigated the link between obesity and metabolic tumour volume and metabolic tumour activity in the same cohort of OAC patients. The number of the patients dropped down to 30 (24 males and 6 females) as only these patients had their diagnostic PET-CT scan performed in St. James's hospital. Following diagnostic PET-CT scan, computer-aided measurements were obtained. This study included the standard uptake value (SUV) based on metabolic tumor volume (MTV) for all patients that this data was available for. All data for this part of the study was obtained from Dr. Vinod Malik in St. James's hospital. Dr. Malik provided us with metabolic tumor volume (MTV) and SUVmax measurements, which represent tumor tissue showing active FDG uptake *in vivo.* Published studies show that the more aggressive, metastatic tumours are associated with high FDG uptake therefore a higher SUVmax in non-small cell lung cancer (NSCLC) and breast cancer [288, 352]. In this study, high epithelial GAPDH expression was significantly correlated with high metabolic tumour volume suggesting a high expression of GAPDH in a potentially more aggressive tumour phenotype. Chung *et al* showed that the MTV has a potential value in predicting short-term outcome and disease free survival in patients with pharyngeal cancers [353]. In their study, the MTVs of primary sites with or without neck nodes were measured in 82 patients. By univariate analyses they reported that patients with high MTV

showed a significantly lower number of complete response/no recurrence than did patients with low MTV [353]. In SCC, Seol *et al* reported a significant decrease of MTV in between before and during CRT showing a decrease in MTV in response to therapy [354] suggesting a correlation between a decreasing MTV and less aggressive tumour.

In this study, high SUVmax values (above the median value in this cohort of OAC patients) were significantly correlated with increasing VFA and above median SUVmax was significantly associated with poor survival. It is well published that high metabolic tumour activity is associated with poor survival (including in OAC), however there are no published studies showing the link between visceral obesity and high metabolic tumour activity in OAC. Similarly, in this study, high epithelial ENO3 expression was positively associated with high SUVmax. This association has never been shown. Overall, we suggest that there may be a potential positive link between obesity, glycolysis, and high metabolic tumour activity *in vivo* and poor overall disease-specific survival in this cohort of OAC patients.

Our present study has several limitations. Firstly, the sample size was limited to only 48 patients. In order to have a better understanding how visceral obesity influences development and progression of OAC, and possibly more significant findings could be achieved with higher population size. Secondly, due to recent OAC tumour samples used for the construction of these tissue microarrays, for many of the patients the follow-up and the survival data was only available for 2-3 years. Therefore, this lack of long-term observation might have contributed to the non-significant correlations between metabolic parameters and survival. It would be beneficial to calculate the overall disease-specific survival when the five-year follow up data becomes available.

Chapter 6

Delineation whether visceral adiposity results in metabolic shift in glucose metabolism and changes in mitochondrial metabolism in oesophageal adenocarcinoma

6.1 Introduction

Most cancer cells undergo changes in their metabolism in order to survive. Published studies show a number of different pathways contributing to this altered metabolic activity in cancer cells [355] (Figure 6.1) Cancer cells generate energy in the form of ATP, in order to produce precursors for macromolecule biosynthesis to support cell growth and to manage the oxidizing effects of their metabolism by reducing the impact of reactive oxygen species (ROS) [355]. Novel therapeutic approaches have been designed targeting cancer cell glycolysis, ranging from the use of nonmetabolizable glucose analogs blocking critical steps in the pathway, such as those catalyzed by lactate dehydrogenase (LDH), hexokinase 2 (HK2) or the monocarboxylate transporters (MCT) that export lactate to the external microenvironment [355, 356], however, these strategies did not have a significant impact. The amount of glucose taken up by a cancer cell greatly exceeds its requirement for ATP, suggesting that the glucose metabolism entails far more than just ATP generation [355].

Nicotinamide adenine dinucleotide phosphate (NADPH) is critical for rapid tumour cell growth and their survival [356]. Tumour cells are able to raise their intracellular NADPH levels by increasing flux through an alternative route of glucose metabolism called the pentose phosphate pathway (PPP). The PPP, produces ribose sugars for nucleotide biosynthesis and NADPH that serves as reducing potential for the synthesis of macromolecules [355, 356]. The regulation of cellular hydrogen potential is a key step that controls cell proliferation, migration and cellular balance of all mammalian cells. The low extracellular pH has been shown to be a hallmark of malignant cells [357]. The extracellular acidic stress in which tumour cells evolve and adapt is a consequence of poor blood supply, low oxygen availability, increased metabolism of glucose and production of lactic acid [357-359]. Low oxygen levels in the tumor leads to proton (H) accumulation. The amount of H within solid tumours is the consequence of oncogene activation tumour suppressor loss, adaptation to hypoxia and the ability of tumour cells to produce lactic acid and carbonic acid that are generated by a shift in glucose metabolism from oxidative phosphorylation (OXPHOS) to glycolysis (Figure 6.1). HIF1A, induces the expression of glycolytic enzymes consequently elevating the

glycolytic metabolic flux for ATP generation [355]. Additionally, in a low oxygen environment, hypoxic tumour cells develop supplemental hydrogen potential regulating systems such as the membrane-associated carbonic anhydrases CAIX and CAXII, which create an environment supportive of cancer cell survival [358, 360].

Lynam-Lennon *et al* for the first time demonstrated that co-culture of oesophageal adenocarcinoma cells with ACM from viscerally-obese OAC patients resulted in an altered metabolic profile and that can drive mitochondrial dysfunction and altered energy metabolism in EAC cells *in vitro* (224). This study showed that ACM-induced mitochondrial dysfunction was accompanied by altered expression of 19 mitochondrial-associated genes and significantly reduced intracellular ATP levels. Moreover, ACM from obese OAC patients, induced a metabolic shift to glycolysis.

Based on the evidence from this study, the aim in this Chapter is to investigate whether ACM and/or hypoxia induce a metabolic shift in glucose metabolism and alters mitochondrial function, which is vital prior to investigating the effect of novel therapeutic targets in this setting.

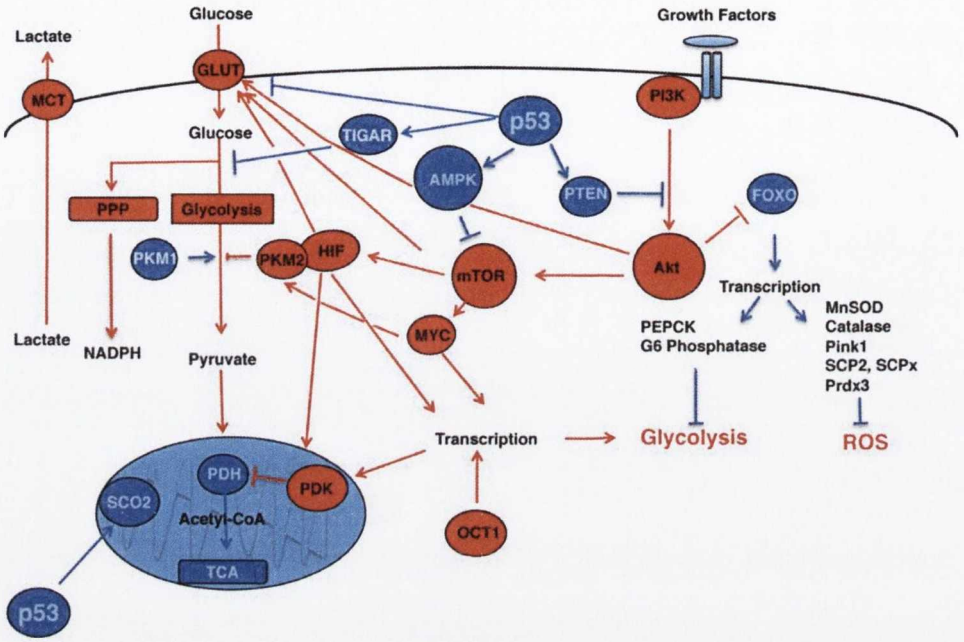


Figure 6.1 Oncogenic and tumor-suppressive pathways contributing to the cellular transformation. The accelerated rate of aerobic glycolysis is driven by molecular activities that synergistically promote cellular transformation (highlighted in red). These promoter activities are countered by the suppressors of cellular transformation (highlighted in dark blue). The engagement of growth factor receptors stimulates phosphatidylinositol-3-phosphate kinase (PI3K), which activates Akt1. Activated Akt1 subsequently up-regulates glycolysis and activates mTOR while inactivating forkhead box subfamily O (FOXO). In the absence of FOXOs, transcription of factors that usually inhibit glycolysis and control ROS are blocked. mTOR activation stimulates translation of growth-related proteins such as Myc and increases HIF transcriptional activity. HIF1 activation drives the expression of glucose transporters, glycolytic enzymes, and pyruvate dehydrogenase kinase (PDK), which inhibits the entry of pyruvate into the tricarboxylic acid (TCA) cycle via pyruvate dehydrogenase (PDH). The production of lactate by lactate dehydrogenase (LDH) is increased due to an increased pyruvate production by glycolysis. Adapted from Cairns *et al.*, 2011 [355].

6.2. Aims and objectives

The aim of this chapter was to investigate whether obesity and hypoxia are associated with a shift in glucose metabolism and changes in mitochondrial function.

Specific Objectives:

- Investigate whether ACM induces a metabolic shift in glucose metabolism and mitochondrial respiration by utilizing RT^2 Profiler PCR Arrays
- Investigate the role of obesity in the metabolic shift and changes in mitochondrial metabolism
- Investigating the feasibility of using cobalt chloride ($CoCl_2$) to induce hypoxia in oesophageal adenocarcinoma cells
- Investigate the role of hypoxia in glucose metabolism and oxidative phosphorylation and its link with obesity

6.3 Results

6.3.1 Assessment of lactate secretion levels by OE33 cells following co-culture with adipose conditioned media

OE33 cells were co-cultured with ACM that was prepared from visceral fat collected from OAC patients who underwent oesophagectomy for oesophageal cancer at St. James's hospital and stored in the designated OAC biobank. Cells were co-cultured with ACM for 24 hours in humidified atmosphere with 5% CO_2 at 37^0C. Secreted lactate levels were measured using lactate assay kit (Sigma-Aldrich). Lactate levels secreted by OE33 cells were significantly higher following co-culture of cells with ACM from obese compared to non-obese OAC patients (239.9 ±26.97 versus 497.7 ±64.09, n=10 per group, $p<0.01$) (Figure 6.2). Patients were segregated into two groups with obese VFA cut off value of 163.8 cm^2 in males and 80.1 cm^2 in females, Patient demographics summarized in Table 6.1.

Table 6.1 Patient demographics for preparation of ACM for lactate assay secretion study

n=20	Mean (S.D.) or n (%) as appropriate
Morphology (OAC)	20 (100%)
Male: female	15: 5 (75%: 25%)
Age	65.3 (10.91)
Normal weight: overweight and obese	10: 10 (50%: 50%)
Normal weight VFA (cm^2)	45.85 (18.55)
Overweight and obese VFA (cm^2)	287 (59.8)

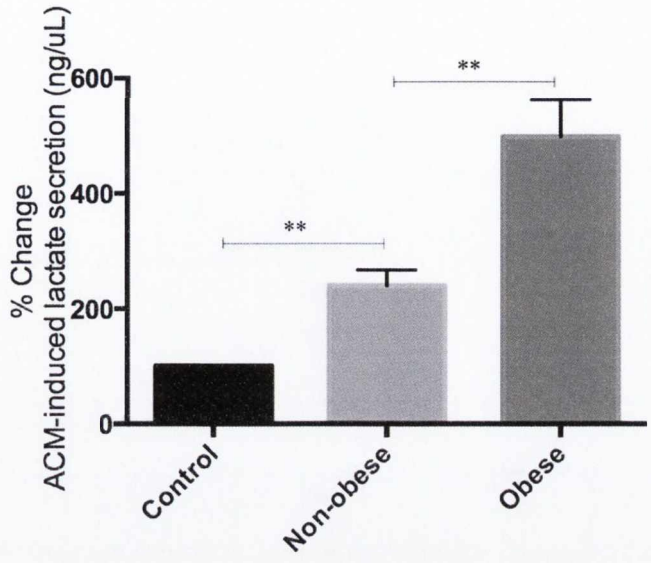


Figure 6.2 Adipose conditioned media induces lactate secretion. A significantly higher level of secreted lactate was observed following co-culture of OE33 cells with ACM from viscerally obese compared to non-obese OAC patients, where patients were segregated into two groups based on an obese VFA cut off value of 163.8 cm^2 in males and 80.1 cm^2 in females (n=10, $p<0.01$). Statistical test used was Mann-Whitney U test. $P<0.01$(**). Error bar denotes mean ± S.E.M.

6.3.2 Assessment whether co-culture of oesophageal adenocarcinoma cells with ACM result in metabolic shift in glucose metabolism

The experiment was performed using the Seahorse XFe24 analyser. OE33 cells were seeded into XFe24 Seahorse plate, at a density of 10,000 cells/well. Cells were serum depleted (0.5% FBS) 5 hours after seeding and incubated overnight at 5% CO_2 at 37^0C. The following day, cells were treated with ACM from viscerally obese patients or M199 media (negative control). 24 hours following treatment, glycolysis in the cells was measured by Seahorse XFe24 analyser. Experimental set up and analysis are described in Chapter 2.18.4

Seahorse XFe technology was applied because it is designed to measure glycolytic activity via measuring the extracellular acidification rate (ECAR) of the media, and it provides quantifiable metabolic data. We measured changes in extracellular acidification rate (ECAR) in OE33 cells following 24 hour co-culture with ACM compared to M199

media only cultured cells, (100% versus 127 ±11.02%, n=10 in each group, $p<0.001$) (Figure 6.3).

The control group was set to 100% and the treatment group (ACM) was calculated as percentage change compared to the control (M199).

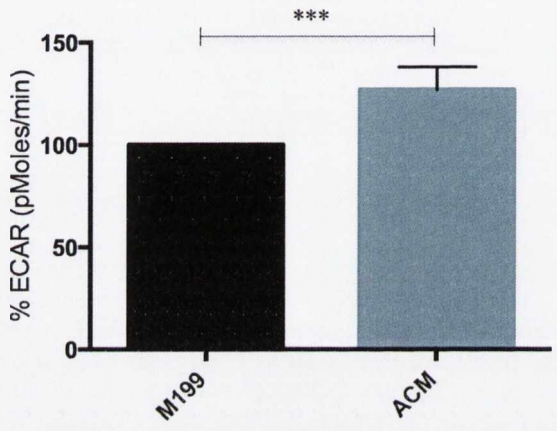


Figure 6.3 Co-culture of ACM with oesophageal adenocarcinoma cells results in a metabolic shift *in-vitro*. There was a significant increase in in glycolytic activity (%ECAR) in OE33 cells treatment with ACM compared to media only (M199) treated cells ($p<0.001$, n=10). Statistical test used was Mann Whitney U test. $p<0.001$ (***). Error bar denotes mean ± S.E.M.

6.3.3 Delineating the expression of human glucose metabolism associated gene expression in response to ACM treatment

To analyse the expression of 84 human genes associated with glucose metabolism, the Human Glucose Metabolism RT^2 Profiler PCR Arrays were used (Section 2.13). OE33 cells were co-cultured with ACM for 24 hours prior RNA extraction. Fold expression of all target genes was normalised relative to the media only treated OE33 cells. The cut-off for differential gene expression was defined by either a relative 2-fold upregulation or 2-fold downregulation. 15 out of 21 glycolysis, 3 out of 7 gluconeogenesis and 4 out of 6 glucose metabolism genes were significantly upregulated in OE33 cells following 24-hour co-culture with ACM (Table 6.2). 25 out of 29 genes in TCA cycle, and 8 out of 11

genes in the pentose phosphate pathway were significantly upregulated following co-culture of cells with ACM (Table 6.3). 9 out of 16 genes associated with glycogen metabolism were significantly upregulated (Table 6.4), therefore in total, 71.4% of genes associated with glucose metabolism were significantly upregulated in OE33 cells that were co-cultured with ACM compared to untreated control. PC, PCK1 and PCK2 were highlighted in red as the genes were associated to two pathways: gluconeogenesis (Table 6.2) and TCA cycle (Table 6.3). PGM1, PGM2 and PGM3 genes were highlighted in green as same genes were associated with two pathways: glycolysis (Table 6.2) and glycogen degradation (Table 6.4).

A panel of 10 genes, which exhibited the greatest significant fold upregulation (more than two fold upregulation following treatment of cells with ACM, compared to M199 media treated cells) were selected. These genes (ALDOB, ENO3, PGM1, PGM2, PC, PDK1, PCK2, H6PD, RBKS, TKT) were subsequently validated *in –vitro* using patient samples.

Table 6.2 Glucose metabolism gene microarray screen between media only and ACM co-cultured OE33 cells: the effect of ACM on the genes of glycolysis, gluconeogenesis and glucose metabolism

Functional Group	Gene	Expression*
Glycolyis	ALDOA	3.41
	ALDOB	7.88
	ALDOC	1.99
	BPGM	2.78
	ENO1	2.24
	ENO2	2.07
	ENO3	4.93
	GALM	0.45
	GCK	0.43
	GPI	2.01
	HK2	3.06
	HK3	0.49
	PFKL	2.76
	PGAM2	0.25
	PGK1	2.83
	PGK2	-0.32
	PGM1	2.49
	PGM2	3.4
	PGM3	2.41
	PKLR	8.56
	TPI1	2.14
Gluconeogenesis	FBP1	1.79
	FBP2	-1.24
	G6PC	2.69
	G6PC3	3.25
	PC	3.76
	PCK1	1.78
	PCK2	1.82
Glucose Metabolism	PDK1	4.58
	PDK2	2.57
	PDK3	-0.19
	PDK4	4.14
	PDP2	1.73
	PDPR	3.15

B2M = Endogenous Control Gene

* Relative Expression (e.g. expression of ALDOA is 3.41 times greater in ACM co-cultured than media only cultured OE33 cells). Upregulation/downregulation greater than two fold was considered to be significant

Table 6.3 Glucose metabolism gene microarray screen between media only and ACM co-cultured OE33 cells: the effect of ACM on the genes of TCA cycle

Functional Group	Gene	Expression*
Tricarboxylic Acid Cycle (TCA)	ACLY	1.79
	ACO1	4.85
	ACO2	5.19
	CS	2.86
	DLAT	2.7
	DLD	3.28
	DLST	2.51
	FH	2.36
	IDH1	4.44
	IDH2	10.22
	IDH3A	2.52
	IDH3B	3.06
	IDH3G	3.81
	MDH1	0.53
	MDH1B	0.05
	MDH2	2.15
	OGDH	2.57
	PC	3.76
	PCK1	1.78
	PCK2	1.82
	PDHA1	3.48
	PDHB	2.88
	SDHA	2.12
	SDHB	2.64
	SDHC	2.78
	SDHD	2.47
	SUCLA2	2.4
	SUCLG1	2.38
	SUCLG2	2.21
Pentose Phospate Pathway	G6PD	2.81
	H6PD	7.57
	PGLS	3.86
	PRPS1	2.07
	PRPS1L1	17.72
	PRPS2	1.3
	RBKS	1.23
	RPE	2.07
	RPIA	2.5
	TALDO1	2.97
	TKT	2.61

B2M = Endogenous Control Gene

* Relative Expression (e.g. expression of ALCY 1.79 times greater in ACM co-cultured than media only cultured OE33 cells). Upregulation/downregulation greater than two fold was considered to be significant

Table 6.4 Glucose metabolism gene microarray screen between media only and ACM co-cultured OE33 cells: the effect of ACM on the genes of glycogen metabolism

Functional Group	Gene	Expression*
Glycogen Metabolism		
Glycogen Synthesis	GBE1	4.9
	GYS1	1.85
	GYS2	0.03
	UGP2	-0.74
Glycogen Degradation	AGL	2.88
	PGM1	2.49
	PGM2	3.4
	PGM3	2.41
	PYGL	1.88
	PYGM	0.2
Regulation of Glycogen Metabolism	GSK3A	2.39
	GSK3B	4.1
	PHKA1	2.66
	PHKB	-1.39
	PHKG1	1.57
	PHKG2	2.68

B2M = Endogenous Control Gene

* Relative Expression (e.g. expression of GBE1 4.9 times greater in ACM co-cultured than media only cultured OE33 cells). Upregulation/downregulation greater than two fold was considered to be significant

6.3.3.1 Validation of glucose metabolism associated genes in OE33 cells co-cultured with ACM

A list of ten significantly upregulated genes following co-culture with ACM were selected from the glucose metabolism RT^2 Profile PCR Arrays (Section 2.11) for validation with SYBR green dye based qPCR (Section 2.12). OE33 cells were co-cultured with ACM from 5 different OAC patients (Table 6.1) and cDNA was synthesized for the validation study. The cell culture set up, RNA isolation and cDNA synthesis were identical to the ones described in Section 2.7 and Section 2.9 respectively.

There was a significant upregulation of glycolysis associated genes ALDOB, ENO3, PGM1 and PGM2 in ACM treated cells compared to media only treated control (1.394 ±0.1237, 1.288 ±1.001, 1.125 ±0.0494, 1.222 ±0.2219, respectively versus 0.8940 ±0.0525, n=5 in each group, $p<0.05$) (Figure 6.4a, Figure 6.4b, Figure 6.4c and Figure 6.4d respectively). Gluconeogenesis associated PC and glucose metabolism associated PDK1 were upregulated following co-culture with ACM (1.23 ±0.0919 and 1.494 ±0.1316, respectively versus 0.894 ±0.0525, n=5 in each group, $p<0.05$ (Figure 6.4e and Figure 6.4f respectively). There was no significant increase in pentose phosphate associated gene H6PD in ACM co-cultured OE33 cells compared to M199 media only treated cells (1.14 ±0.8984 versus 0.894 ±0.0525, n=5 in each group, $p=0.0635$) (Figure 6.5a). There was a significant increase in pentose phosphate associated genes RBKS and TKT in ACM co-cultured cells compared to media only treated control (1.213 ±0.0972 and 1.14 ±0.0694 respectively, versus 0.8940 ±0.0525, n=5 in each group, $p<0.05$) (Figure 6.5b and Figure 6.5c respectively). There was a significant higher expression of TCA cycle associated gene PCK2 in ACM co-cultured cells compared to control (1.248 ±0.1424 versus 0.8940 ±0.0525, n=5 in each group, $p<0.05$) (Figure 6.5d).

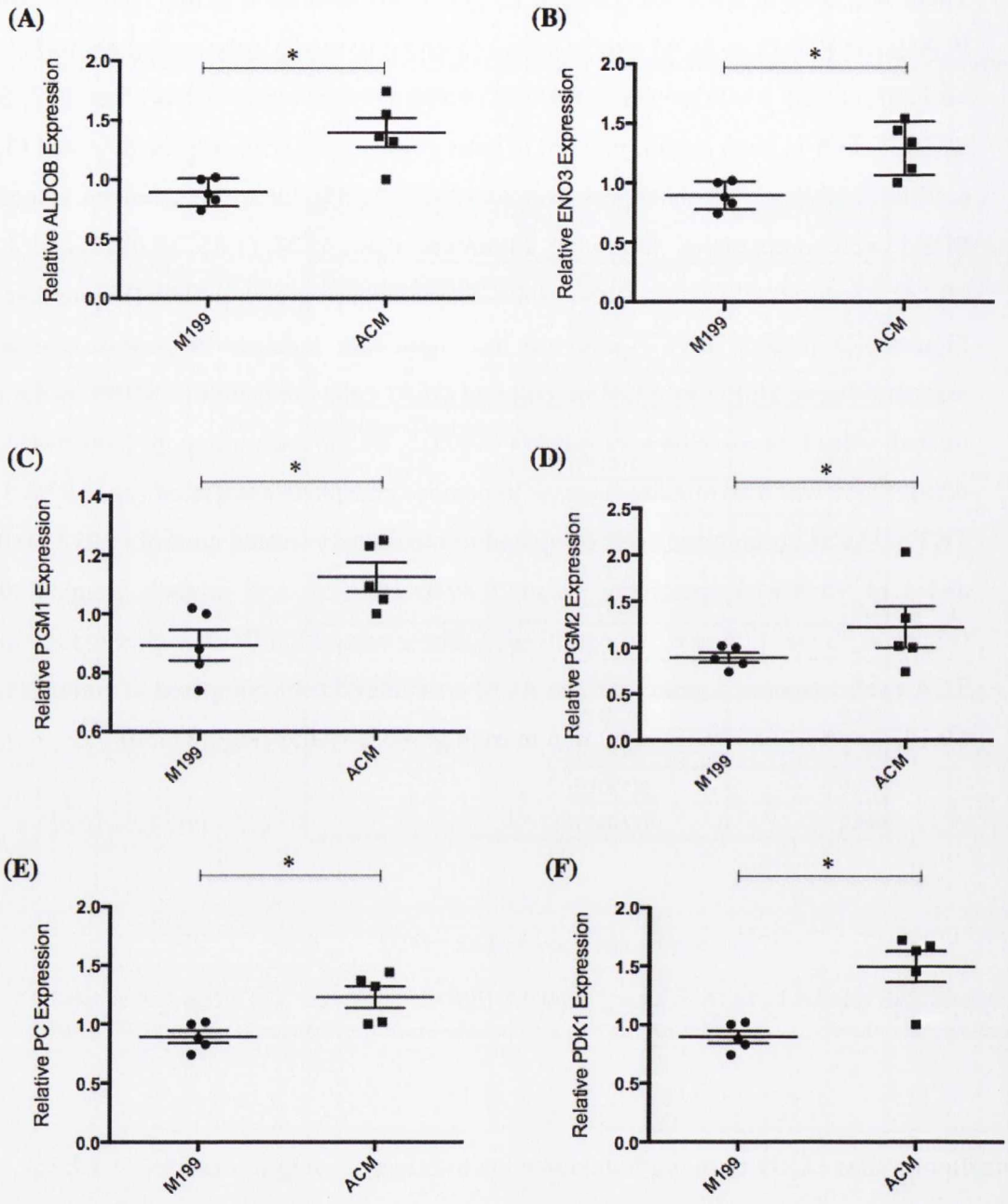


Figure 6.4 Glucose metabolism, glycolysis and TCA cycle associated genes are expressed at significantly higher level in ACM co-cultured OE33. qPCR analysis reveal that glycolysis associated genes (A) ALDOB, (B) ENO3, (C) PGM1 and (D) PGM2 were expressed at significantly higher level in ACM co-cultured OE33 cells compared to M199 media only treated cells ($p<0.05$, n=5 in each group). (E) Glycogenesis/TCA cycle associated PC and (F) glucose metabolism associated PDK1, were both expressed at significantly higher levels in OE33 cells co-cultured with ACM compared to media only treated control ($p<0.05$, n=5 in each group). Statistical test used was Mann Whitney U test. $p<0.05$ (*). Error bar denotes mean ± S.E.M

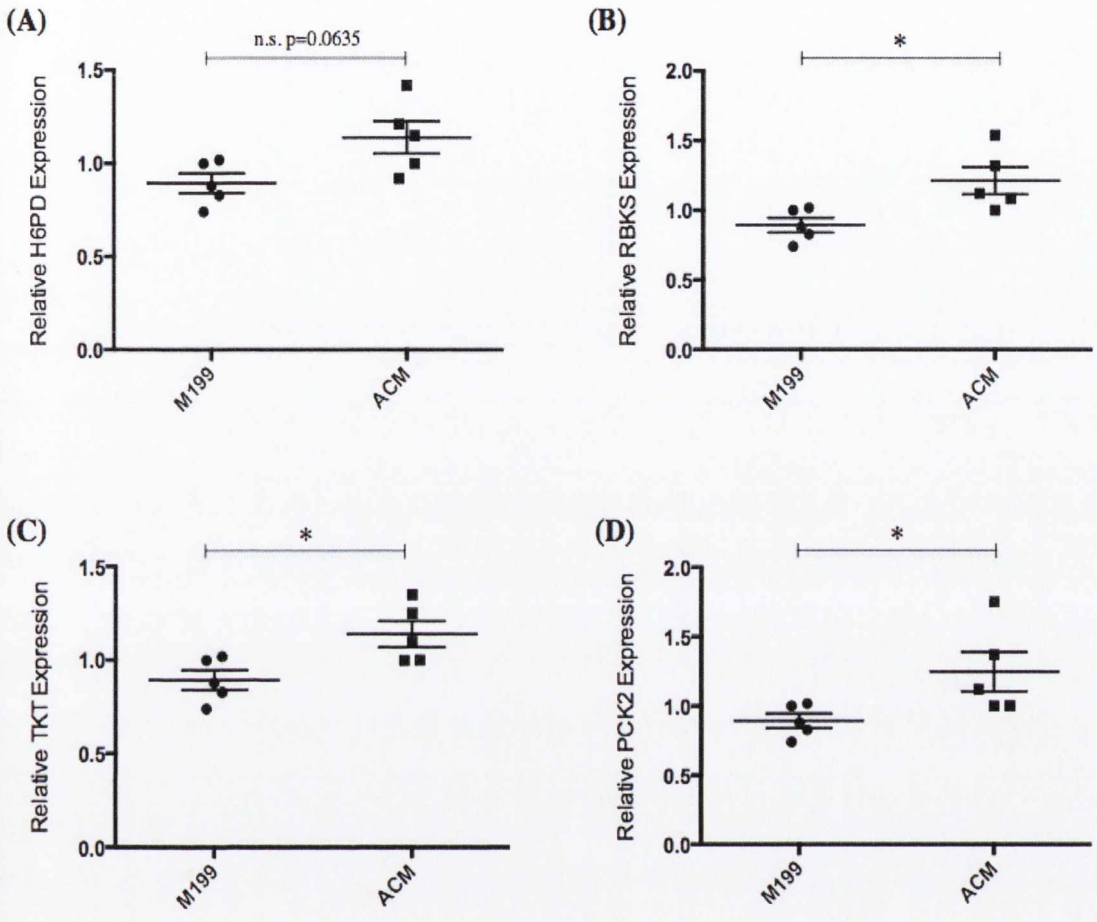


Figure 6.5 Pentose phosphate pathway and TCA cycle associated gene expression in ACM co-cultured OE33 cells compared to media only treated control. qPCR analysis reveal that there was no significant difference in expression levels of pentose phosphate pathway associated (A) H6PD in ACM co-cultured and media only treated cells, however, there was a significant increase in (B) RBKS (C) TKT expression in ACM-co-cultured OE33s. There was a significant increase in TCA associated (D) PCK2 in ACM co-cultured OE33 cells compared to M199 media only treated cells ($p<0.05$, $n=5$ in each group). Statistical test used was Mann Whitney U test. $p<0.05$ (*). Error bar denotes mean ± S.E.M.

6.3.3.2 Validation of glucose metabolism associated genes in OAC tumour biopsies

Biopsy samples were collected from the main specimen post-surgical resection from OAC patients as described in Section 2.4. The patient demographic is summarized in Table 4.3. RNA was isolated as described in Section 2.6 and gene expression was measured by real time by qPCR as described in Section 2.12. Details for gene primer

probes used were summarized in Table 2.3. The RQ value for one patient sample was set as the calibrator to allow normalisation of the data set. Gene expression levels were compared in tumours from obese versus non-obese OAC patients with obese VFA cut off value of 163.8 cm^2 in males and 80.1 cm^2 in females, n=10 in each group.

Glycolysis associated genes ALDOB and ENO3 were expressed at significantly higher levels in viscerally obese compared to non-obese OAC patients (2.523 ±0.3651 versus 1.565 ±0.2135 and 2.354 ±0.3159 versus 1.377 ±0.1766 respectively, n=10 in each group, $p<0.05$) (Figure 6.6a and Figure 6.6b respectively). There was no significant difference in expression levels of glycolysis associated genes PGM1 and PGM2 in obese compared to non-obese OAC patients (1.498 ±0.1564 versus 1.278 ±0.2857 and 1.734 ±0.2041 versus 1.756 ±0.2334 respectively, n=10 in each group, p=0.1184 and p=0.9262 respectively) (Figure 6.6c and Figure 6.6d respectively). There was no significant difference in expression of glycolysis/TCA cycle associated PC gene in viscerally obese compared to non-obese OAC patients (1.622 ±0.284 versus 1.253 ±0.121, n=10 in each group, p=0.492) (Figure 6.6e). Glucose metabolism associated PDK1 gene was expressed at significantly higher level in viscerally obese compared to non-obese OAC patients (2.524 ±0.2902 versus 1.392 ±0.1929, n=10 in each group, $p<0.01$) (Figure 6.6f). Pentose phosphate pathway associated gene H6PD was expressed at significantly higher level in viscerally obese OAC patients (2.094 ±1.577 versus 1.545 ±0.1481, n=10 in each group, $p<0.05$) (Figure 6.7a). There was no significant difference in expression levels of pentose phosphate pathway associated genes RBKS and TKT in obese compared to non-obese OAC patients (1.705 ±0.2973 versus 1.358 ±0.1894 and 2.102 ±0.317 versus 1.725 ±0.3134, n=10 in each group, p=0.4042 and p=0.288 respectively) (Figure 6.7b and Figure 6.7c respectively). There was no significant difference in expression in TCA cycle associated PCK2 gene in viscerally obese compared to non-obese OAC patients (1.734 ±0.2041 versus 1.756 ±0.234, n=10 in each group, p=0.9262) (Figure 6.7d).

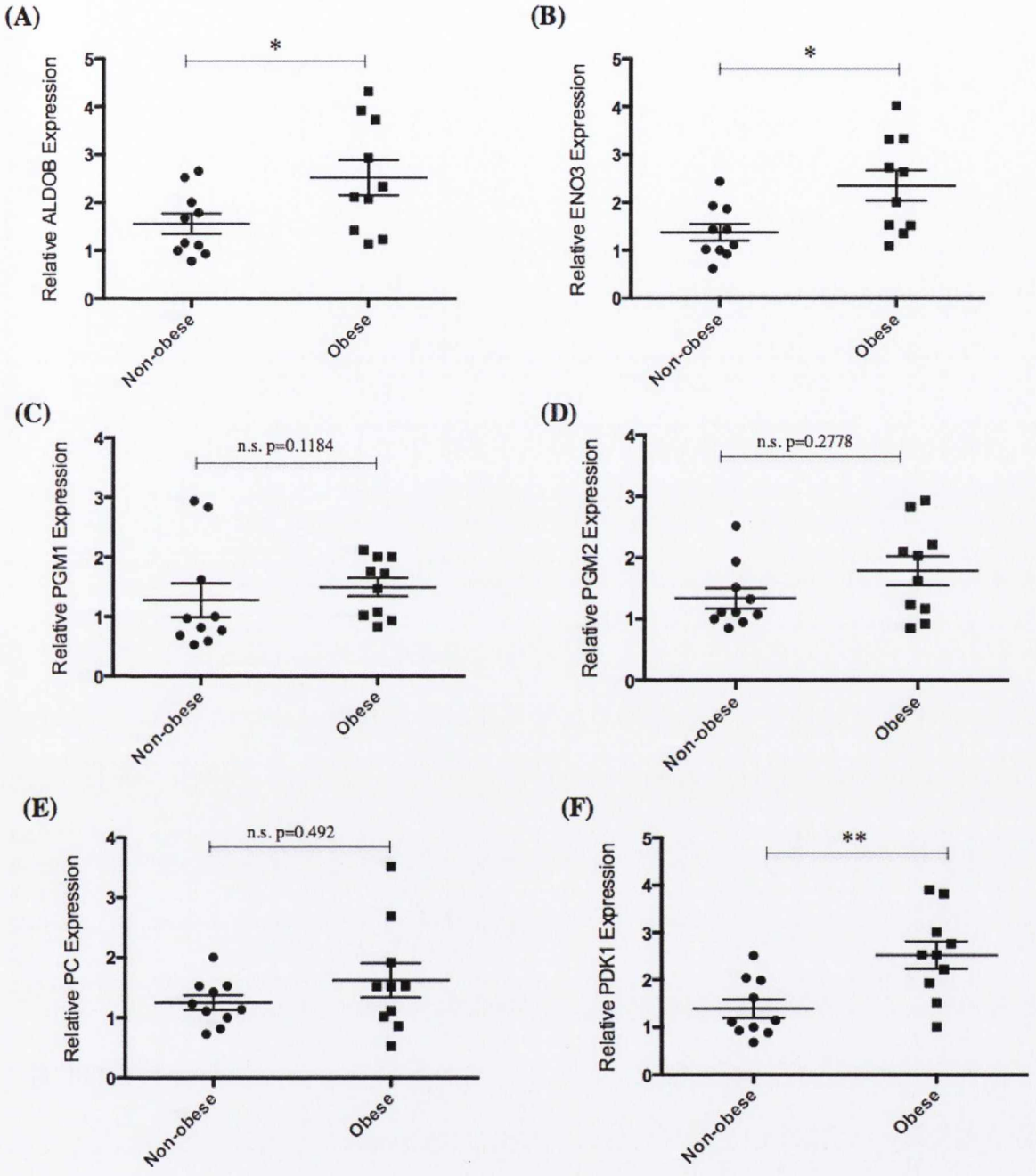


Figure 6.6 Assessment of **glucose metabolism, glycolysis and TCA cycle associated genes in viscerally obese and non-obese OAC patient tumour.** qPCR analysis reveal that glycolysis associated genes (A) ALDOB and (B) ENO3 were expressed at significantly higher level in viscerally obese compared to non-obese OAC patients ($p<0.05$, $n=10$ in each group). There was no significant difference in relative expression levels of (C) PGM1 and (D) PGM2 in obese compared to non-obese OAC patients, $p=0.1184$ and $p=0.9262$ respectively, $n=10$ in each group). (E) There was no differential expression of glycogenesis/TCA cycle associated PC in obese patients. (F) Glucose metabolism associated PDK1, was expressed at significantly higher level in OAC tumours from viscerally obese patients ($p<0.01$, $n=10$ in each group). Statistical test used was Mann Whitney U test. $p<0.05$ (*), $p<0.01$(**). Error bar denotes mean ± S.E.M.

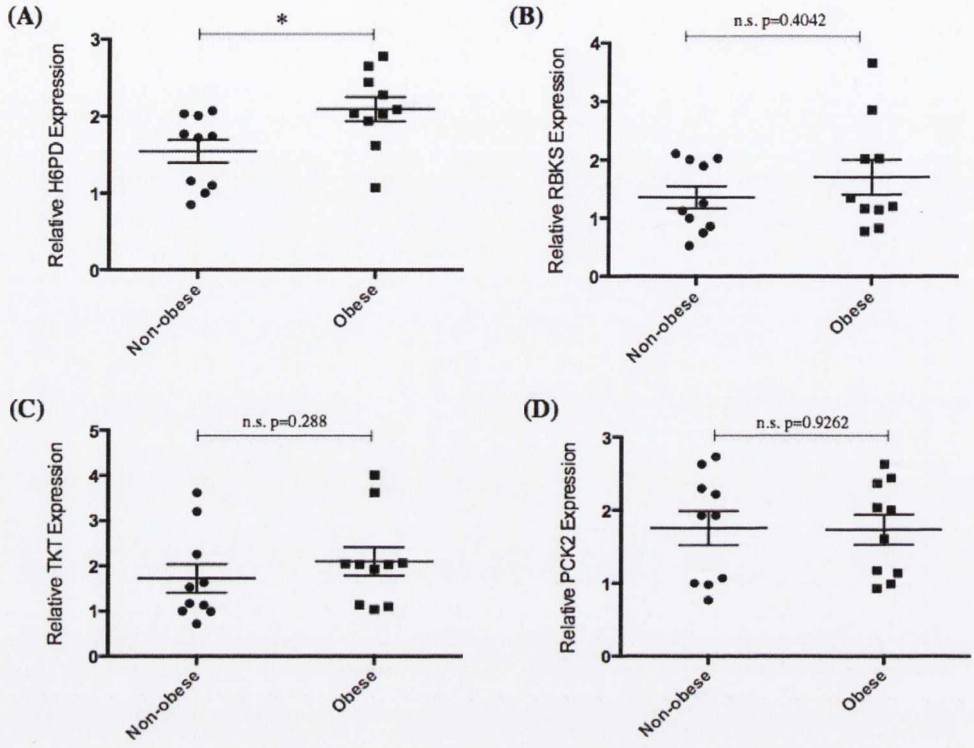


Figure 6.7 Pentose phosphate pathway and TCA cycle associated gene expression in OAC patient tumour. qPCR analysis reveal (A) phosphate pathway associated was expressed at significantly higher level in viscerally obese compared to non-obese patients ($p<0.05$, $n=10$ in each group). There was no difference in the expression levels of (B) RBKS and (C) in obese and non-obese OAC tumour ($p=0.4042$ and $p=0.288$ respectively, $n=10$ in each group). There no significant difference in TCA associated PCK2 expression between viscerally obese and non-obese OAC patient tumour ($p=0.9262$, $n=10$ in each group). Statistical test used was Mann Whitney U test. $p<0.05$ (*). Error bar denotes mean ± S.E.M.

6.3.4 Delineation of human mitochondrial energy metabolism associated genes on OE33 cells cultured with ACM

To analyse the expression of 84 human genes associated with human mitochondrial metabolism, Human Mitochondrial Energy Metabolism Plus RT^2 Profiler PCR Arrays were used. OE33 cells were co-cultured with ACM for 24 hours prior RNA extraction. Fold expression of all target genes was normalised relative to the media only treated OE33 cells. The cut-off for differential gene expression was defined by either a relative 2-fold upregulation or 2-fold downregulation. 28/32 genes in Complex I (Table 6.5), 4/4 genes in complex II (Table 6.6), 10/12 genes in Complex III (Table 6.6), 12/14 genes in Complex V (Table 6.6) and 8/9 pathway activity signature genes (Table 6.7) were

significantly upregulated in ACM co-cultured cells compared to M199 media only treated OE33 cells.

A panel of 10 genes, which exhibited the greatest fold upregulation (more than two fold upregulation following treatment of cells with ACM, compared to M199 media treated cells), was selected. These genes (NDUFA1, NDUFA8, NDUFA11, NDUFS2, COX5B, COX6C, ATP5G2, ATP5L, CYB561D1, HSPA1B) were subsequently validated *in – vitro* using patient samples

Table 6.5 Human mitochondrial function gene microarray screen between media only and ACM co-cultured OE33 cells: the effect of ACM on Complex I gene expression.

Functional Group	Gene	Expression*
Complex I	NDUFA1	7.2
	NDUFA10	2.79
	NDUFA11	3.6
	NDUFA2	1.93
	NDUFA3	2.37
	NDUFA4	3.65
	NDUFA5	2.14
	NDUFA6	1.07
	NDUFA8	3.9
	NDUFAB1	2.59
	NDUFB10	2.33
	NDUFB2	3.6
	NDUFB3	1.61
	NDUFB4	3.12
	NDUFB5	4.27
	NDUFB6	2.31
	NDUFB7	2.04
	NDUFB8	2.92
	NDUFB9	3.6
	NDUFC1	2.42
	NDUFC2	2.61
	NDUFS1	2.53
	NDUFS2	3.19
	NDUFS3	3.15
	NDUFS4	3.6
	NDUFS5	0.16
	NDUFS6	2.28
	NDUFS7	3.23
	NDUFS8	3.54
	NDUFV1	3.92
	NDUFV2	2.97
	NDUFV3	2.61

B2M = Endogenous Control Gene

Relative Expression (e.g. expression of NDUFA1 is 7.2 times greater in ACM co-cultured than media only cultured OE33 cells). Upregulation/downregulation greater than two fold was considered to be significant

Table 6.6 Human mitochondrial function gene microarray screen between media only and ACM co-cultured OE33 cells: the effect of ACM on Complex II, Complex III and Complex V gene expression.

Functional Group	Gene	Expression*
Complex II	SDHA	3.01
	SDHB	2.28
	SDHC	2.86
	SDHD	5.73
Complex III	COX4I1	3.07
	COX5A	2.42
	COX5B	3.24
	COX6A1	3.66
	COX6A2	-4.89
	COX6B1	4.12
	COX6C	7.88
	COX7A2	2.13
	COX7A2L	3.29
	COX7B	2.53
	COX8A	1.92
	CYC1	4.3
Complex V	ATP5A1	1.9
	ATP5B	2.3
	ATP5C1	2.52
	ATP5F1	4.37
	ATP5G1	0.83
	ATP5G2	3.81
	ATP5G3	2.74
	ATP5H	2.23
	ATP5I	2.25
	ATP5J	2.68
	ATP5J2	2.43
	ATP5L	3.03
	ATP5O	2.03
	PPA1	2.59

B2M = Endogenous Control Gene

Relative Expression (e.g. expression of SDHA is 3.01 times greater in ACM co-cultured than media only cultured OE33 cells). Upregulation/downregulation greater than two fold was considered to be significant

Table 6.7 Human mitochondrial function gene microarray screen between media only and ACM co-cultured OE33 cells: the effect of ACM on Pathway activity signature genes.

Functional Group	Gene	Expression*
Pathway Activity Signature Genes	ARRDC3	4.05
	ASB1	3.95
	CYB561D1	2.6
	DNAJB1	3.23
	EDN1	2.73
	GADD45B	3.89
	HSPA1A	1.5
	HSPA1B	2.38
	LRP5L	2.58

B2M = Endogenous Control Gene

Relative Expression (e.g. expression of ARRDC3 is 4.05 times greater in ACM co-cultured than media only cultured OE33 cells). Upregulation/downregulation greater than two fold was considered to be significant

6.3.4.1 Validation of human mitochondrial function associated genes in OE33 cells co-cultured with ACM

A list of ten significantly upregulated genes following co-culture with ACM were selected from the human mitochondrial function RT^2 Profile PCR Arrays for validation with SYBR green dye based qPCR. Genes selected were NDUFA1, NDUFA8, NDUFA11 and NDUFS2 which were associated with Complex I, Complex III associated COC5B and COX6C, Complex V associated ATP5G2 and ATP5L and pathway activity signature genes CYB561D1 and HSPA1B. OE33 cells were co-cultured with ACM from 5 different OAC patients (Table 6.1) and cDNA was synthesized for the validation study. The cell culture set up, RNA isolation and cDNA synthesis were identical to the ones described in Section 2.7 and Section 2.11 respectively.

There was no significant change in NDUFA1, NDUFA8, NDUFA8 and NDUFS2 in ACM treated cells compared to M199 control (1.11 ±0.0482, 1.2 ±0.0932, 1.107 ±0.0513 and 1.181 ±0.082 respectively, versus M199 control 0.904 ±0.0923, p=0.1508, p=0.0556, p=0.1508 and p=0.0952 respectively, n=5 in each group) (Figure 6.8a, Figure 6.8b, Figure 6.8c and Figure 6.8d respectively).

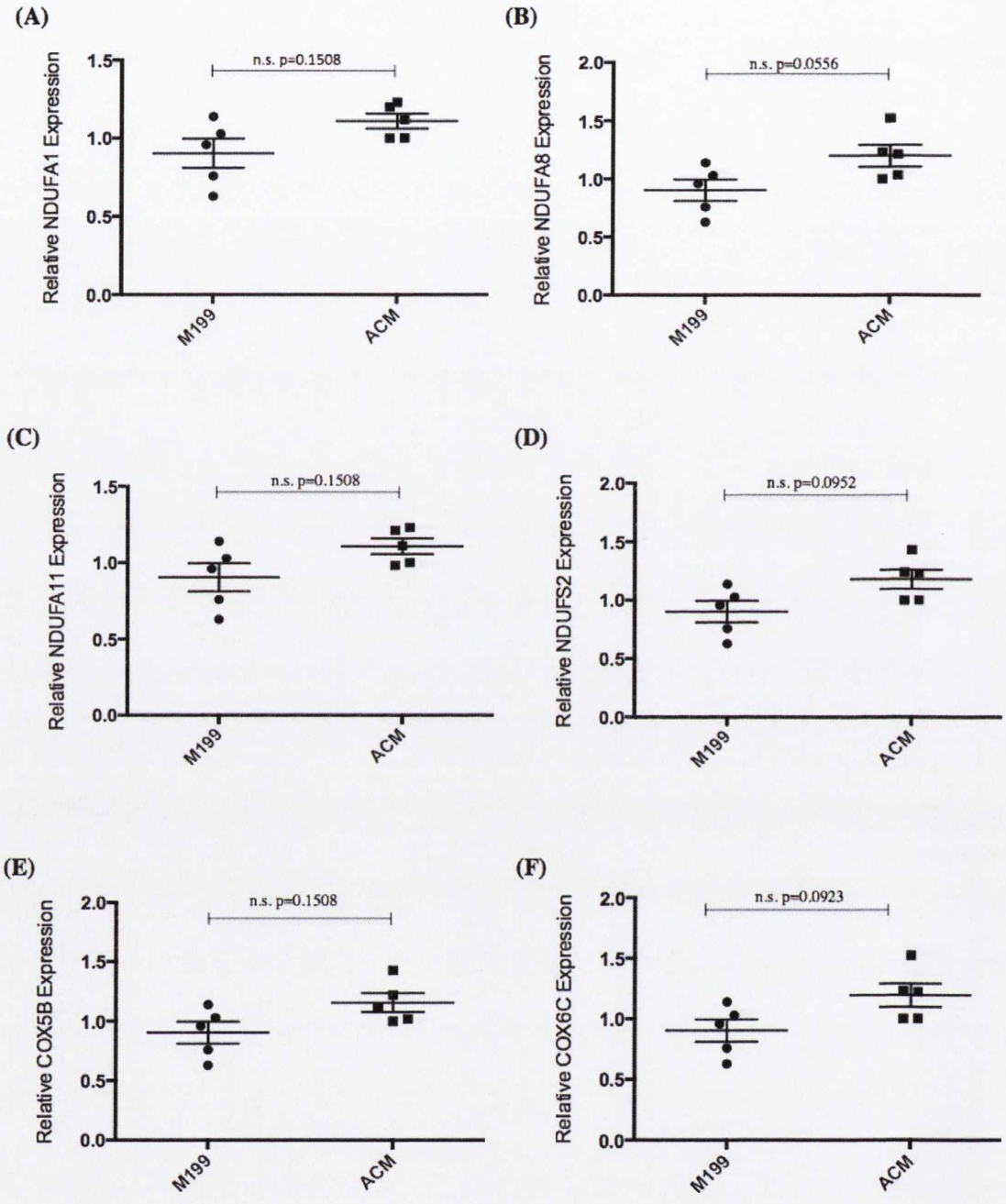


Figure 6.8 Mitochondrial energy metabolism associated gene expression: Complex I and Complex III are not upregulated by co-culture of OE33 cells with ACM qPCR analysis reveal that (A) NDUFA1, (B) NDUFA8, (C) NDUFA11 and (D) NDUFS2 expression levels were not higher in ACM co-cultured OE33 cells compared to M199 media only treated cells (p-0.1508, p=0.0556, p=0.1508 and p=0.0952 respectively, n=5 in each group). (E) There was no significant difference in Complex III associated COX5B and (F) COX6C in ACM co-cultured OE33 cells compared to M199 media only treated cells (p=0.1508 and p=0.0952 respectively, n=t in each group). Statistical test used was Mann Whitney U test. Error bar denotes mean ± S.E.M.

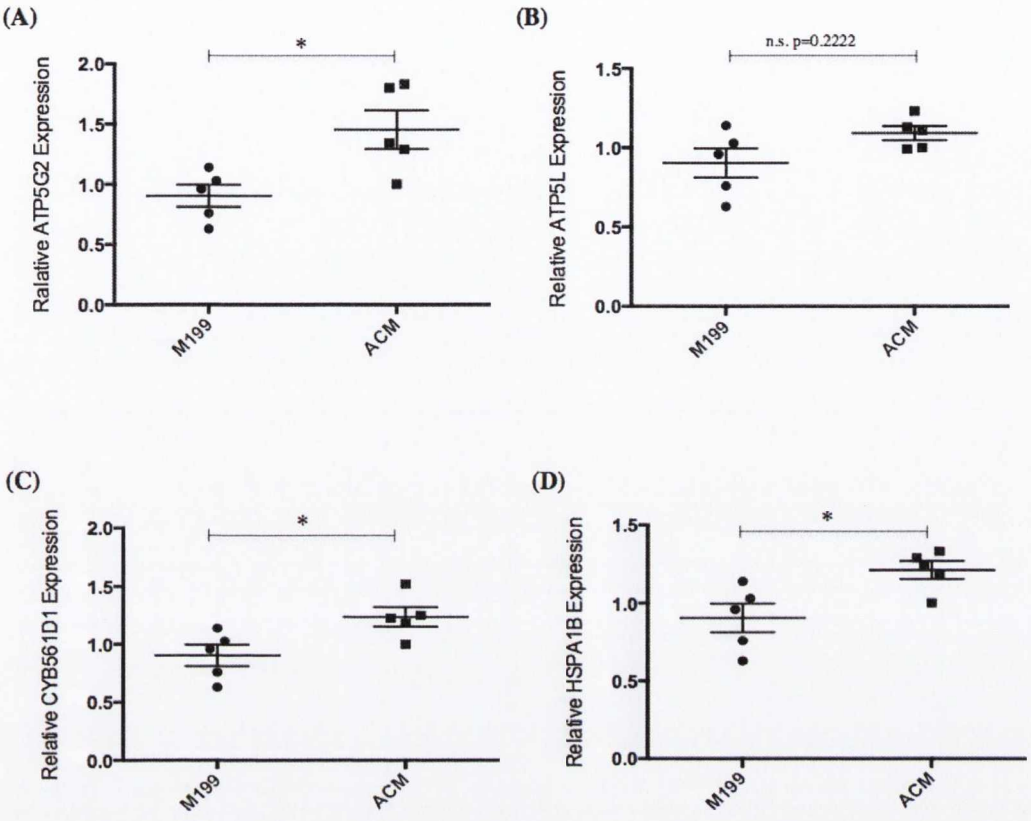


Figure 6.9 Mitochondrial energy metabolism associated gene expression: Complex V and pathway activity signature genes are upregulated by co-culture of OE33 cells with ACM. qPCR analysis reveal that (A) Complex V associated ATP5G was expressed at significantly higher level in ACM co-cultured cells compared to M199 media cultured cells ($p<0.05$, n=5 in each group). (B) There was no significant difference in expression levels of ATP5L in ACM compared to M199 media treated cells (p=0.2222). (C) CYB561D1 and (D) HSPA1B expression levels were significantly higher in ACM co-cultured OE33 cells compared to M199 media only treated cells ($p<0.05$, n=5 in each group). p=0.1508 and p=0.0952 respectively, n=5 in each group). Statistical test used was Mann Whitney U test. $p<0.05$(*).Error bar denotes mean ± S.E.M.

6.3.4.2 Validation of human mitochondrial function associated genes in OAC tumour

Biopsy samples were collected from the main specimen post-surgical resection from OAC patients as described in Section 2.4. The patient demographic is summarized in Table 4.3. RNA was isolated as described in Section 2.6 and gene expression was

measured in real time by qPCR as described in Section 2.12. Details for gene primer probes used were summarized in Table 2.3. The RQ value for one patient sample was set as the calibrator to allow normalisation of the data set. Gene expression levels were compared in tumour from obese versus non-obese OAC patients with obese VFA cut off value of 163.8 cm^2 in males and 80.1 cm^2 in females, n=10 in each group.

Complex I associated genes NDUFA1 and NDUFA8 were expressed at significantly higher levels in the tumour from viscerally obese compared to non-obese OAC patients (1.354 ±0.0681 versus 1.077 ±0.0409 and 1.35 ±0.0981 versus 0.962 ±0.1252 respectively, $p<0.05$ and $p<0.01$ respectively, n=10 in each group) (Figure 6.10a and Figure 6.810 respectively). There was no difference in the expression levels of NDUFA11 and NDUFS2 between obese and non-obese OAC patients (1.129 ±0.0745 versus 0.9643 ±0.1162 and 1.1588 ±0.106 versus 1.129 ±0.109 respectively, p=0.4727 and p=0.7796 respectively, n=10 in each group) (Figure 6.10c and Figure 6.10d respectively). There was no significant difference in Complex III associated COX5B gene expression between obese and non-obese groups (1.5888 ±0.106 versus 1.278 ±0.0819, n=10 in each group, p=0.0627) (Figure 6.8e), however, there was a significant increase in COX6C levels in viscerally obese compared to non-obese OAC patients (1.78 ±0.1334 versus 1.176 ±0.049, n=10 in each group, $p<0.001$) (Figure 6.8f). There was no significant difference in the expression levels of ATP5G2 between viscerally obese and non-obese OAC patients (1.255 ±0.1851 versus 1.195±0.4192, n=10 in each group, p=0.984) (Figure 6.11a), however, ATP5L expression was significantly higher in obese group of patients (1.918 ±0.1744 versus 1.258 ±0.0559, n=10 in each group, $p<0.001$) (Figure 6.11b). There was no significant difference in pathway signature gene expression CYB561D1 and HSPA1B between obese and non-obese OAC patients (1.325 ±0.1098 versus 1.289 ±0.1818 and 0.994 ±0.05529 versus 0.9685 ±0.1163 respectively, n=10 in each group, p=0.8357 and p=0.6706 respectively) (Figure 6.11c and Figure 6.11d respectively).

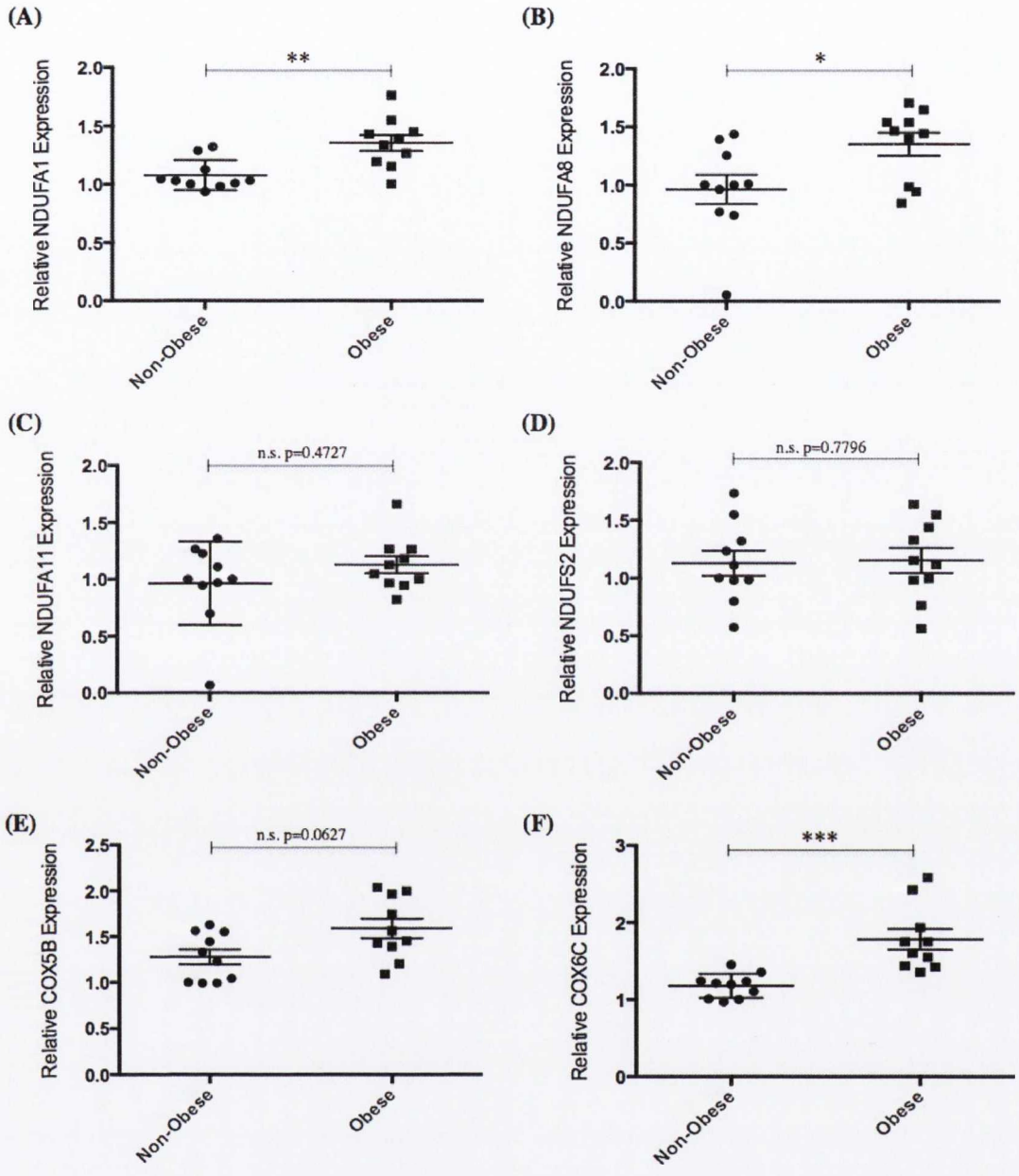


Figure 6.10 Mitochondrial energy metabolism associated gene expression: Complex I and Complex III associated gene expression in AOC patient tumour. qPCR analysis reveal that Complex I associated genes (A) NDUFA1 and (B) NDUFA8 were significantly upregulated in the tumour from viscerally obese compared to non-obese OAC patients ($p<0.05$, $n=10$ in each group). There was no significant difference in the (C) NDUFA11 and (D) NDUFS2 expression levels between the tumour from viscerally obese and non-obese patients ($p=0.4727$ and $p=0.7796$ respectively, $n=10$ in each group). (E) There was no significant difference in Complex III associated COX5B expression between obese and non-obese groups ($p=0.0627$, $n=10$ in each group), however, (F) COX6C expression level was significantly higher in viscerally obese compared to non-obese OAC patients ($p<0.001$). Statistical test used was Mann Whitney U test. $p<0.05$(*), $p<0.001$(***).Error bar denotes mean ± S.E.M.

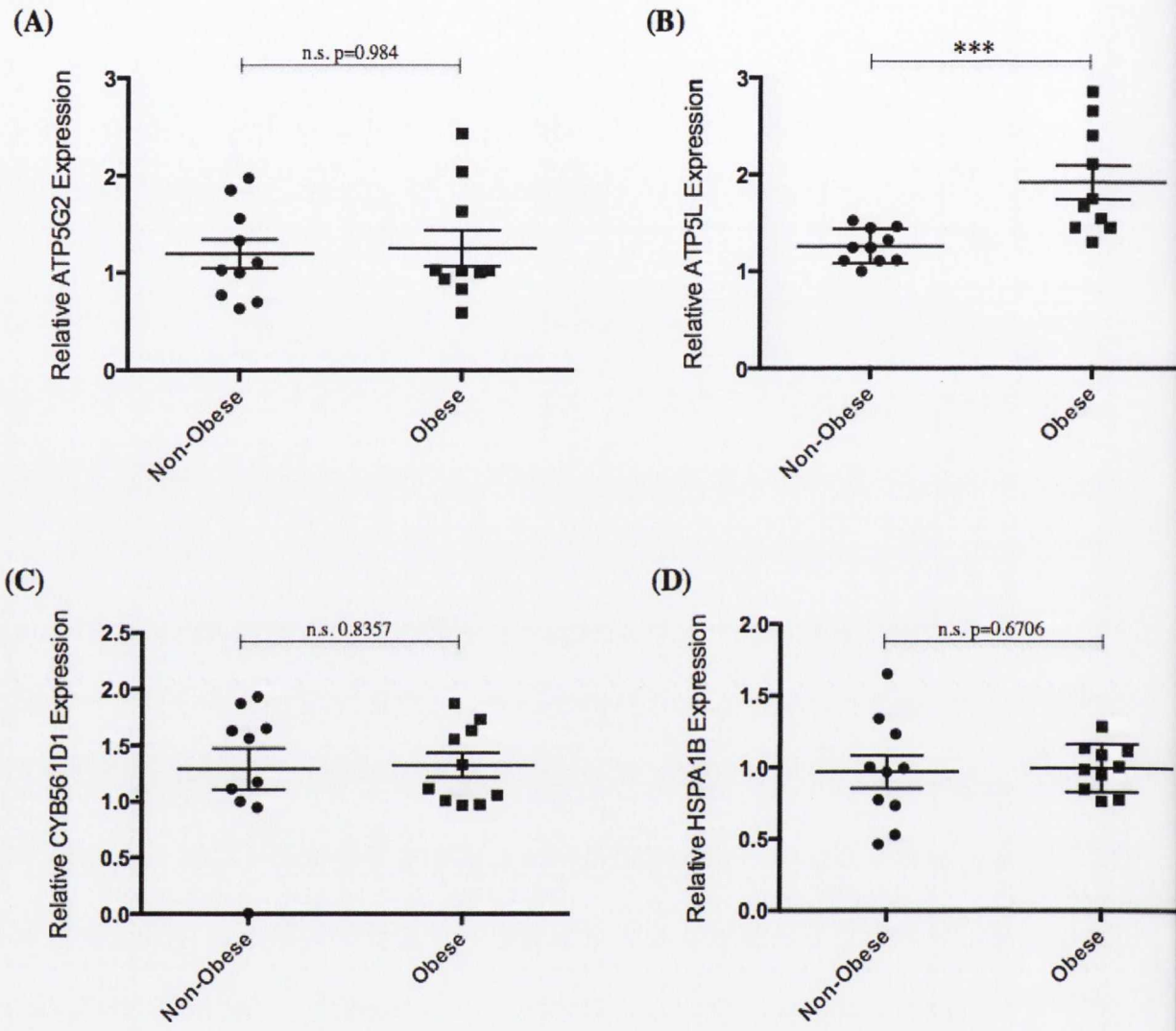


Figure 6.11 Mitochondrial energy metabolism associated gene expression: Complex V and pathway activity signature gene expression in the OAC tumour. qPCR analysis reveal that (A) there was no significant difference between Complex V associated ATP5G expression in the tumour from viscerally obese and non-obese OAC patients ($p=0.984$, $n=10$ in each group), however, (B) there a significant difference in expression levels of ATP5L in the tumour from the obese compared to non-obese OAC patients ($p<0.001$, $n=10$ in each group). There was no significant difference in the expression of pathway activity signature genes (C) CYB561D1 and (D) HSPA1B in obese compared to non-obese OAC patients ($p=0.8357$ and $p=0.6706$ respectively, $n=10$ in each group). Statistical test used was Mann Whitney U test. $p<0.001$(***). Error bar denotes mean ± S.E.M.

6.3.5 Investigation of the effect of hypoxia on metabolic activity in oesophageal adenocarcinoma

6.3.5.1 Determining the optimum concentration of $CoCl_2$ to induce hypoxia in oesophageal adenocarcinoma

Hypoxia and hypoxic-mediated signaling play an important role in the pathology of cancer. It has been noted in the literature that many hypoxia-regulated genes control substrate supply for glucose transporters as well as other cellular metabolic pathways [361]. Cancer cells reprogram their metabolic phenotype to a preferential reliance on glycolysis for ATP generation. This switch in cancer cell metabolism is seen in many types of cancer cells [361]. Hypoxic chamber is a reliable experimental device that can create and maintain a hypoxic environment for cell culture experiments. However, for functional experiments measuring glycolytic activity and mitochondrial respiration using SeaHorse XFe24 analyser, we were unable to place the XFe analyser inside the hypoxic chamber. Published studies show that hypoxia can be induced in cell line models using $CoCl_2$ [362], therefore this approach was optimized and employed in this study.

The level of HIF1A protein expression was measured in OE33 cells following 24-hour treatment with $CoCl_2$ at a range of concentrations (1-100 μM). Protein was isolated from OE33 cells as described in Section 2.14.1. Protein concentration was measured by BCA assay (Section 2.15). 30 μg of protein was loaded per sample and the western blot procedure was performed as described in Section 2.17. Single bands at the expected molecular weight of 132 kDa were observed. β-actin was used to normalize for total protein content and was observed at molecular weight of approximately 42 kDa. Following protein band densitometry and normalization of data to β-actin, significant upregulation in HIF1A level was observed following treatment of OE33 cells with 100 μM of $CoCl_2$. This experiment was independently repeated three times (Figure 6.12).

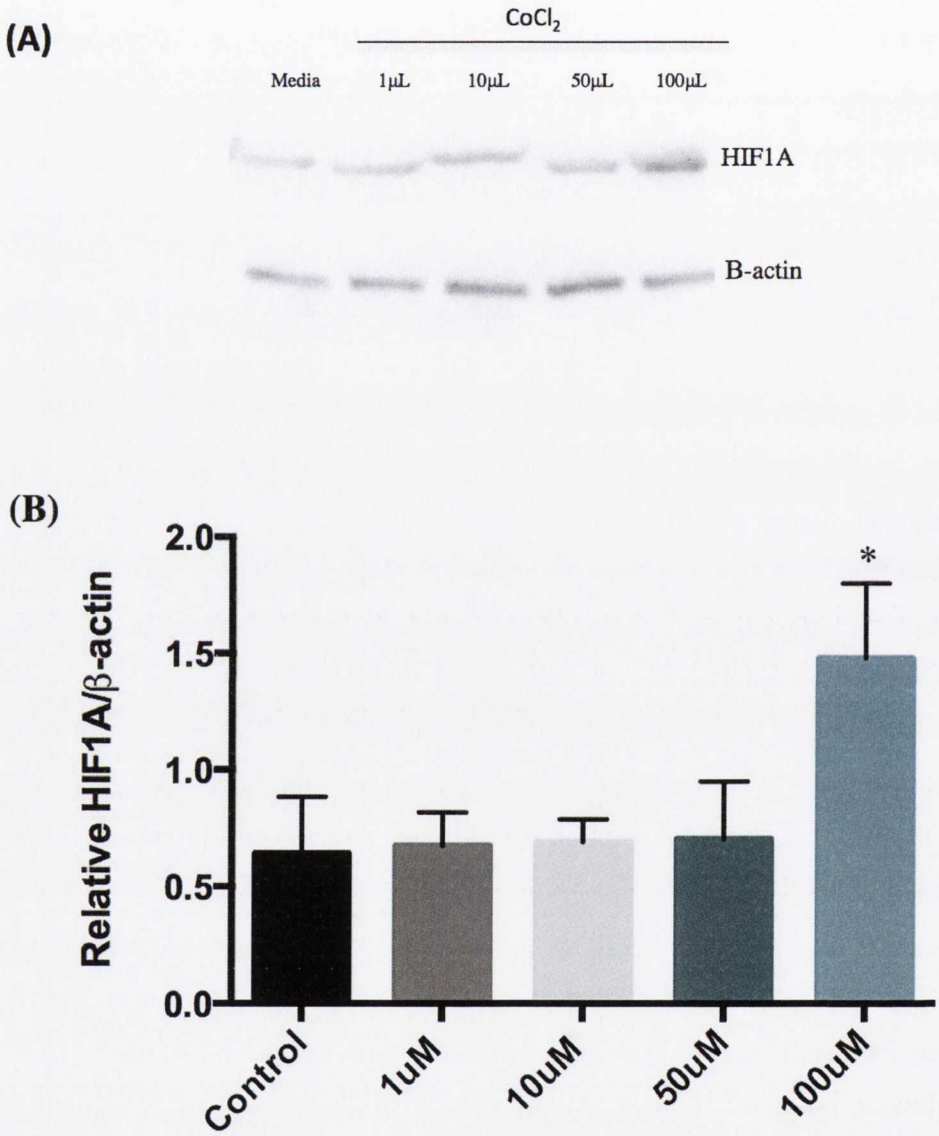


Figure 6.12 HIF1A protein levels are significantly increased following 24-hour treatment of OE33 cells with 100 μM of $CoCl_2$. (A) Representative image of western blot for HIF1A expression following treatment with $CoCl_2$ (1-100 μM). (B) Relative HIF1A expression was significantly higher following 100 μM $CoCl_2$ treatment compared to media treated control cells. Statistical test used was one-way ANOVA with Tukey's Multiple comparison Test. $P<0.05$(*). Error bar denotes mean ±S.E.M.

6.3.5.2 Investigation of $CoCl_2$ effect on glycolysis and oxidative phosphorylation in oesophageal adenocarcinoma cells

Effect of $CoCl_2$ on glycolysis and oxidative phosphorylation was investigated using Seahorse XFe24 Analyser. Briefly, OE33 cells were seeded into Seahorse XFe24 plate, at a density of 10,000 cells/well. Cells were serum depleted overnight (0.5% FBS, 5 hours after seeding). The following day, OE33 cells were treated with 4 different concentrations of $CoCl_2$ (1-100μM). 24 hours following treatment, Seahorse XFe24 experiment was run as described in Section 2.18.4. Experiment was run once in order to investigate whether $CoCl_2$ is able to induce changes in glycolysis and mitochondrial respiration in OE33 cells and at what concentrations this effect could be potentially achieved.

$CoCl_2$ showed an induction of glycolysis in OE33 cells in a dose-dependent manner, with the optimum increase in glycolytic activity (ECAR) at the concentration of 50 μM (Figure 6.13a). $CoCl_2$ induced changes in mitochondrial metabolism (OCR) however the changes were not in a dose-dependent manner (Figure 6.13b).

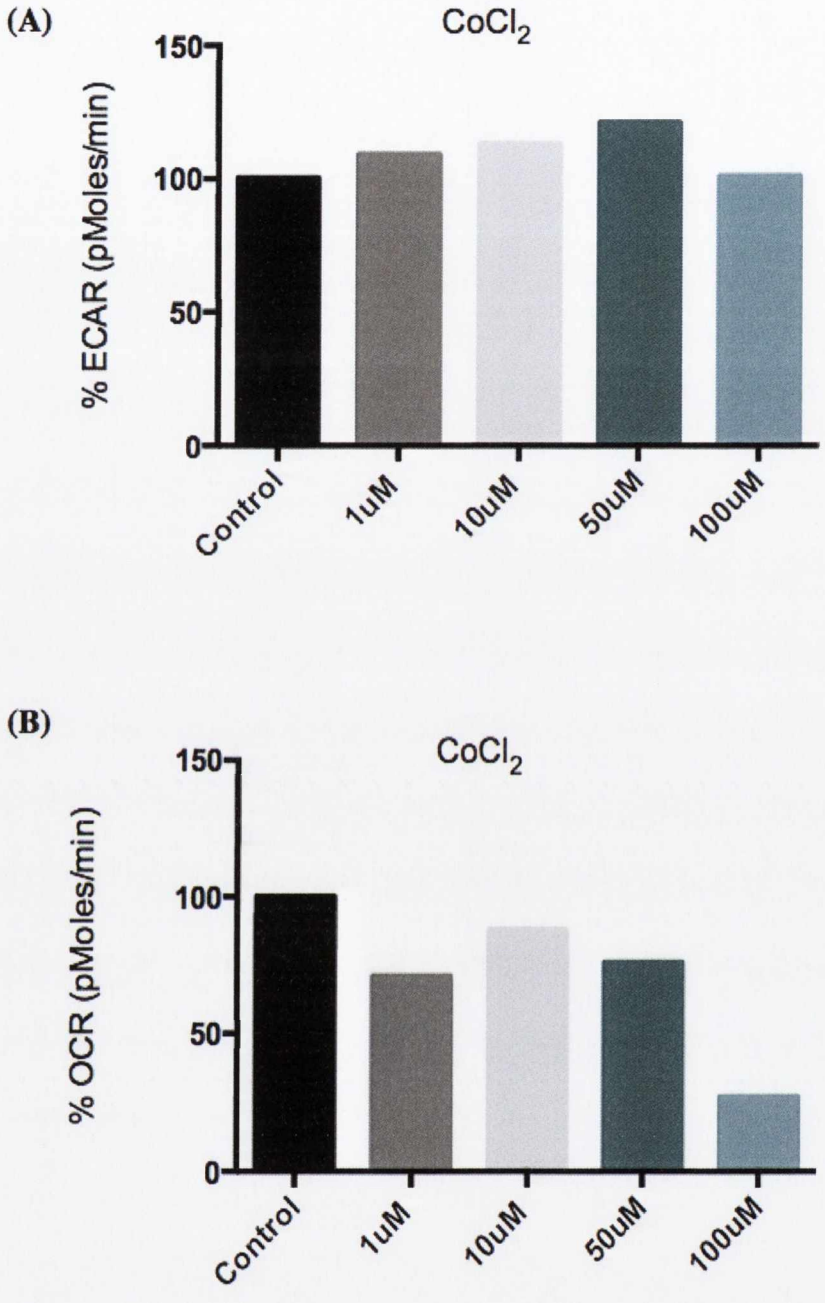


Figure 6.13 Investigating the ability of $CoCl_2$ to induce changes in glycolysis and mitochondrial respiration in oesophageal adenocarcinoma cells *in vitro*. Seahorse XFe24 experiment reveals that (A) $CoCl_2$ induces glycolysis at dose-dependent manner with the optimum concentration of 50uM. (B) $CoCl_2$ shoed alterations in mitochondrial respiration activity, however, there was no dose-dependent trend. Experiment was run once to determine the optimum concentration of $CoCl_2$ for follow up experiments, therefore no statistical analysis were used.

6.3.5.3 Investigation of the optimum time required for $CoCl_2$ to induce hypoxia in oesophageal adenocarcinoma cells

OE33 cells were treated with two different concentrations of $CoCl_2$ 50 μM and 100 μM. RNA was isolated at 0, 2, 4, 6, 8 and 24 hours following treatment. The cell culture set up, RNA isolation and cDNA synthesis were identical to the ones previously described.

qPCR analysis revealed that the optimum time required for $CoCl_2$ to induce hypoxia in OE33 cells was 8 hours, in both concentrations with the highest HIF1A levels observed at 8 hours. $CoCl_2$ significantly induced hypoxia at both 50 μM ($p<0.01$) and 100 μM ($p<0.05$), however the induction was more significant when 50 μM concentration was used (Figure 6.14). Interestingly, elevated HIF1A levels remained elevated at the 24-hour time-point, however, the cells treated with 50 μM of $CoCl_2$ retained HIF1A at a higher level at 24 hours (1.873 ±0.2470 versus 1.417 ±0.1615, with 25% loss of HIF1A between 8 hour and 24 hour time-points) than cells treated with 100 μM of $CoCl_2$ (1.567 ±0.2367 versus 0.7833 ±0.2367, with 50.02% of HIF1A expression between 8 hour and 24 hour time-points) (Figure 6.14).

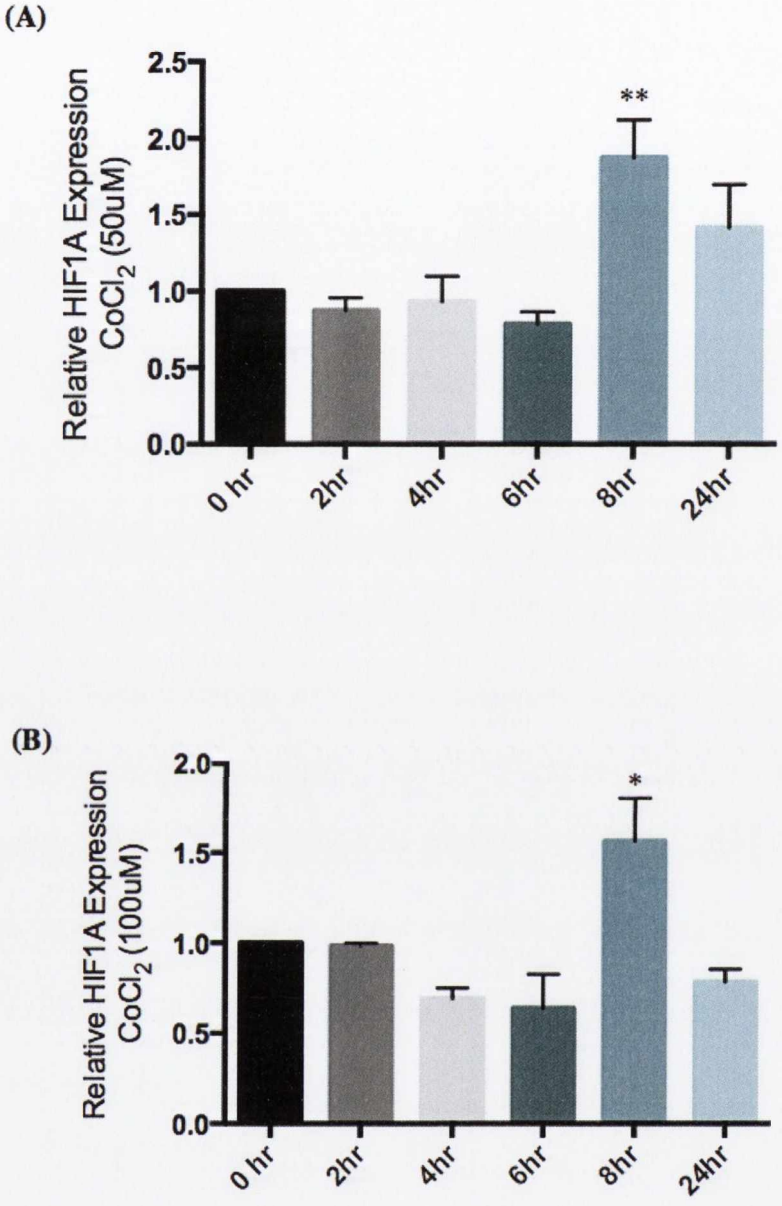


Figure 6.14 The optimum time required for $CoCl_2$ to induce hypoxia in OE33 cells is 8 hours. qPCR results revealed that (A) Treatment of OE33 cells with 50μM of $CoCl_2$ significantly elevated HIF1A levels at 8 hour time-point ($p<0.01$, n=3). (B) Treatment of OE33 cells with 100 μM of $CoCl_2$ significantly induced hypoxia at 8 hour time-point ($p<0.05$, n=3). Statistical test used was one-way ANOVA with Tukey's Multiple comparison Test. $p<0.05$(*), $p<0.01$(**). Error bar denotes mean ±S.E.M.

6.3.5.4 Assessment of HIF1A expression in OAC tumour and its association with visceral obesity

Biopsy samples were collected from the main specimen post-surgical resection from OAC patients as described in Section 2.4. The patient demographic is summarized in Table 4.5. RNA was isolated as described in Section 2.6 and gene expression was measured in real time by qPCR as described in Section 2.10. Expression of HIF1A was assessed. The RQ value for one patient sample was set as the calibrator to allow normalisation of the data set. Gene expression levels were compared in tumour from obese versus non-obese OAC patients with obese VFA cut off value of 163.8 cm^2 in males and 80.1 cm^2 in females, n=10 in each group.

HIF1A expression was significantly higher in tumour from viscerally obese compared to non-obese OAC patients (2.722 ±0.3192 versus 1.732 ±0.2430, n=10 in each group, $p<0.05$) (Figure 6.15).

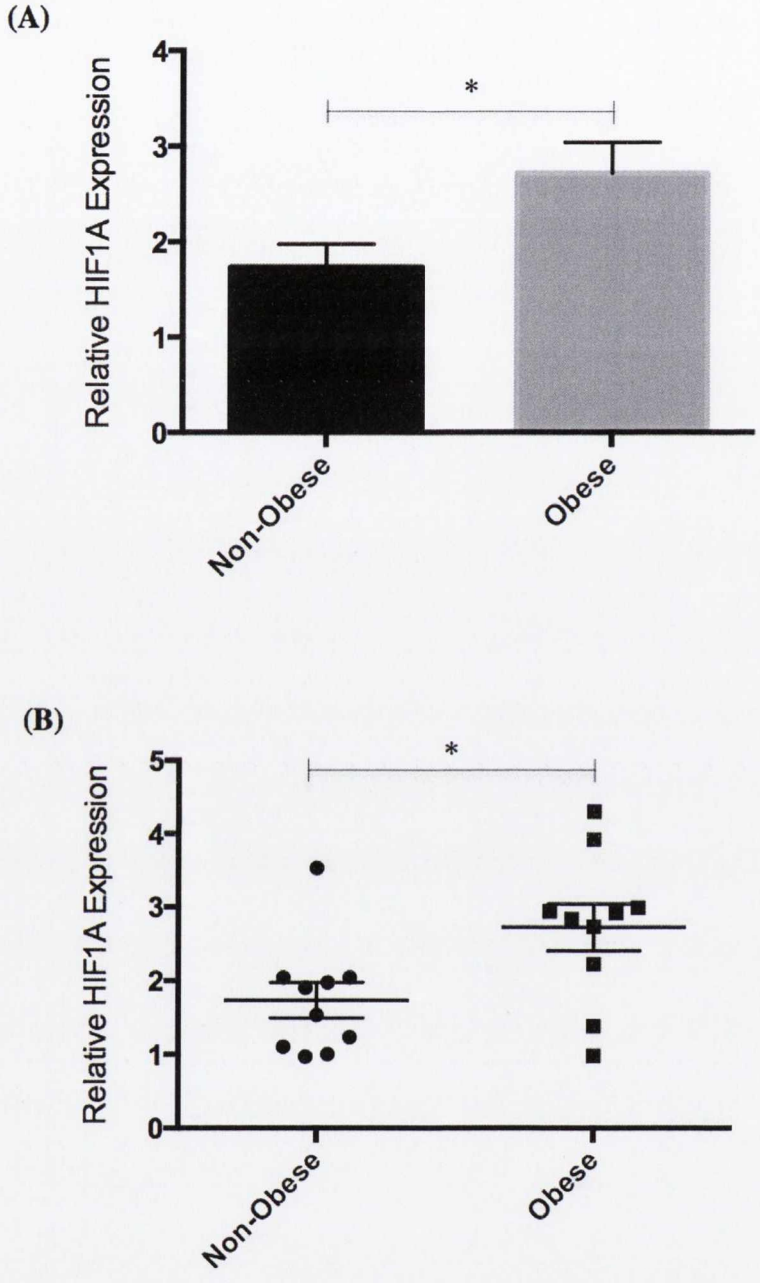


Figure 6.15 HIF1A expression is significantly higher in tumour from viscerally obese compared to non-obese OAC patients. (A) HIF1A expression was significantly higher in tumour from viscerally obese compared to non-obese OAC patients. (B) The distribution of HIF1A expression across OAC patient tumour biopsies shown by scatter plot. n=10 in each group. Statistical test used was Man-Whitney U test. $p<0.05$(*). Error bar denotes mean ± S.E.M.

6.4 Discussion

Visceral obesity has a strong association with both the incidence and mortality of esophageal adenocarcinoma (EAC). Alteration in mitochondrial energy metabolism is one of the new emerging hallmarks of cancer [168, 322]. In this study, we examined whether visceral obesity drives metabolic shift in glucose metabolism and results in mitochondrial dysfunction in OAC. Additionally, the ability of $CoCl_2$ to induce hypoxia in oesophageal adenocarcinoma cells and the effect of hypoxia in cancer cell metabolism was examined.

Accurate assessment of obesity status is crucial for elucidating the pathophysiological role of obesity in OAC, therefore in this study we have used a newly established CT-determined VFA cut-off for classifying visceral obesity in patients with OAC [310]. It has been previously shown that ACM from obese OAC patients has a distinct metabolic profile and was able to alter tumour metabolism, with ACM from obese OAC patients inducing a metabolic shift in glucose metabolism [248]. This study showed that ACM from both obese and non-obese OAC patients significantly induced lactate secretion in OE33 cells, however, there was a significant difference between lactate secretion levels in viscerally obese and non-obese patients suggesting that obesity is potentially associated with metabolic shift in glucose metabolism in this cohort of OAC patients. Lactate levels were not measured in ACM prior experiment. It is expected that ACM prepared using omental fat from different OAC patients contain different levels of lactate. Therefore, for future experiments it would be beneficial to measure lactate levels before co-culture with OAC cell lines and dilute ACM samples appropriately to normalise ACM to lactate levels.

Lactate has been previously shown to be the end product of glycolysis [363], therefore we hypothesised that the increase in lactate secretion in oesophageal adenocarcinoma cells was a result of ACM-induced glycolysis. Following Seahorse XFe24 analysis, this study showed that ACM from viscerally obese OAC patients significantly induced glycolysis in OE33 cells, suggesting that co-culture of OE33 cells with ACM from viscerally obese OAC patients resulted in the shift of glucose metabolism. This result was supported by a recent study by Lynam-Lennon *et al* who showed that ACM from viscerally obese OAC patients altered metabolic profile and resulted in mitochondrial

dysfunction in OAC cells *in vitro* [175].

Following treatment of OE33 cells with ACM from viscerally obese OAC patients, The Human Glucose Metabolism RT^2 Profiler and Human Mitochondrial Function RT^2 Profiler PCR Array data showed that a number of glucose metabolism (Table 6.2-64) and mitochondrial function associated genes (Table 6.5-6.7) were significantly upregulated (upregulation greater than two fold relative to media only treated cells) following co-culture with ACM from viscerally obese OAC patients. 10 significantly altered genes from each panel were validated *in vitro* and in *vivo.* Glucose metabolism associated ALDOB, ENO3, PDK1 and H6PD were upregulated both *in vitro,* where OE33 cells were co-cultured with ACM from viscerally obese patients (n=5), and *in vitro*, in OAC patient tumour biopsies (10 obese and 10 non-obese patients).

PDK1 has been shown to be a HIF1A target that antagonizes the function of Pyruvate dehydrogenase (PDH), a key rate-limiting enzyme for pyruvate conversion to acetyl-coA and entry into the TCA cycle. PDK1-dependent inhibition of PDH reduces the conversion of pyruvate to acetyl-CoA, leading to reduced flow of glucose-derived pyruvate into the TCA cycle, especially under hypoxic conditions [364, 365]. This study showed that PDK1 expression was significantly higher following co-culture of OE33 cells with ACM from viscerally obese OAC patients and in the tumour from viscerally obese OAC patients. Dupuy *et al* showed that HIF1A and PDK1 promote glycolytic metabolism in liver- metastatic breast cancer cells and that elevated PDK1 expression is required for efficient formation of liver metastases [364]. Interestingly, in this study we showed that HIF1A, similarly as PDK1 expression, was significantly higher in tumours from viscerally obese compared to non-obese OAC patients, confirming a potential link between the two and suggesting an association with visceral obesity.

ENO3 expression was significantly higher in ACM co-cultured OE33 cells and in the tumour of viscerally obese OAC patients. This result was in line with literature where ENO3 has been shown to be associated with energy metabolism in cancer cells and this result is supported by previous findings in Chapter 4, where the level of ENO3 was significantly higher in tumour tissue from viscerally obese OAC patients and high epithelial ENO3 expression was positively correlated with increasing BMI suggesting the role in obesity-induced glycolysis. This study reports that glycolysis associated ALDOB expression was significantly higher following co-culture of OE33 cells with ACM and

ALDOB expression was significantly higher in tumour from viscerally obese OAC patients. ALDOB has been shown to be upregulated in colorectal, stomach, liver and renal cancers [366].

Pentose pathway associated H6PD was also significantly upregulated *in vitro* and in tumour from viscerally obese OAC patients. H6PD has been shown to be a member of pentose pathway which allows tumour cells to raise their intracellular NADPH, critical for rapid tumour growth and survival. The pentose phosphate pathway produces ribose sugars for nucleotide biosynthesis and NADPH that serves as reducing potential for the synthesis of macromolecules (555, 556).

The electron transport chain plays a central role in oxidative phosphorylation and it has been shown that respiratory impairment plays a key role in tumourigenesis [236, 367]. Complex I associated NDUFA1 and NDUFA8 were significantly upregulated both in vitro, following co-culture of OE33 cells with ACM and in vivo, in tumour from viscerally obese OAC patients, suggesting their association with inducing changes in mitochondrial metabolism. It has been shown that Complex I is the entry point for most electrons into the respiratory chain, therefore complex I has been suggested as the rate-limiting step in electron transfer [367, 368] and mitochondrial DNA (mtDNA) mutations in genes encoding complex I subunits have been found in various cancer cells [239]. This study reveals that Complex III associated COX6C expression was also significantly elevated *in vitro*, following co-culture of oesophageal adenocarcinoma cells with ACM from viscerally obese OAC patients. COX6C levels were also significantly higher *in vivo*, in tumour from viscerally obese OAC patients, suggesting a potential role of COX6C in alterations in mitochondrial metabolism in this study. It has been shown that Complex III has a link with a role in carcinogenesis. It has been reported that an increase in superoxide radicals inactivates complex III resulting in the impairment of mitochondrial respiration in rat hepatomas [243]. Complex III alterations have been linked to breast, colorectal and ovarian cancer [369, 370].

This study reported that mitochondrial pathway activity associated ATP5L expression was also significantly induced in vitro, following co-culture of OE33 cells with ACM and in vivo in OAC tumour biopsies from viscerally obese patients indicating a potential association with obesity in OAC, and a positive association with metabolic shift in glucose metabolism.

HIF1A has been shown to be a major regulator of oxygen homeostasis within cells [276]. This study reported an increase in epithelial expression of HIF1A in overweight and obese compared to normal weight OAC patients (Chapter 4). An increase in HIF1A expression has been previously shown in adipose tissue and adipocytes [332, 371, 372]. An increase in HIF1A has also been shown to be associated with more aggressive disease phenotype, increase in inflammation that may stimulate cancer development [373] and poor overall survival in colorectal cancer [313, 374]. This study showed that $CoCl_2$ induced hypoxia significantly increased glycolysis (ECAR) in oesophageal adenocarcinoma cells and that the level of HIF1A expression was significantly higher in viscerally obese compared to non-obese OAC patients suggesting a positive association with obesity and induction of metabolic shift in glucose metabolism *in vitro*.

$CoCl_2$ was also shown to induce hypoxia in oesophageal adenocarcinoma cells and to alter glycolysis in these cells. This observation was of a high importance for the following part of the study, where the activity of potential inhibitors of glycolysis can be investigated in the hypoxic conditions.

Chapter 7

Assessment of the anti-cancer potential of novel 5-lipoxygenase targeted inhibitors in models of oesophageal adenocarcinoma

7.1 Introduction

Major improvements to treatment regimes have been implemented in treatment of oesophageal adenocarcinoma over the last decade, particularly in the case of neoadjuvant CRT, there are still many patients who do not befit from such treatment modalities [375]. In recent years, an increasing proportion of cancer research focused on the developing of molecular therapies that target tumour-dependent processes such as tumour cell growth, in order to compliment standard treatment regimen [376, 377].

Eicosanoid signaling pathways including lipoxygenases have been strongly implicated in inflammation and cancer development in breast, prostate and colorectal cancers [73, 299]. The involvement of 5LOX in cancer progression is now widely supported by a growing body of literature and an increase of 5LOX activity has been shown to be associated with a number of cancer types including pancreatic, prostate, breast, renal, and colorectal cancers [73, 378-380]. It has been previously suggested that 5LOX inhibitors, such as commercially available REV 5901, induce apoptosis via a downregulation of Bcl-2 and downregulation of ERK1/2 and PI3K-Akt pathways [87, 378]. More recent evidence by Sarveswaran *et al* suggests that 5LOX induced apoptosis in prostate cancer cells occurs via an alternate suppression on protein kinase C-epsilon and not by mechanisms solely dependent on pro-survival signals Akt and ERK [91]. Furthermore, Meng *et al* reported that 5LOX inhibition resulted in prostate cancer tumour mass in mouse models, leading to a less aggressive tumour phenotype [89], suggesting that inhibition of 5LOX has the potential to target pro-tumour mechanisms.

It has been mentioned at numerous points throughout this thesis the importance of targeting glycolysis in oesophageal adenocarcinoma. We have already shown a positive association between obesity and glycolysis, and a positive association between upregulation of glycolysis markers and poor disease-specific survival. Proof from this study, alongside with poor prognosis of the disease, suggests the need for new inhibitors of both glycolysis and the 5LOX. In this study we tested a number of novel small molecule inhibitors. Our collaborator Dr. Maloney from the National Institutes of Health

(NIH) in Maryland, US, provided us with a novel inhibitor of 5LOX named NIH4. Our second collaborator Dr. Sheridan from the School of Pharmacy in Trinity College Dublin, provided us with a panel of 17 small molecule compounds and natural plant extracts (Named HS1-HS17) with potential anti-glycolytic and anti-5LOX activity. The novel inhibitors were used to explore the inhibition of 5-lipoxygenase and glycolysis pathways in OAC and compared to the efficacy of commercially available inhibitors of glycolysis and 5LOX, which have been previously shown to have anti-5LOX and anti-glycolytic effect is cancer models. Zileuton, the only inhibitor of 5LOX approved by the FDA, has been shown to suppress prostate cancer metastasis by upregulating E-cadherin and paxillin [89]. Ketoconazole, a dual inhibitor of lactate dehydrogenase (LDHA) and 5LOX, has also been shown to reduce hepatic metastases from the human pancreatic carcinoma RWP-2 in the nude mouse model [381]. Inhibition of 5LOX activity by another commercially available inhibitor of 5LOX, MK886 has also been shown to block 5-HETE production and to induce apoptosis in both hormone-responsive and nonresponsive human prostate cancer cells [88]. In published studies, 5LOX protein expression has been reported to be increased in esophageal cancer and the 5LOX inhibitor REV5901 induced esophageal cancer cells to undergo apoptosis, suggesting its potential as a target in OAC [72]. Commercially available inhibitors of glycolysis, were selected with the aim to target glycolysis at various stages of the cycle. The list of inhibitors and their targets was depicted in Table 7.1. The glycolytic inhibitors currently available are not very potent therefore, *in vivo,* high concentrations are required. Development of new generations of glycolytic inhibitors with high potency, stability, and good safety profiles represent an important research area in this field.

7.2 Aims and objectives

The aim of this chapter was to investigate the anti-cancer effects of commercially available inhibitors of glycolysis and 5LOX and to determine whether novel inhibitors of 5-LOX (small molecule inhibitor and natural extracts) were more effective anti-cancer agents than the commercial inhibitors available.

Specific Objectives:

- To investigate anti-cancer efficacy of commercially available and novel inhibitors of glycolysis and 5LOX in the OE33 cell model, through measurement of effects to cell viability, proliferation and glycolytic activity

- To compare and contrast the effect of novel 5LOX inhibitor on glycolysis in OE33 cell model in the presence of oxygen and in hypoxic environment

- To investigate the effect of novel inhibitors to 5LOX metabolite production in *ex vivo* cultured OAC biopsies

- To investigate the effect of novel small molecule inhibitors of 5LOX on glucose metabolism and mitochondrial function in OE33 cell model

- To assess the effect of novel inhibitor of 5LOX treatment on the immuno-oncology secretory profile markers of OAC patient biopsies cultured *ex vivo*

7.3 Results

7.3.1 Oesophageal adenocarcinoma cell viability following treatment with potential glycolytic and 5-lipoxygenase inhibitors

OE33 cells were treated with four doses (0.1 μM, 1μM, 10 μM and 25 μM) of commercial inhibitors of glycolysis and 5LOX (Table 7.1) and novel inhibitors of glycolysis and 5LOX (Table 7.2) for 24 hours. Cell viability was assessed by MTT – cell viability assay by seeding OE33 cells into 96-well plate and treating with vehicle control or treatment (drug treatments dissolved in M199 media (0.5% FBS) for a total treatment time of 24 hours, as described in Section 2.18.1. Non-linear regression analysis was used to determine the IC_{50}, inhibitory concentration required to reduce viability of the cells by 50% of the observed range of response for each compound (Table 7.1 and Table 7.2). Cell viability was measured in the presence and the absence of oxygen (in the hypoxic chamber), however there was no significant difference in cell viability observed between two different conditions. Cell viability following commercially available and novel inhibitor treatment was measured in oesophageal adenocarcinoma cell line OE33 (described in Section 2.3) in both normoxia (21% O_2) and hypoxia (0.5% O_2). Cell viability was measured by three independent experiments.

Table 7.1 IC_{50} doses for OE33 viability by commercially available inhibitors of glycolysis pathway and 5LOX determined by non-linear regression analysis

Inhibitor	Target	IC_{50} (μM)
Potassium Dichloracetate	PDK1	10.31 ±0.16
3-Amino Benzoic Acid	LDHA	11.24 ±0.27
Sodium Oxamate	LDH	9.73 ±0.09
REV5901	5LOX	11.64 ±0.13
2-Deoxy D-Glucose	Glycolysis	11.02 ±0.14
Ketoconazole	5LOX/ THXS	9.76 ± 0.05
Zileuton	5LOX	>25*
Bromopyruvic Acid	HK2	12.02 ±0.18
MK886	5LOX	10.04 ±0.08

*Cannot determine IC_{50} accurately as dose escalation study did not reach 50% reduction of cell viability

Table 7.2 IC_{50} doses for OE33 viability by commercially available inhibitors of glycolysis pathway and 5LOX determined by non-linear regression analysis

Inhibitor	Target/Source	IC_{50} (μM)
HS1	Indane	11.41 ±0.05
HS2	Chemical	>25*
HS3	Chemical	>25*
HS4	Chemical	>25*
HS5	Chemical	24.05 ±0.12
HS6	Chemical**	10.04 ±0.07
HS7	Extract	16.93 ±0.11
HS8	Extract	>25*
HS9	Extract	23.03 ±0.18
HS10	Extract	11.05 ±0.19
HS11	Extract	20.04 ±0.21
HS12	Extract	13.5 ±0.15
HS13	Chemical	16.82 ±0.13
HS14	Chemical	18.04 ±0.08
HS15	Chemical	12.05 ±0.04
HS16	Chemical	15.83 ±0.17
HS17	Chemical	18.04 ±0.06
NIH4	5LOX	10.08 ±0.09

*Cannot determine IC_{50} accurately as dose escalation study did not reach 50% reduction of cell viability
** Chemical compound with shown anti-5LOX activity in breast cancer cell line
Indane= the structure of the compound was composed of two parts, each part occurring in nature, containing an indane core and anti-inflammatory/immunomodulatory fragment.
Chemical= chemical structures
Extract=lyophilised plant extracts from plants-benzophenones.

7.3.2 Oesophageal adenocarcinoma cell proliferation following treatment with potential glycolytic and 5-lipoxygenase inhibitors

Following the compound screening by cell proliferation assay, OE33 cells were treated with three doses (1μM, 10 μM and 25 μM) of commercial inhibitors of glycolysis and 5LOX and three novel inhibitors with the lowest IC_{50} values (Section 7.3.1). Cell proliferation was assessed by BrdU incorporation. The amount of BrdU incorporation in cells correlates with the amount of DNA synthesis, experimental set up was similar to the one of MTT assay and was described in Section 2.18.2. Non-linear regression analysis was used to determine the inhibitory concentration required to reduce the proliferative

capacity of the cells by 50% of the observed range of response for each compound (Table 7.3). Cell viability was measured in a parallel experiment with hypoxic environment (0.5% O_2) created by 50 μM of $CoCl_2$, the dose that has been shown to be sufficient to induce HIF1A expression in OE33 cells in Section 6.3.5.3.

Commercially available inhibitors of 5LOX, with the exception of Zileuton, significantly reduced OE33 cell proliferation following 24-hour treatment, at the dose of 10 μM (Figure 7.2). Zileuton, significantly reduced OE33 cell proliferative activity at the concentration of 25 μM (Figure 7.2b). Commercially available inhibitors of glycolysis: potassium dichloracetate, 3-amino-benzoic acid, sodium oxamate, 2-deoxy-D-glucose, bromopyruvic acid and a novel small molecule inhibitor HS1, significantly reduced cell proliferation (compared to 0.25% DMSO treated cells) (Figure 7.3). Following treatment of OE33 cells with commercially available and novel inhibitors of glycolysis and 5LOX, in chemically induced hypoxic conditions (50 μM $CoCl_2$), there was no difference in OE33 cell proliferation observed between cells cultured in hypoxic (0.5% O_2) and normoxic (21% O_2) environment (Table 7.4).

Table 7.3 IC_{50} doses for OE33 cell proliferation by commercially available and novel inhibitors of glycolysis pathway and 5LOX determined by non-linear regression analysis

Commercial Inhibitor	Target	IC_{50} (μM)
Potassium Dichloracetate	PDK1	12.78 ±0.07
3-Amino Benzoic Acid	LDHA	11.98 ±0.22
Sodium Oxamate	LDH	11.71 ±0.19
REV5901	5LOX	12.03 ±0.19
2-Deoxy D-Glucose	Glycolysis	13.12 ±0.08
Ketoconazole	5LOX/ THXS	9.88 ±0.07
Zileuton	5LOX	23.03 ±0.23
Bromopyruvic Acid	HK2	9.04 ±0.16
MK886	5LOX	10.14 ±0.28
Novel Inhibitor	Target	IC50 (μM)
HS1	Blinded	13.41 ±0.07
HS6	Potential 5LOX	10.96 ±0.12
NIH4	5LOX	10.18 ±0.16

Table 7.4 OE33 cell proliferation following 24-hour treatment in normoxic and hypoxic conditions

Commercial Inhibitor	% Reduction (21% O_2)	% Reduction (0.5% O_2)
Potassium Dichloracetate	52.77 ±6.389	51.83 ±7.32
3-Amino Benzoic Acid	50.41 ±6.224	50.32 ±11.23
Sodium Oxamate	54.02 ±5.576	52.32 ±6.67
REV5901	51.61 ±12.68	51.02 ±11.63
2-Deoxy D-Glucose	53.13 ±6.556	51.93 ±6.84
Ketoconazole	49.35 ±2.285	47.95 ±5.92
Zileuton	48.3 ±7.272	51.03 ±11.23
Bromopyruvic Acid	49.99 ±5.176	47.92 ±8.32
MK886	50.26 ±5.716	48.58 ±4.73
Novel Inhibitor	**21% O_2**	**0.5% O_2**
HS1	56.47 ±5.289	53.66 ±7.85
HS6	54.91 ±7.257	52.92 ±4.42
NIH4	52.83 ±3.255	50.01 ±6.44

7.3.3 Assessing 5LOX activity in OAC *ex vivo*

The aim of this experiment was to delineate whether the novel 5LOX inhibitor NIH4, and the potential 5LOX inhibitor HS6, could inhibit 5LOX enzyme activity in OAC tumour. The endogenous production of LTB4 by OAC tumour biopsies cultured *ex vivo* and the effect of the two novel inhibitors was also investigated by ELISA. Due to the limited size and numbers of treatment-naive biopsies available, it was only possible to test two compounds therefore only two novel compounds were selected. The inhibitors that we brought forward to *ex vivo* study were HS6 and NIH4. Fresh biopsies were collected from the clinic and cut into equally sized pieces. Each piece of tissue was cultured for 24 hours in *ex vivo* medium, as described in Section 2.19.1, with either vehicle control (0.1% DMSO), 10 μM HS6 or 10μM NIH4. Biopsies from 10 OAC patients were treated. The biopsy tissue pieces were homogenised and total protein concentration was determined by BSA assay to normalize protein secretions detected to the size of biopsy pieces. LTB4 secretion by tumour biopsies was found to be significantly decreased following treatment with NIH4 ($p<0.01$) but not by HS6 ($p=0.1601$) (Figure 7.1).

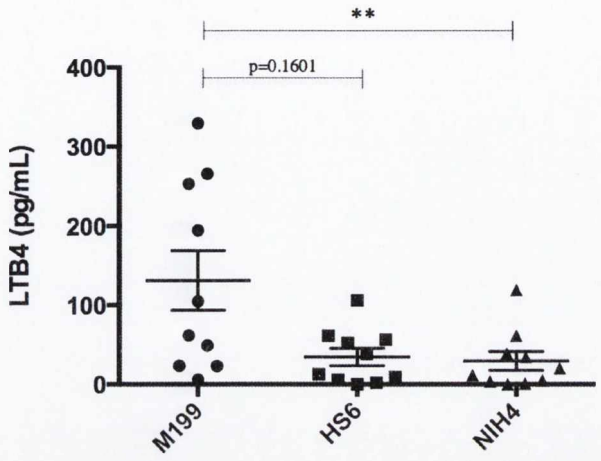


Figure 7.1 OAC tumour LTB4 secretion is decreased following 5LOX inhibitor treatment. Fresh tumour biopsies were cultured *ex vivo* for 24 hours in combination with either vehicle control (M199 media/0.25% DMSO) or 10 μM HS6 or 10 μM NIH4 (n=10) and TCM was assessed by ELISA for endogenous LTB4 production. Both inhibitors showed a reduction in LTB4 secretion, however, only NIH4 showed a statistically significant effect ($p<0.01$). Statistical test used was Kruskal-Wallis test with Dunn's Comparison Test: $p<0.01$ (**). Error denotes mean ±S.E.M.

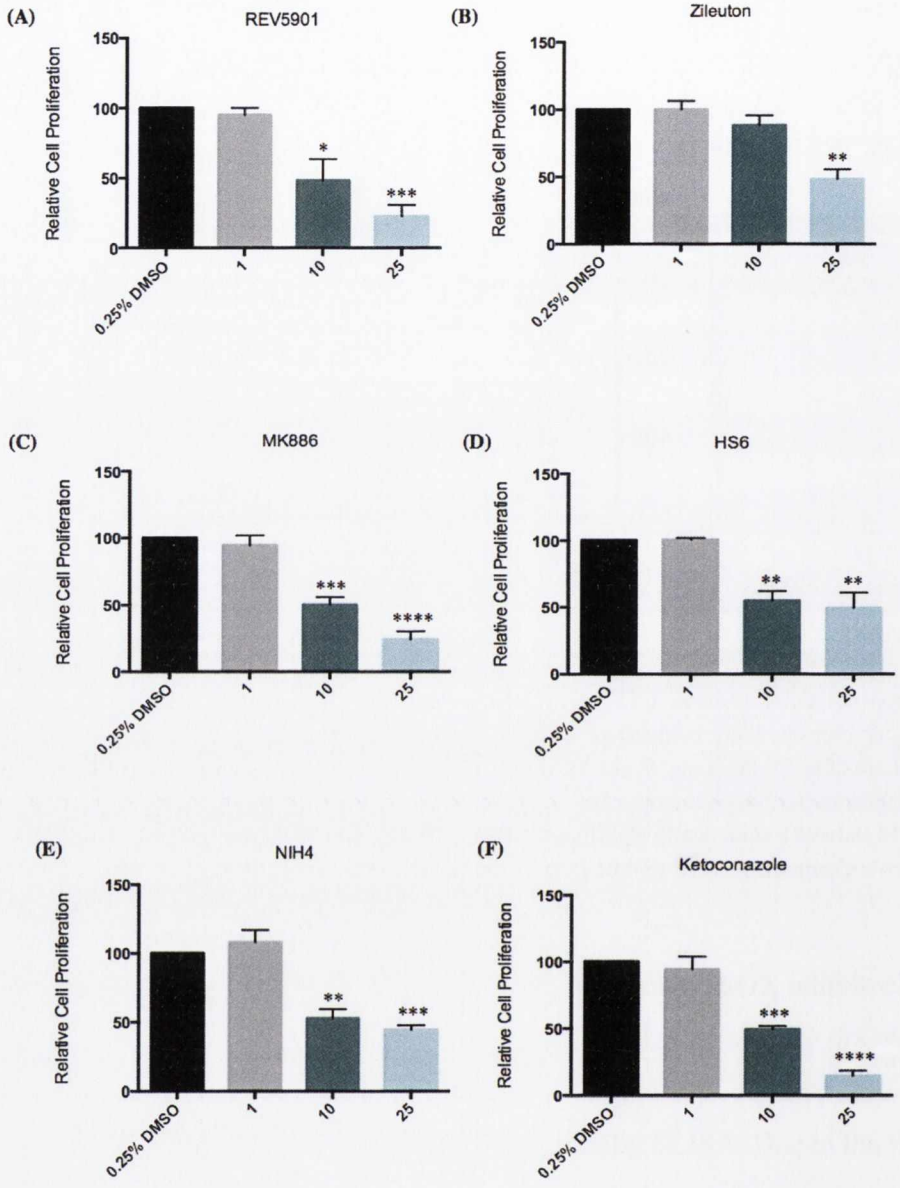


Figure 7.2 5LOX inhibitors, with the exception of Zileuton, significantly reduced OE33 cell proliferation at dose of 10 µM. Following 24-hour treatment of OE33 cells with commercially available and novel small molecule inhibitors of 5LOX reduced oesophageal adenocarcinoma cell proliferative activity at dose-dependent manner (A) REV5901 significantly reduced cell proliferation at dose of 10 µM ($p<0.05$) compared to untreated control (0.25% DMSO), (B) Zileuton had no effect at the dose of 10 µM, however, it significantly reduced cell proliferation at 25 µM concentration. The rest of the commercially available inhibitors all significantly reduced cell proliferation at the dose of 10 µM (C) MK886 ($p<0.001$) and (F) Ketoconazole ($p<0.001$). Novel small molecule inhibitors of 5LOX were successful at reducing cell proliferation at dose of 10 µM (D) HS6 ($p<0.01$) and (E) NIH4 ($p<0.01$). Statistical test used was one-way ANOVA with Tukey's Multiple Comparison Test: n=3, $p<0.05$(*), $p<0.01$(**), $p<0.001$(***), $p<0.0001$(****). Error bar denotes mean ±S.E.M.

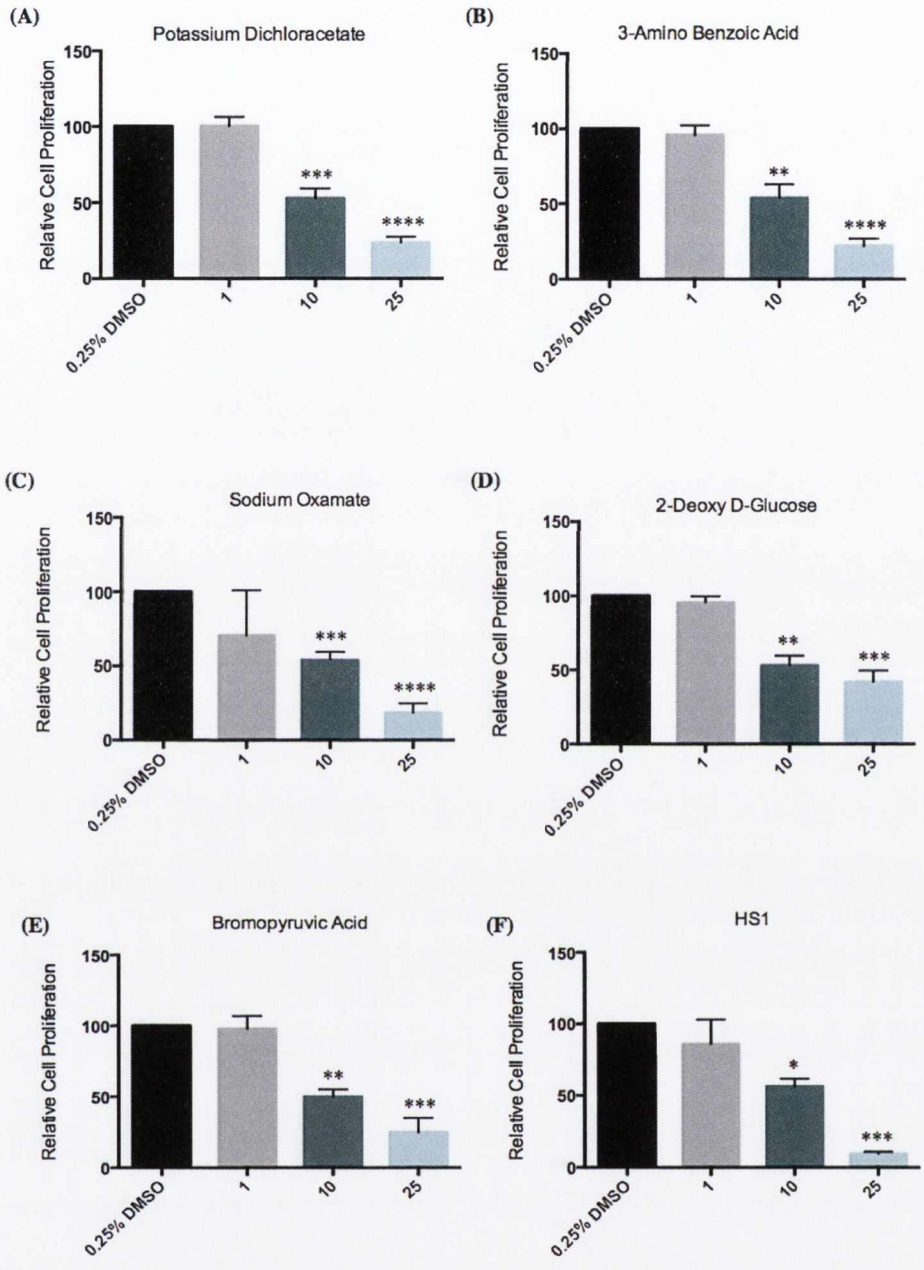


Figure 7.3 Glycolysis pathway inhibitors significantly reduce OE33 cell proliferation at dose of 10 µM. Following 24-hour treatment of OE33 cells with commercially available and novel small molecule inhibitors of glycolysis, oesophageal adenocarcinoma cell proliferative activity was reduced in dose-dependent manner, with significant reduction reached at the dose of 10 µM: (A) Potassium Dichloracetate ($p<0.001$), (B) 3-Amino Benzoic Acid ($p<0.01$), (C) Sodium Oxamate ($p<0.001$), (D) 2-Deoxy D-Glucose ($p<0.01$), (E) Bromopyruvic Acid ($p<0.01$) and (E) HS1 ($p<0.05$), when compared to untreated control (0.25% DMSO). Statistical test used was one-way ANOVA with Tukey's Multiple Comparison Test: n=3, $p<0.05$(*), $p<0.01$(**), $p<0.001$(***), $p<0.0001$(****). Error bar denotes mean ±S.E.M.

7.3.4 Effect of glycolytic and 5LOX inhibitors on ECAR in oesophageal adenocarcinoma cells

This experiment was performed using Seahorse XFe24 analyser. OE33 cells were seeded into 20 out of 24 available wells and treated with a dose of 10 μM of commercially available and novel small molecule inhibitors of glycolysis and 5LOX, in the presence and the absence of ACM. 24 hours following treatment, changes in glycolytic activity (ECAR) and mitochondrial metabolism (OCR) were measured. The full experimental setup using Seahorse XFe24 analyser described in Section 2.18.4. We previously showed that 24-hour co-culture of OE33 cells with ACM from viscerally obese OAC patients induced glycolysis in the cells (Chapter 6). The aim of this experiment was to investigate whether the inhibitors of glycolysis and 5LOX were able to alter glycolysis and mitochondrial metabolism in OE33 cells and whether the alterations were maintained or became more significant following induction of glycolysis by ACM (co-culture of cells with ACM from viscerally obese OAC patients). Levels of ECAR and OCR in OE33 cells treated with 0.1% DMSO were set to 100% and results were expressed as a percentage change relative to DMSO control.

Results revealed that co-culture of OE33 cells with ACM for 24 hours lead to a significant increase in glycolytic activity in OE33 cells in 9 out of 12 independent experiments (n=5) (Figure 7.4 and Figure 7.5) compared to glycolytic activity in cells treated with 0.1% DMSO. Following treatment of cells with the inhibitors of 5LOX, with the exception of REV1509 and Zileuton, glycolytic activity in the cells was significantly reduced in both, cells co-cultured in 0.1% DMSO and ACM (Figure 7.4). Treatment of OE33 cells with REV1509 lead to a significant reduction of ECAR in the cells compared to media only (0.1% DMSO) control (100% versus 72.37 ±6.74%, n=5, $p<0.05$) (Figure 7.4a). REV1509 had no significant effect on glycolytic activity in OE33 cells when used in combination with ACM and compared to ACM only treated cell control (133.0 ±9.007% versus 113.4 ±3.381%, n=5 in each group, p=0.1262) (Figure 7.4a). Following treatment of OE33 cells with 10 μM dose of Zileuton, there were no significant alterations in glycolysis when compared to 0.1% DMSO treated cells (100% versus 83.97 ±7.02%, n=5 in each group, p=0.2996) (Figure 7.4b) and when the treatment was administered in the presence of ACM and compared to ACM only treated cells (121.5 ±4.33 versus 139.4 ±9.325, n=5 in each group, p=0.2154) (Figure 7.4b). MK886, commercially available

inhibitor of 5LOX, significantly reduced glycolysis in OE33 cells compared to vehicle control (100% versus 55.67 ±3.997%, n=5 in each group, $p<0.001$) (Figure 7.4c). The ability of MK886 to reduce glycolysis in OE33 cells was reduced when the cells were treated with the inhibitor in the presence of ACM, however, the reduction was still significant when compared to ACM only treated OE33 cells (188.8 ±8.299 versus 113.6 ±5.04, n=5 in each group, $p<0.05$) (Figure 7.4c). HS6, a potential novel small molecule inhibitor of 5LOX, significantly reduced glycolytic cell activity compared to the cells treated with DMSO only (100% versus 67.77 ±6.64%, n=5 in each group, $p<0.05$), furthermore, the effect was more significant in the presence of ACM, where the cells were treated with the inhibitor in combination with ACM from viscerally obese OAC patients and compared to the cells treated with ACM alone (88.94 ±10.42 versus 140.5 ±9.32, n=5 in each group, $p<0.01$) (Figure 7.4d). NIH4, a novel small molecule inhibitor of 5LOX, significantly reduced glycolytic OE33 cell activity compared to the cells treated with 0.1% DMSO (100% versus 50.91 ±3.12, n=5 in each group, $p<0.05$), furthermore, the effect of NIH4 was more significant when measured in the presence of ACM and compared to the glycolytic activity in ACM only treated cells (96.13 ±7.12 versus 163.1 ±18.72, n=5 in each group, $p<0.01$) (Figure 7.4e). Ketoconazole, a commercially available dual inhibitor of 5LOX and thromboxane synthase, significantly reduced ECAR in OE33 cells compared to DMSO control, following 24-hour treatment (100% versus 61.53 ±3.558%, n=5 in each group, $p<0.01$), and the effect was maintained following co-culture of cells with the inhibitor in the presence of ACM (83.79 ±7.571% versus 137.57 ±16.16%, n=5 in each group, $p<0.01$) (Figure 7.4f). Following 24 treatment of OE33 cells with potassium dichloracetate (PDA), commercially available inhibitor of PDK1, lead to a significant reduction of ECAR in the cells compared to 0.1% DMSO control (100% versus 70.99 ±6.472, n=5, $p<0.01$) however it had no significant effect on glycolytic activity in OE33 cells when used in combination with ACM and compared to the activity in ACM only treated cells (94.52 ±5.818% versus 112.6 ±4.26%, n=5 in each group, $p=0.18$) (Figure 7.4a). 3-aminobenzoic acid, a commercially available inhibitor of LDHA, significantly reduced ECAR in OE33 cells compared to DMSO control, following 24-hour treatment (100% versus 69.41 ±2.04%, n=5 in each group, $p<0.05$), and the effect was maintained following co-culture of cells with the inhibitor in the presence of ACM (101.7 ±5.654% versus 132.6 ±12.64%, n=5 in each group, $p<0.05$) (Figure 7.5b). Sodium oxamate, a commercially available inhibitor of lactate dehydrogenase (LDH), significantly reduced glycolytic activity in OE33 cells compared

to 0.1% DMSO control, following 24-hour treatment (100% versus 63.25 ±6.662%, n=5 in each group, $p<0.01$), furthermore, the effect of sodium oxamate was greater following co-culture of cells with the inhibitor in the presence of ACM and compared to the cells treated with ACM alone (72.65 ±8.169% versus 113.6 ±5.04%, n=5 in each group, $p<0.001$) (Figure 7.5c). 2-deoxy D-glucose, showed no significant effect on OE33 cell glycolytic activity, when compared to 0.1% DMSO treated cells (100% versus 73.88 ±6.116%, n=5 in each group, $p=0.1508$), or in combination with ACM and compared to ACM only treated control group (107.9 ±6.371% versus 136.1 ±13.81, n=5 in each group, $p=0.1094$) (Figure 7.5d). Bromopyruvic acid, significantly reduced ECAR in OE33 cells following 24-hour treatment (100% versus 49.93 ±2.52%, n=5 in each group, $p<0.05$), however, the effect was reduced following treatment of cells in combination with ACM, compared to ACM only treated group (129.3 ±13.71% versus 163.1 ±18.72, n=5 in each group, $p=0.2121$) (Figure 7.5e). HS1, a novel chemical small molecule inhibitor of glycolysis, significantly reduced ECAR in OE33 cells following 24-hour treatment, compared to DMSO control (100% versus 67.82 ±6.56%, n=5 in each group, $p<0.05$), and the effect was maintained following co-culture of cells with the inhibitor in the presence of ACM and compared to ACM only treated control (98.91 ±7.18% versus 142 ±10.81%, n=5 in each group, $p<0.05$) (Figure 7.5f).

None of the inhibitors used in this study, nor the ACM, showed alterations in mitochondrial metabolism in OE33 cells following 24-hour treatment (data not shown).

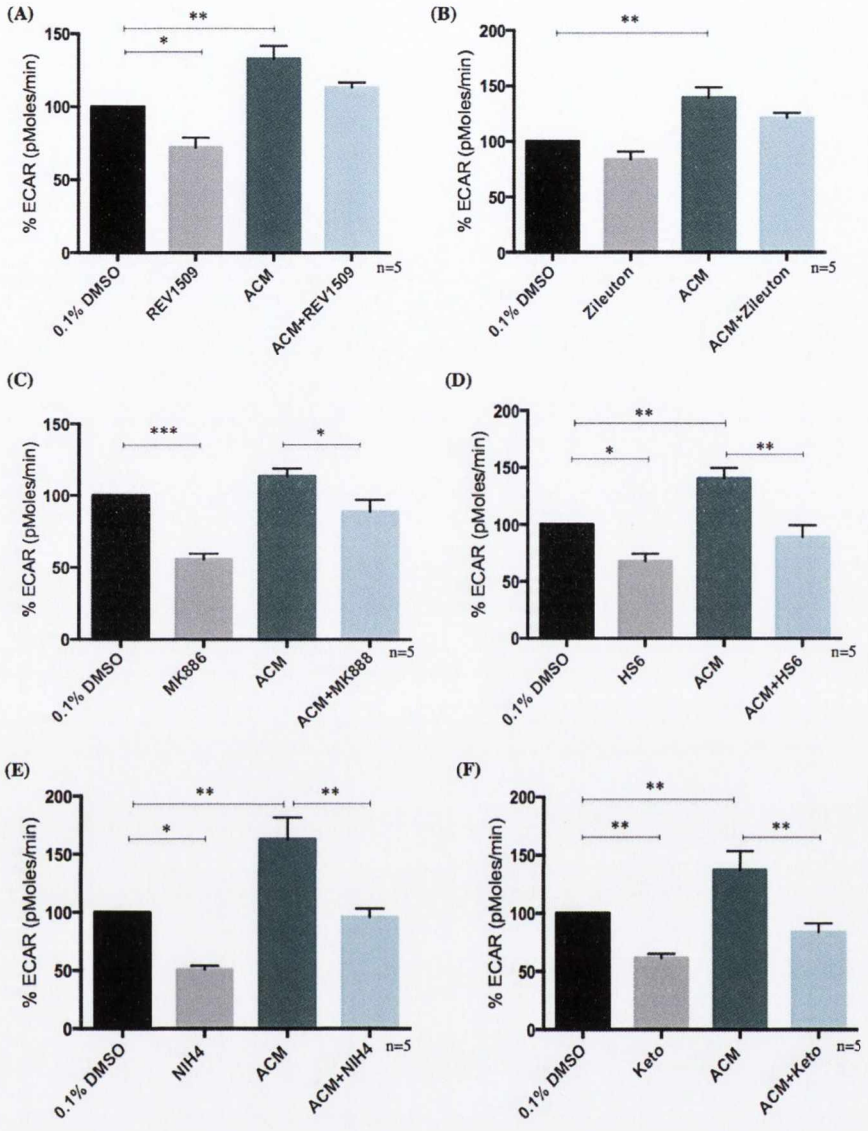


Figure 7.4 Inhibitors of 5LOX, with the exception of Zileuton, reduce glycolysis in OE33 cells. Following 24-hour treatment of OE33 cells with 10 μM dose of commercially available and novel small molecule inhibitors of 5LOX, oesophageal adenocarcinoma cell glycolytic activity was reduced by (A) REV1509 ($p<0.05$), however, REV1509 had no significant effect on glycolytic activity in OE33 cells when used in combination of ACM and compared to ACM only treated cell control ($p=0.1262$). (B) Zileuton, showed no significant alterations in ECAR in the presence or the absence of ACM ($p=0.2154$ and $p=0.2996$ respectively). (C) MK886 showed a significant reduction in ECAR in OE33 cells compared to DMSO control however, the ability of MK886 to alter ECAR in OE33 cells was reduced following treatment in combination with ACM ($p<0.01$ versus $p<0.05$ respectively). (D) Following treatment of cells with HS6, glycolytic cell activity was significantly reduced when compared to the cells treated with DMSO only ($p<0.05$), and HS6 was more effective in reducing glycolytic cell activity in the presence of ACM ($p<0.01$). (E) NIH4, showed a significant reduction in ECAR in OE33 cells and this effect was more statistically significant following treatment of cells with the inhibitor in combination with ACM ($p<0.05$ and $p<0.01$ respectively). (F) Ketoconazole, showed a significant reduction in ECAR in OE33 cells following 24-hour treatment, and the effect was maintained following co-culture of cells with the inhibitor in the presence of ACM ($p<0.05$). Statistical test used was one-way ANOVA with Tukey's Multiple Comparison Test: n=3, $p<0.05$(*), $p<0.01$(**), $p<0.001$(***). Error bar denotes mean ±S.E.M.

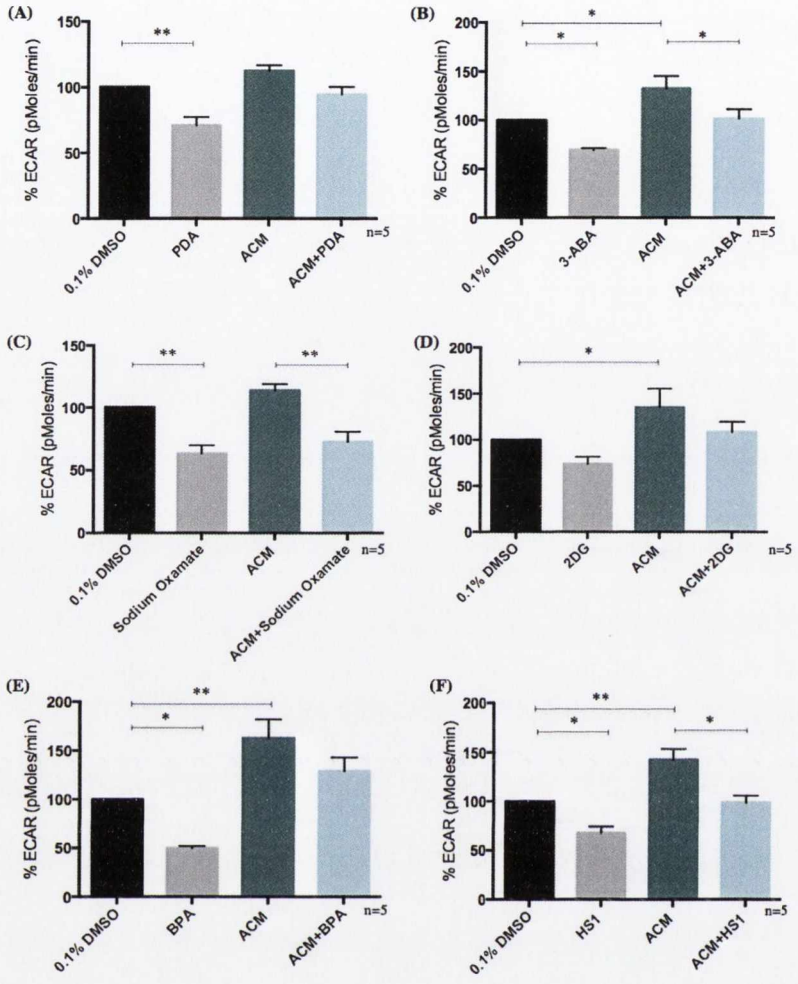


Figure 7.5 Inhibitors of glycolysis, with the exception of 2-Deoxy D-Glucose, reduce glycolysis in OE33 cells. Following 24-hour treatment of OE33 cells with 10 μM dose of commercially available and novel small molecule inhibitors of 5LOX, oesophageal adenocarcinoma cell glycolytic activity was altered. (A) PDA significantly reduced ECAR in OE33 cells ($p<0.01$), however, it had no significant effect on glycolysis in OE33 cells following treatment in combination with ACM ($p=0.18$). (B) 3-aminobenzoic acid significantly reduced ECAR in OE33 cells compared to 0.1% DMSO control, and the effect was maintained following co-culture of cells with the inhibitor in the presence of ACM ($p<0.05$). (C) Sodium oxamate significantly reduced glycolytic activity in OE33 cells compared to 0.1% DMSO control, and the effect the inhibitor was greater following co-culture of cells with the inhibitor in the presence of ACM and compared to the cells treated with ACM alone ($p<0.01$ and $p<0.001$ respectively). (D) There was no significant effect on OE33 cell glycolytic activity following 2-Deoxy D-glucose treatment, in the presence or the absence of ACM ($p= 0.1094$ and $p=0.1508$ respectively). (E) Bromopyruvic acid significantly reduced ECAR in OE33 cells following treatment ($p<0.05$), however, the effect was reduced following treatment of cells in combination with ACM ($p=0.2121$). (F) HS1 significantly reduced ECAR in OE33 cells following treatment, and the effect was maintained following co-culture of cells with the inhibitor in the presence of ACM ($p<0.05$). Statistical test used was one-way ANOVA with Tukey's Multiple Comparison Test: n=3, $p<0.05$(*), $p<0.01$(**), $p<0.001$(***). Error bar denotes mean ±S.E.M.

7.3.5 Effect of novel inhibitors of 5LOX on glycolysis and mitochondrial metabolism in oesophageal adenocarcinoma cells in hypoxia

This part of the study was performed using Seahorse XFe24 analyser. OE33 cells were seeded into available wells on the Seahorse plate and treated with a dose of 10 μM of novel small molecule inhibitors of 5LOX, HS6 and NIH4, in the presence and the absence of ACM and in the presence and absence of oxygen. Hypoxia (0.5% O_2) was chemically induced by treating the cells in the "hypoxia-designated wells" with a dose of 50 μM of $CoCl_2$. 24 hours following treatment, changes in glycolytic activity (ECAR) and mitochondrial metabolism (OCR) were measured. The full experimental setup using Seahorse XFe24 analyser was described in Section 2.18.4. In Section 7.3.5, we showed that 24-hour treatment of OE33 with ACM induced glycolysis in OE33 cells and that HS6 and NIH4 effect on ECAR in the cells was maintained or enhanced in the presence of ACM from viscerally obese OAC patients. The aim in this part of the study was to investigate whether the alterations in glycolysis by the novel small molecule inhibitors of 5LOX were further affected by the lack of oxygen (0.5% O_2). Experiment was repeated independently 3 times.

Results revealed that the ability of HS6 to reduce glycolysis in OE33 cells was reduced in the hypoxic conditions (61.44 ±2.057% versus 55.24 ±8.886%, n=3 in each group, $p<0.001$and $p<0.01$respectively) when compared to media only treated cells (M199/0.1% DMSO) (Figure 7.6a). Following 24-hour treatment of cells with NIH4, glycolysis in OE33 cells was significantly reduced in the hypoxic (50 μM of $CoCl_2$) compared to oxygenated environment (40.79 ±5.082% versus 72.82 ±3.326%, n=3 in each group, $p=0.7404$ versus $p<0.001$) (Figure 7.6b). Furthermore, ACM-induced glycolytic activity in OE33 cells was significantly reduced following 24-hour treatment of cells with NIH4 in hypoxic compared to normoxic environment ($p<0.01$ and $p=0.2253$ respectively). In conclusion, hypoxia had no effect on HS6 ability to alter glycolysis in O33 cells (Figure 7.6a). NIH4 exhibited significantly greater effect in reducing glycolysis in OE33 cells in hypoxic (0.5% O_2) compared to normoxic (21% O_2) conditions (40.79 ±5.082% versus 72.82 ±3.326%, n=3 in each group, $p=0.001$), furthermore, NIH4 significantly reduced ACM-induced glycolysis in OE33 cells in the hypoxic compared to normoxic environment (79.943 ±2.195% versus 99.43 ±2.4%, n=3 in each group, $p<0.05$) (Figure 7.6b).

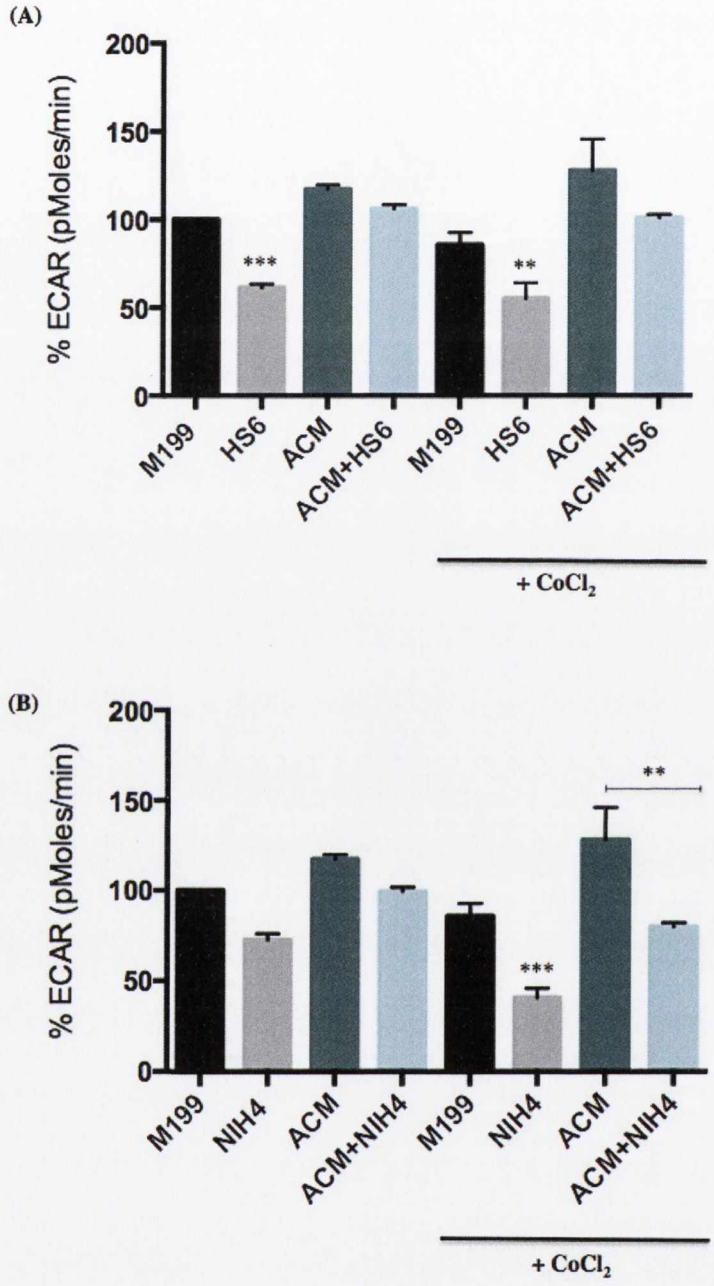


Figure 7.6 Hypoxia induces the ability of NIH4, but not HS6 of reducing ECAR in OE33 cells. Following 24-hour treatment of OE33 cells with 10 μM dose of novel small molecule inhibitors, ACM and $CoCl_2$, glycolytic activity in the cells was measured by Seahorse XFe24 analyser. (A) HS6 ability of to reduce glycolysis in OE33 cells was reduced in the absence compared to normal levels of oxygen ($p<0.001$and $p<0.01$respectively). (B) NIH4 significantly reduced glycolysis in OE33 cells in hypoxic (0.5% O_2) compared to normoxic (21% O_2) conditions ($p=0.001$). Furthermore, NIH4 significantly reduced ACM-induced glycolysis in OE33 cells in the hypoxic compared to normoxic ($p<0.05$). Statistical test used was one-way ANOVA with Tukey's Multiple Comparison Test: n=3, $p<0.05$(*), $p<0.01$(**), $p<0.001$(***). Error bar denotes mean ±S.E.M.

7.3.6 Human Glucose Metabolism Arrays: alterations in OE33 gene expression following novel 5-lipoxygenase inhibitor treatment

Having demonstrated that novel small molecule inhibitors HS6 and NIH4 had functional effects on OE33 cell proliferation and lead to changes in OE33 cell glycolytic activity, Human Glucose Metabolism RT^2 profiler arrays were used to determine which genes associated with glucose metabolism were altered. We have already shown that adipose conditioned media resulted in metabolic shift in human glucose and mitochondrial metabolism in oesophageal adenocarcinoma cell model (Chapter 6). To follow up from that experimental set up, we were interested whether our novel inhibitors of 5LOX are able to reduce this shift in metabolic tumour metabolism in oesophageal adenocarcinoma cells.

OE33 cells were prepared as described in Section 2.13 and were treated for 24 hours with 0.1% DMSO as a vehicle control and either ACM alone or with ACM in combination with one of the selected inhibitors (i.e. HS6 or NIH4). The HS6 and NIH4 compounds were used at a dose of 10 μM because this was the concentration at which biological activity was observed *in vitro*. RNA was isolated as described in Section 2.7 and gene expression was measured in real time by qPCR as described in Section 2.11. RQ value of B2M gene was set as calibrator to allow normalization of the data set. Gene changes were only reported if transcript was amplified prior cycle 35. Values were displayed as fold regulation and the threshold value greater than 2 indicated differential gene expression compared to control.

Alterations of 15/21 glycolysis, 3/7 gluconeogenesis, 4/6 glucose metabolism, 25/29 TCA cycle and 9/16 glycogen metabolism associated genes were upregulated following treatment of OE33 with ACM from viscerally obese OAC patients, compared to media only treated OE33 cells (Table 7.5). Overall, 71% of glucose metabolism associated genes were significantly upregulated (greater than 2 fold change relative to media only control) following treatment with ACM. HS6 and NIH4 showed a significant reduction of 6/84 (7.14%) and 16/84 (19.05%) glucose metabolism associated genes when used in combination with ACM and compared to ACM only treated OE33 cells (Table 7.5). This screen was only carried out for n=2 for each ACM and each compound and were used to indicate potential gene targets for follow up validations.

Table 7.5 List of OE33 gene alterations following ACM and 5LOX inhibitor treatment

Functional Group	Gene	ACM	HS6 +ACM	NIH4 +ACM	Functional Group	Gene	ACM	HS6+ ACM	NIH4 +ACM
Glycolysis	ALDOA				Tricarboxylic Acid	IDH3B			
	ALDOB				Cycle (TCA)	IDH3G			
	ALDOC				(Continued)	MDH1			
	BPGM					MDH1B			
	ENO1					MDH2			
	ENO2					OGDH			
	ENO3					PC			
	GALM					PCK1			
	GCK					PCK2			
	GPI					PDHA1			
	HK2					PDHB			
	HK3					SDHA			
	PFKL					SDHB			
	PGM2					SDHC			
	PGK1					SDHD			
	PGK2					SUCLA2			
	PGM1					SUCLG1			
	PGM2					SUCLG2			
	PGM3				Pentose Phosphate	G6PD			
	PKLR				Pathway	H6PD			
	TPI1					PGLS			
Gluconeogenesis	FBP1					PRPS1			
	FBP2					PRPS1L 1			
	G6PC					PRPS2			
	G6PC3					RBKS			
	PC					RPE			
	PCK1					RPIA			
	PCK2					TALDO 1			
Glucose Metabolism	PDK1					TKT			
	PDK2				Glycogen Synthesis	GBE1			
	PDK3					GYS1			
	PDK4					GYS2			
	PDP2					UGP2			
	PDPR				Glycogen Degradation	AGL			
Tricarboxylic Acid	ACLY					PGM1			
Cycle (TCA)	ACO1					PGM2			
	ACO2					PGM3			
	CS					PYGL			
	DLAT					PYGM			
	DLD				Regulation of Glycogen	GSK3A			
	DLST				Metabolism	GSK3B			
	FH					PHKA1			
	IDH1					PHKB			
	IDH2					PHKG1			
	IDH3A					PHKG2			

Red = upregulation >2 fold, green = downregulation of <-2 and grey = no alteration to gene expression

7.3.7 Validation of selected genes from human glucose metabolism genes from Human Glucose Metabolism RT^2 Profiler arrays

OE33 cells were treated with 0.1% DMSO, ACM or either HS6 or NIH4 in the presence of ACM, for 24 hours (n=5). Expression of selected glucose metabolism associated genes chosen from the human glucose metabolism RT^2 profiler array were investigated by SYBR-based qPCR, using primer sets detailed in Section 2.12. Gene expression was determined using ΔΔCt method as described in Section 2.10 and values were graphed relative to control expression. ACM treated cells were the control group for this part of the study. Human glucose metabolism associated gene expression was compared between the ACM alone treated OE33 cells and HS6 or NIH4 treated cells, where the inhibitors were used in combination with ACM (ACM from the same patients as the control group). The aim of this part of the study was to investigate whether the two novel small molecule inhibitors were able to reduce ACM-induced, human glucose metabolism associated gene expression in oesophageal adenocarcinoma cell line. ACM-induced glucose metabolism associated gene expression was previously validated in Section 6.3.3.1, therefore, gene expression in media only (0.1% DMSO) treated cells was not included in this part of the study.

There was no significant difference in ALDOB expression in OE33 cells following treatment with HS6 and NIH4 compared to ACM only treated cells ($p=0.093$ and $p=0.1101$ respectively, n=5 in each group) (Figure 7.7a). ENO3 expression was significantly downregulated in the cells following treatment with NIH4 ($p<0.05$), however, there was no difference in ENO3 expression following treatment with HS6 ($p=0.01982$) (Figure 7.7b). There was no difference in glycolysis and glycogen degradation associated PGM1 expression following treatment with HS6 and NIH4 compared to ACM only treated cells ($p=0.9221$ and $p=991$ respectively) (Figure 7.7c), however PGM2 gene expression was significantly downregulated in the cells following treatment with NIH4 ($p<0.05$), but not HS6 ($p>0.9999$) (Figure 7.7d). Gluconeogenesis and TCA cycle associated PC expression was not affected in OE33 cells following HS6 or NIH4 treatment ($p>0.9999$ and $p=0.1427$ respectively) (Figure 7.7e), however, glucose metabolism associated PDK1 gene expression was significantly downregulated in the oesophageal adenocarcinoma cells following NIH4 ($p<0.05$), but not following HS6 treatment ($p=0.2315$) (Figure 7.7f). Treatment of OE33 cells with HS6 and NIH4 had no

effect on the expression levels of pentose phosphate pathway associated H6PD ($p>0.9999$ following both treatments) (Figure 7.8a), RBKS ($p>0.9999$ and $p=0.2135$ respectively) (Figure 7.8b), TKT ($p=0.8641$ and $p=0.1009$ respectively) (Figure 7.8c) or PCK2 ($p>0.9999$ following both treatments). Overall, novel 5LOX inhibitor NIH4, significantly reduced ACM-induced ENO3, PGM2 and PDK1 expression in OE33 cells following 24-hour treatment. HS6 failed to reduce ACM-induced glucose metabolism associated gene expression in OE33 cells. Kruskal-Wallis test was used to determine whether the medians of two groups (HS6 and NIH4 treatment) differ to control group (ACM).

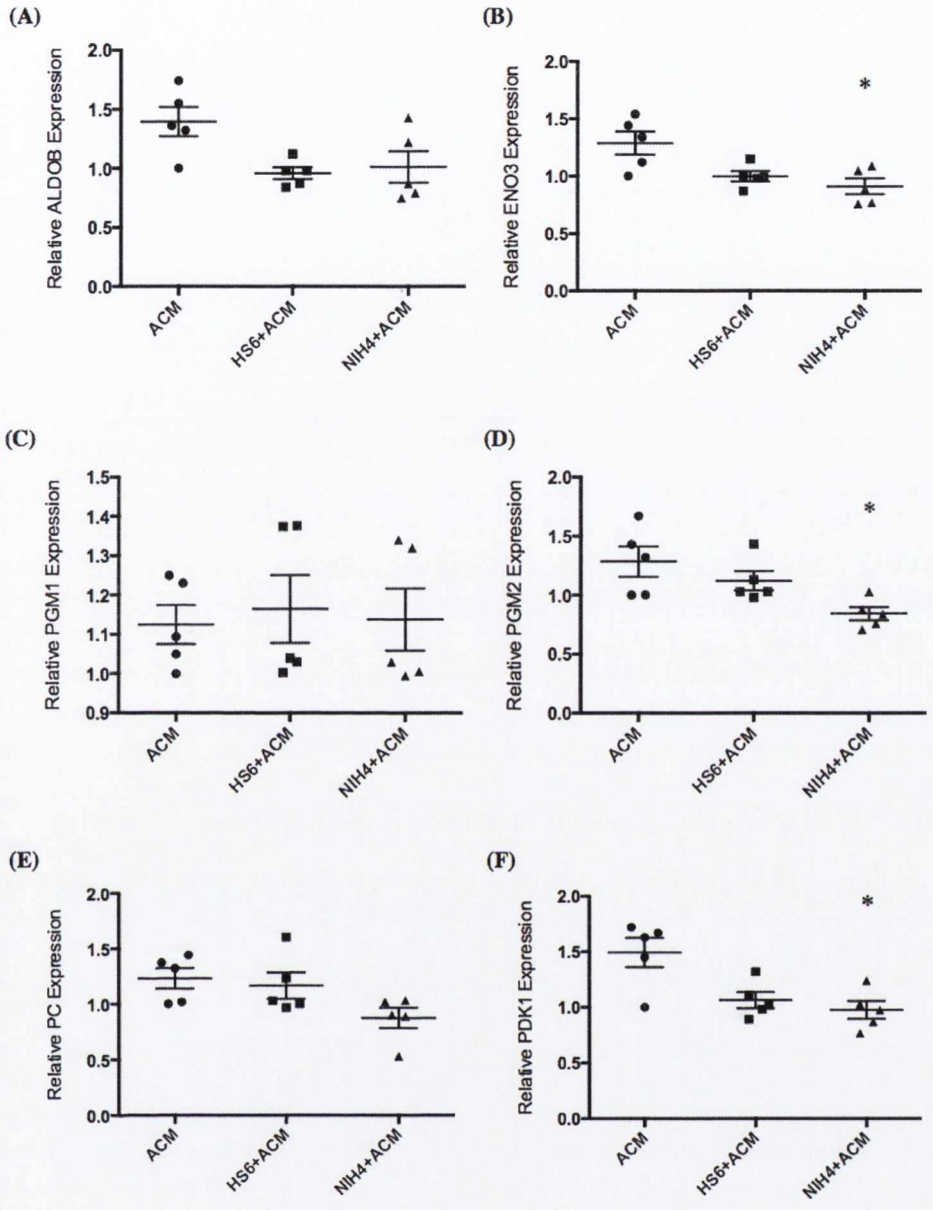


Figure 7.7 Validation of glucose metabolism, glycolysis and TCA cycle associated gene expression following treatment with novel small molecule inhibitors HS6 and NIH4. OE33 cells were treated with ACM and either HS6 or NIH4 in the presence of ACM, for 24 hours (n=5). Expression of glucose metabolism associated genes, chosen from the human glucose metabolism RT^2 profiler array, was investigated by SYBR-based qPCR. (A) There was no significant difference in ALDOB expression in OE33 cells following treatment with HS6 and NIH4 compared to ACM only treated cells ($p=0.093$ and $p=0.1101$ respectively). (B) ENO3 expression was significantly downregulated in the cells following treatment with NIH4 ($p<0.05$), however, there was no difference in ENO3 expression following treatment with HS6 ($p=0.01982$). (C) There was no difference in PGM1 expression following treatment with HS6 and NIH4 compared to ACM only treated cells ($p=0.9221$ and $p=991$ respectively), however, (D) PGM2 gene expression was significantly downregulated in the cells following treatment with NIH4 ($p<0.05$), but not HS6 ($p>0.9999$). (E) PC expression was not affected in OE33 cells following HS6 or NIH4 treatment ($p>0.9999$ and $p=0.1427$ respectively), however, (F) PDK1 gene expression was significantly downregulated in OE33 cells following treatment with NIH4 ($p<0.05$), but not HS6 ($p=0.2315$). Statistical test used was Kruskal-Wallis test with Dunn's Multiple comparison Test. $p<0.05$ (*). Error denotes mean ±S.E.M.

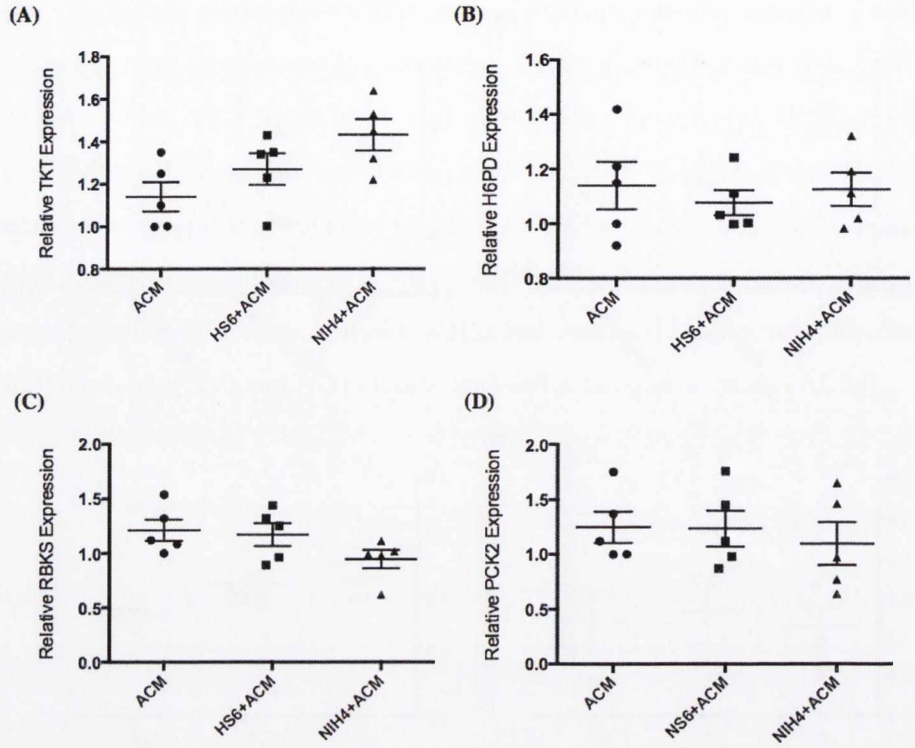


Figure 7.8 Validation of pentose phosphate pathway and TCA cycle associated gene expression following treatment with novel small molecule inhibitors HS6 and NIH4. OE33 cells were treated with ACM and either HS6 or NIH4 in the presence of ACM, for 24 hours (n=5). Expression of glucose metabolism associated genes, chosen from the human glucose metabolism RT^2 profiler array, was investigated by SYBR-based qPCR. (A) There was no significant difference in H6PD expression levels in OE33 cells following treatment with HS6 and NIH4 ($p>0.9999$ following both treatments). (B) There was no significant difference in RBKS expression levels in OE33 cells following treatment with HS6 and NIH4 ($p>0.9999$ and $p=0.2135$ respectively) compared to ACM control. (C) The was no significant difference in TKT expression levels in OE33 cells following treatment with HS6 and NIH4 ($p=0.8641$ and $p=0.1009$ respectively) and (D) Similarly, there was no significant difference in PCK2 expression levels in OE33 cells following treatment with HS6 and NIH4 ($p>0.9999$ following both treatments). Statistical test used was Kruskal-Wallis test with Dunn's Multiple comparison Test. $p<0.05$ (*). Error denotes mean ±S.E.M.

7.3.8 Human Mitochondrial Function Arrays: alterations in OE33 gene expression following novel 5-lipoxyhenase inhibitor treatment

Having demonstrated that the novel 5-LOX inhibitors HS6 and NIH4 significantly reduced ACM-induced gene upregulation in Human Glucose Metabolism RT^2 profiler arrays, Human Mitochondrial Function RT2 profiler arrays were used to determine whether HS6 and NIH4 have an effect on mitochondrial metabolism.

OE33 cells were prepared as previously described in Section 2.13 and were treated for 24 hours with 0.1% DMSO as a vehicle control and either ACM alone or with ACM in combination with one of the selected inhibitors (i.e. HS6 or NIH4). The HS6 and NIH4 compounds were used at a dose of 10 μM, as in Section 7.3.6, because this was the concentration at which biological activity was observed *in vitro*. RNA was isolated as described in Section 2.7 and gene expression was measured in real time by qPCR as described in Section 2.11. RQ value of B2M gene was set as calibrator to allow normalization of the data set. Gene changes were only reported if transcript was amplified before the cycle 35. Values were displayed as fold regulation and the threshold value greater than 2 indicated differential gene expression compared to control.

Alterations of 28/32 Complex I, 4/4 Complex II, 10/12 genes Complex III, 12/14 Complex V and 8/9 pathway activity signature associated genes were upregulated following treatment of OE33 with ACM from viscerally obese OAC patients, compared to media only treated OE33 cells (Chapter 6). Overall, 73.8% human mitochondrial metabolism associated genes were significantly upregulated (greater than 2 fold change relative to media only control) following treatment with ACM. NIH4 showed a significant reduction of 10/84 (11.9%) mitochondrial metabolism associated genes when used in combination with ACM and compared to ACM only treated OE33 cells (Table 7.6). This screen was only carried out for n=2 for each ACM and each compound and were used to indicate potential gene targets for follow up validations.

Table 7.6 List of OE33 gene alterations following 5LOX inhibitor treatment

Functional Group	Gene	ACM	HS6 +ACM	NIH4 +ACM	Functional Group	Gene	ACM	HS6 +ACM	NIH4 +ACM
Complex I	NDUFA1				Complex III	COX4I1			
	NDUFA10					COX5A			
	NDUFA11					COX5B			
	NDUFA2					COX6A1			
	NDUFA3					COX6A2			
	NDUFA4					COX6B1			
	NDUFA5					COX6C			
	NDUFA6					COX7A2			
	NDUFA8					COX7A2L			
	NDUFAB1					COX7B			
	NDUFB10					COX8A			
	NDUFB2					CYC1			
	NDUFB3				Complex V	ATP5A1			
	NDUFB4					ATP5B			
	NDUFB5					ATP5C1			
	NDUFB6					ATP5F1			
	NDUFB7					ATP5G1			
	NDUFB8					ATP5G2			
	NDUFB9					ATP5G3			
	NDUFC1					ATP5H			
	NDUFC2					ATP5I			
	NDUFS1					ATP5J			
	NDUFS2					ATP5J2			
	NDUFS3					ATP5L			
	NDUFS4					ATP5O			
	NDUFS5					PPA1			
	NDUFS6				Pathway Activity	ARRDC3			
	NDUFS7				Signature Genes	ASB1			
	NDUFS8					CYB561D1			
	NDUFV1					DNAJB1			
	NDUFV2					EDN1			
	NDUFV3					GADD45B			
Complex II	SDHA					HSPA1A			
	SDHB					HSPA1B			
	SDHC					LRP5L			
	SDHD								

Red = upregulation >2 fold, green = downregulation of <-2 and grey = no alteration to gene expression

7.3.9 Validation of selected genes from human Mitochondrial Metabolism RT^2 Profiler arrays

OE33 cells were treated with 0.1% DMSO, ACM or either HS6 or NIH4 in the presence of ACM, for 24 hours (n=5). Expression of human mitochondrial metabolism associated genes chosen from the human mitochondrial metabolism RT^2 profiler arrays were investigated by SYBR-based qPCR, using primer sets detailed in Section 2.11. The experimental set up and analysis was identical to the one in Section 7.3.7. ACM treated cells were used as a control group and human mitochondrial metabolism associated gene expression was compared between the ACM alone treated OE33 cells and HS6 or NIH4 treated cells, where the inhibitors were used in combination with ACM. The aim of this part of the study was to investigate whether the two novel small molecule inhibitors HS6 and NIH4 were able to reduce ACM-induced, human mitochondrial function associated gene expression in OE33 cells. ACM-induced human mitochondrial metabolism associated gene expression was previously validated in Section 6.3.4.1, therefore, gene expression in media only (0.1% DMSO) treated cells was not included in this part of the study.

HS6 failed to reduce ACM-induced human mitochondrial metabolism associated gene expression in OE33 cells ($p>0.05$) (Figure 7.9 and Figure 7.10). Similarly, NIH4, novel small molecule inhibitor of 5LOX, failed to reduce ACM-induced upregulation of Complex I associated NDUFA1 ($p=0.2025$) (Figure 7.9a), NDUFA8 ($p=0.9641$) (Figure 7.9b), NDUFA11 ($p>0.9999$) (Figure 7.9c) and NDUFS2 ($p=0.7739$) (Figure 7.9d). Treatment of cells with NIH4 had no effect on the expression levels of Complex V associated ATP5L ($p>0.9999$) (Figure 7.9b), and pathway activity signature genes CYB561D1 and HSPA1B ($p>0.9999$ in each group) (Figure 7.10c and Figure 7.10d respectively). However, NIH4 significantly reduced ACM-induced Complex III associated gene expression in OE33 cells, COX5B ($p<0.05$) (Figure 7.9e) and COX6C ($p<0.05$) (Figure 7.9f) compared to ACM alone treated cells. Complex V associated ATP5G2 expression was reduced in the OE33 cells following treatment with NIH4, however, it failed to reach significance ($p=0.059$) (Figure 7.10a).

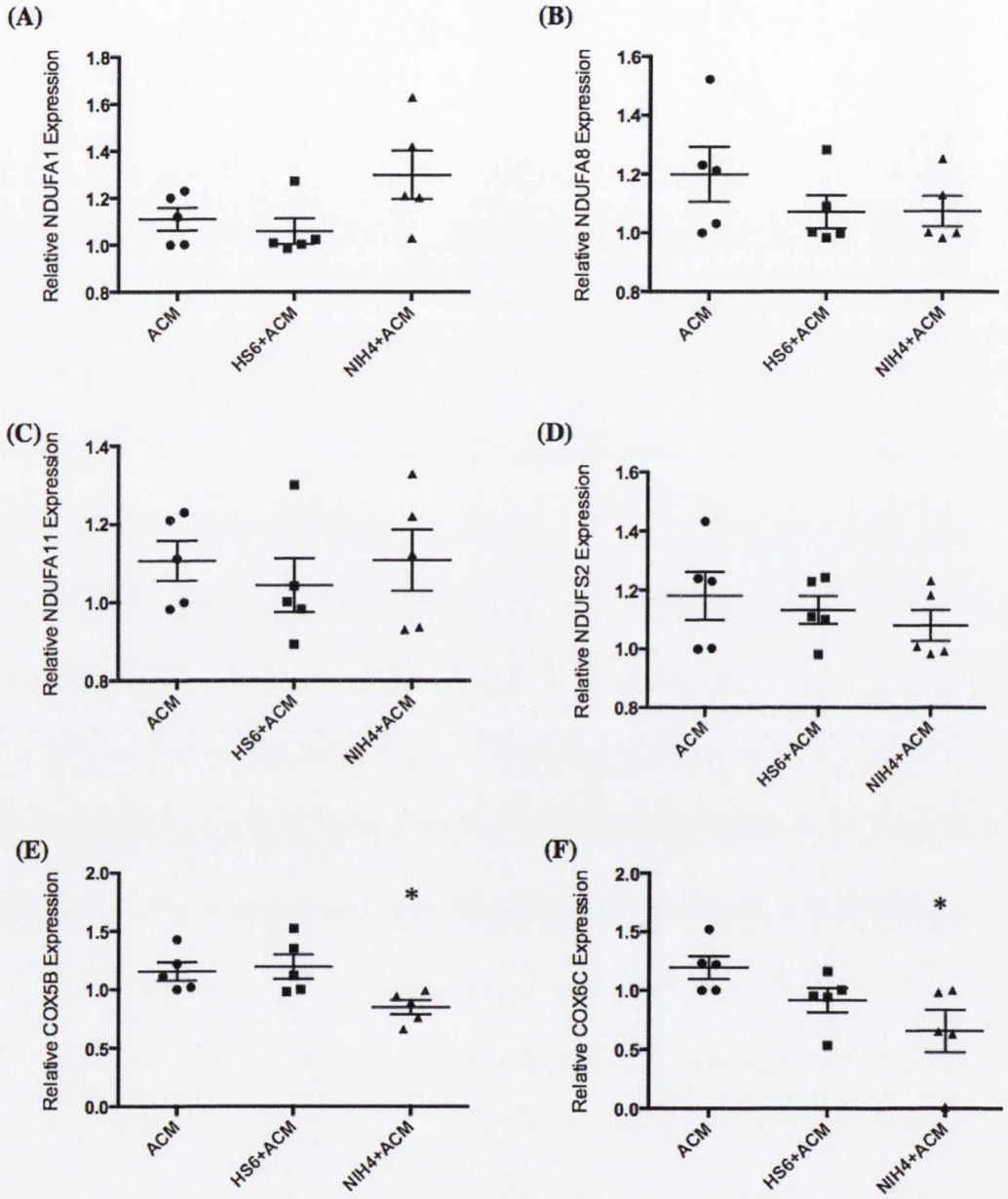


Figure 7.9 Complex I and Complex III associated gene expression in OE33 cells following treatment with novel small molecule inhibitors HS6 and NIH4. (A-D) HS6 and NIH4 failed to reduce Complex I associated human mitochondrial metabolism gene expression ($p>0.05$) in OE33 cells. (E-F) HS6 failed to reduce ACM induced COX5B and COX6C expression in OE33 cells ($p=0.9994$ and $p=0.2283$ respectively), however NIH4 significantly reduced ACM-induced COX5B and COX6C ($p<0.05$) expression in OE33 cells. Statistical test used was Kruskal-Wallis test with Dunn's Multiple comparison Test. $p<0.05$ (*). Error denotes mean ±S.E.M.

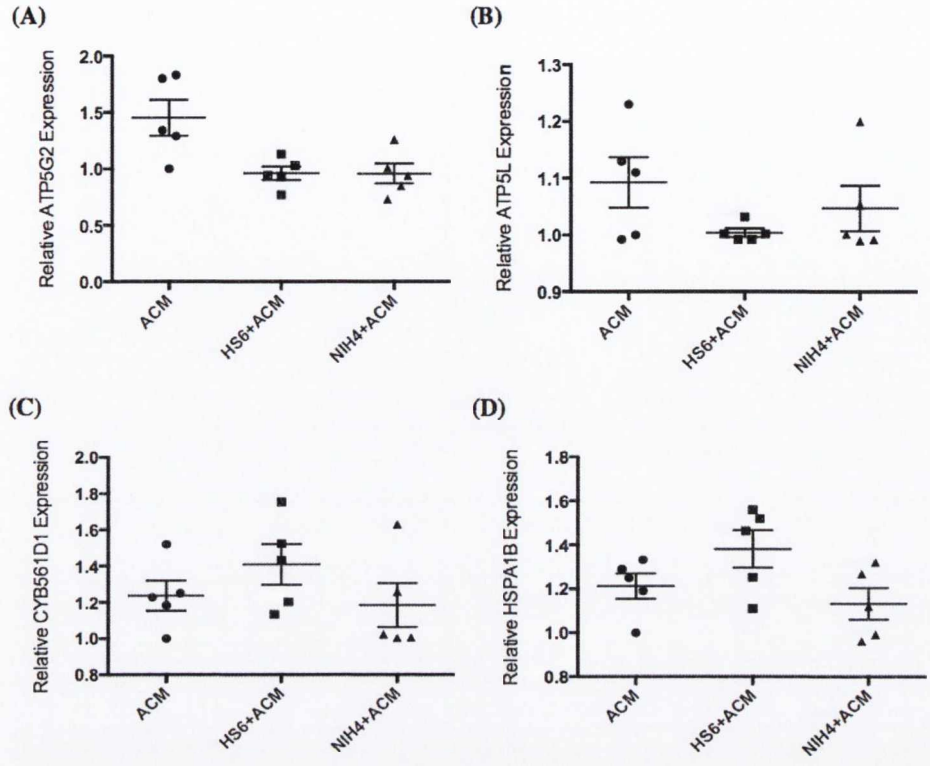


Figure 7.10 Complex V and Pathway Activity associated gene expression in OE33 cells following treatment with novel small molecule inhibitors HS6 and NIH4. Treatment of OE33 cells with HS6 and NIH4 had no significant effect on (A) ATP5G, (B) ATP5L, (C) CYB561D1 and (D) HSP1B expression in OE33 cells ($p>0.05$). Statistical test used was Kruskal-Wallis test with Dunn's Multiple comparison Test. $p<0.05$ (*). Error denotes mean ±S.E.M.

7.3.10 Investigation of pathways altered *ex vivo* using oesophageal tumour explants

Fresh biopsies were collected from the clinic and cut into equally sized pieces. Each piece of tissue was cultured for 24 hours in *ex vivo* medium as described in Section (Section 2.19.1) with either vehicle control (0.1% DMSO), 10 μM HS6 or 10μM NIH4. Biopsies from 10 treatment-naive OAC patients were collected treated, however, only 5 were used for OLINK targeted protein discovery and samples from all 10 patients were used for downstream validations. For Olink proteomics immunoassays, biopsies from 3 overweight and obese (60%) and 2 normal weight (40%) OAC patients were used. Fresh diagnostic tumour biopsies did not have their VFA measurements calculated, therefore, obesity status of these patients was based on their BMI. Patients with BMI $\geq$ 25 kg/m^2 were considered to be overweight and obese BMI $\leq$25 kg/m^2 were considered to be

normal weight [WHO, 2014]. For validation experiments, sample number was increased to n=10, diagnostic OAC biopsies from 6 (60%) overweight and obese and 4 (40%) from normal weight patients.

The biopsy tissue pieces were homogenized and total protein concentration was determined by BSA assay to normalize protein secretions detected to the size of biopsy pieces. In order to discover and validate OAC related protein biomarkers, Proseek® Multiplex Inflammation I ^{96x96} and Oncology II ^{96x96} multiplex OAC immunoassay enabling analysis of 92 inflammation-related protein markers was used. Biomarkers associated with cell proliferation, cell differentiation and adhesion, apoptosis, angiogenesis, exploratory, immune response, metastasis and tumour specific markers were included in the panel.

Tissue conditioned media (TCM) and protein lysates from the three treatment groups (vehicle control, HS6 and NIH4) from 5 treatment-naive OAC patients, were shipped to OLINK Proteomics, Uppsala, Sweden for analysis.

Samples were analysed using Proximity Extension Assay (PEA) technology where due to innovative dual recognition, DNA-coupled methodology enables high multiplex and rapid throughout biomarker analysis, described in more detail in Section 2.25.

The raw data received from OLINK contained normalized protein expression (NPX) values (Log2 scale) for all samples. Values below limit of detection were flagged and were not used for statistical analysis. Normalized Protein expression values (NPX) for all proteins were returned as raw values for statistical analysis. NPX is on a log2 scale therefore an increase in one NPX corresponds to a doubling of the concentration. All samples sent to OLINK Proteomics were blinded and the samples of 2 patients were included in duplicate in order to measure the reproducibility and quality of the experiment. Statistical analysis was performed by Olink biostatistician, who helped us to customize statistical analysis based on our experimental setup (Appendix II).

Only samples that passed quality control and proteins with over 75% detectability were used in the analysis. ANOVA was used in order to find proteins that were different in three treatment groups and Tukey post hoc test was performed for all significant hits.

Following statistical data analysis, clustering heat maps were generated using data obtained from inflammation (INF) and oncology (ONC2) panels (Figure 7.11 and Figure

7.13 respectively). Left color bar indicates control in red (TCM from OAC biopsies treated with M199 media), D1 in green (TCM from OAC biopsies treated with HS6) and D2 in blue (TCM collected from OAC biopsies treated with NIH4).Clustering heat maps for both INF and ONC2 panels showed a pattern of red (control) and green (HS6) clustering together, whereas samples flagged in blue (NIH4 treatment) were seen clustering closely together and separate from red and green (control and HS6 treatment). All significant hits (samples with significant statistical difference in protein expression levels between treatment groups) were graphically represented on both heat maps. The clustering of control and HS6 treatments was more prominent in ONC2 panel.
All significant data was presented in boxplots, showing significantly altered proteins after Benjamini-Hochberg correction.

Data presented as NPX value relative to vehicle control (M199/0.1% DMSO). Vehicle control was labelled 'Cont', HS6 treatment group 'D1' and NIH4 treatment group 'D2'. In the INF panel, secreted VEGFA levels were significantly lower in TCM following 24-hour incubation of biopsy with 10 μM of NIH4 compared to vehicle control (n=5 in each group, $p<0.01$) (Figure 7.12a). There was no significant difference in VEGFA secretion following 24-hour treatment of OAC biopsy with 10 μM of HS6, compared to vehicle control (n=5 in each group, $p=0.9999$) (Figure 7.12a). Secreted TGF-alpha levels were significantly lower in TCM following biopsy treatment with NIH4, compared to vehicle control (n=5 in each group, $p<0.001$) (Figure 7.12b). There was no significant difference in secreted TGF-alpha levels following 24-hour treatment of OAC biopsy with 10 μM of HS6, compared to vehicle control n=5 in each group, $p=0.1323$) (Figure 7.12b). Similarly, secreted SCF levels were significantly lower in TCM following biopsy treatment with NIH4, compared to vehicle control (n=5 in each group, $p<0.05$) (Figure 7.12c) and MCP3 levels were significantly lower in TCM following treatment with NIH4 (n=5 in each group, $p<0.01$) (Figure 7.12d). Only 4/92 (4.35%) tumour-secreted proteins were significantly altered following 24-hour treatment with NIH4 and there were no significant protein alterations following 24-hour treatment with HS6.
In the ONC2 panel (similarly like in INF panel) VEGFA and TGF-alpha levels were significantly lower in TCM following 24-hour incubation of biopsy with 10 μM of NIH4 compared to vehicle control (n=5 in each group, $p<0.01$) (Figure 7.14c and Figure 7.14f respectively). Additionally, five proteins were significantly lower in TCM following 24-hour incubation of biopsy with 10 μM of NIH4 compared to vehicle control: CTSV

($p<0.001$) (Figure 7.14d); WISP1, SCF and CYR61 ($p<0.01$), (Figure 7.14a, Figure 7.14b and Figure 7.15a respectively) and ESM1 ($p<0.05$) (Figure 7.14e). Interestingly, there was no significant difference in expression levels of TFPL, AR, TNFRSF19, and ABL1 in TCM following 24-hour incubation of biopsy with 10 μM of NIH4 or HS6 and vehicle control. However, there was a significant difference in these protein levels between HS6 and NIH treatment groups ($p<0.01$) (Figure 7.15b-Figure 7.15e respectively). To conclude, 7/92 (7.61%) tumour-secreted proteins were significantly altered in ONC2 panel following 24-hour treatment with NIH4 relative to vehicle control and 4/92 (4.35%) proteins were significantly altered following NIH4 treatment relative to HS6 treatment group.

Due to the heterogeneity in patient samples and low sample numbers, there was a large number of proteins that were altered but the significance was not reached. The cut-off point of P value was set to $p=0.05$, therefore proteins with p value greater than 0.05, relative to vehicle control, were excluded. Full list of all protein alterations in INF and ONC2 panels in Appendix II.

NPX range in pg/mL were determined using reference range standard curve provided by OLINK. A standard curve with a reference range of the protein (pg/mL) for each of the 92 biomarkers for each panel was provided on OLINK website (http://www.olink.com/proseek-multiplex/complete-biomarker-list/).

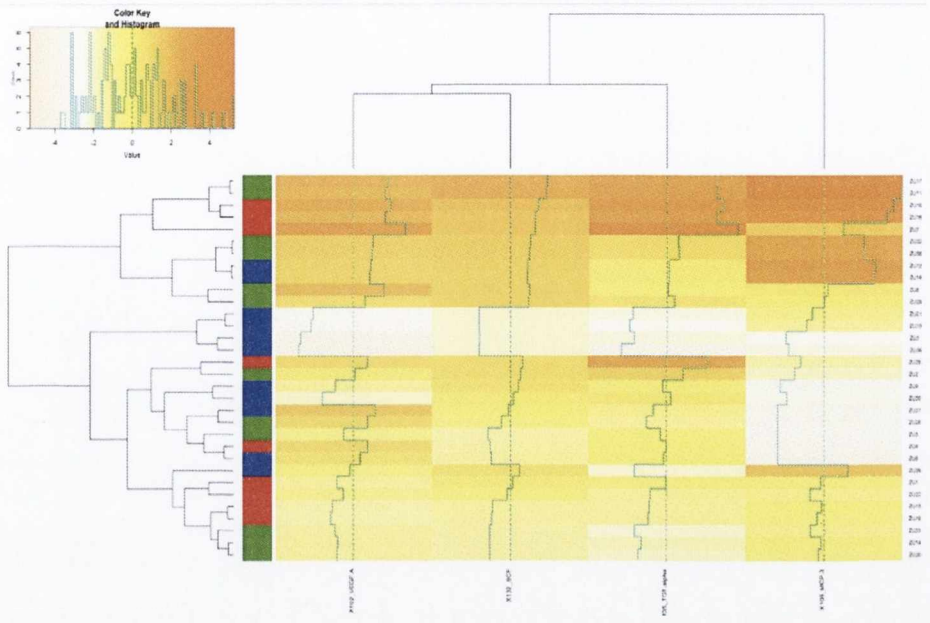


Figure 7.11 Clustering heat map of NPX-levels of significantly altered proteins on the INF panel. Color bar on the left indicates TCM from OAC biopsies treated with media only (shown in red), D1 treatment (TCM from OAC biopsy treated with HS6, shown in green) and D2 treatment (TCM from OAC biopsy treated with NIH4, shown in blue). A pattern of red (control) and green (HS6) is clustering closer together, whereas samples labelled in blue (NIH4 treatment) are clustering closely together and separate from red and green (control and HS6 treatment). Four significant hits (samples with significant statistical difference in protein expression levels between treatment groups) are marked using green vertical lines.

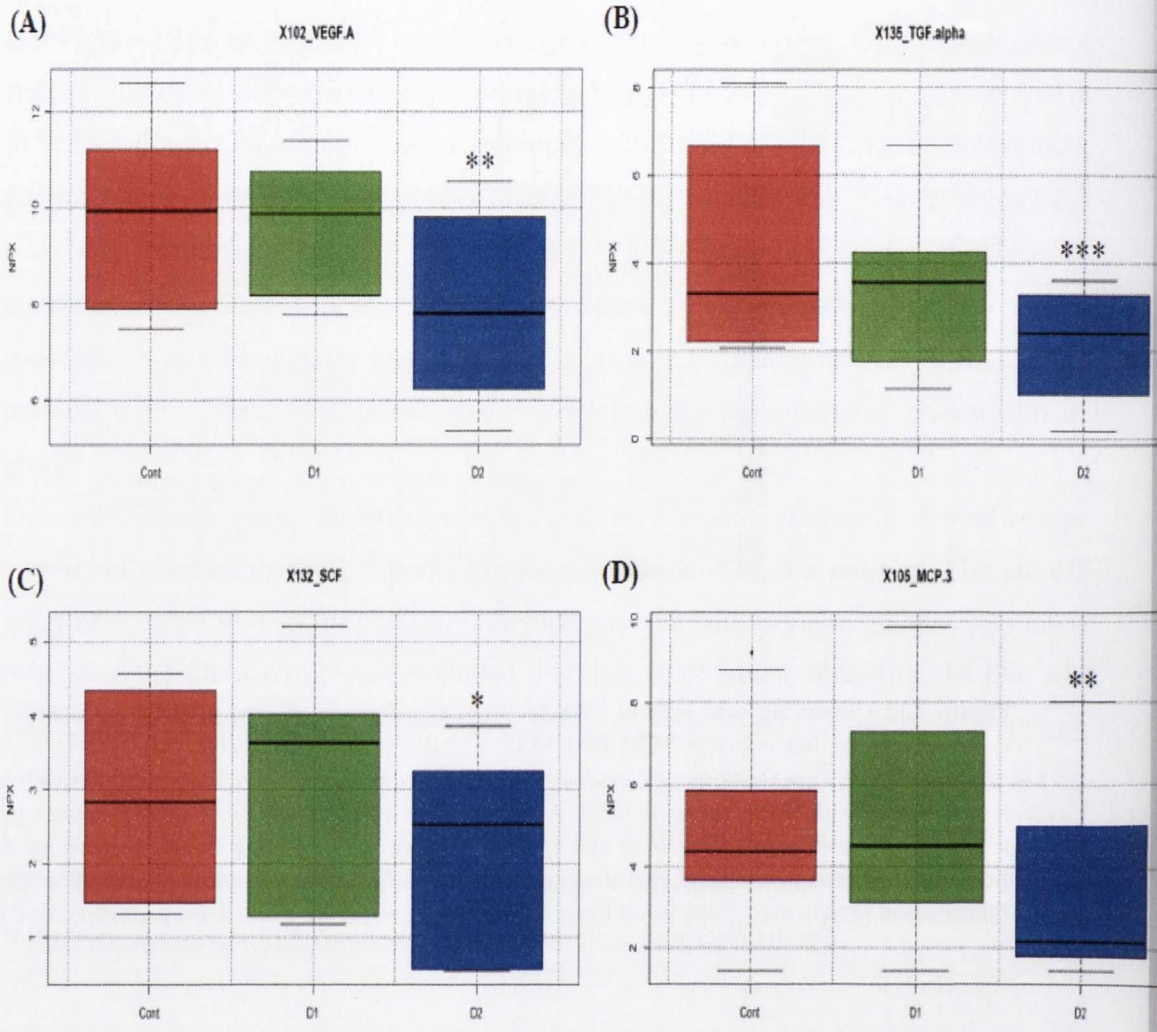


Figure 7.12 Assessment of inflammation-related protein marker secretions by *ex vivo* cultured biopsies following novel 5LOX inhibitor treatment: INF panel. Tumour biopsies were cultured *ex vivo* for 24 hours with 10 μM of HS6 or 10 μM of NIH4 treatment and TCM was analysed using Proximity Extension Assay (PEA) technology. (A) Tumour-secreted VEGFA levels were significantly lower in TCM following 24-hour incubation of biopsy with 10 μM of NIH4 compared to vehicle control ($p<0.01$), however, there was no significant difference in secreted VEGFA levels following 24-hour treatment of OAC biopsy with 10 μM of HS6, compared to vehicle control ($p>0.05$). (B) Tumour-secreted TGF-alpha levels were significantly lower in TCM following 24-hour biopsy culture with 10 μM of NIH4, compared to vehicle control ($p<0.001$), however, there was no significant difference in secreted TGF-alpha levels following 24-hour treatment of OAC biopsy with 10 μM of HS6, compared to vehicle control ($p>0.05$). (C) Similarly, tumour-secreted SCF levels were significantly lower in TCM following biopsy treatment with 10 μM of NIH4, compared to vehicle control ($p<0.05$), however, there was no significant difference in secreted SCF levels following 24-hour treatment of OAC biopsy with 10 μM of HS6 ($p>0.05$). (D) Tumour-secreted MCP3 levels were significantly lower in TCM following biopsy treatment with 10 μM of NIH4, compared to vehicle control ($p<0.05$), and there was no significant difference in secreted MCP3 levels following 24-hour treatment of OAC biopsy with 10 μM of HS6 ($p>0.05$). Statistical test used was ANOVA with Tukey post hoc test. $p<0.05$ (*), $p<0.01$(**), $p<0.001$(***). Error bar denotes mean ±S.E.M.

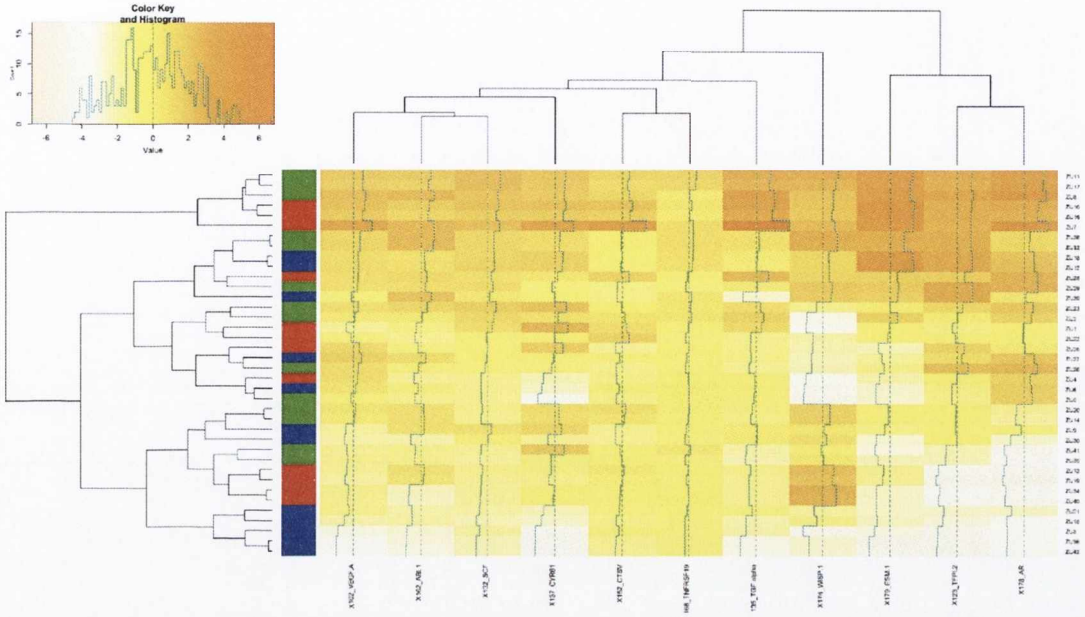


Figure 7.13 Clustering heat map of NPX-levels of significantly altered proteins on the ONC2 panel. Color bar on the left indicates TCM from OAC biopsies treated with media only (shown in red), D1 treatment (TCM from OAC biopsy treated with HS6, shown in green) and D2 treatment (TCM from OAC biopsy treated witj NIH4, shown in blue). A pattern of red (control) and green (HS6) is clustering closer together, whereas samples labelled in blue (NIH4 treatment) are clustering closely together and separate from red and green (control and HS6 treatment). Eleven significant hits (samples with significant statistical difference in protein expression levels between treatment groups) are marked using green vertical lines.

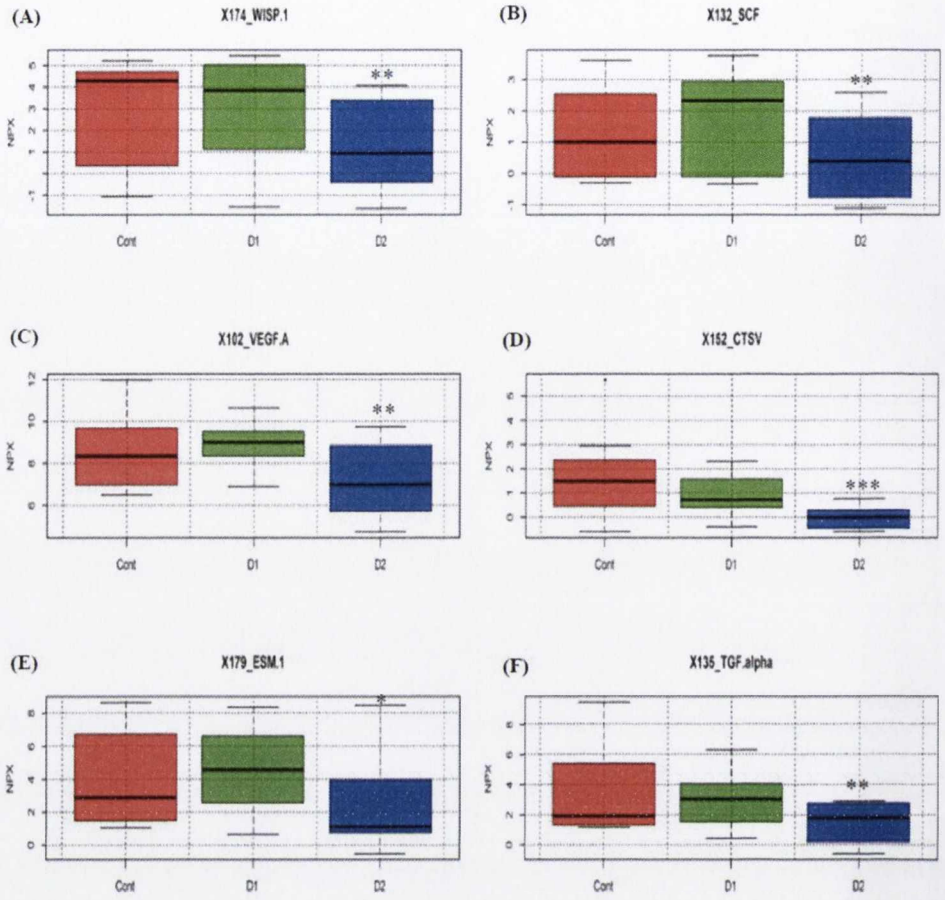


Figure 7.14 Assessment of inflammation-related protein marker secretions by *ex vivo* cultured biopsies following novel 5LOX inhibitor treatment: ONC2 panel. Tumour biopsies were cultured *ex vivo* for 24 hours with 10 μM of HS6 or 10 μM of NIH4 treatment and TCM was analysed using Proximity Extension Assay (PEA) technology. (A) Tumour-secreted WISP1 levels were significantly lower in TCM following 24-hour incubation of biopsy with 10 μM of NIH4 compared to vehicle control ($p<0.01$), however, there was no significant difference in secreted WISP1 levels following 24-hour treatment of OAC biopsy with 10 μM of HS6, compared to vehicle control ($p>0.05$). (B) Similarly like on INF panel, tumour-secreted SCF levels were significantly lower in TCM following 24-hour biopsy culture with 10 μM of NIH4, compared to vehicle control ($p<0.01$), however, there was no significant difference in secreted SCF levels following 24-hour treatment of OAC biopsy with 10 μM of HS6, compared to vehicle control ($p>0.05$) and (C) tumour-secreted VEGFA levels were significantly lower in TCM following biopsy treatment with 10 μM of NIH4, compared to vehicle control ($p<0.01$), but there was no significant difference in secreted VEGFA levels following 24-hour treatment of OAC biopsy with 10 μM of HS6 ($p>0.05$). (D) Tumour-secreted CTSV levels were significantly lower in TCM following biopsy treatment with 10 μM of NIH4, compared to vehicle control ($p<0.001$), and there was no significant difference in secreted CTSV levels following 24-hour treatment of OAC biopsy with 10 μM of HS6 ($p>0.05$). (E) tumour-secreted ESM1 levels were significantly lower in TCM following biopsy treatment with 10 μM of NIH4, compared to vehicle control ($p<0.05$), but there was no significant difference in secreted ESM1 levels following 24-hour treatment of OAC biopsy with 10 μM of HS6 ($p>0.05$). (F) Similarly like on INF panel, tumour-secreted TGF-alpha levels were significantly lower in TCM following biopsy treatment with 10 μM of NIH4, compared to vehicle control ($p<0.01$), and there was no significant difference in secreted CTSV levels following 24-hour treatment of OAC biopsy with 10 μM of HS6 ($p>0.05$). Statistical test used was ANOVA with Tukey post hoc test. $p<0.05$ (*), $p<0.01$(**), $p<0.001$(***). Error bar denotes mean ±S.E.M.

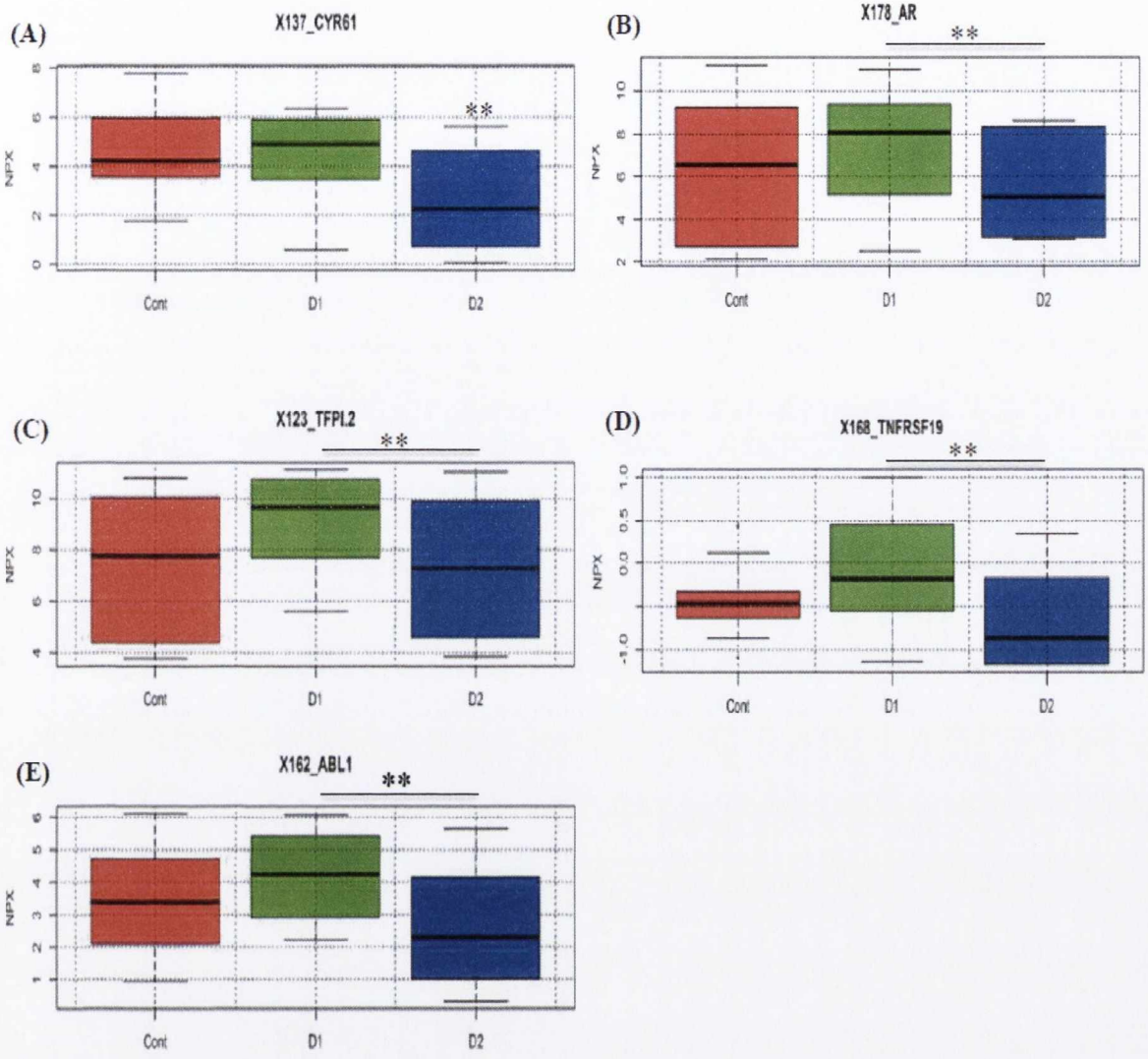


Figure 7.15 Assessment of inflammation-related protein marker secretions by *ex vivo* cultured biopsies following novel 5LOX inhibitor treatment: ONC2 panel. Tumour biopsies were cultured *ex vivo* for 24 hours with 10 μM of HS6 or 10 μM of NIH4 treatment and TCM was analysed using Proximity Extension Assay (PEA) technology. (A) Tumour-secreted CYR61 levels were significantly lower in TCM following 24-hour incubation of biopsy with 10 μM of NIH4 compared to vehicle control ($p<0.01$), however, there was no significant difference in secreted WISP1 levels following 24-hour treatment of OAC biopsy with 10 μM of HS6, compared to vehicle control ($p>0.05$). (B) There was no significant difference in AR levels between TCM following 24-hour biopsy culture with 10 μM of NIH4, compared to vehicle control ($p>0.05$), however, there secreted AR levels were significantly lower in TCM following 24-hour treatment of OAC biopsy with 10 μM of HS6, compared to the levels in TCM following HS6 treatment ($p<0.01$). Similarly there was no significant difference in (C) TFPL2 (D) TNFRSF19, (E) ABL1 levels between TCM following 24-hour biopsy culture with 10 μM of NIH4, compared to vehicle control ($p>0.05$), however, secreted levels of these proteins were significantly lower in TCM following 24-hour treatment of OAC biopsy with 10 μM of HS6, compared to the levels in TCM following HS6 treatment ($p<0.01$). Statistical test used was ANOVA with Tukey post hoc test. $p<0.05$ (*), $p<0.01$(**), $p<0.001$(***). Error bar denotes mean ±S.E.M.

7.3.11 Validation of pathways altered *ex vivo* using oesophageal tumour explants

Tissue conditioned media and OAC tumour tissue protein lysates, the same samples used in Section 7.3.3 and Section 7.5.4.1. Briefly, fresh biopsies from 10 treatment-naive OAC patients were collected from the clinic and cut into equally sized pieces. Each piece of tissue was cultured for 24 hours in *ex vivo* medium, as described in Section 2.19.1, with either vehicle control (0.1% DMSO), 10 μM HS6 or 10μM NIH4. The biopsy tissue pieces were homogenised and total protein concentration was determined by BSA assay to normalize protein secretions detected to the size of biopsy pieces. OAC tumour-secreted levels of VEGF, were measured in TCM, by DuoSet ELISA. Analysis of NIH4 treated biopsies versus vehicle control treated biopsies by paired Wilcoxon signed rank test revealed a significant relationship between NIH4 treatment and decreased VEGF levels ($p<0.05$, $n=10$) (Figure 7.16), validating OLINK Proteomics data (Figure 7.14). Validation data correlated with array data. NIH4 significantly reduced secreted VEGF levels in both OLINK array and validation ELISA. Similarly, HS6 treatment failed to have an effect on VEGF secretion at both experiments setups.

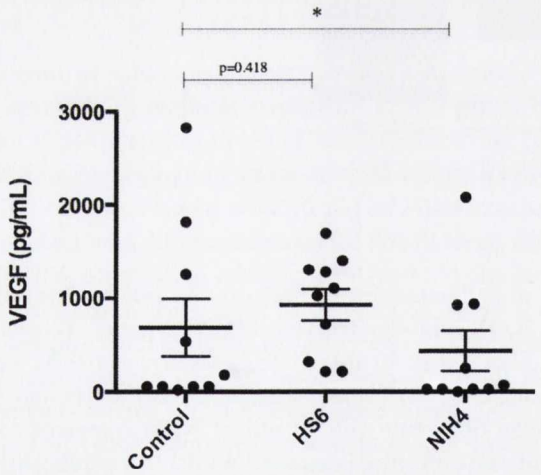


Figure 7.16 Validation of VEGF secretions by ex *vivo* cultured biopsies following novel 5LOX inhibitor treatment. Tumour biopsies were cultured ex vivo for 24 hours with novel 5LOX inhibitors by ELISA. Comparison of tumour-secreted VEGF levels in NIH4 cultured biopsies and vehicle control, revealed a significant reduction of VEGF levels following 24-hour treatment with NIH4 ($p<0.05$, $n=10$ in each group), however, there was no significant difference if secreted VEGF levels in TCM following biopsy treatment with HS6 ($p=0.418$, $n=10$ in each group). Statistical test used was Kruskal-Wallis test with Dunn's Multiple comparison Test. $p<0.05$ (*). Error denotes mean ±S.E.M.

7.3.12 Association between secreted levels of LTB4 and VEGF by OAC patient biopsies *ex vivo*

The endogenous production of LTB4 by OAC tumour biopsies cultured *ex vivo* was measured by ELISA in Section 7.3.3 and OAC tumour-secreted levels of VEGF, were measured in TCM, by DuoSet ELISA in Section 7.3.11. Data from both experiments was combined in order to investigate whether there was an association between tumour-secreted levels of LTB4 (the metabolite of 5LOX) and VEGF. Results showed a positive association between increasing levels of LTB4 and VEGF in TCM from media only (vehicle control) co-cultured OAC biopsies ($r=0.4327$, $p<0.05$, $n=10$ in each group) (Figure 7.18a). Similarly, there was a positive association between tumour-secreted levels of the metabolite of 5LOX and VEGF in TCM from OAC biopsies following 24-hour treatment with NIH4 ($r=0.5111$, $p<0.05$, $n=10$ in each group) (Figure 7.18b).

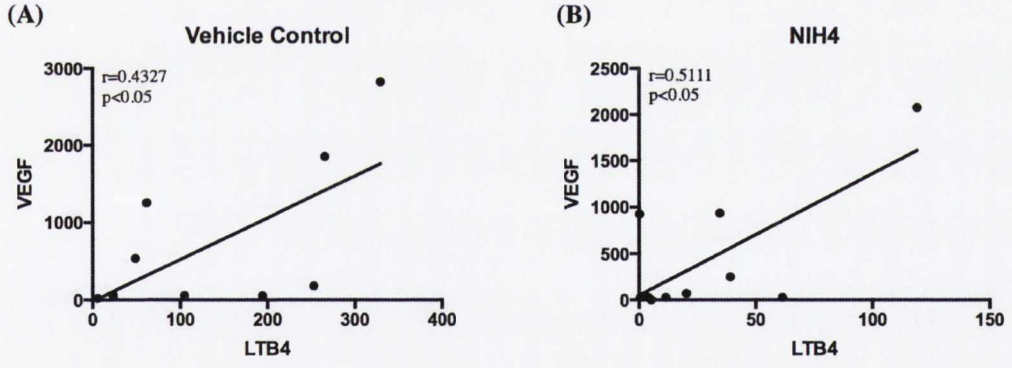


Figure 7.17 There is a significant association between tumor secretion levels of LTB4 and VEGF. Endogenous production of LTB4, by OAC tumor biopsies cultured *ex vivo,* and OAC tumor-secreted levels of VEGF, were previously measured in TCM. Data from both experiments was combined in aim to determine the association between tumor-secreted levels of LTB4 and VEGF. (A) Results showed a significant positive association between increasing levels of LTB4 and VEGF in TCM from media only cultured OAC biopsies ($r=0.4327$, $p<0.05$, $n=10$ in each group). (B) There was a positive association between tumor-secreted levels of the metabolite of 5LOX and VEGF in TCM from OAC biopsies following 24-hour treatment with NIH4 ($r=0.5111$, $p<0.05$, $n=10$ in each group). Statistical test used was Spearman's test. $p<0.05(*)$.

In summary, 2 best in class novel inhibitors of 5LOX (HS6 and NIH4) were selected from a large panel of novel inhibitors. Two novel inhibitors of 5LOX: HS6 and NIH4 were more effective at reducing ACM-induced glycolysis in esophageal adenocarcinoma cell model than commercially available FDA approved Zyleuton (inhibitor of 5LOX used in treatment of asthma). Interestingly, NIH4 was more effective in reducing glycolysis in OE33 cells in hypoxic environment. Additionally, NIH4 was effective in reducing ACM-induced metabolic shift in glucose and mitochondrial metabolism in OE33 cells. In the *ex vivo* study, NIH4 significantly reduced 12 OAC explant-secreted pro-tumourigenic and pro-inflammatory proteins.

7.4 Discussion

In an effort to combat rising rates of OAC, a large proportion of research efforts have focused on identifying novel molecular targets involved in pro-tumourigenic pathways [101], with the aim to boost treatment response to currently used treatment strategies. The contribution of 5LOX and glycolysis pathways has been previously reported to drive carcinogenesis, and inhibition of these pathways has been reported to be a potential anti-cancer therapy in lung, prostate and colon cancers [299, 382, 383]. In this novel study, new structural classes of 5LOX and glycolytic inhibitors, identified by our collaborators (Dr. Maloney, NIH, Bethesda, MI and Dr. Sheridan, School of Pharmacy, Trinity College Dublin, Ireland) were used to explore the inhibition of 5-lipoxygenase and glycolysis pathways in OAC.

Assessment of drug effects on cancer cell viability and proliferation in vitro is often one of the first stages of preclinical investigation with novel therapeutics. In this study we compared the effect of commercially available inhibitors of 5LOX and glycolysis with novel therapeutics provided by Dr. Maloney and Dr. Sheridan. High positive expression of 5LOX in OE33 cells was previously confirmed at mRNA and protein level in the department (data not shown), therefore indicating their potential susceptibility to such targeted therapies. In this study, REV5901 was shown to potentially inhibit OE33 cell viability and proliferation with IC_{50} values of 11.64μM and 12.03 μM respectively. Research studies from other groups suggest that REV5901 reducing cancer cell proliferation by triggering cell cycle arrest, and subsequently cell death, via intrinsic apoptotic pathway [87] . Ketoconazole and MK886 showed similar potency in decreasing cell viability with IC_{50} values of 9.76 μM and 10.04 μM respectively, and cell proliferation with IC_{50} values of 9.88 μM and 10.14 μM respectively. Zileuton was markedly less potent at reducing both OE33 cell viability with IC_{50} value not reached at dose of 25 μM and IC_{50} of proliferative cell activity was reached at concentration of 23.03 μM. Novel small molecule inhibitors of 5LOX, HS6 and NIH4 showed a reduction in cell viability with IC_{50} values of 10.04 μM and 10.08 μM respectively, and reduction in cell proliferation at IC_{50} 10.96 μM and 10.18 μM respectively. Commercially available inhibitors of glycolysis, potassium dichloracetate, 3-aminobenzoic acid, sodium oxamate

2-Deoxy D-glucose and bromopyruvic acid inhibited OE33 cell viability with IC_{50} values between 9.73 μM -12.02 μM. Furthermore, OE33 cell viability was significantly reduced following 24-hour treatment with novel small molecule inhibitors (HS1, HS5, HS7-HS17) with IC_{50} values between 11.05 μM -24.05 μM. Commercially available inhibitors of glycolysis inhibited OE33 cell proliferation with IC_{50} values between 9.04 μM -13.41 μM. Commercially available and novel inhibitors of 5LOX and glycolysis were used in the further experiments at a 10 μM concentration.

Following the measurement of endogenous production of LTB4 in OAC tumor explants, NIH4 was confirmed to be an inhibitor of 5LOX, due to a significant decrease in LTB4 (a metabolite of 5LOX) levels secreted following 24-hour culture of OAC tumor with this inhibitor. HS6 has been shown to be a potential inhibitor of 5LOX due to a decrease in LTB4 secretion by OAC tumor following 24-hour culture with HS6, however, while HS6 did appear to reduce LTB4 expression a significant decrease was not reached ($p=0.1601$). As HS6 was reported to have potential anti-5LOX activity, it was selected, alongside the confirmed 5-LOX inhibitor NIH4, for further analysis.

The Seahorse XFe24 analyser was used to investigate the ability of commercially available and novel inhibitors of 5LOX to alter glycolysis in OE33 cells and whether the alterations were maintained or became more significant following induction of glycolysis by ACM (co-culture of cells with ACM from viscerally obese OAC patients). Results revealed that MK886 and Ketoconazole significantly reduced glycolysis (ECAR) in OE33 cells following 24-hour treatment with Ketoconazole maintaining the same level of reduction in the presence of ACM. Interestingly, novel inhibitors HS6 and NIH4, both significantly reduced ECAR levels following 24-hour treatment ($p<0.05$), and the reduction was significantly greater following treatment of OE33 cells in the presence of ACM ($p<0.01$), suggesting that the novel inhibitors could potentially be more beneficial in reducing obesity driven glycolysis in OAC. The commercially available inhibitors of glycolysis, 3-amino benzoic acid (inhibitor of LDHA) and sodium oxamate (inhibitor of LDH), both significantly reduced ECAR in OE33 cells following 24-hour treatment ($p<0.05$ and $p<0.01$ respectively) and maintained the same level of inhibition in the presence of ACM from viscerally obese OAC patients. Novel inhibitor HS1, similar to 3-aminobenzoic acid, significantly reduced ECAR in OE33 cells following 25-hour treatment and the effect was maintained in the presence of ACM. The novel inhibitor, HS1, was shown to be potentially more effective in reducing glycolysis in OE33 cells

compared to commercially available 2DG, bromopyruvic acid and potassium dichloracetate.

Following the findings in this study, that HS6 and NIH4 may be potentially more effective in reducing obesity-induced glycolysis in OE33 cells, we investigated whether alterations in glycolytic OE33 cell activity by the novel inhibitors of 5LOX were further affected by the lack of oxygen (0.5% O_2). Results showed that NIH4 had a significantly greater effect in reducing glycolysis in OE33 cells under hypoxic (0.5% O_2) conditions ($p=0.001$), and that NIH4 significantly reduced ACM-induced glycolysis in OE33 cells in the hypoxic compared to normoxic environment ($p<0.05$). This result is in line with recent evidence that 5LOX induction may be associated with hypoxia [384]. Gonsalves *et al* showed that hypoxia mediates the expression of 5LOX activating protein (FLAP), a key enzyme in leukotriene formation in human pulmonary microvascular endothelial and human brain endothelial cells [384].

In order to investigate the effect of ACM from viscerally obese OAC patients was able to alter genes involved in the regulation mitochondrial metabolism in OE33 cells, we used RT² Profiler™ PCR Human Glucose Metabolism Arrays. Additionally, we were interested whether the novel inhibitors of 5LOX (HS6 and NIH4) were able to reverse ACM-induced changes in OE33 cells. For this part of the study, OE33 cells were treated for 24 hours with ACM, HS6, and NIH4, RNA was isolated and synthesised cDNA was used for the arrays. Results revealed that overall, 71% of glucose metabolism associated genes were significantly upregulated (greater than 2 fold change relative to media only control) following treatment with ACM, suggesting a positive association between obesity and glycolysis in OAC. This data is in line with a recent study demonstrating that ACM from obese OAC patients was able to alter tumor metabolism, supporting the metabolic shift in glucose metabolism [103]. Additionally, NIH4 showed a significant reduction of 6/84 (7.14%) and 16/84 (19.05%) glucose metabolism associated genes when used in combination with ACM and compared to ACM only treated OE33 cells. Top ten potential gene targets (altered by the greatest fold change) were further validated in OE33 cell line following treatment with NIH4 in the presence of ACM. Validation studies supported findings from the human glucose metabolism arrays.

Additionally to investigation of ACM and novel inhibitor-induced changes in glucose metabolism in OE33 cells, we were interested whether ACM from viscerally obese OAC

patients was able to alter genes involved in mitochondrial metabolism in OE33 cells. For this part of the study we used RT² Profiler™ PCR Human Glucose Metabolism Arrays. The experimental set up was identical to the one used in glucose metabolism arrays. OE33 cells were treated for 24 hours with ACM, HS6, and NIH4, RNA was isolated and synthesised cDNA was used for the arrays. Results showed that following treatment of OE33 cells with ACM, 73.8% human mitochondrial metabolism associated genes were significantly upregulated (greater than 2 fold change relative to media only control). 10/84 (11.9%) mitochondrial metabolism associated genes were upregulated when used in combination with ACM and compared to ACM only treated OE33 cells. Consequently, reduction of Complex III associated COX5B and COX6C levels following 24-hour treatment of OE33 cells with NIH4 were validated in OE33 cells ($p<0.05$), suggesting a potential role of NIH4 in altering glucose metabolism in esophageal adenocarcinoma cells. It has been shown that alterations in Complex III have been linked with breast, colorectal and ovarian cancers (99-101), therefore, NIH4 may be a novel inhibitor of interest in mitochondrial metabolism associated alterations.

As another route of investigation, we explored the effect of 5LOX inhibitor treatment on pro-tumourigenic secretions by OAC tumor biopsies cultured *ex vivo* by Proseek® Inflammation I ^{96x96} and Oncology II ^{96x96} multiplex immunoassay. While *in vitro* models are critical for pre-clinical drug testing, they are not representative of the heterogeneity of an *in vivo* tumor. Therefore, in contrast to testing the effect of the inhibitors in OE33 cell line, the *ex vivo* tumor biopsy culture model offered a unique opportunity to study the effect of novel 5LOX inhibitors in tumor cells and intact peritumoural stroma. Although this study consisted of small number of biopsies (5 for each treatment group), a number of significant associations were observed, providing some insight into the molecular pathways altered by novel inhibitors of 5LOX. Notably, HS6 did not appear to alter pro-tumourigenic protein secretion *ex-vivo*, however, NIH4 treatment was found to significantly decrease VEGFA, TGF-alpha, SCF, MCP3, WISP1, SCF, CTSV, ESM1 and CYR61 relative to vehicle control. Moreover, an additional four secreted protein markers were lower in TCM following 24-hour biopsy treatment with 10μM NIH4 compared to TCM following treatment with HS6. These proteins were TFPL2, AR, TNFRSF19 and ABL1. A large number of proteins were altered following biopsy treatment with NIH4, however, failed to reach significance due to small sample numbers and sample heterogeneity.

VEGFA, a growth factor, has been shown to induce endothelial cell proliferation, promote cell migration, to inhibit apoptosis and to induce permeabilization of blood vessels. It has been shown to be involved in inflammation-related diseases such as inflammatory bowel disease, rheumatoid arthritis and neuroinflammation [385, 386].

TGF-alpha, the second growth factor expression, that was downregulated following biopsy treatment with NIH4, have been shown to play an important role in stem cells restoration in neurodegenerative disorders [386, 387]. It has also been described to be involved in several inflammation-related diseases such as inflammatory bowel disease, hepatitis C [388], and the expression of TGF-alpha in cancers including breast [20], colorectal [389] and head and neck cancers [390].

Stem cell factor (SCF) was significantly downregulated following 24-hour co-culture of OAC biopsy with NIH4. SCF has been shown to be a mediator of numerous biological functions in hematopoiesis, melanogenesis, erythropoiesis, spermatogenesis, and carcinogenesis [391]. Esposito *et al* examined the expression and function of SCF in 17 normal and 26 cancerous pancreatic tissues as well as in 6 pancreatic cell lines [392]. This study suggested that pancreatic cancer cells might have the capacity to recruit mast cells to the tumor mass via SCF production and thereafter, mast cells might potentiate tumor invasion and angiogenesis through their effects on the extracellular matrix [392]. Elpek *et al* mast cell density (MCD) in tumor specimens from 53 esophageal SCC patients and reported that MCD were associated with the depth of wall invasion, lymph node metastasis, and tumor progression, suggesting that MCD may have a role in the angiogenesis of these tumours and might be responsible for their aggressive behavior [393].

Published studies show monocyte chemotactic protein-3 (MCP-3) to be a potent chemoattractant for a variety of leukocytes including monocytes, eosinophils, basophils, DC, NK cells and activated T lymphocytes [394]. Dendritic cells and distinct T lymphocyte populations play an important role in acquiring tumor immunity, therefore, MCP-3 may be an appealing antitumor agent [395]. Study by Hu *et al* suggested that the transfection of chemokine MCP-3 gene could induce anti-colorectal cancer immunity, however, they concluded that the tumor growth could not be inhibited completely by merely MCP-3 gene transfection [396]. In this study, MCP-3 secretion by OAC tumor was significantly reduced by NIH4, suggesting a potential anti-inflammatory role.

OAC tumor secreted levels of protease cathepsin V (CTSV) were significantly reduced following 24-hour NIH4 treatment. Published studies show that proteases contribute to

tumor invasion and metastasis by degrading basement membranes and extracellular matrix (ECM) [397]. CTSV overexpression has been observed in many cancers including breast, colorectal, prostate, lung and liver cancers [397]. The ability of NIH4 to significantly reduce OAC tumor secreted CTSV levels suggest a potential anti-cancer effects in OAC.

Published studies show endothelial cell specific molecule-1 (ESM-1) to be upregulated in tissue and serum from colorectal cancer patients and suggested that breast, colorectal, prostate, lung and liver cancers [398, 399]. Elpek *et al* showed that knocking down ESM-1 by siRNA decreased cell survival. This study also showed that overexpression of ESM-1 in human colon carcinoma cells enhanced cell proliferation through the Akt-dependent activation of NF-κB pathway. This study also demonstrated a positive involvement ESM-1 in cell survival, cell cycle progression, migration, invasion and EMT during tumor invasion in colorectal cancer. Based on the results of this published study in human colorectal cancer ESM-1 may be a useful therapeutic target for colorectal cancer. ONC2 multiplex array data showed that ESM1 was secreted by OAC tumor and its secretion levels were significantly reduced following 24-hour treatment with NIH4, therefore, once again suggesting a pro-tumourigenic effect of this inhibitor in OAC.

Cysteine-rich 61 (Cyr61) is a member of the CCN (Cyr61/CTGF/Nov) protein family and it has a role in cell adhesion, migration, proliferation, and survival [400]. Jeong *et al* assessed the Cyr61 expression in 6 colorectal cancer cell lines and 20 sets of paired normal and colorectal cancer tissues and reported that all cancer cell lines expressed Cyr61 and among the 20 cases of paired normal and tumor tissues, greater Cyr61 expression was observed in 16 (80%) tumor tissues than in normal tissues. They also reported high Cyr61 expression was associated with significantly poorer survival [401]. Study by Sun *et al* reported that Cyr61 induces proliferation and migration of prostate cancer cells and *in vivo* study using a prostate cancer mouse model further demonstrated that Cyr61 was also involved in facilitating metastasis [402].

Olink platform enabled us to have a better understanding of pro-inflammatory and pro-tumourigenic proteins altered in esophageal adenocarcinoma and provided us with a better insight in therapeutic efficacy of novel inhibitors of 5LOX. The ability of 5LOX inhibitor to reduce SCF and potentially have an effect on cancer stemness forms a starting point for future studies.

A positive association between the levels of LTB4 and VEGF in the *ex vivo* study indicate a potential role of 5LOX in more aggressive disease phenotype. Reduction of 5LOX in the *ex vivo* study resulted in reduction of other pro-tumourigenic markers including pro-angiogenic VEGF, pro-inflammatory TGF-alpha and stem cell factor contributing to cancer stemness. We suggest that targeting 5LOX we could potentially reduce a number of other pro-tumourigenic factors. Moreover, a positive association between tumor-secreted levels of the metabolite of 5LOX and VEGF in TCM from OAC biopsies following 24-hour treatment with NIH4 indicate the efficacy of NIH4 in targeting VEGF, which is associated with poor prognosis is esophageal cancer [402].

In conclusion, in this study we have shown that the novel 5LOX inhibitor NIH4 can induce specific anti-proliferative effects on OE33 cells, unlike some commercially available inhibitors such as Zileuton. NIH4 was shown to reduce 5LOX activity in OAC biopsies by reduction of LTB4 production, indicating the efficacy of NIH4 in targeting 5LOX in OAC. Through *in vitro* and *ex vivo* experiments, NIH4 has been found to have potential anti-cancer effects through mechanisms of altered glycolysis and mitochondrial function. Interestingly, NIH4 was not only able to reduce glycolysis in esophageal adenocarcinoma cell model, but it was even more efficacious in the hypoxic environment. This is an important finding as most novel inhibitors and commercially available drugs fail in the absence of oxygen (for example in less oxygenated areas like tumor core).

Chapter 8

Assessment of the role of ENO3 and PKM2 in an esophageal adenocarcinoma cell model driven by adipose conditioned medium: therapeutic targeting of a specific pathway

8.1 Introduction

RNA interference (RNAi) has been shown to be a useful tool to investigate the function of genes in mammalian cells *in vitro* [402]. Following this finding, the usage of small interfering RNAs (siRNAs) were the focus of many research groups, with the aim to reduce the expression of individual genes of interest in order to establish the link between gene identity, gene function and its role in the disease [403]. siRNAs are highly specific, and therefore are widely used for target validation and pathway analysis studies [404].

In this study, we aimed to investigate the role of two enzymes in the glycolysis pathway: ENO3 and PKM2, in OAC *in vitro* using a targeted knock out approach. The two enzymes were selected for the gene silencing study based on the findings in published studies and the significant findings in the previous chapters of this thesis.

Accumulating evidence shows that activity of the PKM2 is closely related to tumorigenesis. Sun *et al* investigated the relationship between PKM2 expression, tumor invasion and the prognosis of patients with lung adenocarcinoma [405]. This study reported that PKM2 expression was significantly associated with reduced patient survival. They used siRNA technology to investigate the effect of targeted PKM2 knockout on tumor growth at the cellular level. *In vitro*, siRNA-mediated PKM2 knockdown significantly inhibited cell proliferation, glucose uptake, ATP generation and fatty acid synthesis of A549 cells, while increasing mitochondrial respiratory capacity of the cells increased. It has also been shown that PKM2 knockout significantly inhibited the expression of the glucose transporter GLUT1, metalloproteinase 2 (MMP-2) and vascular endothelial growth factor (VEGF), which are important in degradation of the extracellular matrix and angiogenesis respectively [405]. These observations show that PKM2 is able to activate both glycolysis and lipid synthesis, thereby regulating cell proliferation and invasion [405]. Additionally, Golberk *et al* investigated the role of PKM2 in NCI-60, a panel of human tumor cell lines that were previously characterized and were broadly used in drug screening [406]. The constituent cell lines in NCI-60 panel represented multiple types of cancer, including brain, breast, colon, lung, ovarian, renal

and skin cancers. This study showed that silencing PKM2 induced apoptosis in all cancer cell lines in NCI-60 panel.

Enolase 3 (ENO3) was of interest in this study as it has been previously shown to be a glycolytic enzyme associated with energy metabolism in cancer cells, however, a very limited number of published studies focused on a targeted knock out of ENO3 as a potential therapy. We have demonstrated previously that ENO3 expression was significantly higher in tumor biopsies from viscerally obese compared to normal weight OAC patients, and that the epithelial protein expression of ENO3 in tissue microarrays constructed from tumor of AOC patients, was significantly higher in obese compared to normal weight patients (Chapter 4). Therefore, due to the potential link between ENO3 and obesity-driven OAC, it was selected for assessment of its potential suitability as a targeted therapy.

8.2 Aims and objectives

The aim of this chapter was to investigate the role of ENO3 and PKM2 in OAC *in vitro* using a targeted knockout approach. It was hoped that this work would provide the insight into the relevance of targeting these two enzymatic pathways as therapeutic approach in OAC.

Specific objectives:

- To optimise and validate silencing protocol for ENO3 and PKM2 in OE33 cells
- To investigate whether silencing of ENO3 and PKM2 in OE33 cells alters proliferative cell activity in real time, using xCELLigence platform
- To assess the efficacy of novel inhibitors HS6 and NIH4 in ENO3 and PKM2 transfected cells in real time using xCELLigence platform
- To investigate the role of ENO3 and PKM2 in glycolysis in OE33 cells using a Seahorse XFe24 analyser

8.3 Results

8.3.1 siRNA-mediated ENO3 and PKM2 knockdown in OE33 cells *in vitro*

The optimization of siRNA-targeted OE33 cell transfection protocol was attempted by two different methods: fast-forward and reverse transfection. In the fast-forward transfection, plating and transfection of cells were performed on the same siRNAs were diluted in serum-free culture medium and the transfection reagent was added to the diluted nucleic acid in order to produce reagent–nucleic acid complexes. The cells were seeded and the complexes were added directly to the freshly seeded cells (Figure 8.1a). In a reverse transfection, cells were plated 24 hours prior to transfection. OE33 cells were seeded in culture medium containing serum and antibiotics the day before transfection and incubated under normal growth conditions. The following day, siRNA was diluted in serum-free culture medium and transfection reagent was added directly to the diluted siRNA to produce reagent-nucleic acid complexes (Figure 8.1b).

Silencing of ENO3 and PKM2 were carried out for 10nM and 30nM concentrations of siRNA. A negative control was set up for each concentration, which utilized a scrambled RNA control. Transfection experiments were done in duplicate to allow assessment of ENO3 and PKM2 at gene and protein level. The reverse transfection procedure (Section 2.3.3) was optimized successfully following a number of changes in the optimization step, including the change of the cell seeding numbers and change of transfection reagent. The main changes in optimization steps were described in Table 8.1. Forward transfection protocol was not optimized successfully. OE33 cells which had undergone forward transfection protocol, yielded insufficient quantities of RNA and protein to bring forward for validation and downstream analysis. The transfection of ENO3 and PKM2 were validated at the gene level via qPCR and at the protein level by Western blot.

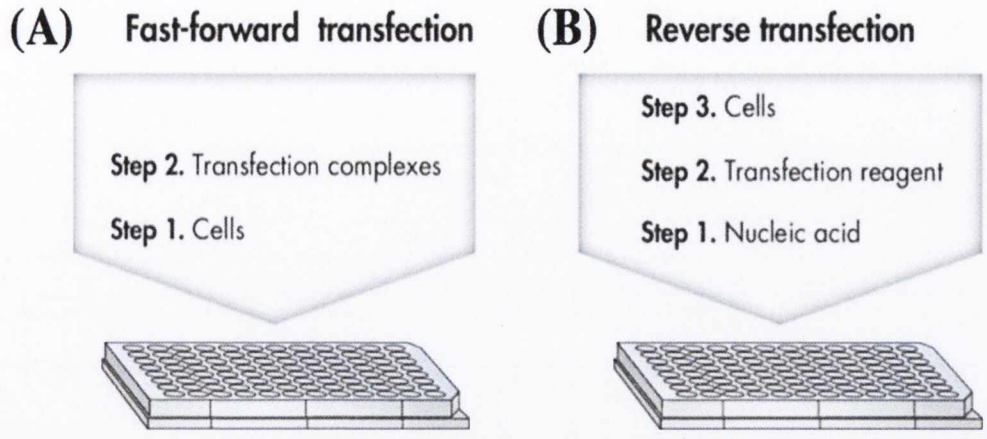


Figure 8.1 Two methods of siRNA-targeted transfection *in vitro.* (A) Fast-forward transfection method involving plating and transfection of on the same day. siRNA is diluted in serum-free culture medium and transfection reagent was added to the diluted nucleic acid (NA) to produce reagent–NA complexes. The cells are seeded and then complexes are added directly to the freshly seeded cells. (B) Reverse transfection protocol where the cells are plated 24 hours prior to transfection. Cells are seeded in culture medium containing serum and antibiotics the day before transfection and incubated under normal growth conditions. The following day DNA or siRNA is diluted in serum-free culture medium and transfection reagent is added directly to the diluted siRNA to produce reagent–NA complexes. Figure adapted from https://www.qiagen.com/ie/resources/molecular-biology-methods/transfection/ (809).

Table 8.1 Variations on the protocols trialed in order to achieve ENO3 and PKM2 knockout in OE33 cells

Optimisation Step	Result
Cell Seeding at 300,000 cells/well	✗
Cell Seeding at 200,000/well	✗
Cell Seeding at 150,000/well	✓
Transfection reagent HyPerfect	✗
Transfection reagent RNA-iMAX	✓

8.3.1.1 Relative expression of ENO3 and PKM2 in OE33 cells silenced for these genes

Targeted silencing of ENO3 and PKM2 for 24 hours in OE33 cells, revealed no difference in gene expression levels between the transfected groups and their relative scrambled RNA control groups, data not shown. A reduction of ENO3 (26%) was achieved at the gene level at 48 hours, when compared to the scrambled control ($p<0.05$, $n=3$ in each group) (Figure 8.2a). A 100% knockdown of ENO3 was achieved at 72 hours. There was no ENO3 expression detected in OE33 cells following 72 hours knockdown (Figure 8.2b). However, CT levels of 18S (endogenous control), were similar in both scrambled RNA control and siRNA groups (14.93 ±2.14 versus 12.74 ±1.19 respectively). PKM2 knockdown in OE33 cells showed a very similar result. A partial knockdown of PKM2 (27%) was achieved at the gene level following 48 hour silencing when compared to the scrambled control ($p<0.05$, $n=3$ in each group) (Figure 8.2c) and 100% knockdown of PKM2 was achieved at 72 hours. No PKM2 expression was detected in OE33 cells following 72 hours knockdown (Figure 8.1d). However, CT levels of 18S, were similar in both scrambled RNA control and siRNA groups (13.62 ±1.7 versus 13.12 ±2.17 respectively).

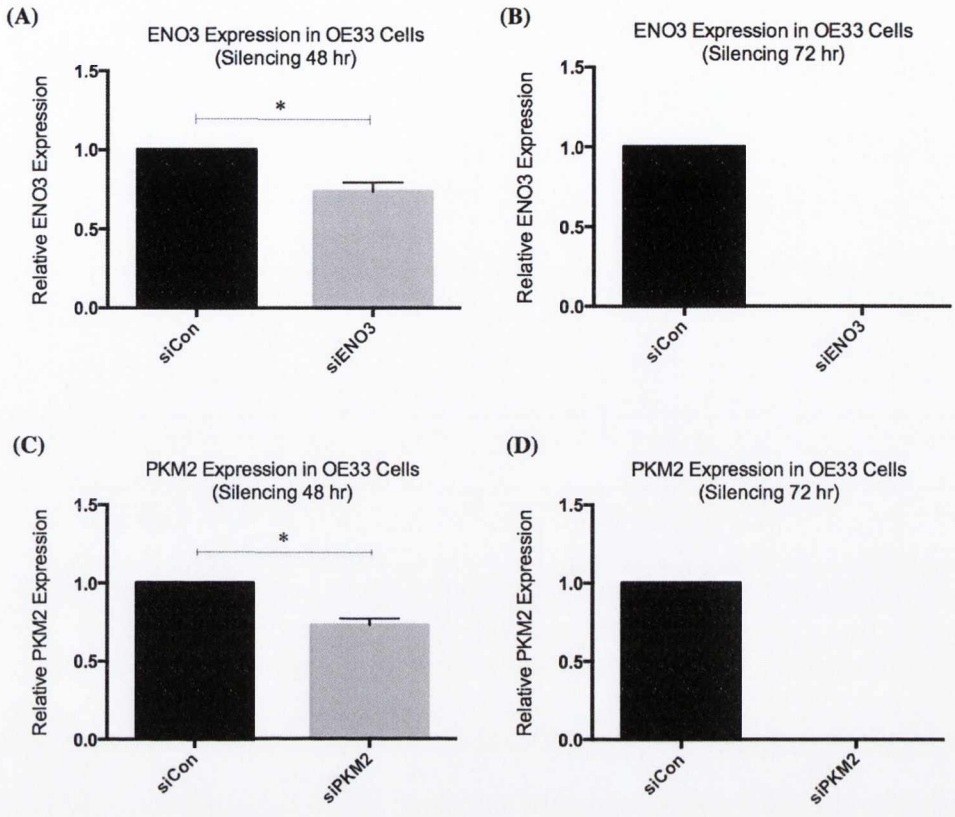


Figure 8.2 A 100% knock down knockdown of ENO3 and PKM2 gene expression in OE33 cells is achieved at 72 hours. Cells were reverse-transfected for ENO3 and PKM2, RNA was isolated at 24 hour, 48 hour and 72 hour time-points and relative gene expression was assessed by qPCR. Scrambled RNA control (siCon) was set to 1 and changes in ENO3 and PKM2 expression following gene transfection were calculated as fold change relative to siCon. There was no difference in ENO3 or PKM2 levels between scrambled control and gene silenced groups at 24-hour time-point (data not shown). (A) A partial, but statistically significant knockdown of ENO3, was achieved at 48 hours when compared to the scrambled control ($p<0.05$, $n=3$ in each group). (B) A 100% knock down of ENO3 was achieved at 72 hours. (C) A partial, but statistically significant knockdown of PKM2, was achieved in OE33 cells following 48-hour silencing when compared to its relative scrambled control ($p<0.05$, $n=3$ in each group). (D) A 100% knock down of PKM2 was achieved at 72 hours. Statistical test used was paired student t-test. $p<0.05$(*). Statistical analysis were not done for (C) and (D) due to the values being identical in each group. Error bar denotes mean ± S.E.M.

8.3.1.2 Assessment of ENO3 and PKM2 protein expression in OE33 cells following targeted transfection

Experimental set up used for silencing of ENO3 and PKM2 was described in the previous section. Protein was isolated from transfected OE33 cells at 48-hour and 72-hour time points. Protein concentration was measured by BCA assay (Section 2.15). 30 μg of protein was loaded per sample and the western blot procedure was performed as described in Section 2.17. Single bands at the expected molecular weight of 47 kDa were observed for ENO3 (Figure 8.3a) and 58kDa for PKM2 (Figure 8.3b). β-actin was used to normalize for total protein content and was observed at molecular weight of approximately 42 kDa. Western blot analysis for both, ENO3 and PKM2, validate the results from Section 8.3.1.1 where the relative expression of ENO3 and PKM2 in siRNA treated OE33 cells was measured at gene level.

A slight reduction of ENO3 was achieved following 10 nM siRNA treatment and a total a depletion of ENO3 was observed following 30 nM siRNA treatment at 48 hours, when compared to the scrambled control (Figure 8.3a). A 100% knock down of ENO3 was achieved at 72 hours following 10 nM and 30 nM siRNA treatments, compared to their scrambled RNA control (Figure 8.3a). A very similar level of PKM2 expression was observed following treatment with siRNA for 48 and 72 hours. A slight reduction of PKM2 was achieved following 10 nM siRNA treatment and a total a depletion of PKM2 was observed following 30 nM siRNA treatment at 48 hours, when compared to the scrambled control (Figure 8.3b). A complete knockdown of PKM2 was achieved at 72 hours following 10 nM and 30 nM siRNA treatments, compared to their scrambled RNA control (Figure 8.3b). Single bands of β-actin bands were observed at a molecular weight of approximately of 42kDa. The size of the β-actin bands were of a similar size indicating that the same amount of protein was loaded to all wells. The concentration of 10 nM siRNA and 72 hour time point were selected for further studies, because 10nM that achieved complete depletion of both ENO3 and PKM2.

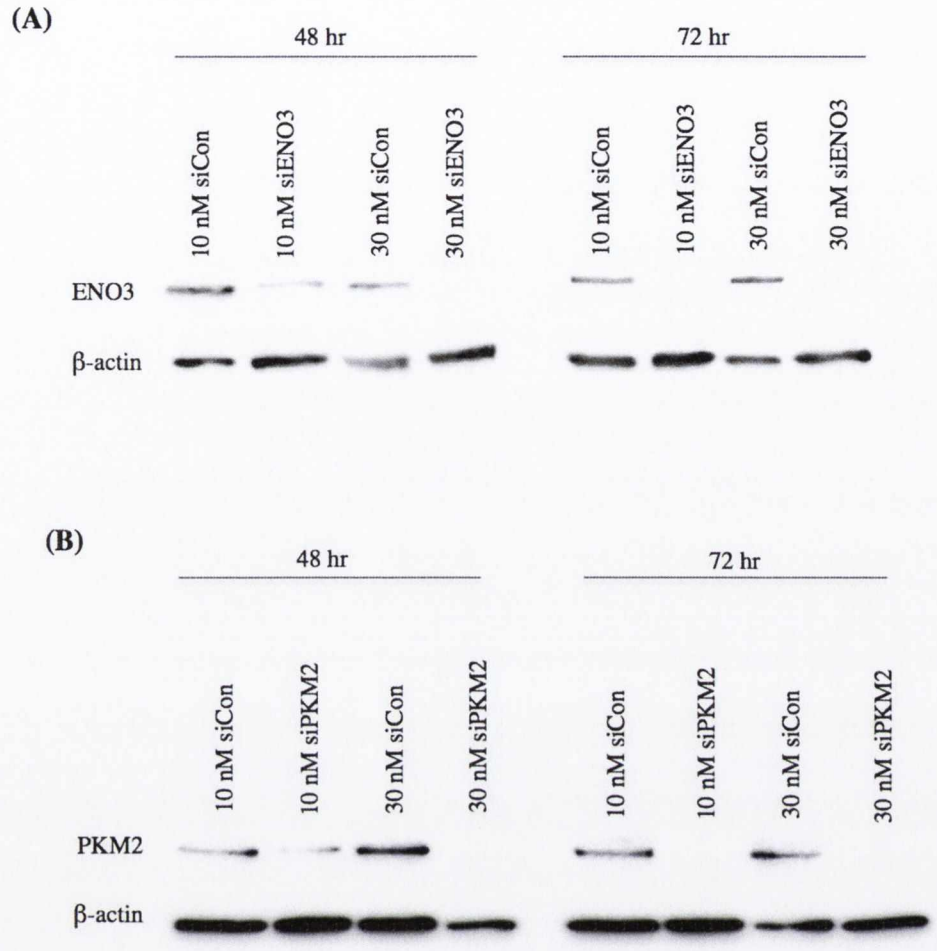


Figure 8.3 A 100% knockdown of ENO3 and PKM2 protein expression in OE33 cells is achieved at 72 hours. Cells were reverse-transfected for ENO3 and PKM2, protein was isolated at 48 hour and 72 hour time-points and protein levels in OE33 cells were assessed by Western Blot. (A) Western blot stained for ENO3 and β-actin showing the different time points and concentrations of siRNA and scrambled RNA control. Partial knockdown of ENO3 was achieved at 10 nM ENO3 at 48 hours and a 100% knock down of ENO3 was achieved at 30 nM siRNA treaetment at 72 hours. (B) Western blot stained for PKM2 and β-actin showing the different time points and concentrations of siRNA and scrambled RNA control. Partial knockdown of PKM2 was achieved at 10 nM PKM2 at 24 hours and a 100% knock down of PKM2 was achieved at 30 nM siRNA treatment at 72 hours.

8.3.2 Assessment of efficacy of novel small molecule inhibitors following silencing of ENO3 and PKM2 in OE33 cells

The xCELLigence™ RTCA DP (Real Time Cell Analyser Dual Plate) uses a 16-well E-plate to measure cell proliferation in real time. The well surface of the E-plate is covered by a layer of microelectrode sensors. When cells adhere and proliferate on the surface of each well, impedance signals are recorded by xCELLigence software. This platform offers a real time cellular assay to measure changes in cell proliferation in response to stimuli or inhibitors. We explored the use of this technology to assess the effect of ENO3 and PKM2 silencing in OE33 cells. We also tested ENO3 and PKM2 silenced cells in combination with ACM and two small molecule inhibitors: HS6 and NIH4.

OE33 cells were reverse transfected in T75 flasks for 72 hours and seeded into the 16-wel E-plate and the xCELLigence machine was set to record the impedance signals on the plate every 30 minutes. The rate of cell adherence and cell growth were determined by calculating the slope between two time points. The outline of the experiment can be seen in a representative image generated by xCELLigence software (Figure 8.4a). Cells were seeded, allowed to adhere (4-5 hours approximately) and serum depleted overnight (0.5% FBS/M199 media). Cells were treated directly into the wells of the E-plate at approximately 26-27 hours following seeding of cells and following the minimum 12 hours of serum depletion. Cell proliferation was recorded immediately following drug or ACM treatment and ceased after 72 hours or when a decline of cell proliferation was observed. Cell proliferation in OE33 cells treated with ACM and HS6 was only measured 60 hours due to a cell growth inhibition at that time point (Figure 8.4). Results indicate the utility of the xCELLigence platform to investigate the functional effect of novel inhibitors of 5LOX, ACM and the role of ENO3 and PKM2 in OE33 cell proliferation. The slope values calculated by the xCELLigence software as shown in Figure 8.4 indicate that ACM from 3 different patients induced OE33 cell proliferation and both novel inhibitors HS6 and NIH4 markedly reduced ACM-induced cell proliferation (Figure 8.4b and Figure 8.4c respectively). xCELLigence data in Figure 8.5 shows that ENO3 and PKM2 have a functional role in OE33 cell proliferation. Although very preliminary, the slope values calculated by the xCELLigence software indicate that silencing of ENO3, PKM2 and the combination of both, markedly reduce OE33 cell proliferative activity when compared to scrambled RNA control. Following transfection of ENO3 and PKM2,

ACM was still able to drive cell proliferation and treatment of transfected cells reduced ACM-induced cell proliferation to a similar extent like in OE33 cells that did not undergo transfection (Figure 8.4). Moreover, HS6 and NIH4 markedly reduced siENO3 and siPKM2 cell proliferation in the absence of ACM, but the inhibition of cell proliferation by HS6 and NIH4 was the greatest in OE33 cells with a combined ENO3 and PKM2 knockout (Figure 8.5a).

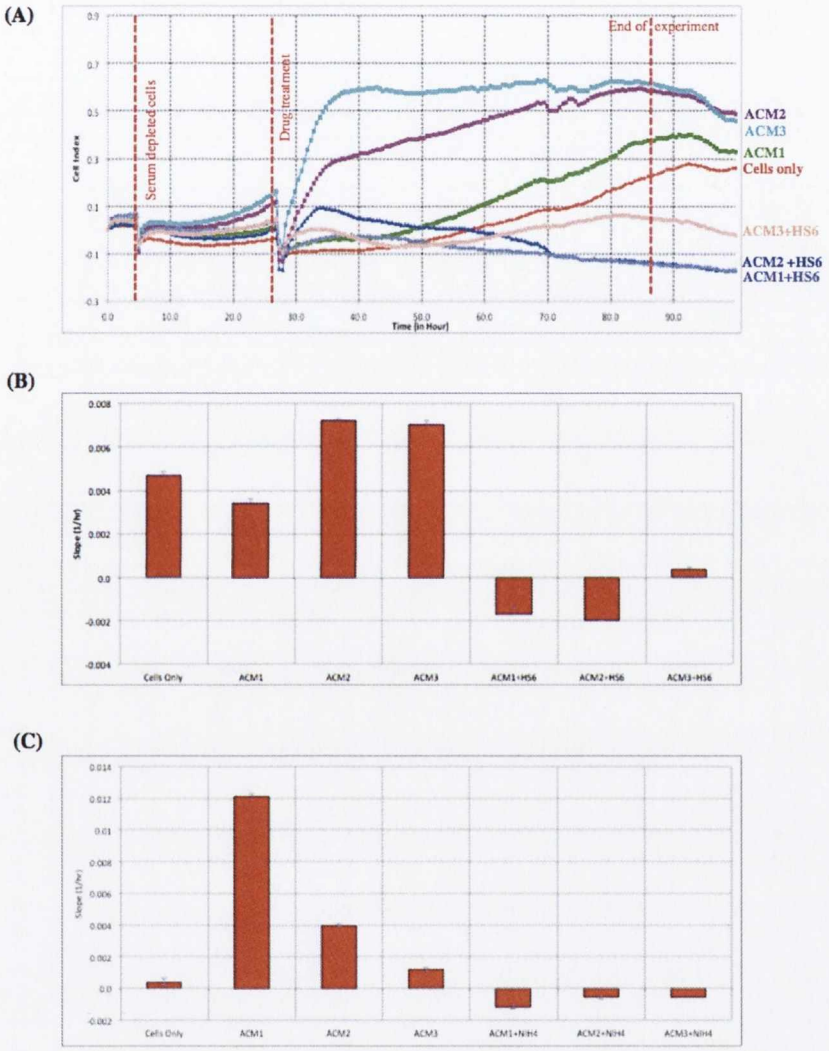


Figure 8.4 Preliminary results indicate the utility of the xCELLigence platform to investigate the functional effect of novel inhibitors of 5LOX treatment on OE33 cells. (A) OE33 cells were serum depleted and treatment was added before 30 hours as indicated in the xCELLigence raw data line graph. Data was normalized just after the drug treatment (i.e. Delta CI=1 for all treatment groups) and the rate of cell growth (i.e. slope) was calculated between 27-87 hours. (B) ACM from 3 different viscerally obese OAC patients induced OE33 cell proliferation and HS6 markedly reduced ACM-induced cell proliferation. (C) ACM from 3 different viscerally obese OAC patients induced OE33 cell proliferation and NIH4 markedly reduced ACM-induced cell proliferation. No statistical analysis was performed.

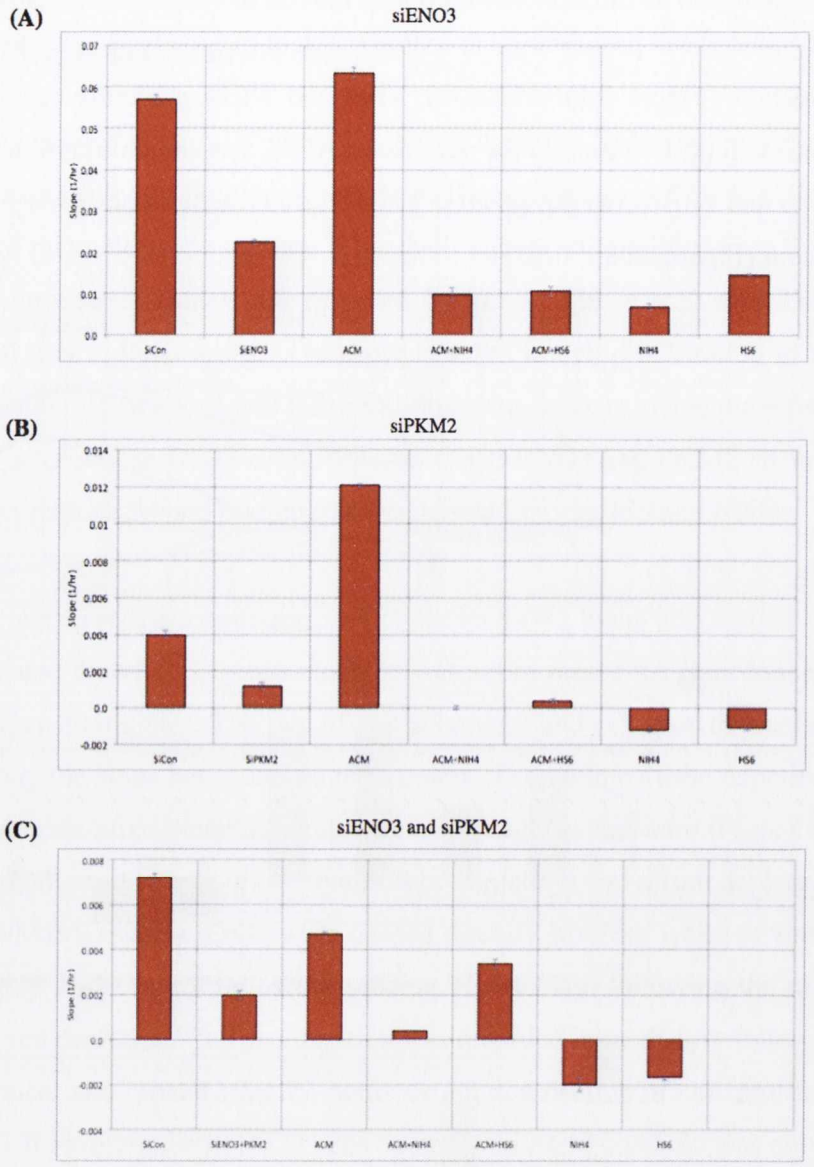


Figure 8.5 Preliminary results indicate the utility of the xCELLigence platform to investigate the functional effect of novel inhibitors of 5LOX treatment on OE33 cells following ENO3 and PKM2 knockout. ENO3, PKM2 and combination of both ENO3/PKM2 silenced cells were serum depleted and treatment was added before 30 hours. Data was normalized just after the drug treatment (i.e. Delta CI=1 for all treatment groups) and the rate of cell growth (i.e. slope) was calculated between 27-87 hours. The slope values calculated by the xCELLigence software indicate that (A) Silencing of ENO3, (B) PKM2 and (C) ENO3/PKM2, markedly reduce OE33 cell proliferative activity when compared to scrambled RNA control. Following transfection of ENO3 and PKM2, ACM was still able to drive cell proliferation and treatment of transfected cells reduced ACM-induced cell proliferation. (C) Inhibition of OE33 cell proliferation by HS6 and NIH4 was the greatest in OE33 cells with a combination ENO3 and PKM2 transfection. No statistical analysis was performed.

8.3.3 Assessment of ENO3 and PKM2 role in glycolysis *in vitro*

This experiment was performed using OE33 cells silenced for ENO3, PKM2 and the combination of both. Silencing of genes was achieved by siRNA treatment for 72 hours. A negative control was set up for each treatment, which utilized a scrambled RNA control. The reverse transfection procedure was described in more detail in Section 2.3.3. OE33 cells were transfected in T75 flasks and following 72 hour treatment were seeded Seahorse XFe24 analyser plates. The full experimental setup using Seahorse XFe24 analyser described in Section 2.18.4. We previously showed that 24-hour co-culture of OE33 cells with ACM from viscerally obese OAC patients induced glycolysis in the cells (Chapter 6). The aim of this experiment was to investigate whether silencing of ENO3, PKM2 and the combination of both, have an effect on glycolysis in OE33 cells. We also investigated the efficacy of novel inhibitors HS6 and NIH4 in target-transfected cells compared to RNA scrambled control cells. Each set of results contains data from at least three independent experiments. Following transfection of OE33 for ENO3 and PKM2, alongside to seeding the cells for Seahorse analysis, the level of gene knock out was measured by qPCR and 100% knock out was confirmed each time.

8.3.3.1 Assessment of ENO3 and PKM2 role in glycolysis *in vitro*

Following Seahorse Analyser XFe24 analysis, the ECAR reading for control cells treated with scrambled RNA control (siCon) were set to 100% and changes in glycolytic OE33 activity following transection with ENO3 and PKM2 were measured relative to siCon. Results showed that silencing of ENO3, PKM2 and the combination of both ENO3/PKM2, resulted in a significant reduction of glycolysis in OE33 cells when compared to scrambled RNA control treated cells (100% versus 63.17 ±2.903, 57.67 ±2.343 and 49.33 ±4.145 respectively, n=6 in each group, $p<0.0001$) (Figure 8.6). Moreover, there was a significant reduction in glycolysis in OE33 cells between cells silenced for ENO3 and cells silenced for ENO3/PKM2 (63.17 ±2.903 versus 49.33 ±4.145, n=6 in each group, $p<0.05$) (Figure 8.6).

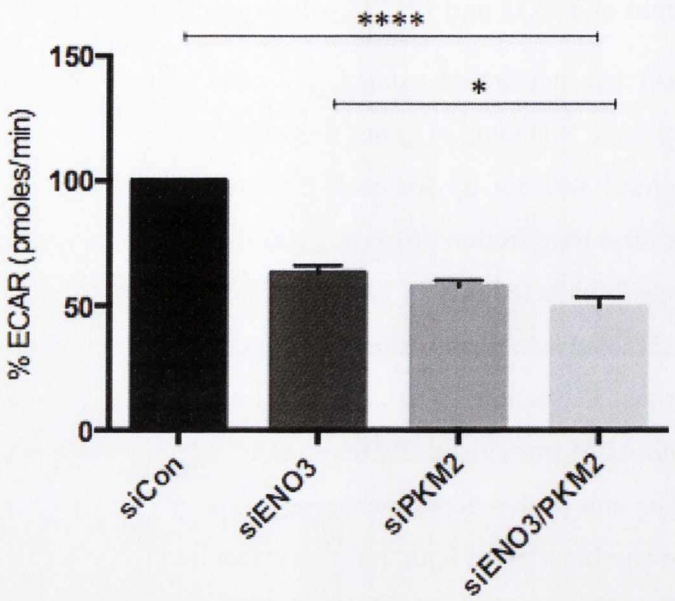


Figure 8.6 Silencing of ENO3 and PKM2 significantly reduces glycolysis in OE33 cells. Glycolysis in OE33 cells following silencing for ENO3 and PKM2 was measured by Seahorse Analyser XFe24 analyser. Changes in glycolytic OE33 activity following transfection was expressed relative to siCon. Results show that silencing of ENO3, PKM2 and the combination of both ENO3/PKM2, resulted in a significant reduction of glycolysis in OE33 cells when compared to siCon treated cells ($p<0.0001$, $n=6$). There was a significant reduction in glycolysis in OE33 cells between cells silenced for ($p<0.05$, $n=6$). Statistical test used was one-way ANOVA with Tukey's Multiple Comparisons Test: $p<0.05$ (*), $p<0.0001$ (****). Error bar denotes mean ±S.E.M.

8.3.3.2 Assessment of ENO3 and PKM2 role in ACM-driven glycolysis *in vitro*

ACM-induced glycolysis in OE33 cells in ENO3 and PKM2 transfected cells was measured by Seahorse XFe24 analyser. Changes in ACM-induced glycolysis was measured following transfection with siENO3, siPKM2 or the combination of both siENO3/siPKM2 were expressed relative to ACM treated siCon OE33 cells. Results show that silencing of ENO3, PKM2 and the combination of both ENO3/PKM2, resulted in a significant reduction of glycolysis in OE33 cells when compared to siCon cells treated with ACM (170 ±11.72 versus 110.1 ±4.301, 66 ±3.916 and 43.33 ±7.709 respectively, $n=6$ in each group, $p<0.0001$) (Figure 8.7). There was a significant reduction in ACM-induced glycolysis in OE33 cells between cells silenced for ENO3 and PKM2 (110.1 ±4.301 versus 43.33 ±7.709, $n=6$ in each group, $p<0.01$) and between cells silenced for ENO3 and the combination of ENO3 and PKM2 (110.1 ±4.301 versus 66 ±3.9, $n=6$ in each group, $p<0.0001$) (Figure 8.7).

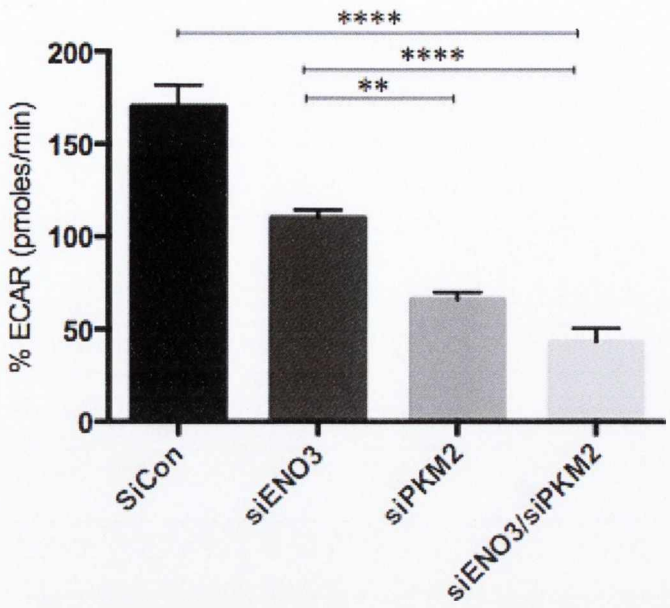


Figure 8.7 Silencing of ENO3 and PKM2 significantly reduces ACM-induced glycolysis in OE33 cells. ACM-induced glycolysis in OE33 cells following silencing for ENO3 and PKM2 was measured by Seahorse XFe24 analyser. Changes in glycolytic OE33 activity in transfected cells following 24-hour ACM treatment was expressed relative to siCon OE33 cells co-cultured with ACM. Results show that silencing of ENO3, PKM2 and the combination of both ENO3/PKM2, resulted in a significant reduction in ACM-induced glycolysis in OE33 cells when compared to ACM treated siCon OE33 cells ($p<0.0001$, n=6). There was a significant reduction in ACM-induced glycolysis in OE33 cells between cells silenced for ENO3 and PKM2 ($p<0.01$, n=6) and cells silenced for ENO3 and the combination of both ENO3 and PKM2 ($p<0.0001$, n=6). Statistical test used was one-way ANOVA with Tukey's Multiple Comparisons Test: $p<0.01$ (**), $p<0.0001$ (****). Error bar denotes mean ±S.E.M.

8.3.3.3 Effect of novel inhibitors of 5LOX on glycolysis in OE33 cells following transfection of ENO3, PKM2 and the combination of both ENO3 and PKM2

Results from the previous section showed that silencing of ENO3 and PKM2 in OE33 lead to a significant reduction in glycolysis in OE33 cells. In this part of the study the aim was to delineate whether silencing of ENO3 and PKM2 had an effect on the efficacy of the two novel inhibitors: HS6 and NIH4. The experimental set-up was identical to the one described in the previous Section 6.3.3, with the addition of the inhibitors in this part of the study. Glycolytic activity in the cells was measured by Seahorse XFe24 analyser. Effect of ACM and NIH4 on glycolysis in OE33 cells was compared between the cells treated with scrambled RNA control (siCon) and between the cells with siRNA. NIH4 reduced glycolysis in OE33 cells treated with scrambled RNA control ($p<0.05$) however had no significant effect on siENO3 transfected OE33 cells ($p=0.6211$). Co-culture of

cells with ACM from viscerally obese OAC patients significantly induced glycolysis in OE33 cells treated with siCon, however the ability of ACM to induce glycolysis was lost in PKM2 transfected cells ($p<0.0001$ and $p=0.645$). NIH4 significantly reduced ACM-induced glycolysis in siCon treated OE33 cells ($p<0.0001$), however, the ability of the inhibitor to reduce ACM-induced glycolysis was lost in siENO3 transfected cells ($p=0.981$). The effect of NIH4 and HS6 on glycolysis was assessed in ENO3, PKM2 and ENO3/PKM2 –silenced cells and the results were very similar following knockout of all genes (data shown in Appendix VIII). An upregulation of a pathway, in this case glycolysis, was required in order for the inhibitors to have a biological effect.

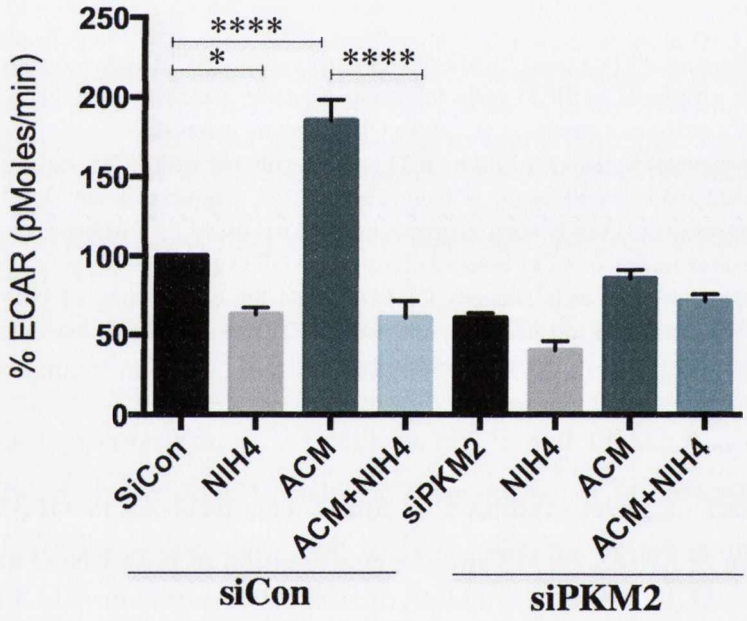


Figure 8.8 Effect of ACM and HIH4 on glycolytic activity in OE33 cells following transfection of ENO3, PKM2 and the combination of both. Following 72 transfection with 10 μM siRNA, treatment OE33 cells were seeded into the Seahorse XFe 24 plates and treated with 10 μM dose of NIH4. , Glycolytic activity in the cells was measured by Seahorse XFe24 analyser. Effect of ACM and NIH4 on glycolytic OE33 cell activity was compared within cells treated with scrambles RNA control (siCon) and cells with siRNA. (A) NIH4 reduced glycolysis in OE33 cells treated with scrambled RNA control ($p<0.05$) however had no significant effect on siENO3 transfected OE33 cells ($p=0.6211$). ACM significantly induced glycolysis in OE33 cells treated with siCon and in siENO3, however the ability of ACM to induce glycolysis was significantly reduced in siENO3 transfected cells ($p<0.0001$ and $p=0.645$ respectively). NIH4 significantly reduced ACM-induced glycolysis in siCon treated OE33 cells ($p<0.0001$), however, the inhibitor had no biological effect due to the glycolysis reduction in OE33 cells following silencing of PKM2 ($p=0.981$).

8.4 Discussion

It has been widely documented that cancer cells use metabolic reprogramming for their growth and survival [322]. Rapidly proliferating cancer cells favor incomplete glucose metabolism, producing large amounts of lactate to sustain cell growth [407]. In published studies, ENO3 and PKM2 expression has been reported to be upregulated in many cancers [408, 409]. In this study, we had previously shown that ENO3 and PKM2 gene expression was significantly higher in tumor from viscerally obese compared to non-obese patients, and epithelial protein expression of both ENO3 and PKM2 was significantly higher in obese compared to normal weight patients (Chapter 4). Therefore, we hypothesized that these two enzymes were associated with obesity-driven OAC cancer. The aim of this study was to investigate the role of ENO3 and PKM2 in OAC cancer *in vitro* by silencing approach.

In this study, we successfully silenced ENO3 and PKM2 in esophageal adenocarcinoma cell model (OE33 cells) by reverse transfection. Firstly, we investigated the role of the two genes in OE33 cell proliferation in real time, using the xCELLigence platform. Although very preliminary, data showed that silencing of ENO3 and PKM2 markedly reduced cell proliferation. Following treatment of OE33 cells with ACM from viscerally obese OAC patients, proliferation of ENO3 and PKM2 transfected cells was markedly increased. However, the ability of cells to proliferate was decreased in the cells where the combination of both genes was silenced. Moreover, novel inhibitors HS6 and NIH4, markedly reduced proliferation of cells where ENO3 and PKM2 were silenced. Additionally, proliferation of OE33 cells was further reduced following HS6 and NIH4 treatment following the silencing of combination of both genes. This result was supported by a the previous study by Goldberk *et al* where silencing of PKM2 has been shown to reduce cell proliferation and induce apoptosis in vitro in a number of cancers, including brain, breast, colon, lung, ovarian, renal, and skin [406].

Following investigation of ENO3 and PKM2 role in cell proliferation, we investigated whether silencing of the two genes had an effect on glucose metabolism in OE33 cells. Seahorse XFe24 analysis revealed that silencing of ENO3, PKM2 and the combination of both ENO3 and PKM2 in OE33 cells, resulted in a significant reduction of glycolysis

in the transfected cells when compared to scrambled RNA treated cells. Following the proof that silencing of the two genes results in reduce glycolytic activity in OE33 cells, we investigated whether silencing of the two genes reduce ACM-induced glycolysis in OE33 cells. OE33 cells transfected for ENO3, PKM2 and the combination of both, were co-cultured with ACM prior Seahorse XFe24 analysis. Results showed that silencing of ENO3, PKM2 and the combination of both ENO3 and PKM2, resulted in a significant reduction in ACM-induced glycolysis in OE33 cells when compared to ACM treated cells that were transfected with silencing control. There was also a significant reduction in ACM-induced glycolysis in OE33 cells between the cells silenced for ENO3 and PKM2 versus the cells silenced for the combination of both genes. Since PKM2 has been shown to be the key enzyme catalyzing the final step of glycolysis [269], we already hypothesized that silencing of the gene should potentially reduce glycolysis in esophageal cancer *in vitro*. However, the finding that glycolysis was further reduced following transfection of PKM2 in combination with ENO3 was novel.

In summary, ENO3 and PKM2 have a positive association with proliferation and glycolysis in esophageal adenocarcinoma cells *in vitro*. Targeting of multiple genes in combination, suggest a potential benefit to achieve a greater targeted response. ACM from viscerally obese OAC patients have a positive association with proliferation and glycolysis in OE33 cells. Targeting multiple genes in combination in obese esophageal adenocarcinoma patients, suggest a potentially better targeted response. Additionally, it would be beneficial to investigate whether PKM2 and ENO3 contribute to OAC invasiveness. Same experimental set up and xCELLigence migration plates could be used to determine whether ACM induces OE33 migratory capacity, what is the optimum time for ACM to induce cancer cell migration and whether silencing of ENO3 and PKM2 genes in OE33 cells result in changes in cell migration and invasiveness. It would be beneficial to determine whether silencing the combination of both genes have a greater effect on OE33 cell migratory capacity rather than silencing them individually.

Chapter 9

Concluding Discussion

9.1 Concluding discussion

In recent years, there has been a dramatic increase in the incidence of esophageal adenocarcinoma, with the second and third highest rates in Europe in males and females respectively. Despite major improvements to patient outcomes through improved CRT regimes, fewer than 20% of esophageal cancer patients survive longer than 5 years following their diagnosis.

Current research predominantly shows that obesity can alter tumor metabolism [410], therefore is associated with poor prognosis in esophageal adenocarcinoma [411]. In published studies, metabolically active fat has been reported to produce and secrete inflammatory cytokines by adipocytes or infiltrating macrophages [146, 412]. Therefore adipose tissue, visceral fat in particular, is an important initiator of the microenvironment favorable for tumor development [146].

This study showed a potential link between obesity and poor prognosis in esophageal adenocarcinoma. We found that the glucose transporter protein GLUT4 and glycolysis associated enzymes HK2, PKM2 GAPDH and ENO3 were all significantly higher in treatment-naive OAC tumor biopsies from viscerally obese compared to non-obese patients, suggesting that glycolysis is upregulated and a more active process in obese OAC patients. Following an immunohistochemical study, 5LOX epithelial expression was also significantly higher in overweight and obese OAC patients, in OAC tissue microarrays, showing elevated 5LOX in obese OAC patients at gene and protein level. In published studies, obesity has been linked with poor prognosis in esophageal cancer [330].

In the OAC patient cohort, with the obesity status based on BMI measurement, Kaplan Meier survival analysis revealed that individuals expressing high levels of GLUT4, HK2 and GAPDH were associated with poor 5-year post-operative OAC-specific survival. This suggests that the epithelial expression of the glucose transporter protein GLUT4 and the markers of glycolysis HK2 and GAPDH are associated with poor outcome in OAC patients. The expression of glucose transporter proteins and markers of glycolysis was also used to assess 5-year disease specific survival in a newly constructed cohort of OAC tissue microarrays, however there were no significant findings recorded. This may be due to a small sample size of only 46 patients. Moreover, due to recent OAC tumor samples

used for the construction of these tissue microarrays, for many of the patients the follow-up and the survival data was only available for up to 3 years. The lack of long-term observation might have contributed to the non-significant correlations between metabolic parameters and survival.

Published studies show HIF1A to be a major regulator of anaerobic metabolism. In the hypoxic environment, there is a shift from aerobic to anaerobic metabolism, in order to facilitate cellular energy production [236]. HIF1A has been shown to be a principal gene coordinating this shift, by inducing a number of glucose transporters and glycolytic enzymes [276]. We showed a significant association between HIF1A and obesity. HIF1A was expressed at significantly higher levels in OAC tumours from viscerally obese compared to non-obese patients. Additionally, epithelial HIF1A was higher in overweight and obese compared to non-obese OAC patients in OAC tissue micro arrays stained for HIF1A. Its expression was significantly higher in non-leading edge (NLE) of tumor than in the more vascularized leading edge (LE). Published studies show, that oxygen levels, blood and nutrient supply are lower in the core of the tumor compared to the surrounding tissues [302]. High HIF1A expression was also significantly associated with nodal and venous involvement suggesting its role in tumor aggressiveness. Most importantly, high epithelial HIF1A expression was significantly associated with significantly reduced 5-year disease-specific survival in the cohort of OAC patients where the obesity status is based on BMI measurement. Our findings are in line with other published studies in other cancer types, for example, an immunohistochemical study by Baba *et al* where the link between HIF1A and poor disease prognosis was shown in 731 colorectal cancer patients and HIF1A expression was significantly associated with shorter disease-specific survival and overall survival [313].

Additionally, this study showed that a potential link between obesity and an increase in EMT. We showed a significantly higher expression of SNAI1, SNAI2 and MMP9 and a significantly lower level of β-catenin in the tumor of overweight and obese compared to normal weight OAC patients. Downregulated β-catenin levels are consistent with activation of EMT. Activation of EMT has been previously shown to result in a poor prognosis of the disease, by facilitating cancer metastasis [339]. Although there was no significant difference between the 5 year disease specific survival of overweight and obese versus normal weight OAC patients observed in immunohistochemical study,

Kaplan Meier analysis indicated that individuals with lover levels of these adhesion molecules had a trend towards the lower probability of survival. Higher expression of genes coding for SNAI1, SNAI2 and MMP9 suggest a positive association with higher metastatic potential and poor prognosis [173, 326]. This suggests that overweight and obese individuals are at higher risk of tumor metastasis and poor prognosis. Obesity status for the OAC patients used in the tissue microarray study was determined by BMI. This simple index of weight-for-height is commonly used to assess obesity, however, it is not an accurate measurement of abnormal or excessive fat accumulation. BMI measurement does not distinguish fat mass from lean body mass components. This was an important limitation of the study, because the distribution of fat tissue differs greatly between individuals [343], and we were interested in viscerally obese patients in particular. In order to have a better insight of the impact of visceral obesity in OAC, we constructed a new cohort of OAC tissue microarrays with obesity status of the patients based on the VFA. Gender-specific threshold level of VFA of $\geq$163.8 cm^2 for men and $\geq$80.1 cm^2 for women as previously determined by Doyle *et al* [310]. GLUT4, HK2 and GAPDH levels were significantly higher in epithelium of obese compared to non-obese OAC patients. This was an important result indicating a strong link between visceral obesity in this cohort of patients, because significant levels of expression were observed in a small population of only 46 subjects. Epithelial expression of 5LOX was markedly higher in obese compared to non-obese OAC patients, but failed to reach significance. However, we seen a significant positive correlation between the increasing levels of 5LOX and increasing VFA measurement. Epithelial 5LOX expression was previously significantly positively correlated with increasing BMI is OAC patients, however, a positive correlation of expression with VFA indicates a strong association with visceral obesity rather than obesity as a whole.

Following the study investigating the link between obesity and glycolysis, hypoxia and 5LOX, we investigated whether there is a link between the expression of those markers and metabolic tumor activity. Following grading of OAC tissue microarrays and correlating the data with SUVmax and MTV we observed an association between glucose transporter proteins, markers of glycolysis and 5LOX and tumor metabolism in OAC. Epithelial GLUT4 and HK2 expression was positively correlated with SUVmax, suggesting that metabolically active tumours express higher levels of these markers. A positive association between epithelial GAPDH expression and SUVmax was also

observed, however this just failed to reach significance. This result indicates that metabolically active tumours express higher levels of GAPDH in this cohort of OAC patients. In the newly constructed cohort of OAC tissue microarrays (obesity status based on VFA), we observed that high epithelial ENO3 expression was positively associated with high SUVmax. Strong epithelial GAPDH expression was significantly correlated with high metabolic tumor volume, supporting the data from the previous cohort of patients, where an increase in epithelial GAPDH expression was positively associated with high SUVmax but failed to reach significance. This data suggested a higher expression of GAPDH to be present in a potentially more aggressive tumor phenotype. A study published by Seol *et al* shows a significant decrease in MTV in response to therapy in SCC [354], suggesting a correlation between a decreasing MTV and less aggressive tumor. We conclude that SUVmax may be a potential predictor of the level of metabolic tumor activity in OAC. Additionally, GLUT4, HK2, ENO3 and GAPDH may be used as potential markers to determine the level of metabolic activity of OAC tumor.

In the past decade, an increasing proportion of cancer research has focused on the development of molecular therapies that target tumor-dependent processes such as tumor cell growth, in order to complement standard treatment regimen (671). We already demonstrated that 5LOX expression was associated with visceral obesity in OAC at both gene and protein level, in two different cohorts of OAC patients, therefore, we hypothesized that 5LOX may be an attractive druggable target in OAC. Since the expression of 5LOX in OE33, esophageal adenocarcinoma cells, was previously confirmed at mRNA and protein level in the department, we used this cell model to carry out *in vitro* screening. We selected two novel inhibitors of 5LOX, NIH4 and HS6, for this part of the study. We confirmed that HS6 and NIH4 were active inhibitors of 5LOX by measuring the endogenous production of LTB4 in tissue conditioned media (TCM) from OAC tumor explants, following 24-hour culture of 10 treatment-naive OAC biopsies. NIH4 significantly decreased secreted levels of LTB4 (a metabolite of 5LOX), following 24-hour culture of OAC tumor with this inhibitor, and HS6 decreased LTB4 secretion by OAC tumours following 24-hour culture, however, statistical significance was not reached. In another preliminary study carried out by an independent group in Trinity College Dublin, HS6 was shown to have anti-5LOX activity in breast cancer cells, therefore, it was selected alongside NIH4 for further analysis.

Results showed that the two novel 5LOX inhibitors, HS6 and NIH4, were more effective at reducing cell viability, proliferation and glycolysis in OE33 cells when compared to other commercially inhibitors of 5LOX, such as Zileuton. This was a significant finding because Zileuton is the only inhibitor of 5LOX approved by the FDA, approved for use in asthma. Other inhibitors of 5LOX, such as REV5901, MK886 and Ketoconazole, all reduced the viability and proliferation of OE33 cells at very similar IC_{50} values. Following the measurement of glycolysis in OE33 cells by Seahorse XFe24 analyser, it was clear that inhibition of 5LOX with the commercial inhibitors significantly reduced tumor glycolysis. Notably, while zileuton did not have an effect on glycolysis, the novel 5LOX inhibitors, HS6 and NIH4, were more superior then other commercially available inhibitors of 5LOX. The novel inhibitors not only significantly reduced ECAR levels following 24-hour treatment, but the reduction was significantly greater following treatment of OE33 cells in the presence of ACM, suggesting that the novel inhibitors are potentially more superior in reducing obesity-driven glycolysis in OAC. Following the finding that HS6 and NIH4 may be potentially more effective in reducing obesity-induced glycolysis in OE33 cells, we showed that alterations in glycolytic OE33 cell activity by the novel inhibitors of 5LOX were further affected by oxygen depletion (0.5% O_2). NIH4 was significantly more effective in reducing glycolysis in OE33 and in the cells with ACM-induced glycolysis, under hypoxic (0.5% O_2) conditions. This result was supported by a recent study by Gonsalves *et al* where 5LOX induction was shown to be associated with hypoxia [384]. It was shown that hypoxia mediates the expression of 5LOX activating protein (FLAP), a key enzyme in leukotriene formation in human pulmonary microvascular endothelial and human brain endothelial cells [384].

Following *in vitro* studies confirming that the novel inhibitors of 5LOX were more effective than commercially available compounds in reducing ACM-induced glycolysis, we used Human Glucose Metabolism and RT^2 Profiler PCR Arrays in order to assess efficacy of the two inhibitors in altering genes associated with glucose and glycogen metabolism. Following treatment of OE33 cells with HS6 and NIH4 in the presence and the absence of ACM and measuring glucose metabolism associated gene expression, we discovered a number of genes altered by ACM and the two drugs. We showed that ACM was responsible for upregulation of 71% of glucose metabolism associated genes present on Human Glucose Metabolism RT^2 Profiler PCR Array. ACM-induced glucose metabolism-associated gene induction once again suggests a positive link between

obesity and glycolysis in OAC. Additionally, NIH4 showed a significant reduction of 22 (26.19%) of glucose metabolism associated genes when used in combination with ACM and compared to ACM only treated OE33 cells. A panel of 10 genes that showed the most significant upregulation following treatment of cells with ACM and the greatest reduction following drug treatment, were selected for further validation. In the validation study, OE33 cells were treated with ACM from 5 different viscerally obese OAC patients and compared to media only treated control, in the presence and the absence of ACM. The levels of ENO3, PGM2 and PDK1 were significantly higher in OE33 cells following 24-hour co-culture with ACM. 24-hour treatment of OE33 cells with NIH4 in the presence of ACM, significantly reduced expression of the genes compared to ACM only treated cells. Therefore the validation analysis confirmed that ENO3, PGM2 and PDK1 were upregulated by obesity (ACM from viscerally obese OAC patients) and that the novel inhibitor of 5LOX, NIH4, was able to reduce this ACM upregulated glycolysis. This result suggests once again that 5LOX is an attractive potential target in order to reduce glycolysis in OAC.

A published study by Miyazono *et al* showed that mitochondrial function is altered in Barrett's oesophagus and suggests an important role in the subsequent progression to OAC [413]. Mutations in the mtDNA D-loop region have been shown to occur frequently in OAC supporting the hypothesis that oxidative damage might be a mechanism for the induction of OAC [414, 415]. In this study, we used Human Mitochondrial Metabolism RT^2 Profiler PCR Arrays in order to investigate whether ACM alters human mitochondrial function and whether novel inhibitors of 5LOX were able to reverse these ACM-caused alterations. Results showed that treatment of OE33 cells with ACM from viscerally obese OAC patients, upregulated 73.8% human mitochondrial metabolism associated genes in the human mitochondrial metabolism array. Treatment of cells with NIH4, reduced 11.9% mitochondrial metabolism associated genes when used in combination with ACM and compared to ACM only treated OE33 cells. Consequently, in the validation study, reduction of Complex III associated COX5B and COX6C levels following 24-hour treatment of OE33 cells with NIH4 were validated in OE33 cells ($p<0.05$), suggesting a potential role of NIH4 in altering glucose metabolism in OAC. Published studies show, that alterations in Complex III are linked with breast, colorectal and ovarian cancers [369, 416], therefore, NIH4 may be a novel inhibitor of interest to target mitochondrial energy metabolism in OAC.

Following proof that NIH4 was able to reverse ACM-induced glycolysis and alterations in mitochondrial metabolism, an *ex vivo* study was set up to delineate which oncogenic genes in particular were altered by the novel inhibitors of 5LOX. We explored the effect of 5LOX inhibition on pro-tumourigenic secretions by OAC tumor biopsies cultured *ex vivo,* by Proseek® Multiplex Inflammation I and Oncology II ^{96x96} immunoassays. The use of *ex vivo* samples are more superior than the usage of *in vitro* models, as *in vitro* models are not representative of the heterogeneity of an *in vivo* tumor. Therefore, the *ex vivo* tumor biopsy culture model provided us with a unique opportunity to study the effect of novel 5LOX inhibitors in OAC tumor cells and intact peritumoural stroma. The immune assay experiment consisted of small number of biopsies (5 for each treatment group), a number of significant or alterations showing a positive trend, even though not reaching the statistical significance, were observed. This study provided us with some insight into the molecular pathways altered by novel inhibitors of 5LOX. HS6 did not appear to alter pro-tumourigenic protein secretion *ex-vivo*, however, treatment of OAC tissue with NIH4, was found to significantly decrease secreted levels of VEGFA, TGF-alpha, SCF, MCP3, WISP1, CTSV, ESM-1 and CYR61 in OAC tumor. An additional 23 secreted protein markers in INF panel and 28 secreted proteins in ONC2 panel were lower in TCM following 24-hour biopsy treatment with NIH4, however, failed to reach statistical significance. We propose that statistical significance was not reached due to small sample size and sample heterogeneity. The eight significantly altered markers following treatment of tumor with NIH4, were recorded to be altered in various cancers and inflammation-related conditions. For example, VEGFA, TGF-alpha and SCF levels were measured in both INF and ONC2 panels and the secretion levels of all three proteins were significantly reduced following NIH4 treatment in both panels. VEGFA, a growth factor, has been previously shown to induce endothelial cell proliferation, promote cell migration, to inhibit apoptosis and to induce permeabilization of blood vessels. Additionally, VEGFA has been shown to be involved in inflammation-related diseases such as IBD, rheumatoid arthritis and neuroinflammation [386, 417, 418]. Similarly, secreted levels of TGF-alpha, the second growth factor expression, were downregulated following 24-hour OAC biopsy treatment with NIH4. Published studies show TGF-alpha to be overexpressed in inflammation-related diseases such as IBD, hepatitis C, Crohn's disease [386, 419, 420], and high expression of TGF-alpha is observed in cancers such as breast [20], colorectal [389] and head and neck [390]. NIH4 significantly reduced OAC tumor secreted SCF levels. Published studies show SCF to be a mediator of many

biological functions including carcinogenesis [391]. Esposito *et al* investigated the role of SCF in pancreatic cancer and concluded that pancreatic cancer cells may have the capacity to recruit mast cells to the tumor mass via SCF production and thereafter, mast cells might potentially initiate tumor invasion and angiogenesis through their effects on the extracellular matrix [392]. Following this finding by Esposito *et al* we looked whether mast cell recruitment or their density had an effect on the outcome of the disease in esophageal cancer. Elpek *et al* showed that mast cell density (MCD) was positively associated with the depth of wall invasion, lymph node metastasis, and tumor progression in esophageal SCC, suggesting that MCD may have a role in the angiogenesis of these tumours and might be responsible for their aggressive behavior [393]. Therefore, targeting SCF may potentially reduce mast cell recruitment into the tumor mass. NIH4 also reduced secretion of a number of pro-inflammatory and pro-tumourigenic proteins including MCP3, WISP1, CTSV, ESM-1 and CYR61 in OAC tumor, once again suggesting a potential role as anti-inflammatory and anti-cancer agent.

To conclude, results from Inflammation I and Oncology II multiplex immunoassay suggests that NIH4 exhibits anti-inflammatory and anti-tumourigenic effects by downregulating a number of growth factors, cytokines, pro-inflammatory and pro-tumourigenic factors.

Following investigation of the NIH4-altered genes in the Inflammation I and Oncology II panel, we selected VEGFA for validation in a larger number of samples. The samples included 10 sets of TCMs (TCM from pre-treatment OAC biopsies treated with media alone, HS6 or NIH4). 5 out of 10 sets of TCMs were the same samples used for Olink Oncology II immunoassay and 5 sets of brand new TCMs, prepared under identical set up as the original 5 sets of samples. Olink immunoassay results were successfully validated by VEGFA sandwich ELISA. Secreted VEGFA levels were significantly lower in TCM from OAC biopsies treated with NIH4 compared to media only treated control. Successful validation of the marker confirms that the Olink Oncology II immunoassay provided us with accurate and reproducible data.

Utilizing the same 10 *ex vivo* samples (TCM) showed a positive association between the levels of LTB4 and VEGFA, suggesting a potential role of 5LOX in more aggressive disease phenotype. Moreover, a positive association between tumor-secreted levels of the metabolite of 5LOX (LTB4) and VEGFA in TCM from OAC biopsies following

treatment with NIH4, once again indicate the efficacy of NIH4 in targeting. VEGF, which is associated with poor prognosis is esophageal cancer [421].

In the final chapter of this study, we investigated the efficacy of novel inhibitors NIH4 and HS6, following silencing of genes associated with glycolysis in OAC. Published studies predominantly show that cancer cells use metabolic reprogramming in order to proliferate and survive [407]. Rapidly proliferating cancer cells have been show to favor incomplete glucose metabolism, producing large amounts of lactate to sustain cell growth [407]. In published studies, ENO3 and PKM2 expression has been documented to be upregulated in many cancers [409]. We had previously shown that high ENO3 and PKM2 gene expression was significantly higher in tumor from viscerally obese compared to non-obese OAC patients. Following immunohistochemical study of 120 OAC patients, we also reported significantly higher epithelial expression of ENO3 and PKM2 in tumor from obese compared to normal weight patients. Therefore, we hypothesized that these two enzymes were associated with obesity-driven OAC cancer and that the novel inhibitors would revert OAC-induced glycolysis. We successfully silenced ENO3 and PKM2 in OE33 cells by reverse transfection, treated the cells with media alone, inhibitors alone or inhibitors in the presence of ACM and ACM alone, and showed cell proliferation in real-time. Firstly, we showed that silencing of ENO3 and PKM2 markedly reduced cell proliferation. Following treatment of OE33 cells with ACM from viscerally obese OAC patients, proliferation of ENO3 and PKM2 transfected cells was markedly increased. Moreover, the ability of cells to proliferate was decreased in the cells where the combination of both genes was silenced in OE33 cells. Novel inhibitors HS6 and NIH4, markedly reduced proliferation of cells in which ENO3 and PKM2 were silenced. Proliferation of OE33 cells was further reduced following HS6 and NIH4 treatment following the silencing of combination of both genes. This result was supported by a the previous study by Golberk *et al* where silencing of PKM2 has been shown to reduce cell proliferation and induce apoptosis in vitro in a number of cancers, including brain, breast, colon, lung, ovarian, renal, and skin [406]. Following delineation of ENO3 and PKM2 role in cell proliferation, we showed that silencing of the two genes has an effect on glycolysis in OE33 cells. Seahorse XFe24 analysis revealed that silencing of ENO3, PKM2 and the combination of both, resulted in a significant reduction of glycolysis in the transfected cells when compared to scrambled RNA treated cells. This experiment was repeated only three times, and due to the nature of the experiment (measuring glycolysis in live cells results in large variability between independent experiments) and

observed a significant result, we suggest a strong link between ENO3 and PKM2 and glycolysis in OAC. Following the findings that silencing of the two genes results in reduce glycolytic activity in OE33 cells, we showed that silencing of ENO3 and PKM2 in combination, prevents ACM-induced glycolysis in OE33 cells. Since published studies report PKM2 to be the key enzyme catalyzing the final step of glycolysis, we hypothesized that silencing of PKM2 should potentially reduce glycolysis in esophageal cancer *in vitro*. We proved the hypothesis, however, the finding that glycolysis was further reduced following transfection of PKM2 in combination with ENO3 was novel.

In conclusion, in this thesis we showed that glycolysis, hypoxia and 5-lipoxygenase are involved in OAC and are associated with obesity. High expression of markers of glycolysis, hypoxia and 5LOX are associated with more aggressive cancer type and poor OAC-specific survival. Assessment of novel 5LOX inhibitors in both *in vitro* and *ex vivo* models of OAC have indicated the involvement of these pathways in the regulation of cell growth and survival. It is important to note that all statistical analysis in this study were performed using univariate analysis, therefore, significant association between glycolysis, OXPHOS, hypoxia and 5-lipoxygenas, obesity and overall outcome of the disease addressed in this study was seen using univariate analysis. Relationship between variables will need to be taken in consideration and multivariate analysis will need to be performed in order to get more realistic picture and strengthen the data. However, based on univariate data, we suggest that targeting 5LOX may be a therapeutic strategy in the treatment of OAC, particularly in respect to glycolysis. Further studies are required to determine whether 5LOX are preferentially expressed in early or later stages of the disease, and at what point of the disease targeting this enzyme would be the most efficacious.

9.2 Future directions

In this project we have shown a number of associations between 5LOX expression and OAC. We have shown the link between epithelial 5LOX expression and its link to obesity, and poor OAC-specific survival. We have also shown that higher expression of 5LOX was observed in tumor from obese OAC patients, once again suggesting the link between 5LOX and obesity in OAC. While 5LOX immune regulation has been previously investigated in asthma, COPD and cancer, it has not been investigated in OAC. Following the Olink Oncology II immune assay results and indication that novel inhibitor of 5LOX have a potential anti-inflammatory effects, future studies should concentrate on delineating the link between 5LOX and inflammation. Isolation of immune cells from digested OAC tumor and adipose tissue and investigation whether they have 5LOX activity and respond to 5LOX treatment, would be beneficial.

Our findings reveal significant alterations to angiogenic factor VEGFA in tumor biopsies treated with novel inhibitor of 5LOX. It would be interesting to examine the effect of overexpression of 5LOX enzyme in OAC cells injected into a mouse xenograft model has on tumor growth. Additionally, would be interesting to investigate whether the novel inhibitor of 5LOX could affect the size of the tumor and vessel formation.

Finally, the link between glucose transporter proteins, markers of glycolysis, hypoxia and 5LOX and obesity was investigated in a newly constructed cohort of tissue microarrays, with the obesity status based on VFA measurement. We have seen a significant association between these markers and visceral obesity. Small sample size of only 48 patients and significant association suggests a very strong link between obesity and glycolysis, hypoxia and 5LOX in OAC. However, no significant associations were seen between expression of these markers and clinical and pathological parameters, including disease-specific survival. Since the sample size was small and the follow up data available for 2-3 years only, we could not see the full picture in relation to expression of these markers and disease prognosis. It would be beneficial to increase sample size and to re-calculate 5-year OAC specific survival when follow-up data becomes available.

References

Uncategorized References

1. Zhang, Y., *Epidemiology of esophageal cancer.* World J Gastroenterol, 2013. **19**(34): p. 5598-606.

2. Peters, C.J. and R.C. Fitzgerald, *Systematic review: the application of molecular pathogenesis to prevention and treatment of oesophageal adenocarcinoma.* Aliment Pharmacol Ther, 2007. **25**(11): p. 1253-69.

3. Torre, L.A., et al., *Global cancer statistics, 2012.* CA Cancer J Clin, 2015. **65**(2): p. 87-108.

4. de Jonge, P.J., et al., *Barrett's oesophagus: epidemiology, cancer risk and implications for management.* Gut, 2014. **63**(1): p. 191-202.

5. Kamangar, F., et al., *Environmental causes of esophageal cancer.* Gastroenterol Clin North Am, 2009. **38**(1): p. 27-57, vii.

6. Hou, J.C. and J.E. Pessin, *Ins (endocytosis) and outs (exocytosis) of GLUT4 trafficking.* Curr Opin Cell Biol, 2007. **19**(4): p. 466-73.

7. Pennathur, A., et al., *Oesophageal carcinoma.* The Lancet, 2013. **381**(9864): p. 400-412.

8. Sharma, N. and K.Y. Ho, *Risk Factors for Barrett's Oesophagus.* Gastrointest Tumors, 2016. **3**(2): p. 103-108.

9. Edge, S.B. and C.C. Compton, *The American Joint Committee on Cancer: the 7th Edition of the AJCC Cancer Staging Manual and the Future of TNM.* Annals of Surgical Oncology, 2010. **17**(6): p. 1471-1474.

10. Schmidt, C.W., *A Change in the Air: Smoking Bans Gain Momentum Worldwide.* Environmental Health Perspectives, 2007. **115**(8): p. A412-A415.

11. Cho, J.W., et al., *Lymph Node Metastases in Esophageal Carcinoma: An Endoscopist's View.* Clinical Endoscopy, 2014. **47**(6): p. 523-529.

12. Rice, T.W., et al., *Esophageal carcinoma: depth of tumor invasion is predictive of regional lymph node status.* Ann Thorac Surg, 1998. **65**(3): p. 787-92.

13. Gall, A., et al., *Bacterial Composition of the Human Upper Gastrointestinal Tract Microbiome Is Dynamic and Associated with Genomic Instability in a Barrett's Esophagus Cohort.* PLoS ONE, 2015. **10**(6): p. e0129055.

14. Abnet, C.C., et al., *Non-steroidal anti-inflammatory drugs and risk of gastric and oesophageal adenocarcinomas: results from a cohort study and a meta-analysis.* British Journal of Cancer, 2009. **100**(3): p. 551-557.

15. Farrow, D.C., et al., *Use of aspirin and other nonsteroidal anti-inflammatory drugs and risk of esophageal and gastric cancer.* Cancer Epidemiol Biomarkers Prev, 1998. **7**(2): p. 97-102.

16. Key, T.J., *Fruit and vegetables and cancer risk.* British Journal of Cancer, 2011. **104**(1): p. 6-11.

17. Long, E. and I.L.P. Beales, *The role of obesity in oesophageal cancer development.* Therapeutic Advances in Gastroenterology, 2014. **7**(6): p. 247-268.

18. Sun, F., et al., *Staging accuracy of endoscopic ultrasound for esophageal cancer after neoadjuvant chemotherapy: a meta-analysis and systematic review.* Dis Esophagus, 2015. **28**(8): p. 757-71.

19. Meyers, B.F., et al., *The utility of positron emission tomography in staging of potentially operable carcinoma of the thoracic esophagus: results of the American College of Surgeons Oncology Group Z0060 trial.* J Thorac Cardiovasc Surg, 2007. **133**(3): p. 738-45.

20. Ciardiello, F., et al., *Expression of transforming growth factor alpha (TGF alpha) in breast cancer.* Ann Oncol, 1991. **2**(3): p. 169-82.

21. DeMeester, S.R., *Epidemiology and Biology of Esophageal Cancer.* Gastrointestinal Cancer Research : GCR, 2009. **3**(2 Suppl 1): p. S2-S5.

22. Schwarz, R.E. and D.D. Smith, *Clinical impact of lymphadenectomy extent in resectable esophageal cancer.* J Gastrointest Surg, 2007. **11**(11): p. 1384-93; discussion 1393-4.

23. Altorki, N.K., et al., *Total number of resected lymph nodes predicts survival in esophageal cancer.* Ann Surg, 2008. **248**(2): p. 221-6.

24. Quail, D.F. and J.A. Joyce, *Microenvironmental regulation of tumor progression and metastasis.* Nature medicine, 2013. **19**(11): p. 1423-1437.

25. Facciabene, A., et al., *Tumour hypoxia promotes tolerance and angiogenesis via CCL28 and T(reg) cells.* Nature, 2011. **475**(7355): p. 226-30.

26. Escribese, M.M., M. Casas, and A.L. Corbi, *Influence of low oxygen tensions on macrophage polarization.* Immunobiology, 2012. **217**(12): p. 1233-40.

27. Murdoch, C., A. Giannoudis, and C.E. Lewis, *Mechanisms regulating the recruitment of macrophages into hypoxic areas of tumors and other ischemic tissues.* Blood, 2004. **104**(8): p. 2224-34.

28. Samuels, Y. and T. Waldman, *Oncogenic Mutations of PIK3CA in Human Cancers.* Current topics in microbiology and immunology, 2010. **347**: p. 21-41.

29. Glasgow, E. and L. Mishra, *Transforming growth factor-β signaling and ubiquitinators in cancer.* Endocrine-related cancer, 2008. **15**(1): p. 10.1677/ERC-07-0168.

30. Whitaker, J.W., et al., *Integrative Omics Analysis of Rheumatoid Arthritis Identifies Non-Obvious Therapeutic Targets.* PLoS ONE, 2015. **10**(4): p. e0124254.

31. Peschansky, V.J. and C. Wahlestedt, *Non-coding RNAs as direct and indirect modulators of epigenetic regulation.* Epigenetics, 2014. **9**(1): p. 3-12.

32. Shenouda, S.K. and S.K. Alahari, *MicroRNA function in cancer: oncogene or a tumor suppressor?* Cancer Metastasis Rev, 2009. **28**(3-4): p. 369-78.

33. Jung, H.M., et al., *Tumor suppressor miR-375 regulates MYC expression via repression of CIP2A coding sequence through multiple miRNA–mRNA interactions.* Molecular Biology of the Cell, 2013. **24**(11): p. 1638-1648.

34. Lou, F., et al., *Esophageal Cancer Recurrence Patterns and Implications for Surveillance.* Journal of thoracic oncology : official publication of the International Association for the Study of Lung Cancer, 2013. **8**(12): p. 1558-1562.

35. Parry, K., et al., *Prognosis and Treatment After Diagnosis of Recurrent Esophageal Carcinoma Following Esophagectomy with Curative Intent.* Annals of Surgical Oncology, 2015. **22**: p. 1292-1300.

36. Su, X.-D., et al., *Prognostic factors in patients with recurrence after complete resection of esophageal squamous cell carcinoma.* Journal of Thoracic Disease, 2014. **6**(7): p. 949-957.

37. Lagergren, J., *Adenocarcinoma of oesophagus: what exactly is the size of the problem and who is at risk?* Gut, 2005. **54 Suppl 1**: p. i1-5.

38. Blot, W.J., et al., *Rising incidence of adenocarcinoma of the esophagus and ngastric cardia.* JAMA, 1991. **265**(10): p. 1287-1289.

39. Saber, H. and M. Ghanei, *Extra-Esophageal Manifestations of Gastroesophageal Reflux Disease: Controversies Between Epidemiology and Clicnic.* The Open Respiratory Medicine Journal, 2012. **6**: p. 121-126.

40. Yang, P.C. and S. Davis, *Incidence of cancer of the esophagus in the US by histologic type.* Cancer, 1988. **61**(3): p. 612-7.

41. Vaezi, M.F. and J.E. Richter, *Role of acid and duodenogastroesophageal reflux in gastroesophageal reflux disease.* Gastroenterology, 1996. **111**(5): p. 1192-9.

42. Naini, B.V., et al., *Barrett's oesophagus diagnostic criteria: endoscopy and histology.* Best Practice & Research Clinical Gastroenterology, 2015. **29**(1): p. 77-96.

43. Powell, J., et al., *Continuing rising trend in oesophageal adenocarcinoma.* Int J Cancer, 2002. **102**(4): p. 422-7.

44. Reid, B.J., et al., *Endoscopic biopsy can detect high-grade dysplasia or early adenocarcinoma in Barrett's esophagus without grossly recognizable neoplastic lesions.* Gastroenterology, 1988. **94**(1): p. 81-90.

45. Conteduca, V., et al., *Barrett's esophagus and esophageal cancer: an overview.* Int J Oncol, 2012. **41**(2): p. 414-24.

46. Pennathur, A., R.J. Landreneau, and J.D. Luketich, *Surgical aspects of the patient with high-grade dysplasia.* Semin Thorac Cardiovasc Surg, 2005. **17**(4): p. 326-32.

47. Attwood, S.E., et al., *Medical or surgical management of GERD patients with Barrett's esophagus: the LOTUS trial 3-year experience.* J Gastrointest Surg, 2008. **12**(10): p. 1646-54; discussion 1654-5.

48. Corey, K.E., S.M. Schmitz, and N.J. Shaheen, *Does a surgical antireflux procedure decrease the incidence of esophageal adenocarcinoma in Barrett's esophagus[quest] A meta-analysis.* Am J Gastroenterol, 2003. **98**(11): p. 2390-2394.

49. O'Farrell, N.J., et al., *Evolving changes in the management of early oesophageal adenocarcinoma in a tertiary centre.* Ir J Med Sci, 2013. **182**(3): p. 363-9.

50. Allum, W.H., et al., *Guidelines for the management of oesophageal and gastric cancer.* Gut, 2011. **60**(11): p. 1449-72.

51. Rouvelas, I., et al., *Survival after surgery for oesophageal cancer: a population-based study.* Lancet Oncol, 2005. **6**(11): p. 864-70.

52. Lagergren, J. and P. Lagergren, *Oesophageal cancer.* Bmj, 2010. **341**: p. c6280.

53. Murphy, T.J., N. Ravi, and J.V. Reynolds, *Treatment options for esophageal cancer.* Expert Opin Pharmacother, 2008. **9**(18): p. 3197-210.

54. Reynolds, J.V., et al., *Long-term outcomes following neoadjuvant chemoradiotherapy for esophageal cancer.* Ann Surg, 2007. **245**(5): p. 707-16.

55. van Hagen, P., et al., *Preoperative Chemoradiotherapy for Esophageal or Junctional Cancer.* New England Journal of Medicine, 2012. **366**(22): p. 2074-2084.

56. Pech, O., et al., *Long-term results and risk factor analysis for recurrence after curative endoscopic therapy in 349 patients with high-grade intraepithelial neoplasia and mucosal adenocarcinoma in Barrett's oesophagus.* Gut, 2008. **57**(9): p. 1200-6.

57. Reynolds, J.V., et al., *Modern oncologic and operative outcomes for oesophageal cancer treated with curative intent.* Ir Med J, 2011. **104**(8): p. 235-8.

58. Reynolds, J.V., et al., *Evolving progress in oncologic and operative outcomes for esophageal and junctional cancer: Lessons from the experience of a high-volume center.* The Journal of Thoracic and Cardiovascular Surgery, 2012. **143**(5): p. 1130-1137.e1.

59. Hayakawa, Y., et al., *Oesophageal adenocarcinoma and gastric cancer: should we mind the gap?* Nat Rev Cancer, 2016. **16**(5): p. 305-318.

60. Pectasides, E., *Genomic Alterations and Targeted Therapy in Gastric and Esophageal Adenocarcinoma.* Clin Ther, 2016. **38**(7): p. 1589-99.

61. Uzunoglu, F.G., A.M. Koenig, and J.R. Izbicki, *The potential for targeting HER2 therapeutically in esophageal cancer - a grasp at straws?* Expert Opin Ther Targets, 2014. **18**(12): p. 1421-6.

62. Bang, Y.J., et al., *Trastuzumab in combination with chemotherapy versus chemotherapy alone for treatment of HER2-positive advanced gastric or gastro-oesophageal junction cancer (ToGA): a phase 3, open-label, randomised controlled trial.* Lancet, 2010. **376**(9742): p. 687-97.

63. Hanawa, M., et al., *EGFR protein overexpression and gene amplification in squamous cell carcinomas of the esophagus.* Int J Cancer, 2006. **118**(5): p. 1173-80.

64. Kim, M.A., et al., *EGFR in gastric carcinomas: prognostic significance of protein overexpression and high gene copy number.* Histopathology, 2008. **52**(6): p. 738-46.

65. Sunpaweravong, P., et al., *Epidermal growth factor receptor and cyclin D1 are independently amplified and overexpressed in esophageal squamous cell carcinoma.* J Cancer Res Clin Oncol, 2005. **131**(2): p. 111-9.

66. Waddell, T., et al., *Epirubicin, oxaliplatin, and capecitabine with or without panitumumab for patients with previously untreated advanced oesophagogastric cancer (REAL3): a randomised, open-label phase 3 trial.* Lancet Oncol, 2013. **14**(6): p. 481-9.

67. Dutton, S.J., et al., *Gefitinib for oesophageal cancer progressing after chemotherapy (COG): a phase 3, multicentre, double-blind, placebo-controlled randomised trial.* The Lancet Oncology, 2014. **15**(8): p. 894-904.

68. Shih, C.H., et al., *Vascular endothelial growth factor expression predicts outcome and lymph node metastasis in squamous cell carcinoma of the esophagus.* Clin Cancer Res, 2000. **6**(3): p. 1161-8.

69. Peng, J., et al., *Prognostic significance of vascular endothelial growth factor expression in esophageal carcinoma: a meta-analysis.* J buon, 2013. **18**(2): p. 398-406.

70. Enzinger, P.C., et al., *Multicenter phase 2: Capecitabine (CAP) + oxaliplatin (OX) + bevacizumab (BEV) + trastuzumab (TRAS) for patients (pts) with metastatic esophagogastric cancer (MEGCA).* J Clin Oncol (Meeting Abstracts), 2015. **33**(15_suppl): p. 4038-.

71. Hardwick, J.P., et al., *Eicosanoids in metabolic syndrome.* Adv Pharmacol, 2013. **66**: p. 157-266.

72. Hoque, A., et al., *Increased 5-lipoxygenase expression and induction of apoptosis by its inhibitors in esophageal cancer: a potential target for prevention.* Carcinogenesis, 2005. **26**(4): p. 785-91.

73. Wang, D. and R.N. Dubois, *Eicosanoids and cancer.* Nat Rev Cancer, 2010. **10**(3): p. 181-93.

74. Woods, J.W., et al., *5-Lipoxygenase is located in the euchromatin of the nucleus in resting human alveolar macrophages and translocates to the nuclear envelope upon cell activation.* J Clin Invest, 1995. **95**(5): p. 2035-46.

75. Mancini, J.A., et al., *5-lipoxygenase-activating protein is an arachidonate binding protein.* FEBS Letters, 1993. **318**(3): p. 277-281.

76. Schwenk, U. and J.-M. Schröder, *5-Oxo-eicosanoids Are Potent Eosinophil Chemotactic Factors.: FUNCTIONAL CHARACTERIZATION AND STRUCTURAL REQUIREMENTS.* Journal of Biological Chemistry, 1995. **270**(25): p. 15029-15036.

77. Samuelsson, B. and C.D. Funk, *Enzymes involved in the biosynthesis of leukotriene B4.* J Biol Chem, 1989. **264**(33): p. 19469-72.

78. Knab, L.M., P.J. Grippo, and D.J. Bentrem, *Involvement of eicosanoids in the pathogenesis of pancreatic cancer: the roles of cyclooxygenase-2 and 5-lipoxygenase.* World J Gastroenterol, 2014. **20**(31): p. 10729-39.

79. Peters-Golden, M., M.M. Gleason, and A. Togias, *Cysteinyl leukotrienes: multi-functional mediators in allergic rhinitis.* Clin Exp Allergy, 2006. **36**(6): p. 689-703.

80. Gounari, F., et al., *Loss of adenomatous polyposis coli gene function disrupts thymic development.* Nat Immunol, 2005. **6**(8): p. 800-9.

81. Kwong, L.N. and W.F. Dove, *APC and its modifiers in colon cancer.* Advances in experimental medicine and biology, 2009. **656**: p. 85-106.

82. Cheon, E.C., et al., *Mast cell 5-lipoxygenase activity promotes intestinal polyposis in APCDelta468 mice.* Cancer Res, 2011. **71**(5): p. 1627-36.

83. Goodman, J.E., et al., *Arachidonate lipoxygenase (ALOX) and cyclooxygenase (COX) polymorphisms and colon cancer risk.* Carcinogenesis, 2004. **25**(12): p. 2467-72.

84. Mashima, R. and T. Okuyama, *The role of lipoxygenases in pathophysiology; new insights and future perspectives.* Redox Biol, 2015. **6**: p. 297-310.

85. Chen, X., et al., *Overexpression of 5-Lipoxygenase in Rat and Human Esophageal Adenocarcinoma and Inhibitory Effects of Zileuton and Celecoxib on Carcinogenesis.* Clinical Cancer Research, 2004. **10**(19): p. 6703-6709.

86. Tsukada, T., K. Nakashima, and S. Shirakawa, *Arachidonate 5-lipoxygenase inhibitors show potent antiproliferative effects on human leukemia cell lines.* Biochem Biophys Res Commun, 1986. **140**(3): p. 832-6.

87. Steinhilber, D., et al., *5-Lipoxygenase: Underappreciated Role of a Pro-Inflammatory Enzyme in Tumorigenesis.* Frontiers in Pharmacology, 2010. **1**: p. 143.

88. Ghosh, J. and C.E. Myers, *Inhibition of arachidonate 5-lipoxygenase triggers massive apoptosis in human prostate cancer cells.* Proceedings of the National Academy of Sciences of the United States of America, 1998. **95**(22): p. 13182-13187.

89. Meng, Z., et al., *Inhibitor of 5-lipoxygenase, zileuton, suppresses prostate cancer metastasis by upregulating E-cadherin and paxillin.* Urology, 2013. **82**(6): p. 1452.e7-14.

90. Matsuyama, M., et al., *Expression of lipoxygenase in human prostate cancer and growth reduction by its inhibitors.* Int J Oncol, 2004. **24**(4): p. 821-7.

91. Sarveswaran, S., et al., *Inhibition of 5-lipoxygenase triggers apoptosis in prostate cancer cells via down-regulation of protein kinase C-epsilon.* Biochimica et biophysica acta, 2011. **1813**(12): p. 2108-2117.

92. Ding, X.Z., et al., *Lipoxygenase inhibitors abolish proliferation of human pancreatic cancer cells.* Biochem Biophys Res Commun, 1999. **261**(1): p. 218-23.

93. De Pergola, G. and F. Silvestris, *Obesity as a Major Risk Factor for Cancer.* Journal of Obesity, 2013. **2013**: p. 291546.

94. Ramos-Nino, M.E., *The Role of Chronic Inflammation in Obesity-Associated Cancers.* ISRN Oncology, 2013. **2013**: p. 697521.

95. Zhang, Y., *Epidemiology of esophageal cancer.* World Journal of Gastroenterology : WJG, 2013. **19**(34): p. 5598-5606.

96. Melhado, R.E., D. Alderson, and O. Tucker, *The Changing Face of Esophageal Cancer.* Cancers, 2010. **2**(3): p. 1379-1404.

97. Calle, E.E. and R. Kaaks, *Overweight, obesity and cancer: epidemiological evidence and proposed mechanisms.* Nat Rev Cancer, 2004. **4**(8): p. 579-591.

98. Reid, B.J., et al., *Barrett's oesophagus and oesophageal adenocarcinoma: time for a new synthesis.* Nat Rev Cancer, 2010. **10**(2): p. 87-101.

99. Kang, Y.E., et al., *The Roles of Adipokines, Proinflammatory Cytokines, and Adipose Tissue Macrophages in Obesity-Associated Insulin Resistance in Modest Obesity and Early Metabolic Dysfunction.* PLoS One, 2016. **11**(4): p. e0154003.

100. Donohoe, C.L., S.L. Doyle, and J.V. Reynolds, *Visceral adiposity, insulin resistance and cancer risk.* Diabetology & Metabolic Syndrome, 2011. **3**: p. 12-12.

101. Donohoe, C.L., et al., *The role of obesity in gastrointestinal cancer: evidence and opinion.* Therapeutic Advances in Gastroenterology, 2014. **7**(1): p. 38-50.

102. Renehan, A.G., et al., *Body-mass index and incidence of cancer: a systematic review and meta-analysis of prospective observational studies.* Lancet, 2008. **371**(9612): p. 569-78.

103. Lynam-Lennon, N., et al., *Excess visceral adiposity induces alterations in mitochondrial function and energy metabolism in esophageal adenocarcinoma.* BMC Cancer, 2014. **14**(1): p. 907.

104. Steffen, A., et al., *Anthropometry and esophageal cancer risk in the European prospective investigation into cancer and nutrition.* Cancer Epidemiol Biomarkers Prev, 2009. **18**(7): p. 2079-89.

105. MacInnis, R.J., et al., *Body size and composition and the risk of gastric and oesophageal adenocarcinoma.* Int J Cancer, 2006. **118**(10): p. 2628-31.

106. *Trends in adult body-mass index in 200 countries from 1975 to 2014: a pooled analysis of 1698 population-based measurement studies with 19·2 million participants.* The Lancet, 2016. **387**(10026): p. 1377-1396.

107. Lobstein, T., et al., *Child and adolescent obesity: part of a bigger picture.* Lancet (London, England), 2015. **385**(9986): p. 2510-2520.

108. Lifshitz, F., *Obesity in Children.* Journal of Clinical Research in Pediatric Endocrinology, 2008. **1**(2): p. 53-60.

109. Huang, L., R.-L. Wu, and A.M. Xu, *Epithelial-mesenchymal transition in gastric cancer.* American Journal of Translational Research, 2015. **7**(11): p. 2141-2158.

110. Fontana, L., et al., *Visceral fat adipokine secretion is associated with systemic inflammation in obese humans.* Diabetes, 2007. **56**(4): p. 1010-3.

111. Lafontan, M., *Fat cells: afferent and efferent messages define new approaches to treat obesity.* Annu Rev Pharmacol Toxicol, 2005. **45**: p. 119-46.

112. Xu, H., et al., *Chronic inflammation in fat plays a crucial role in the development of obesity-related insulin resistance.* J Clin Invest, 2003. **112**(12): p. 1821-30.

113. Booth, F.W., C.K. Roberts, and M.J. Laye, *Lack of exercise is a major cause of chronic diseases.* Comprehensive Physiology, 2012. **2**(2): p. 1143-1211.

114. Irving, B.A., et al., *Effect of exercise training intensity on abdominal visceral fat and body composition.* Med Sci Sports Exerc, 2008. **40**(11): p. 1863-72.

115. Park, A., W.K. Kim, and K.-H. Bae, *Distinction of white, beige and brown adipocytes derived from mesenchymal stem cells.* World Journal of Stem Cells, 2014. **6**(1): p. 33-42.

116. Saely, C.H., K. Geiger, and H. Drexel, *Brown versus white adipose tissue: a mini-review.* Gerontology, 2012. **58**(1): p. 15-23.

117. Cinti, S., *Transdifferentiation properties of adipocytes in the adipose organ.* Am J Physiol Endocrinol Metab, 2009. **297**(5): p. E977-86.

118. Kim, S.H. and J. Plutzky, *Brown Fat and Browning for the Treatment of Obesity and Related Metabolic Disorders.* Diabetes Metab J, 2016. **40**(1): p. 12-21.

119. Wu, C., et al., *Activating Brown Adipose Tissue for Weight Loss and Lowering of Blood Glucose Levels: A MicroPET Study Using Obese and Diabetic Model Mice.* PLoS ONE, 2014. **9**(12): p. e113742.

120. Castro, A.V.B., et al., *Obesity, insulin resistance and comorbidities – Mechanisms of association.* Arquivos brasileiros de endocrinologia e metabologia, 2014. **58**(6): p. 600-609.

121. Cypess, A.M. and C.R. Kahn, *Brown fat as a therapy for obesity and diabetes.* Current opinion in endocrinology, diabetes, and obesity, 2010. **17**(2): p. 143-149.

122. Berg, J. M., Tymoczko, J. L. & Stryer, L. Biochemistry. (W.H.Freeman & Co Ltd, 2006).

123. Shellock, F.G., M.S. Riedinger, and M.C. Fishbein, *Brown adipose tissue in cancer patients: possible cause of cancer-induced cachexia.* J Cancer Res Clin Oncol, 1986. **111**(1): p. 82-5.

124. Jones, L.P., et al., *Abnormal Mammary Adipose Tissue Environment of Brca1 Mutant Mice Show a Persistent Deposition of Highly Vascularized Multilocular Adipocytes.* Journal of cancer science & therapy, 2011(Suppl 2): p. 004.

125. van Marken Lichtenbelt , W.D., et al., *Cold-Activated Brown Adipose Tissue in Healthy Men.* New England Journal of Medicine, 2009. **360**(15): p. 1500-1508.

126. Shuster, A., et al., *The clinical importance of visceral adiposity: a critical review of methods for visceral adipose tissue analysis.* The British Journal of Radiology, 2012. **85**(1009): p. 1-10.

127. Heus, C., et al., *Visceral obesity, muscle mass and outcome in rectal cancer surgery after neo-adjuvant chemo-radiation.* Int J Surg, 2016. **29**: p. 159-64.

128. Beddy, P., et al., *Association of visceral adiposity with oesophageal and junctional adenocarcinomas.* Br J Surg, 2010. **97**.

129. Doyle, S.L., et al., *Establishing computed tomography–defined visceral fat area thresholds for use in obesity-related cancer research.* Nutrition Research. **33**(3): p. 171-179.

130. Yoshizumi, T., et al., *Abdominal fat: standardized technique for measurement at CT.* Radiology, 1999. **211**(1): p. 283-6.

131. Maurovich-Horvat, P., et al., *Comparison of anthropometric, area- and volume-based assessment of abdominal subcutaneous and visceral adipose tissue volumes using multi-detector computed tomography.* Int J Obes (Lond), 2007. **31**(3): p. 500-6.

132. Klein, S., et al., *Waist circumference and cardiometabolic risk: a consensus statement from Shaping America's Health: Association for Weight Management and Obesity Prevention; NAASO, The Obesity Society; the American Society for Nutrition; and the American Diabetes Association.* Am J Clin Nutr, 2007. **85**(5): p. 1197-202.

133. Hu, F.B., *Obesity and mortality: watch your waist, not just your weight.* Arch Intern Med, 2007. **167**(9): p. 875-6.

134. Vander Heiden, M.G., L.C. Cantley, and C.B. Thompson, *Understanding the Warburg Effect: The Metabolic Requirements of Cell Proliferation.* Science (New York, N.Y.), 2009. **324**(5930): p. 1029-1033.

135. Pattabiraman, D.R. and R.A. Weinberg, *Tackling the cancer stem cells – what challenges do they pose?* Nature reviews. Drug discovery, 2014. **13**(7): p. 497-512.

136. Rani, B., et al., *Role of the tissue microenvironment as a therapeutic target in hepatocellular carcinoma.* World Journal of Gastroenterology : WJG, 2014. **20**(15): p. 4128-4140.

137. Lin, E.W., et al., *The Tumor Microenvironment in Esophageal Cancer.* Oncogene, 2016. **35**(41): p. 5337-5349.

138. Maciel, T.T., I.C. Moura, and O. Hermine, *The role of mast cells in cancers.* F1000Prime Reports, 2015. **7**: p. 09.

139. Crawford, S., *Anti-inflammatory/antioxidant use in long-term maintenance cancer therapy: a new therapeutic approach to disease progression and recurrence.* Therapeutic Advances in Medical Oncology, 2014. **6**(2): p. 52-68.

140. Rahman, M., et al., *Inhibition of COX-2 in Colon Cancer Modulates Tumor Growth and MDR-1 Expression to Enhance Tumor Regression in Therapy-Refractory Cancers In Vivo.* Neoplasia (New York, N.Y.), 2012. **14**(7): p. 624-633.

141. Jana, D., et al., *Role of Cyclooxygenase 2 (COX-2) in Prognosis of Breast Cancer.* Indian Journal of Surgical Oncology, 2014. **5**(1): p. 59-65.

142. Godwin, P., et al., *Targeting Nuclear Factor-Kappa B to Overcome Resistance to Chemotherapy.* Frontiers in Oncology, 2013. **3**: p. 120.

143. Arora, S., et al., *Honokiol: a novel natural agent for cancer prevention and therapy.* Current molecular medicine, 2012. **12**(10): p. 1244-1252.

144. Hoesel, B. and J.A. Schmid, *The complexity of NF-κB signaling in inflammation and cancer.* Molecular Cancer, 2013. **12**: p. 86-86.

145. Mantovani, A., et al., *Cancer-related inflammation.* Nature, 2008. **454**(7203): p. 436-444.

146. Catalán, V., et al., *Adipose tissue immunity and cancer.* Frontiers in Physiology, 2013. **4**: p. 275.

147. Ribeiro, R., et al., *Obesity and prostate cancer: gene expression signature of human periprostatic adipose tissue.* BMC Medicine, 2012. **10**(1): p. 108.

148. Trayhurn, P., *Hypoxia and adipocyte physiology: implications for adipose tissue dysfunction in obesity.* Annu Rev Nutr, 2014. **34**: p. 207-36.

149. Trayhurn, P., B. Wang, and I.S. Wood, *Hypoxia in adipose tissue: a basis for the dysregulation of tissue function in obesity?* Br J Nutr, 2008. **100**(2): p. 227-35.

150. Ye, J., *Emerging Role of Adipose Tissue Hypoxia in Obesity and Insulin Resistance.* International journal of obesity (2005), 2009. **33**(1): p. 54-66.

151. Cancello, R., et al., *Reduction of macrophage infiltration and chemoattractant gene expression changes in white adipose tissue of morbidly obese subjects after surgery-induced weight loss.* Diabetes, 2005. **54**(8): p. 2277-86.

152. Nizet, V. and R.S. Johnson, *Interdependence of hypoxic and innate immune responses.* Nature reviews. Immunology, 2009. **9**(9): p. 609-617.

153. Mamlouk, S. and B. Wielockx, *Hypoxia-inducible factors as key regulators of tumor inflammation.* Int J Cancer, 2013. **132**(12): p. 2721-9.

154. Semenza, G.L., *Hypoxia-inducible factor 1 and cancer pathogenesis.* IUBMB Life, 2008. **60**(9): p. 591-7.

155. Yang, Z.J., et al., *The Role of Autophagy in Cancer: Therapeutic Implications.* Molecular cancer therapeutics, 2011. **10**(9): p. 1533-1541.

156. Wigerup, C., S. Påhlman, and D. Bexell, *Therapeutic targeting of hypoxia and hypoxia-inducible factors in cancer.* Pharmacology & Therapeutics, 2016. **164**: p. 152-169.

157. Masoud, G.N. and W. Li, *HIF-1α pathway: role, regulation and intervention for cancer therapy.* Acta Pharmaceutica Sinica B, 2015. **5**(5): p. 378-389.

158. Semenza, G.L., *Targeting HIF-1 for cancer therapy.* Nat Rev Cancer, 2003. **3**(10): p. 721-732.

159. Lemoine, A.Y., S. Ledoux, and E. Larger, *Adipose tissue angiogenesis in obesity.* Thromb Haemost, 2013. **110**(4): p. 661-8.

160. Ferrara, N. and R.S. Kerbel, *Angiogenesis as a therapeutic target.* Nature, 2005. **438**(7070): p. 967-74.

161. Ye, J., *Emerging role of adipose tissue hypoxia in obesity and insulin resistance.* Int J Obes (Lond), 2009. **33**(1): p. 54-66.

162. Gomez-Ambrosi, J., et al., *Involvement of serum vascular endothelial growth factor family members in the development of obesity in mice and humans.* J Nutr Biochem, 2010. **21**(8): p. 774-80.

163. Rupnick, M.A., et al., *Adipose tissue mass can be regulated through the vasculature.* Proc Natl Acad Sci U S A, 2002. **99**(16): p. 10730-5.

164. Cao, Y., *Angiogenesis modulates adipogenesis and obesity.* J Clin Invest, 2007. **117**(9): p. 2362-8.

165. Kanneganti, T.D. and V.D. Dixit, *Immunological complications of obesity.* Nat Immunol, 2012. **13**(8): p. 707-12.

166. Olefsky, J.M. and C.K. Glass, *Macrophages, inflammation, and insulin resistance.* Annu Rev Physiol, 2010. **72**: p. 219-46.

167. Shapiro, H., et al., *Adipose tissue foam cells are present in human obesity.* J Clin Endocrinol Metab, 2013. **98**(3): p. 1173-81.

168. Hanahan, D. and R.A. Weinberg, *The hallmarks of cancer.* Cell, 2000. **100**(1): p. 57-70.

169. Hanahan, D. and R.A. Weinberg, *Hallmarks of cancer: the next generation.* Cell, 2011. **144**(5): p. 646-74.

170. Donohoe, C.L., et al., *Emerging Concepts Linking Obesity with the Hallmarks of Cancer.* Trends Endocrinol Metab, 2017. **28**(1): p. 46-62.

171. Lysaght, J., et al., *Pro-inflammatory and tumour proliferative properties of excess visceral adipose tissue.* Cancer Lett, 2011. **312**(1): p. 62-72.

172. Lysaght, J., et al., *T lymphocyte activation in visceral adipose tissue of patients with oesophageal adenocarcinoma.* Br J Surg, 2011. **98**(7): p. 964-74.

173. Allott, E.H., et al., *MMP9 expression in oesophageal adenocarcinoma is upregulated with visceral obesity and is associated with poor tumour differentiation.* Mol Carcinog, 2013. **52**(2): p. 144-54.

174. Allott, E.H., et al., *Elevated Tumor Expression of PAI-1 and SNAI2 in Obese Esophageal Adenocarcinoma Patients and Impact on Prognosis.* Clin Transl Gastroenterol, 2012. **3**: p. e12.

175. Lynam-Lennon, N., et al., *Excess visceral adiposity induces alterations in mitochondrial function and energy metabolism in esophageal adenocarcinoma.* BMC Cancer, 2014. **14**: p. 907.

176. Kong, D., et al., *Cancer Stem Cells and Epithelial-to-Mesenchymal Transition (EMT)-Phenotypic Cells: Are They Cousins or Twins?* Cancers (Basel), 2011. **3**(1): p. 716-29.

177. Kalcheim, C., *Epithelial-Mesenchymal Transitions during Neural Crest and Somite Development.* J Clin Med, 2015. **5**(1).

178. Lamouille, S., J. Xu, and R. Derynck, *Molecular mechanisms of epithelial–mesenchymal transition.* Nature reviews. Molecular cell biology, 2014. **15**(3): p. 178-196.

179. Liu, X., et al., *Loss of E-cadherin and epithelial to mesenchymal transition is not required for cell motility in tissues or for metastasis.* Tissue Barriers, 2014. **2**(4): p. e969112.

180. Scanlon, C.S., et al., *Biomarkers of Epithelial-Mesenchymal Transition in Squamous Cell Carcinoma.* Journal of Dental Research, 2013. **92**(2): p. 114-121.

181. Scarpa, E., et al., *Cadherin Switch during EMT in Neural Crest Cells Leads to Contact Inhibition of Locomotion via Repolarization of Forces.* Dev Cell, 2015. **34**(4): p. 421-34.

182. Wheelock, M.J., et al., *Cadherin switching.* Journal of Cell Science, 2008. **121**(6): p. 727-735.

183. Youn, Y.-H., J. Hong, and J.M. Burke, *Cell Phenotype in Normal Epithelial Cell Lines with High Endogenous N-Cadherin: Comparison of RPE to an MDCK Subclone.* Investigative ophthalmology & visual science, 2006. **47**(6): p. 2675-2685.

184. Larue, L. and A. Bellacosa, *Epithelial-mesenchymal transition in development and cancer: role of phosphatidylinositol 3[prime] kinase//AKT pathways.* Oncogene, 0000. **24**(50): p. 7443-7454.

185. Talbot, L.J., S.D. Bhattacharya, and P.C. Kuo, *Epithelial-mesenchymal transition, the tumor microenvironment, and metastatic behavior of epithelial malignancies.* International Journal of Biochemistry and Molecular Biology, 2012. **3**(2): p. 117-136.

186. Hasan, M.R., et al., *Slug is a predictor of poor prognosis in esophageal squamous cell carcinoma patients.* PLoS One, 2013. **8**(12): p. e82846.

187. Ye, X., et al., *Distinct EMT programs control normal mammary stem cells and tumour-initiating cells.* Nature, 2015. **525**(7568): p. 256-260.

188. Uygur, B. and W.-S. Wu, *SLUG promotes prostate cancer cell migration and invasion via CXCR4/CXCL12 axis.* Molecular Cancer, 2011. **10**: p. 139-139.

189. Shrivastava, S., et al., *Identification of molecular signature of head and neck cancer stem-like cells.* Scientific Reports, 2015. **5**: p. 7819.

190. Tsukasa, K., et al., *Slug contributes to gemcitabine resistance through epithelial-mesenchymal transition in CD133(+) pancreatic cancer cells.* Hum Cell, 2015. **28**(4): p. 167-74.

191. Tanaka, Y., et al., *Prognostic impact of EMT (epithelial-mesenchymal-transition)-related protein expression in endometrial cancer.* Cancer Biology & Therapy, 2013. **14**(1): p. 13-19.

192. ElMoneim, H.M.A. and N.M. Zaghloul, *Expression of e-cadherin, n-cadherin and snail and their correlation with clinicopathological variants: an immunohistochemical study of 132 invasive ductal breast carcinomas in Egypt.* Clinics, 2011. **66**(10): p. 1765-1771.

193. Côme, C., et al., *Roles of the transcription factors snail and slug during mammary morphogenesis and breast carcinoma progression.* Journal of Mammary Gland Biology and Neoplasia, 2004. **9**(2): p. 183-193.

194. Uchikado, Y., et al., *Slug Expression in the E-cadherin preserved tumors is related to prognosis in patients with esophageal squamous cell carcinoma.* Clin Cancer Res, 2005. **11**(3): p. 1174-80.

195. Metallo, C.M. and M.G.V. Heiden, *Understanding metabolic regulation and its influence on cell physiology.* Molecular cell, 2013. **49**(3): p. 388-398.

196. Hanahan, D. and Robert A. Weinberg, *Hallmarks of Cancer: The Next Generation.* Cell, 2011. **144**(5): p. 646-674.

197. Mergenthaler, P., et al., *Sugar for the brain: the role of glucose in physiological and pathological brain function.* Trends in neurosciences, 2013. **36**(10): p. 587-597.

198. Cheong, H., et al., *Therapeutic targets in cancer cell metabolism and autophagy.* Nature biotechnology, 2012. **30**(7): p. 10.1038/nbt.2285.

199. Pelicano, H., et al., *Glycolysis inhibition for anticancer treatment.* Oncogene, 2006. **25**(34): p. 4633-46.

200. Zhao, F.-Q. and A.F. Keating, *Functional Properties and Genomics of Glucose Transporters.* Current Genomics, 2007. **8**(2): p. 113-128.

201. Schurmann, A., *Insight into the "odd" hexose transporters GLUT3, GLUT5, and GLUT7.* Am J Physiol Endocrinol Metab, 2008. **295**(2): p. E225-6.

202. Aparicio, L.M., et al., *Glucose transporter expression and the potential role of fructose in renal cell carcinoma: A correlation with pathological parameters.* Mol Med Rep, 2010. **3**(4): p. 575-80.

203. Carvalho, K.C., et al., *GLUT1 expression in malignant tumors and its use as an immunodiagnostic marker.* Clinics, 2011. **66**(6): p. 965-972.

204. Sawayama, H., et al., *High Expression of Glucose Transporter 1 on Primary Lesions of Esophageal Squamous Cell Carcinoma is Associated with Hematogenous Recurrence.* Annals of Surgical Oncology, 2014. **21**(5): p. 1756-1762.

205. Tohma, T., et al., *Overexpression of glucose transporter 1 in esophageal squamous cell carcinomas: a marker for poor prognosis.* Dis Esophagus, 2005. **18**(3): p. 185-9.

206. Chiba, I., et al., *Clinical significance of GLUT-1 expression in patients with esophageal cancer treated with concurrent chemoradiotherapy.* Oncology Letters, 2011. **2**(1): p. 21-28.

207. Piątkiewicz, P., et al., *NK cell count and glucotransporter 4 (GLUT4) expression in subjects with type 2 diabetes and colon cancer.* Diabetology & Metabolic Syndrome, 2016. **8**: p. 38.

208. Acharya, S., et al., *Downregulation of GLUT4 contributes to effective intervention of estrogen receptor-negative/HER2-overexpressing early stage breast disease progression by lapatinib.* Am J Cancer Res, 2016. **6**(5): p. 981-95.

209. Garrido, P., et al., *Loss of GLUT4 induces metabolic reprogramming and impairs viability of breast cancer cells.* J Cell Physiol, 2015. **230**(1): p. 191-8.

210. Wilson, J.E., *Isozymes of mammalian hexokinase: structure, subcellular localization and metabolic function.* J Exp Biol, 2003. **206**(Pt 12): p. 2049-57.

211. Gao, Y., et al., *Overexpression of metabolic markers HK1 and PKM2 contributes to lymphatic metastasis and adverse prognosis in Chinese gastric cancer.* Int J Clin Exp Pathol, 2015. **8**(8): p. 9264-71.

212. Li, W., et al., *Expression patterns of three regulation enzymes in glycolysis in esophageal squamous cell carcinoma: association with survival.* Med Oncol, 2014. **31**(9): p. 118.

213. Anderson, M., et al., *Hexokinase 2 promotes tumor growth and metastasis by regulating lactate production in pancreatic cancer.* Oncotarget, 2016.

214. Dai, W., et al., *By reducing hexokinase 2, resveratrol induces apoptosis in HCC cells addicted to aerobic glycolysis and inhibits tumor growth in mice.* Oncotarget, 2015. **6**(15): p. 13703-13717.

215. Hatoum, D. and E.M. McGowan, *Recent Advances in the Use of Metformin: Can Treating Diabetes Prevent Breast Cancer?* BioMed Research International, 2015. **2015**: p. 548436.

216. Fang, R., et al., *MicroRNA-143 (miR-143) Regulates Cancer Glycolysis via Targeting Hexokinase 2 Gene.* The Journal of Biological Chemistry, 2012. **287**(27): p. 23227-23235.

217. Zhang, X., et al., *Nuclear PKM2 expression predicts poor prognosis in patients with esophageal squamous cell carcinoma.* Pathol Res Pract, 2013. **209**(8): p. 510-5.

218. Israelsen, W.J. and M.G. Vander Heiden, *Pyruvate kinase: Function, regulation and role in cancer.* Semin Cell Dev Biol, 2015. **43**: p. 43-51.

219. Ugurel, S., et al., *Tumor type M2 pyruvate kinase (TuM2-PK) as a novel plasma tumor marker in melanoma.* Int J Cancer, 2005. **117**(5): p. 825-30.

220. Weinberger, R., et al., *The pyruvate kinase isoenzyme M2 (Tu M2-PK) as a tumour marker for renal cell carcinoma.* Eur J Cancer Care (Engl), 2007. **16**(4): p. 333-7.

221. Peng, X.C., et al., *Comparative proteomic approach identifies PKM2 and cofilin-1 as potential diagnostic, prognostic and therapeutic targets for pulmonary adenocarcinoma.* PLoS One, 2011. **6**(11): p. e27309.

222. Landt, S., et al., *Tumor-specific correlation of tumor M2 pyruvate kinase in pre-invasive, invasive and recurrent cervical cancer.* Anticancer Res, 2010. **30**(2): p. 375-81.

223. Fatela-Cantillo, D., et al., *Prognostic value of plasmatic tumor M2 pyruvate kinase and carcinoembryonic antigen in the survival of colorectal cancer patients.* Tumour Biol, 2012. **33**(3): p. 825-32.

224. Zhang, J.Y., et al., *Critical protein GAPDH and its regulatory mechanisms in cancer cells.* Cancer Biol Med, 2015. **12**(1): p. 10-22.

225. Caradec, J., et al., *Is GAPDH a relevant housekeeping gene for normalisation in colorectal cancer experiments?* Br J Cancer, 2010. **103**(9): p. 1475-6.

226. Bazzocco, S., et al., *Highly Expressed Genes in Rapidly Proliferating Tumor Cells as New Targets for Colorectal Cancer Treatment.* Clin Cancer Res, 2015. **21**(16): p. 3695-704.

227. Puzone, R., et al., *Glyceraldehyde-3-phosphate dehydrogenase gene over expression correlates with poor prognosis in non small cell lung cancer patients.* Mol Cancer, 2013. **12**(1): p. 97.

228. Shedden, K., et al., *Gene expression-based survival prediction in lung adenocarcinoma: a multi-site, blinded validation study.* Nat Med, 2008. **14**(8): p. 822-7.

229. Lee, E.S., et al., *Prediction of recurrence-free survival in postoperative non-small cell lung cancer patients by using an integrated model of clinical information and gene expression.* Clin Cancer Res, 2008. **14**(22): p. 7397-404.

230. Tomida, S., et al., *Relapse-related molecular signature in lung adenocarcinomas identifies patients with dismal prognosis.* J Clin Oncol, 2009. **27**(17): p. 2793-9.

231. Roepman, P., et al., *An immune response enriched 72-gene prognostic profile for early-stage non-small-cell lung cancer.* Clin Cancer Res, 2009. **15**(1): p. 284-90.

232. Okayama, H., et al., *Identification of genes upregulated in ALK-positive and EGFR/KRAS/ALK-negative lung adenocarcinomas.* Cancer Res, 2012. **72**(1): p. 100-11.

233. Botling, J., et al., *Biomarker discovery in non-small cell lung cancer: integrating gene expression profiling, meta-analysis, and tissue microarray validation.* Clin Cancer Res, 2013. **19**(1): p. 194-204.

234. Hjerpe, E., et al., *Metabolic markers GAPDH, PKM2, ATP5B and BEC-index in advanced serous ovarian cancer.* BMC Clin Pathol, 2013. **13**(1): p. 30.

235. Revillion, F., et al., *Glyceraldehyde-3-phosphate dehydrogenase gene expression in human breast cancer.* Eur J Cancer, 2000. **36**(8): p. 1038-42.

236. Zheng, J.I.E., *Energy metabolism of cancer: Glycolysis versus oxidative phosphorylation (Review).* Oncology Letters, 2012. **4**(6): p. 1151-1157.

237. Sharma, L.K., et al., *Mitochondrial respiratory complex I dysfunction promotes tumorigenesis through ROS alteration and AKT activation.* Hum Mol Genet, 2011. **20**(23): p. 4605-16.

238. Dasgupta, S., et al., *Mitochondrial DNA Mutations in Respiratory Complex-I in Never-Smoker Lung Cancer Patients Contribute to Lung Cancer Progression and associated with EGFR gene mutation.* Journal of cellular physiology, 2012. **227**(6): p. 2451-2460.

239. Chatterjee, A., E. Mambo, and D. Sidransky, *Mitochondrial DNA mutations in human cancer.* Oncogene, 2006. **25**(34): p. 4663-74.

240. Kluckova, K., et al., *Mitochondrial complex II, a novel target for anti-cancer agents.* Biochim Biophys Acta, 2013. **1827**(5): p. 552-64.

241. Janeway, K.A., et al., *Defects in succinate dehydrogenase in gastrointestinal stromal tumors lacking KIT and PDGFRA mutations.* Proc Natl Acad Sci U S A, 2011. **108**(1): p. 314-8.

242. Pollard, P.J., et al., *Accumulation of Krebs cycle intermediates and over-expression of HIF1alpha in tumours which result from germline FH and SDH mutations.* Hum Mol Genet, 2005. **14**(15): p. 2231-9.

243. Boitier, E., et al., *Impairment of the mitochondrial respiratory chain activity in diethylnitrosamine-induced rat hepatomas: possible involvement of oxygen free radicals.* Cancer Res, 1995. **55**(14): p. 3028-35.

244. Liu, V.W., et al., *High incidence of somatic mitochondrial DNA mutations in human ovarian carcinomas.* Cancer Res, 2001. **61**(16): p. 5998-6001.

245. Polyak, K., et al., *Somatic mutations of the mitochondrial genome in human colorectal tumours.* Nat Genet, 1998. **20**(3): p. 291-3.

246. Tseng, L.M., et al., *Mitochondrial DNA mutations and mitochondrial DNA depletion in breast cancer.* Genes Chromosomes Cancer, 2006. **45**(7): p. 629-38.

247. Phelan, J.J., et al., *Differential expression of mitochondrial energy metabolism profiles across the metaplasia-dysplasia-adenocarcinoma disease sequence in Barrett's oesophagus.* Cancer Lett, 2014. **354**(1): p. 122-31.

248. Lynam-Lennon, N., et al., *Altered mitochondrial function and energy metabolism is associated with a radioresistant phenotype in oesophageal adenocarcinoma.* PLoS One, 2014. **9**(6): p. e100738.

249. Al Ghouleh, I., et al., *Oxidases and peroxidases in cardiovascular and lung disease: new concepts in reactive oxygen species signaling.* Free Radic Biol Med, 2011. **51**(7): p. 1271-88.

250. Jonckheere, A.I., J.A.M. Smeitink, and R.J.T. Rodenburg, *Mitochondrial ATP synthase: architecture, function and pathology.* Journal of Inherited Metabolic Disease, 2012. **35**(2): p. 211-225.

251. Berridge, M.V., P.M. Herst, and A.S. Tan, *Metabolic flexibility and cell hierarchy in metastatic cancer.* Mitochondrion, 2010. **10**(6): p. 584-8.

252. Warburg, O., *On the origin of cancer cells.* Science, 1956. **123**(3191): p. 309-14.

253. Vander Heiden, M.G., L.C. Cantley, and C.B. Thompson, *Understanding the Warburg effect: the metabolic requirements of cell proliferation.* Science, 2009. **324**(5930): p. 1029-33.

254. Sonnenschein, C. and A.M. Soto, *The aging of the 2000 and 2011 Hallmarks of Cancer reviews: A critique.* Journal of biosciences, 2013. **38**(3): p. 651-663.

255. Cantor, J.R. and D.M. Sabatini, *Cancer Cell Metabolism: One Hallmark, Many Faces.* Cancer discovery, 2012. **2**(10): p. 881-898.

256. Liberti, M.V. and J.W. Locasale, *The Warburg Effect: How Does it Benefit Cancer Cells?* Trends Biochem Sci, 2016. **41**(3): p. 211-8.

257. Alfarouk, K.O., et al., *Glycolysis, tumor metabolism, cancer growth and dissemination. A new pH-based etiopathogenic perspective and therapeutic approach to an old cancer question.* Oncoscience, 2014. **1**(12): p. 777-802.

258. Vogelstein, B. and K.W. Kinzler, *Cancer genes and the pathways they control.* Nat Med, 2004. **10**(8): p. 789-99.

259. Hu, Y., et al., *K-ras(G12V) transformation leads to mitochondrial dysfunction and a metabolic switch from oxidative phosphorylation to glycolysis.* Cell Res, 2012. **22**(2): p. 399-412.

260. Denko, N.C., *Hypoxia, HIF1 and glucose metabolism in the solid tumour.* Nat Rev Cancer, 2008. **8**(9): p. 705-13.

261. Majmundar, A.J., W.J. Wong, and M.C. Simon, *Hypoxia-inducible factors and the response to hypoxic stress.* Mol Cell, 2010. **40**(2): p. 294-309.

262. Duvel, K., et al., *Activation of a metabolic gene regulatory network downstream of mTOR complex 1.* Mol Cell, 2010. **39**(2): p. 171-83.

263. Levine, A.J. and A.M. Puzio-Kuter, *The control of the metabolic switch in cancers by oncogenes and tumor suppressor genes.* Science, 2010. **330**(6009): p. 1340-4.

264. Lu, C.W., et al., *Induction of pyruvate dehydrogenase kinase-3 by hypoxia-inducible factor-1 promotes metabolic switch and drug resistance.* J Biol Chem, 2008. **283**(42): p. 28106-14.

265. Sun, Q., et al., *Mammalian target of rapamycin up-regulation of pyruvate kinase isoenzyme type M2 is critical for aerobic glycolysis and tumor growth.* Proc Natl Acad Sci U S A, 2011. **108**(10): p. 4129-34.

266. Dang, C.V., et al., *The interplay between MYC and HIF in cancer.* Nat Rev Cancer, 2008. **8**(1): p. 51-6.

267. Pelicano, H., et al., *Glycolysis inhibition for anticancer treatment.* Oncogene, 0000. **25**(34): p. 4633-4646.

268. Patra, K.C., et al., *Hexokinase 2 is required for tumor initiation and maintenance and its systemic deletion is therapeutic in mouse models of cancer.* Cancer cell, 2013. **24**(2): p. 213-228.

269. Dong, G., et al., *PKM2 and cancer: The function of PKM2 beyond glycolysis.* Oncology Letters, 2016. **11**(3): p. 1980-1986.

270. Soltany-Rezaee-Rad, M., et al., *Overexpression of FOXO3, MYD88, and GAPDH Identified by Suppression Subtractive Hybridization in Esophageal Cancer Is Associated with Autophagy.* Gastroenterology Research and Practice, 2014. **2014**: p. 185035.

271. Peshavaria, M. and I.N. Day, *Molecular structure of the human muscle-specific enolase gene (ENO3).* Biochemical Journal, 1991. **275**(Pt 2): p. 427-433.

272. Baba, Y., et al., *HIF1A overexpression is associated with poor prognosis in a cohort of 731 colorectal cancers.* Am J Pathol, 2010. **176**(5): p. 2292-301.

273. Fillies, T., et al., *HIF1-alpha overexpression indicates a good prognosis in early stage squamous cell carcinomas of the oral floor.* BMC Cancer, 2005. **5**(1): p. 84.

274. Lock, F.E., et al., *Targeting carbonic anhydrase IX depletes breast cancer stem cells within the hypoxic niche.* Oncogene, 2013. **32**(44): p. 5210-9.

275. McDonald, P.C. and S. Dedhar, *Carbonic anhydrase IX (CAIX) as a mediator of hypoxia-induced stress response in cancer cells.* Subcell Biochem, 2014. **75**: p. 255-69.

276. Ziello, J.E., I.S. Jovin, and Y. Huang, *Hypoxia-Inducible Factor (HIF)-1 Regulatory Pathway and its Potential for Therapeutic Intervention in Malignancy and Ischemia.* The Yale Journal of Biology and Medicine, 2007. **80**(2): p. 51-60.

277. Semenza, G.L., *HIF-1 mediates metabolic responses to intratumoral hypoxia and oncogenic mutations.* The Journal of Clinical Investigation, 2013. **123**(9): p. 3664-3671.

278. Solaini, G., et al., *Hypoxia and mitochondrial oxidative metabolism.* Biochimica et Biophysica Acta (BBA) - Bioenergetics, 2010. **1797**(6–7): p. 1171-1177.

279. Wang, D. and R.N. DuBois, *Eicosanoids and cancer.* Nature reviews. Cancer, 2010. **10**(3): p. 181-193.

280. Chen, X., et al., *Overexpression of 5-lipoxygenase in rat and human esophageal adenocarcinoma and inhibitory effects of zileuton and celecoxib on carcinogenesis.* Clin Cancer Res, 2004. **10**(19): p. 6703-9.

281. Tafani, M., et al., *The Interplay of Reactive Oxygen Species, Hypoxia, Inflammation, and Sirtuins in Cancer Initiation and Progression.* Oxidative Medicine and Cellular Longevity, 2016. **2016**: p. 3907147.

282. Jun, Y.J., et al., *Clinicopathologic significance of GLUT1 expression and its correlation with Apaf-1 in colorectal adenocarcinomas.* World Journal of Gastroenterology : WJG, 2011. **17**(14): p. 1866-1873.

283. Schwartzenberg-Bar-Yoseph, F., M. Armoni, and E. Karnieli, *The Tumor Suppressor p53 Down-Regulates Glucose Transporters GLUT1 and GLUT4. Gene Expression.* Cancer Research, 2004. **64**(7): p. 2627-2633.

284. Jones, R.G. and C.B. Thompson, *Tumor suppressors and cell metabolism: a recipe for cancer growth.* Genes & Development, 2009. **23**(5): p. 537-548.

285. Quail, D.F. and J.A. Joyce, *Microenvironmental regulation of tumor progression and metastasis.* Nat Med, 2013. **19**(11): p. 1423-1437.

286. Calvo, M.B., et al., *Potential Role of Sugar Transporters in Cancer and Their Relationship with Anticancer Therapy.* International Journal of Endocrinology, 2010. **2010**: p. 205357.

287. Sahiner, I. and G.U. Vural, *Positron emission tomography/computerized tomography in lung cancer.* Quantitative Imaging in Medicine and Surgery, 2014. **4**(3): p. 195-206.

288. Gallamini, A., C. Zwarthoed, and A. Borra, *Positron Emission Tomography (PET) in Oncology.* Cancers, 2014. **6**(4): p. 1821-1889.

289. Benveniste, M.F.K., et al., *FDG PET-CT Aids in the Preoperative Assessment of Patients with Newly Diagnosed Thymic Epithelial Malignancies.* Journal of thoracic oncology : official publication of the International Association for the Study of Lung Cancer, 2013. **8**(4): p. 10.1097/JTO.0b013e3182835549.

290. Bai, B., J. Bading, and P.S. Conti, *Tumor Quantification in Clinical Positron Emission Tomography.* Theranostics, 2013. **3**(10): p. 787-801.

291. Yoo Ie, R., et al., *Prognostic value of SUVmax and metabolic tumor volume on 18F-FDG PET/CT in early stage non-small cell lung cancer patients without LN metastasis.* Biomed Mater Eng, 2014. **24**(6): p. 3091-103.

292. Groheux, D., et al., *Performance of FDG PET/CT in the clinical management of breast cancer.* Radiology, 2013. **266**(2): p. 388-405.

293. Olson, A.L., *Regulation of GLUT4 and Insulin-Dependent Glucose Flux.* ISRN Molecular Biology, 2012. **2012**: p. 856987.

294. Patra, K.C. and N. Hay, *Hexokinase 2 as oncotarget.* Oncotarget, 2013. **4**(11): p. 1862-1863.

295. Gao, Y., et al., *Overexpression of metabolic markers HK1 and PKM2 contributes to lymphatic metastasis and adverse prognosis in Chinese gastric cancer.* International Journal of Clinical and Experimental Pathology, 2015. **8**(8): p. 9264-9271.

296. Xie, J., C. Dai, and X. Hu, *Evidence That Does Not Support Pyruvate Kinase M2 (PKM2)-catalyzed Reaction as a Rate-limiting Step in Cancer Cell Glycolysis.* J Biol Chem, 2016. **291**(17): p. 8987-99.

297. Wolfson-Stofko, B., T. Hadi, and J.S. Blanchard, *Kinetic and Mechanistic Characterization of the Glyceraldehyde 3-Phosphate Dehydrogenase from Mycobacterium tuberculosis.* Archives of biochemistry and biophysics, 2013. **540**(0): p. 10.1016/j.abb.2013.10.007.

298. Capello, M., et al., *alpha-Enolase: a promising therapeutic and diagnostic tumor target.* Febs j, 2011. **278**(7): p. 1064-74.

299. Rao, C.V., N.B. Janakiram, and A. Mohammed, *Lipoxygenase and Cyclooxygenase Pathways and Colorectal Cancer Prevention.* Current colorectal cancer reports, 2012. **8**(4): p. 316-324.

300. Wisastra, R. and F.J. Dekker, *Inflammation, Cancer and Oxidative Lipoxygenase Activity are Intimately Linked.* Cancers, 2014. **6**(3): p. 1500-1521.

301. Gerlee, P. and A.R.A. Anderson, *DIFFUSION-LIMITED TUMOUR GROWTH: SIMULATIONS AND ANALYSIS.* Mathematical biosciences and engineering : MBE, 2010. **7**(2): p. 385-400.

302. Hojfeldt, J.W. and K. Helin, *Regional tumour glutamine supply affects chromatin and cell identity.* Nat Cell Biol, 2016. **18**(10): p. 1027-1029.

303. Takalkar, A.M., G. El-Haddad, and D.L. Lilien, *FDG-PET and PET/CT - Part II.* The Indian Journal of Radiology & Imaging, 2008. **18**(1): p. 17-36.

304. McDonald, P.C., et al., *Recent Developments in Targeting Carbonic Anhydrase IX for Cancer Therapeutics.* Oncotarget, 2012. **3**(1): p. 84-97.

305. Lou, Y., et al., *Targeting tumor hypoxia: suppression of breast tumor growth and metastasis by novel carbonic anhydrase IX inhibitors.* Cancer Res, 2011. **71**(9): p. 3364-76.

306. Ilie, M., et al., *High levels of carbonic anhydrase IX in tumour tissue and plasma are biomarkers of poor prognostic in patients with non-small cell lung cancer.* Br J Cancer, 2010. **102**(11): p. 1627-35.

307. Choschzick, M., et al., *Overexpression of carbonic anhydrase IX (CAIX) is an independent unfavorable prognostic marker in endometrioid ovarian cancer.* Virchows Arch, 2011. **459**(2): p. 193-200.

308. Klatte, T., et al., *Carbonic anhydrase IX in bladder cancer: a diagnostic, prognostic, and therapeutic molecular marker.* Cancer, 2009. **115**(7): p. 1448-58.

309. Tafreshi, N.K., et al., *Chapter 13: Carbonic Anhydrase IX as an Imaging and Therapeutic Target for Tumors and Metastases.* Sub-cellular biochemistry, 2014. **75**: p. 221-254.

310. Doyle, S.L., et al., *Establishing computed tomography-defined visceral fat area thresholds for use in obesity-related cancer research.* Nutr Res, 2013. **33**.

311. Jung, U.J. and M.-S. Choi, *Obesity and Its Metabolic Complications: The Role of Adipokines and the Relationship between Obesity, Inflammation, Insulin Resistance, Dyslipidemia and Nonalcoholic Fatty Liver Disease.* International Journal of Molecular Sciences, 2014. **15**(4): p. 6184-6223.

312. Trayhurn, P., *Hypoxia and adipose tissue function and dysfunction in obesity.* Physiol Rev, 2013. **93**(1): p. 1-21.

313. Baba, Y., et al., *HIF1A Overexpression Is Associated with Poor Prognosis in a Cohort of 731 Colorectal Cancers.* The American Journal of Pathology, 2010. **176**(5): p. 2292-2301.

314. Lynam-Lennon, N., et al., *Altered mitochondrial function and energy metabolism is associated with a radioresistant phenotype in oesophageal adenocarcinoma.* PLoS One, 2014. **9**.

315. Jose, C., N. Bellance, and R. Rossignol, *Choosing between glycolysis and oxidative phosphorylation: A tumor's dilemma?* Biochimica et Biophysica Acta (BBA) - Bioenergetics, 2011. **1807**(6): p. 552-561.

316. Matsuyama, T., et al., *Expression of hypoxia-inducible factor-1alpha in esophageal squamous cell carcinoma.* Cancer Sci, 2005. **96**(3): p. 176-82.

317. Liu, J., et al., *Epithelial-to-mesenchymal transition in human esophageal cancer associates with tumor progression and patient's survival.* Int J Clin Exp Pathol, 2014. **7**(10): p. 6943-9.

318. Hoque, A., et al., *Increased 5-lipoxygenase expression and induction of apoptosis by its inhibitors in esophageal cancer: a potential target for prevention.* Carcinogenesis, 2005. **26**(4): p. 785-791.

319. Freemerman, A.J., et al., *Metabolic reprogramming of macrophages: glucose transporter 1 (GLUT1)-mediated glucose metabolism drives a proinflammatory phenotype.* J Biol Chem, 2014. **289**(11): p. 7884-96.

320. Moon, J.S., et al., *mTORC1-Induced HK1-Dependent Glycolysis Regulates NLRP3 Inflammasome Activation.* Cell Rep, 2015. **12**(1): p. 102-15.

321. Wolf, A., et al., *Hexokinase 2 is a key mediator of aerobic glycolysis and promotes tumor growth in human glioblastoma multiforme.* J Exp Med, 2011. **208**(2): p. 313-26.

322. Phan, L.M., S.-C.J. Yeung, and M.-H. Lee, *Cancer metabolic reprogramming: importance, main features, and potentials for precise targeted anti-cancer therapies.* Cancer Biology & Medicine, 2014. **11**(1): p. 1-19.

323. Larue, L. and A. Bellacosa, *Epithelial-mesenchymal transition in development and cancer: role of phosphatidylinositol 3' kinase/AKT pathways.* Oncogene, 2005. **24**(50): p. 7443-54.

324. Jiang, Y.G., et al., *Role of Wnt/beta-catenin signaling pathway in epithelial-mesenchymal transition of human prostate cancer induced by hypoxia-inducible factor-1alpha.* Int J Urol, 2007. **14**(11): p. 1034-9.

325. Heerboth, S., et al., *EMT and tumor metastasis.* Clinical and Translational Medicine, 2015. **4**: p. 6.

326. Allott, E.H., et al., *Elevated tumor expression of PAI-1 and SNAI2 in obese esophageal adenocarcinoma patients and impact on prognosis.* Clin Transl Gastroenterol, 2012. **3**.

327. Liu, L., et al., *ZEB1 Upregulates VEGF Expression and Stimulates Angiogenesis in Breast Cancer.* PLoS One, 2016. **11**(2): p. e0148774.

328. Lin, C.Y., et al., *Matrix metalloproteinase-9 cooperates with transcription factor Snail to induce epithelial-mesenchymal transition.* Cancer Sci, 2011. **102**(4): p. 815-27.

329. Despres, J.P., et al., *Abdominal obesity and the metabolic syndrome: contribution to global cardiometabolic risk.* Arterioscler Thromb Vasc Biol, 2008. **28**(6): p. 1039-49.

330. Chen, Q., H. Zhuang, and Y. Liu, *The association between obesity factor and esophageal caner.* Journal of Gastrointestinal Oncology, 2012. **3**(3): p. 226-231.

331. Favaretto, F., et al., *GLUT4 defects in adipose tissue are early signs of metabolic alterations in Alms1GT/GT, a mouse model for obesity and insulin resistance.* PLoS One, 2014. **9**(10): p. e109540.

332. He, Q., et al., *Regulation of HIF-1α activity in adipose tissue by obesity-associated factors: adipogenesis, insulin, and hypoxia.* American Journal of Physiology - Endocrinology and Metabolism, 2011. **300**(5): p. E877-E885.

333. Allott, E.H., et al., *MMP9 expression in oesophageal adenocarcinoma is upregulated with visceral obesity and is associated with poor tumour differentiation.* Mol Carcinog, 2013. **52**.

334. Kim, Y.H., et al., *TWIST1 and SNAI1 as markers of poor prognosis in human colorectal cancer are associated with the expression of ALDH1 and TGF-beta1.* Oncol Rep, 2014. **31**(3): p. 1380-8.

335. Liu, J., et al., *Epithelial-to-mesenchymal transition in human esophageal cancer associates with tumor progression and patient's survival.* International Journal of Clinical and Experimental Pathology, 2014. **7**(10): p. 6943-6949.

336. Sanchez-Tillo, E., et al., *ZEB1 represses E-cadherin and induces an EMT by recruiting the SWI/SNF chromatin-remodeling protein BRG1.* Oncogene, 2010. **29**(24): p. 3490-500.

337. Cathcart, J., A. Pulkoski-Gross, and J. Cao, *Targeting matrix metalloproteinases in cancer: Bringing new life to old ideas.* Genes & Diseases, 2015. **2**(1): p. 26-34.

338. Gonzalez, D.M. and D. Medici, *Signaling mechanisms of the epithelial-mesenchymal transition.* Science signaling, 2014. **7**(344): p. re8-re8.

339. Kalluri, R. and R.A. Weinberg, *The basics of epithelial-mesenchymal transition.* The Journal of Clinical Investigation, 2009. **119**(6): p. 1420-1428.

340. Doyle, S.L., et al., *Visceral obesity, metabolic syndrome, insulin resistance and cancer.* Proc Nutr Soc, 2012. **71**.

341. Wells, J.C.K. and M.S. Fewtrell, *Measuring body composition.* Archives of Disease in Childhood, 2006. **91**(7): p. 612-617.

342. Grignol, V.P., et al., *Increased visceral to subcutaneous fat ratio is associated with decreased overall survival in patients with metastatic melanoma receiving anti-angiogenic therapy.* Surg Oncol, 2015. **24**(4): p. 353-8.

343. Kim, J.H., et al., *Impact of intra-abdominal fat on surgical outcome and overall survival of patients with gastric cancer.* International Journal of Surgery, 2014. **12**(4): p. 346-352.

344. Yoshikawa, K., et al., *Visceral fat area is superior to body mass index as a predictive factor for risk with laparoscopy-assisted gastrectomy for gastric cancer.* Surgical Endoscopy, 2011. **25**(12): p. 3825-3830.

345. Sahakyan, K.R., et al., *Normal-Weight Central Obesity: Implications for Total and Cardiovascular Mortality.* Ann Intern Med, 2015. **163**(11): p. 827-35.

346. Obata, Y., et al., *Impact of visceral fat on gene expression profile in peripheral blood cells in obese Japanese subjects.* Cardiovascular Diabetology, 2016. **15**: p. 159.

347. Wang, H.K., et al., *Visceral fat accumulation is associated with different pathological subtypes of renal cell carcinoma (RCC): a multicentre study in China.* BJU Int, 2014. **114**(4): p. 496-502.

348. Ness-Abramof, R. and C.M. Apovian, *Waist circumference measurement in clinical practice.* Nutr Clin Pract, 2008. **23**(4): p. 397-404.

349. Pahk, K., et al., *Predictive Role of Functional Visceral Fat Activity Assessed by Preoperative F-18 FDG PET/CT for Regional Lymph Node or Distant Metastasis in Patients with Colorectal Cancer.* PLoS ONE, 2016. **11**(2): p. e0148776.

350. Kinahan, P.E. and J.W. Fletcher, *PET/CT Standardized Uptake Values (SUVs) in Clinical Practice and Assessing Response to Therapy.* Seminars in ultrasound, CT, and MR, 2010. **31**(6): p. 496-505.

351. Shankar, L.K., et al., *Consensus recommendations for the use of 18F-FDG PET as an indicator of therapeutic response in patients in National Cancer Institute Trials.* J Nucl Med, 2006. **47**(6): p. 1059-66.

352. Song, B.-I., et al., *Prognostic Value of Primary Tumor Uptake on F-18 FDG PET/CT in Patients with Invasive Ductal Breast Cancer.* Nuclear Medicine and Molecular Imaging, 2011. **45**(2): p. 117-124.

353. Chung, M.K., et al., *Metabolic tumor volume of [18F]-fluorodeoxyglucose positron emission tomography/computed tomography predicts short-term outcome to radiotherapy with or without chemotherapy in pharyngeal cancer.* Clin Cancer Res, 2009. **15**(18): p. 5861-8.

354. Seol, K.H. and J.E. Lee, *PET/CT planning during chemoradiotherapy for esophageal cancer.* Radiation Oncology Journal, 2014. **32**(1): p. 31-42.

355. Cairns, R.A., et al., *Cancer cell metabolism.* Cold Spring Harb Symp Quant Biol, 2011. **76**: p. 299-311.

356. Jiang, P., W. Du, and M. Wu, *Regulation of the pentose phosphate pathway in cancer.* Protein Cell, 2014. **5**(8): p. 592-602.

357. Swietach, P., et al., *The chemistry, physiology and pathology of pH in cancer.* Philosophical Transactions of the Royal Society B: Biological Sciences, 2014. **369**(1638): p. 20130099.

358. Chiche, J., M.C. Brahimi-Horn, and J. Pouysségur, *Tumour hypoxia induces a metabolic shift causing acidosis: a common feature in cancer.* Journal of Cellular and Molecular Medicine, 2010. **14**(4): p. 771-794.

359. Gatenby, R.A. and R.J. Gillies, *Why do cancers have high aerobic glycolysis?* Nat Rev Cancer, 2004. **4**(11): p. 891-899.

360. Sedlakova, O., et al., *Carbonic anhydrase IX, a hypoxia-induced catalytic component of the pH regulating machinery in tumors.* Frontiers in Physiology, 2014. **4**(400).

361. Jang, M., S.S. Kim, and J. Lee, *Cancer cell metabolism: implications for therapeutic targets.* Experimental & Molecular Medicine, 2013. **45**(10): p. e45.

362. Piret, J.P., et al., *CoCl2, a chemical inducer of hypoxia-inducible factor-1, and hypoxia reduce apoptotic cell death in hepatoma cell line HepG2.* Ann N Y Acad Sci, 2002. **973**: p. 443-7.

363. Rogatzki, M.J., et al., *Lactate is always the end product of glycolysis.* Front Neurosci, 2015. **9**: p. 22.

364. Dupuy, F., et al., *PDK1-Dependent Metabolic Reprogramming Dictates Metastatic Potential in Breast Cancer.* Cell Metabolism, 2015. **22**(4): p. 577-589.

365. Kim, J.-w., et al., *HIF-1-mediated expression of pyruvate dehydrogenase kinase: A metabolic switch required for cellular adaptation to hypoxia.* Cell Metabolism, 2006. **3**(3): p. 177-185.

366. Sanders, E. and S. Diehl, *Analysis and interpretation of transcriptomic data obtained from extended Warburg effect genes in patients with clear cell renal cell carcinoma.* Oncoscience, 2015. **2**(2): p. 151-186.

367. Sharma, L.K., et al., *Mitochondrial respiratory complex I dysfunction promotes tumorigenesis through ROS alteration and AKT activation.* Human Molecular Genetics, 2011. **20**(23): p. 4605-4616.

368. Sharma, L.K., J. Lu, and Y. Bai, *Mitochondrial Respiratory Complex I: Structure, Function and Implication in Human Diseases.* Current medicinal chemistry, 2009. **16**(10): p. 1266-1277.

369. Owens, K.M., et al., *Impaired OXPHOS Complex III in Breast Cancer.* PLoS ONE, 2011. **6**(8): p. e23846.

370. Bénit, P., S. Lebon, and P. Rustin, *Respiratory-chain diseases related to complex III deficiency.* Biochimica et Biophysica Acta (BBA) - Molecular Cell Research, 2009. **1793**(1): p. 181-185.

371. Lin, Q. and Z. Yun, *The Hypoxia-Inducible Factor Pathway in Adipocytes: The Role of HIF-2 in Adipose Inflammation and Hypertrophic Cardiomyopathy.* Frontiers in Endocrinology, 2015. **6**: p. 39.

372. Lee, Y.S., et al., *Increased adipocyte O2 consumption triggers HIF-1alpha, causing inflammation and insulin resistance in obesity.* Cell, 2014. **157**(6): p. 1339-52.

373. Gomez-Roman, N., et al., *Hypoxia-inducible factor 1 alpha is required for the tumourigenic and aggressive phenotype associated with Rab25 expression in ovarian cancer.* Oncotarget, 2016. **7**(16): p. 22650-22664.

374. Müller-Edenborn, K., et al., *Hypoxia attenuates the proinflammatory response in colon cancer cells by regulating IκB.* Oncotarget, 2015. **6**(24): p. 20288-20301.

375. Kuwano, H., et al., *Guidelines for Diagnosis and Treatment of Carcinoma of the Esophagus April 2012 edited by the Japan Esophageal Society.* Esophagus, 2015. **12**(1): p. 1-30.

376. Wang, H., et al., *The Challenges and the Promise of Molecular Targeted Therapy in Malignant Gliomas().* Neoplasia (New York, N.Y.), 2015. **17**(3): p. 239-255.

377. Vanneman, M. and G. Dranoff, *Combining immunotherapy and targeted therapies in cancer treatment.* Nat Rev Cancer, 2012. **12**(4): p. 237-251.

378. Knab, L.M., P.J. Grippo, and D.J. Bentrem, *Involvement of eicosanoids in the pathogenesis of pancreatic cancer: The roles of cyclooxygenase-2 and 5-lipoxygenase.* World Journal of Gastroenterology : WJG, 2014. **20**(31): p. 10729-10739.

379. Sarveswaran, S., et al., *Inhibition of 5-lipoxygenase triggers apoptosis in prostate cancer cells via down-regulation of protein kinase C-epsilon.* Biochim Biophys Acta, 2011. **1813**(12): p. 2108-17.

380. Bishayee, K. and A.R. Khuda-Bukhsh, *5-lipoxygenase antagonist therapy: a new approach towards targeted cancer chemotherapy.* Acta Biochim Biophys Sin (Shanghai), 2013. **45**(9): p. 709-19.

381. Tzanakakis, G.N., et al., *The preventive effect of ketoconazole on experimental metastasis from a human pancreatic carcinoma may be related to its effect on prostaglandin synthesis.* Int J Gastrointest Cancer, 2002. **32**(1): p. 23-30.

382. Cesari, I.M., et al., *Methyl Jasmonate: Putative Mechanisms of Action on Cancer Cells Cycle, Metabolism, and Apoptosis.* International Journal of Cell Biology, 2014. **2014**: p. 572097.

383. Li, L., et al., *Combined inhibition of glycolysis, the pentose cycle, and thioredoxin metabolism selectively increases cytotoxicity and oxidative stress in human breast and prostate cancer.* Redox Biology, 2015. **4**: p. 127-135.

384. Gonsalves, C.S. and V.K. Kalra, *Hypoxia-mediated expression of 5-lipoxygenase-activating protein involves HIF-1alpha and NF-kappaB and microRNAs 135a and 199a-5p.* J Immunol, 2010. **184**(7): p. 3878-88.

385. Alkim, C., et al., *Angiogenesis in Inflammatory Bowel Disease.* International Journal of Inflammation, 2015. **2015**: p. 970890.

386. Lange, C., et al., *Vascular endothelial growth factor: a neurovascular target in neurological diseases.* Nat Rev Neurol, 2016. **12**(8): p. 439-454.

387. Carpentier, P.A. and T.D. Palmer, *Immune Influence on Adult Neural Stem Cell Regulation and Function.* Neuron, 2009. **64**(1): p. 79-92.

388. Colotta, F., et al., *Cancer-related inflammation, the seventh hallmark of cancer: links to genetic instability.* Carcinogenesis, 2009. **30**(7): p. 1073-1081.

389. Tanaka, S., et al., *Immunoreactive transforming growth factor alpha is commonly present in colorectal neoplasia.* The American Journal of Pathology, 1991. **139**(1): p. 123-129.

390. Grandis, J.R. and D.J. Tweardy, *TGF-alpha and EGFR in head and neck cancer.* J Cell Biochem Suppl, 1993. **17f**: p. 188-91.

391. Ray, P., et al., *Signaling of c-kit in dendritic cells influences adaptive immunity.* Annals of the New York Academy of Sciences, 2010. **1183**: p. 104-122.

392. Esposito, I., et al., *The stem cell factor-c-kit system and mast cells in human pancreatic cancer.* Lab Invest, 2002. **82**(11): p. 1481-92.

393. Elpek, G.O., et al., *The prognostic relevance of angiogenesis and mast cells in squamous cell carcinoma of the oesophagus.* J Clin Pathol, 2001. **54**(12): p. 940-4.

394. Baggiolini, M., *Chemokines and leukocyte traffic.* Nature, 1998. **392**(6676): p. 565-568.

395. Wetzel, K., et al., *MCP-3 (CCL7) delivered by parvovirus MVMp reduces tumorigenicity of mouse melanoma cells through activation of T lymphocytes and NK cells.* Int J Cancer, 2007. **120**(6): p. 1364-71.

396. Hu, J.-Y., et al., *Transfection of colorectal cancer cells with chemokine MCP-3 (monocyte chemotactic protein-3) gene retards tumor growth and inhibits tumor metastasis.* World Journal of Gastroenterology, 2002. **8**(6): p. 1067-1072.

397. Tan, G.-J., et al., *Cathepsins mediate tumor metastasis.* World Journal of Biological Chemistry, 2013. **4**(4): p. 91-101.

398. Ji, N.Y., et al., *Identification of endothelial cell-specific molecule-1 as a potential serum marker for colorectal cancer.* Cancer Sci, 2010. **101**(10): p. 2248-53.

399. Delehedde, M., et al., *Endocan in Cancers: A Lesson from a Circulating Dermatan Sulfate Proteoglycan.* International Journal of Cell Biology, 2013. **2013**: p. 705027.

400. Krupska, I., E.A. Bruford, and B. Chaqour, *Eyeing the Cyr61/CTGF/NOV (CCN) group of genes in development and diseases: highlights of their structural likenesses and functional dissimilarities.* Human Genomics, 2015. **9**: p. 24.

401. Jeong, D., et al., *Cyr61 Expression is associated with prognosis in patients with colorectal cancer.* BMC Cancer, 2014. **14**: p. 164-164.

402. Sun, Z.J., et al., *Involvement of Cyr61 in growth, migration, and metastasis of prostate cancer cells.* Br J Cancer, 2008. **99**(10): p. 1656-67.

403. Elbashir, S.M., et al., *Duplexes of 21-nucleotide RNAs mediate RNA interference in cultured mammalian cells.* Nature, 2001. **411**(6836): p. 494-8.

404. Jackson, A.L. and P.S. Linsley, *Recognizing and avoiding siRNA off-target effects for target identification and therapeutic application.* Nat Rev Drug Discov, 2010. **9**(1): p. 57-67.

405. Sun, H., et al., *Knockdown of PKM2 Suppresses Tumor Growth and Invasion in Lung Adenocarcinoma.* Int J Mol Sci, 2015. **16**(10): p. 24574-87.

406. Goldberg, M.S. and P.A. Sharp, *Pyruvate kinase M2-specific siRNA induces apoptosis and tumor regression.* The Journal of Experimental Medicine, 2012. **209**(2): p. 217-224.

407. Li, C., et al., *Metabolic reprogramming in cancer cells: glycolysis, glutaminolysis, and Bcl-2 proteins as novel therapeutic targets for cancer.* World Journal of Surgical Oncology, 2015. **14**: p. 15.

408. Chaika, N.V., et al., *Differential Expression of Metabolic Genes in Tumor and Stromal Components of Primary and Metastatic Loci in Pancreatic Adenocarcinoma.* PLoS ONE, 2012. **7**(3): p. e32996.

409. Cui, Y., et al., *Upregulation of glucose metabolism by NF-kappa B2/p52 mediates enzalutamide resistance in castration resistant prostate cancer cells.* Endocrine-related cancer, 2014. **21**(3): p. 435-442.

410. Hopkins, B.D., M.D. Goncalves, and L.C. Cantley, *Obesity and Cancer Mechanisms: Cancer Metabolism.* J Clin Oncol, 2016. **34**(35): p. 4277-4283.

411. Pischon, T. and K. Nimptsch, *Obesity and Risk of Cancer: An Introductory Overview.* Recent Results Cancer Res, 2016. **208**: p. 1-15.

412. Divella, R., et al., *Obesity and cancer: the role of adipose tissue and adipo-cytokines-induced chronic inflammation.* Journal of Cancer, 2016. **7**(15): p. 2346-2359.

413. Miyazono, F., et al., *Mutations in the mitochondrial DNA D-Loop region occur frequently in adenocarcinoma in Barrett's esophagus.* Oncogene, 2002. **21**(23): p. 3780-3.

414. Hibi, K., et al., *Mitochondrial DNA alteration in esophageal cancer.* Int J Cancer, 2001. **92**(3): p. 319-21.

415. Sharma, H., et al., *Mutations in the mitochondrial DNA D-loop region are frequent in cervical cancer.* Cancer Cell International, 2005. **5**: p. 34-34.

416. Gaude, E. and C. Frezza, *Defects in mitochondrial metabolism and cancer.* Cancer & Metabolism, 2014. **2**: p. 10-10.

417. Ferrante, M., et al., *The role of vascular endothelial growth factor (VEGF) in inflammatory bowel disease.* Inflamm Bowel Dis, 2006. **12**(9): p. 870-8.

418. Afuwape, A.O., S. Kiriakidis, and E.M. Paleolog, *The role of the angiogenic molecule VEGF in the pathogenesis of rheumatoid arthritis.* Histol Histopathol, 2002. **17**(3): p. 961-72.

419. Sato, Y., et al., *Hepatitis C virus core protein promotes proliferation of human hepatoma cells through enhancement of transforming growth factor alpha expression via activation of nuclear factor-kappaB.* Gut, 2006. **55**(12): p. 1801-8.

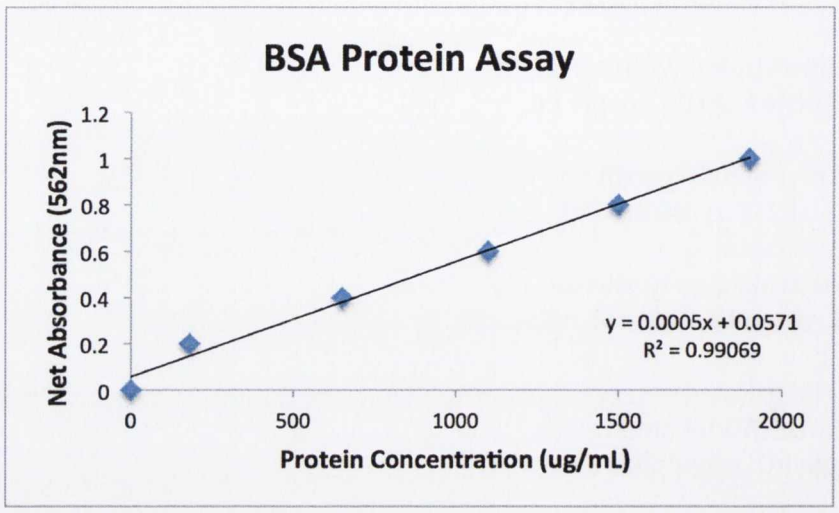
420. Hormi, K., et al., *Transforming growth factor-alpha and epidermal growth factor receptor in colonic mucosa in active and inactive inflammatory bowel disease.* Growth Factors, 2000. **18**(2): p. 79-91.

421. Dreikhausen, L., et al., *Association of angiogenic factors with prognosis in esophageal cancer.* BMC Cancer, 2015. **15**: p. 121.

Appendices

Appendix I

Representative BSA standard curve used in BSA protein quantification assay



Appendix II

Figure 1 List of biomarkers measured by Proseek Multiplex Inflammation I Arrays

		Sample types							Analytical measurement					Precision	
		Signal-to-background (2^{NPX})				Relative 2^{NPX} to EDTA			pg/mL				log10		
Target	UniProt No	ACD	EDTA	Heparin	Serum	ACD	Heparin	Serum	LOD	LLOQ	ULOQ	Hook	Range	Intra-assay	Inter-assay
Adenosine Deaminase (ADA)	P00813	45	58	47	58	77%	80%	99%	0.48	0.48	31250	125000	4.8	5%	29%
Artemin (ARTN)	Q5T4W7	NR	1	NR	1	NR	NR	102%	0.24	0.48	31250	62500	4.8	7%	18%
Axin-1 (AXIN1)	O15169	4	9	3	4	50%	30%	42%	61	61	62500	250000	3.0	6%	19%
Beta-nerve growth factor (Beta-NGF)	P01138	3	3	2	4	95%	81%	123%	0.48	0.48	15625	31250	4.5	6%	14%
Brain-derived neurotrophic factor (BDNF)	P23560	16	21	16	23	75%	76%	109%						6%	10%
Caspase 8 (CASP-8)	Q14790	3	3	3	5	84%	105%	154%	0.48	0.48	31250	62500	4.8	7%	22%
C-C motif chemokine 4 (CCL4)	P13236	37	68	56	99	55%	82%	146%	1.9	1.9	31250	62500	4.2	6%	17%
C-C motif chemokine 19 (CCL19)	Q99731	1014	1128	870	1249	90%	77%	111%	15	15	31250	62500	3.3	8%	15%
C-C motif chemokine 20 (CCL20)	P78556	169	184	132	139	91%	72%	75%	7.6	7.6	15625	15625	3.3	7%	13%
C-C motif chemokine 23 (CCL23)	P55773	322	384	313	358	84%	81%	93%	31	31	31250	62500	3.0	6%	13%
C-C motif chemokine 25 (CCL25)	O15444	71	82	73	95	86%	89%	115%	3.8	3.8	62500	125000	4.2	6%	18%
C-C motif chemokine 28 (CCL28)	Q9NRJ3	3	4	2	4	75%	60%	111%	61	122	1000000	1000000	3.9	7%	14%
CD40L receptor (CD40)	P25942	399	463	452	646	86%	98%	140%	0.01	0.01	3906	15625	5.4	5%	21%
CUB domain-containing protein 1 (CDCP1)	Q9H5V8	7	8	7	9	81%	87%	107%	0.12	0.12	7812	31250	4.8	6%	24%
C-X-C motif chemokine 1 (CXCL1)	P09341	135	422	713	1301	32%	169%	308%	3.8	7.6	15625	15625	3.3	6%	15%
C-X-C motif chemokine 5 (CXCL5)	P42830	336	3011	5114	9171	11%	170%	305%	0.95	0.95	7812	15625	3.9	7%	13%
C-X-C motif chemokine 6 (CXCL6)	P80162	50	177	409	840	28%	231%	475%	7.6	31	15625	31250	2.7	8%	14%
C-X-C motif chemokine 9 (CXCL9)	Q07325	54	68	59	68	80%	87%	100%	0.95	0.95	3906	7812	3.6	6%	12%
C-X-C motif chemokine 10 (CXCL10)	P02778	378	505	378	546	75%	75%	108%	7.6	7.6	15625	31250	3.3	7%	11%
C-X-C motif chemokine 11 (CXCL11)	O14625	94	308	578	850	31%	188%	276%	7.6	31	15625	15625	2.7	7%	14%
Cystatin D (CST5)	P28325	86	97	89	101	88%	91%	104%	1.9	1.9	15625	31250	3.9	5%	21%
Delta and Notch-like epidermal growth factor-related recep (DNER)	Q6NFT8	181	201	181	220	90%	90%	109%	0.95	1.9	31250	62500	4.2	5%	26%
Eotaxin-1 (CCL11)	P51671	247	294	307	318	84%	104%	108%	3.8	3.8	31250	62500	3.9	5%	14%
Eukaryotic translation initiation factor 4E binding protein 1 (4E-BP1)	Q13541	14	102	12	61	14%	12%	59%						6%	23%
Fibroblast growth factor 5 (FGF-5)	Q8NF90	2	2	2	2	90%	76%	104%	1.9	1.9	31250	125000	4.2	7%	14%
Fibroblast growth factor 19 (FGF-19)	O95750	387	477	394	503	81%	83%	105%	7.6	7.6	15625	31250	3.3	6%	19%
Fibroblast growth factor 21 (FGF-21)	Q9NSA1	30	39	35	35	76%	89%	89%	31	31	62500	500000	3.3	8%	21%
Fibroblast growth factor 23 (FGF-23)	Q9GZV9	27	38	33	9	71%	86%	22%	122	122	62500	62500	2.7	9%	26%
Fms-related tyrosine kinase 3 ligand (Flt3L)	P49771	405	493	410	532	82%	83%	108%	0.01	0.01	977	3906	4.8	6%	15%
Fractalkine (CX3CL1)	P78423	58	70	64	101	84%	92%	145%	15.3	15.3	15625	31250	3.0	7%	24%
Glial cell line-derived neurotrophic factor (hGDNF)	P39905	5	5	3	4	92%	51%	85%	0.01	0.01	1953	3906	5.1	7%	12%
Hepatocyte growth factor (HGF)	P14210	85	130	67	198	66%	52%	153%	7.6	7.6	125000	125000	3.9	6%	16%
Interferon gamma (IFN-gamma)	P01579	2	2	2	2	104%	89%	103%	15.3	15.3	62500	62500	3.6	7%	17%
Interleukin-1 alpha (IL-1 alpha)	P01583	NR	NR	3	2	NR	NR	NR	0.48	0.95	31250	125000	4.5	7%	18%
Interleukin-2 (IL-2)	P60568	NR	NR	NR	2	NR	NR	NR	30.5	30.5	1000000	1000000	4.5	9%	16%
Interleukin-2 receptor subunit beta (IL-2RB)	P14784	NR	2	2	2	NR	96%	101%	15	31	250000	1000000	3.9	7%	19%
Interleukin-4 (IL-4)	P05112	NR	2	NR	2	NR	NR	115%	0.24	0.24	7812	15625	4.5	7%	16%
Interleukin-5 (IL-5)	P05113	4	2	3	2	175%	126%	105%	3.8	3.8	15625	62500	3.6	7%	17%
Interleukin-6 (IL-6)	P05231	28	31	31	40	90%	99%	128%	0.12	0.12	3906	15625	4.5	6%	8%
Interleukin-7 (IL-7)	P13232	3	7	4	19	45%	64%	283%	0.24	0.24	7812	15625	4.5	6%	18%
Interleukin-8 (IL-8)	P10145	41	69	73	129	60%	106%	188%	0.03	0.03	3906	7812	5.1	6%	15%
Interleukin-10 (IL-10)	P22301	7	10	8	10	75%	77%	105%	0.48	0.48	62500	125000	5.1	7%	12%
Interleukin-10 receptor subunit alpha (IL-10RA)	Q13651	3	2	2	2	137%	94%	105%	3.8	7.6	250000	500000	4.5	6%	19%
Interleukin-10 receptor subunit beta (IL-10RB)	Q08334	61	75	71	79	81%	95%	105%	0.12	0.12	1953	3906	4.2	5%	31%
Interleukin-12 subunit beta (IL-12B)	P29460	12	14	10	16	87%	74%	111%	0.12	0.12	3906	3906	4.5	6%	18%
Interleukin-13 (IL-13)	P35225	NR	NR	NR	NR	NR	NR	NR	7.6	7.6	62500	500000	3.9	14%	26%

Figure 2 List of biomarkers measured by Proseek Multiplex Inflammation I Array (Continued)

		Sample types							Analytical measurement					Precision	
		Signal-to-background (2^{NPX})				Relative 2^{NPX} to EDTA			pg/mL				log10		
Target	UniProt No	ACD	EDTA	Heparin	Serum	ACD	Heparin	Serum	LOD	LLOQ	ULOQ	Hook	Range	Intra-assay	Inter-assay
Interleukin-15 receptor subunit alpha (IL-15RA)	Q13261	2	2	2	2	93%	84%	112%	0.95	0.95	7812	15625	3.9	6%	20%
Interleukin-17A (IL-17A)	Q16552	NR	2	2	2	NR	93%	109%	3.8	7.6	62500	62500	3.9	8%	17%
Interleukin-17C (IL-17C)	Q9P0M4	4	5	4	5	81%	81%	110%	31	31	125000	500000	3.3	6%	18%
Interleukin-18 (IL-18)	Q14116	124	153	133	164	81%	87%	108%	0.06	0.06	15625	15625	5.4	6%	19%
Interleukin-18 receptor 1 (IL-18R1)	Q13478	93	115	102	132	81%	89%	115%	0.06	0.06	7812	15625	5.1	5%	26%
Interleukin-20 (IL-20)	Q9NYY1	2	2	1	2	97%	79%	103%	7.6	15	62500	125000	3.6	7%	22%
Interleukin-20 receptor subunit alpha (IL-20RA)	Q9UHF4	NR	2	NR	2	NR	NR	99%	1.9	1.9	125000	125000	4.8	6%	22%
Interleukin-22 receptor subunit alpha-1 (IL-22 RA1)	Q8N6P7	NR	4	3	3	NR	79%	87%	0.24	0.24	3906	15625	4.2	7%	23%
Interleukin-24 (IL-24)	Q13007	NR	2	2	2	NR	116%	108%	1.9	3.8	31250	125000	3.9	6%	29%
Interleukin-33 (IL-33)	O95760	NR	2	NR	2	NR	NR	97%	3.8	3.8	31250	125000	3.9	9%	26%
Latency-associated peptide transforming growth factor beta 1 (LAP TGF-beta-1)	P01137	81	183	190	352	44%	104%	192%	61	61	500000	500000	3.9	7%	24%
Leukemia inhibitory factor (LIF)	P15018	48	38	60	22	126%	158%	57%	3.8	7.6	15625	31250	3.3	7%	18%
Leukemia inhibitory factor receptor (LIF-R)	P42702	6	8	7	9	75%	83%	107%	30.5	15.3	62500	250000	3.3	7%	26%
Macrophage colony-stimulating factor 1 (CSF-1)	P09603	235	264	227	297	89%	86%	113%	0.004	0.01	1953	3906	5.4	5%	25%
Macrophage inflammatory protein 1-alpha (MIP-1 alpha)	P10147	5	7	5	9	71%	74%	129%	0.06	0.06	488	977	3.9	6%	14%
Matrix metalloproteinase-1 (MMP-1)	P03956	3	9	6	9	28%	68%	93%	1.9	3.8	15625	31250	3.6	5%	19%
Matrix metalloproteinase-10 (MMP-10)	P09238	104	103	117	145	101%	114%	141%	0.95	0.95	15625	62500	4.2	5%	28%
Monocyte chemotactic protein 1 (MCP-1)	P13500	1064	1213	1063	1494	88%	88%	123%	0.03	0.03	1953	3906	4.8	6%	13%
Monocyte chemotactic protein 2 (MCP-2)	P80075	363	610	488	982	60%	80%	161%	0.06	0.06	3906	7812	4.8	6%	8%
Monocyte chemotactic protein 3 (MCP-3)	P80098	4	5	6	6	78%	110%	120%	0.48	0.48	1953	3906	3.6	7%	17%
Monocyte chemotactic protein 4 (MCP-4)	Q99616	5	8	9	15	59%	111%	189%	7.6	7.6	3906	3906	2.7	6%	11%
Natural killer cell receptor 2B4 (CD244)	Q9BZW8	60	75	67	81	81%	90%	108%	0.06	0.06	7812	15625	5.1	5%	24%
Neurotrophin-3 (NT-3)	P20783	4	5	2	4	75%	37%	78%	0.12	0.12	3906	7812	4.5	6%	13%
Neurturin (NRTN)	Q99748	NR	2	NR	2	NR	NR	109%	3.8	7.6	15625	62500	3.3	9%	15%
Oncostatin-M (OSM)	P13725	6	14	12	37	46%	86%	272%	0.03	0.03	977	3906	4.5	5%	12%
Osteoprotegerin (OPG)	O00300	1205	1385	1103	1520	87%	80%	110%	0.24	0.48	31250	62500	4.8	6%	12%
Programmed cell death 1 ligand 1 (PD-L1)	Q9NZQ7	6	5	5	6	135%	99%	124%	3.8	3.8	500000	1000000	5.1	9%	25%
Protein S100-A12 (EN-RAGE)	P80511	8	4	12	35	196%	274%	825%	122	122	500000	1000000	3.6	8%	17%
Signaling lymphocytic activation molecule (SLAMF1)	Q13291	6	7	6	8	82%	89%	113%	31	31	1000000	1000000	4.5	9%	21%
SIR2-like protein 2 (SIRT2)	Q8IXJ6	8	36	8	20	23%	21%	57%	7.6	15.3	62500	250000	3.6	6%	22%
STAM-binding protein (STAMPB)	O95630	10	25	9	17	39%	37%	67%	7.6	7.6	31250	62500	3.6	5%	27%
Stem cell factor (SCF)	P21583	334	368	356	418	91%	97%	113%	1.9	3.8	15625	31250	4	5%	20%
Sulfotransferase 1A1 (ST1A1)	P50225	3	2	5	5	122%	228%	183%	244	244	125000	500000	2.7	6%	25%
T cell surface glycoprotein CD5 (CD5)	P06127	21	23	20	24	90%	89%	104%	0.06	0.12	3906	15625	4.5	5%	22%
T cell surface glycoprotein CD6 isoform (CD6)	Q8WWJ7	19	23	21	22	84%	91%	98%	0.24	0.24	7812	31250	4.2	6%	23%
Thymic stromal lymphopoietin (TSLP)	Q969D9	NR	2	NR	2	NR	NR	94%	3.8	3.8	15625	62500	3.8	6%	20%
TNF-beta (TNFB)	P01374	13	14	13	16	93%	91%	114%	0.24	0.48	15625	15625	4.5	6%	22%
TNF-related activation-induced cytokine (TRANCE)	O14788	23	27	23	29	83%	84%	106%	3.8	3.8	31250	125000	3.9	7%	24%
TNF-related apoptosis-inducing ligand (TRAIL)	P50591	383	425	382	484	90%	90%	114%	0.95	0.95	31250	31250	4.5	5%	17%
Transforming growth factor alpha (TGF-alpha)	P01135	3	3	3	11	90%	81%	342%	0.48	0.48	3906	31250	3.9	6%	27%
Tumor necrosis factor (Ligand) superfamily, member 12 (TWEAK)	Q4ACW9	410	537	432	669	76%	80%	124%	1.9	1.9	125000	500000	4.8	6%	11%
Tumor necrosis factor (TNF)	P01375	8	5	7	7	177%	158%	153%	0.48	0.48	3906	15625	3.9	9%	11%
Tumor necrosis factor ligand superfamily member 14 (TNFSF14)	O43557	5	6	7	23	74%	119%	378%	0.95	1.9	15625	31250	3.9	6%	15%
Tumor necrosis factor receptor superfamily member 9 (TNFRSF9)	Q07011	74	84	76	95	88%	91%	114%	0.03	0.03	3906	3906	5.1	5%	21%
Urokinase-type plasminogen activator (uPA)	P00749	1227	1408	1306	1346	87%	93%	96%	0.12	0.12	7812	15625	4.8	5%	11%
Vascular endothelial growth factor A (VEGF-A)	P15692	1218	1909	1608	3004	64%	84%	157%	0.06	0.06	7812	15625	5.1	6%	8%

Figure 3 List of biomarkers measured by Proseek Multiplex Oncology II Arrays

		Sample types						Endogenous Interference	Analytical measurement					Precision	
		Normal plasma levels (NPX)			Relative to EDTA plasma (%)			(mg/mL)	pg/mL				log10	% CV	
Target	UniProt No	10th %tile	Median	90th %tile	ACD	Heparin	Serum	Haemolysate	LOD	LLOQ	ULOQ	Hook	Range	Intra	Inter
5'-nucleotidase (5'-NT)	P21589	8.3	8.9	9.7	105	137	142	7.5	0.5	0.5	62 500	62 500	5.1	6.6	23
A disintegrin and metalloproteinase with thrombospondin motifs 15 (ADAM-TS 15)	Q8TE58	3.1	4.1	4.7	86	56	27	15	15	30	125 000	250 000	3.6	7.6	14
Alpha-taxilin (TXLNA)	P40222	1.5	2.3	3.3	49	32	46	3.8	7.6	7.6	31 250	125 000	3.6	7.3	13
Amphiregulin (AR)	P15514	1.6	2.0	2.9	93	83	121	15	1.9	15	15 625	31 250	3.0	8.8	12
Annexin A1 (ANXA1)	P04083	1.3	2.0	3.5	97	171	232	0.9	976	976	125 000	500 000	2.1	7.8	16
Carbonic anhydrase 9 (CA9)	Q16790	2.1	2.8	3.9	102	101	125	7.5	1.9	1.9	15 625	31 250	3.9	8.2	14
Carboxypeptidase E (CPE)	P16870	3.1	3.6	4.1	87	78	102	15	15	15	125 000	500 000	3.9	8.5	16
Carcinoembryonic antigen-related cell adhesion molecule 1 (CEACAM1)	P13688	6.8	7.4	7.8	95	98	118	15	7.6	7.6	125 000	125 000	4.2	4.9	13
Carcinoembryonic antigen-related cell adhesion molecule 5 (CEACAM5)	P06731	1.7	2.7	3.7	95	88	109	15	7.6	15	31 250	125 000	3.3	11	20
Cathepsin L2 (CTSV)	O60911	3.2	3.7	4.4	96	78	105	15	61	61	7 812	15 625	2.1	8.8	11
CD160 antigen (CD160)	O95971	4.3	5.0	5.6	94	102	118	15	0.1	0.2	7 812	31 250	4.5	7.6	16
CD27 antigen (CD27)	P26842	7.5	7.9	8.6	95	100	109	15	0.1	0.2	7 812	7 812	4.5	7.2	12
CD48 antigen (CD48)	P09326	6.3	6.7	7.2	90	109	119	15	7.6	7.6	31 250	125 000	3.6	6.6	14
CD70 antigen (CD70)	P32970	3.5	4.2	5.0	95	96	165	7.5	15	30	125 000	250 000	3.6	7.2	15
Cornulin (CRNN)	Q9UBG3	4.6	5.6	6.5	99	104	112	15	1.9	1.9	3 906	15 625	3.3	9.4	16
C-type lectin domain family 4 member K (CD207)	Q9UJ71	2.1	2.6	3.4	102	101	111	7.5	7.6	7.6	125 000	250 000	4.2	8.2	14
C-X-C motif chemokine 13 (CXCL13)	O43927	7.1	8.0	9.3	100	82	132	15	7.6	7.6	15 625	15 625	3.3	6.1	11
Cyclin-dependent kinase inhibitor 1 (CDKN1A)	P38936	0.8	1.1	1.9	60	39	44	15	NA	NA	NA	NA	NA	7.3	12
Delta-like protein 1 (DLL1)	O00548	8.5	9.0	9.4	94	103	117	15	1.9	1.9	31 250	125 000	4.2	7.8	15
Disintegrin and metalloproteinase domain-containing protein (ADAM8)	P78325	3.5	4.0	4.4	104	112	153	15	15	30	62 500	125 000	3.3	7.0	16
Endothelial cell-specific molecule 1 (ESM-1)	Q9NQ30	7.0	7.7	8.7	60	53	82	7.5	7.6	15	15 625	31 250	3.0	9.6	14
Ephrin type-A receptor 2 (EPH2)	P29317	1.6	1.9	2.2	98	101	124	15	7.6	7.6	62 500	125 000	3.9	8.0	15
FAS-associated death domain protein (FADD)	Q13158	0.8	1.0	1.7	85	87	128	1.9	7812	7812	1 000 000	1 000 000	2.1	7.2	13
Fc receptor-like B (FCRLB)	Q8IAA4	1.0	1.6	2.8	101	76	103	15	7.8	3.8	125 000	125 000	4.5	8.5	13
Fibroblast growth factor-binding protein 1 (FGF-BP1)	Q14512	6.0	6.2	6.7	116	98	117	15	7.6	30	62 500	125 000	3.3	5.7	13
Folate receptor alpha (FR-alpha)	P15328	6.2	6.6	7.1	97	96	122	7.5	0.5	0.95	7 812	125 000	3.9	8.1	15
Folate receptor gamma (FR-gamma)	P41439	2.6	9.2	12	97	103	130	3.8	0.1	0.11	7 812	125 000	4.8	7.8	13
Furin (FURIN)	P09958	2.6	3.3	4.0	93	96	143	15	61	61	125 000	125 000	3.3	7.4	15
Galectin-1 (Gal-1)	P09382	5.6	6.1	6.5	95	106	118	15	31	61	125 000	250 000	3.3	5.3	14
Glypican-1 (GPC1)	P35052	4.0	4.5	5.1	89	99	121	15	122	488	250 000	500 000	2.7	7.7	13
Granzyme B (GZMB)	P10144	1.4	2.3	3.0	95	73	92	3.8	1.0	0.95	7 812	7 812	3.9	9.1	13
Granzyme H (GZMH)	P20718	2.7	3.6	4.5	99	107	124	1.9	3.8	7.6	15 625	31 250	3.3	7.7	16
Hepatocyte growth factor (HGF)	P14210	5.4	5.8	6.7	72	54	156	15	7.6	15	125 000	125 000	3.9	8.5	15
ICOS ligand (ICOSLG)	O75144	3.8	4.3	4.8	98	137	148	7.5	7.6	7.6	31 250	125 000	3.6	5.7	15
Insulin-like growth factor 1 receptor (IGF1R)	P08069	3.0	3.3	3.8	95	97	144	15	7.6	15	500 000	500 000	4.5	7.9	15
Integrin alpha-V (ITGAV)	P06756	3.4	3.8	4.3	87	88	109	7.5	7.6	15	31 250	125 000	3.3	5.5	13
Integrin beta-5 (ITGB5)	P18084	7.6	8.2	8.8	56	57	68	15	1.9	15	125 000	125 000	3.9	7.3	13
Interferon gamma receptor 1 (IFN-gamma-R1)	P15260	3.2	3.6	3.9	94	102	121	15	3.8	7.6	31 250	125 000	3.6	7.3	15
Interleukin-6 (IL-6)	P05231	1.9	3.0	4.1	99	96	129	15	0.02	0.05	3 906	7 812	4.8	8.3	12
Kallikrein-11 (hK11)	Q9UBX7	4.6	5.1	5.6	93	105	118	15	15	15	7 812	31 250	2.7	7.8	13
Kallikrein-13 (KLK13)	Q9UKR3	2.2	3.3	3.9	116	88	96	15	1.9	1.9	7 812	125 000	3.6	7.3	16
Kallikrein-14 (hK14)	Q9P0G3	5.9	6.8	7.4	95	65	97	15	15	30	31 250	31 250	3.0	9.4	15
Kallikrein-8 (hK8)	O60259	6.0	6.5	7.0	90	106	112	15	3.8	7.6	7 812	125 000	3.0	7.0	14
Ly6/PLAUR domain-containing protein 3 (LYPD3)	Q95274	3.7	4.1	4.7	95	104	115	15	15	30	31 250	125 000	3.0	6.3	13
Melanoma-derived growth regulatory protein (MIA)	Q16674	9.4	9.9	10	97	72	104	15	0.95	3.8	3 906	7 812	3.0	7.4	12
Mesothelin (MSLN)	Q13421	1.9	2.7	3.0	100	109	129	15	244	488	500 000	1 000 000	3.0	6.5	20
Methionine aminopeptidase 2 (MetAP2)	P50579	2.42	2.9	4.0	46	16	92	0	244	244	62 500	125 000	2.4	7.2	12
MHC class I polypeptide-related sequence A/B (MIC A/B)	Q29983, Q29980	1.15	4.1	4.9	101	103	132	15	0.95	1.9	3 906	125 000	3.3	6.4	17
Midkine (Mk)	P21741	5.2	6.0	7.2	49	39	53	15	15	15	7 812	125 000	2.7	9.6	15

Figure 4 List of biomarkers measured by Proseek Multiplex Oncology II Arrays (Continued)

		Sample types						Endogenous interference	Analytical measurement					Precision	
		Normal plasma levels (NPX)			Relative to EDTA plasma (%)			(mg/mL)	pg/mL				log10	% CV	
Target	UniProt No	10th %tile	Median	90th %tile	ACD	Heparin	Serum	Haemolysate	LOD	LLOQ	ULOQ	Hook	Range	Intra	Inter
Mothers against decapentaplegic homolog 5 (MAD homolog 5)	Q99717	3.1	3.8	4.2	100	18	97	15	30	30	62 500	125 000	3.3	7.4	13
Mucin-16 (MUC-16)	Q8WX07	3.8	4.8	6.7	86	102	127	15	0.03	0.03	1 250	1 250	4.5	7.9	15
Nectin-4 (PVRL4)	Q96NY8	5.6	5.9	6.3	92	97	119	15	0.47	0.47	7 812	7 812	4.2	7.5	15
Pancreatic prohormone (PPY)	P01298	2.0	4.1	5.9	91	91	52	7.5	244	244	62 500	125 000	2.4	9.7	16
Podocalyxin (PODXL)	O00592	3.9	4.3	4.5	97	105	114	7.5	7.6	7.6	31 250	125 000	3.6	4.6	16
Pro-epidermal growth factor (EGF)	P01133	3.7	4.3	6.6	30	140	727	15	0.47	0.95	7 812	7 812	3.9	9.0	11
Protein CYR61 (CYR61)	O00622	3.8	5.0	6.3	170	51	174	15	7.6	30	125 000	500 000	3.6	9.2	14
Protein S100-A11 (S100A11)	P31949	3.0	3.4	4.0	103	108	152	15	3.8	7.6	7 812	125 000	3.0	6.3	14
Protein S100-A4 (S100A4)	P26447	2.5	3.1	3.8	69	96	203	0	122	244	125 000	125 000	2.7	7.0	13
Proto-oncogene tyrosine-protein kinase receptor Ret (RET)	P07949	2.8	3.6	4.4	170	178	228	7.5	7.6	30	125 000	250 000	3.6	7.7	16
Receptor tyrosine-protein kinase erbB-2 (ERBB2)	P04626	6.7	7.1	7.5	91	99	120	15	0.5	0.47	31 250	31 250	4.8	7.4	15
Receptor tyrosine-protein kinase erbB-3 (ERBB3)	P21860	7.6	8.1	8.4	93	88	116	15	0.95	1.9	31 250	125 000	4.2	6.2	16
Receptor tyrosine-protein kinase erbB-4 (ERBB4)	Q15303	4.5	5.0	5.4	97	99	122	15	3.8	7.6	7 812	31 250	3.0	6.3	15
R-spondin-3 (RSPO3)	Q9BXY4	2.4	3.2	3.8	71	71	67	15	1.9	1.9	15 625	31 250	3.9	9.9	13
Secretory carrier-associated membrane protein 3 (SCAMP3)	O14828	1.2	1.6	2.6	87	88	101	0.5	122	244	125 000	500 000	2.7	8.2	15
Seizure 6-like protein (SEZ6L)	Q9BYH1	5.3	5.8	6.2	94	109	127	15	122	244	125 000	250 000	2.7	7.4	15
SPARC (SPARC)	P09486	5.6	5.9	6	66	113	144	15	30	61	125 000	1 000 000	3.3	5.0	11
Stem cell factor (SCF)	P21583	8.2	8.8	9.4	92	99	113	7.5	0.95	0.95	31 250	125 000	4.5	7.3	13
Syndecan-1 (SYND1)	P18827	5.4	6.1	7.0	90	101	131	15	7.6	15	125 000	125 000	3.9	7.7	14
T-cell leukemia / lymphoma protein 1A (TCL1A)	P56279	3.5	5.2	7.8	54	83	59	3.8	1.9	7.6	62 500	125 000	3.9	9.1	14
TGF-beta receptor type-2 (TGFR-2)	P37173	6.5	7.2	7.6	90	100	121	15	0.95	0.95	7 812	125 000	3.9	8.3	14
Tissue factor pathway inhibitor 2 (TFPI-2)	P48307	7.1	7.7	8.4	73	88	90	15	0.95	0.95	7 812	15 625	3.9	8.8	13
T-lymphocyte surface antigen Ly-9 (LY9)	Q9HBG7	4.9	5.3	5.8	94	106	122	15	0.47	0.47	31 250	31 250	4.8	6.5	14
TNF-related apoptosis-inducing ligand (TRAIL)	P50591	4.5	5.5	6.1	94	99	118	15	0.47	0.47	7 812	125 000	4.2	7.6	15
Toll-like receptor 3 (TLR3)	O15455	1.8	2.0	2.4	98	87	372	3.8	0.95	0.95	7 812	7 812	3.9	7.7	14
Transforming growth factor alpha (TGF-alpha)	P01135	6.3	6.6	7.0	101	103	117	15	7.6	7.6	62 500	125 000	3.9	5.2	16
Transmembrane glycoprotein NMB (GPNMB)	Q14956	7.0	7.3	7.7	98	97	121	15	1.9	7.6	31 250	31 250	3.6	7.9	12
Tumor necrosis factor ligand superfamily member 13 (TNFSF13)	O75888	7.3	7.9	8.5	78	82	101	7.5	7.6	30	250 000	250 000	3.9	7.9	13
Tumor necrosis factor ligand superfamily member 6 (FASLG)	P48023	8.0	8.7	9.4	114	100	120	15	0.03	0.03	7 812	15 625	5.4	8.9	13
Tumor necrosis factor receptor superfamily member 19 (TNFRSF19)	Q9NS68	3.8	4.3	4.8	87	99	137	7.5	0.47	1.9	7 812	7 812	3.6	7.8	15
Tumor necrosis factor receptor superfamily member 4 (TNFRSF4)	P43489	2.4	3.1	3.6	95	99	127	7.5	0.47	0.95	7 812	7 812	3.9	7.5	15
Tumor necrosis factor receptor superfamily member 6B (TNFRSF6B)	O95407	3.4	4.1	5.1	89	70	154	15	7.6	15	31 250	125 000	3.3	8.5	13
Tyrosine-protein kinase ABL1 (ABL1)	P00519	1.6	2.0	2.6	80	60	82	3.8	0.95	1.9	62 500	250 000	4.5	8.2	18
Tyrosine-protein kinase Lyn (LYN)	P07948	1.0	1.3	1.8	84	56	78	3.8	7.6	15	7 812	7 812	2.7	5.6	13
WAP four-disulfide core domain protein 2 (WFDC2)	Q14508	6.8	7.2	7.6	97	106	121	15	7.6	7.6	31 250	125 000	3.6	6.8	13
Vascular endothelial growth factor A (VEGF-A)	P15692	8.6	9.1	9.7	71	88	153	15	0.11	0.11	7 812	15 625	4.8	8.3	13
Vascular endothelial growth factor receptor 2 (VEGFR-2)	P35968	6.2	6.8	7.2	103	94	114	15	7.6	7.6	31 250	125 000	3.6	6.4	19
Vascular endothelial growth factor receptor 3 (VEGFR-3)	P35916	5.8	6.5	6.8	92	101	129	15	122	244	250 000	1 000 000	3.0	6.1	14
VEGF-co regulated chemokine 1 (CXL17)	Q6UXB2	2.9	4.4	5.2	81	79	57	7.5	7.6	30	125 000	250 000	3.6	8.6	20
Vimentin (VIM)	P08670	1.7	2.9	5.1	73	363	644	0.5	976	976	1 000 000	1 000 000	3.0	8.6	15
Wnt inhibitory factor 1 (WIF-1)	Q9Y5W5	4.7	5.3	5.9	87	98	109	15	15	30	125 000	500 000	3.6	9.1	15
WNT1-inducible-signaling pathway protein 1 (WISP-1)	O95388	3.6	4.2	5.0	74	116	212	15	3.8	15	31 250	31 250	3.3	8.2	15
Xaa-Pro aminopeptidase 2 (XPNPEP2)	O43895	6.1	7.4	7.9	100	101	116	7.5	7.6	15	62 500	125 000	3.6	5.6	15

*U/µl

Figure 5 Complete list of biomarkers measured by Proseek Multiplex Inflammation I and Oncology II Arrays. Statistical analysis used was ANOVA

Protein (INF)	p-value	BH adjusted	Protein (ONC)	p-value	BH adjusted
X102_VEGF.A	0.0003666	0.0113874	X174_WISP.1	0.0003388	0.009371935
X135_TGF.alpha	0.0004211	0.0113874	X132_SCF	0.0003468	0.009371935
X132_SCF	0.000589	0.0113874	X123_TFPI.2	0.0003905	0.009371935
X105_MCP.3	0.0012687	0.0183961	X102_VEGF.A	0.0007893	0.014207245
X156_HGF	0.005545	0.0631728	X152_CTSV	0.001387	0.019972171
X110_OPG	0.0068734	0.0631728	X137_CYR61	0.00224	0.026074809
X154_CXCL5	0.0086334	0.0631728	X179_ESM.1	0.0025351	0.026074809
X112_uPA	0.0102661	0.0631728	X135_TGF.alpha	0.003631	0.032678642
X149_IL.10RB	0.0113577	0.0631728	X162_ABL1	0.0048946	0.039156459
X187_TNFRSF9	0.0114034	0.0631728	X178_AR	0.0059803	0.043058068
X183_MCP.2	0.0125791	0.0631728	X168_TNFRSF19	0.0071677	0.046915615
X118_AXIN1	0.0130702	0.0631728	X111_SYND1	0.0095773	0.052092942
X158_IL.24	0.016588	0.074008	X110_TNFRSF6B	0.010117	0.052092942
X128_CXCL1	0.0224041	0.0921551	X161_MK	0.0102088	0.052092942
X189_TWEAK	0.0238332	0.0921551	X156_HGF	0.0108527	0.052092942
X184_CASP.8	0.0266978	0.0938297	X136_FURIN	0.0123464	0.055558959
X133_IL.18	0.0275018	0.0938297	X117_IFN.gamma.R1	0.0131306	0.055611821
X151_IL.18R1	0.0358756	0.115599	X163_FGF.BP1	0.0149696	0.059878365
X107_CDCP1	0.0447368	0.1292336	X108_TNFSF13	0.0158349	0.06000597
X155_TRANCE	0.0463388	0.1292336	X130_ERBB2	0.0188071	0.067705466
X116_IL.17A	0.0481679	0.1292336	X165_LYN	0.0206558	0.06897037
X115_MCP.1	0.0490196	0.1292336	X143_EPHA2	0.0210743	0.06897037
X192_STAMPB	0.0588581	0.1484248	X101_TXLNA	0.0240469	0.075277316
X161_MMP.10	0.0657434	0.1588798	X196_FR.alpha	0.0263063	0.078918816
X168_CXCL6	0.078966	0.1819451	X183_CXCL13	0.0276531	0.079640889
X142_MMP.1	0.0815616	0.1819451	X159_DKN1A	0.0316081	0.086316489
X167_Flt3L	0.0904762	0.1893562	X153_CD27	0.0323687	0.086316489
X194_ADA	0.091644	0.1893562	X139_FADD	0.0355851	0.091504564
X138_TNFSF14	0.097181	0.1893562	X115_SCAMP3	0.0407097	0.10058616
X164_CCL23	0.0979429	0.1893562	X120_TRAIL	0.0419109	0.10058616
X126_OSM	0.1040154	0.1946095	X131_ERBB3	0.0433396	0.100659608
X137_CCL11	0.1269143	0.2300322	X158_5..NT	0.0514119	0.115676724
X108_CD244	0.131941	0.2318963	X145_Gal.1	0.0535574	0.116852569
X120_TRAIL	0.1430219	0.234408	X169_CRNN	0.0568459	0.12037946
X181_LIF	0.1453257	0.234408	X172_TNFRSF4	0.0637673	0.13117848
X173_CCL28	0.1474325	0.234408	X141_PVRL4	0.0785333	0.157066596
X196_CSF.1	0.1506359	0.234408	X122_GPC1	0.0913602	0.177782086
X111_LAP.TGF.beta.1	0.1535777	0.234408	X118_ITGAV	0.1041812	0.193565615
X169_CXCL10	0.1661708	0.2471258	X129_IGF1R	0.104848	0.193565615
X165_CD5	0.183774	0.2664723	X182_WFDC2	0.114004	0.204530155
X172_SIRT2	0.1939915	0.274427	X142_FASLG	0.1164686	0.204530155
X176_CD40	0.2068908	0.2857064	X106_CEACAM1	0.123426	0.208948637
X122_CXCL9	0.2190136	0.2954137	X140_MetAP.2	0.1247888	0.208948637
X190_CCL20	0.2270611	0.2993078	X160_DLL1	0.1464984	0.239724647
X131_CD6	0.2746101	0.3539419	X133_SPARC	0.1574653	0.247799912
X191_ST1A1	0.3088709	0.3894459	X121_hK11	0.1583166	0.247799912
X117_CXCL11	0.3220419	0.3974134	X151_MIA	0.1724233	0.264137804
X177_IL.33	0.3476907	0.4201262	X157_ADAM.8	0.1762811	0.264421656
X113_IL.6	0.3669189	0.4343122	X164_TLR3	0.2049435	0.301141414
X170_4E.BP1	0.4339152	0.5033416	X149_GPNMB	0.2129564	0.306657186
X101_IL.8	0.6470087	0.7358138	X193_GZMB	0.2204761	0.306774654

Figure 6 Complete list of biomarkers measured by Proseek Multiplex Inflammation I and Oncology II Arrays. Statistical Analysis used was ANOVA (Continued)

X157_IL.12B	0.6870602	0.7663364	X191_MUC.16	0.2215595	0.306774654
X125_IL.1.alpha	0.7975284	0.8692334	X107_MSLN	0.2274931	0.309047241
X145_CCL19	0.8092862	0.8692334	X116_LY9	0.2374402	0.316586977
X166_MIP.1.alpha	0.8417594	0.8721493	X138_hK14	0.2436017	0.318896792
X175_EN.RAGE	0.8420752	0.8721493	X144_ITGB5	0.2831004	0.363986205
X123_CST5	0.9532566	0.9607611	X114_CD48	0.3959387	0.500133143
X130_CCL4	0.9607611	0.9607611	X175_CXL17	0.48828	0.603511051
			X134_GZMH	0.4945438	0.603511051
			X189_CEACAM5	0.5094971	0.611396579
			X150_CA9	0.526761	0.621566537
			X173_MIC.A.B	0.5352379	0.621566537
			X167_VIM	0.5614204	0.641623263
			X109_EGF	0.6333572	0.696298835
			X113_IL.6	0.6336725	0.696298835
			X188_FR.gamma	0.6382739	0.696298835
			X177_S100A11	0.6862059	0.737415345
			X128_S100A4	0.7256994	0.768387627
			X170_TCL1A	0.8273283	0.863299126
			X105_KLK13	0.8494477	0.873717662
			X124_hK8	0.9115278	0.924366172
			X195_ANXA1	0.9898303	0.98983027